

申 报	系列：教师
	专业：材料学
	职称：教授

业绩成果材料

（申报人的业绩成果材料包括论文、科研项目、获奖以及其他成果等）

单 位（二级单位） 材料与能源学院

姓 名 林雅铃

材料核对人：

单位盖章：

核对时间：

华南农业大学制

目 录

一、教学研究业绩

1. 教学研究项目

- 1.1 在制药工程专业设立“创新学分”的探索研究（校级教改项目） 1
- 1.2 药物分析（校级质量工程） 3
- 1.3 课程育人与科研育人相结合——《药物分析》研究性教学探索（校级教改项目） 4
- 1.4 深度学习视域下《药物分析》课程线上线下混合式教学模式探索（广东省高等教育学会研究课题） 10

2. 教改论文

- 2.1 基于离子氢键的聚硅氧烷超分子弹性体的制备及其实验设计（C类） 11
- 2.2 聚丙烯酰胺季铵盐大分子药物的环境毒性评价及其实验设计（C类） 21

二、科研项目

1. 主持

- 1.1 两亲性大分子季铵盐的合成及其对水稻纹枯病菌的抑制作用与机理（国家自然科学基金项目，31772202）有关佐证材料 31
- 1.2 两亲性大分子季铵盐的合成及其在水稻纹枯病防治中的应用研究（广州市科技计划项目，201704020084）有关佐证材料 33
- 1.3 两亲性聚硅氧烷接枝季铵盐的合成及其在香蕉枯萎病防治中的应用（广东省科技计划项目，2016A020210105）有关佐证材料 37

1.4 甜菜碱型两性离子聚合物的合成及其在甜菜夜蛾无公害防治中的应用（教育部博士点新教师基金项目，20124404120025）有关佐证材料.....	40
1.5 含聚硅氧烷两亲性大分子季铵盐的合成及其在香蕉枯萎病防治中的应用（广州市科技计划项目，201803020015）有关佐证材料	43
1.6 基于微区分离与动态可逆键的人工心脏瓣膜用超分子弹性体（广东省自然科学基金，2023A1515011264）有关佐证材料	49
1.7 人工心脏瓣膜用抗凝抗钙化聚氨酯弹性体（其他纵向，20240010）有关佐证材料.....	54
1.8 聚合物材料的生物相容性评价（横向项目，h20220413）有关佐证材料	57
1.9 覆铜板基板树脂材料的开发研究（横向项目，h20240612）有关佐证材料	63
2. 主要参加	
2.1 基于抑制昆虫雌性生殖干细胞分化活性的骆驼蓬碱构效（教育部博士点博导项目，20134404110019）有关佐证材料	66

三、论文、著作等

1. 检索证明	67
2. 以第一作者发表本专业论文情况	
2.1. Synergistic enhancement of the robustness of multifunctional polyurethane via an ionic noncovalent cross-linking network and aromatic disulfides (<i>Chemical Engineering Journal</i> , 2024)	72
2.2 Surface-imprinted polysiloxane with recognition ability based on an	

ITO layer for rapid detection of <i>Fusarium oxysporum</i> f. sp. <i>cubense</i> by the naked eye (<i>ACS Applied Materials & Interfaces</i> , 2024)	86
2.3 Amphiphilic polysiloxane graft guanidine salts with a combination of low environmental toxicity and high antifungal activity (<i>European Polymer Journal</i> , 2024)	96
2.4 Fluorine-containing amphiphilic quaternary ammonium salts for the suppression of Banana fusarium wilt (<i>Reactive & Functional Polymers</i> , 2023)	105
2.5 Polymeric diallyl quaternary ammonium salts for inhibiting banana <i>Fusarium</i> wilt (<i>Reactive & Functional Polymers</i> , 2022)	115
2.6 Molecularly Imprinted Photonic Crystals Based on Fusaric Acid for the Detection of Banana <i>Fusarium</i> Wilt (<i>ACS Applied Polymer Materials</i> , 2021)	121
2.7 The interactions between bovine serum albumin and carboxybetaine-functionalized polysiloxanes in solution (<i>Colloid and Polymer Science</i> , 2016)	129
2.8 Synthesis and antimicrobial activities of polysiloxane-containing quaternary ammonium salts on bacteria and phytopathogenic fungi (<i>Reactive & Functional Polymers</i> , 2014)	138
2.9 多臂星形聚乙二醇-聚乳酸嵌段共聚物的降解特性 (<i>高分子材料科学与工程</i> , 2013)	147

3. 以通讯作者发表本专业论文情况

3.1 Polyacrylamide quaternary ammonium salts based on stable adsorption in soil and its application on the control of soil-borne fungal disease (<i>European Polymer Journal</i> , 2024)	154
3.2 Antifungal mechanisms of polymeric quaternary ammonium salts	

against conidia of <i>Fusarium oxysporum</i> f. sp. <i>cubense</i> , race 4 (<i>European Journal of Plant Pathology</i> , 2023)	161
3.3 超声细胞粉碎法快速提取真菌中的麦角甾醇 (<i>南京农业大学学报</i> , 2021)	176
3.4 Polydimethylsiloxane-polymethacrylate block copolymers containing quaternary ammonium salts against <i>Fusarium oxysporum</i> f. sp. <i>cubense</i> race 4 in soil: Antifungal activities and pot experiments (<i>Reactive & Functional Polymers</i> , 2021)	186
3.5 Anti- <i>Rhizoctonia solani</i> activity by polymeric quaternary ammonium salt and its mechanism of action (<i>Reactive & Functional Polymers</i> , 2018)	196
3.6 Polymeric quaternary ammonium salt activity against <i>Fusarium oxysporum</i> f. sp. <i>cubense</i> race 4: Synthesis, structure-activity relationship and mode of action (<i>Reactive & Functional Polymers</i> , 2017)	206

四、科研成果

1. 知识产权

1.1. 专利授权证书：大分子季铵盐在抑制水稻纹枯病菌菌核萌发中的用途 (专利号：201610278530.1)	216
1.2. 专利授权证书：嵌段大分子季铵盐在抑制香蕉枯萎病菌生长中的用途 (专利号：201610278195.5)	218
1.3. 专利授权证书：非渗透性的聚硅氧烷的无规共聚物及其制备方法和应用 (专利号：202011328953.2)	220
1.4. 专利授权证书：具有两嵌段结构的含氟大分子季铵盐及其制备方法和应用 (专利号：202210337163.3)	222

五、其他业绩

1. 指导学生学科竞赛

- 1.1. 指导学生参加学科竞赛（广东省第十届大学生材料创新大赛总决赛 三等奖，2020 年）..... 224

2. 近五年本科评教有 3 个学期以上在本单位排名前 10%的证明材料 225

华南农业大学2013年度教育教学改革与研究一般、自筹项目一览表

序号	项目名称	项目负责人	项目类别
1	单片机课程网络教学资源建设与考核方式改革	邓小玲	一般项目
2	《企业网组网实验》课程的优化研究	韩方珍	一般项目
3	国际班双语教学PBL教学模式研究与实践	张霞	一般项目
4	《包装印刷工艺实验》课程的整合设计与教学实践	范小平	一般项目
5	基于研究型实验的《化学生物学》实验教学的探索与实践	熊亚红	一般项目
6	园林专业《园林工程学》课程实践教学改革创新研究	汤辉	一般项目
7	《汽车构造》精品课程建设的研究与实践	武涛	一般项目
8	专业大类教学模式《概率论与数理统计》课程教学改革与实践	徐小红	一般项目
9	教师角色理论在《植物学》实验课程教学组织中的应用研究	白玫	一般项目
10	《植物制片与形态结构》课程内容体系改革和优化的研究与实践	梁社坚	一般项目
11	《大学物理》实验教学模式改革的研究	刘勇	一般项目
12	院级实验教学示范中心公共创新平台运行模式的探讨	黄九九	一般项目
13	高校移动网络教学模式探索与研究	曾鸣	一般项目
14	基于Moodle的《大学计算机基础》课程在线学习平台的设计与应用研究	杨磊	一般项目
15	基于移动计算技术的高等教育信息化服务体系的研究与探索	梁茹冰	一般项目
16	《汽车试验学》课程改革与实践研究	吴伟斌	一般项目
17	《森林生态学》双语课程教学资源整合与实践	贾小容	一般项目
18	《生物质能源工程》课程教学改革与探索	王明峰	一般项目
19	《环境保护与可持续发展》课程教学改革与实践	赵本良	一般项目
20	《食品生物技术》“快捷式”教学过程探索与实践	陈忠正	一般项目
21	本科生推荐免试研究生后期质量跟踪调查与信息反馈——基于地方重点院校的实证研究	孟成民	一般项目
22	基于网络平台的高等农业院校参与公益性农技推广人员培训的模式研究	宋欢	一般项目
23	师生互动环节在《毛泽东思想和中国特色社会主义理论体系概论》课程中的方法设计与应用研究	崔慧霞	一般项目
24	我校大类招生人才培养模式下本科生专业分流机制优化研究	刘春桃	一般项目
25	工商管理本科应用型人才培养的问题与对策研究——以华南农业大学为例	郭萍	一般项目
26	阳光体育运动下的普通高校耐力跑课程的教学设计改革与实践	周华锋	一般项目
27	《创业管理》课程教学内容体系改革和整体优化研究与实践	杨学儒	一般项目
28	文化素质教育课程建设与教学改革——基于大学生心理素质教育课程建设与教学改革研究	宋迎秋	一般项目
29	基于文化创意产业特点的《基础写作》课程教学研究	王青	一般项目
30	社会化背景下学校社区工作的育人功能研究	李敏	一般项目
31	高校人才培养与企业需求有效对接的研究——以法学专业为例	郑大睿	一般项目
32	基于珠三角会展经济发展的《展示设计》课程教学改革研究	李女仙	一般项目
33	构建“华农文库”，推动华南农业大学学科建设	何建新	一般项目
34	汉语言文学专业百篇作文训练培养模式研究	韦盛年	一般项目
35	高校《思想道德修养与法律基础》课师生互动教学模式的效果评估指标体系研究	张机	一般项目
36	电子沙盘模拟在管理类专业课程实验教学中的应用研究	张程	一般项目
37	中外合作办学项目教学质量监控体系的构建与实践——基于华南农业大学的实证研究	魏旭娇	一般项目
38	基于WebQuest的大学英语研究性教学模式的建构与实践	仇如慧	一般项目
39	视觉化下的英语口语教学研究	魏清华	一般项目
40	基于校企联合培养模式的财会专业学生创业教育研究	刘卫民	一般项目
41	基于自建专门用途英语（ESP）教学语料库的词块研究——探索大学英语教师向ESP教师转型的途径	秦建华	一般项目
42	以校园文化讲坛为载体的大学生文化素质教育模式的创新与实践	汪路勇	一般项目
43	新人才培养方案指导下的法学专业课程整合与优化	李文丽	一般项目
44	高校思政课对话教学模式的建构与研究	蔡小婷	一般项目
45	创意思维训练模式在动画剧作教学中的实践	王柯	一般项目
46	以创新型人才培养为目标的艺术素质教育改革的研究与实践	石娟娟	一般项目
47	优化整合校内媒体资源建设广播电视编导专业教育实训基地	王敏	一般项目
48	基于企业合作的动画专业实践教学研究与实施	吴祝元	一般项目
49	开放·交叉·融合——普通高校体育课双语教学模式的研究与实践	单宇	一般项目
50	基于协同创新的高校校企合作人才培养模式研究	欧阳倩兰	一般项目
51	高校校园文化品牌培育模式的研究与实践	张春苑	一般项目
52	教学团队建设的研究与实践——以A系列课程《创业学》为例	陈建	一般项目
53	少学时条件下的课程教学改革研究——以《工程光学》课程教学为例	刘建斌	自筹项目
54	《食品工程原理课程设计》课程的教学改革	李雁	自筹项目
55	基于聚合算子决策的学科交叉课程设计培养方案	刘鹏飞	自筹项目
56	茶艺美学资源开发及《茶艺学》教学内容体系改革研究与实践	张凌云	自筹项目

57	适于高等农业院校的入侵生物学教学课程体系的构建与探索	陆永跃	自筹项目
58	高等教育大众化视域下大学生学习动力系统分析与构建研究	房三虎	自筹项目
59	基于DUS三性判定的农事训练模式的探索与实践	徐振江	自筹项目
60	《摄影测量学》课程实践教学模式创新和实践教学基地建设改革与实践	王长委	自筹项目
61	农林院校化学类专业开放性实验室的管理与改革实践	温青	自筹项目
62	在制药工程专业设立“创新学分”的探索研究	林雅铃	自筹项目
63	《植物检疫学》课程教学改革探索	胡琼波	自筹项目
64	《生物统计附试验设计》课程教学改革与实践	张哲	自筹项目
65	以问题求解能力为核心的渐进式程序设计实验教学改革研究与实践	林毅申	自筹项目
66	工科类工业设计专业产品设计表现技法课程实践教学改革	郭晓燕	自筹项目
67	高等农业院校统计学专业实践教学的研究和探讨	肖莉	自筹项目
68	动物科学学院《微生物学》课程教学团队的改革与建设	刘丽	自筹项目
69	工程训练模式下教学管理的创新与实践	任春涛	自筹项目
70	面向卓越工程师教育培养的电子科学与技术专业实践教学体系研究	罗霞	自筹项目
71	以培养应用能力为导向的《生物防治》课程教学改革与实践	许小霞	自筹项目
72	《食品工艺原理》课程教学改革的实践与探索	赵雷	自筹项目
73	基于学生综合能力培养的机械实验课程改革探索与实践	甄文斌	自筹项目
74	以实践教学改革为核心的道路与桥梁工程应用型人才培养模式研究	黄俐	自筹项目
75	《环境化学》课程教学内容与教学过程的优化建设	蒋成爱	自筹项目
76	《土壤化学分析》实验课实验方法的改进与探索	赵兰凤	自筹项目
77	精品课程《森林经理学》信息技术服务体系的构建与实践	王本洋	自筹项目
78	《生物化学实验》课程教学改革与实践	蒋珺	自筹项目
79	大学生课外学术创新能力培养模式的探索与实践	许益鏖	自筹项目
80	学研结合的《动物营养与饲料学》实践教学探索与实践	叶慧	自筹项目
81	基于创新能力培养的实验教学改革与实践——以《动物遗传学》课程为例	刘满清	自筹项目
82	以兴趣培养为核心的《植物学》课程教学的改革	龚维	自筹项目
83	非英语专业大学生英语学习“动机缺失”研究	彭英	自筹项目
84	我校专门用途英语（ESP）课程建设研究	李飞武	自筹项目
85	基于高校学生社区的社会工作专业校本实践平台建设研究	周志荣	自筹项目
86	《制度经济学》课程设计创新与教学体系改革实践	何一鸣	自筹项目
87	大学英语分层教学模式下《跨文化交际》作为拓展课程的教学实践与探索	赵勇	自筹项目
88	综合性高校音乐学科改造与特色建设的研究与实践	胡远慧	自筹项目
89	历史学专业课程中教学方法的创新研究	殷小平	自筹项目
90	英语分层教学模式下学生需求、认知风格与自我效能的分析与应对策略研究	吕丽珊	自筹项目
91	《马克思主义基本原理概论》课教学设计研究	黄浩	自筹项目
92	高校校外实践模式、创业教育对大学生就业影响研究	李尚蒲	自筹项目

2019年、2020年校级课程立项汇总表

学院名称	课程类别	课程名称	课程负责人	立项时间
材料与能源学院	课程思政	基础化学实验AⅢ (物理化学实验)	丁唯嘉	2019
材料与能源学院	课程思政	无机化学	刘晓璐	2019
材料与能源学院	课程思政	无机功能材料	倪春林	2019
材料与能源学院	大国三农	农业新能源与新材料	简秀梅	2019
材料与能源学院	线下课程	无机及分析化学实验	倪春林	2020
材料与能源学院	线上线下混合式	有机化学 (公共课)	李春远	2020
材料与能源学院	线上线下混合式	家具设计	郭 琼	2020
材料与能源学院	线上线下混合式	药物分析	林雅铃	2020
材料与能源学院	线上线下混合式	(药物)毒理学	王 磊	2020
材料与能源学院	线上线下混合式	基础化学实验Ⅱ	肖 勇	2020
创新创业学院	课程思政	大学生创新创业基础	顾美霞	2019
电子工程学院	课程思政	微电子技术基础 (双语)	刘洪山	2019
电子工程学院	全英课程	光纤通信	徐初东	2019
电子工程学院	线上线下混合式	人工智能技术智慧农业应用导论	韩宇星	2020
电子工程学院	线上线下混合式	光电图像处理技术	杨初平	2020
动物科学学院	大国三农	农科大学生创新创业基础与实践	何冬梅	2019
动物科学学院	全英课程	蚕业经济与管理	刘吉平	2019
动物科学学院	线下课程	动物生产学	孙宝丽	2020
动物科学学院	线下课程	家畜环境卫生学	吴银宝	2020
动物科学学院	线下课程	动物营养与饲料综合实验	曹庆云	2020
动物科学学院	线上线下混合式	家畜育种学	张 哲	2020
工程基础教学与训练中心	大国三农	农用无人机工程技能通识训练课	卢玉华	2019
工程基础教学与训练中心	线上线下混合式	工程制图	文 晟	2020
工程基础教学与训练中心	线上线下混合式	工程力学B	陈海波	2020
工程学院	大国三农	精准农业航空技术与应用	兰玉彬	2019
工程学院	线上线下混合式	单片机原理及接口技术	魏德仙	2020
工程学院	线上线下混合式	自动控制原理	张铁民	2020
公共管理学院	课程思政	田野调查与社会实践	廖 杨	2019
公共管理学院	线下课程	社会工作导论	卓彩琴	2020
公共管理学院	线下课程	土地信息系统	王 枫	2020
公共管理学院	线下课程	公共政策学	武玉坤	2020
公共管理学院	线上线下混合式	田野调查与社会实践	廖 杨	2020

033

项目编号: JG19 1 06

华南农业大学教育教学研究和改革项目

申 报 书

项目名称 课程育人与科研育人相结合——

《药物分析》研究性教学探索

项目负责人 林雅铃

职 称 副教授

工作单位 材料与能源学院 (盖章)

移动电话 13380097023

电子邮箱 linyaling@scau.edu.cn

申报日期 2019-06-13

华南农业大学 教务处 制

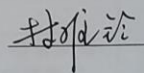
2019 年 6 月

211

申请者的承诺与成果使用授权

本人自愿申报华南农业大学教育教学改革项目，承诺对所填写的《申报书》所涉及各项内容的真实性负责，保证没有知识产权争议。课题申请如获准立项，在研究工作中，接受华南农业大学教务处及本人所在单位的管理，并对以下约定信守承诺：

- 1.遵守相关法律法规。遵守我国著作权法和专利法等相关法律法规；遵守我国政府签署加入的相关国际知识产权规定。
- 2.遵循学术研究的基本规范，恪守学术道德，维护学术尊严。研究过程真实，不得以任何方式抄袭、剽窃或侵吞他人学术成果，杜绝伪注、伪造、篡改文献和数据等学术不端行为；成果真实，不重复发表研究成果；维护社会公共利益，不以项目名义牟取不当利益。
- 3.遵守华南农业大学教育教学改革项目有关管理规定以及华南农业大学财务规章制度。
- 4.凡因项目内容、成果或研究过程引起的法律、学术、产权或经费使用问题引起的纠纷，责任由相应的项目研究人员承担。
- 5.项目获批后务必按项目计划要求及时开展研究工作，确保研究工作如期完成。
- 6.同意华南农业大学或其授权（委托）单位有权基于公益需要公布、使用、宣传《项目申请·评审书》内容及相关成果。

项目负责人（签章）： 

2019 年 6 月 19 日

六、单位、评审小组及学校意见

所在单位意见:

同意推荐.

(公章)

单位负责人签字:

2019年 6月 24日



张俊双

评审小组意见:

同意立项

评审小组长签字:

2019年 月 日

张俊亮

学校主管部门意见:

同意立项

签章:

2019年 月 日



附件： 2021年度校级质量工程暨教改项目验收结果

序号	项目类别	项目名称	负责人	所在单位	验收结果	备注
1	一流专业	生态学	章家恩	资源环境学院	验收通过	已入选国家一流专业建设点
2	一流专业	食品质量与安全	孙远明	食品学院	验收通过	已入选国家一流专业建设点
3	一流专业	植物保护	徐汉虹	农学院	验收通过	已入选国家一流专业建设点
4	大学生校外实践教育基地	华南农业大学广东海印股份有限公司实践教学基地	刘辉	公共管理学院	验收通过	
5	大学生校外实践教育基地	华南农业大学上达电子（深圳）股份有限公司实践教学基地	杨卓鸿	材料与能源学院	验收通过	
6	大学生校外实践教育基地	华南农业大学广州博物馆实践教学基地	赵飞	人文与法学学院	暂缓通过	延迟结题
7	大学生校外实践教育基地	华南农业大学索菲亚家居股份有限公司实践教育基地	孙瑾	材料与能源学院	验收通过	
8	大学生校外实践教育基地	华南农业大学通联支付广东分公司实践教学基地	左伟	经济管理学院	验收通过	
9	大学生实践教学基地	华南农业大学广东粤建设计研究院有限公司校外实践教育基地	闫恩诚	水利与土木工程学院	验收通过	
10	实验教学示范中心	工程通识训练实验教学示范中心	陶冶	基础实验与实践训练中心	验收通过	
11	实验教学示范中心	生物质材料与能源实验教学示范中心	胡传双	材料与能源学院	验收通过	
12	实验教学示范中心	工业设计实验教学示范中心	高锐涛	工程学院	验收通过	
13	实验教学示范中心	基于云平台的计算机实验教学示范中心	田绪红	数学与信息学院、软件学院	验收通过	
14	战略新兴产业特色专业	信息与计算科学	蔡贤资	数学与信息学院、软件学院	验收通过	
15	战略新兴产业特色专业	环境设计	郑欣	艺术学院	验收通过	
16	教学团队	制药工程系列实践课程教学团队	倪春林	材料与能源学院	验收通过	
17	教学团队	面向非遗文创的设计学跨专业课程群教学团队	曾智林	艺术学院	验收通过	
18	教学团队	百篇作文教学团队	王瑛	人文与法学学院	验收通过	
19	教学团队	经济管理专业《统计学原理》教学团队	谭莹	经济管理学院	验收通过	
20	教学团队	岭南城乡特色营造实践教学团队	卢丹梅	林学与风景园林学院	验收通过	
21	教学团队	压花艺术教学团队	陈国菊	园艺学院	验收通过	
22	教学团队	国际经济与贸易教学团队	熊启泉	经济管理学院	验收通过	
23	教学团队	刑事法实践教学团队	杜国明	人文与法学学院	验收通过	
24	教学团队	音乐表演专业教学团队	郑颜文	艺术学院	验收通过	
25	在线开放课程	传统园林技艺	高伟	林学与风景园林学院	验收通过	
26	在线开放课程	最优化方法	张昕	数学与信息学院、软件学院	验收通过	

序号	项目类别	项目名称	负责人	所在单位	验收结果	备注
27	在线开放课程	电视摄像	李俊良	艺术学院	验收通过	
28	在线开放课程	发展社会学	程启军	公共管理学院	验收通过	
29	在线开放课程	微生物学	马金成	生命科学学院	暂缓通过	延迟结题
30	在线开放课程	电机学	孙振刚	工程学院	验收通过	
31	在线开放课程	水力学	韦未	水利与土木工程学院	验收通过	
32	在线开放课程	结构力学	唐贵和	水利与土木工程学院	验收通过	
33	在线开放课程	机械制造基础	刘天湖	工程学院	验收通过	
34	在线开放课程	形势与政策	项赠	马克思主义学院	验收通过	
35	专业认证	木材科学与工程	胡传双	材料与能源学院	验收通过	已通过SWST认证
36	专业认证	网络工程	周敏	数学与信息学院、软件学院	验收通过	已通过IEET认证
37	专业认证	土木工程	刘爱华	水利与土木工程学院	验收通过	已通过IEET认证
38	专业认证	建筑学	吴运江	水利与土木工程学院	验收通过	
39	产业学院	华南农业大学华顺农林产业学院	曹藩荣	园艺学院	验收通过	
40	精品视频公开课(选题)	生活中的数据分析	杨德贵	数学与信息学院、软件学院	验收通过	
41	精品资源共享课	广告管理	张蓓	经济管理学院	验收通过	
42	精品资源共享课	林业经济学	李怡	经济管理学院	验收通过	
43	精品资源共享课	兽医外科手术学(双语)	李守军	兽医学院	验收通过	
44	精品资源共享课	水污染控制工程	崔理华	资源环境学院	验收通过	
45	线上线下结合精品课程	动物学	李海云	动物科学学院	验收通过	
46	线上线下结合精品课程	人类学与现代生活(基于微信平台的精品视频公开课改造)	廖杨	公共管理学院	验收通过	
47	特色专业	社会学	廖杨	公共管理学院	验收通过	
48	教学研究与改革项目	基于云课堂的混合式教学在《药剂学实验》中的应用研究与实践	胡洋	材料与能源学院	验收通过	
49	教学研究与改革项目	国际认证背景下新工科专业的品牌化建设与实践——以家具专业为例	易欣	材料与能源学院	验收通过	
50	教学研究与改革项目	《物理化学》教学中落实“课程思政”理念的改革与探索	秦为为	材料与能源学院	验收通过	
51	教学研究与改革项目	基于校企联合培养基地的实践教学改革创新	孙理超	材料与能源学院	验收通过	
52	教学研究与改革项目	新媒体平台在《有机化学》课程教学改革中的应用	李兆栋	材料与能源学院	验收通过	
53	教学研究与改革项目	《无机化学》课程思政的建设与实践	刘晓璐	材料与能源学院	验收通过	

序号	项目类别	项目名称	负责人	所在单位	验收结果	备注
54	教学研究与改革项目	基于雨课堂及精品网课资源的农业院校公共有机化学混合式教学改革	丁唯嘉	材料与能源学院	验收通过	
55	教学研究与改革项目	基于国际标准培养木材科学与工程新工科专业特色人才的研究与实践	古今	材料与能源学院	验收通过	
56	教学研究与改革项目	新工科背景下化工原理虚拟仿真实验教学改革与实践	袁腾	材料与能源学院	验收通过	
57	教学研究与改革项目	课程育人与科研育人相结合——《药物分析》研究性教学探索	林雅铃	材料与能源学院	验收通过	
58	教学研究与改革项目	基于“互联网+”技术在基础化学实验教学的改革与实践	肖勇	材料与能源学院	验收通过	
59	教学研究与改革项目	基于速课微课堂教学平台的物理化学教学难点突破研究	陈明洁	材料与能源学院	验收通过	
60	教学研究与改革项目	校企合作背景下材料化学专业人才培养模式探讨	张超群	材料与能源学院	验收通过	
61	教学研究与改革项目	多媒体网络技术在基础化学实验教学中的应用探索	唐小兰	材料与能源学院	验收通过	
62	教学研究与改革项目	结合从业上岗证培训的“实验动物学”课程的改革与实践	余文兰	测试中心（实验动物中心）	验收通过	
63	教学研究与改革项目	基于能力结构的卓越农林教师教学发展模式研究	朱蕾	党委教师工作部、人力资源处	验收通过	
64	教学研究与改革项目	高校创新创业教育的慕课体系建设研究	曾璇	党委学生工作部（党委研究生工作部）	验收通过	
65	教学研究与改革项目	《舞蹈鉴赏》课程中“艺术+思政”的改革探索与实践研究	殷舒	党委学生工作部（党委研究生工作部）	验收通过	
66	教学研究与改革项目	艺术类专业人才培养的创新创业教育改革研究	陈志远	党委学生工作部（党委研究生工作部）	验收通过	
67	教学研究与改革项目	基于人工智能背景下的教学教务管理信息化探索与研究	王宣琳	党政办公室（研究室）	暂缓通过	延迟结题
68	教学研究与改革项目	知识传授、文化传承、价值引领三位一体的课程思政教学改革与创新——以大学物理基础课程为例	徐初东	电子工程学院（人工智能学院）	验收通过	
69	教学研究与改革项目	《数字电子技术》课程思政建设研究	赵文锋	电子工程学院（人工智能学院）	验收通过	
70	教学研究与改革项目	可编程器件原理与应用实验在线课程建设与应用	徐海涛	电子工程学院（人工智能学院）	验收通过	
71	教学研究与改革项目	《物联网技术导论》课程校企协同育人机制创新实践研究	贾维卿	电子工程学院（人工智能学院）	验收通过	
72	教学研究与改革项目	结合企业实训的实践教学体系的创新与研究	徐梅宣	电子工程学院（人工智能学院）	验收通过	
73	教学研究与改革项目	新工科背景下通信工程专业多方协同育人模式改革与实践	俞龙	电子工程学院（人工智能学院）	验收通过	
74	教学研究与改革项目	《养羊学》课程内容优化及微课、翻转课堂在教学实践中的应用研究	柳广斌	动物科学学院	验收通过	
75	教学研究与改革项目	基于蚕病学课程的全英教学和管理模式研究	孙京臣	动物科学学院	验收通过	
76	教学研究与改革项目	在生物化学课程中构建低年级大学生研究性学习引导机制研究	孙加节	动物科学学院	验收通过	
77	教学研究与改革项目	学分制模式下动物科学专业人才培养方案的修订	吴银宝	动物科学学院	验收通过	
78	教学研究与改革项目	新时代背景下产业学院本科生实践能力提升机制研究——以华南农大一温氏集团产业学院为例	何小敏	动物科学学院	验收通过	
79	教学研究与改革项目	通过丝绸文化课程提升大学生对中华文化自信	陈芳艳	动物科学学院	验收通过	



广东省高等教育学会
2022年度高等教育研究课题
(一般课题)

结题证书

课题编号: 22GYB060

课题名称: 深度学习视域下《药物分析》课程线上线下
混合式教学模式探索

课题承担单位: 华南农业大学

课题主持人: 林雅铃

课题组成员: 聂燕芳、宋高鹏、霍理坚、高永峰

获得等级: 合格

该课题经审核准予结项, 特发此证。

广东省高等教育学会

2024年11月25日



中国高等教育学会实验室管理工作分会会刊
中文核心期刊
RCCSE中国权威学术期刊

ISSN 1002-4956
CN 11-2034/T
CODEN SJYGAR

实验技术与管理

Shiyan Jishu yu Guanli

Experimental Technology and Management

10
2022

第39卷 第10期
Vol. 39 No.10

月刊

中西亚地区野外科学观测台站建设实践

现代极地科考破冰船实验室管理

改良标记点线栓法建立大鼠脑缺血再灌注模型

六自由度液体旋转晃动实验平台设计

往复式杆套类柱面摩擦副的摩擦磨损模拟试验机研制

悬索桥模型结构设计及其动力学分析

2021年重庆市实验室生物安全管理现状调查分析

我国医药卫生相关科技创新基地建设简析

ISSN 1002-4956



9 771002 495224

10>

中华人民共和国教育部主管

清华大学主办

主管：中华人民共和国教育部
主办：清华大学

主编：吕志刚

副主编：彭远红

编辑部主任：彭远红（兼）

编辑：张文杰 彭远红 张利芳

孙浩 杨荫茜

编务：杨荫茜 陈昕

发行：段然 吴岩

封面题字：刘仙洲院士、清华大学原第一副校长，
1963年题

编辑：《实验技术与管理》编辑部

地址：北京市海淀区清华大学科技服务楼

邮编：100084

在线投稿：http://syjl.cbpt.cnki.net

编辑部电话：010-62783005

邮箱：sjg@tsinghua.edu.cn

广告电话：010-62788738

订刊发行电话：010-62792635

邮箱：syjsygl@tsinghua.edu.cn

出版与发行：清华大学出版社有限公司

地址：北京市海淀区双清路学研大厦A座6层

邮编：100084

印刷：北京卓诚恒信彩色印刷有限公司

发行范围：国内外公开发行

国际标准连续出版物号：ISSN 1002-4956

国内统一连续出版物号：CN 11-2034/T

国际期刊编码：CODEN SJYGAR

广告发布登记：京海市监广登字20200045号

出版日期：10月20日

定价：26.00元/期 全年12期 312.00元

收录本刊内容的国内外数据库与媒体：

- 中国学术期刊(光盘版)
- 中国核心期刊(遴选)数据库
- 万方数据资源系统数字化期刊群
- 中国期刊网
- 中国学术期刊综合评价数据库
- 中国期刊全文数据库
- 中文科技期刊数据库
- 中文电子期刊服务
- 中国学术期刊文摘(中文版)
- 中国科技论文在线
- 美国《剑桥科学文摘》(CSA)
- 美国《化学文摘(网络版)》(CA)
- 美国《乌利希期刊指南(网络版)》(Ulrichsweb)
- 英国《世界陶瓷文摘(网络版)》(WCA)
- 日本《日本科学技术振兴机构数据库(中国)》(JST China)
- 美国《艾博思科数据库》(EBSCOhost)

目次

第39卷 第10期(总第314期) 2022年10月

特约专栏——高水平实验室建设

- 中亚地区野外科学观测台建设实践.....洪永欣, 张新, 郝丽静, 等 1
现代极地科考破冰船实验室管理.....陈清满, 廖周鑫, 沈悦 6

实验技术与方法

- 页岩气开发水基钻屑的生物急性毒性测试研究
.....朱天莉, 宋娇, 黄涛, 等 12
基于脑电实验的高铁调度员工作负荷识别方法
.....张光远, 邓一平, 王亚伟 18
基于 COMSOL 的光学压力传感器的仿真与实验
.....杨福铃, 梁帅, 李艳 24
不同卸围压速率下灰岩卸荷力学特性试验研究.....周传涛 30

基于离子氢键的聚硅氧烷超分子弹性体的制备及其实验设计

-林雅铃, 霍理坚, 莫家亨, 等 36
改良标记点线栓法建立大鼠脑缺血再灌注模型

-王梦洁, 李炜健, 宋心怡, 等 42
茶多酚功能化的还原氧化石墨烯的制备和生物性能

-郝丽英, 罗萌, 康茂萍 49
水压致裂煤体分区渗流试验装置及教学实验方法设计

-张村, 宋子玉, 刘晨熙, 等 54
基于注意力残差网络的甲状腺结节分类研究.....杨行, 惠雨, 李菁菁, 等 59
山梨酰胺对侧小麦种子萌发的影响.....陈蔚燕, 李建忠 65

虚拟仿真技术

- 螺纹连接松动机理有限元仿真分析.....何佳龙, 郭继超, 李雨露, 等 69
基于忆阻器的多模式识别 CNN 电路设计.....陈鑫辉, 王宇轩, 张跃军, 等 75
一种改进型 RetinaFace 的遮挡人脸检测算法.....党宏社, 狄国栋, 张逸德 80
基于 ANSYS 的海上风机雷电电磁暂态虚拟仿真实验
.....张萍, 杨晓磊, 李永健, 等 86
融合随机游走 MFPT 特征的链接预测仿真与实证分析

-伍杰华, 高学勤, 王涛, 等 91
基于数字孪生技术的智能医学影像实验室构建及应用
.....陈珊珊, 汪红志, 夏天, 等 101

仪器设备研制

- 六自由度液体旋转晃动实验平台设计.....王志亮, 周炳红, 孙志斌 108
往复杆套类柱面摩擦副的摩擦磨损模拟试验机研制
.....高雷雷, 姜浩, 李肖, 等 115

实验教学研究与管理

- 组合夹具设计“虚实结合”实验平台开发.....尚振国, 蔡卫国, 安相华, 等 122
热蒸汽改性 FeS₂ 制备及光催化降解罗丹明 B 综合实验
.....王海涛, 邹菁, 江吉周 130

期刊基本参数: CN11-2034/T * 1963 * m * A4 * 248 * zh * P * ¥26.00 * 6500 * 44 * 2022-10

基于离子氢键的聚硅氧烷超分子弹性体的制备及其实验设计

林雅铃¹, 霍理坚¹, 莫家亨², 赵 颖², 张安强²

(1. 华南农业大学 材料与能源学院, 广东 广州 510642;
2. 华南理工大学 材料科学与工程学院, 广东 广州 510641)

摘 要: 基于非共价键构建超分子弹性体是近年来超分子领域研究的热点之一, 其中离子氢键因其结构简单且性能可控而受到重视。通过将该领域最新科研成果引入实验教学, 设计、制备了两类结构相似但性能迥异的超分子弹性体, 通过 FT-IR、¹H-NMR、GPC、流变行为、力学性能及自愈合效率等表征手段, 建立了超分子弹性体的结构与性能关系。该实验内容涵盖了聚合物合成与改性、制备方案设计和实施、聚合物结构表征等诸多环节, 具有一定的综合性与探索性, 有利于提高学生的综合素质, 以及科研与创新能力。

关键词: 超分子弹性体; 离子键-氢键; 流变特性

中图分类号: TQ33 文献标识码: A 文章编号: 1002-4956(2022)10-0036-06

Experimental design and preparation of polysiloxane supramolecular elastomer based on ionic hydrogen bond

LIN Yaling¹, HUO Lijian¹, MO Jiaheng², ZHAO Ying², ZHANG Anqiang²

(1. College of Material and Energy, South China Agricultural University, Guangzhou 510642, China; 2. School of Materials Science and Engineering, South China University of Technology, Guangzhou 510641, China)

Abstract: Supramolecular elastomers based on non-covalent bonds is one of the hotspots recently in the field of supramolecular, in which the ionic hydrogen bond associations have attract much attention for their simple structure and controllable properties. By introducing the latest scientific research achievements in this field into experimental teaching, two serials supramolecular elastomers with similar structures but different properties are designed and prepared, and relationship between structure and properties is established based on FT-IR, ¹H-NMR, GPC, rheological behavior, mechanical properties and self-healing efficiency. The experimental content covers many subjects such as polymer synthesis and modification, preparation scheme design and implementation, polymer structure characterization and so on, it is comprehensive and exploratory to a certain extent, and is conducive to improve students' comprehensive quality, scientific research and innovation ability.

Key words: supramolecular elastomer; ionic hydrogen bond; rheological behaviors

将材料领域的最新科研成果引入本科探索性实验教学, 是科研与教学结合的重要方式之一, 在此过程

中应注意科研成果的前沿性与学生认知水平及实验教学条件的匹配^[1]。基于可逆键(如: 氢键^[2]、配位键^[3-4]、

收稿日期: 2022-05-06

基金项目: 国家自然科学基金项目(51473051、31772202、52073098); 广东省教育厅质量工程项目(GD2019-185); 华南农业大学教育教学改革与研究重点项目(JG19106); 华南理工大学教学研究项目(2021-C9213066); 华南理工大学探索性实验项目(2021-C9212110)

作者简介: 林雅铃(1978—), 女, 福建罗源, 博士, 副教授, 主要研究领域为大分子药物与超分子弹性体, linyaling@scau.edu.cn。

通信作者: 张安强(1976—), 男, 湖南安仁, 博士, 教授, 主要研究方向为功能高分子材料, aqzhang@scut.edu.cn。

引文格式: 林雅铃, 霍理坚, 莫家亨, 等. 基于离子氢键的聚硅氧烷超分子弹性体的制备及其实验设计[J]. 实验技术与管理, 2022, 39(10): 36-41.

Cite this article: LIN Y L, HUO L J, MO J H, et al. Experimental design and preparation of polysiloxane supramolecular elastomer based on ionic hydrogen bond[J]. Experimental Technology and Management, 2022, 39(10): 36-41. (in Chinese)

离子键^[5-6]或可逆共价键^[7-8]等)构建超分子弹性体(supramolecular elastomers),是弹性体领域的热点和重要方向之一^[9]。以可穿戴的柔性传感为例,要求柔性基材可多次动态弯折、易于贴合皮肤、无不适感、生物相容性好以及与传感器黏合好等^[10],而这些恰好是超分子弹性体区别与传统共价交联弹性体的优势^[11-13]。

基于此要求,本文提出了以主链柔顺且生物相容性好的聚二甲基硅氧烷(PDMS)为基材,在其侧基上引入廉价且无毒的羧酸和伯胺,合成得到氨基接枝聚硅氧烷(APS)和羧基接枝聚硅氧烷(包括:不饱和羧基接枝聚硅氧烷(UCS)与饱和羧基接枝聚硅氧烷(SCS)),通过调控有机酸和有机碱的相互作用强度,使二者之间在产生氢键的同时发生质子转移,形成具有较强相互作用的离子氢键(ionic hydrogen bonds, IHBs),继而通过调节二者的混合比例,制备得到基于离子氢键交联且具有不同黏弹特性的聚硅氧烷超分子弹性体^[12]。该方案解决了传统共价交联的聚硅氧烷弹性体无自黏性、模量较高且不易调节、不能自愈等问题,可为柔性可穿戴传感器提供良好的弹性体基材^[13]。

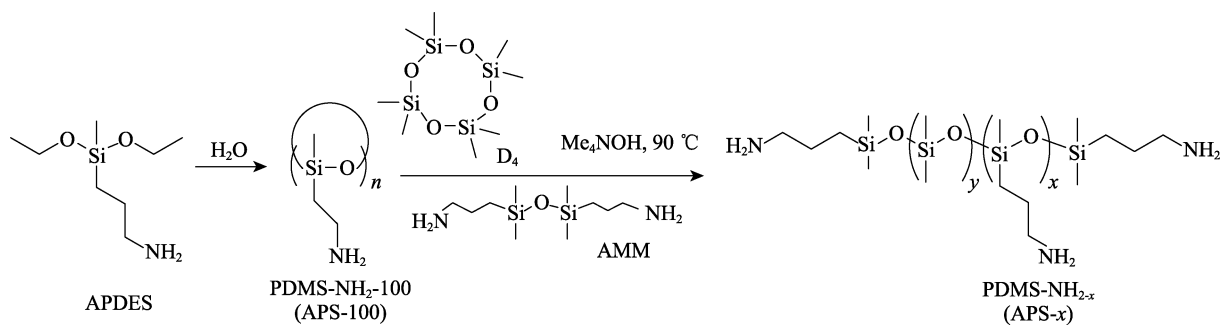


图1 氨基接枝聚硅氧烷(APS-x)的合成路线

在单口瓶中加入 APDES、过量的去离子水,升温至 50 °C,磁力搅拌 4 h 后在 120 °C、1 mbar 下减压蒸馏 2 h 除去副产物乙醇和多余的水,得到无色透明黏稠状液体 APS-100,产率约为 95%。

APS-x 的分子量和接枝密度由 APS-100、D₄和封头剂 AMM 三者投料配比给出,其中 AMM 在控制分子量的同时带有氨基,在合成分子量不大的 APS 时还应该考虑其对氨基接枝密度的影响,从而更精准控制氨基接枝密度。APS 的分子量和接枝密度与 APS-100、D₄和封头剂 AMM 三者投料质量比由式(1)给出:

$$\begin{cases} m_{\text{APS-100}} = 117 \frac{Ma - 148 - 100a}{43a + 74} \\ m_{\text{D}_4} = M - 248 - m_{\text{APS-100}} \\ m_{\text{AMM}} = 248 \end{cases} \quad (1)$$

式中, $m_{\text{APS-100}}$ 、 m_{D_4} 和 m_{AMM} 、分别表示 APS-100、D₄和 AMM 的投料量(g); M 为所合成的 APS-x 的设

1 实验部分

1.1 实验试剂

八甲基环四硅氧烷(D₄, 99%),美国道康宁公司;3-氨丙基甲基二乙氧基硅烷(APDES, 96%),山东曲阜化工有限公司;1,3-双(3-氨基丙基)-1,1,3,3-四甲基二硅氧烷(AMM, 99%),四甲基氢氧化铵·五水合物(Me₄NOH·5H₂O, 97%),马来酸酐(MAH, 99%),琥珀酸酐(SAH, 99%),3-氨丙基三甲氧基硅烷(APTMS, 99%),均为上海麦克林生化科技有限公司产品;其余试剂均为常规分析纯,广州化学试剂厂。

1.2 样品制备

1.2.1 氨基接枝聚硅氧烷(APS)的合成

氨基接枝聚硅氧烷是双端和侧基都接枝有氨基丙基的聚二甲基硅氧烷。其合成分为两步:先合成全侧氨丙基聚硅氧烷(APS-100, 100表示100%的硅氧烷单元上都接枝氨基),继而与八甲基环四硅氧烷(D₄)和封头剂 AMM 调聚,得到一定氨基接枝密度以及分子量的氨基接枝聚硅氧烷(APS-x, x 表示 $x\%$ 的硅氧烷单元上接枝有氨基),其合成路线如图1所示。

计数均分子量; a 为氨基的比例($a = x/(x+y)$, $0 < a < 1$)。

根据以上公式,以接枝率为10%,分子量为10 kDa的氨基接枝聚硅氧烷(记为 APS-10-10 kDa)为例,说明其合成过程:将 APS-100(31 g)、封头剂 AMM(6.2 g)和催化剂 Me₄NOH·5H₂O(1.2 g,占单体总质量约0.5%)加入500 mL三口烧瓶,通入氮气,升温至90 °C,敞口机械搅拌1 h除去体系中微量的水分。接着加入 D₄(213 g),装上冷凝管继续反应10 h。升温至160 °C并保持1.5 h分解催化剂,得到无色透明粗产物。将得到的粗产物在160 °C、1 mbar条件下减压蒸馏2 h除去低沸点杂质,得到均一无色透明液体 APS-10-10 kDa,产率为95%。

1.2.2 羧基硅油(UCS和SCS)的合成

不饱和羧基接枝聚硅氧烷(UCS)和饱和羧基接枝聚硅氧烷(SCS)由 APS-x 在无溶剂条件下分别与马来酸酐(MAH)和琥珀酸酐(SAH)反应得到,其合成路线如图2所示。

以接枝率为 10% 的羧基硅油的合成为例, 在烧杯中加入一定量的 APS-10-10 kDa, 升温至 80 °C, 开动机械搅拌, 缓慢加入氨基的 1.05 eq 的 MAH 或 SAH,

继续搅拌 10 min, 得到淡黄色黏稠液体 UCS-10 或 SCS-10。

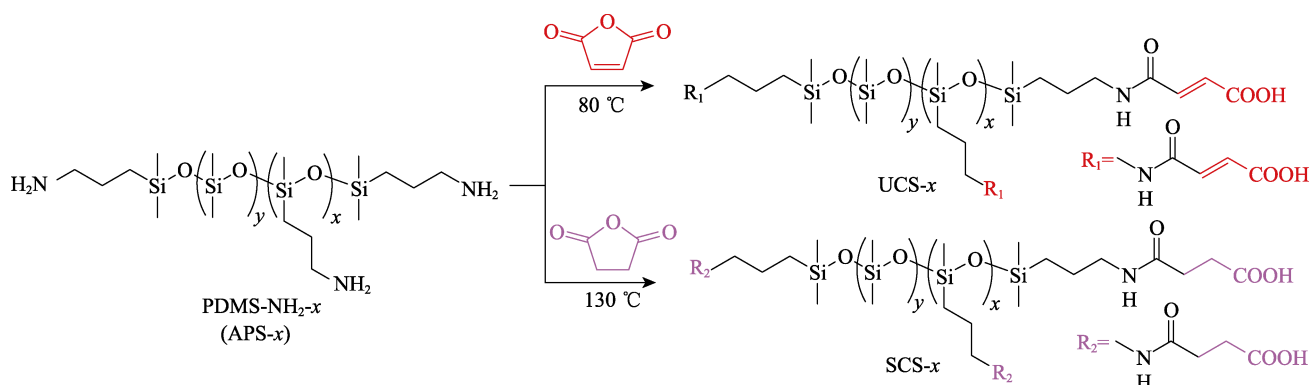


图 2 不饱和羧基接枝聚硅氧烷 (UCS) 与饱和羧基接枝聚硅氧烷 (SCS) 的合成路线

1.2.3 聚硅氧烷超分子弹性体的制备

在 APS 和对应的 UCS 控制羧基和氨基的比值为 1 : 1 的条件下, 在室温无溶剂条件下直接混合, 机械搅拌 5~10 min 至均一透明黏稠液体, 倒入聚四氟乙烯模具中, 抽真空排除气泡后放入 60 °C 真空烘箱 48 h, 得到无色透明弹性薄膜, 其代号为 APS-UCS-x, 例如: APS-UCS-10 表示 UCS-10 和 APS-10 按 $n(-\text{COOH}) : n(-\text{NH}_2) = 1 : 1$ 混合而得到的产物。

如果将 APS 和对应的 SCS 控制羧基和氨基的比值为 1 : 1 的条件下, 在室温无溶剂条件下直接混合, 所得产物标记为 APS-SCS-x。

1.2.4 羧基与伯胺基之间离子氢键作用结合力常数的测定

为了更准确表征超分子弹性体内不同结构的羧基与伯胺基之间的离子氢键作用, 参照文献[12]的方法合成得到 3-氨丙基三甲氧基硅烷 (APTMS) 与 MAH 或 SAH 的酰胺化产物 (APTMS-MA 和 APTMS-SA, 其结构分别如图 7 所示)。采用核磁滴定的方法测定和计算羧基与伯胺基之间的离子氢键作用强度, 简述如下: 将 APTMS、APTMS-MA 及 APTMS-SA 分别溶于氘代 DMSO 中, 将 APTMS 浓度固定为 0.12 mol/L, 向 APTMS 溶液中分别加入不同量的 APTMS-MA (或 APTMS-SA), 使核磁管中的 APTMS/APTMS-MA (或 APTMS/APTMS-SA) 浓度比为 0.12 mol/L : 0.02 mol/L 至 0.12 mol/L : 0.12 mol/L 之间的多个浓度, 并测定相应的核磁氢谱, 以 APTMS 中紧邻 $-\text{NH}_2$ 的亚甲基的核磁位移为观察对象, 按照文献[14]所述方法计算 APTMS 与 APTMS-MA (或 APTMS-SA) 之间的结合力常数 K_1 (或 K_2), 以此分别作为 APS 与 UCS (或 SCS) 之间的羧基与伯胺基之间的离子氢键作用强度。

1.3 测试与表征

用傅立叶变换红外光谱仪 (美国赛默飞 Nicolet iS5) 测定样品的红外光谱; 用核磁共振仪 (德国布鲁克 Avance III-600) 测定样品的核磁氢谱 (以氘代氯仿或氘代 DMSO 为溶剂, 室温下测试); 用凝胶渗透色谱仪 (美国 Waters515-2414) 测定样品的分子量和分子量分布 (以单分散 PS 为标样, 氯仿作为流动相, 流速为 1 mL/min, 柱温 40 °C, 其中, APS 样品中含有反应性的伯胺基, 在进行 GPC 测试前需用间甲苯异氰酸酯进行封端处理); 用平板流变仪 (奥地利安东帕 MCR102) 测试弹性体的流变行为; 用恒温恒湿拉力试验机 (东莞科建 KJ-2091) 测试弹性体样品的拉伸应力应变特性。

将 50 mm×10 mm×1 mm 样条用锋利的刀片从中间划开, 小心拼接, 在不受外力作用下水平放置, 待其进行自愈合, 愈合效率定义为

$$\text{愈合效率} = \text{TS}_{\text{healed}} / \text{TS}_{\text{virgin}} \times 100\% \quad (2)$$

式中, $\text{TS}_{\text{virgin}}$ 和 $\text{TS}_{\text{healed}}$ 表示样品愈合前后的拉伸强度。

2 结果与分析

2.1 APS-x、UCS-x 和 SCS-x 的结构表征

为便于说明, 下文以接枝率为 10% 的不同阶段产物为例进行说明, 图 3(a) 为接枝率为 10% 的 APS-10、UCS-10 和 SCS-10 的红外图谱对比。可以看到在所有的样品中, 有 2966 cm^{-1} 和 2906 cm^{-1} 处的甲基上的 C—H 伸缩振动吸收峰、1262 cm^{-1} 处的变形振动吸收峰以及 1096 cm^{-1} 和 1026 cm^{-1} 伸缩振动双驼峰, 这些特征吸收峰表明这 3 种产物具有相同的聚硅氧烷主链。1614 cm^{-1} 为 APS 接枝伯胺上 N—H 弯曲振动吸收峰, 3300~3200 cm^{-1} 范围内为 UCS 和 SCS 接枝羧基上 O—H 振动吸收峰, 1714 cm^{-1} 和 1725 cm^{-1} 分别是 UCS-10

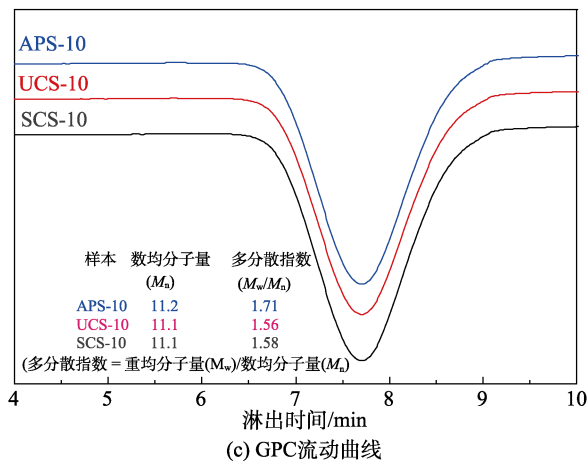
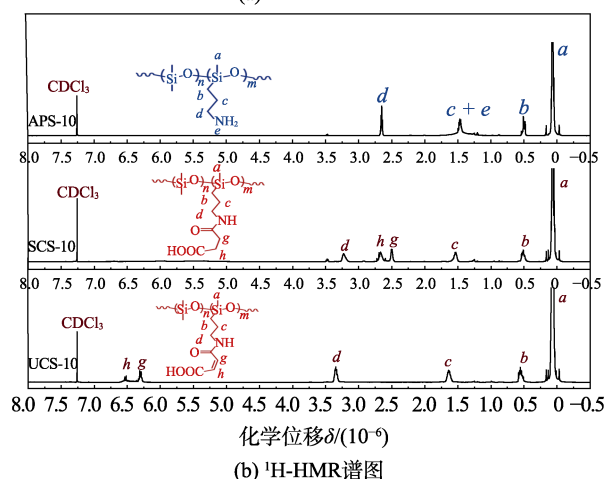
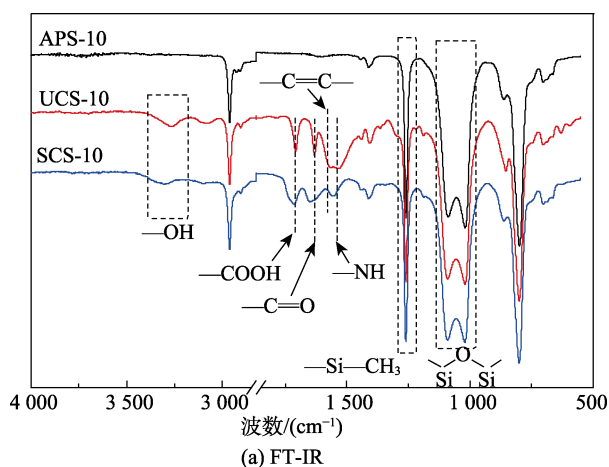


图3 APS-10、UCS-10和SCS-10的FT-IR、¹H-NMR谱图和GPC流动曲线

和SCS-10接枝羧基上C=O的伸缩振动吸收峰, 1640 cm⁻¹和1652 cm⁻¹分别是UCS和SCS接枝酰胺基上C=O的伸缩振动吸收峰, 1445 cm⁻¹是酰胺基上N—H的弯曲振动吸收峰, 这些特征吸收峰表明羧基成功接枝到聚硅氧烷主链上。此外, 在1800~1750 cm⁻¹处没有酸酐的特征吸收峰, 表明体系中酸酐已反应完全。

图3(b)是APS-10、UCS-10和SCS-10的¹H-NMR谱图。其中, δ0.46~0.55、δ1.40~1.50和δ2.63~2.68分

别对应APS-10中氨基上离硅原子由近到远3个亚甲基上的质子峰; δ0.50~0.58、δ1.57~1.68和δ3.29~3.38分别对应UCS-10中离硅原子由近到远3个亚甲基上的质子峰, 相比APS-10, 受到酰胺基的影响这3个质子峰均向低场移动, 且越靠近酰胺基位移越大; δ0.46~0.57、δ1.48~1.61和δ3.16~3.27则分别对应SCS-10中离硅原子由近到远3个亚甲基上的质子峰, 虽然同样受到酰胺基的影响, 但是位移程度比UCS-10的稍小。δ2.45~2.56和δ2.60~2.72分别是酰胺基和羧基中间两个亚甲基的质子峰。核磁测试结果说明氨基全部转化为对应的不饱和或者饱和羧基, 且没有酸酐的残留。

图3(c)是APS-10、UCS-10和SCS-10的GPC曲线、分子量以及分子量分布数据, 可见三者的数均分子量与设计值(10×10³)十分接近。需要注意的是, 直接测量得到的APS-10分子量并非其真实值, 这是因为在测量前需要用间甲苯基异氰酸酯(mTI)把氨基封端(防止伯胺基与色谱柱填料发生反应), 这将会稍微增大分子量。

2.2 两种超分子产物(APS-UCS和APS-SCS)的结构表征与分子模拟

2.2.1 两种超分子产物(APS-UCS和APS-SCS)的结构表征

将APS-10与UCS-10(或SCS-10)在无溶剂条件下直接混合, 得到的两种产物, 分别标记为: APS-UCS-10、APS-SCS-10, 图4是其FT-IR谱图, 由图可见, APS-10与UCS-10或SCS-10混合后, 1750~1700 cm⁻¹处羧基上C=O伸缩振动吸收峰消失, 同时出现1560 cm⁻¹处的羧酸盐振动吸收峰, 这表明氨基和羧基发生酸碱中和反应且不再有羧基剩余。实验发现, APS-UCS-10为无色透明的弹性体薄膜, 而APS-SCS-10产物为黏稠状液体。

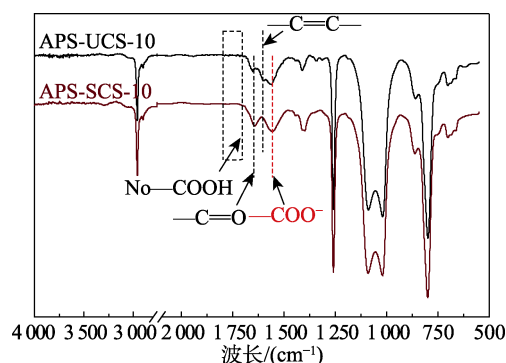


图4 APS-UCS-10和APS-SCS-10的FT-IR谱图

图5是APS-UCS-10和APS-SCS-10的流变行为主曲线, 在25℃的参考温度下, APS-UCS-10整个测试频率范围内都处于橡胶平台: 即储能模量G' > 损耗模量G'', 随着频率的增加, G'小幅上升, G''则出现显

著上升；而在整个测试频率范围内，APS-SCS-10 的主曲线都呈现 $G' < G''$ 的特征，表现为黏流态的液体。

如前所述，UCS 和 SCS 的差异仅仅在于聚硅氧烷所接枝的羧基中含的是 C=C 双键还是 C—C 单键，其产物的性能却迥然不同，这主要是两个体系中离子氢键的作用强度相差较大造成的：在氨基基团结构不变的条件下，影响氨基与羧基之间离子氢键强度的主要因素是羧基的酸性（常用羧基电离常数的负对数，pKa 值来表示）。其中，含有不饱和 C=C 双键的马来酸与含有 C—C 单键的琥珀酸的 pKa 值分别为 1.92 和 4.21，前者的电离常数较后者高了两个数量级，即 UCS 具有更强的酸性，导致 APS-UCS 体系中的离子氢键强度更高，更有利于构建稳定的交联体系，表现在宏观上，APS-UCS 为交联弹性体，而 APS-SCS 为黏性流体（如图 5 所示）。

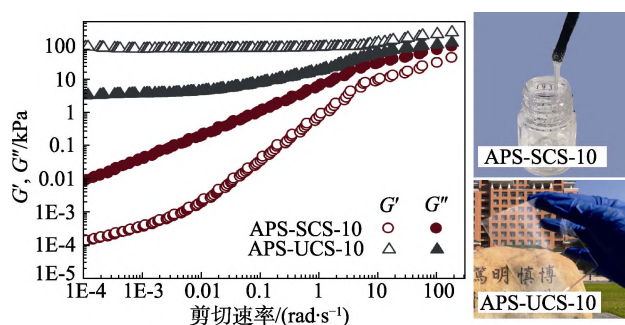


图 5 APS-UCS-10 和 APS-SCS-10 的流变主曲线及产物外观

2.2.2 两种不同结构羧基与氨基之间离子氢键作用强度的小分子模拟

为了更清晰地表征两种不同结构羧基与氨基之间的离子氢键作用强度，使得学生更直观地了解羧基酸性强弱对其与氨基之间相互作用强度的影响，考虑到大分子结构和作用力的复杂性，引入小分子模拟物 APTMS、APTMS-MA 和 APTMS-SA（结构如图 6 所示），利用核磁滴定可用于测定化合物间的非共价相互作用的强度^[12,14]，结果如图 6 所示。

对于 APTMS 和 APTMS-MA 组合，随着 APTMS-MA 浓度的从 0.02 mol/L 上升到 0.12 mol/L，APTMS 中紧邻 NH₂ 的亚甲基的化学位移从 2.51 移动到 2.77，通过最小二乘法拟合算得结合常数 K_1 为 45.5 L/mol；对于 APTMS 和 APTMS-SA 组合，其化学位移从 2.51 移动到 2.69，算得结合常数 K_2 为 7.25 L/mol。结合常数是可逆非共价相互作用强度的良好度量，不饱和羧基与氨基的结合常数远大于饱和羧基与氨基的结合常数说明前者组合产生的离子氢键强度更强。

2.3 APS-UCS 的力学性能和自愈合特性表征

APS-UCS 的拉伸测试结果如图 7 所示。随着氨基和羧基接枝率的提高，APS-UCS 的拉伸强度和杨氏模量也显著增加，而断裂伸长率则从 900% 急剧下降到 260%；自愈合效率也随之下降。这主要是因为离子氢键交联密度的提高会增加链间相互作用力和限制聚硅氧烷主链的运动，在提高拉伸强度和模量的同时降低

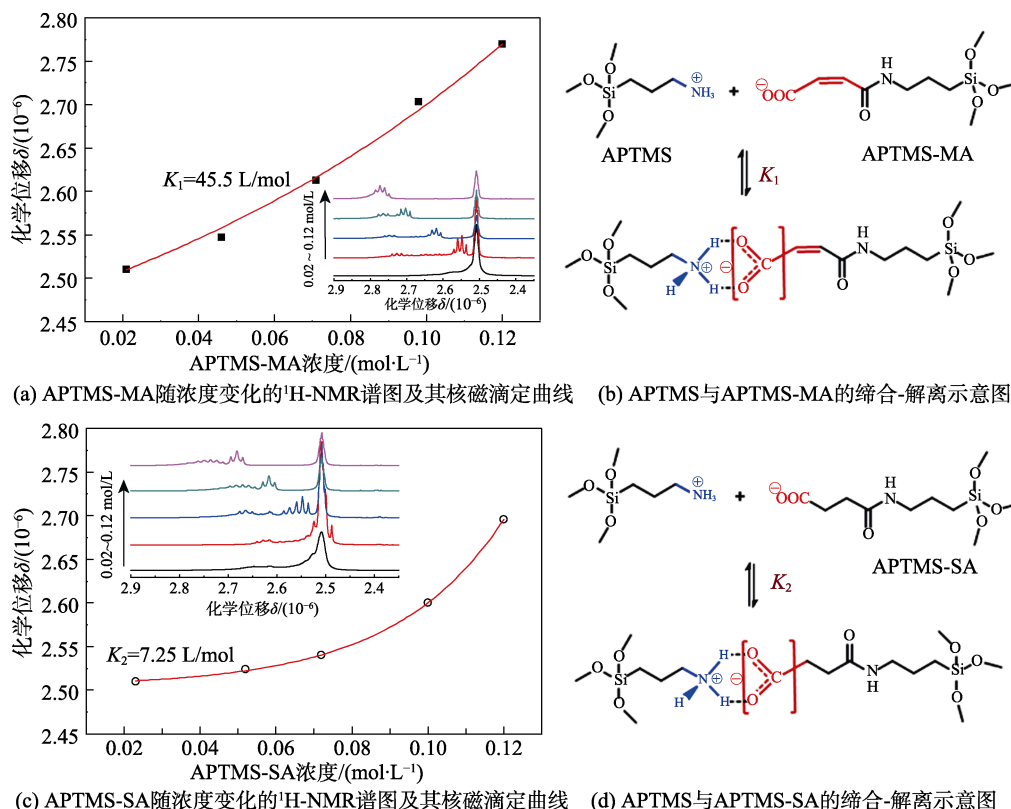


图 6 APTMS-MA 和 APTMS-SA 随浓度变化的 ¹H-NMR 谱图、核磁滴定曲线及其缔合-解离示意图

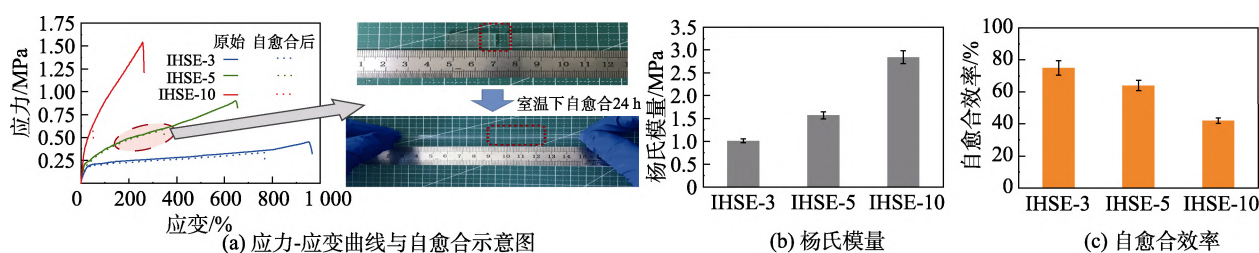


图7 APS-UCS-x 的应力-应变曲线、杨氏模量、自愈合效率

了扯断伸长率;自愈合的机理在于离子氢键的断裂、迁移和重组,同时还跟界面的扩散有关,这些过程受链段运动能力控制,随着聚合物链运动能力的下降,其自愈合的效率也会降低。

3 结语

通过两步法合成了氨基接枝聚硅氧烷 (APS-x),利用 APS 与马来酸酐或琥珀酸酐在无溶剂条件下反应获得 UCS-x 和 SCS-x。通过 FT-IR、 $^1\text{H-NMR}$ 和 GPC 表征证明合成产物能准确符合预先设计值。APS 与 UCS 在无溶剂条件下简单共混能获得离子氢键超分子弹性体,而同样条件下 APS 与 SCS 的共混则得到弹性体,流变行为表征亦清晰证实了上述结果;通过引入小分子模型化合物,结合核磁滴定,较好地解释了 APS-UCS 和 APS-SCS 体系产物性能差异的原因。APS-UCS 的拉伸强度和模量随着氨基和羧基接枝率的提高而降低,而室温自愈合能力则表现出相反的趋势。

该实验大大丰富了传统弹性体制备的实验内容,涵盖了材料的设计、合成到制备、性能分析与验证,既增强了实验的综合性,也提高了学习难度和要求。通过该实验,学生能够掌握聚合物结构表征的常用方法,更深入理解高分子材料结构与性能之间的构效关系,分析和解决问题的能力也都得到了有效的提升。

参考文献 (References)

- [1] 陈世良, 黄亦军, 黄嘉驰. 教师科研项目融入高分子专业实验教学的探索与实践[J]. 实验技术与管理, 2020, 37(9): 170-173, 178.
- [2] 张安强, 陆合承, 王炼石. 基于氢键作用的超分子弹性体材料的研究进展[J]. 高分子材料科学与工程, 2012, 28(2): 161-164.
- [3] MOZHDEHI D, AYALA S, CROMWELL O R, et al. Self-healing multiphase polymers via dynamic metal-ligand interactions[J]. Journal of the American Chemical Society, 2014, 136(46): 16128-16131.

- [4] LEI Y F, HUANG Q P, SHAN S J, et al. A stretchable and rapidly self-healable polysiloxane elastomer based on reversible aluminum- amino coordination[J]. New Journal of Chemistry, 2019, 43, 17441-17445.
- [5] LEI Y F, HUANG W Y, HUANG Q P, et al. A novel polysiloxane elastomer based on reversible aluminum-carboxylate coordination[J]. New Journal of Chemistry, 2019, 43, 261-268.
- [6] XU C H, CAO L M, LIN B, et al. Design of self-healing supramolecular rubbers by introducing ionic cross-links into natural rubber via a controlled vulcanization[J]. ACS Applied Materials & Interfaces, 2016, 8, 17728-17737.
- [7] GARCÍA F, SMULDERS M M J. Dynamic covalent polymers[J]. Journal of Polymer Science Part A Polymer Chemistry, 2016, 54, 3551-3577.
- [8] ZOU W, DONG J, LUO Y, et al. Dynamic covalent polymer networks: From old chemistry to modern day innovations[J]. Advanced Materials, 2017, 29(14): 1606100.
- [9] 莫家亨, 陈心渝, 傅育槟, 等. 基于可逆键构筑超分子弹性体的研究进展[J]. 弹性体, 2019, 29(6): 67-75.
- [10] DROZDOV A D, CHRISTIANSEN J D. Multi-cycle deformation of supramolecular elastomers: Constitutive modeling and structure-property relations[J]. International Journal of Engineering Science, 2018, 133: 311-335.
- [11] WEI S M, YOU Y, MA Y Y, et al. Bi-layer supramolecular polydimethylsiloxane elastomer film: Synthesis, characterization, and application in wound dressing on normal and diabetic rat[J]. Reactive and Functional Polymers, 2019, 141, 21-32.
- [12] MO J H, CHEN X Y, FU Y B, et al. A solvent-free, transparent, self-healing polysiloxanes elastomer based on unsaturated carboxyl-amino ionic hydrogen bonds[J]. Polymer, 2021, 228, 123903.
- [13] MAI D D, MO J H, SHAN S J, et al. Self-healing, self-adhesive strain sensors made with carbon nanotubes/polysiloxanes based on unsaturated carboxyl-amine ionic interactions[J]. ACS Applied Materials & Interfaces, 2021, 13(41): 49266-49278.
- [14] CORTESE J, SOULIÉ-ZIAKOVIC C, LEIBLER L. Binding and supramolecular organization of homo- and heterotelechelic oligomers in solutions[J]. Polymer Chemistry, 2014, 5(1): 116-125.

智慧实验室



安全准入管理系统

安全准入学习 | 考试自动阅卷
准入资格管理 | 准入门禁联动



大型仪器共享管理系统

预约授权使用 | 数据统计分析
账单汇总推送 | 数据一键上报



实验动物管理系统

实验培训考试 | 动物伦理审查
动物实验申请 | 动物订购寄养



环境监测管理系统

温湿度监测 | 气体监测
多级智能预警 | 实验室声光报警

可视化数据中心



试剂耗材管理系统

耗材档案管理 | 采购自动入库
领用审核出库 | 库存管理预警

智能终端

独特的蓝牙方案：仪器共享行业创新研发，150多家客户成熟应用，不受限于网络，不受限于地域。

智慧的人脸识别方案：人脸识别、语音交互、联动控制、AI人脸智能追踪。



蓝牙版电源控制器



网络版电源控制器



人脸识别终端



蓝牙版电脑控制器



网络版电脑控制器



智慧人脸门牌



智能门禁



动物管理手持终端



冰箱锁



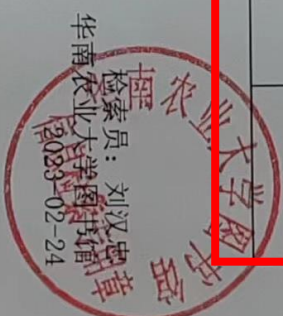
环境监测



10	ammonium salts against conidia of Fusarium oxysporum f. sp. cubense, race 4	PATHOLOGY 出版年: 2022 卷期: 页码: - 文献类型: Article; Early Access	通讯作者	B类	华南农业大学	SCI	IF2-year=2.224 IF5-year=2.262 (2021)	农林科学 3区 Top期刊: 否 (2022)
11	Polymeric diallyl quaternary ammonium salts for inhibiting banana Fusarium wilt	REACTIVE & FUNCTIONAL POLYMERS 出版年: 2022 MAR 卷期: 172 文献号: 105174 文献类型: Article	第一作者	B类	华南农业大学	SCI	IF2-year=4.966 IF5-year=4.266 (2021)	工程技术 3区 Top期刊: 否 (2022)
12	基于离子氢键的聚硅氧烷超分子弹性体的制备及其实验设计	实验技术与管理 出版年: 2022 卷期: 39 10 页码: 36-41 文献类型: Article	第一作者	C类	华南农业大学	北大核心		

说明: 本表按照《华南农业大学学术评价方案(试行)》划分。

报告免责声明: 如未盖章, 报告无效





中国高等教育学会实验室管理工作分会会刊
中文核心期刊
中国科技核心期刊
科技期刊世界影响力指数(WJCI)科学技术综合学科01区
RCCSE中国权威学术期刊

ISSN 1002-4956
CN 11-2034/T
CODEN SJYGAR

实验技术与管理

Shiyan Jishu yu Guanli

Experimental Technology and Management

8

2024

第41卷 第8期
Vol. 41 No. 8

月刊

高分辨液相色谱质谱联用仪在蛋白质化学修饰中的应用

基于异构图和语义融合的实体关系抽取

竖直接管内三种粉体抑爆剂对聚乙烯燃爆火焰传播的影响

基于VRX的无人水面船智能控制虚拟仿真实验平台设计

基于液压储能器的制动能量回收试验台研制

聚乙烯醇/SAPO-34混合基质膜制备及渗透汽化性能综合实验教学设计

基于遗传算法的元胞自动机复杂楼宇人员疏散模型

ISSN 1002-4956



08>

9 771002 495248

中华人民共和国教育部主管

清华大学主办

主管：中华人民共和国教育部

主办：清华大学

主编：王玉军

副主编：彭远红

编辑部主任：彭远红（兼）

编辑：张文杰 彭远红 张利芳 孙浩

责任编辑：孙浩

编务：陈昕

发行：吴岩

封面题字：刘仙洲院士、清华大学原第一副校长、
1963年题

编辑：《实验技术与管理》编辑部

地址：北京市海淀区双清路学研大厦B座908

邮编：100084

在线投稿：<http://syjl.cbpt.cnki.net>

编辑部电话：010-62783005

邮箱：sjg@tsinghua.edu.cn

广告电话：010-62788738

订刊发行电话：010-62792635

邮箱：syjsygl@tsinghua.edu.cn

出版与发行：清华大学出版社有限公司

地址：北京市海淀区双清路学研大厦A座6层

邮编：100084

印刷：北京卓诚恒信彩色印刷有限公司

发行范围：国内外公开发行

国际标准连续出版物号：ISSN 1002-4956

国内统一连续出版物号：CN 11-2034/T

国际期刊编码：CODEN SJYGAR

广告发布登记：京海市监广登字20200045号

出版日期：8月20日

定价：30.00元/期 全年12期 360.00元

收录本刊内容的国内外数据库与媒体：

- 中国学术期刊(光盘版)
- 中国核心期刊(遴选)数据库
- 万方数据资源系统数字化期刊群
- 中国期刊网
- 中国学术期刊综合评价数据库
- 中国期刊全文数据库
- 中文科技期刊数据库
- 中文电子期刊服务
- 中国学术期刊文摘(中文版)
- 中国科技论文在线
- 美国《剑桥科学文摘》(CSA)
- 美国《化学文摘(网络版)》(CA)
- 美国《乌利希期刊指南(网络版)》(Ulrichsweb)
- 英国《世界陶瓷文摘(网络版)》(WCA)
- 日本《日本科学技术振兴机构数据库(中国)》(JST China)
- 美国《艾博思科数据库》(EBSCOhost)

目次

第41卷 第8期(总第336期) 2024年8月

特约专栏——蛋白质化学修饰研究进展

高分辨液相色谱质谱联用仪在蛋白质化学修饰中的应用

汪会玲, 孟祥高, 肖凤萍, 等 1

实验技术与方法

Gleeble 高温拉伸样品标距段的选定对拉伸曲线的影响

赵冠琳, 吴东亭, 刘树帅, 等 15

基于异构图和语义融合的实体关系抽取 唐贤伦, 丁河长, 唐瑜泽, 等 22

超声空化诱导煤微观孔隙损伤的原位测试技术研究

李傲, 王玉娟, 郭晓阳, 等 30

海洋食品酶解物改善精神疲劳功能性评价的综合实验设计

张恬恬, 马磊, 邹宏宇, 等 36

基于透明物体深度补全的机器人抓取实验设计

张倩, 朱美强, 王惠, 等 43

竖直管道内三种粉体抑爆剂对聚乙烯燃爆火焰传播的影响

苏明清, 多英全, 陈思凝, 等 53

基于三维建模的喷油器流量系数在线测试 董全, 王迪, 周谈庆, 等 60

[Emim]NTF₂/MIL-53(Al)复合材料制备及其硫酸羟基氯喹吸附性能探索型实验
设计 李正杰, 刘苗, 刘忆贤, 等 66

聚丙烯酰胺季铵盐大分子药物的环境毒性评价及其实验设计

林雅铃, 吴明阳, 张卫, 等 77

双级可转导叶压气机性能研究 王忠义, 李政, 王瑞浩, 等 82

基于双折射晶体透镜的自干涉全息成像系统 许灿华, 薛孔松, 范德峰, 等 88

矿物分选中低阶多孔煤的药剂吸附及表征实验设计

解维伟, 周玲娟, 王立明, 等 96

核电领域高阻抗纯水体系 IR 降控制的研究 蔡双雨, 雷应, 曹健, 等 104

虚拟仿真技术

井底流固耦合环境下 PDC 钻头切削齿冷却仿真实验

王京印, 耿明磊, 廖华林 111

基于 VRX 的无人水面船智能控制虚拟仿真实验平台设计

张宇, 李洪宇, 王宗省 121

基于 Unity 3D 的瓦斯燃烧与烟气排放仿真实验建设

李乃良, 王利军, 刘常松, 等 129

断层破碎带隧道结构破坏离散元数值试验 杨青林, 李醒, 王永雷 136

仪器设备研制

高铁司机警觉度监测与干预穿戴装置研制 史磊, 周文慧, 魏方传, 等 143

期刊基本参数: CN11-2034/T * 1963 * m * A4 * 259 * zh * P * ¥30.00 * 6500 * 36 * 2024-08

基于液压储能器的制动能量回收试验台研制·····徐平, 马宗正, 王赛飞, 等	150
动水条件下煤岩单轴蠕变试验监测装置研制·····杨东辉, 张星星, 陈晓鹏, 等	156
一种用于缆上控制与保护装置(IC-CPD)测试的剩余电流模拟系统设计 ·····陈聪, 倪峰, 李春	161
液位控制实训平台设计·····王振浩, 专祥涛	169

实验教学研究与管理

区域综合能源系统两阶段鲁棒优化实验案例教学 ·····邵振国, 林勇棋, 陈煜超, 等	175
多孔有机笼膜材料纳滤机理的分子模拟教学实验设计 ·····刘捷, 谭晓艳, 薛亚楠, 等	182
基于高精度激光光斑质心定位技术的教学实验设计 ·····沈利荣, 张文博, 隆嘉瑾, 等	188
聚乙烯醇/SAPO-34 混合基质膜制备及渗透汽化性能综合实验教学设计 ·····蔡卫滨, 宋美洁, 焦健, 等	195
基于实际工程项目的装配参数视觉检测实践教学设计与实现 ·····杨义, 陈宗涛, 徐刚, 等	201
创新型传热学导热系数教学实验的设计与实践·····孙始财, 谷林霖	208
集成 AI 大语言模型的在线编程实验平台设计与实现 ·····厉旭杰, 顾雨辰, 姚持恩	215
LSTM 智能导向的电子信息技术教改探索·····包建荣, 秦艺鹏, 刘超, 等	222

实验室环境健康与安全

标杆管理理论在高校实验室安全管理中的应用 ·····范寒寒, 朱久娟, 冯嘉靖, 等	230
基于遗传算法的元胞自动机复杂楼宇人员疏散模型 ·····白鹏, 刘楠, 董卓龙, 等	236

实验室建设与管理

新工科背景下提高教学类仪器设备利用率的探索与实践——以吉林大学工程 训练中心为例·····丁连涛, 吴彤, 刘思含, 等	244
实验技术队伍先进技术集群建设·····郑娜, 吴哲敏, 徐丽, 等	251
地方院校实验室科研用房绩效考核改革与实践——以徐州医科大学为例 ·····赵冲, 郑友广, 徐红岩	255

· 广告索引 ·

江苏埃德伯格电气有限公司(封二)
2024 年《实验技术与管理》征订单(后一)
外应环球科技(北京)有限公司(封三)
上海万欣计算机信息科技有限公司(封底)



《实验技术与管理》
微信公众号

实验技术与管理

第十二届编辑委员会名单

主任: 曾嵘

顾问: (按姓名拼音排序)

陈小明 程建平 高松 邱爱慈 瞿振元
席葆树 周玉 周远清 朱静

副主任: (按姓名拼音排序)

毕卫民 董林 胡国庆 蒋兴浩 金永东
李长利 刘克新 孙小平 唐睿康 王海洁
王小力 王玉军 席海涛 熊宏齐 张社荣
钟代笛 朱臻 宗俊峰

编委: (按姓名拼音排序)

蔡以兵 曹蓓 陈越 陈晓猛 陈心浩
丁元明 董华青 董绍辉 杜华云 冯建刚
盖宏伟 郭庆 郭建中 韩英霞 郝志强
侯珏 黄富贵 蒋开东 蒋文春 康传红
赖延清 李崧 李格升 李立光 李鹏健
李天书 李向阳 梁勇 刘锋 刘刚
刘哲 刘红军 刘兼唐 刘崎峰 刘琦晖
刘雯杰 刘拥军 芦燕 罗茂斌 马国杰
马国玉 毛昌杰 毛继泽 孟兆磊 牛晓滨
彭远红 任志波 邵岚 邵光辉 沈勇
沈清明 沈如群 孙胜春 唐俊峰 汪必琴
王建 王强 王耀峰 王哲强 王中亮
魏永前 闻毓民 吴卫 吴雁 吴祝武
向坚持 熊龙彪 许燕滨 薛凌云 杨立成
杨立功 杨小兵 杨旭静 杨原志 姚丽华
姚作芳 于江华 余自中 袁洪学 占金华
张东 张莉 张巍 张文 张淑峰
张明生 张若好 张新生 章明卓 赵国
赵冬梅 钟华勇 周晔 朱正茂 朱仁青
庄志鸿

特邀编委: (按姓名拼音排序)

敖天其 毕大强 蔡峥 陈小鸿 丁建伟
冯建跃 桂南 韩小涛 金仁东 林文文
雷敬炎 李赛 李震彪 史天贵 唐国强
王兵 王杰 邢志 姚文清 袁志
张云怀 章立军 钟茂华

特别支持单位

江苏埃德伯格电气有限公司 董事长 杨勇
上海万欣计算机信息科技有限公司 总经理 谢卫民
中国分析测试协会高校分析测试分会 秘书长 施文清
清华四川能源互联网研究院 副院长 曹宗相
浙江清华长三角研究院 副院长 冯叶成

聚丙烯酰胺季铵盐大分子药物的环境毒性评价及其实验设计

林雅铃¹, 吴明阳¹, 张卫¹, 孙凯伦², 张安强²

(1. 华南农业大学 材料与能源学院, 广东 广州 510642;

2. 华南理工大学 材料科学与工程学院, 广东 广州 510641)

摘要: 聚丙烯酰胺季铵盐 (PAM-QAS) 是丙烯酰胺 (AM) 与丙烯酰胺季铵盐 (AM-QAS) 的无规共聚物, 因兼具聚丙烯酰胺的土壤改良特性和大分子季铵盐的抑菌特性, 在抑制土壤病原真菌、改良和修复病土等领域有良好的应用前景。但人们对季铵盐具有较高环境毒性的传统认识, 极大地限制了这类新型大分子药物的应用。如何结合 PAM-QAS 的应用环境, 综合、客观地评价其环境毒性, 是大分子药物设计和应用中亟待解决的问题。通过在 PAM-QAS 中修饰荧光基团直观地观察其在土壤中的吸附与淋溶特性, 以及结合土壤吸附和淋溶实验用鱼类经口急性毒性实验和蚯蚓毒性实验评价 PAM-QAS 经土壤吸附后的实际环境毒性, 为 PAM-QAS 的田间应用提供了一定科学依据。该实验内容涉及聚合物结构表征与应用、大分子药物在复杂环境下的定性检测, 以及药物的环境毒性评价等诸多环节, 具有一定的综合性与探索性, 有利于提高学生的综合素质、科研能力和创新能力。

关键词: 聚丙烯酰胺季铵盐; 荧光基团修饰; 土壤吸附特性; 环境毒性评价

中图分类号: TQ33 **文献标识码:** A **文章编号:** 1002-4956(2024)08-0077-05

将药物的评价标准与实际应用条件相结合, 客观评价药物的综合性能, 一直是药物分析和评价领域的难题, 将这些领域的研究成果引入本科探索性实验教学, 是科研与教学结合的重要方式。在此过程中, 应注意测试标准的普适性与实际应用环境的有机结合, 以及学生认知水平与实验教学条件的匹配^[1]。聚丙烯酰胺季铵盐 (PAM-QAS) 是丙烯酰胺 (AM) 与丙烯酰胺季铵盐 (AM-QAS) 的无规共聚物, 因兼具聚丙烯酰胺的土壤改良特性^[2-4]和大分子季铵盐的抑菌特性^[5-6], 在抑制土壤的病原真菌^[7]、改良和修复病土^[8]等领域有良好的应用前景。但基于人们关于传统小分子季铵盐具有广谱抑菌活性^[9-13], 具有较高环境毒性的惯性思维, 往往也认为大分子季铵盐也具有较高环境毒性, 这极大地限制了这类新型大分子药物的应用。

针对上述问题, 我们设计了多个可直观表现 PAM-QAS 低环境毒性的实验。首先, 在 PAM-QAS 的聚合过程中引入极少量的乙烯基荧光单体, 得到荧光修饰

的聚丙烯酰胺季铵盐 (PAM-QAS-FL), 通过土壤淋溶实验证实 PAM-QAS-FL 在土壤中具有有良好的吸附和难迁移特性; 其次, 结合 PAM-QAS 的土壤吸附与淋溶实验, 用斑马鱼毒性实验 (鱼类急性毒性实验) 证实 PAM-QAS 经土壤吸附后, 极大地降低了对环境水体的影响; 最后, 用蚯蚓毒性实验证实吸附了 PAM-QAS 的土壤对蚯蚓的毒性极低。本综合实验内容涵盖了功能聚合物的荧光特性表征、结合实际应用条件和国家标准开展实验设计等诸多环节, 还具有一定的趣味性, 能够使学生较为系统地学习功能高分子材料的分子设计、结构表征及应用等方面知识, 训练灵活掌握大分子药物和功能高分子材料学科的研究方法与思维方式。

1 实验部分

1.1 实验材料

N, N-二甲基十二烷基苄基氯化铵 (商品名: 苯扎

收稿日期: 2024-02-28

基金项目: 国家自然科学基金项目 (31772202); 广州市科技计划项目 (201803020015); 广东省高等教育教学改革项目 (2022-397); 广东省高等教育学会课题 (22GYB060); 华南理工大学探索性实验项目 (2021-11)

作者简介: 林雅铃 (1978—), 女, 福建罗源, 博士, 副教授, 主要研究领域为大分子药物与超分子弹性体, linyaling@scau.edu.cn。

通信作者: 张安强 (1976—), 男, 湖南安仁, 博士, 教授, 主要研究方向为功能高分子材料, aqzhang@scut.edu.cn。

引文格式: 林雅铃, 吴明阳, 张卫, 等. 聚丙烯酰胺季铵盐大分子药物的环境毒性评价及其实验设计[J]. 实验技术与管理, 2024, 41(8): 77-81.

Cite this article: LIN Y L, WU M Y, ZHANG W, et al. Environmental toxicities evaluation and experimental design of polymeric drugs based on polyacrylamide quaternary ammonium salts[J]. Experimental Technology and Management, 2024, 41(8): 77-81. (in Chinese)

氯铵, BC), >99%, 麦克林生化科技有限公司产品。根据季铵盐结构的不同, 聚丙烯酰胺季铵盐 (PAM-QAS) 分为 PAM-BB 和 PAM-BC 两种, 对应的荧光基团产物 (PAM-QAS-FL), 也分为 PAM-BB-FL 和 PAM-BC-FL, 其结构如图 1 所示, 均参考文献[8]合成。实验用土取自华南农业大学科研基地农场 (菜园土), 风干

后去除非土物质, 碾碎, 过 20 目筛, 备用。土壤的理化性质如下: pH 5.54, 有机质含量 21.1 g/kg, 全 N、P、K 含量分别为 824、108、226 mg/kg。斑马鱼购于上海市费曦生物科技有限公司, 全长 2 ± 0.5 cm, 体重 0.2 ± 0.1 g。蚯蚓品种为赤子爱胜蚓 (*Eisenia foetida*), 购于河北省鑫伊达蚯蚓养殖场, 全长 5~8 cm, 体重 0.3~0.6 g。

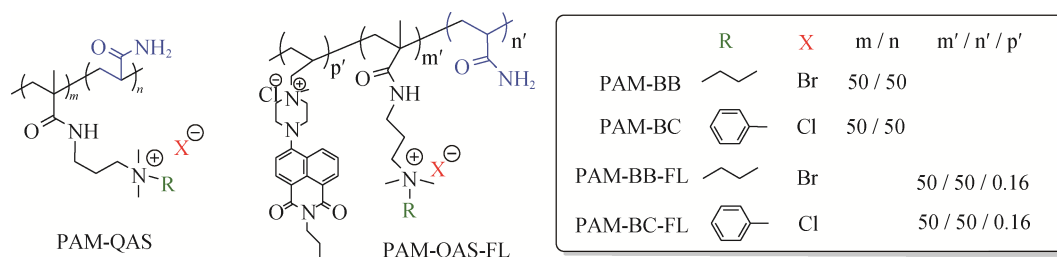


图 1 PAM-QAS (PAM-BB 和 PAM-BC) 和 PAM-QAS-FL (PAM-BB-FL 和 PAM-BC-FL) 的结构示意图

1.2 土壤淋溶实验

根据 PAM-QAS 在土壤中的常用施用量 (0.2 g/kg 干土), 预先把 PAM-QAS (或 PAM-QAS-FL) 按 3 倍常用施用量 (0.6 g/kg 干土) 与风干并过筛的土壤混合均匀 (阳性对照为苯扎氯铵/BC, 阴性对照为不加任何药物), 然后将 700 g 混合土壤装入内径为 4 cm、长度为 30 cm、带有出口控制阀的玻璃柱中 (装置如图 2 所示), 需边轻微振动边添加土壤以实现均匀填充, 最后用石英砂覆盖土柱的上表面。加入 0.01 mol/L CaCl_2 溶液使土柱中水分达到饱和, 以去除土壤颗粒中存在的空气, 平衡 24 h 后, 在 24 h 内于每个土柱上滴加 320 mL (相当于 255 mm/ 24 h 的“特大暴雨”级别的降雨量) 的人工降雨 (去离子水), 收集土柱淋出液, 静置 12 h 后, 得到土壤淋溶液。当混入药物为 PAM-QAS-FL 时, 淋溶液浓缩后用荧光分光光度计测定其荧光吸收特性; 当混入药物为 PAM-QAS 时, 在收集的淋溶液中加入斑马鱼, 以评价 PAM-QAS 土壤淋溶液对斑马鱼的急性毒性。

1.3 PAM-QAS 对斑马鱼的急性毒性实验

参照《GB/T 31270.12—2014: 鱼类急性毒性试验》

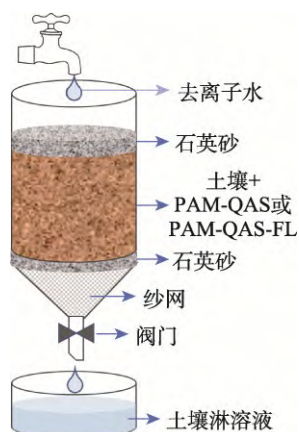


图 2 土壤淋溶装置示意图

测试 PAM-QAS 在不同条件下 (直接投入、土壤淋溶液、药物与水土混合物) 对水生生物斑马鱼的急性毒性, 选用 $2.0 \sim 2.2$ cm 体长和 $0.2 \sim 0.3$ g 体重的斑马鱼作为实验对象。

在直接投入条件下, 以 PAM-BB、PAM-BC 和 BC 作为实验药物, 重铬酸钾为参照毒物, 不含任何药物的清水为对照组。在预实验中, 将重铬酸钾、BC、PAM-BB 和 PAM-BC 的浓度设置为 0 、 0.01 、 0.1 、 1.0 、 10 和 100 mg/L, 以确定导致斑马鱼 $0 \sim 100\%$ 死亡率时的浓度范围。每个处理组放入 7 尾鱼, 每隔 24 h 记录斑马鱼的存活情况。预实验中, 浓度为 100 mg/L 的处理组即为限度实验, 若此测试浓度下 7 尾鱼全部存活, 则证明所测试药物对斑马鱼无急性毒性。根据预实验 96 h 毒性结果, 在正式实验中, 将药物在 $10 \sim 100$ mg/L 区间配置成不同浓度持续进行, 记录 96 h 鱼的死亡率。根据毒力方程求出 BC、PAM-BB 和 PAM-BC 对斑马鱼的半数致死浓度 LC_{50} [14]。

针对土壤淋溶液环境, 以 PAM-BB、PAM-BC 和 BC 作为实验药物, 参照本文 1.2 节中所述方法获得土壤淋溶液, 每组放入 7 尾鱼, 每组重复三次。空白对照组为不含药物土壤的淋溶液, 其他条件与实验组相同。以每公斤干土中所含的药物为基础, 估算所得淋溶液在 96 h 后对斑马鱼的半数致死浓度, 为了与 LC_{50} 相区分, 采用 LC_{50L} 来表示, 下标 “L” 表示淋溶液。

针对水土共混环境, 以 PAM-BB、PAM-BC 和 BC 作为实验药物, 将其加入到水土比约为 $5:1$ 的模拟鱼塘水中, 充分混匀后静置 24 h 后, 每组放入 7 尾鱼, 每组重复三次。空白对照组为不含药物的水溶液, 其他条件与实验组相同。观察并记录 96 h 后斑马鱼的中毒症状和死亡率, 所得的对斑马鱼的半数致死浓度标记为 LC_{50S} , 下标 “S” 表示含土壤的水土共混环境。

1.4 PAM-QAS 对蚯蚓的急性毒性实验

参照 GB/T31270.12—2014, 选取二月龄以上、体重在 0.4 ± 0.1 g 的健康赤子爱胜蚓。在进行实验之前, 在室内对蚯蚓培养 7 d 以上。配制由 10% 泥炭藓、68% 50~100 μm 的石英砂、20% 高岭土、2% 碳酸钙组成的人工土壤, 调节其 pH 值至 6.0 ± 0.5 , 加入蒸馏水调节人工土壤含水量为 30%~35%。以 PAM-BB、PAM-BC 和 BC 作为实验药物, 按一定比例间距设置 6 个浓度组和 1 个空白对照组, 每个浓度重复三组。不同处理组分别放入蚯蚓 10 条, 用保鲜膜封好瓶口并扎小孔, 将烧杯置于 20 ± 2 $^{\circ}\text{C}$ 、湿度 80% 左右、光照强度 400~800 lx 的培养箱中。根据蚯蚓 14 d 的死亡率, 计算药物对蚯蚓的毒性 LC_{50} 值及 95% 置信限^[10-11,15]。

2 结果与讨论

2.1 PAM-QAS 在土壤中的淋溶与迁移特性

与诸多小分子药物不同的是, PAM-QAS 自身并没有明显的特征吸收峰, 难以用常规的光谱分析方法表征其在土壤中的吸附、迁移与淋溶特性, 故需在其分子链中共聚极少量的荧光基团 ($<0.2\%$ mol), 得到荧光基团修饰的 PAM-QAS, 即: PAM-QAS-FL。图 3 是 PAM-BB-FL 及含 PAM-BB-FL 土壤的淋溶液的荧光光谱图。由图 3 可以看出, PAM-BB-FL 水溶液在紫外灯下能够发出明亮的绿光, 且在 515 nm 处有最大的荧光强度, 而含 PAM-BB-FL 土壤的淋溶液浓缩后在紫外灯下只有暗蓝色光, 为土壤本身所带荧光物质颜色, 且在 515 nm 处的荧光强度极低。这一实验结果直观地表明, PAM-QAS 在土壤中难以移动, 不容易随水迁移, 可以较长时间稳定地待在土壤中, 有利于长期发挥抑菌作用。

2.2 PAM-QAS 在不同环境下对斑马鱼和蚯蚓的急性毒性

图 4 是 PAM-QAS 和 BC 在不同环境下对斑马鱼和蚯蚓的急性毒性。由图可见, 当按照 GB/T 31270.12—2014 的要求, 将药物直接投入水中来评价药物对鱼类的急性毒性时, 季铵盐类药物都表现出较高的毒性, 其中, BC 的 $\text{LC}_{50} < 1$ mg/L, 表现为高毒, PQDXAM 的 LC_{50} 较 BC 略高一些, 在 1~10 mg/L 间, 但仍属于中毒范畴, 这与文献报道^[9-12]大致吻合, 这也是人们对季铵盐类药物在田间施用感到担忧的一个原因。众所周知, 季铵盐可经由不同途径释放到环境中, 在水体、沉积物、土壤等多种介质中均可检出, 由于其较强的表面活性和非专一性的生物毒性, 对生态环境构成潜在威胁^[12]。PAM-QAS 作为一类新型的具有较大分子量的水溶性大分子季铵盐类药物, 其分子特性及土壤吸附特性与小分子季铵盐存在较大差异, 主要以水溶液与土壤预拌方式施用。鉴于其与土壤之间具有很强的吸附作用^[8], 绝大部分的 PAM-QAS 被土壤有效吸附, 难以被淋溶进入环境水体 (如图 3 所示)。实际上, 图 4 中的蚯蚓急性毒性实验结果也证实了, 经

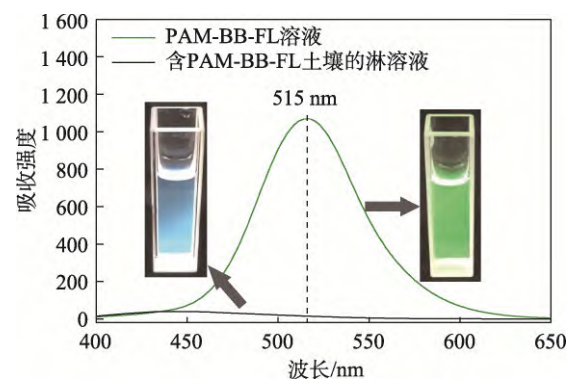


图 3 PAM-BB-FL 在土壤中的淋溶行为

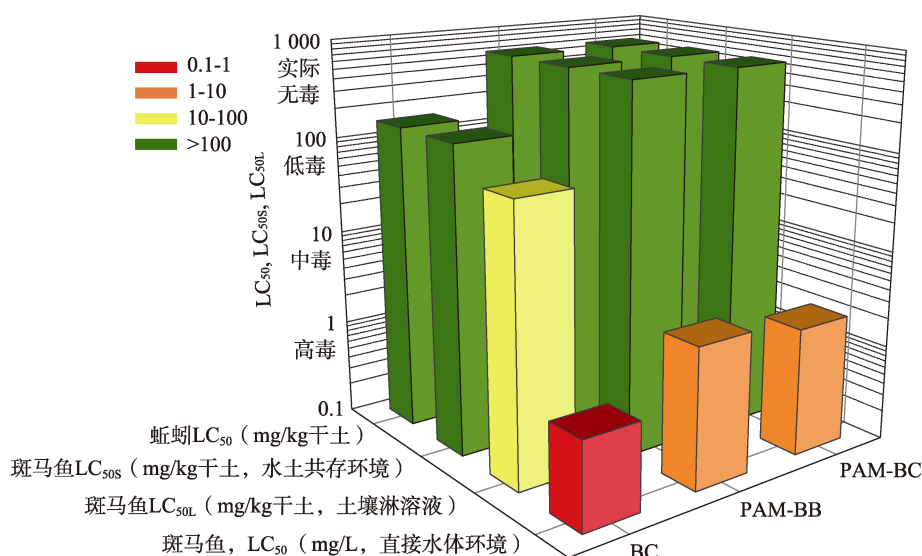


图 4 PAM-QAS 和 BC 在不同环境条件下对斑马鱼和蚯蚓的急性毒性

过与土壤的吸附, PAM-QAS 和 BC 对蚯蚓的急性毒性均处于低毒范畴。相应地, 需要针对不同的施用方式使用不同的鱼类毒性评价方法。

基于上述理念, 我们通过模拟药物在实际生产应用中随雨水渗入地下水以及与水土混合后对环境水体的影响, 引入 LC_{50L} 和 LC_{50S} 两个指标分别用于评价土壤淋溶液和水/土/药混合液的鱼类毒性。我们发现, 由于 PAM-QAS 在土壤中具有较强的吸附和难迁移特性, 大大降低了进入环境水体中的游离药物浓度。由图 4 可见, 在 3 倍田间常用施用量 (即: $0.6 \text{ g}/(\text{kg} \text{ 干土})$) 条件下, PAM-QAS 的土壤淋溶液及水土混合液中, 所有斑马鱼经过 96 h 后均都可以正常存活, 即相应的 LC_{50L} 和 LC_{50S} 均大于 $600 \text{ mg}/(\text{kg} \text{ 干土})$, 说明在田间常用施用量下, PAM-QAS 对鱼类和蚯蚓均是安全的。而在同样的施用量下, BC 的土壤淋溶液和水土共混液中的斑马鱼全部死亡, 说明 PAM-QAS 环境毒性较 BC 显著降低。这与直接施用于水体中所测得的 LC_{50} 有显著差异, 也是更符合实际使用条件的测试结果。我们认为, 这主要得益于聚丙烯酰胺较高的主链分子量及其与土壤之间的良好吸附作用。上述实验结果, 为在土壤中具有较强吸附作用药物 (尤其是大分子药物) 的环境评价, 提供了新的思路和方法。

3 结语

通过模拟药物在实际生产应用中随雨水渗入地下水以及与水土混合后对环境水体的影响, 引入 LC_{50L} 和 LC_{50S} 指标分别用于评价土壤淋溶液和水/土/药混合液的鱼类毒性, 较为准确地建立了 PAM-QAS 的环境毒性评价方法。实验结果表明, 在田间常用施用量为 $0.6 \text{ g}/(\text{kg} \text{ 干土})$ 条件下, PAM-QAS 可在土壤中稳定地吸附和存留, 对鱼类和蚯蚓均是安全的。与小分子季铵盐 BC 相比, 其环境毒性显著降低。

该实验大大丰富了大分子药物的环境毒性评价实验内容, 涵盖了功能聚合物的荧光特性表征、结合实际应用条件和国家标准开展环境毒性评价实验设计等诸多环节, 有助于学生深入理解高分子材料结构与性能之间的构效关系, 灵活掌握药物分析和功能高分子材料学科的研究方法与思维方式。在此过程中, 学生的材料结构表征能力、分析和解决问题能力也得到有效提升。

参考文献 (References)

- [1] 陈世良, 黄亦军, 黄嘉驰. 教师科研项目融入高分子专业实验教学的探索与实践[J]. 实验技术与管理, 2020, 37(9): 170–173, 178.
CHEN S L, HUANG Y J, HUANG J C. Exploration and practice

- of combining scientific research projects with experimental teaching of polymer materials and engineering[J]. Experimental Technology and Management, 2020, 37(9): 170–173, 178. (in Chinese)
- [2] ZHANG H L, WANG G H, DU J, et al. Effects of several polymeric materials on the improvement of the sandy soil under rainfall simulation[J]. Journal of Environmental Management, 2023(345): 118847.
- [3] MAMEDOV A I, HUANG C H, ALIEV F A, et al. Aggregate stability and water retention near saturation characteristics as affected by soil texture, aggregate size and polyacrylamide application [J]. Land Degradation and Development, 2017, 28(2): 543–552.
- [4] KEBEDE B, TSUNEKAWA A, HAREGEWEYN N, et al. Effectiveness of polyacrylamide in reducing runoff and soil loss under consecutive rainfall storms[J]. Sustainability, 2020, 12(4): 1597.
- [5] JIAO Y, NIU L N, MA S, et al. Quaternary ammonium-based biomedical materials: State-of-the-art, toxicological aspects and antimicrobial resistance[J]. Progress in Polymer Science, 2017(71): 53–90.
- [6] LU G Q, WU D C, FU R W. Studies on the synthesis and antibacterial activities of polymeric quaternary ammonium salts from dimethylaminoethyl methacrylate[J]. Reactive and Functional Polymers, 2007, 67(4): 355–366.
- [7] ZHANG A Q, LIU Q Q, LEI Y F, et al. Synthesis and antimicrobial activities of acrylamide polymers containing quaternary ammonium salts on bacteria and phytopathogenic fungi [J]. Reactive and Functional Polymers, 2015(88): 39–46.
- [8] ZHANG W, YU J G, WU M Y, et al. Polyacrylamide quaternary ammonium salts based on stable adsorption in soil and its application on the control of soil-borne fungal disease[J]. European Polymer Journal, 2024(202): 112604.
- [9] TONG Y H, LU P L, ZHANG W Y, et al. The shock of benzalkonium chloride on aerobic granular sludge system and its microbiological mechanism[J]. The Science of the Total Environment, 2023(895): 165010.
- [10] CHEN Y, GEURTS M, SJOLLEMA S B, et al. Acute toxicity of the cationic surfactant C12-benzalkonium in different bioassays: How test design affects bioavailability and effect concentrations[J]. Environmental Toxicology and Chemistry, 2014, 33(3): 606–615.
- [11] WANG Y H, CANG T, ZHAO X P, et al. Comparative acute toxicity of twenty-four insecticides to earthworm, *Eisenia fetida*[J]. Ecotoxicology and Environmental Safety, 2012(79): 122–128.
- [12] 李北兴, 李华, 张大侠, 等. 季铵盐和有机硅助剂对啮虫脉杀虫活性及水生生物毒性的影响[J]. 农药学报, 2017, 19(1): 93–99.
LI B X, LI H, ZHANG D X, et al. Influence of quaternary ammonium and organic silicon adjuvant on insecticidal activity of acetamiprid and environmental toxicity against aquatic organisms[J]. Chinese Journal of Pesticide Science, 2017, 19(1): 93–99. (in Chinese)

- [13] LARSSON Y, MONGELLI A, KISIELIUS V, et al. Microbial biofilm metabolism of benzalkonium compounds (benzyl dimethyl dodecyl ammonium & benzyl dimethyl tetradecyl ammonium chloride)[J]. Journal of Hazardous Materials, 2024(463): 132834.
- [14] EL-HARBAWI M. Toxicity measurement of imidazolium ionic liquids using acute toxicity test[J]. Procedia Chemistry, 2014(9): 40–52.
- [15] 陈吉祥, 于伟丽, 王广友, 等. 氯虫苯甲酰胺对环境生物的急性毒性与安全性评价[J]. 生态毒理学报, 2022, 17(6): 452–461.
- CHEN J X, YU W L, WANG G Y, et al. Acute toxicity and safety evaluation of chlorantraniliprole to environmental organisms[J]. Asian Journal of Ecotoxicology, 2022, 17(6): 452–461 (in Chinese)

Environmental toxicities evaluation and experimental design of polymeric drugs based on polyacrylamide quaternary ammonium salts

LIN Yaling¹, WU Mingyang¹, ZHANG Wei¹, SUN Kailun², ZHANG Anqiang²

(1. College of Materials and Energy, South China Agricultural University, Guangzhou 510642, China;

2. School of Materials Science and Engineering, South China University of Technology, Guangzhou 510641, China)

Abstract: [Objective] Because of the huge damage caused by soil-borne fungal diseases in agriculture, polyacrylamide quaternary ammonium salts (PAM-QAS) have been introduced to control soil-borne fungal diseases, such as banana *Fusarium* wilt, which is caused by *Fusarium oxysporum* f. sp. *cubense* (Foc). As a random copolymer of acrylamide and acrylamide quaternary ammonium salt, PAM-QAS shows significant improvement properties on soil and good antifungal activities against soil-borne fungal diseases, such as Foc. Thus, PAM-QAS has a good application prospect in the control of soil-borne fungal diseases and improving soil. However, traditional small molecular quaternary ammonium salts have been well-known to show high environmental toxicities, greatly limiting their application. Thus, visually evaluating the environmental toxicities of PAM-QAS based on exact application environments has become an urgent issue in the design and application of PAM-QAS. In this work, multiple experiments were designed to visually demonstrate the low environmental toxicity of PAM-QAS. [Methods] To visualize PAM-QAS, a very small amount of a fluorescent group (FL) was introduced into PAM-QAS to obtain fluorescent-labeled PAM-QAS (PAM-QAS-FL). Thus, its adsorption and leaching characteristics in soil could be observed intuitively. From the soil adsorption and leaching experiments, the actual environmental toxicities of PAM-QAS after soil adsorption could be evaluated using fish oral acute toxicity and earthworm toxicity experiments, which gave a good perspective for the field application of PAM-QAS. [Results] The soil adsorption and leaching experiments intuitively showed that under an application rate of 0.6 g per kilogram of dry soil in the field, which was about three times the commonly applied amount, PAM-QAS-FL could be stably adsorbed and retained in the soil, with only a few free PAM-QASs leaching into environmental water. Thus, the impact of PAM-QAS on the environment could be greatly reduced. The fish acute toxicity of simulated rain leaching solution containing PAM-QAS and soil (LC_{50L}), the fish acute toxicity of a suspension containing PAM-QAS and soil (LC_{50S}), and the earthworm toxicity of PAM-QAS (LC_{50}) were all higher than 600 mg per kilogram of dry soil. Meanwhile, the LC_{50L} , LC_{50S} , and LC_{50} (earthworm) for small molecule quaternary ammonium salt (benzalkonium chloride (BC)) were about 70, 150, and 150 mg per kilogram of dry soil, respectively. These results demonstrate that compared with BC, the environmental toxicity of PAM-QAS is significantly reduced, and it is safe for both fish and earthworms. [Conclusions] By simulating the effects of drugs infiltrating groundwater with rainwater and mixing with soil and water in practical production applications, LC_{50L} and LC_{50S} were introduced to evaluate the fish toxicity of soil leaching solutions and water/soil/drug mixtures, respectively. A more accurate environmental toxicity assessment method for PAM-QAS was thus established. This work covers several aspects, such as structure characterization and application of functional polymers, qualitative detection of polymeric drugs in complex environments, and environmental toxicity evaluation of drugs. It is comprehensive and exploratory to a certain extent and is conducive to improving students' comprehensive quality, scientific research, and innovation ability.

Key words: polyacrylamide quaternary ammonium salt; fluorescent group modification; soil adsorption characteristics; environmental toxicity evaluation

(编辑: 张文杰)

智慧可视化管理平台

万欣可视化维视(VIIS维视)智慧管理平台

· 挖掘数据价值 · 赋能综合治理 · 支撑建设决策 · 展示应用成效

应用成果
智慧展示数据

展示



建设管理
科学利用数据

利用

专项
建设

仪器
购置

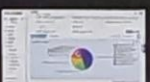
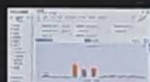
绩效
考核

数据
上报

安全
治理

统计报表
智能分析数据

分析



运行过程
采集使用数据

采集

安全
管控

资源
开放

实验
教学

物联
终端

整合治理
规范基础数据

规范

房间

人员

设备

耗材

安全
信息

万欣高校智慧实验室信息化管理



上海万欣计算机信息科技有限公司

A: 上海市虹口区花园路128号7街区A座3001 T: 400-008-1581 W: <http://www.wanxinsoft.com>



扫码关注万欣

检索证明

根据委托人提供的论文材料，委托人华南农业大学材料与能源学院 林雅铃 1 篇论文收录情况如下表。

序号	论文名称	发表刊物及发表的年月卷期/页码等	作者排名	论文等级	作者文中单位	收录情况	影响因子	中科院大类分区
1	聚丙烯酰胺季铵盐大分子药物的环境毒性评价及其实验设计	实验技术与管理 出版年：2024 卷期： 页码： - 文献号： 文献类型：	第一作者	C 类	华南农业大学 材料与能源学院	北大核心	无	无

说明：论文等级和中科院大类分区按《华南农业大学学术论文评价方案（试行）》划分。

报告免责声明：如未盖章，报告无效

检索员：尹银怀
华南农业大学图书馆

2025-07-11

关于国家自然科学基金资助项目批准及有关事项的通知

林雅铃 先生/女士：

根据《国家自然科学基金条例》的规定和专家评审意见，国家自然科学基金委员会（以下简称自然科学基金委）决定批准资助您的申请项目。项目批准号：

31772202，项目名称：两亲性大分子季铵盐的合成及其对水稻纹枯病菌的抑制作用与机理，直接费用：55.00万元，项目起止年月：2018年01月至2021年12月，有关项目的评审意见及修改意见附后。

请尽早登录科学基金网络信息系统（<https://isisn.nsf.gov.cn>），获取《国家自然科学基金资助项目计划书》（以下简称计划书）并按要求填写。对于有修改意见的项目，请按修改意见及时调整计划书相关内容；如对修改意见有异议，须在计划书电子版报送截止日期前提出。**注意：请严格按照《国家自然科学基金资助项目资金管理办法》填写计划书的资金预算表，其中，劳务费、专家咨询费科目所列金额与申请书相比不得调增。**

计划书电子版通过科学基金网络信息系统（<https://isisn.nsf.gov.cn>）上传，由依托单位审核后提交至自然科学基金委进行审核。审核未通过者，返回修改后再行提交；审核通过者，打印为计划书纸质版（一式两份，双面打印），由依托单位审核并加盖单位公章后报送至自然科学基金委项目材料接收工作组。计划书电子版和纸质版内容应当保证一致。

向自然科学基金委提交和报送计划书截止时间节点如下：

- 1、提交计划书电子版截止时间为**2017年9月11日16点**（视为计划书正式提交时间）；
- 2、提交计划书电子修改版截止时间为**2017年9月18日16点**；
- 3、报送计划书纸质版截止时间为**2017年9月26日16点**。

请按照以上规定及时提交计划书电子版，并报送计划书纸质版，未说明理由且逾期不报计划书者，视为自动放弃接受资助。

附件：项目评审意见及修改意见表

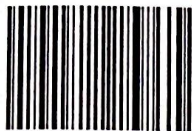
国家自然科学基金委员会
生命科学部
2017年8月17日

表9 科研课题情况
林雅铃 主持的课题

序号	项目名称	评审等级	项目来源	合同经费/实到经费	立项时间	结题时间	课题组总人数	本人排名	是否结题	备注
1	两亲性大分子季铵盐的合成及其对水稻纹枯病菌的抑制作用与机理	A	国家自然科学基金委员会	65.0	2017-08-17	2021-12-31	4	1	是	

科技处审核人及盖章：

年 月 日



201704020084

广州市科技计划项目合同书

批文号:穗科创字(2017)107号

项目编号: 201704020084

广州市科技计划项目 合同书

(前期资助一次性拨付类)

项目名称: 两亲性大分子季铵盐的合成及其在水稻纹枯病防治中的应用研究

计划类别: 产学研协同创新重大专项

专题名称: 民生科技研究

起止时间: 2017-05-01到2019-12-31

承担单位: 华南农业大学材料与能源学院

组织单位: 华南农业大学

责任处室: 社基处

填表日期: 2017-01-17 19:07

广州市科技创新委员会制
(2016年版)



201704020084

广州市科技计划项目合同书

一、项目基本信息表

项目名称		两亲性大分子季铵盐的合成及其在水稻纹枯病防治中的应用研究					
研究类别/所属技术领域		农业与食品/农业生产资料/农药的研制与生产					
承担单位	名称	华南农业大学材料与能源学院					
	通信地址	广州市天河区五山路483号					
	邮政编码	510642	传真	02085282366			
	单位特性	其他	单位类型				
	组织机构代码	45541656-3	统一社会信用代码	暂无			
	法定代表人	陈晓阳	电子邮箱	linyaling@scau.edu.cn			
	联系人	房翊	联系电话	13380055703			
参加单位	序号	名称	单位类型	分工	联系人	联系电话	
	1	华南理工大学	高等院校	(参见项目承担单位与参与单位合作内容)	张安强	133 188 188 95	
(一) 项目负责人							
姓名	林雅铃	性别	女	出生年月	1978-07-15		
国籍	中国	民族	汉族	学位授予国家(或地区)	中国		
学历	博士研究生	学位	博士	手机号码	13380097023		
证件名称	身份证	证件号码	3501231978 07150045	固定电话	020-85280319		
职务	副教授	职称	副高	电子邮箱	linyaling@scau.edu.cn		



八、合同书各方签章

签订地点：广州市越秀区

广州市科技创新委员会（甲方）：

项目经办人（签章）

胡宁

联系电话

83124044

责任处室负责人（签章）

华国彭

（公章）



2017月-06- 05

项目承担单位（乙方）：华南农业大学材料与能源学院

项目负责人（签章）

林雅玲

财务负责人（盖章）

郑晓月

财务负责人联系电话：

8928)402

帐户名：华南农业大学

帐号：3602002609000310520

开户银行：中国工商银行广东省广州市五山支行

法定代表人：（签章）

（Signature of Legal Representative）

（公章）

2017年3月22日

组织单位（丙方）：华南农业大学

项目经办人（签章）

（Signature of Project Officer）

（公章）

2017年3月22日

表9 科研课题情况
林雅铃 主持的课题

序号	项目名称	评审等级	项目来源	合同经费/实到经费	立项时间	结题时间	课题组总人数	本人排名	是否结题	备注
1	两亲性大分子季铵盐的合成及其在水稻纹枯病防治中的应用研究	A	广州市科技局	100.0	2017-04-27	2019-12-31	5	1	是	

科技处审核人及盖章：

年 月 日

受理编号: c1630550100241

项目编号: 2016A020210105

文件编号: 粤科规财字(2016)47号



2016A020210105

广东省省级科技计划项目 合同书

项目名称: 两亲性聚硅氧烷接枝季铵盐的合成及其在香蕉枯萎病防治中的应用

计划类别: 农村科技领域

项目起止时间: 2016-01-01 至 2018-12-31

管理单位(甲方): 广东省科学技术厅

承担单位(乙方): 华南农业大学

乙方主管部门(丙方): 华南农业大学

通讯地址: 广东省广州市天河区五山路483号

邮政编码: 510642

单位电话: 020-38632819

项目负责人: 林雅铃

联系电话: 020-38297109

项目联系人: 林雅铃

联系电话: 020-38297109

广东省科学技术厅
二〇一四年制

九、本合同签约各方

管理单位（甲方）：广东省科学技术厅（盖章）

单位地址：广东省广州市连新路171号

法定代表人（或授权代表）：黄宁生

联系人（经办人）姓名：刘世伟

Email: liusw@gdstc.gov.cn

电话：020-83163909



2016年 9月 1日

承担单位（乙方）：华南农业大学

（盖章）

二级部门：华南农业大学材料与能源学院

单位地址：广东省广州市天河区五山路483号

法定代表人（或法人代理）：陈晓阳

联系人（项目主管）姓名：石睿

Email: 77909213@qq.com

电话：020-85283435

开户单位名称：华南农业大学

开户银行及帐号：广东广州工行五山支行 3602002609000310520

[Handwritten signature]
[Handwritten signature]



2016年 9月 1日

乙方主管部门（丙方）：华南农业大学

（盖章）

单位地址：广东省广州市天河区五山路483号

法定代表人（或法人代理）：陈晓阳

联系人（项目主管）姓名：石睿

Email: 77909213@qq.com

电话：020-85283435

开户单位名称：华南农业大学

开户银行及帐号：广东广州工行五山支行 3602002609000310520

[Handwritten signature]
[Handwritten signature]



2016年 9月 1日

表9 科研课题情况
林雅铃 主持的课题

序号	项目名称	评审等级	项目来源	合同经费/实到经费	立项时间	结题时间	课题组总人数	本人排名	是否结题	备注
1	两亲性聚硅氧烷接枝季铵盐的合成及其在香蕉枯萎病防治中的应用	B	广东省科技厅	15.0	2016-04-22	2018-12-31	3	1	是	

科技处审核人及盖章：

年 月 日

教育部科技发展中心

[首 页](#) | [机构设置](#) | [科研基金](#) | [科技奖励](#) | [科技成果](#) | [产学研合作](#) | [大学科技园](#) | [科技产业化](#) | [计量认证](#) | [教育信息化](#)

2023年5月24日 星期三 [\[公告\]](#) [·2021年《中国教育网络》杂志征订函](#) [·2021年《中国高校科技》杂志征订](#)  站内搜索:

您的位置: 首页 >> 中心工作动态

2012年博士点基金立项课题公布

来源: 教育部科技发展中心

发布时间: 2012-12-18

访问次数:

【字体: 大 中 小】

2012年度高等学校博士学科点专项科研基金课题评审工作结束, 现将批准项目公布。

2012年12月18日

附件: [2012年博士点基金资助课题名单-博导类](#)

[2012年博士点基金资助课题名单-新教师类](#)

[2012年博士点基金资助课题名单-优先发展领域](#)

[2012年博士点基金资助课题名单-与香港研资局研究用途补助金合作项目资助课题](#)

相关信息

没有相关信息

[打印本页](#)

[关闭窗口](#)

客户服务信箱 Fax: 010-62514678 京ICP备: 05004627号



京公网安备 11040202430024号

位来客

Copyright © 2007-2012 版权所有: 教育部科技发展中心 未经书面许可 不得转载本站信息



1	2012年度高等学校博士学科点专项科研基金资助课题名单（新教师类）						
2	序号	课题编号	课题名称	申请学校	申请人	学科组名称	资助额度 (万元)
3	1	20120001120097	Hermite 向量丛的半稳定性	北京大学	陈华一	数学	4
4	2	20120001120098	三维流形的福勒结构及应用	北京大学	王家军	数学	4
			基于Ren的实时及混成连接件建模与验证方				
487	485	20123702120014	测墒补灌条件下小麦水氮高效利用的生理机制研究	山东农业大学	石玉	农林渔牧一组	4
488	486	20124306120006	异源四倍体鲫鲂雌核发育后代的遗传和生殖特性研究	湖南师范大学	覃钦博	农林渔牧一组	4
489	487	20124320120001	稻米垩白度基因CD6的精细定位与克隆	湖南农业大学	雷东阳	农林渔牧一组	4
490	488	20124404120002	基于无线地下传感网的中尺度土壤含水量测定方法	华南农业大学	徐兴	农林渔牧一组	4
491	489	20124404120007	水稻稻瘟病抗性基因Pik-m抗病机理的研究	华南农业大学	王加峰	农林渔牧一组	4
492	490	20124404120008	林木根系形态特征对稳态营养供应的响应机理研究	华南农业大学	何茜	农林渔牧一组	4
493	491	20124404120009	同步深施肥机械精量穴直播水稻的氮素利用效率研究	华南农业大学	潘圣刚	农林渔牧一组	4
494	492	20124404120011	硅提高大豆白粉病抗性的分子机制研究	华南农业大学	沈雪峰	农林渔牧一组	4
495	493	20124404120025	甜菜碱型两性离子聚合物的合成及其在甜菜夜蛾无公害防治中的应用	华南农业大学	林雅铃	农林渔牧一组	4
496	494	20124404120031	水稻细菌性基腐病菌zeamine毒素基因簇的结构来源及关键基因的功能分析	华南农业大学	周佳暖	农林渔牧一组	4
497	495	20125103120008	组蛋白甲基转移酶基因Lhd1调控的水稻开花分子机制研究	四川农业大学	孙昌辉	农林渔牧一组	4
498	496	20125103120011	锌指蛋白基因OsGCZ2在水稻稻瘟病致病过程中的调控机制	四川农业大学	李伟滔	农林渔牧一组	4
499	497	20125103120018	亚热带天然次生林地下碳循环过程对氮沉降的响应	四川农业大学	涂利华	农林渔牧一组	4
500	498	20126518120002	干旱胁迫下棉花叶黄素循环的响应机制及与抗性的关系	石河子大学	张亚黎	农林渔牧一组	4
501	499	20120008120001	降解呕吐毒素有益菌的筛选及其在饲料单端孢霉烯族毒素降解中的应用	中国农业大学	赵丽红	农林渔牧二组	4
502	500	20120014120004	农作物秸秆纤维素清洁分离及功能产品制备研究	北京林业大学	王堃	农林渔牧二组	4
503	501	20120014120006	纳米纤维素基高强度水凝胶制备研究	北京林业大学	杨俊	农林渔牧二组	4

表9 科研课题情况
林雅铃 主持的课题

序号	项目名称	评审等级	项目来源	合同经费/实到经费	立项时间	结题时间	课题组总人数	本人排名	是否结题	备注
1	甜菜碱型两性离子聚合物的合成及其在甜菜夜蛾无公害防治中的应用	B	教育部	4.0	2012-12-28	2015-12-31	9	1	是	

科技处审核人及盖章：

年 月 日

项目编号： 201803020015

广州市科技计划项目 合同书

项目名称： 含聚硅氧烷两亲性大分子季铵盐的合成及其在香蕉枯萎病防治中的应用

计划类别： 民生科技攻关计划

专题名称： 都市型现代农业专题

起止时间： 2018年04月01日 至 2021年03月31日

承担单位： 华南理工大学

组织单位： 华南理工大学

责任处室： 社会发展与基础研究处

填表日期： 2018年02月13日

广州市科技创新委员会
(2017年版)

八、项目承担单位（乙方）与合作单位合作内容

承担单位名称：华南理工大学

任务分工：材料合成与结构表征、材料物理性能表征与生物相容性测试

知识产权分配：双方共享

市科创委经费分配额度（万元）：65.00

自筹经费出资额度（万元）：0.00



合作单位（1）名称：华南农业大学

任务分工：材料生物相容性表征、抑菌实验与抑菌机理与盆栽实验等

知识产权分配：双方共享

市科创委经费分配额度（万元）：35.00

自筹经费出资额度（万元）：0.00



九、合同书各方签章

签订地点：广州市越秀区

广州市科技创新委员会（甲方）：广州市科技创新委员会

项目经办人（签章）：

秀珍

联系电话：

83124044

责任处室负责人（签章）

华国彭



章)

2018-05月10日

项目承担单位（乙方）：华南理工大学

二级部门：华南理工大学材料科学与工程学院

项目负责人（签章）：

张华

财务负责人（签章）：

马红

财务负责人联系电话：87110372

帐户名：华南理工大学

帐号：3602002609000733759

开户银行：工行广州五山支行

法定代表人（签章）：

王迎军



组织单位（丙方）：华南理工大学

项目经办人（签章）：

吴婷婷



联合申报项目协议书

甲方：华南理工大学

乙方：华南农业大学

甲方与乙方经友好协商决定联合申报 2018 年度 广州市科技计划项目(民生科技攻关计划项目) 项目，项目名称：含聚硅氧烷两亲性大分子季铵盐的合成及其在香蕉枯萎病防治中的应用研究。并达成如下合作协议：

第一条：项目研究工作详细分工：

甲方(主持方)：材料合成与结构表征、材料物理性能表征与生物相容性测试；

乙方(参与方)：材料物理性能表征、抑菌实验与抑菌机理、盆栽实验等。

第二条：经费分配：

1、如果本申报项目获批立项，按政府下达的资助经费，甲方、乙方同意此经费分别按政府资助经费的甲方：65 %、乙方：35 %进行分配。

2、甲方在收到 广州市科技创新委员会 下达的资助经费后的一个月将乙方所占经费支付给乙方指定帐户。

账 户：华南农业大学

帐 号：3602002609000310520

开户行：工商银行广州五山支行

第三条：企业配套经费比例：

无。

第四条：知识产权归属：

1. 项目实施过程中所产生的知识产权，优先执行任务下达单位的知识产权管理政策，在此前提下，作如下规定：

①各方独立完成的所有权归各自所有；双方共同完成的由双方共享，具体按照双方的贡献大小进行分配或双方另行商定。

②项目成果的转让，须在双方同意的前提下进行，任何一方不得私自转让或许可实施。

2. 项目成果申报各级奖项，双方单位排名根据具体情况另行商定，人员排

名原则上按贡献大小先后排名。

第五条：合作项目各方应严格遵守共同签订的合作协议书，除因不可抗拒的客观原因，不得中途撤消或中止合同。在合同期内，某方要求修改合同条款，须各方协商，确认后方能生效。

第六条：如合作方因各种原因无法履行合同条款时，由项目负责人报项目主管部门同意后，另寻合作者。

第七条：经批准中途退出合作的一方，应视具体情况将所余经费退回项目主持方，已用经费由项目负责人提出审查报告，报项目主管部门审批。

第八条：合作一方在工作进行中有问题不及时报告，影响项目整体的年度进展者，项目负责人有权缓拨或停拨下一年度经费，并通报项目主管部门。如影响项目整体无法完成者，将承担相关责任，并报主管部门。

第九条：本协议自双方签字盖章之日起生效，至项目完成之日起终止；若合作申请未获资助，本协议自动废止。

大
爆
章

甲方单位（盖章）：

委托代理人：

项目负责人（签字）：

2017年6月9日

南理工
吴婷婷
张书强
科技合同专用章

乙方单位（盖章）：

委托代理人：

项目负责人（签字）：

2017年6月9日

农业大
科技合同专用章
(1)
林明论

表9 科研课题情况
林雅铃 主持的课题

序号	项目名称	评审等级	项目来源	合同经费/实到经费	立项时间	结题时间	课题组总人数	本人排名	是否结题	备注
1	含聚硅氧烷两亲性大分子季铵盐的合成及其在香蕉枯萎病防治中的应用	C	广州市科技局	35.0	2017-10-31	2021-12-31	5	1	是	

科技处审核人及盖章：

年 月 日

受理编号: c23140500001255

项目编号: 2023A1515011264

文件编号: 粤基金字(2023)2号

广东省基础与应用基础研究基金项目 任务书

项目名称: 基于微区分离与动态可逆键的人工心脏瓣膜用超分子弹性体

项目类别: 广东省自然科学基金-面上项目

项目起止时间: 2023-01-01 至 2025-12-31

管理单位(甲方): 广东省基础与应用基础研究基金委员会

依托单位(乙方): 华南理工大学

通讯地址: 广东省广州市天河区广州市天河区五山路381号

邮政编码: 510640

单位电话: 020-87110630

项目负责人: 张安强

联系电话: 020-87112466



(广东科技微信公众号)



(查看任务书信息)



(受理纸质材料二维码)

广东省基础与应用基础研究
基金委员会
二〇二〇年制

五、人员信息

项目负责人

姓名	证件号码	年龄	性别	职称	学历	在项目中承担的任务	所在单位	签名
张安强	432831197610172419	47	男	教授	博士研究生	项目负责人	华南理工大学	张安强

项目组主要成员

姓名	证件号码	年龄	性别	职称	学历	在项目中承担的任务	所在单位	签名
林雅铃	350123197807150045	45	女	副教授	博士研究生	生物相容性与血流动力学评价	华南农业大学	林雅铃
黄皓浩	330222197412061975	49	男	副教授	博士研究生	材料结构表征	华南理工大学	黄皓浩
吴雄辉	430424199409138210	29	男	未取得	博士研究生	材料合成、结构表征与生物相容性评价	华南理工大学	吴雄辉
单世洁	370202199604201128	27	女	未取得	博士研究生	材料合成与结构表征	华南理工大学	单世洁
夏宇	36062220001205003x	23	男	未取得	本科	材料合成、生物相容性与血流动力学评价	华南理工大学	夏宇

六、工作分工及财政经费分配

承担/参与单位名称 (盖章)	工作分工	省级财政科技资金分配 (万元)
华南理工大学	材料合成与结构分析、瓣膜制备	7.00
华南农业大学	生物相容性评价与血流动力学测试。	3.00
	合计	10.00

2023 年度广东省自然科学基金项目申报合作协议书

甲方：华南理工大学

乙方：华南农业大学

甲乙双方本着相互协作的精神，合作申报 2023 年广东省自然科学基金面上项目，项目名称“基于微区分离与动态可逆键的人工心脏瓣膜用超分子弹性体”，经过协商达成如下协议，并由双方共同恪守。

一、 双方负责人：

甲方 华南理工大学 为项目依托单位，项目负责人为 张安强。

乙方 华南农业大学 为项目合作单位，合作方联系人为 林雅铃。

二、 研究分工：

甲方：材料合成与结构表征；

乙方：材料生物相容性与动物实验研究。

三、 研究成果归属：各自所有。

四、 经费分配：

该项目申请经费 10 万元，甲方经费比例 70 %，乙方经费比例 30 %。

本协议一式两份。若本项目未被批准，该协议自动失效；若项目获批，则甲乙双方根据实际获批经费，重新签订正式合作任务书。

甲方：华南理工大学

法人代表/委托代理人：

项目负责人（签章）：

张安强

联系电话：13318818895

2022 年 8 月 18 日

乙方：华南农业大学

法人代表/委托代理人：

项目负责人：

林雅铃

联系电话：13380097023

2022 年 8 月 18 日

科技合同-20230146

表9 科研课题情况
林雅铃 主持的课题

序号	项目名称	评审等级	项目来源	合同经费/实到经费	立项时间	结题时间	课题组总人数	本人排名	是否结题	备注
1	基于微区分离与动态可逆键的人工心脏瓣膜用超分子弹性体	按照个人到位经费定级	广东省基础与应用基础研究基金委员会	3.0	2023-01-01	2025-12-31	1	1	否	

科技处审核人及盖章：

年 月 日

项目编号：20240010

华南理工大学

广东省高性能与功能高分子材料重点实验室开放基金 项目合同书

项目名称：人工心脏瓣膜用抗凝抗钙化聚氨酯弹性体

项目负责人：林雅铃

联系电话：13380097023

起止年月 2024 年 6 月 至 2025 年 5 月

广东省高性能与功能高分子材料重点实验室学术委员会

- 第三条 甲方所设开放基金项目资金来源是其承担的广东省科学技术厅“广东省高性能与功能高分子材料重点实验室开放运行”项目经费，按照科研项目经费管理办法，甲方财务处已扣科研管理费、公摊水电费等间接费用。乙方在收到甲方转入的开放基金课题费用时，不能再重复扣管理费、水电费等任何间接费用。
- 第四条 乙方项目负责人务必于每年十二月底前，报送《广东省高性能与功能高分子材料重点实验室开放基金科研资助计划项目年度进展报告》。
- 第五条 乙方阶段性研究成果或最终研究成果，在出版或发表时，必须注明“广东省高性能与功能高分子材料重点实验室开放基金资助”（英文：The Open Fund for Key Lab of Guangdong High Property and Functional Macromolecular Materials, China）字样。否则，此成果不能视作本项目成果，不予结题。
- 第六条 乙方研究工作完成后必须及时结题，填写《广东省高性能与功能高分子材料重点实验室开放基金资助计划项目总结报告》。
- 第七条 乙方若不能按上述条款执行，未按期完成项目，将终止经费使用，在三年内不得申请新项目。
- 第八条 本合同正式文本一式肆份，甲、乙方各持贰份，自签约之日起生效，各合同具有同等法律效力。

甲方：华南理工大学

签字：

盖章：

乙方：华南农业大学

签字：

盖章：

乙方银行账户信息：汇款时请注明：林雅铃华工省重开放基金项目经费）

账户户名：华南农业大学

银行账号：3602 0026 0900 0310 520

开户银行：中国工商银行广州五山支行

签约日期 年 月 日

表9 科研课题情况
林雅铃 主持的课题

序号	项目名称	评审等级	项目来源	合同经费/实到经费	立项时间	结题时间	课题组总人数	本人排名	是否结题	备注
1	人工心脏瓣膜用抗凝抗钙化聚氨酯弹性体		其他纵向	2.0	2024-06-30	2025-05-31	1	1	否	

科技处审核人及盖章：

年 月 日

合同编号:

技术服务合同

项目名称: 聚合物材料的生物相容性评价

委托方: 华南理工大学
(甲方)

受托方: 华南农业大学
(乙方)

签订时间: 2022年6月 日

签订地点: 广州市

有效期限: 2022年6月15日至2023年12月31日

中华人民共和国科学技术部印制

填 写 说 明

一、本合同为中华人民共和国科学技术部印制的技术服务合同示范文本，各技术合同认定登记机构可推介技术合同当事人参照使用。

二、本合同书适用于一方当事人（受托方）以技术知识为另一方（委托方）解决特定技术问题所订立的合同。

三、签约一方为多个当事人的，可按各自在合同关系中的作用等，在“委托方”、“受托方”项下（增页）分别排列为共同委托人或共同受托人。

四、本合同书未尽事项，可由当事人附页另行约定，并作为本合同的组成部分。

五、当事人使用本合同书时约定无需填写的条款，应在该条款处注明“无”等字样。

技术服务合同

委托方（甲方）： 华南理工大学

住 所 地： 广州市天河区五山路 381 号

法定代表人： 高松

项目联系人： 张安强

联系方式：

通讯地址： 广州市天河区五山路 381 号

电 话： 020-87112466 传真：

电子信箱：

受托方（乙方）： 华南农业大学

住 所 地： 广州市天河区五山路

法定代表人： 刘雅红

项目联系人： 林雅铃

联系方式

通讯地址： 广州市天河区五山路 483 号

电 话： 13380097023 传 真：

电子信箱： linyaling@scau.edu.cn

本合同甲方委托乙方就 聚合物材料的生物相容性评价 项目进行的专项技术服务，并支付相应的技术服务报酬。双方经过平等协商，在真实、充分地表达各自意愿的基础上，根据《中华人民共和国合同法》的规定，达成如下协议，并由双方共同恪守。

1. 技术背景资料：无；
2. 可行性论证报告：无；
3. 技术评价报告：无；
4. 技术标准和规范：无；
5. 原始设计和工艺文件：无；
6. 其他：无；

第十五条：双方约定本合同其他相关事项为：无。

第十六条：本合同一式肆份，具有同等法律效力。

第十七条：本合同经双方签字盖章后生效。

甲方：华南理工大学（盖章）

法定代表人 / 委托代理人：高晓明（签名）

年 月 日

经办人：丁楚怡

乙方：华南农业大学（盖章）

法定代表人 / 委托代理人：刘雅红（签名）

年 月 日

印花税票粘贴处：



（以下由技术合同登记机构填写）

合同登记编号：

--	--	--	--	--	--	--	--	--	--	--	--	--	--	--	--

1. 申请登记人：_____

2. 登记材料：(1) _____

(2) _____

(3) _____

3. 合同类型：_____

4. 合同交易额：_____

5. 技术交易额：_____



技术合同登记机构（印章）

经办人：

年 月 日

表9 科研课题情况
林雅铃 主持的课题

序号	项目名称	评审等级	项目来源	合同经费/实到经费	立项时间	结题时间	课题组总人数	本人排名	是否结题	备注
1	聚合物材料的生物相容性评价		横向	6.0	2022-06-13	2023-12-31	2	1	是	

科技处审核人及盖章：

年 月 日

HX1GHT2024.879

合同编号：

技术开发（合作）合同

项目名称： 覆铜板基板树脂材料的开发研究

甲方： 湖南方锐达科技有限公司

乙方： 华南农业大学

签订时间： 2024 年 7 月 日

签订地点： 湖南省浏阳市经开区康平路 175 号

有效期限： 2024 年 7 月 15 日至 2026 年 7 月 15 日

中华人民共和国科学技术部印制

任一方违反本条，守约方有权终止本合同且无须承担违约责任，且违约方应立即停止违约行为，如导致另一方声誉受损或经济损失的，违约方应当同时承担相应的损害赔偿责任，守约方保留进一步追究违约方法律责任的权利。

第十八条 合作各方约定本合同其他相关事项为：为有效履行本合同，合作各方确定，在本合同有效期内，甲方指定李玉新为甲方项目联系人，乙方指定林雅铃为乙方项目联系人。项目联系人承担以下责任：

1. 及时联络双方项目进展工作，组织双方研讨会；
 2. 一方变更项目联系人的，应当及时并以书面形式通知其合作方。
- 未及时发现并影响本合同履行或造成损失的，应承担相应的责任。

第十九条 本合同一式四份，具有同等法律效力。

第二十条 本合同经合作各方签字盖章后生效。

甲方：湖南方锐达科技有限公司 (盖章)

法定代表人/委托代理人：林雅铃 (签名)

2024年7月5日

乙方：华南农业大学 (盖章)

法定代表人/委托代理人：林雅铃 (签名)

年 月 日

表9 科研课题情况
林雅铃 主持的课题

序号	项目名称	评审等级	项目来源	合同经费/实到经费	立项时间	结题时间	课题组总人数	本人排名	是否结题	备注
1	覆铜板基板树脂材料的开发研究		横向	30.0	2024-07-05	2026-07-15	1	1	否	

科技处审核人及盖章：

年 月 日

表9 科研课题情况
林雅铃 参与的课题

序号	项目名称	评审等级	项目来源	合同经费/实到经费	立项时间	开始时间	结题时间	负责人	课题组总人数	本人排名	是否结题
1	基于抑制昆虫雌性生殖干细胞分化活性的骆驼蓬碱构效关系研究		教育部	12.0	2013-10-28	2014-01-01	2016-12-31	钟国华	9	3	是

科技处审核人及盖章：

年 月 日

检索证明

根据委托人提供的论文材料, 委托人华南农业大学材料与能源学院 林雅铃 9 篇论文收录情况如下表。

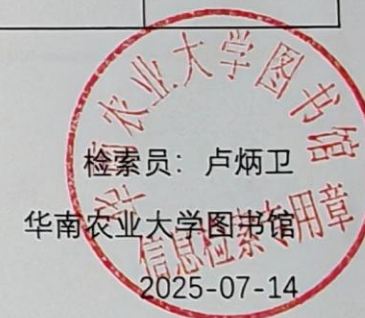
序号	论文名称	发表刊物及发表的年月卷期/页码等	作者排名	论文等级	作者文中单位	收录情况	影响因子	中科院大类分区
1	Synergistic enhancement of the robustness of multifunctional polyurethane via an ionic noncovalent cross-linking network and aromatic disulfides	CHEMICAL ENGINEERING JOURNAL 出版年: 2024 出版日期: FEB 1 卷期: 481 页码: - 文献号: 148229 文献类型: Article	第一作者, 共同通讯作者	T2 类	华南农业大学材料与能源学院	SCI	IF2-year=13.2 IF5-year=13.5 (2024)	材料科学 1 区 Top 期刊: 是 (2025)
2	Surface-Imprinted Polysiloxane with Recognition Ability Based on an ITO Layer for Rapid Detection of Fusarium oxysporum f. sp. cubense by the Naked Eye	ACS APPLIED MATERIALS & INTERFACES 出版年: 2024 出版日期: JUN 21 卷期: 16 26 页码: 33182-33191 文献类型: Article	第一作者, 共同通讯作者	A 类	华南农业大学材料与能源学院	SCI	IF2-year=8.2 IF5-year=8.5 (2024)	材料科学 2 区 Top 期刊: 否 (2025)
3	Amphiphilic polysiloxane graft guanidine salts with a combination of low environmental toxicity and high antifungal activity	EUROPEAN POLYMER JOURNAL 出版年: 2024 出版日期: AUG 7 卷期: 216 页码: -	第一作者, 共同通讯作者	A 类	华南农业大学材料与能源学院	SCI	IF2-year=6.3 IF5-year=6.0 (2024)	化学 2 区 Top 期刊: 否 (2025)

		文献号: 113258 文献类型: Article						
4	Fluorine-containing amphiphilic quaternary ammonium salts for the suppression of Banana fusarium wilt	REACTIVE & FUNCTIONAL POLYMERS 出版年: 2023 出版日期: JAN 卷期: 182 页码: - 文献号: 105488 文献类型: Article	第一作者, 共同通讯作者	B 类	华南农业大学 材料与能源学院	SCI	IF2-year=4.5 IF5-year=4.1 (2023)	工程技术 3 区 Top 期刊: 否 (2023)
5	Polymeric diallyl quaternary ammonium salts for inhibiting banana Fusarium wilt	REACTIVE & FUNCTIONAL POLYMERS 出版年: 2022 出版日期: MAR 卷期: 172 页码: - 文献号: 105174 文献类型: Article	第一作者, 共同通讯作者	B 类	华南农业大学 材料与能源学院	SCI	IF2-year=5.1 IF5-year=4.3 (2022)	工程技术 3 区 Top 期刊: 否 (2022)
6	Molecularly Imprinted Photonic Crystals Based on Fusaric Acid for the Detection of Banana Fusarium Wilt	ACS APPLIED POLYMER MATERIALS 出版年: 2021 出版日期: NOV 12 卷期: 3 11 页码: 5818-5825 文献类型: Article	第一作者, 共同通讯作者	B 类	华南农业大学 材料与能源学院	SCI	IF2-year=4.855 IF5-year=4.855 (2021)	化学 3 区 Top 期刊: 否 (2021)

7	The interactions between bovine serum albumin and carboxybetaine-functionalized polysiloxanes in solution	COLLOID AND POLYMER SCIENCE 出版年: 2016 出版日期: DEC 卷期: 294 12 页码: 2029-2037 文献类型: Article	第一作者, 共同通讯作者	B 类	华南农业大学材料与能源学院	SCI	IF2-year=1.723 IF5-year=1.749 (2016)	化学 3 区 Top 期刊: 否 (2016)
8	Synthesis and antimicrobial activities of polysiloxane-containing quaternary ammonium salts on bacteria and phytopathogenic fungi	REACTIVE & FUNCTIONAL POLYMERS 出版年: 2014 出版日期: DEC 卷期: 85 页码: 36-44 文献类型: Article	第一作者, 共同通讯作者	A 类	华南农业大学资源与环境学院	SCI	IF2-year=2.515 IF5-year=2.535 (2014)	工程技术 2 区 Top 期刊: 否 (2014)
9	多臂星形聚乙二醇-聚乳酸嵌段共聚物的降解特性	高分子材料科学与工程 出版年: 2013 卷期: 页码: - 文献号: 文献类型:	第一作者, 通讯作者	B 类	华南农业大学资源与环境学院	北大核心	无	无

说明: 论文等级和中科院大类分区按《华南农业大学学术论文评价方案(试行)》划分。

报告免责声明: 如未盖章, 报告无效



检索证明

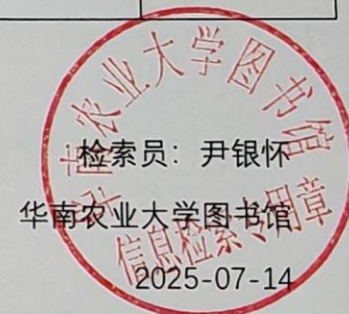
根据委托人提供的论文材料，委托人华南农业大学材料与能源学院 林雅铃 6 篇论文收录情况如下表。

序号	论文名称	发表刊物及发表的年月卷期/页码等	作者排名	论文等级	作者文中单位	收录情况	影响因子	中科院大类分区
1	Polyacrylamide quaternary ammonium salts based on stable adsorption in soil and its application on the control of soil-borne fungal disease	EUROPEAN POLYMER JOURNAL 出版年：2024 出版日期：JAN 5 卷期：202 页码：- 文献号：112604 文献类型：Article	共同通讯作者（倒数第一）	A 类	华南农业大学 材料与能源学院	SCI	IF2-year=6.3 IF5-year=6.0 (2024)	化学 2 区 Top 期刊：否 (2025)
2	Antifungal mechanisms of polymeric quaternary ammonium salts against conidia of Fusarium oxysporum f. sp. cubense, race 4	EUROPEAN JOURNAL OF PLANT PATHOLOGY 出版年：2023 出版日期：FEB 卷期：165 2 页码：317-331 文献类型：Article	通讯作者	B 类	华南农业大学 材料与能源学院	SCI	IF2-year=1.7 IF5-year=1.9 (2023)	农林科学 3 区 Top 期刊：否 (2023)
3	超声细胞粉碎法快速提取真菌中的麦角甾醇	南京农业大学学报 出版年：2021 卷期：44 6 页码：- 文献号： 文献类型：	通讯作者	B 类	华南农业大学 材料与能源学院	北大核心	无	无

4	Perspective Article Polydimethylsiloxane-polymethacrylate block copolymers containing quaternary ammonium salts against <i>Fusarium oxysporum</i> f. sp. <i>cubense</i> race 4 in soil: Antifungal activities and pot experiments	REACTIVE & FUNCTIONAL POLYMERS 出版年: 2021 出版日期: MAR 卷期: 160 页码: - 文献号: 104848 文献类型: Article	共同通讯 作者(倒数第一)	B 类	华南农业大学 材料与能源学院	SCI	IF2-year=4.966 IF5-year=4.266 (2021)	工程技术 3 区 Top 期刊: 否 (2021)
5	Anti-Rhizoctonia solani activity by polymeric quaternary ammonium salt and its mechanism of action	REACTIVE & FUNCTIONAL POLYMERS 出版年: 2018 出版日期: APR 卷期: 125 页码: 1-10 文献类型: Article	共同通讯 作者(倒数第一)	A 类	华南农业大学 材料与能源学院	SCI	IF2-year=3.074 IF5-year=3.076 (2018)	工程技术 2 区 Top 期刊: 否 (2018)
6	Polymeric quaternary ammonium salt activity against <i>Fusarium oxysporum</i> f. sp. <i>cubense</i> race 4: Synthesis, structure-activity relationship and mode of action	REACTIVE & FUNCTIONAL POLYMERS 出版年: 2017 出版日期: MAY 卷期: 114 页码: 13-22 文献类型: Article	通讯作者	A 类	华南农业大学 材料与能源学院	SCI	IF2-year=2.975 IF5-year=2.843 (2017)	工程技术 2 区 Top 期刊: 否 (2017)

说明: 论文等级和中科院大类分区按《华南农业大学学术论文评价方案(试行)》划分。

报告免责声明: 如未盖章, 报告无效





Synergistic enhancement of the robustness of multifunctional polyurethane via an ionic noncovalent cross-linking network and aromatic disulfides

Yaling Lin ^{a,*}, Ning Yu ^{b,1}, Shijie Shan ^b, Anqiang Zhang ^{b,*}

^a College of Materials and Energy, South China Agricultural University, 483 Wushan Rd., Guangzhou 510642, Guangdong, China

^b School of Materials Science and Engineering, South China University of Technology, 381 Wushan Rd., Guangzhou 510641, Guangdong, China

ARTICLE INFO

Keywords:

Ionic noncovalent cross-linking
Mechanical robustness
Self-healing
Recyclability
Multifunctionality

ABSTRACT

The preparation of functional polyurethane materials with high strength, toughness, and excellent self-healing ability is currently challenging. In this study, a multifunctional bi-dynamic supramolecular crosslinked network PU elastomer was successfully prepared by introducing ionic bonds and aromatic disulfide bonds into a PU matrix. The resulting ionic PU elastomers exhibited impressive mechanical properties, including high tensile strength (39.9 ± 4.4 MPa) and excellent elongation at break (1930 ± 345 %). They also demonstrated efficient self-healing capability (94.4 %), recyclability and processability. The distribution of hydrophilic ion bonds within the polymer networks enabled the elastomers to possess water-induced shape memory and antibacterial activity. Additionally, the hydrophilicity of the elastomers provided a self-cleaning ability when used as a coating material. The covalent bonding of the cations with the PU matrix prevented the leaching of bactericidal substances, ensuring good biocompatibility of the ionic PU. Furthermore, a double-layered self-healing composite flexible sensor was developed using the ionic PU as the substrate and carboxylated carbon nanotubes (CNTs-COOH) as the conductive medium to detect human motion. These multifunctional ionic PU elastomers offer great potential for the design and preparation of robust materials with self-healing ability for various applications across multiple fields.

1. Introduction

The development of society has increased the demand for versatile and progressive elastomer materials. PU elastomers have a wide range of raw materials and offer strong control over molecular structure. The unique 'microphase separation' structure of the molecular chain, consisting of soft and hard segments, provides excellent overall performance [1]. These elastomers have adjustable mechanical properties and can be easily produced [2]. They also possess shape memory [3], are non-toxic, highly transparent, and have found widespread applications in various technical fields such as biomedical [4], antifouling and antibacterial coatings [5], intelligent textiles [6], and flexible electronic devices [7–9]. However, due to the complexity and harshness of their usage environment, PU elastomers are susceptible to mechanical damage throughout their lifecycle. If such damage is not repaired promptly, it can lead to a rapid decline in performance and render them unusable. Therefore, integrating self-healing ability and recyclability into elastomers is considered a promising approach to enhance their lifespan,

reduce raw material consumption, and lower carbon emissions [10].

In recent years, researchers have focused on developing reversible dynamic covalent bonds, such as Diels-Alder crosslink bonds [11,12], imine bonds [13,14], acylhydrazone bonds [15,16], and intrinsic self-healing and recyclable elastomers with disulfide bonds [17–19]. Additionally, noncovalent interactions, including hydrogen bonds [20], metal coordinates [21], and ionic bonds [22,23], have also been explored. However, the mechanical strength of materials has often been overlooked in the pursuit of effective self-healing ability. Numerous studies have demonstrated the challenge of balancing the mechanical strength and self-healing properties [24–26]. To enhance the self-healing efficiency and mechanical strength of PU materials, researchers have proposed various strategies. Noncovalent bonds, such as supermolecular self-assembly bonds, offer advantages over covalent bonds due to their dynamic reversibility and physical cross-linking. These bonds can be destroyed and rebuilt, effectively dissipating energy and improving the flexibility, resilience, and self-healing performance of PU materials. Ureidopyrimidone (UPy) is a self-

* Corresponding authors.

E-mail addresses: linyin@scau.edu.cn (Y. Lin), aqzhang@scut.edu.cn (A. Zhang).

¹ These authors contribute equally.

complementary quaternary hydrogen bonding group that has the potential to enhance the mechanical strength and toughness of polymer networks. This is achieved by increasing the noncovalent cross-linking and sacrificial bonds. However, the synthesis of polyurethane or polyurea elastomers with UPy groups is complex and these materials have low solubility in common polar solvents. As a result, they are not suitable for large-scale production and preparation [27,28]. To address this limitation, researchers have proposed the incorporation of a dual dynamic mechanism into a single polymer system. This exciting concept aims to achieve synergistic effects between the two mechanisms, enhancing both self-healing and mechanical properties. Qin and colleagues [29] introduced diazoalkylurea (DU) and aromatic disulfide into the PU matrix to overcome the trade-off between mechanical robustness and room temperature self-healing. The strong hydrogen bonding cross-linking points improved the robustness of the cross-linking structure, while the rapid chemical decomposition of disulfide bonds contributed to the kinetics of the cross-linking network. The obtained PU elastomer had high tensile strength (14.08 MPa), high toughness (64.6 MJ/m³), and excellent self-healing ability (~81 % at room temperature). Sun et al. [21] investigated the combination of disulfide exchange and metal coordination interaction. The introduction of coordinate covalent bonds disrupted the hydrogen bond sequence, resulting in the destruction of the hard phase. This disruption was beneficial for disulfide exchange. The material exhibited a tensile strength of 9.4 ± 0.1 MPa and a self-healing efficiency of 96.6 ± 1.5 %. Wu et al. [30] synthesized a supramolecular elastomer with exceptional toughness (14.7 MJ/m³) and high tensile properties (1700 %) by incorporating strong metal coordinate covalent bonds and weak tetrahydrogen bonds into the molecule. However, the mechanical strength was only 2.6 MPa. Despite significant advancements in the development of high-strength, high-toughness self-healing materials in recent years, there are still numerous challenges in achieving simultaneous high strength, high toughness, and self-healing capabilities in polymer materials.

Ionic bonds, with their strong noncovalent bond interaction (50–250 kJ/mol), play a crucial role in enhancing energy dissipation through bond fracture, thereby toughening materials. However, there have been limited studies on how to enhance PU through interchain ionic bonds. In this study, we present a novel approach that involves the introduction of dynamic disulfide bonds, which contain rigid benzene ring structures, and ionic chain extenders into prepolymers. This leads to the formation of PU ionomers, enabling the development of room temperature self-healing and recyclable PU elastomers with exceptional mechanical strength. In this study, it was observed that ionic interactions displayed a higher interaction strength compared to the relatively weaker π - π stacking interactions and hydrogen bonds. The presence of ionic groups in the polymer matrix resulted in the formation of clusters, which in turn enhanced the physical crosslinking by dispersing within the soft polyester network domain [31]. The dithio diphenylamine, with its rigid structure consisting of two benzene rings, exhibited excellent double decomposition ability [32,33]. The PU elastomer obtained in this study demonstrated several desirable properties, including high tensile strength, toughness, self-healing ability, water-induced shape memory, antibacterial and antifouling properties, and other multifunctional properties. These properties were achieved through a combination of hydrogen bonds, ion interactions, and the dynamic disulfide effect, which induced the formation of soft and hard microphase separation structures in the network. Moreover, the PU elastomers showed good recyclability due to their reversible cross-linking structure, making them suitable for multiple cycles of use. Additionally, the potential application of ionic PU in wearable flexible electronic products was demonstrated by coating a layer of conductive CNT-COOH on the surface of the prepared flexible ionic PU matrix.

2. Experimental section

2.1. Materials

Polytetramethylene ether glycol (PTMG, $M_n = 2000$), isophorone diisocyanate (IPDI, 99 %), ditin butyl dilaurate (DBTDL, 95 %), 3-dimethylaminopropane-1,2-diol (DP, 98 %), 4,4'-thiodianiline (AFD, 98 %), *n*-butyl bromide (99.0 %), castor-oil and carboxylated multiwalled carbon nanotubes (CNTs-COOH, 95 % purity, length: 10–30 μ m, -COOH: ~3.9 wt%) were purchased from Shanghai Macklin Inc. *Escherichia coli* (*E. coli*), *Staphylococcus albus* (*S. albus*) and human fibroblast cells were provided by South China Agricultural University. Fluorescein isothiocyanate-labelled bovine serum albumin (FITC-BSA) was obtained from Solarbio Science & Technology Co., Ltd. (Beijing, China). Dulbecco's modified Eagle's medium (DMEM) and fetal bovine serum (FBS) were purchased from Hyclone (Thermo Fisher, USA). All chemicals were used without further purification.

2.2. Synthesis of QDP

DP (4.77 g, 40 mmol) and *n*-butyl bromide (8.22 g, 60 mmol) were dissolved in isopropanol (~50 mL) and added into a 100 mL three-neck round-bottom flask equipped with magnetic stirring and condensation reflux. The system was heated to 75 °C and stirred for 24 h in a N₂ atmosphere. Appropriate amounts of water and chloroform were added to the product for extraction, and the extraction was repeated to obtain the aqueous phase three times to fully extract the final product. The aqueous phase was evaporated to remove water, resulting in a transparent and colorless liquid. The sample was dried in a 60 °C oven for 12 h and had a yield of approximately 90 %. For convenience, this product was named QDP.

2.3. Synthesis of PU-QDPx-SS

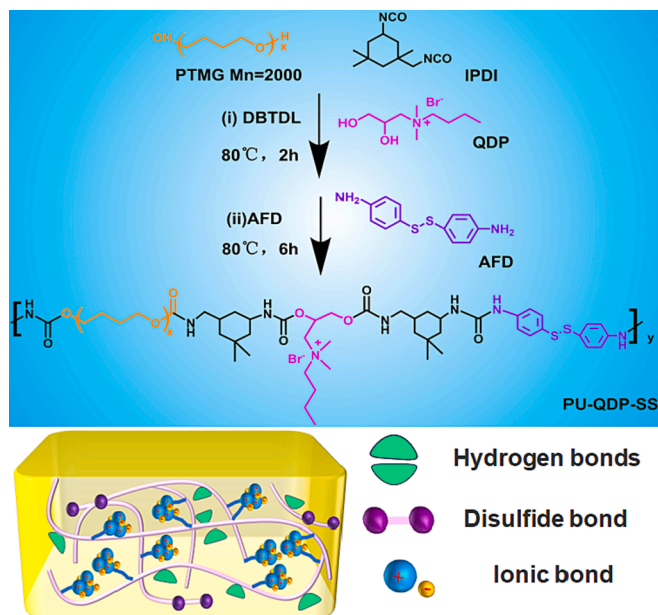
QDP was added dropwise to a mixture of IPDI and DBTDL in anhydrous N, N-dimethylformamide (DMF) (50 mL) at 80 °C for 2 h under stirring with the protection of a nitrogen atmosphere, and then AFD was added for another 6 h of reaction. The resultant mixture was poured into a mold and then maintained at 60 °C for 24 h. The obtained ionic PU were named PU-QDP_x-SS ($x = 3/1$ or $2/2$). The amount of each reactant is listed in Table S1. PU-DP_x-SS ($x = 3/1$ or $2/2$), PU-DP, PU-QDP and PU-SS were synthesized similarly. Their synthetic routes are shown in Scheme 1, Schemes S1 and S2.

2.4. Electrospinning of EPU-QDP_{3/1}-SS

A 10 mL medical syringe was used to draw 10-mL of a THF/DMF (1/1, v/v) PU-QDP_{3/1}-SS solution with a concentration of 10 % (w/w). The syringe was connected to the 19 # flat mouth spinneret, the positive and negative electrodes of the high-voltage power supply were connected to the positions of the nozzle and the receiving device, and the solution propulsion flow rate was controlled through a micro-injection pump. The extrusion rate was 3 mL/h. The positive voltage of spinning was 15 kV, the distance between the receiver and the spinneret was adjusted to 12 cm, and the electrospinning process lasted for 1 h at room temperature. After the spinning was completed, the collected nanofiber film was placed in a vacuum drying oven at 30 °C for 48 h and repeatedly weighed until the fiber film was at constant weight. Record the fiber membrane obtained by electrospinning as EPU-QDP_{3/1}-SS.

2.5. Fabrication of the self-healable electrode film

First, 10 mg of CNTs was added to 20 mL of ethanol and sonicated for 10 min to obtain a uniform dispersion. Second, the obtained CNT dispersion (1 g) was sprayed onto the surface of EPU-QDP_{3/1}-SS (40 mm \times 60 mm) using an air compressor equipped with a spray gun (DUN-30



Scheme 1. Schematic diagram of the preparation process of PU-QDP-SS.

L, Anjieshun, China) at a pressure of 0.5 MPa and a distance of 20 cm. The sample was placed in a 60 °C vacuum oven and cured for 24 h to remove residual solvents. The mold was peeled off to obtain a carbon nanotube ionic PU composite film, denoted as EPU-CNT.

2.6. Characterizations

The NMR spectra were obtained from a Bruker AVANCE III HD 600 using methanol- d_4 as the solvent. The FTIR spectra of the samples were acquired with a Thermo Nicolet iS5 spectrometer (Thermo Scientific, USA) with a ZnSe ATR accessory. The TGA curves were measured on a Netzsch TG 209 F1. The samples (~10 mg) were heated from 30 °C to 900 °C at a rate of 20 °C/min in a N_2 atmosphere. XRD measurements (D8 Advance, Bruker, Germany) were taken to determine the phase structure and composition of the ionic PU, with a 2 θ scanning range of 5–60°. Stress–strain curves were measured on a KJ-1067 tensile test machine with a controlled temperature and humidity chamber (Dongguan Kejian Instrument Co. Ltd., China). The measurements were carried out at room temperature at a stretching speed of 100 mm/min. At least three specimens were tested for each elastomer sample, and the average values with standard errors were calculated. For cyclic tensile tests, both loading and unloading processes were carried out at a strain rate of 100 mm min^{−1} at room temperature. The dissipated energy was evaluated from the closed area between the loading–unloading curves. The toughness was acquired by integrating the area under the stress–strain curves. DMA (dynamic mechanical thermal spectrometer) (Mettler Toledo Star 1 system) from Mettler Toledo was used to evaluate the dynamic properties. The measurements were carried out in a temperature range of −100 °C to 50 °C with a heating rate of 5 °C/min at a frequency of 1 Hz. Rheological sweeping curves were measured with an Anton Paar MCR 102 rheometer (Austria) equipped with a stainless-steel parallel-plate geometry (diameter: 25 mm). For temperature sweeping tests, a constant frequency of 1 Hz and 1 % strain were applied, and the temperature was increased from 20 °C to 160 °C at a heating speed of 2 °C/min. The stress relaxation behavior was tested in parallel plate mode on an Anton Paar MCR-102 rheometer; a circular specimen with a diameter of 35 mm and a thickness of 1 mm was initially equilibrated at the set temperature for 10 min, and then a strain of 1.5 % was applied to the sample. The relaxation modulus changes over time were recorded at a constant temperature. X-ray photoelectron spectroscopy (XPS) of samples was recorded by a Thermo Fisher Scientific ESCALAB 250xi.

The energy scanning range was 0–1300 eV, the step size was 1 eV, and analysis was performed using the Advantage software system. The films were tested using a Raman spectroscopy (HJY LabRAM Aramis) with a laser wavelength of 785 nm and silicon wafer calibration. The micro-phase separation structure of polyurethane was observed with a Bruker NT-MDT Prima atomic force microscope (AFM). Transmission electron microscopy (TEM) characterization were carried out on JEM 2100F (JEOL) electron microscope. Ultrathin sections about 200 nm in thickness of the samples were cut by an ultramicrotome Leica EMUC6 under liquid nitrogen atmosphere. Scanning electron microscopy (SEM) of the morphology of the film was carried out using ZEISS EVO 18 Special Edition (Merlin, Carl Zeiss Jena, Germany) at 1000× magnification. The surface morphology of ionic PU after immersion was examined using a three-dimensional optical profilometer (UP Dual Model, RTEC, USA). The sample film was vacuum-dried at room temperature for 24 h and placed on the platform of a contact angle measuring instrument (DSA25, Krüss Company, Germany). Deionized water was added dropwise onto the film surface using a microsyringe. The shape of the droplet was recorded using a camera and analyzed using software to obtain the contact angle. The test was repeated at least three times for each sample.

2.7. Antifouling assay

After UV sterilization, all samples were cultured with FITC-BSA solution (0.05 mg/mL) in the dark at 37 °C for 2 h. Afterward, the samples were gently rinsed with PBS to remove unadhered proteins. Finally, the adhesion of proteins on the surface were observed by fluorescent inverted microscope (Olympus IX73). To further clarify the adhesion level of FITC-BSA, ImageJ software was used to evaluate the relative fluorescence intensity (RFI) results (setting the RFI of PU-SS to 100 %).

2.8. Antimicrobial activities

The antibacterial performance of ionic PU was measured using the plate counting method [34]. The experimental bacteria were *S. albus* and *E. coli*. The bacteria were inoculated in lysogeny broth and incubated overnight under shaking at 37 °C and 150 rpm to reach the growth index stage. The number of live bacteria in this bacterial solution should be $(1 \sim 5) \times 10^5$ CFU/mL. A bacterial suspension (100 μ L) was dripped onto the sample surface and then covered with the sterile polyethylene film (2 x 2 cm²) to make the bacterial suspension evenly spread across the surface. After incubation at 37 °C for 24 h, all samples were washed with 5 mL of sterilized PBS, and then the number of CFUs was counted. Each colony determination test was repeated independently more than 3 times. For comparison, polyethylene film was used as the control group.

2.9. Cytotoxicity evaluation

To evaluate the cytotoxicity of PU-QDP_{3/1}-SS elastomers on human fibroblasts through MTT experiments [35], human dermal fibroblasts (3×10^5) in 1 mL of DMEM supplemented with 10 % fetal bovine serum were cultured in a 24-well plate for 72 h. The membrane was cut into 10 x 10 mm² squares and sterilized under a UV lamp for 30 min, and the sample was immersed in 30 mL of PBS at pH 7.4 for 24 h to obtain the leachate. Then, 20 μ L leachate was added and cultured at 37 °C for 12, 24 and 48 h, respectively; 20 μ L PBS with pH 7.4 was added in the control group. Next, 100 μ L of the MTT solution (5 g/L PBS) was added to each well. After being placed at 37 °C for 4 h, 100 μ L dimethyl sulfoxide (DMSO) was added to each well, and the optical density (OD) value at 490 nm was measured with a microplate reader (Spectra Max M5, Molecular Devices, USA). All measurements were repeated three times.

2.10. Sensing performance

The EPU-CNT film with a size of 10 mm x 30 mm x 0.5 mm was

attached onto the finger or wrist of a volunteer. Copper tapes at both ends of the film were used to connect the film with output metallic wires, and commercial tapes were used to firmly fix the film with the finger/wrist. As a result, the real-time electrical signal changes of this film during stretching were recorded through the digital source table.

3. Results and discussion

3.1. Structural characterization of ionic PU and thermodynamic properties

Fig. S1 presents the ^1H NMR spectra of DP and QDP following the quaternary ammonium reaction. The triplet peak at 2.50 ppm and the quartet peak at 2.19 ppm were assigned to the methylene protons directly attached to the nitrogen atom. After reacting DP with n-butyl

bromide, the resonating protons for these methylene protons were observed at 3.44 ppm due to increased electronegativity. The signals corresponding to the methyl and methylene protons of the butyl groups appeared in the range of 0.97–1.79 ppm. These results indicate the successful transformation of QDP into a quaternary ammonium compound. The structure of the ionic PU was analyzed using FTIR spectroscopy, as shown in Fig. 1a. Strong peaks were observed in the range of 1750 cm^{-1} and 1600 cm^{-1} . Specifically, the peaks at 1718 cm^{-1} and 1633 cm^{-1} were assigned to the carbonyl tensile vibration peaks of nonhydrogen bond and disordered hydrogen bond carbamate bonds, respectively. Additionally, the peaks at 1692 cm^{-1} and 1652 cm^{-1} were attributed to the ordered and disordered hydrogen bond urea bond carbonyl tensile vibration peaks (gray area), respectively [21,28]. Notably, no-NCO stretching vibration peak was observed near 2230 cm^{-1} (Fig. S2), indicating the complete depletion of the highly active

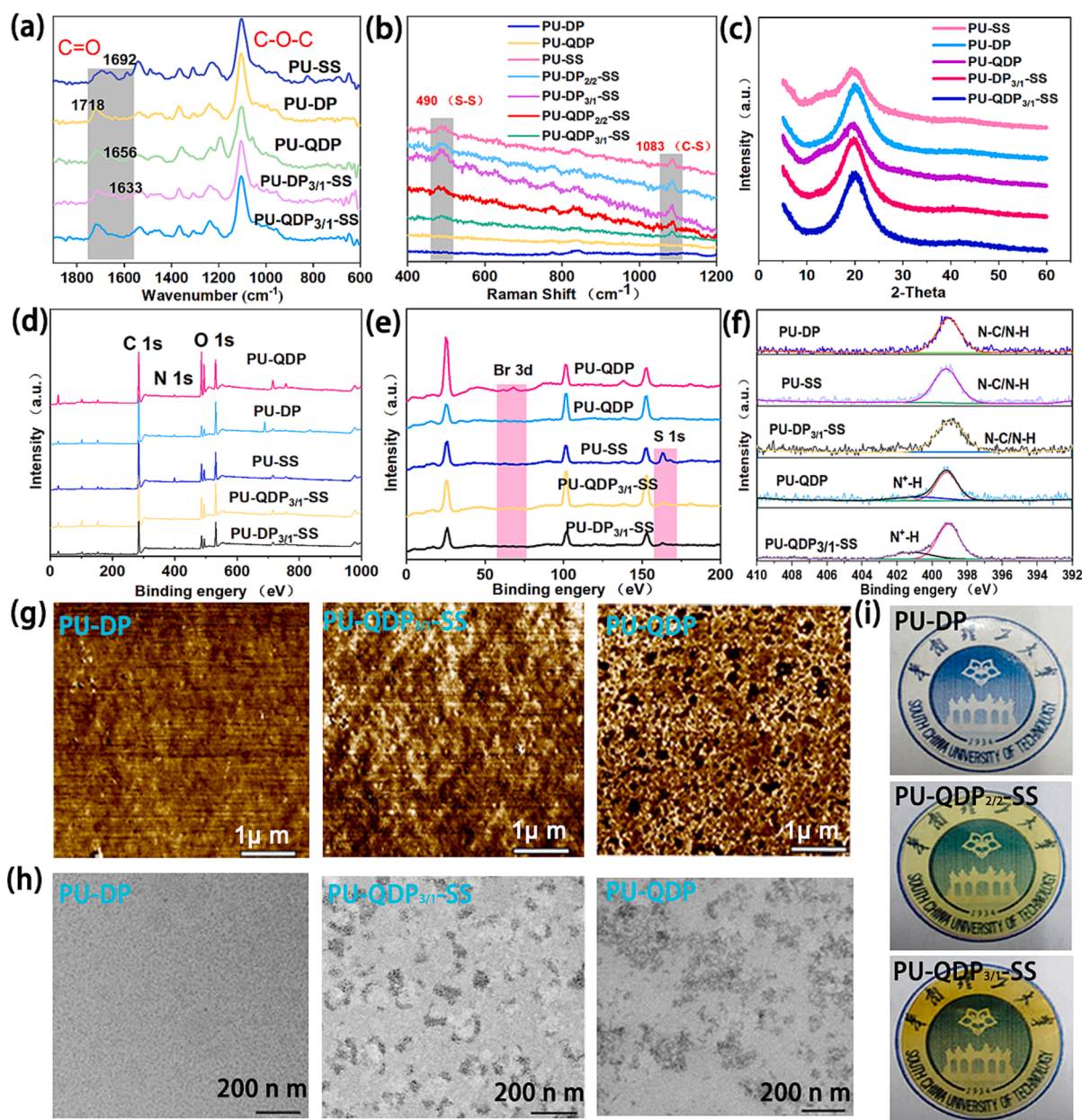


Fig. 1. (a) FTIR spectra of the ionic noncovalent interaction-enhanced PU with dynamic aromatic disulfides. (b) Raman spectra of the PU samples. (c) XRD curves of the PU-DP, PU-QDP, PU-SS, PU-DP_{3/1}-SS and PU-QDP_{3/1}-SS samples. (d) (e) XPS wide-scan spectra of PU-DP, PU-QDP, PU-SS, PU-DP_{3/1}-SS and PU-QDP_{3/1}-SS samples. (f) XPS N1s signals of the PU samples. (g) AFM 2D analysis of the PU samples. (h) TEM images of PU samples. (i) Digital optical images of the PU-DP, PU-DP_{2/2}-SS and PU-QDP_{3/1}-SS samples.

isocyanate bond.

Based on the Raman spectrum in Fig. 1b, the absorption peak of the S-S bond in PU-SS, PU-DP_{3/1}-SS and PU-QDP_{3/1}-SS was observed at 490 cm⁻¹, and the characteristic peak at 1083 cm⁻¹ was C-S. However, the PU-DP and PU-QDP samples did not show any evident characteristic peak at 490 cm⁻¹ and 1083 cm⁻¹, indicating the successful introduction of disulfide bonds in the polymers. The XPS spectrum of ionic PU, shown in Fig. 1d and e, revealed that all PU samples were mainly composed of C, N, and O elements, with corresponding binding energies appearing at 284, 400, and 532 eV, respectively. In comparison, the signals for Br3d (~68 eV) were observed in PU-QDP_{3/1}-SS and PU-QDP, while S1s (~163 eV) appeared in PU-SS, PU-QDP_{3/1}-SS, and PU-DP_{3/1}-SS. In Fig. 1f, the N1s peak of PU-QDP and PU-QDP_{3/1}-SS, which contained quaternary ammonium ionic groups consisted of two components: N⁺-C (~402 eV) and N-C/N-H (~399 eV). However, the N1s peak of PU-DP, PU-SS and PU-DP_{3/1}-SS without quaternization only had N-C/N-H (~399 eV). After quaternization, the electron cloud density of N decreased, causing its binding energy to increase [36]. Therefore, based on the above analysis, ionic PU was successfully synthesized. The microphase separation, a structural characteristic of polyurethane, is influenced by various factors and affects its performance. Atomic force microscopy (AFM) was used to examine the microphase separation morphology of ionic PU. Fig. 1g shows the presence of discontinuous areas where bright (hard segments) and dark regions (soft segments) are

observed, indicating the microphase separation of the soft and hard segments of PU. The microphase separation in ionic PU is more pronounced compared to PU-DP due to the formation of ion clusters and aggregation of hard segments [37,38]. TEM was employed to further investigate the microstructure of the ionic PU. Fig. 1h clearly shows the presence of hard domains in the microphase separation of the membrane. These dark regions are nanoclusters, while the bright regions correspond to the soft segments where PTMG is located. In contrast, PU-DP did not exhibit significant differences in brightness. The presence of ion clusters promotes the formation of microphase separation, consistent with the AFM results. The XRD pattern in Fig. 1c indicates a macroscopic homogeneous amorphous structure in ionic PU, resulting in excellent transparency (Fig. 1i).

The storage modulus and loss factor (tan δ) of various materials were measured using DMA within different temperature ranges. In Fig. 2a, the addition of ionic bonds increased the storage modulus of ionic PU. This could be attributed to the enhanced interaction between chain segments due to the presence of ionic bonds, which limited their mobility and flexibility. For polytetrahydrofuran, the T_g of all samples was concentrated within the range of -69 °C to -65 °C. When the temperature exceeded T_g, a significant decrease in the storage modulus was observed, indicating the condition for shape memory [39]. Fig. 2b and c depict the TGA curves of the ionic PU under a N₂ atmosphere. The starting decomposition temperatures (T_{Start}) of the PU-DP, PU-QDP and

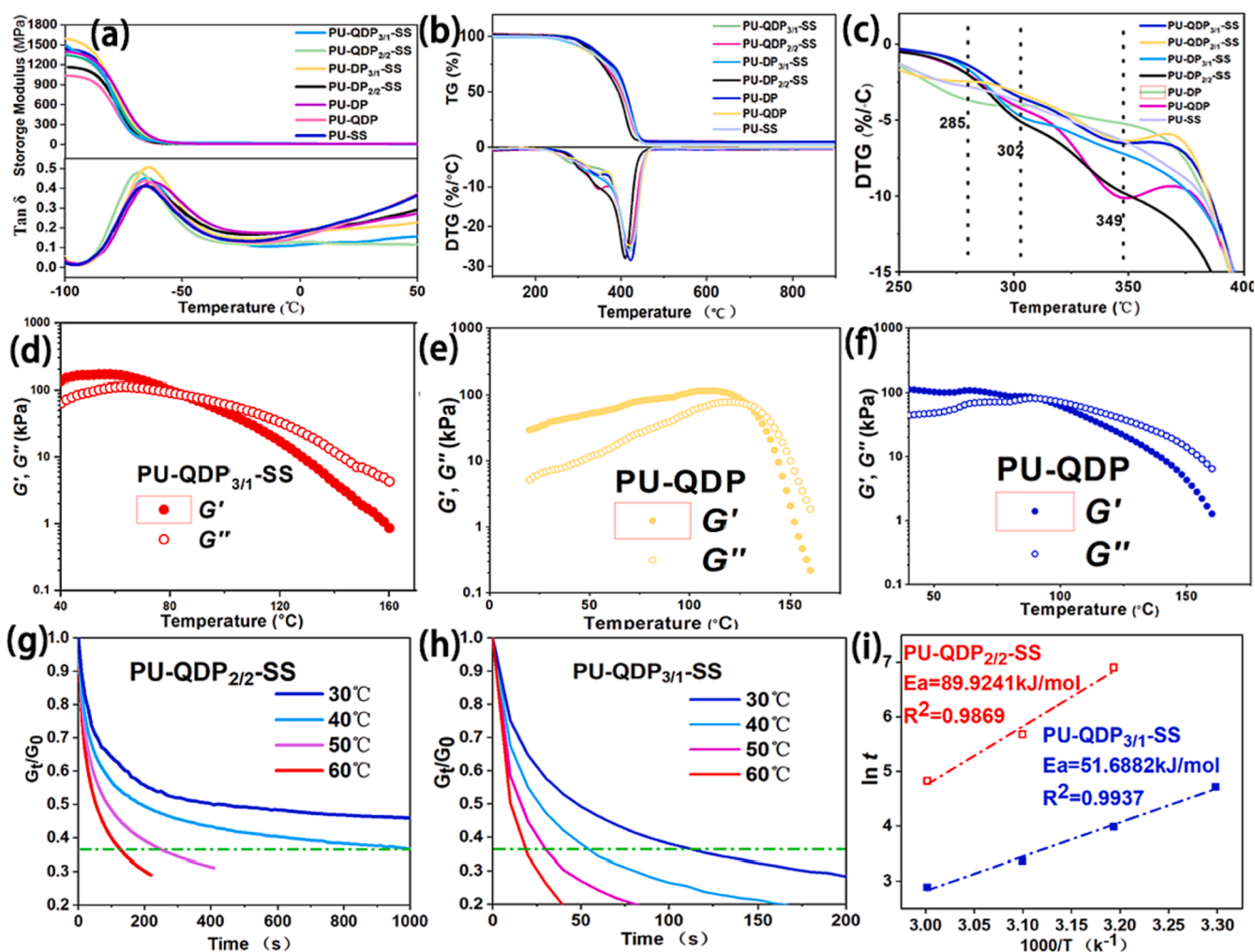


Fig. 2. (a) Overlaid plots of the storage modulus and tan δ against temperature of ionic PU from the DMA tests. (b-c) TGA curves of ionic PU. (d-f) Storage modulus (G') and loss modulus (G'') against temperature of PU-QDP_{3/1}-SS, PU-QDP and PU-SS from the temperature sweeping tests of rheology analysis. (g-h) Normalized stress relaxation experiments of the PU-QDP_{2/2}-SS and PU-QDP_{3/1}-SS under different conditions. (i) Linear fitting of relaxation time at different temperatures according to the Arrhenius law.

PU-SS samples were 392.4 °C, 399.1 °C and 373.6 °C, respectively. These differences can be attributed to the heat resistance of the quaternary ammonium groups in the polyurethane formulation (Table S2). As the degree of [DP]/[AFD] (or [QDP]/[AFD]) increased from 2/2 to 3/1, the T_{start} values of PU-QDP_x-SS were higher than those of the corresponding PU-DP_x-SS. The introduction of quaternary ammonium led to improved thermal stabilities of the PU.

The viscous flow transition temperature of PU-SS was approximately 142 °C, as shown in Fig. 2d–f. However, for ionized PU-QDP, the viscous flow transition temperature occurred at a lower temperature due to the physical cross-linking effects produced by ion interactions. When the system contained both aromatic disulfide and ion bonds, the viscous flow transition temperature reached 92 °C, potentially due to the synergistic effect of the two dynamic bonds. From Fig. 2g and h, it can be observed that a lower temperature correlated with a larger friction within the molecular chain and a more difficult stress relaxation. According to the Maxwell model of viscoelastic fluids, the relaxation time is defined as the time corresponding to the decay of the modulus to the original value of 37 % (1/e) [40]. As shown in Fig. 2g and h and Fig. S3 show the relaxation times of PU-QDP_{3/1}-SS, PU-DP_{3/1}-SS, PU-QDP_{2/2}-SS and PU-DP_{2/2}-SS at 50 °C, which are 32 s, 51 s, 228 s and 312 s, respectively. The relaxation time decreased with increasing ion content. The relationship between the characteristic relaxation time (s) and

temperature followed the Arrhenius formula. Fig. 2i and Fig. S4, display the activation energies E_a of PU-QDP_{3/1}-SS, PU-QDP_{2/2}-SS, PU-DP_{3/1}-SS and PU-DP_{2/2}-SS calculated from the slope, which were 51.6, 89.9, 24.9 and 69.9 kJ/mol, respectively. A lower activation energy provided a greater topological rearrangement and resulted in good healing performance due to rapid exchange reactions.

3.2. Mechanical properties and self-healing behaviors

By introducing ionic bonds and aromatic disulfide bonds, a dynamic double cross-linked structure was formed in PU-QDP-SS, resulting in significant improvement in its mechanical properties. Fig. 3(a–c) illustrates that ionic PU exhibited higher tensile strength, elongation at break, and toughness compared to nonionized PU. Among the variants, PU-QDP_{3/1}-SS demonstrated the highest elongation at break (1930 %), tensile strength (39.9 MPa), and toughness (288.0 MPa). In an ionized PU network, anions and cations interacted directionally within a specific range, forming ion clusters of a certain scale. The strong polarity of ion bonds facilitated the formation of microphase separation structures in non-polar soft phases, while the physical crosslinking effect of hard aggregates enhanced both tensile strength and stretchability. Additionally, the incorporation of a small amount of rigid disulfide structure increased spatial hindrance and further restricted the segmental

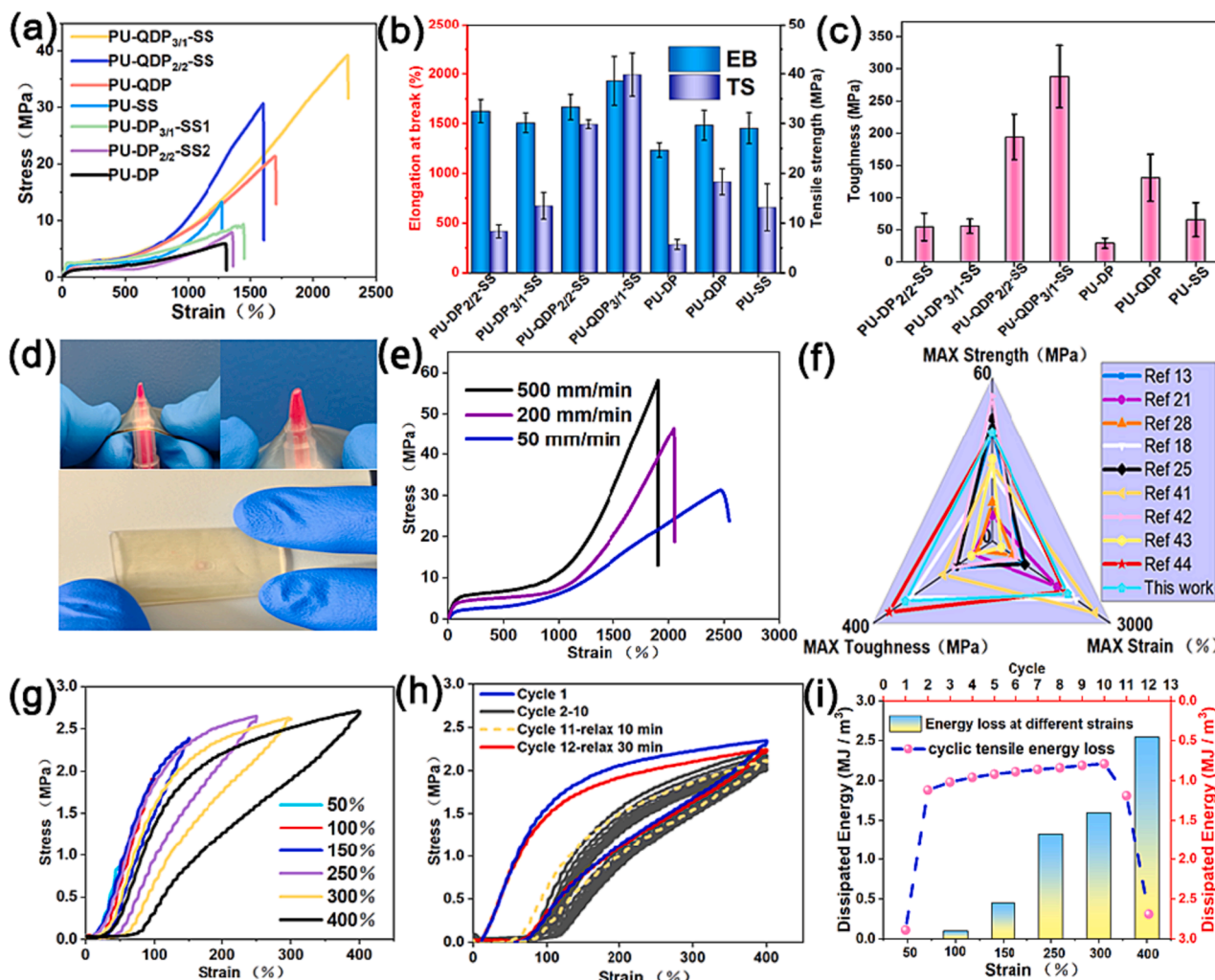


Fig. 3. (a) Typical stress-strain curves of ionic PU. (b) Tensile strength and breaking elongation. (c) Toughness. (d) Photographic images of PU-QDP_{3/1}-SS puncture resistance. (e) Tensile stress-strain curves of PU-QDP_{3/1}-SS specimens under different deformation rates. (f) Comparison of tensile strength, elongation at break, and toughness of PU-QDP_{3/1}-SS with data from other literature. (g) Successive cyclic tensile behavior of PU-QDP_{3/1}-SS at different strains. (h) Consecutive cyclic tensile curves of PU-QDP_{3/1}-SS at a strain of 400%. (i) Cyclic tensile energy loss value.

movement of PU. This resulted in a more regular chain arrangement, thereby enhancing the robustness of hard segments in the PU matrix. In contrast, nonionized PU solely relied on polymer chain entanglement and intermolecular hydrogen bonds between urethane and urea groups, leading to insufficient mechanical strength due to the absence of hard domains. A sample from the PU-QDP_{3/1}-SS series demonstrated excellent mechanical robustness, successfully resisting puncture from a writing pen (Fig. 3d). The stress-strain behaviors of PU varied depending on the frequency of stress transfer. When subjected to low stretching speeds, PU molecular chains were able to unfold more easily, thereby improving its stretchability. However, at high stretching rates, the molecular chains of PU were unable to fully stretch within a short period of time, resulting in chain aggregation and a significant increase in modulus and tensile strength (Fig. 3e). Among several self-healing PU

reported in [9,13,18,21,25,28,41–43], the tensile strength and toughness values of ionic PU were particularly noteworthy (Fig. 3f).

Cyclic tensile tests were performed to investigate the deformation recovery and recoverable energy dissipation capability. Fig. 3g illustrates the single cyclic stress-strain curves of PU-QDP_{3/1}-SS at various strains (50 %, 100 %, 150 %, 250 %, 300 %, and 400 %) during the successive tensile process. It is evident that the hysteresis loop becomes more pronounced with increasing tensile strain. Furthermore, Fig. 3i provides quantification results for the lag region. The energy dissipated by the material increases from 0.01 to 2.54 MJ/m³ as the deformation (elongation) rises from 100 to 400 %. This indicates that PU-QDP_{3/1}-SS effectively dissipates strain energy resulting from the breaking of ionic bonds, S-S bonds, and H-bonds during stretching-retraction cycles at different strains. During the cyclic stretching process with a fixed strain

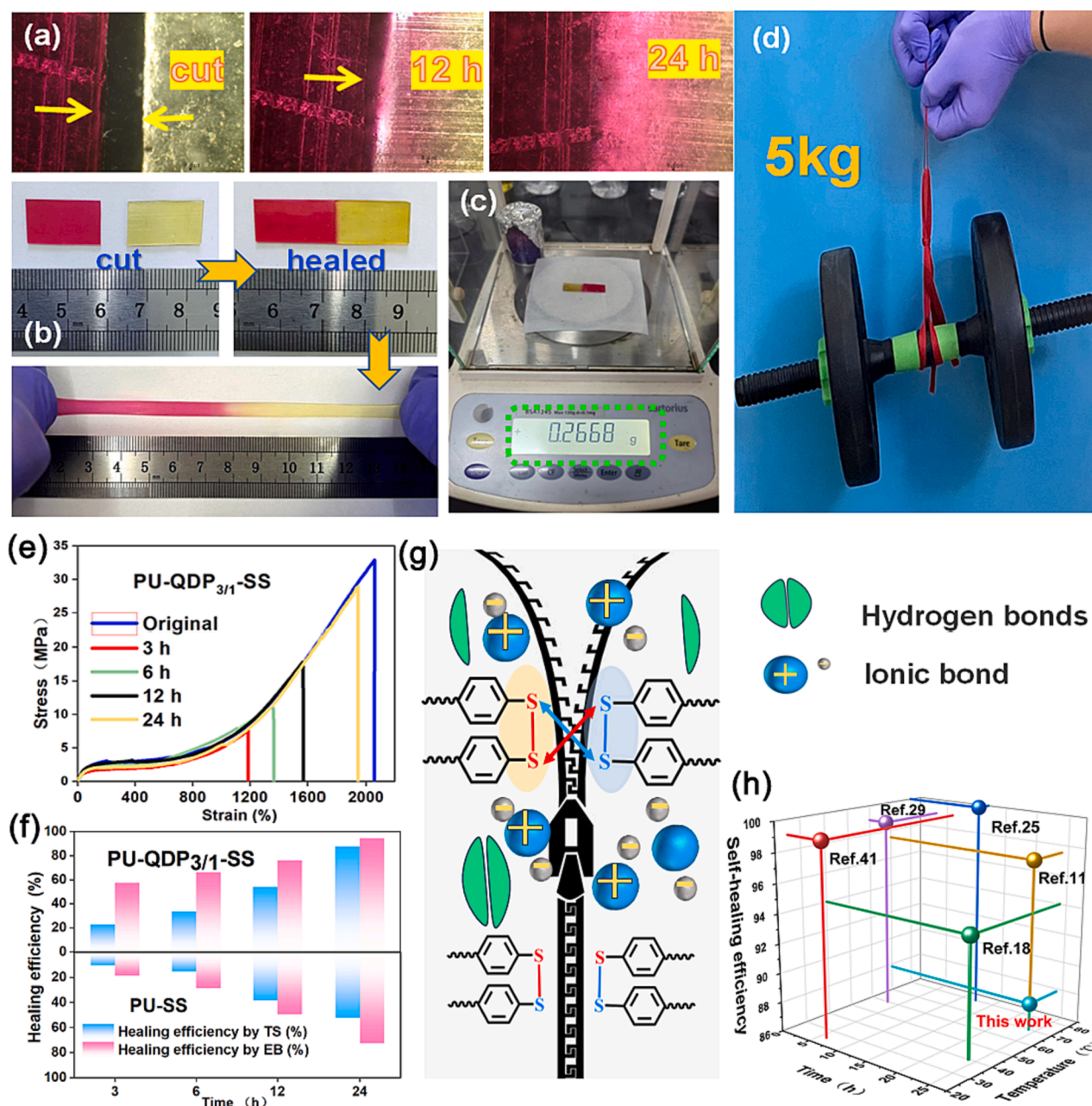


Fig. 4. (a) Digital images of the fracture-healing process of PU-QDP_{3/1}-SS under an optical microscope. (b) Healed PU-QDP_{3/1}-SS sample stretched to ~500 %. (c) Weighing the mass of PU-QDP_{3/1}-SS with an electronic balance. (d) Photograph of the PU-QDP_{3/1}-SS lifting a 5 kg dumbbell. (e) Stress-strain curves of the self-healing PU-QDP_{3/1}-SS under different healing times. (f) Healing efficiency of PU-QDP_{3/1}-SS and PU-SS under different repair conditions. (g) Self-healing mechanism. (h) Comparison of the self-healing efficiency, temperature and time of PU-QDP_{3/1}-SS with other literature data.

of 400 %, the energy dissipated in the 1st cycle was 2.89 MJ/m³, which was four times higher than the dissipated energy in the 10th cycle (0.68 MJ/m³). This difference can be attributed to the partially unrecovered dissociated dynamic bonds from the first cycle (Fig. 3h and i). After a resting time of 30 min (Fig. 3h), the hysteresis loop of the PU-QDP_{3/1}-SS almost returned to its original state, and the energy dissipated also reached 94 % of the initial situation, demonstrating excellent elastic restorability. This time-dependent self-recovery property primarily relies on the reversible dissociation/reassociation of relatively weak H-bonds, ion clusters, and S-S bonds in the dynamic hard domains.

To express the self-repairing behavior of our prepared samples more intuitively, a pristine and a methyl red dyed PU film were respectively cut into two pieces and then placed directly at 70 °C for a period of time without any external force. After 24 h, the incision on the surface was almost completely repaired (Fig. 4a). The healed sample exhibited a certain level of tensile strength and elongation, capable of stretching up to 5 times its own length (~2.5 cm) (Fig. 4b). Furthermore, a sample weighing 0.2688 g could withstand a weight of 5 kg of dumbbells without sustaining any damage (Fig. 4d). Additionally, its load-bearing capacity was found to be 18,600 times its own weight (Fig. 4c).

The self-healing efficiency refers to the percentage of recovery to the original sample. After being subjected to a temperature of 70 °C for 24 h, the tensile strength and tensile rate of the sample showed a self-healing efficiency of 87.8 % and 94.4 % respectively, as depicted in Fig. 4e and f. This indicates that PU-QDP_{3/1}-SS possesses a good self-healing ability. Additionally, Fig. S5 demonstrates that reducing the temperature significantly decreases the healing efficiency. For instance, when the healing time was 24 h at 50 °C, the self-healing efficiency of the sample was equivalent to that achieved by heating to 70 °C for 12 h. Furthermore, the self-healing efficiency of PU-QDP_{3/1}-SS is substantially higher than that of PU-SS, as shown in Fig. 4f. Fig. 4g provides a schematic diagram illustrating the self-healing process of PU-QDP_{3/1}-SS samples. The self-healing ionic PU sample primarily consists of ordinary

hydrogen bonds, ion interactions, and aromatic disulfide bonds within the main chain. When exposed to a temperature of 70 °C, the small-sized anions and cations on the polymer chain are attracted to each other, leading to diffusion at the interface. This local diffusion enhances the overall segmental motion of the polymer chains. The rapid diffusion of small-sized anions promotes the double decomposition reaction of disulfide bonds, which is crucial for crack healing. However, the presence of a single aromatic disulfide bond in PU-SS, which is locked in the hard domain, affects the self-healing efficiency due to the tightly arranged hard segments. Therefore, the self-healing performance of PU-QDP_{3/1}-SS is a result of the combined action of ionic bonds and disulfide bonds. In comparison to experimental data in the literature, the self-healing efficiency of ion elastomers was not particularly remarkable (Fig. 4h). This can be attributed to the strong ion interactions and the structure of the biphenyl ring, which hindered chain segment motion.

3.3. Shape memory properties

The storage modulus of the PU-QDP_{3/1}-SS sample showed a significant dependence on temperature. By disrupting the dynamic ionic and disulfide bonds, the sample could rearrange its network topology, leading to shape memory behavior under appropriate programming. Fig. 5a provides a visual representation of the strong correlation between shape memory behavior and temperature. It is evident that a flat sample can be gradually transformed into a cubic shape by heating it to 90 °C and then cooling it to room temperature. The stretching chain's limited relaxation allows for the maintenance of macroscopic deformation at room temperature [2]. When subjected to additional heating and cooling cycles, each deformed part of the sample exhibited simultaneous recovery to its initial state (Fig. 5a). However, the lack of control mechanisms for thermally induced shape memory processes has significantly impeded their widespread application on a large scale. The distinguishing feature of water-induced shape memory is the precise

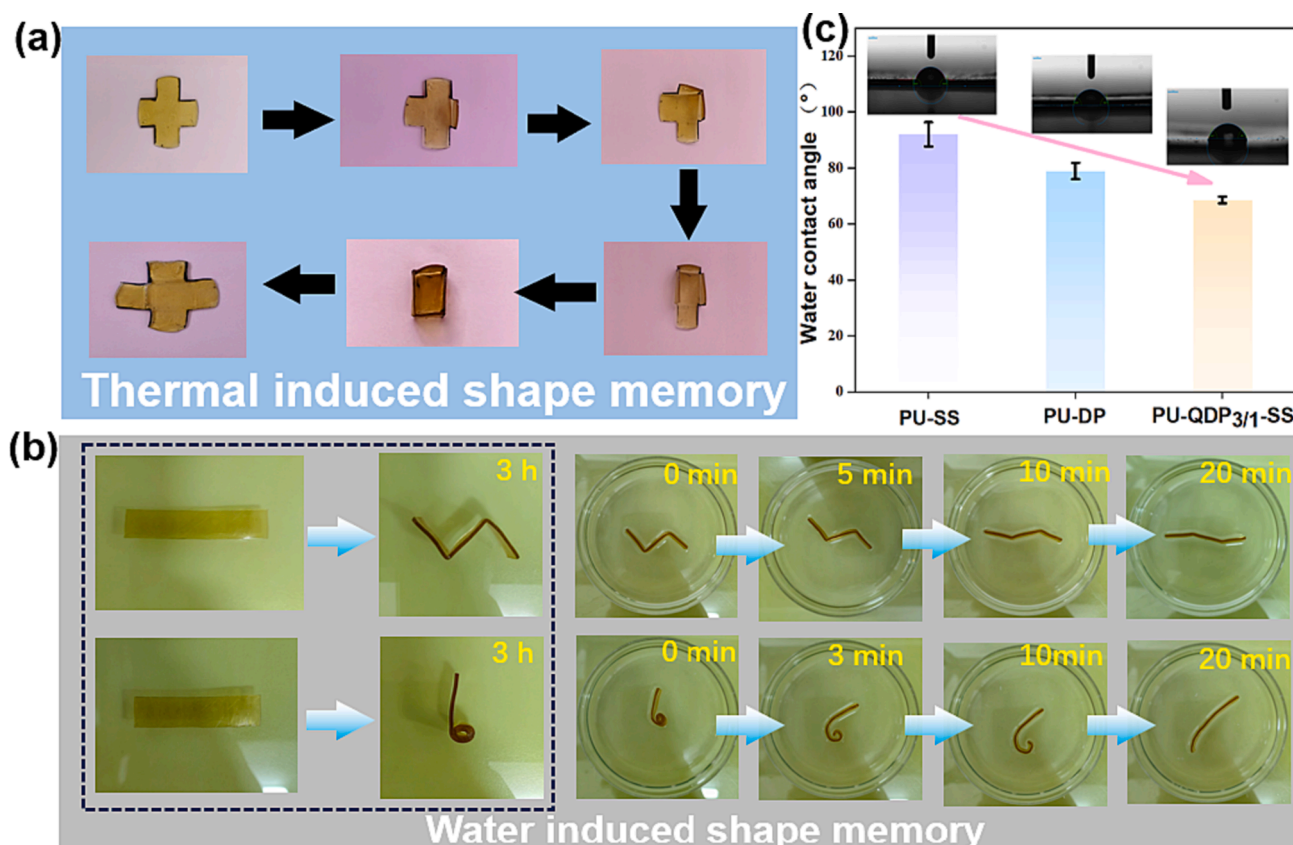


Fig. 5. (a) and (b) Photographs showing the shape memory behavior of PU-QDP_{3/1}-SS in heat and water. (c) Water contact angle of PU-SS, PU-DP and PU-QDP_{3/1}-SS.

control over the order of deformation, which introduces a control switch in addition to the traditional heat-induced shape memory.

The original straight specimens PU-QDP_{3/1}-SS were initially bent into a temporary shape (Fig. 5b) at 90 °C and then cooled back to room temperature (20 °C) to fix the shape. At room temperature, the shape of the elastomer remained unchanged without any additional stimulation. Subsequently, the deformed specimens were immersed in water (~5 °C) to observe the water-induced shape recovery process. It was observed that all the specimens could recover their original shape after being immersed for more than 20 min. The excellent hydrophilicity of the ion segment of ionic PU facilitated the quick absorption of water molecules by PU in the aqueous environment. These absorbed water molecules then participated in the hydration of ions. Consequently, with the

assistance of water molecules, both ionic and hydrogen bonds rapidly dissociated, leading to the destruction of the hard phase and providing the necessary structural conditions for the reconstruction of a new temporary shape. Fig. 5c illustrates that the water contact angle of PU is 68°, which is lower than that of nonionized PU, indicating the contribution of ions to the hydrophilicity of the material.

3.4. Self-cleaning characteristics

Ionic PU elastomers can be used as coatings to firmly bond with substrates, such as glass and metal [44]. However, due to the hydrophilic properties of ionic PU, it leads to a high surface energy and is easily contaminated by substances with low surface energy, such as

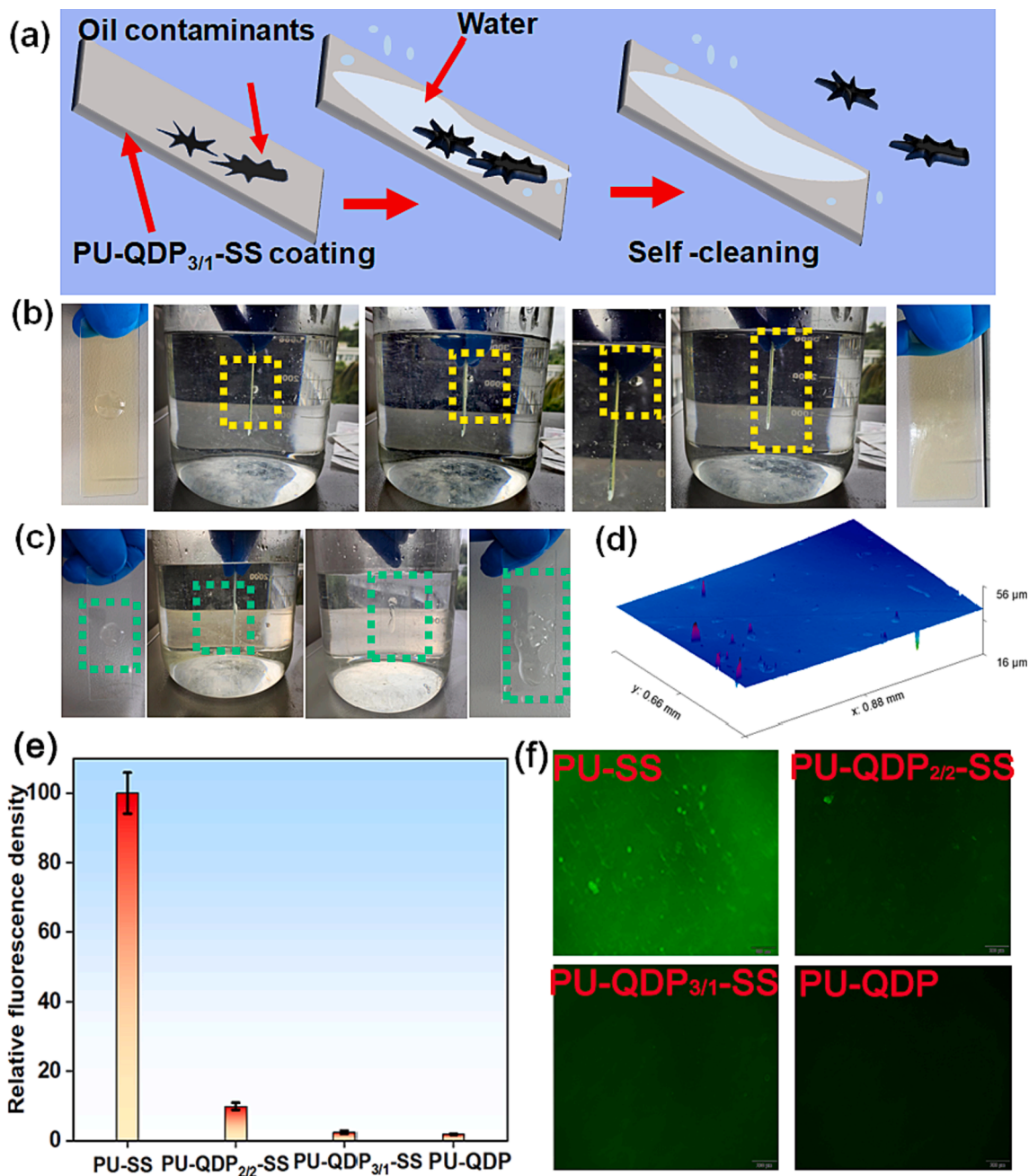


Fig. 6. (a) Schematic diagram of the self-cleaning of the PU-QDP_{3/1}-SS coating. (b) Digital photo of the separation process of castor oil in water by the PU-QDP_{3/1}-SS coating. (c) Digital photos of a glass plate adhering to castor oil in water. (d) 3D contour map of the PU-QDP_{3/1}-SS membrane surface after soaking in water for 72 h. (e) Relative fluorescence density of different types of ionic PU. (f) Fluorescence photos of BSA-FITC protein adsorption on different ionic PU sample surfaces. Scale bar: 200 μm.

various oil stains. Therefore, the antifouling performance of ionic PU coatings is crucial in practical applications [23]. The self-cleaning performance of PU-QDP_{3/1}-SS was evaluated by conducting tests. Castor oil was added dropwise onto a glass plate coated with ionic PU. When the glass plate was submerged in water, the hydrophilic PU-QDP_{3/1}-SS coating surface quickly interacted with a layer of water molecules (Fig. 6a and b). The oil stain on the glass plate formed a ball in the water, gradually sliding off the ionic PU coating surface and floating in the water, leaving a clean surface. In contrast, when the uncoated glass plate was immersed in water, the oil stains remained on the surface and could not be removed, leading to surface contamination (Fig. 6c). SEM images, microscope magnified views, and three-dimensional optical contour line diagrams (Fig. 6d and Fig. S6) demonstrated that after 72 h of immersion in water, the coating surface remained smooth and crack-free, exhibiting excellent water stability. These findings indicate the potential application of this coating in the field of antifouling coatings.

Fig. 6e and f present both qualitative and quantitative results of BSA-FITC protein adsorption on the ionic PU surfaces. The stained protein images (Fig. 6f) reveal a significant amount of green BSA-FITC protein adsorbed on the surface of PU-SS. The adsorption capacity of BSA-FITC protein decreases noticeably with the increase in ion bond content, and fluorescence signals are barely observable on the surface of PU-QDP. By using the fluorescence intensity of PU-SS as the baseline (100 %), the relative fluorescence intensity of ionic PU was calculated (Fig. 6e). It can be deduced that the relative absorbance of the PU-QDP surface is the smallest (<1.3 %), indicating that the hydrophilicity of the substrate surface effectively resists protein adsorption.

3.5. Recyclability, antimicrobial activity and cytotoxicity evaluation

Ionic PU offers the advantage of reconstructing network topology through postprocessing techniques such as solvent-assisted recovery and heat recovery. Fig. 7a demonstrates the process where the PU-QDP_{3/1}-SS

sample is cut into small pieces, rapidly dissolved in organic solvents (such as THF and DMF) for 20 min, dried in a vacuum at 50 °C, and finally transformed into the original transparent film, which can also be recovered through heating. Additionally, Fig. 7b illustrates how the ionic PU fragments acquire a heart shape when subjected to hot working at 100°C. Cationic polymers possess broad-spectrum bactericidal properties and do not exhibit bacterial resistance. The antibacterial mechanism of these polymers can be summarized as follows: firstly, cationic polymers adhere to the negatively charged cell membrane of bacteria through electrostatic interactions. Secondly, the hydrophobic alkyl chains of the polymers are inserted into the lipid layer of the bacterial membranes, resulting in leakage of the cytoplasm and subsequent bacterial death [45]. The antibacterial activity of ionic PUs was studied using the plate counting method. Fig. 7b and c show the antibacterial rates of the raw and recycled elastomer films. The antibacterial rate was calculated by Eq. (1):

$$\text{Antibacterial rate (\%)} = \frac{CFU(\text{control}) - CFU(\text{sample})}{CFU(\text{control})} \times 100 \quad (1)$$

The study found that the ionized PU (PU-QDP-SS series) exhibited antibacterial properties, with antibacterial rates of 98.36 % and 99.93 % against *E. coli* and *S. albus*, respectively. The antibacterial rate of recycled PU-QDP_{3/1}-SS against the two types of bacteria did not show significant change. The distribution of quaternary ammonium cations on the polymer remained unaffected by the recovery process of the antibacterial elastomer through thermoforming, indicating that its antibacterial performance was not compromised. Furthermore, the structural differences between *E. coli* and *S. albus* led to the cell membrane of *S. albus* being more susceptible to damage caused by cation charge interference, resulting in higher antibacterial activity of the elastomers against *S. albus* compared to *E. coli* [46].

Electrospinning is a fiber preparation technology known for its

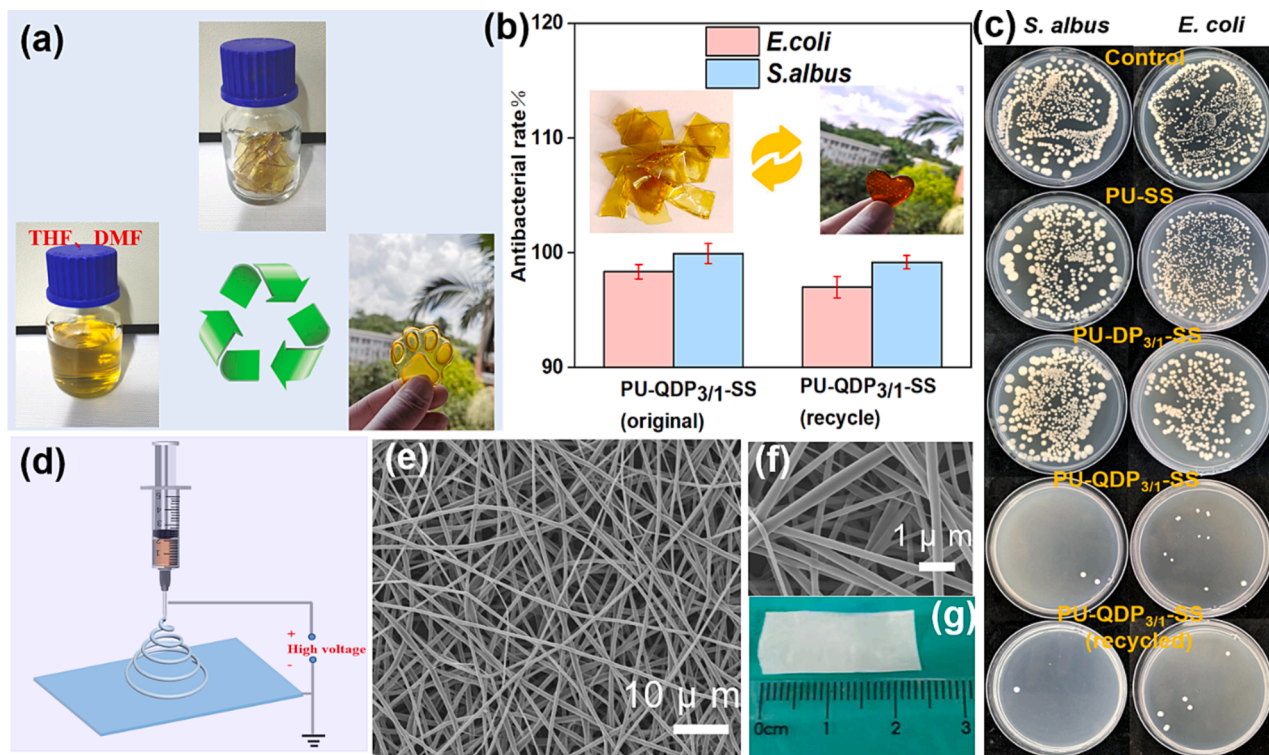


Fig. 7. (a). Process for recycling the PU-QDP_{3/1}-SS elastomer, where the elastomer was cut into pieces and dissolved in DMF and then cast into a cat claw shape. (b) Antibacterial rate of the original and recycled PU-QDP_{3/1}-SS samples. Illustration: chopped PU-QDP_{3/1}-SS and thermoplasticized it into a heart shape at 100 °C. (c) Plate photos of the antibacterial efficiency and bacterial colony count determined by the plate counting method. (d) Schematic diagram of PU-QDP_{3/1}-SS electrospinning. (e-g) SEM images and digital photo of the electrospun film.

simple process and high repeatability. In this study, the processability of PU-QDP_{3/1}-SS was investigated using electrospinning technology (Fig. 7d). The morphology and digital photo of the electrospun PU film were observed through SEM, as depicted in Fig. 7e–g. The fiber size was uniformly distributed without any defects, and the electrospun fiber membrane exhibited a smooth surface morphology. Our research highlights the potential applications of ionic PUs in various fields, particularly in the biomedical sector.

Calculate the relative growth rate (RGRs) of dermal fibroblasts based on the 490 nm OD value obtained by the MTT assay to evaluate the cytotoxicity of ionic PU. The RGR values for PU-SS, PU-DP_{3/1}-SS, and PU-QDP_{3/1}-SS membranes were determined to be 92 %, 92 %, and 88 %, respectively. These results indicate that the synthesized ionic PU membranes exhibit low cytotoxicity (Fig. 8a and Table S3). The morphology of normal fibroblasts stained with the live/dead kit after 48 h is depicted in Fig. 8b and c. All cells exhibited strong green fluorescence signals, and the fibroblasts displayed the typical fusiform (diffusion) morphology. These findings confirm that the ionic PU membranes do not generate cytotoxic byproducts. *E. coli* was chosen as the model microorganism to demonstrate the contact antibacterial properties of the ionic PU membrane using the inhibition zone method. A sterilized PU-QDP_{3/1}-SS (with a diameter of 20 mm) was placed on an agar plate containing the *E. coli* strain (at a concentration of 10⁵ CFUs/mL) and then incubated at 37 °C for 24 h. As depicted in Fig. 8d, no inhibition zone was observed around the PU films, indicating that antimicrobial properties required direct contact between the biocidal surface and microorganisms. Since the quaternary ammonium was attached to the PU systems through reactions, there was no release of antimicrobial agents. Without the release of antimicrobial agents, these films could prevent contamination of the environment and long-term antibacterial activity. The surface zeta potential of the membrane (Fig. 8e) revealed that PU-QDP_{3/1}-SS had a positive charge on its surface, but these cations did not leach out. Thus, these films exhibited both surface antibacterial properties and good biocompatibility.

3.6. Sensing performance

Due to its unique mechanical and self-healing properties, the self-healing ionic PU can be used as a flexible conductive substrate or as a composite material with conductive materials for flexible wearable electronic devices and human motion detection [47–49]. A flexible stretchable strain sensor based on ionic PU was obtained by spraying CNTs-COOH as conductive fillers on the surface of EPU-QDP_{3/1}-SS (Fig. 9a). The electrospun ionic PU frameworks in Fig. 9-b1 exhibited smooth surfaces and similar diameters, forming different pore sizes. When CNTs precipitated onto the surface of the porous framework, they densely stacked and connected to create a network, establishing a continuous conductive pathway for current transmission (Fig. 9-b2 and b3). Additionally, the fiber mesh structure of the sensor contributed to its excellent sensing performance, enabling high sensitivity (gauge factor (GF)) over a wide strain range. Fig. S7 demonstrates that EPU-CNT acted as a wire to light up LED bulbs. Notably, the CNTs-COOH formed ion interactions with the ionic PU, significantly enhancing the interfacial adhesion between the two materials. The study investigated the self-healing behavior of CNTs as conductive fillers on the surface of ionic PU films. Initially, the resistance of the original sample was measured as 1.0 K Ω using a multimeter (Fig. 9c, original sample). To assess the impact of damage, a cut mark was made on the EPU-CNT conductive film using a razor blade, resulting in the disconnection of CNTs on both sides of the cut. This led to a reading of 0 on the electricity meter, indicating the loss of conductivity in the EPU-CNT conductive film (Fig. 9c, the sample with a cut mark). However, when the damaged film was allowed to heal at room temperature for 10 s and 1 min, the resistance value gradually approached the initial value, suggesting a recovery of conductivity. Fig. 9d illustrates that the resistance-time curve exhibited a sharp increase in the peak value when the EPU-CNT film had a cut mark, indicating a discontinuity in the circuit transmission of the separated part. Conversely, when the separated parts came into contact again, the transmission path was reconstructed,

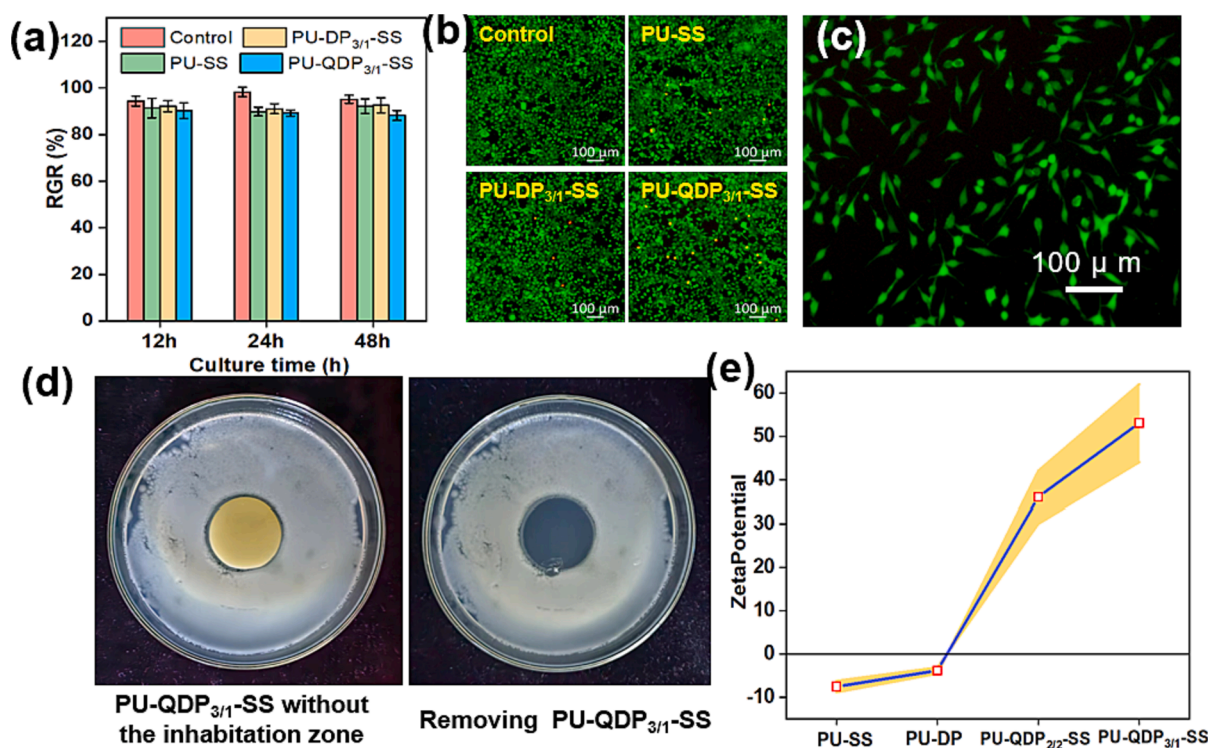


Fig. 8. (a) Relative growth rate (RGR %) of the fibroblasts cultured in the extracted leachate of PU-QDP_{3/1}-SS. (b) Morphology under a microscope of the cells cultivated after 48 h (c) Microscopic enlarged view of the spindle-forming fibroblasts. (d) Inhibition zones of the PU-QDP_{3/1}-SS films against *E. coli*. (e) Surface zeta potential of ionic PU.

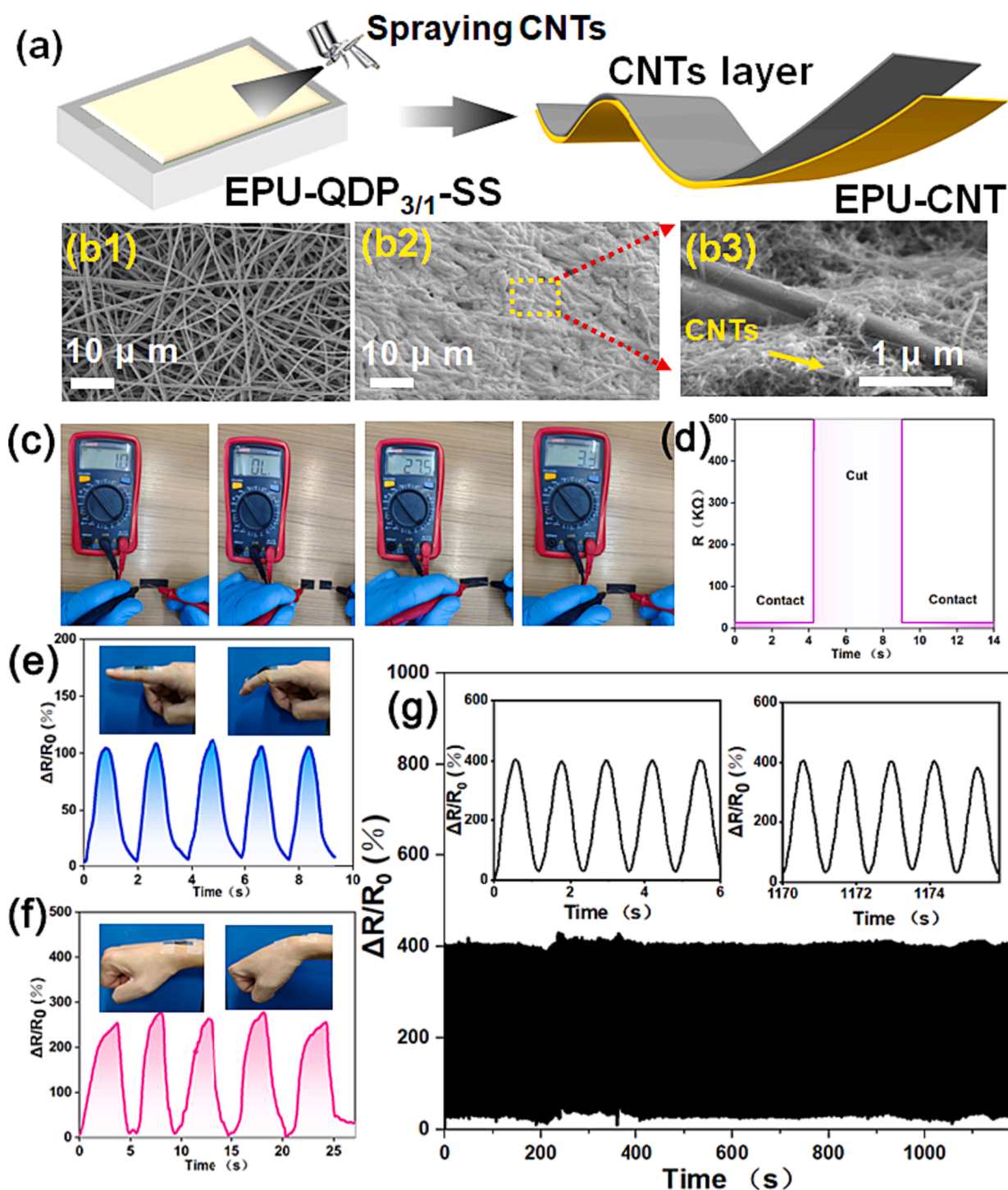


Fig. 9. (a) Preparation process of EPU-CNT flexible composite materials. (b) SEM images of electrospun ion PU and EPU-CNT. (c) Measurement of the resistance of the EPU-CNT composite flexible sensor with a multimeter in the initial state, state with a cut mark, and state when healing at room temperature for 10 s and 1 min. (d) Electrical resistance changes of EPU-CNT during the cut-reconnection. (e) Change rate of relative resistance when detecting the bending motion of the human index finger. (f) Change rate of relative resistance when detecting the bending motion of the human wrist. (g) Response stability of the strain sensor at a constant strain of 50 % for 1000 cycles.

demonstrating the restoration of conductivity in the EPU-CNT membrane.

The changes in the relative resistance of flexible sensors within the tensile strain range of 0–400 % $\Delta R/R_0$ and GF values are depicted in Fig. S8. The stretching process can be divided into two strain regions: 0–200 % and 200–400 %. The corresponding GFs for these regions are 7.52 and 4.31, respectively. As the strain amplitude increases, the slope

of the curve decreases and GF decreases, indicating an increase in resistance during the stretching process. Fig. 9e and f demonstrate the sensor's response to different bending angles of the fingers and wrists. In addition, $\Delta R/R_0$ increased with increasing bending angle. The results illustrated that the strain sensor based on EPU-CNT has high sensitivity in a wide sensing range. Stability is another important parameter for strain sensors, and the response stability of the strain sensor was

evaluated by continuously monitoring the resistance change under constant deformation for 1000 cycles. The results displayed a uniform response curve waveform for each deformation, as shown in Fig. 9g, indicating that the sensor exhibited good stable strain response. Overall, real-time monitoring of $\Delta R/R_0$ changes was achieved with accuracy, highlighting the potential of EPU-CNT as a sensitive self-repairing wearable strain sensor for monitoring various human activities.

4. Conclusions

In this study, a self-healing ionic PU with ionic bonds and an aromatic disulfide structure was synthesized. The formation of ion clusters through the aggregation of anions and cations resulted in physical cross-linking networks. The combination of these ion clusters and dynamic aromatic disulfide bonds effectively addressed the trade-off between mechanical robustness and healing efficiency. Compared to PU without cationic noncovalent interactions, the PU-QDPx-SS exhibited a high decomposition temperature and demonstrated high tensile strength (39.9 ± 4.4 MPa), elongation at break (1930 ± 345 %), and toughness (288 ± 48.4 MPa). The self-healing efficiency of the PU-QDP_{3/1}-SS after 24 h reached 94.4 %. Furthermore, biological experiments showed that even the recovered PU-QDP_{3/1}-SS samples exhibited excellent contact killing and antibacterial activity. The quaternary ammonium attached to the PU system through a reaction and did not release antibacterial agents, ensuring good biocompatibility. The presence of ionic bonds also demonstrated the water-induced shape memory ability of the ionic PU, which, due to its high hydration ability resulting from hydrophilicity, also exhibited self-cleaning ability as a coating material. Finally, the study explored the practical application of composite films assembled using CNTs-COOH as conductive materials and EPU-QDP_{3/1}-SS as substrates in flexible wearable strain sensors. This research presents a novel approach for designing flexible, multifunctional, high-strength, and high-toughness elastomers.

Author contributions

This manuscript was written through contributions of all authors. All authors have given approval to the final version of the manuscript.

CRediT authorship contribution statement

Yaling Lin: Writing – review & editing, Writing – original draft, Supervision, Project administration, Methodology. **Ning Yu:** Writing – original draft, Methodology, Investigation, Data curation. **Shijie Shan:** Writing – original draft, Methodology. **Anqiang Zhang:** Writing – review & editing, Supervision, Project administration, Funding acquisition, Conceptualization.

Declaration of competing interest

The authors declare that they have no known competing financial interests or personal relationships that could have appeared to influence the work reported in this paper.

Data availability

Data will be made available on request.

Acknowledgements

The authors acknowledge the financial support from the National Natural Science Foundation of China (No. 52073098, 31772202) and the Natural Science Foundation of Guangdong Province (No. 2022A1515011570, 2023A1515011264).

Appendix A. Supplementary data

Supplementary data to this article can be found online at <https://doi.org/10.1016/j.cej.2023.148229>.

References

- [1] Y. Zhang, Y. Li, H. Wang, Z. Zhang, Y. Feng, Q. Tian, N. Li, J. Mei, J. Su, H. Tian, Measuring the microphase separation scale of polyurethanes with a vibration-induced emission-based ratiometric “fluorescent ruler”, *ACS Appl. Mater. Interfaces*. 11 201939351–39358, <https://doi.org/10.1021/acsami.9b13193>.
- [2] S. Yang, S. Wang, X. Du, Z. Du, X. Cheng, H. Wang, Mechanically robust self-healing and recyclable flame-retarded polyurethane elastomer based on thermoreversible crosslinking network and multiple hydrogen bonds, *Chem. Eng. J.* 391 (2020) 123544, <https://doi.org/10.1016/j.cej.2019.123544>.
- [3] C. Liu, H. Yang, L. Shen, L. Shi, Q. Yin, Y. Bao, J. Ma, Mechanically robust waterborne polyurethane with excellent room temperature self-healing and shape memory performance, *Eur. Polym. J.* 196 (2023) 112288, <https://doi.org/10.1016/j.eurpolymj.2023.112288>.
- [4] S. Wendels, L. Avérous, Biobased polyurethanes for biomedical applications, *Bioact. Mater.* 6 (2021) 1083–1106, <https://doi.org/10.1016/j.bioactmat.2020.10.002>.
- [5] H. Guo, L. Song, J. Hu, T. Lin, X. Li, H. Yu, D. Cheng, Y. Hou, X. Zhan, Q. Zhang, Enhanced antifouling strategy with a strong synergistic effect of fluorescent antifouling and contact bacteriostasis using 7-amino-4-methylcoumarin, *Chem. Eng. J.* 420 (2021) 127676, <https://doi.org/10.1016/j.cej.2020.127676>.
- [6] Y. Dai, K. Qi, K. Ou, Y. Song, Y. Zhou, M. Zhou, H. Song, J. He, H. Wang, R. Wang, Ag nw-embedded coaxial nanofiber-coated yarns with high stretchability and sensitivity for wearable multi-sensing textiles, *ACS Appl. Mater. Interfaces* 15 (2023) 11244–11258, <https://doi.org/10.1021/acsami.2c20322>.
- [7] N. Jiang, X. Chang, D. Hu, L. Chen, Y. Wang, J. Chen, Y. Zhu, Flexible, transparent, and antibacterial ionogels toward highly sensitive strain and temperature sensors, *Chem. Eng. J.* 424 (2021) 130418, <https://doi.org/10.1016/j.cej.2021.130418>.
- [8] W.B. Ying, Z. Yu, D.H. Kim, K.J. Lee, H. Hu, Y. Liu, Z. Kong, K. Wang, J. Shang, R. Zhang, J. Zhu, R. Li, Waterproof, highly tough, and fast self-healing polyurethane for durable electronic skin, *ACS Appl. Mater. Interfaces* 12 (2020) 11072–11083, <https://doi.org/10.1021/acsami.0c00443>.
- [9] Z. Liu, W. Guo, W. Wang, Z. Guo, L. Yao, Y. Xue, Q. Liu, Q. Zhang, Healable strain sensor based on tough and eco-friendly biomimetic supramolecular waterborne polyurethane, *ACS Appl. Mater. Interfaces* 14 (2022) 6016–6027, <https://doi.org/10.1021/acsami.1c21987>.
- [10] Z. Guo, X. Lu, X. Wang, X. Li, J. Li, J. Sun, Engineering of chain rigidity and hydrogen bond cross-linking toward ultra-strong, healable, recyclable, and water-resistant elastomers, *Adv. Mater.* 35 (2023), <https://doi.org/10.1002/adma.202300286>.
- [11] P.K. Behera, S.K. Raut, P. Mondal, S. Sarkar, N.K. Singha, Self-healable polyurethane elastomer based on dual dynamic covalent chemistry using diels-alder “click” and disulfide metathesis reactions, *ACS Appl. Polym. Mater.* 3 (2021) 847–856, <https://doi.org/10.1021/acsp.0c01179>.
- [12] Y. Song, J. Li, G. Song, L. Zhang, Z. Liu, X. Jing, F. Luo, Y. Zhang, Y. Zhang, X. Li, Self-healing polyurethane elastomers with high mechanical properties based on synergistically thermo-reversible and quadruple hydrogen bonds, *ACS Appl. Polym. Mater.* 5 (2023) 1302–1311, <https://doi.org/10.1021/acsp.0c01849>.
- [13] Z. Shi, J. Kang, L. Zhang, Water-enabled room-temperature self-healing and recyclable polyurea materials with super-strong strength, toughness, and large stretchability, *ACS Appl. Mater. Interfaces* 12 (2020) 23484–23493, <https://doi.org/10.1021/acsami.0c04414>.
- [14] M. Grosjean, D. Berne, S. Caillol, V. Ladmiral, B. Nottet, Dynamic peg-pla/hydroxyurethane networks based on imine bonds as reprocessable elastomeric biomaterials, *Biomacromolecules* (2023), <https://doi.org/10.1021/acs.biomac.3c00229>.
- [15] R. Liang, H. Zhang, Y. Wang, J. Ye, L. Guo, L. He, X. Li, T. Qiu, X. Tuo, Dual dynamic network system constructed by waterborne polyurethane for improved and recoverable performances, *Chem. Eng. J.* 442 (2022) 136204, <https://doi.org/10.1016/j.cej.2022.136204>.
- [16] X. Zhu, K. Han, C. Li, J. Wang, J. Yuan, Z. Pan, M. Pan, Tough, photoluminescent, self-healing waterborne polyurethane elastomers resulting from synergistic action of multiple dynamic bonds, *ACS Appl. Mater. Interfaces*. 15 (2023) 19414–19426, <https://doi.org/10.1021/acsami.3c00333>.
- [17] C. Liu, Q. Yin, Q. Yuan, L. Hao, L. Shi, Y. Bao, B. Lyu, J. Ma, A wear-resistant, self-healing and recyclable multifunctional waterborne polyurethane coating with mechanical tunability based on hydrogen bonding and an aromatic disulfide structure, *Polym. Chem.* 13 (2022) 5647–5658, <https://doi.org/10.1039/D2PY00958G>.
- [18] F. Dong, X. Yang, L. Guo, Y. Wang, H. Shaghaleh, Z. Huang, X. Xu, S. Wang, H. Liu, Self-healing polyurethane with high strength and toughness based on a dynamic chemical strategy, *J. Mater. Chem. A* 10 (2022) 10139–10149, <https://doi.org/10.1039/D2TA00802E>.
- [19] K. Chang, H. Jia, S. Gu, A transparent, highly stretchable, self-healing polyurethane based on disulfide bonds, *Eur. Polym. J.* 112 (2019) 822–831, <https://doi.org/10.1016/j.eurpolymj.2018.11.005>.
- [20] G. Wu, J. Li, Q. Zhang, H. Zhang, Synergistic effect of multiple hydrogen bond and disulfide bond on healing waterborne conductive polyurethane composite, *Polymer* 258 (2022) 125240, <https://doi.org/10.1016/j.polymer.2022.125240>.

- [21] Y. Li, W. Guo, W. Li, X. Liu, H. Zhu, J. Zhang, X. Liu, L. Wei, A. Sun, Tuning hard phase towards synergistic improvement of toughness and self-healing ability of poly(urethane urea) by dual chain extenders and coordinative bonds, *Chem. Eng. J.* 393 (2020) 124583, <https://doi.org/10.1016/j.cej.2020.124583>.
- [22] Z. Wei, Z. Liu, X. Fu, Y. Wang, A. Yuan, J. Lei, Effect of crystalline structure on water resistance of waterborne polyurethane, *Eur. Polym. J.* 157 (2021) 110647, <https://doi.org/10.1016/j.eurpolymj.2021.110647>.
- [23] H. Luo, H. Wei, L. Wang, Q. Gao, Y. Chen, J. Xiang, H. Fan, Anti-smudge and self-cleaning characteristics of waterborne polyurethane coating and its construction, *J. Colloid. Interface. Sci.* 628 (2022) 1070–1081, <https://doi.org/10.1016/j.jcis.2022.08.017>.
- [24] D. Wang, Z. Wang, S. Ren, J. Xu, C. Wang, P. Hu, J. Fu, Molecular engineering of a colorless, extremely tough, superiorly self-recoverable, and healable poly(urethane-urea) elastomer for impact-resistant applications, *Mater. Horiz.* 8 (2021) 2238–2250, <https://doi.org/10.1039/d1mh00548k>.
- [25] H. Xu, J. Tu, J. Ji, L. Liang, H. Li, P. Li, X. Zhang, Q. Gong, X. Guo, Ultra-high-strength self-healing supramolecular polyurethane based on successive loose hydrogen-bonded hard segment structures, *Eur. Polym. J.* 177 (2022) 111437, <https://doi.org/10.1016/j.eurpolymj.2022.111437>.
- [26] W. Yang, Y. Zhu, T. Liu, D. Puglia, J.M. Kenny, P. Xu, R. Zhang, P. Ma, Multiple structure reconstruction by dual dynamic crosslinking strategy inducing self-reinforcing and toughening the polyurethane/nanocellulose elastomers, *Adv. Funct. Mater.* 33 (2023) 2213294, <https://doi.org/10.1002/adfm.202213294>.
- [27] X. Chen, Q. Zhong, C. Cui, L. Ma, S. Liu, Q. Zhang, Y. Wu, L. An, Y. Cheng, S. Ye, X. Chen, Z. Dong, Q. Chen, Y. Zhang, Extremely tough, puncture-resistant, transparent, and photoluminescent polyurethane elastomers for crack self-diagnose and healing tracking, *ACS Appl. Mater. Interfaces* 12 (2020) 30847–30855, <https://doi.org/10.1021/acsami.0c07727>.
- [28] J. Xu, X. Wang, X. Zhang, Y. Zhang, Z. Yang, S. Li, L. Tao, Q. Wang, T. Wang, Room-temperature self-healing supramolecular polyurethanes based on the synergistic strengthening of biomimetic hierarchical hydrogen-bonding interactions and coordination bonds, *Chem. Eng. J.* 451 (2023) 138673, <https://doi.org/10.1016/j.cej.2022.138673>.
- [29] Y. Xu, S. Zhou, Z. Wu, X. Yang, N. Li, Z. Qin, T. Jiao, Room-temperature self-healing and recyclable polyurethane elastomers with high strength and superior robustness based on dynamic double-crosslinked structure, *Chem. Eng. J.* 466 (2023) 143179, <https://doi.org/10.1016/j.cej.2023.143179>.
- [30] X. Wu, J. Wang, J. Huang, S. Yang, Robust, stretchable, and self-healable supramolecular elastomers synergistically cross-linked by hydrogen bonds and coordination bonds, *ACS Appl. Mater. Interfaces* 11 (2019) 7387–7396, <https://doi.org/10.1021/acsami.8b20303>.
- [31] K.I. Winey, Designing tougher elastomers with ionomers, *Science* 358 (2017) 449–450, <https://doi.org/10.1126/science.aap8114>.
- [32] C. Zhang, H. Liang, D. Liang, Z. Lin, Q. Chen, P. Feng, Q. Wang, Renewable castor-oil-based waterborne polyurethane networks: simultaneously showing high strength, self-healing, processability and tunable multishape memory, *Angew. Chem. Int. Ed.* 60 (2021) 4289–4299, <https://doi.org/10.1002/anie.202014299>.
- [33] S. Kim, H. Jeon, S. Shin, S. Park, J. Jegal, S.Y. Hwang, D.X. Oh, J. Park, Superior toughness and fast self-healing at room temperature engineered by transparent elastomers, *Adv. Mater.* 30 (2018) 1705145, <https://doi.org/10.1002/adma.201705145>.
- [34] Q. Xu, Z. Zheng, B. Wang, H. Mao, F. Yan, Zinc ion coordinated poly(ionic liquid) antimicrobial membranes for wound healing, *ACS Appl. Mater. Interfaces* 9 (2017) 14656–14664, <https://doi.org/10.1021/acsami.7b01677>.
- [35] Z. Luo, H. Cui, J. Guo, J. Yao, X. Fang, F. Yan, B. Wang, H. Mao, Poly(ionic liquid)/ce-based antimicrobial nanofibrous membrane for blocking drug-resistance dissemination from mrsa-infected wounds, *Adv. Funct. Mater.* 31 (2021) 2100336, <https://doi.org/10.1002/adfm.202100336>.
- [36] Y. Wang, R. Chen, T. Li, P. Ma, H. Zhang, M. Du, M. Chen, W. Dong, Antimicrobial waterborne polyurethanes based on quaternary ammonium compounds, *Ind. Eng. Chem. Res.* 59 (2020) 458–463, <https://doi.org/10.1021/acs.iecr.9b04828>.
- [37] C. Yu, M. Salzano De Luna, A. Russo, I. Adamiano, F. Scherillo, Z. Wang, X. Zhang, H. Xia, M. Lavorgna, Role of diisocyanate structure on self-healing and anticorrosion properties of waterborne polyurethane coatings, *Adv. Mater. Interfaces* 8 (2021) 2100117, <https://doi.org/10.1002/admi.202100117>.
- [38] Q. Qu, J. He, Y. Da, M. Zhu, Y. Liu, X. Li, X. Tian, H. Wang, High toughness polyurethane toward artificial muscles, tuned by mixing dynamic hard domains, *Macromolecules* 54 (2021) 8243–8254, <https://doi.org/10.1021/acs.macromol.1c01098>.
- [39] X. Wang, J. Xu, Y. Zhang, T. Wang, Q. Wang, Z. Yang, X. Zhang, High-strength, high-toughness, self-healing thermosetting shape memory polyurethane enabled by dual dynamic covalent bonds, *Polym. Chem.* 13 (2022) 3422–3432, <https://doi.org/10.1039/D2PY00564F>.
- [40] J. Rong, J. Zhong, W. Yan, M. Liu, Y. Zhang, Y. Qiao, C. Fu, F. Gao, L. Shen, H. He, Study on waterborne self-healing polyurethane with dual dynamic units of quadruple hydrogen bonding and disulfide bonds, *Polymer* 221 (2021) 123625, <https://doi.org/10.1016/j.polymer.2021.123625>.
- [41] J. Chen, Y. Gao, L. Shi, W. Yu, Z. Sun, Y. Zhou, S. Liu, H. Mao, D. Zhang, T. Lu, Q. Chen, D. Yu, S. Ding, Phase-locked constructing dynamic supramolecular ionic conductive elastomers with superior toughness, autonomous self-healing and recyclability, *Nat. Commun.* 13 (2022), <https://doi.org/10.1038/s41467-022-32517-4>.
- [42] Z. Zheng, D. Liang, H. Deng, F. Xie, X. Chen, Y. Luo, C. Zhang, Castor oil-based, robust, non-leaching and durable antibacterial waterborne polyurethane/polyhexamethylene guanidine composites prepared via an electrostatic self-assembly strategy, *Chem. Eng. J.* 462 (2023) 142060, <https://doi.org/10.1016/j.cej.2023.142060>.
- [43] H. Wu, Y. Chen, W. Zhu, Y. Shangguan, Q. Zheng, Highly adhesive and tough thermoplastic polyurethanes using a furandicarboxamide rigid chain extender with noncovalent interactions, *ACS Appl. Polym. Mater.* 5 (2023) 3515–3523, <https://doi.org/10.1021/acsapm.3c00198>.
- [44] C. Li, P. Wang, D. Zhang, S. Wang, Near-infrared responsive smart superhydrophobic coating with self-healing and robustness enhanced by disulfide-bonded polyurethane, *ACS Appl. Mater. Interfaces* 14 (2022) 45988–46000, <https://doi.org/10.1021/acsami.2c08496>.
- [45] H. Yang, L. Jin, D. Zhao, Z. Lian, M. Appu, J. Huang, Z. Zhang, Antibacterial and antibiofilm formation activities of pyridinium-based cationic pillar[5]arene against pseudomonas aeruginosa, *J. Agric. Food. Chem.* 69 (2021) 4276–4283, <https://doi.org/10.1021/acs.jafc.1c01032>.
- [46] S. He, M. Hou, S. Shan, R. Li, N. Yu, Y. Lin, A. Zhang, Synthesis and anti-bacterial/fungal activities of amphiphilic polysiloxanes primary ammonium salts, *Reactive Funct. Polymers* 183 (2023) 105495, <https://doi.org/10.1016/j.reactfunctpolym.2022.105495>.
- [47] T. Guan, X. Wang, Y. Zhu, L. Qian, Z. Lu, Y. Men, J. Li, Y. Wang, J. Sun, Mechanically robust skin-like poly(urethane-urea) elastomers cross-linked with hydrogen-bond arrays and their application as high-performance ultrastretchable conductors, *Macromolecules* 55 (2022) 5816–5825, <https://doi.org/10.1021/acs.macromol.2c00492>.
- [48] E.K. Boahen, B. Pan, H. Kweon, J.S. Kim, H. Choi, Z. Kong, D.J. Kim, J. Zhu, W. B. Ying, K.J. Lee, D.H. Kim, Ultrafast, autonomous self-healable iontronic skin exhibiting piezo-ionic dynamics, *Nat. Commun.* 13 (2022), <https://doi.org/10.1038/s41467-022-35434-8>.
- [49] X. Xun, Z. Zhang, X. Zhao, B. Zhao, F. Gao, Z. Kang, Q. Liao, Y. Zhang, Highly robust and self-powered electronic skin based on tough conductive self-healing elastomer, *ACS Nano* 14 (2020) 9066–9072, <https://doi.org/10.1021/acsnano.0c04158>.

Surface-Imprinted Polysiloxane with Recognition Ability Based on an ITO Layer for Rapid Detection of *Fusarium oxysporum* f. sp. *cubense* by the Naked Eye

Yaling Lin,^{*,§} Rui Li,[§] Ning Yu, Jianjun Chen, and Anqiang Zhang^{*}



Cite This: *ACS Appl. Mater. Interfaces* 2024, 16, 33182–33191



Read Online

ACCESS |

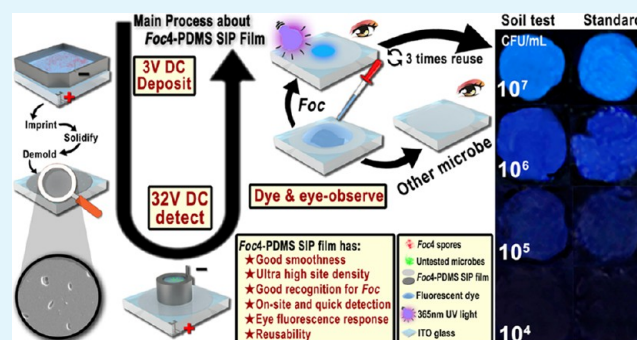
Metrics & More

Article Recommendations

Supporting Information

ABSTRACT: Direct observation by the naked eye of fluorescence-stained microbes adsorbed on surface imprinted polymers (SIPs) is highly challenging and limited by speed, accuracy and the semiquantitative nature of the method. In this study, we tested for the presence of spores of *Fusarium oxysporum* f. sp. *cubense* race 4 (*Foc4*), which cause severe banana Fusarium wilt disease and reduces the area of banana plants. This kind of spore can become dormant in soil, which means that the detection of secreted molecules (molecular imprinting) in soil may be inaccurate; detection methods such as polymerase chain reaction (PCR) and Raman spectroscopy are more accurate but time-consuming and inconvenient. Therefore, a semiquantitative and rapid SIP detection method for *Foc4* was proposed. Based on the ITO conductive layer, a reusable and naked-eye-detectable *Foc4*-PDMS SIP film was prepared with a site density of approximately 9000 mm⁻². Adsorption experiments showed that when the *Foc4* spore concentration was between 10⁴ to 10⁷ CFU/mL, the number of *Foc4* spores adsorbed and the fluorescence intensity were strongly correlated with the concentration and could be fully distinguished by the naked eye after fluorescence staining. Adsorption tests on other microbes showed that the SIP film completely recognized only the *Foc* series. All the results were highly consistent with the naked-eye observations after fluorescence staining, and the results of the *Foc4*-infected soil experiment were also close to the ideal situation. Taken together, these results showed that *Foc4*-PDMS SIPs have the ability to rapidly and semiquantitatively detect the concentration of *Foc* in soil, which can provide good support for banana cultivation. This method also has potential applications in the detection of other fungal diseases.

KEYWORDS: on-site rapid detection, surface imprinted polymers, naked eye, fluorescence staining, *Fusarium oxysporum* f. sp. *cubense*



1. INTRODUCTION

In the past few decades, due to the development of material and biochemical science and technology, related detection technologies for small molecules, macromolecules, viruses, and microbes have rapidly developed.^{1–9} In these studies, imprinted polymers (IPs), including molecular imprinted polymers (MIPs) and surface imprinted polymers (SIPs), which simulate antigen–antibody binding effects, serve as on-site rapid detection materials with simple sensing capabilities.¹⁰

Fusarium oxysporum f. sp. *cubense* (*Foc*) is a plant fungus that causes banana Fusarium wilt disease in vast regions of the world and is capable of long-term dormancy; in particular, race 1 (*Foc1*) and race 4 (*Foc4*) of the *Foc* series pose great harm.¹¹ Banana fusarium wilt disease caused by *Foc4* and *Foc1* is a devastating disease faced by the banana industry worldwide, but suitable disease-resistant varieties and effective treatment measures for this disease are lacking. Therefore, it is particularly important to use rapid and accurate detection techniques for banana fusarium wilt to identify pathogenic fungi and control the spread of this disease. On the other hand,

banana Fusarium wilt disease has also led to a large number of abandoned banana fields and a continuous reduction in banana planting areas. Studies have shown that the number of pathogenic fungi in the soil is positively correlated with disease severity. Therefore, timely detection of the amount of *Foc* in the soil is highly important for banana field replanting. The current mainstream detection methods for fungal spores are coating plates, polymerase chain reaction (PCR), and spectral analysis.^{12,13} For the detection of *Foc*, the coating plate wastes much time and high-end manpower; PCR technology is the most common technology, but due to cross contamination and incorrect nucleic acid sequences (DNA and RNA),¹⁴ it is

Received: April 17, 2024

Revised: June 12, 2024

Accepted: June 13, 2024

Published: June 21, 2024



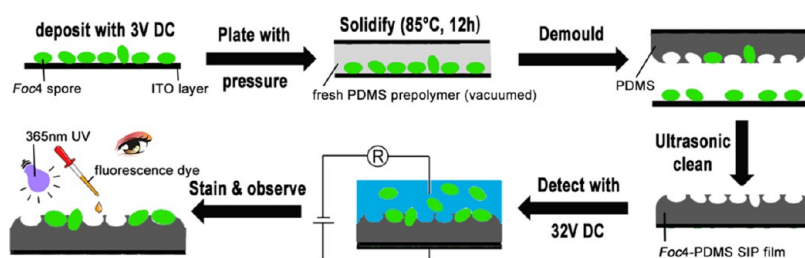


Figure 1. Complete process of preparation, adsorption, and detection of the *Foc4*-PDMS SIP film.

not completely reliable, and Raman spectroscopy instruments are very expensive and inconvenient to carry, which means that a new method must be proposed, and imprinting technology, especially IP, is much more suitable for the above conditions. Therefore, to quickly obtain reliable detection data on site, the use of MIPs to detect small molecules secreted by *Foc* with the naked eye has been considered.¹⁵ However, Compared with hyphae, *Foc* spore secretes a limited amount of small molecules in specific environments, and in most cases, it only undergoes normal metabolism and even directly enters a dormant state, which results in a minimum metabolic rate;¹¹ this makes the detection of small molecules such as fusaric acid (FA) based on MIP ineffective, and without PCR, the detection of secreted proteins such as those secreted in xylem protein (SIX) is also considered difficult.¹⁶ Inexpensive SIPs usually allow for rapid microbe detection,¹⁷ which means that SIPs are more suitable for detecting *Foc* spores than MIPs; therefore, the preparation of whole-cell SIPs and the establishment of good detection methods are absolute priorities.

The preparation of *Foc4*-PDMS SIPs and related detection methods face daunting challenges, which mainly include (1) the dispersion of microbial sedimentary layers, (2) changes in the size of imprinted sites caused by the death and dehydration of microbes during the preparation of SIP, (3) surface recognition efficiency and recognition accuracy, (4) rapid detection and sensing, especially by the naked eye, and (5) the reusability of thin smooth films.¹⁸

Many strategies have been designed to address these issues. In the initial research, a large number of scholars used glutaraldehyde to fix cells and sizes of imprint sites and then measured the adsorption capacity of imprinted polymers by using QCM.^{19–21} The application of conductive electrochemical cell SIPs enables rapid preparation, and impedance is subsequently used to detect microbial suspensions, which greatly increases the detection efficiency.^{22–24} Zhu et al.²⁵ improved the preparation of electrochemical SIPs and obtained electrodes with surface-grafted quaternary ammonium salt-imprinted polymers, which had a detection limit as low as 2 CFU/mL for *Escherichia coli* and *Staphylococcus albus*. More detection methods, such as PDMS microfluidic chip sensing²⁶ and heat transfer,^{27–29} are being explored. Ren and Zare³⁰ reported that when a modified surface is more lipophilic, more microorganisms can be adsorbed. Gennaro et al.³⁰ used electrostatic relaxation technology on adsorbed brewing yeast, indicating that in addition to surface geometric information, deeper surface information is transferred to the imprinted polymer film layer, which explains the enhanced adhesion of yeast under the action of imprinted polymers³¹ and explains why surface imprinted polymers can distinguish ABO blood groups.³² Fluorescence staining is a good auxiliary method that is sometimes used to assist in impedance detection and heat transfer detection,^{33,34} and faster on-site

detection has also been achieved via this method. Dulay et al.³⁵ labeled *E. coli* with fluorescent proteins, and the number of effectively recognized *E. coli* on the imprinted membranes was determined. Gao et al.³⁶ used AO/EB fluorescent dyes to stain tumor cells on the imprinted polymer with antibodies and achieved efficient capture of tumor cells. Bezdekova et al.³⁷ used magnetic MIP to adsorb *S. aureus* in the milk samples, and the detection limit is approximately 10^3 CFU/mL.

As mentioned above, most of the *Foc4* would be in the state of dormant spores due to the lacking of nutrients and host in real-world soil. This study was guided by rapid on-site naked-eye detection, without any host, the extremely inactive fungus *F. oxysporum* f. sp. *cubense* race 4 (*Foc4*) which spores could be in dormant state for long was selected for imprinting and detection. This kind of spore easily aggregates,³⁸ which is inconsistent with bacteria and single-cell biological spores.^{21,39} This study applied direct voltage to achieve high density and uniform dispersion to facilitate the preparation of SIPs and enhanced recognition by applying a higher voltage. A fluorescent agent that can strongly stain *F. oxysporum* is used, and solid fluorescence is used for detection to evaluate the actual effectiveness of fluorescence detection by the naked eye.⁴⁰

2. EXPERIMENTAL SECTION

2.1. Design Strategy for the *Foc4*-PDMS SIP Film. The core idea of this work is to use the good spreadability of the prepolymer and the flexibility of PDMS to prepare a relatively flat *Foc4*-PDMS surface-imprinted polymer layer on a conductive and transparent ITO layer that has been plated on a glass substrate to facilitate the observation of the electrostatic adsorption process of spores on the SIP film under an optical microscope and to collect real-time adsorption statistics. The entire process is shown in Figure 1. The preparation processes for the other fungal SIP films (changing *Foc4* to other fungi and changing the deposition time) and NIP films (without deposition) were nearly the same as those for the *Foc4*-PDMS SIP film.

2.2. Materials. ITO layered glass ($0.2\ \mu\text{m}$, $32\ \Omega$) was obtained from Luoyang Guluo (China), SYLGARD 184 was obtained from Dow Corning (Midland), *F. oxysporum* f. sp. *cubense* race 4. (*Foc4*), *F. oxysporum* f. sp. *cubense* race 1. (*Foc1*), *F. oxysporum* f. sp. *benincasae* (*Fob*), *E. coli* (*E. coli*), and *Staphylococcus albus* (*S. albus*) were obtained from South China Agricultural University, *Saccharomyces* was bought from Angel Yeast Co., Ltd. (China), and *n*-pentane, CaCl_2 , NaCl , NaOH , benzyldimethyldodecylammonium chloride (DDBAC), and Calcofluor White M2R (Fluorescent Brightener 28, FB-28) were obtained from Macklin (Shanghai, China). All chemicals were of analytical grade and used as received.

2.3. Characterization. The characterization instruments used included an optical microscope (XDS200-PH, Phenix Optics, China), a scanning electron microscope (SEM, EVO-18, Zeiss, German), a fluorescence spectrophotometer with a solid holder (F-2700, Hitachi, Japan), a microplate reader (Wellscan Mk3, Thermo LabSystems),

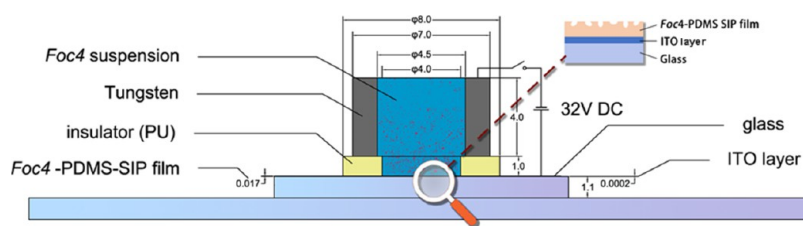


Figure 2. Diagram of the device for *Foc* spore electrodeposition detection (unit: mm).

and a three-dimensional (3D) surface profile instrument (RETC UP Dual Model, RETC).

2.4. Preparation of the *Foc4* Spore Suspension and other Microbe Suspensions. *Foc4*, *Foc1*, *Fob*, and *Staphylococcus* were flushed from solid media to a CaCl_2 solution (0.01 M, pH 7.0) to prepare suspensions, which were then manually counted after dilution to obtain accurate concentrations. *E. coli* was removed from the liquid culture medium directly to prepare a suspension, and a microplate reader was used to determine its concentration. Finally, all the suspensions were sealed at 6 °C for future use.

2.5. Preparation of the *Foc4* Spore Stamp. *Foc4* spore suspension ($1 \times 10^8 \text{ mL}^{-1}$, 15 μL). To be consistent with other papers, all mL^{-1} units in this study were written as CFU/mL, and sterile CaCl_2 solution (0.01 M, 385 μL) was mixed in a sterile centrifuge tube until the prominent uneven white turbidity disappeared. Then, all the well-mixed liquid was carefully transferred to a special tungsten model whose bottom was protected by PDMS on an ITO layer of glass to prevent any damage to the ITO layer and provide insulation protection. Afterward, a 3 V direct current was applied for 60 min, the negative electrode was set on the tungsten model, and the positive electrode was set on the ITO layer. Then, the direct current, the tungsten model, and all the liquid on the ITO layer were removed, and the ITO layer was washed with ultrapure water with a slow current for 2 min to clean the *Foc4* spore layer. Finally, the ITO layer with the *Foc4* spore layer on glass was dried without dust or other microbes for 30 min. The white transparent layer, which was subsequently plated on glass, was the *Foc4* spore stamp, and all steps were carried out at 25 °C.

2.6. Preparation of the *Foc4*-PDMS Surface Imprinted Polymer Film (*Foc4*-PDMS SIP Film, SIP Film) and PDMS Nonimprinted Polymer Film (NIP Film). Components A and B of SYGARD 184 were well mixed at a mass ratio of 10:1 as the prepolymer mixture (prepolymer), and then the mixture was vacuumed at room temperature for 10 min. After the prepolymer was placed at −18 °C for 60 min to ensure that the polymerization activity of the prepolymer was minimized, a pipet was used to accurately aspirate 3.0 μL of the prepolymer and carefully drop it on another clean ITO layer. Then, this ITO layer with the mixture was placed in a clean environment for 15 min to allow the mixture to have full contact with the ITO surface for subsequent operations. With the two pieces of ITO layered glass placing contactless cross, the mixture was scrupulously covered with the well-prepared *Foc4* spore stamp. After all the area between the two pieces of ITO layered glass was filled with the mixture, the ITO-mixture-*Foc*-ITO sandwich was placed in an environment at 85 °C for 12 h. Finally, the two pieces of ITO glass were separated, and the piece of ITO layered glass with the PDMS film was the final detection piece with the *Foc4*-PDMS SIP film. In addition to the use of a clean ITO layer instead of a *Foc4* spore stamp, the preparation steps for the NIP film were the same as those for the SIP film.

2.7. Establishment of the *Foc* Spore Electrodeposition Detection Device. Inspired by a thermal transport sensor,²⁷ a *Foc* spore electrodeposition detection device composed of a glass gasket, ITO glass, *Foc4*-PDMS SIP film, tungsten ring, microbe suspension, polyurethane spacer (insulator), and a downward steady electric field on SIP film was developed. The self-established device with the detection area is shown in Figure 2.

2.8. Adsorption and Detection. In a conventional adsorption experiment at 25 °C, 15 μL of NaCl solution (0.1 M, pH 7.0) and 50

μL of *Foc4* spore suspension were mixed uniformly first, and then the mixture was added to the detection area of the SIP film, and an approximately $1.88 \text{ V}/\mu\text{m}$ ($32 \text{ V}/17 \mu\text{m}$) downward electric field was applied to adsorb the *Foc4* spores. After 60 min of adsorption, the remaining suspension, tungsten ring, and electric field were removed, and the SIP film was washed with ultrapure water under slow flow for 2 min to remove the nonadsorbed *Foc4* spores. Then, the SIP film with adsorbed *Foc4* spores was completely dried in a clean environment. Similar methods will also be used for the adsorption of other microbes for comparison. After adsorption, 50–100 μL of staining solution containing FB-28 and NaOH (1 g/L FB-28, pH = 12.0) was added to the detection area of the SIP film with adsorbed *Foc4* spores, and a piece of sterile cover glass was immediately added to the SIP film to provide the staining solution. After the entire system was put in a dark environment and dyed for 2 min, the cover glass was peeled, and the SIP film was washed with ultrapure water under slow flow for 2 min. Then, all the liquid attached to the SIP film was removed. Then, solid-state fluorescence was used to detect the fluorescence intensity of the detection area with adsorbed *Foc4* spores on the SIP film, and an ultraviolet lamp with a 365 nm wavelength was used for illumination in a dark environment to take photos and observe the sample with the naked eye. The detection and adsorption processes of the other microbes and SIP film were the same as those of *Foc*. All adsorption experiments were repeated 3 times.

2.9. Detection of *Foc* in Soil. After mixing 1 g of sterilized dry soil with 1 mL of a 10^8 CFU/mL *Foc4* spore suspension and leaching with a 20 μm metal filter 3 times, as shown in Figure 3, filtrates with

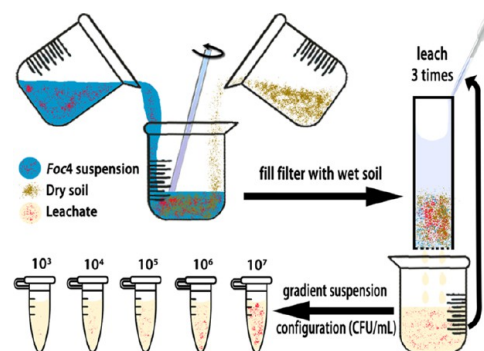


Figure 3. Processing of *Foc4*-soil leachate.

spore concentrations ranging from 10^3 to 10^7 CFU/mL were prepared after counting and adjusting the concentration of the sterile soil extract. The adsorption and detection processes were the same as in Section 2.8.

2.10. Reuse Experiments. The deposited layer was reused after demolding, the ITO layer was reused after thoroughly cleaning the deposited layer by ultrasonication, and the *Foc4*-PDMS SIPs were reused after ultrasonic cleaning. The remaining operating steps were the same as those described in Section 2.8.

3. RESULTS AND DISCUSSION

3.1. Statistics of *Foc4* Spore Number Density on the Deposited Layer. When the *Foc4* spores were deposited, the real-time number density, which varied with time, was

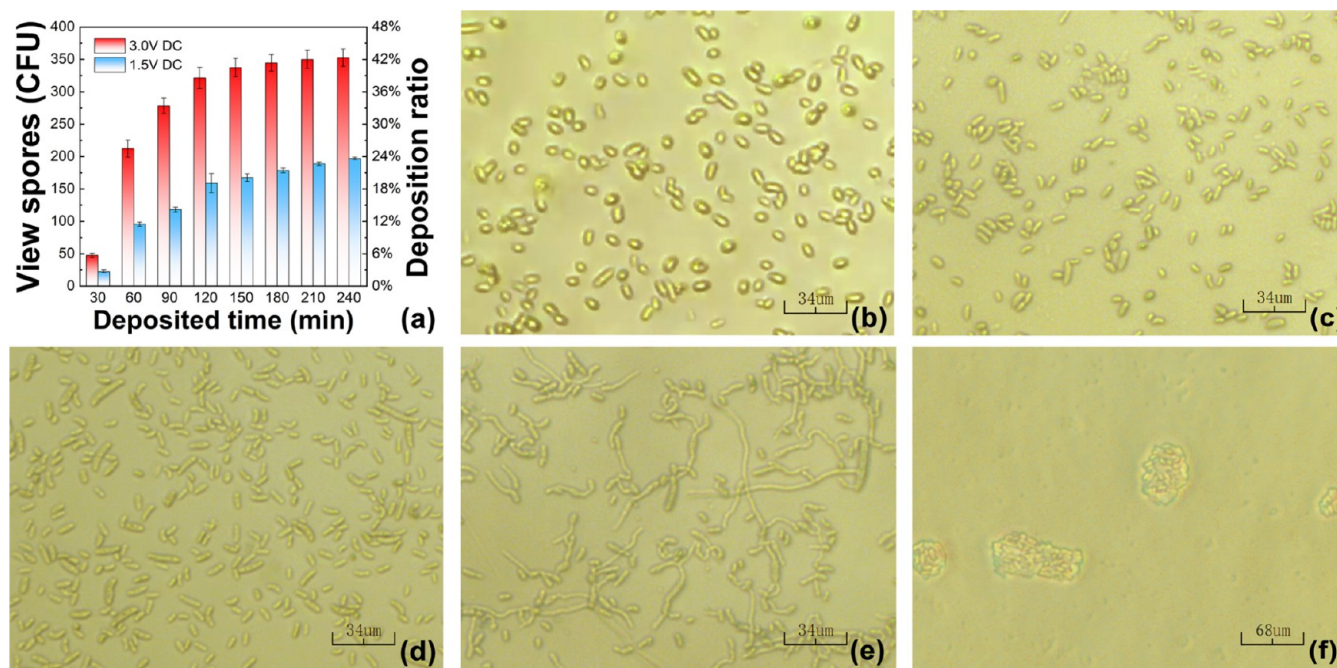
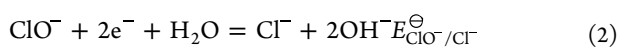
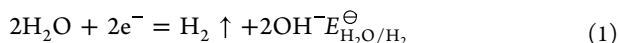


Figure 4. (a) Relationships between *Foc4* spore number density and deposition ratio, voltage, and deposition time; (b) *Foc4* spores deposited at 3 V for 60 min; (c) *Foc4* spores deposited at 3 V for 90 min; (d) *Foc4* spores deposited at 3 V for 120 min; (e) *Foc4* spores deposited at 3 V for 240 min; (f) *Foc4* spores deposited at 120 min without electricity.

determined under an optical microscope by taking micrographs after washing, and the dispersity of the *Foc4* spores could be observed at the same time. To avoid spore death caused by electrochemical reactions, according to eqs 1–3, with a 0.01 mol/L CaCl_2 solution, the lowest voltage at which the reaction begins was 1.54 V in theory, and a pre-experiment indicated that the iron sheet and stainless-steel sheet were all corroded under this voltage. Considering that the pre-experiment of the ITO layer in which the surface potential (E_ζ) cannot be ignored, the reaction began at 3.05 V.



$$E = (E_{\text{H}_2\text{O}/\text{H}_2}^\ominus - E_{\text{ClO}^-/\text{Cl}^-}^\ominus) - \frac{2RT}{nF} \ln[\text{Cl}^-] + E_\zeta \quad (3)$$

The statistical data of the deposition voltage at 3.0 and 1.5 V under the same view area (0.0552 mm^2), which included 3 layers per deposition time from 30 to 240 min, are shown in Figure 4a. According to this figure, for deposition, the 3.0 V voltage was better than the 1.5 V voltage, and the number density of *Foc4* spores increased rapidly first and then increased slowly until it tended to nearly stabilize, which indicated that the best deposition time was between 120 and 240 min, when the number density under 3.0 V of *Foc4* spores was between 5500 and 6500 CFU/ mm^2 . The micrographs shown in Figure 4b–e, which included different deposition times of 60 min, 90, 120 and 240 min, indicated that excessive electrodeposition time led to *Foc4* spore germination. The abovementioned phenomena implied that the best deposition time was approximately 120 min.

Compared with the layer deposited without electricity for 120 min, as shown in Figure 4f, the layer deposited with electricity, as shown in Figure 4d, could significantly disperse *Foc4* spores. Due to the presence of well-dispersed spores, the

subsequent use of a *Foc4* spore surface imprinting polymer, which is sensitive to the shape of a single spore, was convenient. The deposition methods used are shown in Table S1.

3.2. Characterization of the *Foc4*-PDMS SIP Film. After solvent-free film formation with quantitative plating, as shown in Figure S1, the two pieces of ITO glass were cured and separated, and Fourier-transform infrared (FT-IR) was used to ensure that the prepolymer fully reacted. After an electronic microgauge was used to approximately measure the thickness of the film, SEM and optical microscopy were used to obtain micrographs to determine the thickness three times, as shown in Figure 5a,b. Figure 5c shows the NIP film. And at the same time, imprinting sites could also be observed, as shown in Figure 5d–e. Compared with Figure 5f, which shows the SIP film, and Figure 5g, which shows the stamp before the SIP film, the consistency between the positions of the imprinting sites on the SIP film and the positions of the spores on the stamp indicated that the positions of the spores did not change during the preparation of the SIP film. The 3D surface profiling images shown in Figure 5h,i, which also implied that the sizes of the imprinting sites were nearly the same as those of single spores, and the surface density of the imprinted site was $9000 \pm 500 \text{ mm}^{-2}$, as shown in Figure S2.

3.3. Adsorption and Detection of *Foc4* Spores. Due to the negative charge on the spore surface, the spores could be better deposited by applying a voltage. When the device was used to adsorb *Foc4* spores, the adsorption curves shown in Figure 6a,b indicated that the optimal adsorption time was greater than 45 min. Note that in Figure 6b, the adsorption efficiency (η), which was calculated by eq 4, changed sharply when the adsorption time was between 20 and 40 min, possibly because of the permeation of ions in the film, which reduced the resistance to the appropriate value.

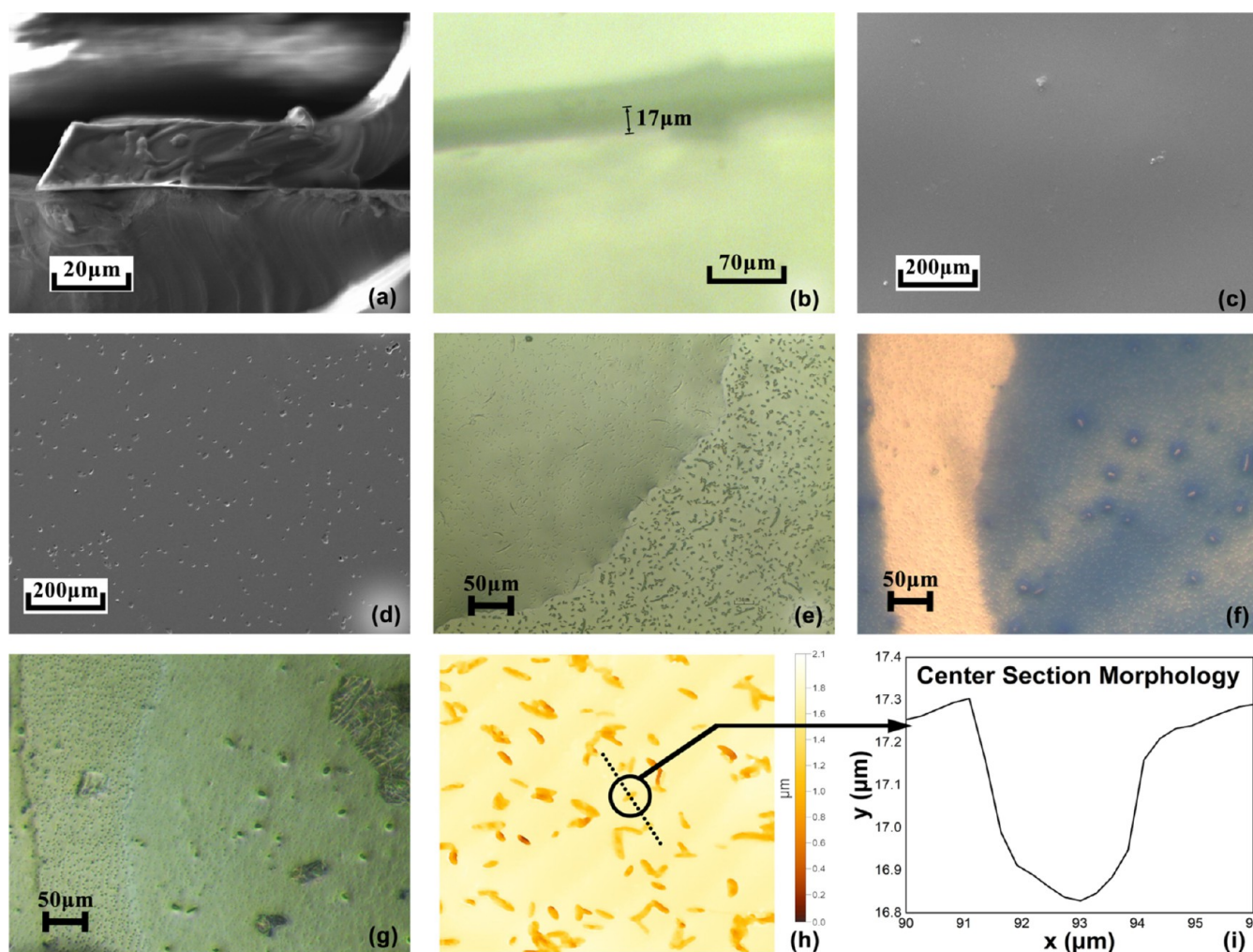


Figure 5. (a) SEM image of the film with a thickness of 17 μm ; (b) optical microscopy image of the film with a thickness of 17 μm ; (c) SEM image of the NIP film; (d) SEM image of the *Foc4*-PMDS SIP film; (e) optical microscopy image of the *Foc4*-PMDS SIP film; (f) marking area before imprinting (stamp); (g) marking area after imprinting (film); (h) 3D surface profiling image of the *Foc4*-PMDS SIP film; (i) site size.

$$\eta = \frac{\text{view number after washing}}{\text{view number before washing}} \times 100\% \quad (4)$$

After converting the number of *Foc4* spores in the view area ($10^4 \sim 2 \times 10^6$ CFU/mL: 0.37775 mm^2 ; $10^7 \sim 2 \times 10^7$ CFU/mL: 0.055224 mm^2) to the number of *Foc4* spores per unit area (CFU/ mm^2), the relationship between the adsorption number/adsorption efficiency and concentration of the *Foc4* suspension was determined, as shown in Figure 6c, and the results demonstrated that the optimal concentration for detection seemed to be between 10^5 and 10^7 CFU/mL. However, Figure 6d–f, which represent the excitation spectrum, emission spectrum and fit curve of the maximum light intensity (420 nm), respectively, showed that after fluorescence staining and analysis of the fluorescence intensity, the absolute degree of deviation from the fluorescence intensity fit curve was much smaller than that of the microscopic statistics fit curve at a spore concentration of 10^4 CFU/mL. Based on this phenomenon, we believe that the statistics are imprecise because an insufficient view area cannot reflect the real distribution of extremely few *Foc4* spores with poor distribution on a small scale, which means that the lower detection limit of this method is between 10^3 and 10^4 CFU/

mL, and the upper detection limit is between 10^7 and 2×10^7 CFU/mL.

In addition to the above results, photos taken by the camera (as shown in Figure 7a–e) strongly indicated that the best detection interval for the naked eye was 10^4 to 10^7 CFU/mL. Long-term tracking by optical microscopy and SEM was subsequently used to prove the effective adsorption of the *Foc4* spores. The adsorption process was successfully tracked (photos are shown in Figure 7f–i, and a video of the adsorption process is shown in Videos S1 and S2), and a static adsorption photo (SIP film produced with 0.1 wt % *n*-pentane), as shown in Figure 7j, was also obtained. These results well illustrated that *Foc4* spores were indeed adsorbed on the SIP film effectively.

3.4. Immunity and Selectivity of the *Foc4*-PDMS SIP Film. To compare the adsorption effects of other microbes with those of *Foc4*, *Foc1*, *Fob*, *E. coli*, and *S. albus*, a concentration of 10^7 CFU/mL was chosen. The statistical results and optical microscopy images of *Foc4*, *Foc1*, and *Fob* shown in Figure 8a–c indicate that the recognition of the *Foc4*-PDMS SIP film was likely based on the morphology of the imprint sites. The ratios of the overlap length and width of the same interval for these three kinds of microbes are shown in Figure S3, and the adsorption ratio (k) was calculated

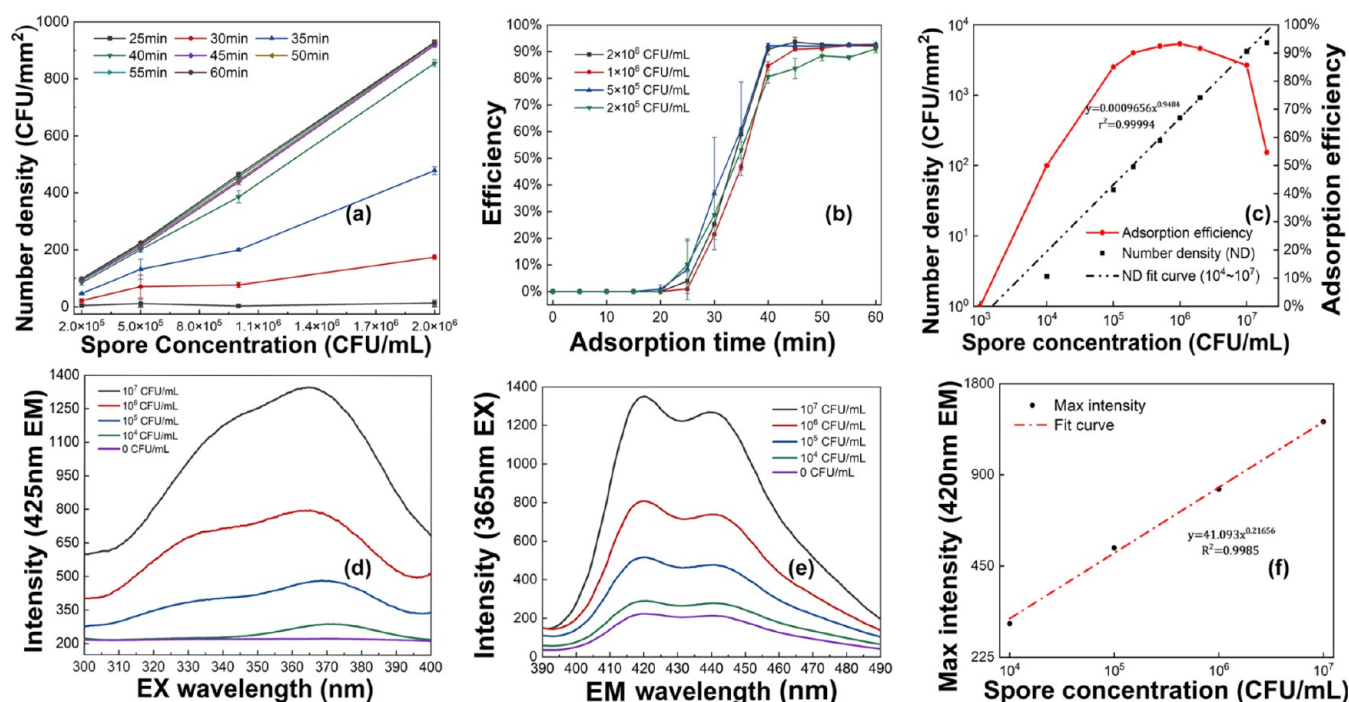


Figure 6. (a) Spore number density of *Foc4* at different concentrations at the same adsorption time; (b) Spore adsorption efficiency of *Foc4* at different adsorption times at the same concentrations; (c) Spore adsorption efficiency and number density of *Foc4* at different concentrations after adsorbing for 60 min; (d) Excitation spectrum after adsorbing for 60 min; (e) Emission spectrum after adsorbing for 60 min; (f) Maximum intensity after adsorbing for 60 min.

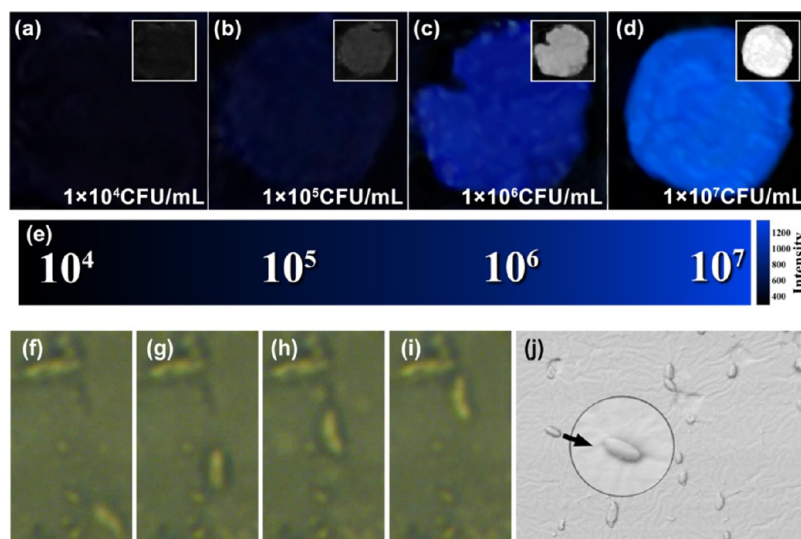


Figure 7. (a–d) Photos taken by camera (naked eye observed) with different *Foc4* spore concentrations; (e) cubic-interpolated light intensity color bar at 420 nm emission; (f–i) adsorption process; (j) static adsorption on film produced with 0.1 wt % *n*-pentane.

according to eq 5, while the η of eq 5 was calculated according to eq 4. All the statistical data were combined and calculated via eqs 4 and 5, the value of k for *Foc4* and *Fob* was 9.88% (7.34–11.36%), while that for *Foc4* and *Foc1* was approximately 100%, which confirmed that the recognition of the *Foc4*-PDMS SIP film was based on the morphology of the imprint sites. Furthermore, the abovementioned phenomena and data indicated that the *Foc4*-PDMS SIP film was not able to distinguish between *Foc4* and *Foc1*; however, considering that *Foc1* is also the main pathogenic fungus of banana Fusarium wilt disease and that the difference in virulence

between *Foc1* and *Foc4* is not significant, recognition was still considered effective.

$$k = \frac{\eta(\text{another microbe})}{\eta(\text{Foc4})} \times 100\% \quad (5)$$

Then, all the chosen microbes were adsorbed via the same methods first and tested via solid-state fluorescence. Figure 8d shows the maximum intensity of the different microbes, which was used to verify the identification mechanism of the *Foc4*-PDMS SIP film.

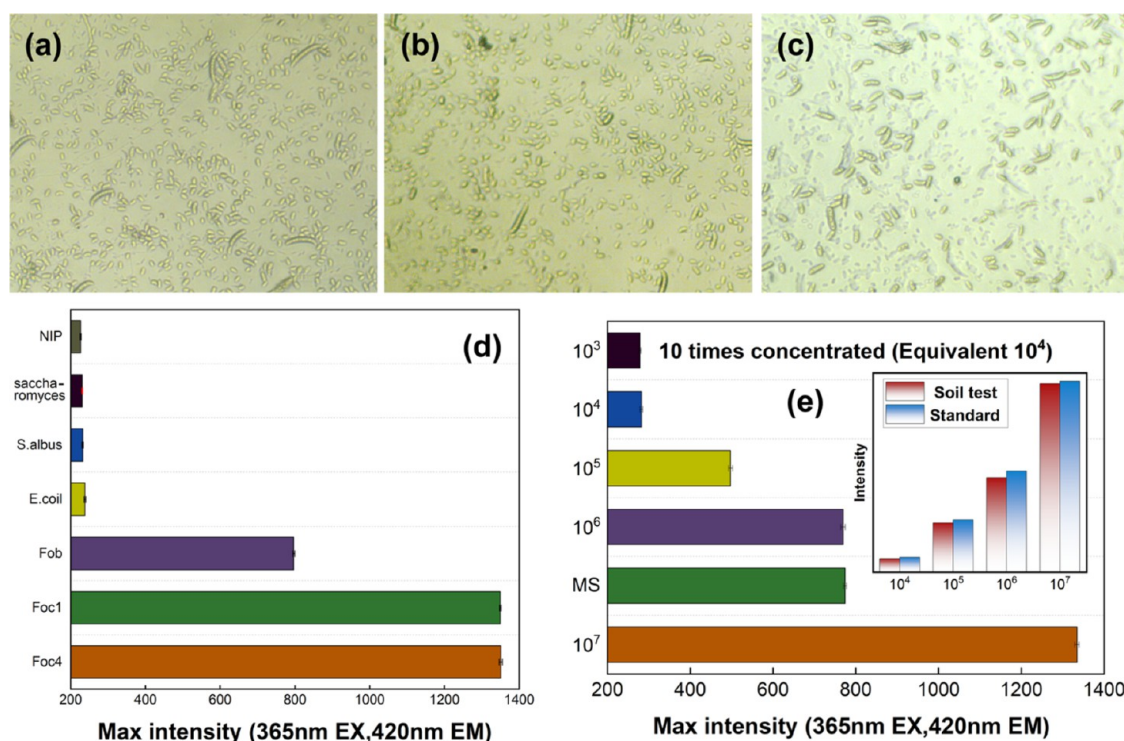


Figure 8. (a) Adsorption of *Foc4*; (b) adsorption of *Foc1*; (c) adsorption of *Fob*; (d) maximum solid-state fluorescence intensity of different microbes and NIP adsorption. (e) Soil detection with MS and different concentrations of *Foc4* spores and comparison with standard data.

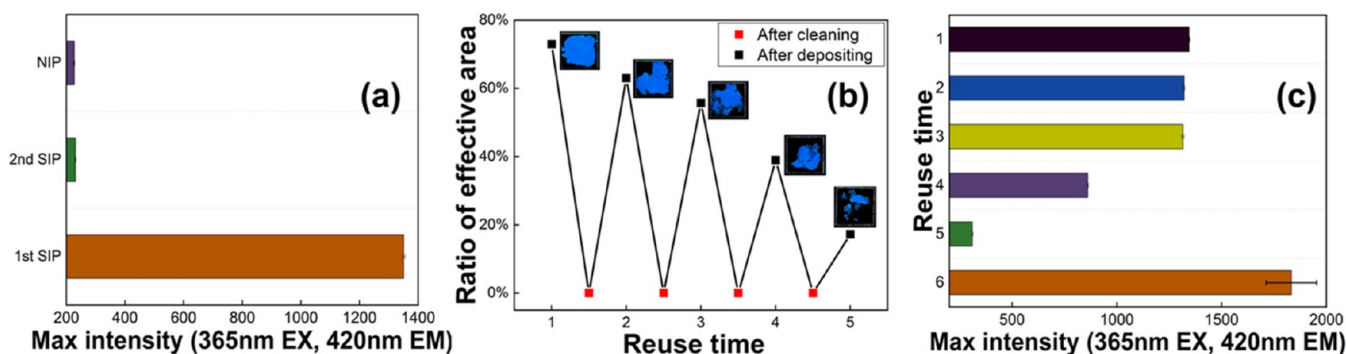


Figure 9. (a) Solid-state fluorescence intensity of NIPs, SIPs (first SIP), and reprint SIPs (second SIP); (b) ratio of the effective area of the ITO layer when reusing; (c) solid-state fluorescence intensity with different reuse times of SIPs.

To verify the detection sensitivity of the film layer in real situations, different concentrations of *Foc4* spores were detected in soil. The detection of 10⁴ to 10⁷ CFU/mL and 10 times the concentration (by centrifugation) of 10³ CFU/mL are shown in Figure 8e. And according to Figure 3, the mixed suspension (MS) with 10⁶ CFU/mL of each type microbe (*Foc4*, *E. coli*, *S. albus*, and *Saccharomyces*) was also prepared, and the result is shown in Figure 8e as well. All results indicate that the *Foc4*-PDMS SIP film had good sensitivity in real situations. One additional clarification is that *Fob* and *Foc* hardly appear in the same piece of land in the real environment, and the toxicity of *Foc1* to bananas is similar to that of *Foc4*, so the results were acceptable with a simple survey of soil history.

3.5. Reuse Experiment. To explore the recycling effect of the ITO layer with deposited spores, a second imprint was generated, as shown in Figure 9a. After a second processing at 85 °C for 12 h and reimprinting, the second *Foc4*-PDMS SIP film was not able to be used to identify *Foc4* spores, which was

similar to the identification of dead *Foc4* spores (treated with 1 g/L DDBAC for 24 h) on the first *Foc4*-PDMS SIP film; this finding indicated that the *Foc4*-deposited layer had no reuse value because an environment with long-term high temperature and low humidity killed all the spores. Due to the inability to reuse the deposited *Foc4* layer, the reuse of ITO layered glass was tested. With ultrasonic cleaning after deposition and subsequent deposition, by fluorescence staining with FB-28, Figure 9b shows that the effective deposition area of the layer decreased with increasing deposition time, so it was considered that the damage to the ITO layer caused by reuse was irreversible, but reusing twice was acceptable. A reuse experiment of the *Foc4*-PDMS SIP film was also carried out, and the solid fluorescence results of this experiment are shown in Figure 9c. The results indicated that when reused no more than 3 times, the *Foc4*-PDMS SIP film exhibited good adsorption. When it was reused 3–5 times, the adsorption capacity of the film rapidly decreased, which might be related to the total time of voltage application and the total time of

water adsorption, which greatly accelerated the failure of the film when the film was about to deform. When it was reused more than 5 times, the film was destroyed by voltage and water. Sketch maps of deformation with water adsorption and destroyed films are shown in Figure S4.

3.6. Contrast Experiment. To show that the *Foc4*-SIP film had a certain degree of specificity, SIP films of *Fob* and *S. albus* were prepared via the same process. Because adsorption kinetic of different microbes has significant differences which causes significant differences of absolute fluorescence intensity of each SIP film, all fluorescence intensity was normalized to relative intensity $I'_{Y/X}$ with eq 6. In this equation, X represents spore suspension corresponding to the SIP film, Y represents spore suspension to be tested, and I represents the absolute fluorescence intensity.

$$I'_{Y/X} = \frac{I_Y - I_{NIP}}{I_X - I_{NIP}} \times 100\% \quad (6)$$

Figure 10 shows that after normalization of fluorescence intensity, each fungi-SIP PDMS film prepared by this method

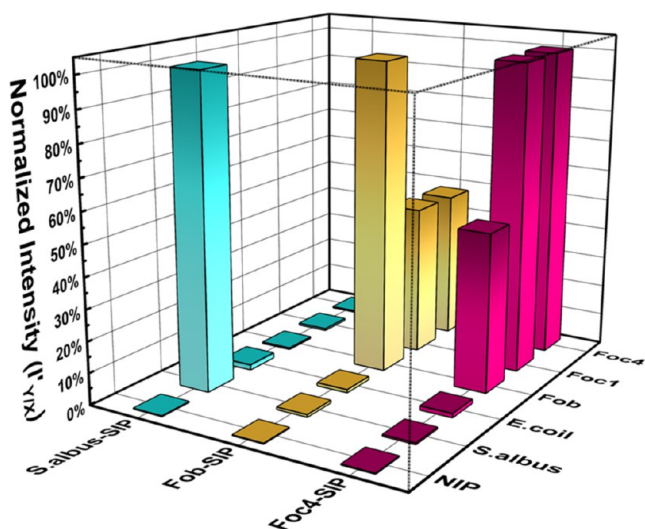


Figure 10. Detection of different SIP films.

has a response to the corresponding fungal spores, and has an incomplete response to spores with similar shapes and sizes. All results indicated that this preparation, adsorption, and detection method has considerable potential for application.

4. CONCLUSIONS

This work demonstrated a preparation strategy for smooth SIP films different from that for other SIP films and showed an easy way to detect *Foc4* spores on site by the naked eye within 1 h (the particular detection range was thought to be limited to *Foc*, including *Foc1* and *Foc4*). Compared with preparations of other microbe-deposited layers that were not easily agglomerated, the difficulty of strongly agglomerating *Foc4* spores was overcome by treatment with a stable low-voltage direct current, which led to the successful preparation of a layer of uniformly dispersed *Foc4* spores. This was the first time that the SIP dynamic adsorption process was recorded. Compared with other detection methods, the advantages of *Foc4* detection methods are as follows: (i) easy operation and visibility to the naked eye, which means that instruments are not necessary; (ii) portable SIP films and staining agents, which have great

potential for real-time and rapid detection; and (iii) easy cleaning, which shows the reusability of SIP films. Benefiting from the advantages of the preparation and detection methods, the efficiency and practicality of the *Foc4*-PDMS SIP film were confirmed. By providing a history of disease, this work may provide a new approach for on-site rapid economic detection of low-activity fungal spores or other low-activity microbes. Above all, with an acceptable limit of detection (LOD), this work has taken a significant step toward identifying microorganisms with the naked eye rather than instrument detection.

■ ASSOCIATED CONTENT

Supporting Information

The Supporting Information is available free of charge at <https://pubs.acs.org/doi/10.1021/acsami.4c06275>.

Deposition and adsorption method (processing method) selection; *Foc4*-PDMS SIP film preparation method selection; thickness selection of *Foc4*-PDMS SIP film; statistics on the length and width of *Foc1*, *Foc4* and *Fob*; explanation of destroy of reused film (PDF)

Adsorption process (MP4)

Demonstration that spores with poor adsorption could be wash by water (MP4)

■ AUTHOR INFORMATION

Corresponding Authors

Yaling Lin – College of Materials and Energy, South China Agricultural University, Guangzhou 510642 Guangdong, China; orcid.org/0000-0002-5289-4304; Email: linyaling@scau.edu.cn

Anqiang Zhang – School of Materials Science and Engineering, South China University of Technology, Guangzhou 510641 Guangdong, China; orcid.org/0000-0001-7499-8406; Email: aqzhang@scut.edu.cn

Authors

Rui Li – School of Materials Science and Engineering, South China University of Technology, Guangzhou 510641 Guangdong, China; orcid.org/0000-0003-4866-5821

Ning Yu – School of Materials Science and Engineering, South China University of Technology, Guangzhou 510641 Guangdong, China; orcid.org/0000-0002-0671-6216

Jianjun Chen – College of Materials and Energy, South China Agricultural University, Guangzhou 510642 Guangdong, China; orcid.org/0009-0003-2872-3817

Complete contact information is available at: <https://pubs.acs.org/doi/10.1021/acsami.4c06275>

Author Contributions

[§]Y.L. and R.L. contributed equally to this work. This manuscript was written through contributions of all authors. All authors have given approval to the final version of the manuscript.

Notes

The authors declare no competing financial interest.

■ ACKNOWLEDGMENTS

The authors acknowledge the financial support from the National Natural Science Foundation of China (Nos. 52073098, 31772202), the Scientific and Technological Planning Project of Guangzhou City (201803020015), and

the Natural Science Foundation of Guangdong Province (Nos. 2022A1515011570, 2023A1515011264).

REFERENCES

- (1) Vlatakis, G.; Andersson, L. I.; Müller, R.; Mosbach, K. Drug assay using antibody mimics made by molecular imprinting. *Nature* **1993**, *361*, 645–647.
- (2) Hu, X.; Li, G.; Huang, J.; Zhang, D.; Qiu, Y. Construction of Self-Reporting Specific Chemical Sensors with High Sensitivity. *Adv. Mater.* **2007**, *19* (24), 4327–4332.
- (3) Gong, C. B.; Wong, K. L.; Lam, M. H. W. Photoresponsive molecularly imprinted hydrogels for the photoregulated release and uptake of pharmaceuticals in the aqueous media. *Chem. Mater.* **2008**, *20* (4), 1353–1358.
- (4) Cumbo, A.; Lorber, B.; Corvini, P. F. X.; Meier, W.; Shahgaldian, P. A synthetic nanomaterial for virus recognition produced by surface imprinting. *Nat. Commun.* **2013**, *4* (1), No. 1503.
- (5) Wangchareansak, T.; Thitithanyanont, A.; Chuakheaw, D.; Gleeson, M. P.; Lieberzeit, P. A.; Sangma, C. Influenza A virus molecularly imprinted polymers and their application in virus subtype classification. *J. Mater. Chem. B* **2013**, *1* (16), 2190–2197.
- (6) Hou, J.; Zhang, H.; Yang, Q.; Li, M.; Jiang, L.; Song, Y. Hydrophilic-Hydrophobic Patterned Molecularly Imprinted Photonic Crystal Sensors for High-Sensitive Colorimetric Detection of Tetracycline. *Small* **2015**, *11* (23), 2738–2742.
- (7) Dinc, M.; Esen, C.; Mizakoff, B. Recent advances on core-shell magnetic molecularly imprinted polymers for biomacromolecules. *TrAC, Trends Anal. Chem.* **2019**, *114*, 202–217.
- (8) Li, Z.-y.; Jing, L.-p.; Gu, L.-l.; Tong, Z.-h.; Du, K.; Zhang, H. Preparation and application of highly sensitive mycobutanil sensor based on molecularly imprinted photonic crystals. *Polymer* **2021**, *228*, No. 123921.
- (9) Kotsiri, Z.; Vidic, J.; Vantarakis, A. Applications of biosensors for bacteria and virus detection in food and water-A systematic review. *J. Environ. Sci.* **2022**, *111*, 367–379.
- (10) Dar, K. K.; Shao, S.; Tan, T.; Lv, Y. Molecularly imprinted polymers for the selective recognition of microorganisms. *Biotechnol. Adv.* **2020**, *45*, No. 107640.
- (11) Ploetz, R. C. Fusarium Wilt of Banana. *Phytopathology* **2015**, *105* (12), 1512–1521.
- (12) Ray, M.; Ray, A.; Dash, S.; Mishra, A.; Achary, K. G.; Nayak, S.; Singh, S. Fungal disease detection in plants: Traditional assays, novel diagnostic techniques and biosensors. *Biosens. Bioelectron.* **2017**, *87*, 708–723.
- (13) Lin, Y. J.; Lin, H. K.; Lin, Y. H. Construction of Raman spectroscopic fingerprints for the detection of Fusarium wilt of banana in Taiwan. *PLoS One* **2020**, *15* (3), No. e0230330.
- (14) Arnheim, N.; Erlich, H. Polymerase Chain Reaction Strategy. *Annu. Rev. Biochem.* **1992**, *61* (1), 131–156.
- (15) Lin, Y.; Feng, X.; Zhang, W.; Li, R.; Zhang, A. Molecularly Imprinted Photonic Crystals Based on Fusaric Acid for the Detection of Banana Fusarium Wilt. *ACS Appl. Polym. Mater.* **2021**, *3* (11), 5818–5825.
- (16) Adusei-Fosu, K.; Dickinson, M. Detecting Fusarium oxysporum f. sp. elaeidis by using loop-mediated isothermal amplification. *J. Plant Pathol.* **2023**, *105* (4), 1637–1643.
- (17) Cui, F.; Zhou, Z.; Zhou, H. S. Molecularly Imprinted Polymers and Surface Imprinted Polymers Based Electrochemical Biosensor for Infectious Diseases. *Sensors* **2020**, *20* (4), No. 996, DOI: 10.3390/s20040996.
- (18) Mamipour, Z.; Nematollahzadeh, A.; Kompany-Zareh, M. Molecularly imprinted polymer grafted on paper and flat sheet for selective sensing and diagnosis: a review. *Microchim. Acta* **2021**, *188* (8), 279.
- (19) Dickert, F. L.; Hayden, G. Bioimprinting of polymers and sol-gel phases. Selective detection of yeasts with imprinted polymers. *Anal. Chem.* **2002**, *74* (6), 1302–1306.
- (20) Ren, K.; Zare, R. N. Chemical Recognition in Cell-Imprinted Polymers. *ACS Nano* **2012**, *6* (5), 4314–4318.
- (21) Werner, M.; Gluck, M. S.; Brauer, B.; Bismarck, A.; Lieberzeit, P. A. Investigations on sub-structures within cavities of surface imprinted polymers using AFM and PF-QNM. *Soft Matter* **2022**, *18* (11), 2245–2251.
- (22) Namvar, A.; Warriner, K. Microbial imprinted polypyrrole/poly(3-methylthiophene) composite films for the detection of Bacillus endospores. *Biosens. Bioelectron.* **2007**, *22* (9–10), 2018–2024.
- (23) Lahcen, A. A.; Arduini, F.; Lista, F.; Amine, A. Label-free electrochemical sensor based on spore-imprinted polymer for Bacillus cereus spore detection. *Sens. Actuators, B* **2018**, *276*, 114–120.
- (24) Yasmeen, N.; Etienne, M.; Sharma, P. S.; El-Kirat-Chatel, S.; Helu, M. B.; Kutner, W. Molecularly imprinted polymer as a synthetic receptor mimic for capacitive impedimetric selective recognition of *Escherichia coli* K-12. *Anal. Chim. Acta* **2021**, *1188*, No. 339177.
- (25) Zhu, L.; Wang, L.; Zhang, X.; Li, T.; Wang, Y.; Riaz, M. A.; Sui, X.; Yuan, Z.; Chen, Y. Interfacial engineering of graphenic carbon electrodes by antimicrobial polyhexamethylene guanidine hydrochloride for ultrasensitive bacterial detection. *Carbon* **2020**, *159*, 185–194.
- (26) Regiart, M.; Rinaldi-Tosi, M.; Aranda, P. R.; Bertolino, F. A.; Villarroel-Rocha, J.; Sapag, K.; Messina, G. A.; Raba, J.; Fernandez-Baldo, M. A. Development of a nanostructured immunosensor for early and in situ detection of Xanthomonas arboricola in agricultural food production. *Talanta* **2017**, *175*, 535–541.
- (27) Eersels, K.; van Grinsven, B.; Ethirajan, A.; Timmermans, S.; Monroy, K. L. J.; Bogie, J. F.; Punniyakoti, S.; Vandenryt, T.; Hendriks, J. J.; Cleij, T. J.; et al. Selective identification of macrophages and cancer cells based on thermal transport through surface-imprinted polymer layers. *ACS Appl. Mater. Interfaces* **2013**, *5* (15), 7258–7267.
- (28) Yongabi, D.; Khorshid, M.; Losada-Pérez, P.; Eersels, K.; Deschaume, O.; D'Haen, J.; D'Haen, J.; Bartic, C.; Hooyberghs, J.; Thoelen, R.; Wübbenhorst, M.; Wagner, P. Cell detection by surface imprinted polymers SIPs: A study to unravel the recognition mechanisms. *Sens. Actuators, B* **2018**, *255*, 907–917, DOI: 10.1016/j.snb.2017.08.122.
- (29) Stilman, W.; Lenzi, M. C.; Wackers, G.; Deschaume, O.; Yongabi, D.; Mathijssen, G.; Bartic, C.; Gruber, J.; Wübbenhorst, M.; Heyndrickx, M.; Wagner, P. Low Cost, Sensitive Impedance Detection of *E. coli* Bacteria in Food-Matrix Samples Using Surface-Imprinted Polymers as Whole-Cell Receptors. *Phys. Status Solidi A* **2021**, *219* (23), No. 2100405, DOI: 10.1002/pssa.202100405.
- (30) Gennaro, A.; Yongabi, D.; Deschaume, O.; Bartic, C.; Wagner, P.; Wübbenhorst, M. Cell detection by surface imprinted polymers (SIPs) — A study of the sensor surface by optical and dielectric relaxation spectroscopy. *IEEE Trans. Dielectr. Electr. Insul.* **2018**, *25* (3), 816–821.
- (31) Hachulka, K.; Lekka, M.; Okrajni, J.; Ambroziak, W.; Wandelt, B. Polymeric sensing system molecularly imprinted towards enhanced adhesion of Saccharomyces cerevisiae. *Biosens. Bioelectron.* **2010**, *26* (1), 50–54.
- (32) Hayden, O.; Mann, K. J.; Krassnig, S.; Dickert, F. L. Biomimetic ABO blood-group typing. *Angew. Chem., Int. Ed.* **2006**, *45* (16), 2626–2629.
- (33) Wang, R.; Wang, L.; Yan, J.; Luan, D.; Tao, S.; Wu, J.; Bian, X. Rapid, sensitive and label-free detection of pathogenic bacteria using a bacteria-imprinted conducting polymer film-based electrochemical sensor. *Talanta* **2021**, *226*, No. 122135.
- (34) Arreguin-Campos, R.; Eersels, K.; Rogosic, R.; Cleij, T. J.; Dilién, H.; van Grinsven, B. Imprinted Polydimethylsiloxane-Graphene Oxide Composite Receptor for the Biomimetic Thermal Sensing of *Escherichia coli*. *ACS Sens.* **2022**, *7* (5), 1467–1475.
- (35) Dulay, M. T.; Zaman, N.; Jaramillo, D.; Mody, A. C.; Zare, R. N. Pathogen-Imprinted Organosiloxane Polymers as Selective Biosensors for the Detection of Targeted *E. coli* **2018** *4* *2* *29* DOI: 10.3390/c4020029.
- (36) Gao, S.; Chen, S.; Lu, Q. Cell-imprinted biomimetic interface for intelligent recognition and efficient capture of CTCs. *Biomater. Sci.* **2019**, *7* (10), 4027–4035.

(37) Bezdekova, J.; Zemankova, K.; Hutarova, J.; Kociova, S.; Smerkova, K.; Adam, V.; Vaculovicova, M. Magnetic molecularly imprinted polymers used for selective isolation and detection of *Staphylococcus aureus*. *Food Chem.* **2020**, 321, No. 126673.

(38) Whitehead, K. A.; Liauw, C. M.; Lynch, S.; El Mohtadi, M.; Amin, M.; Preuss, A.; Deisenroth, T.; Verran, J. Diverse surface properties reveal that substratum roughness affects fungal spore binding. *iScience* **2021**, 24 (4), No. 102333.

(39) Sarkhosh, T.; Mayerberger, E.; Jellison, K.; Jedlicka, S. Development of cell-imprinted polymer surfaces for *Cryptosporidium* capture and detection. *Water Res.* **2021**, 205, No. 117675.

(40) Stewart, A.; Deacon, J. W. Vital fluorochromes as tracers for fungal growth studies. *Biotech. Histochem.* **1995**, 70 (2), 57–65.



Amphiphilic polysiloxane graft guanidine salts with a combination of low environmental toxicity and high antifungal activity

Yaling Lin^{a,*}, Shiqi He^b, Mingyang Wu^a, Meng Hou^a, Rui Li^b, Anqiang Zhang^{b,**}

^a College of Materials and Energy, South China Agricultural University, 483 Wushan Rd., Guangzhou 510642, Guangdong, China

^b School of Materials Science and Engineering, South China University of Technology, 381 Wushan Rd., Guangzhou 510641, Guangdong, China

ARTICLE INFO

Keywords:

Polysiloxane graft guanidine salts
Antifungal activity
Banana Fusarium wilt
Environmental toxicity

ABSTRACT

Banana Fusarium wilt is one of the most serious diseases that restricts the banana industry. How to achieve efficient, low toxicity, and long-term inhibition of pathogenic fungal spores (*Fusarium oxysporum* f. sp. *cubense*, race 4, Foc4) that grow in soil has become a challenge in the field of chemical control of plant diseases in recent years. Based on the special antimicrobial mechanism of guanidine salts, which can effectively inhibit microbes by forming transmembrane stomata on the plasma membrane, we were inspired to introduce hydrophilic guanidine salts to hydrophobic PDMS chains to potentially balance high antimicrobial activity and low environmental toxicity. In this work, a series of novel amphiphilic polysiloxane graft guanidine salts (PDMS-g-GH) were synthesized based on our previous works, i.e., polysiloxane graft primary amine salts (PDMS-g-AH), in which the primary amine salt groups were converted to guanidine salt groups. The molecular weight of the polymer, the grafting density of guanidine salts, the distribution of guanidine salt units on the main chain (random or block), the *in vitro* antifungal activities and the anti-Foc4 activities in soil, the adsorption characteristics in soil, and the environmental toxicity after soil adsorption were systematically studied. The results confirmed that compared with PDMS-g-AH, PDMS-g-GH showed stronger antifungal activity against Foc4 and long-term antifungal activity against Foc4 in soil, but its environmental toxicity was significantly reduced. These results support the potential application of PDMS-g-GH for the prevention and control of banana Fusarium wilt and other soil-borne fungal diseases.

1. Introduction

Banana Fusarium wilt is one of the most common and devastating soilborne diseases in banana-producing regions worldwide and is caused by *Fusarium oxysporum* f. sp. *cubense* (Foc). [1] With regards to the pathogen responsible for banana Fusarium wilt, there are multiple physiological races in which race 4 (Foc4) is the most harmful and can infect almost all banana varieties. [2] Once banana plants are infected with Foc4, the pathogen enters the vascular bundle through the root system, and conventional drugs have little effect on prevention and control; hence, this pathogen is called “banana cancer”. [3] Even worse, the chlamydospores of Foc4 can survive in soil for several years or more. The occurrence of banana Fusarium wilt is significantly related to the concentration of Foc4 spores in soil; [4,5] thus, reducing the concentration of Foc4 in the soil is currently the main goal for the control of

banana Fusarium wilt, and the control and prevention methods include cultivating resistant varieties of banana, crop rotation, soil disinfection, and biological control. [6,7] Among these methods, crop rotation has certain effects, but these effects are highly limited by market factors, such as supply and sales. [6] Soil disinfection, also called soil fumigation, involves the use of disinfectants/fumigants (such as lime nitrogen and chlorine dioxide) to kill almost all microorganisms in the soil, including Foc4; thus, new organic matter needs to be introduced after treatment to restore the soil, [7,8] and it should be noted that both residual and escaping disinfectants can also pollute the environment, and due to the difficulty of long-term retention in the soil, it is almost ineffective in the spread and diffusion of pathogens caused by the transplantation stage of banana plants after soil disinfection. [9] Biological control has been a research hotspot in recent years, and its main prevention and control strategy is to inhibit pathogens while maintaining

* Corresponding author at: College of Materials and Energy, South China Agricultural University, 483 Wushan Rd., Guangzhou 510642, Guangdong, China.

** Corresponding author at: School of Materials Science and Engineering, South China University of Technology, 381 Wushan Rd., Guangzhou 510641, Guangdong, China.

E-mail addresses: linyaling@scau.edu.cn (Y. Lin), aqzhang@scut.edu.cn (A. Zhang).

<https://doi.org/10.1016/j.eurpolymj.2024.113258>

Received 9 May 2024; Received in revised form 19 June 2024; Accepted 20 June 2024

Available online 26 June 2024

0014-3057/© 2024 Elsevier Ltd. All rights reserved, including those for text and data mining, AI training, and similar technologies.

the diversity of soil microbial communities. [7] However, the effectiveness of biological control is influenced by many external factors and is not widely applicable. Thus, an urgent challenge for the control and prevention of banana *Fusarium* wilt should be reducing the concentration of Foc4 in soil while maintaining microbial diversity in soil at the same time. [2,3].

In previous studies, [10–18] it was found that the molecular weight, hydrophilicity and hydrophobicity of the main chain, as well as the sequence structure of the main chain (random or block) of polymeric quaternary ammonium salts (PQASs), had different impacts on the antimicrobial activities of PQASs, and these PQASs showed some commonalities, such as significantly enhanced antimicrobial activity compared to that of the corresponding monomers containing cations, strong adsorption and difficulty migrating in soil; after being adsorbed by soil, their toxicity to the environment was significantly reduced, and their impact on soil microbial populations was relatively small. [12,14–16] For example, both amphiphilic polysiloxane-polyacrylate quaternary ammonium salt block copolymers (S₅Q₅) [12] and hydrophilic polyacrylamide containing quaternary ammonium salt (PAM-X) [15] can effectively adsorb in soil, and their inhibitory effect on Foc4 spores in soil can last for 60–90 d. When a more hydrophobic fluorinated acrylic monomer unit is introduced into the main chain of the polyacrylate quaternary ammonium salts, the anti-Foc4 activity can be significantly enhanced. [14] Unlike commercial small-molecule quaternary ammonium salts (such as benzalkonium chloride/BC), which can significantly destroy soil microbial diversity, the abovementioned PQASs, which have vastly different structures, have relatively small overall impacts on soil microbial populations. [15,16] Although these PQASs are basically nontoxic to earthworms when applied to soil and their soil/water mixtures and soil leaching solutions are almost nontoxic to fish, their acute oral toxicity to fish when directly applied to water is moderate, which hinders their application in the field.

Compared with quaternary ammonium salts, other cationic groups, such as primary ammonium salts and guanidine salts, can increase electrostatic binding to anionic lipopolysaccharides, which strongly disrupts cell wall integrity. [18,19] It was found that polymers containing guanidine salts could effectively inhibit microbes by forming transmembrane stomata on the plasma membrane in contact with microorganisms, which is different from the mechanism of action of QASs, indicating that the guanidine polymer could be effective against microbial activity without severe membrane damage; in other words, the introduction of guanidine salts into polymer chains might be a potential strategy for the synthesis of polymers with low toxicity and high antimicrobial activity. [20–23].

These results also prompt us to consider the following questions: can we simultaneously reduce the environmental toxicity while obtaining higher antifungal activity by introducing different cations into the polymer chain? [24–26] Therefore, in this work, based on previous work, i.e., the synthesis of a series of polydimethylsiloxane-grafted primary amine hydrochlorides (PDMS-g-AH), [16] we attempted to convert the primary amine salt into a guanidine salt, thus affording a series of polydimethylsiloxane-grafted guanidine salts (PDMS-g-GH) with different main chain lengths, main chain structures (random or block), and guanidine salt grafting rates. The inhibitory effects of PDMS-g-GH on Foc4 in culture media and in the soil environment and its environmental toxicity, including its impact on the soil microbial population and fish, and its relationship with polymer structure were also evaluated. In these works, we hope that a novel cationic polymer with low toxicity and high antifungal activity can be obtained.

2. Experimental section

2.1. Materials

1H-Pyrazole-1-carboxamide hydrochloride (HPC, 99 %), N,N-diisopropylethylamine (DIEA, 99 %), and benzalkonium chloride (BC,

99 %) were obtained from Shanghai Macklin Biochemical Technology Co., Ltd. (Shanghai, China).

Fusarium oxysporum f. sp. *cubense* race 4 (Foc4) was donated by the Fungal Laboratory, Department of Plant Pathology, South China Agricultural University. The soil (crushed and screened through a 20-mesh sieve) was taken from the banana field of the scientific research base of South China Agricultural University. The physicochemical properties of the soil are shown in Table S2. Zebrafish with a total length of 2 ± 0.5 cm and a weight of 0.2 ± 0.1 g were purchased from Shanghai Feixi Biotechnology Co., Ltd.

2.2. Synthesis of amphiphilic polysiloxane graft guanidine salts (PDMS-g-GH)

Polysiloxanes grafted with primary ammonium (PDMS-g-AH) with different chain lengths and structures, i.e., random copolymer (PDMS-co-AH) or block copolymer (PDMS-b-AH), as shown in Scheme 1, were synthesized via a thiol-ene “click” reaction between cysteamine hydrochloride and polydimethylsiloxane-polymethylvinylsiloxane (PDMS-PVMS), including random copolymer (PDMS-co-PVMS) and block copolymer (PDMS-b-PVMS), according to our previous work, where the chain lengths of PDMS-co-PVMS or PDMS-b-PVMS are 3, 5, and 8 kDa, and the graft ratios of primary ammonium, which are determined by the contents of PVMS in PDMS-PVMS, are 50 % and 75 %, respectively, as shown in Table S1. [16].

PDMS-g-GH was synthesized via a guanidine reaction between PDMS-g-AH and 1H-pyrazole-1-carboxamide hydrochloride (HPC), as shown in Scheme 1. Predetermined amounts of PDMS-g-AH and HPC were dissolved in 50 g of anhydrous ethanol in a 250 mL three-neck flask, and predetermined amounts of DIEA were added as catalysts under a nitrogen atmosphere. The mixture was reacted for 12 h at 55 °C, and most of the solvent was removed by rotary steaming at 70 °C. Then, the residue was precipitated three times using a mixed solvent of methanol and acetone and finally vacuum dried overnight at 60 °C (approximately 93 % yield).

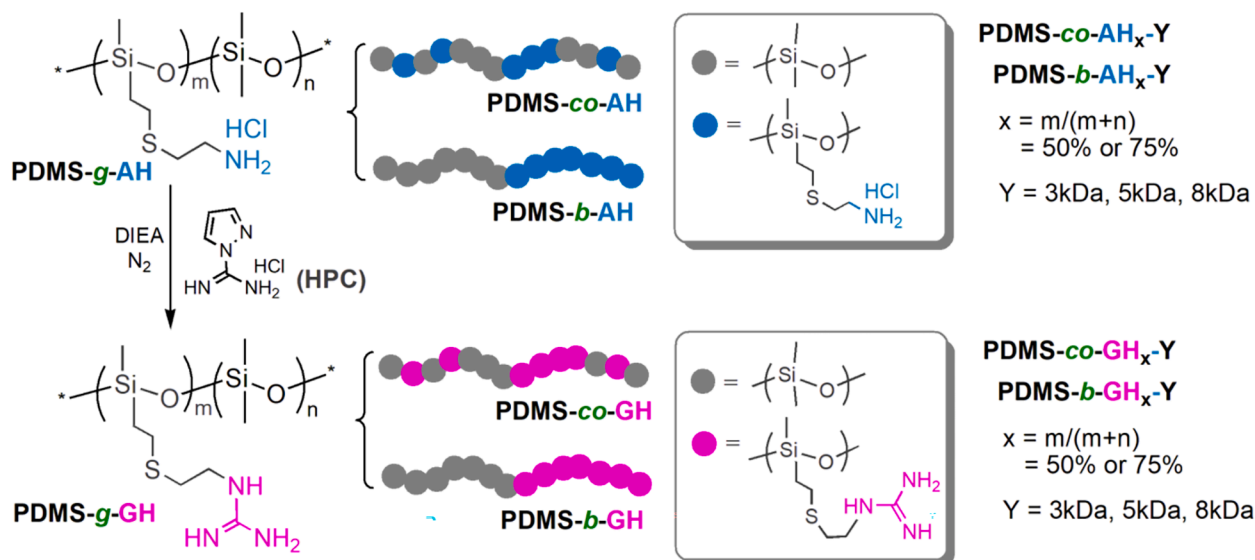
For convenience, PDMS-g-GH with a random structure and block structure are represented as PDMS-co-GH_x-Y and PDMS-b-GH_x-Y, respectively, where x represents the graft ratio of GH in PDMS-g-GH (50 % or 75 %), i.e., m/(m + n) in Scheme 1, and Y is the theoretical molecular weight of PDMS-PVMS (3 kDa, 5 kDa and 8 kDa).

¹H NMR (600 MHz, D₂O, δ , ppm): δ = 0–0.30 (m, 9H, –SiCH₃); 1.03 (t, 2H, –SiCH₂CH₂S–); 2.75 (t, 2H, –SiCH₂CH₂S–); 2.86 (t, 2H, –CH₂SCH₂–), 3.48 (t, 2H, –SCH₂CH₂NH); FT-IR (ν , KBr, cm^{–1}): 3400 (ν_{NH}), 2963 (ν_{asCH} , –CH₃), 1640 (δ C=N), 1095 ($\nu_{\text{Si-O}}$), 1020 ($\nu_{\text{Si-O}}$), 866 ($\nu_{\text{Si(CH}_3)_2}$), 802 ($\nu_{\text{asSi(CH}_3)_2}$).

2.3. Characterization and methods

FT-IR spectra were collected on a Nicolet iS5 Fourier transform infrared spectrometer (Thermo Scientific, USA) equipped with an iD7-ZnSe ATR accessory. ¹H NMR spectra were obtained using a Bruker Avance III HD 600 (Bruker Instrument Corp., Germany) spectrometer with CDCl₃ (for PDMS-PVMS) or D₂O (for PDMS-g-AH or PDMS-g-GH) as the solvent. The critical micelle concentration (CMC) was determined using a DDS-11A conductivity meter (Shanghai Hongyi Instrument Co. Ltd., China). Zeta potentials and particle size distributions were analyzed using a Brookhaven BI-90 Plus particle size analyzer (Brookhaven Instrument Corp., USA) with ultrapure water as the solvent. TEM was performed with a JEM-2100 transmission electron microscope (JEOL, Japan), in which PDMS-g-GH was prepared in a 1 g/L solution with ultrapure water, followed by dropping and drying onto a copper net with a carbon film.

The other methods, including the testing method for the adsorption of PDMS-g-GH in soil, the antifungal assay of PDMS-g-GH on Foc4 (in vitro and in soil), and the biotoxicity evaluation (culturable microbes in soil and fish acute toxicity evaluation), are detailed in the Supporting



Scheme 1. The synthetic route of PDMS-g-AH and PDMS-g-GH.

Information (Parts S2 to S4).

3. Results and discussion

3.1. Structural characterization of PDMS-g-GH

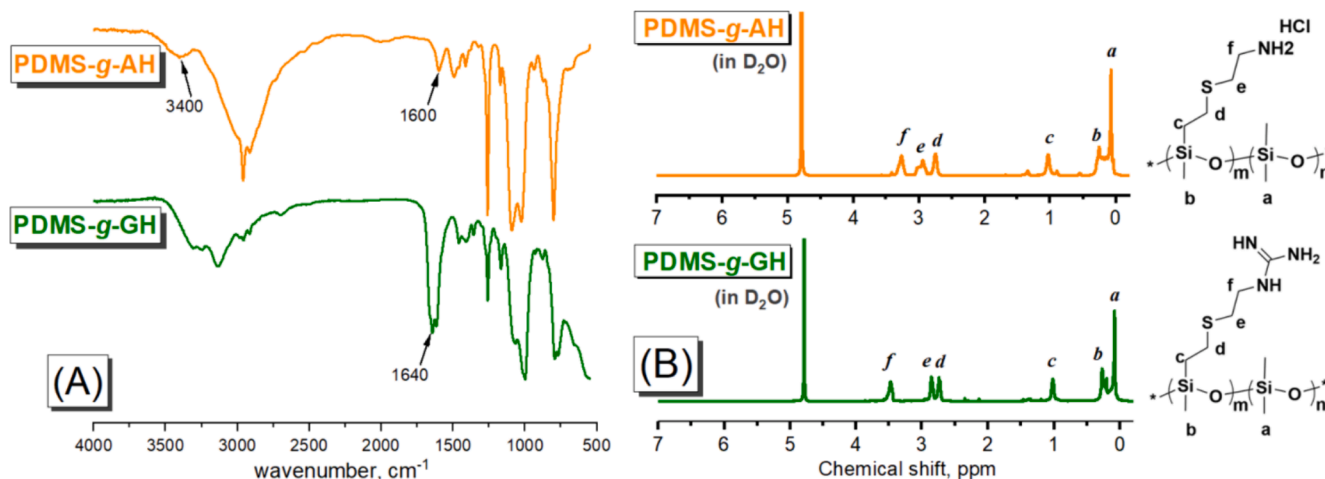
With respect to the guanidine products of PDMS-g-AH, the disappearance of the characteristic peak of the primary ammonium salts and the appearance of the characteristic peak of the guanidine salts could effectively support the synthesis of PDMS-g-GH. As shown in Fig. 1-A, the peak at 1640 cm^{-1} for PDMS-g-GH can be assigned to the guanidine groups, and the protons at 3.48 ppm ($-\text{SCH}_2\text{CH}_2\text{NH}$) (Fig. 1-B) confirmed the successful connection of the guanidine salts to the PDMS chain.

As shown in Scheme 1, there is only one simple side functional group conversion between PDMS-g-AH and PDMS-g-GH, and the molecular weight and molecular weight distribution of PDMS-g-GH are basically consistent with those of PDMS-g-AH, as described in our previous work [16].

3.2. Aggregation characteristics of PDMS-g-GH in water

The critical micelle concentration (CMC) of PDMS-g-GH was measured by the electrical conductivity method. Fig. 2-A shows the CMCs of PDMS-g-GH with different molecular weights and grafting degrees. The CMCs of the block type (PDMS-b-GH) were lower than those of the random type (PDMS-co-GH), while the molecular weights and grafting degrees were the same. Compared with those of PDMS-g-AH, [16] the CMCs of PDMS-g-GH are slightly greater, which might be related to the greater hydrophilicity of the guanidine salts.

The zeta potential and particle morphology of PDMS-g-GH in water are shown in Fig. 2-B and Figure S1, respectively. The results showed that polymers with low molecular weights exhibited low zeta potentials, indicating that it was easier for polymers to aggregate in water. Compared with PDMS-g-AH, [16] PDMS-g-GH with the same structure, i. e., the same chain length and chain structure (random or block), showed a lower zeta potential (Fig. 7-B) and larger particle size. Moreover, at concentrations much greater than the CMC, PDMS-g-GH could form spherical or hollow micelles (Figure S1), and a higher molecular weight would result in a larger diameter of the micelles.

Fig. 1. FTIR spectra (A) and ^1H NMR spectra (B) of PDMS-g-AH and PDMS-g-GH.

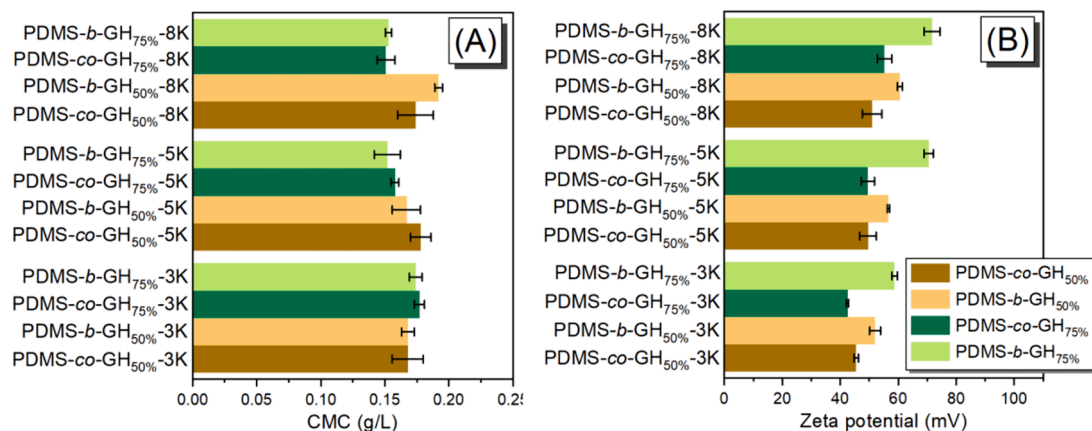


Fig. 2. The critical micelle concentration (CMC) (A) and zeta potentials (B) of PDMS-co-GH and PDMS-b-GH with different molecular weights (3, 5, and 8 kDa) and grafting degrees (50 % and 75 %, respectively). (Vertical bars represent the standard error of the means.).

3.3. The absorption effect of PDMS-g-GH in soil

Fig. 3 shows the sorption kinetics of PDMS-g-GH, PDMS-g-AH and BC in soils. After less than 3h, equilibrium adsorption of the three tested fungicides in soil was observed, after which the concentration of fungicides in the soil was almost unchanged (Fig. 3-A). Moreover, the overall adsorption kinetics of these three fungicides on the soil conformed to a pseudo-second-order model with coefficients of correlation (R^2) above 0.99 (Fig. 3-B). Both the Freundlich and Langmuir models were selected to fit the results (Fig. 3-C, D and Table S3), where the

Freundlich model showed a better regression coefficient (R^2), indicating that the adsorption of PDMS-g-GH, PDMS-g-AH and BC to the tested soil tended to be a multilayer adsorption process. The Freundlich constant ($1/n$) (Table S3) is related to the adsorption strength of the adsorbent: $1/n$ values of 0.1–0.5, 0.5–1.0, and > 1.0 indicate that adsorption is good, easy to adsorb, and difficult to adsorb, respectively. Thus, the $1/n$ values of PDMS-g-GH, PDMS-g-AH and BC are all greater than 0.5, indicating that they can be easily adsorbed in soil. The strong absorption effect of PDMS-g-GH and PDMS-g-AH in soil might be due to two main factors: first, the positive charge carried by the polymers can combine

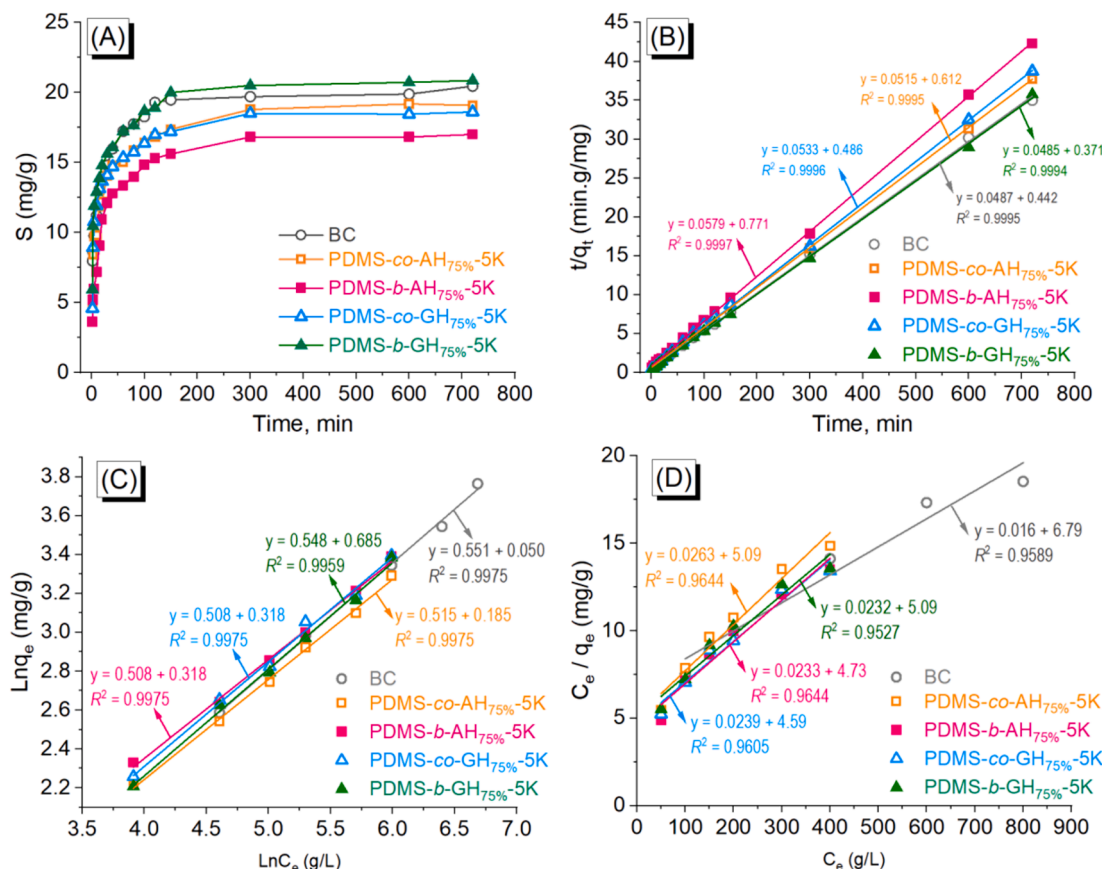


Fig. 3. Sorption kinetics and isotherms of PDMS-g-GH, PDMS-g-AH and BC in soils: (A) relationships between the sampling time and the PDMS-g-GH, PDMS-g-AH and BC concentrations in soils; (B) the pseudo-second-order model fit to the PDMS-g-GH, PDMS-g-AH and BC sorption kinetics data; (C) Freundlich sorption isotherms and (D) Langmuir sorption isotherms.

with the negative charge normally carried by soil particles (such as sludge and sediments); second, the long chain of polymers and the entanglement between polymer chains and soil particles. For BC, the first aspect mentioned above is the main reason.

3.4. Antifungal activities of PDMS-g-GH based on different evaluation methods

According to the different application scenarios of fungicides, there are several commonly used methods for evaluating antifungal activities, such as the TTC coloration method, inhibition of mycelial growth, and the spore counting method, which simulate the antifungal activities of fungicides in soil. The TTC coloration method evaluates the antifungal activity of fungicides when they come into free contact with fungal spores or mycelia in a liquid environment, in which the minimum inhibitory concentration (MIC) and minimum fungicidal concentration (MFC) are used to evaluate the antifungal activities. While for the method of inhibition of mycelial growth, fungal mycelia were cultured on solid or gel cultures containing fungicide, and the 50 % effective concentration (EC_{50}) and 90 % effective concentration (EC_{90}) were used to evaluate the antifungal activities. Since the contact between the mycelia and the culture medium is limited, the results might not reflect the true environment of fungicides in soil.

Considering that fungicides might be used in soil to inhibit soil-borne fungal spores, it is necessary to introduce the soil environment during the testing process. The spore counting method was designed for the application of fungicides in soil. To distinguish it from the aforementioned methods, EC_{50s} and EC_{90s} were used to evaluate the antifungal activities of fungicides in soil; here, the subscript “s” indicates soil.

The *in vitro* antifungal activities of PDMS-g-GH against Foc4, i.e., MIC and MFC and EC_{50} and EC_{90} , are shown in Figs. 4 and 5, respectively. Although the testing methods are different, the general trends of the polymer structure and antifungal activities are similar. For example, for the same molecular weight of the main chain, block polymers and polymers with higher graft rates showed stronger antifungal activities. Additionally, for both PDMS-g-AH and PDMS-g-GH, the MIC and MFC values on Foc4 are much lower than their CMC values, which means that micelles formed by single polymer chains play a dominant role in antifungal activity. Due to the different methods used for testing antifungal activities, the antifungal activities of the polymers were slightly different: PDMS-g-GH-5 K and PDMS-g-GH-8 K showed better antifungal

activities (Fig. 4) based on the MIC and MFC results, while PDMS-g-GH-5 K showed stronger antifungal activities based on the EC_{50} and EC_{90} results (Fig. 5). When the side group of the primary ammonium salt (AH) was converted to a guanidine salt (GH), the antifungal activity significantly increased, and the antifungal activity of PDMS-g-GH was almost double that of PDMS-g-AH.

In the subsequent evaluation of antifungal activities in soil, PDMS-g-AH and PDMS-g-GH, which have main chain molecular weights of 3 k and 5 k and high *in vitro* antifungal activity, respectively, were chosen for further evaluation of their EC_{50s} and EC_{90s} . Fig. 6 shows the 50 % inhibitory concentration (EC_{50s}) and 90 % inhibitory concentration (EC_{90s}) of PDMS-g-GH and PDMS-g-AH in inhibiting Foc4 spores in soil. Compared to the EC_{50} , the EC_{50s} had a much lower value, which is only approximately half of the EC_{50} . Although the *in vitro* anti-Foc4 activity of PDMS-g-GH was much lower than that of BC, the anti-Foc4 activity of PDMS-g-GH in soil was similar to or even greater than that of BC, which might be related to the chemical structure of the guanidine group and the hydrophilic-hydrophobic balance of PDMS-g-GH. Although the antifungal activity of PDMS-g-GH was stronger than that of PDMS-g-AH, these two series of fungicides exhibited a pattern of greater zeta potential and stronger anti-Foc4 activities, in which the block polymers showed greater zeta potential and stronger anti-Foc4 activities than the random polymers (Fig. 7-B), which might be due to the tighter aggregation of cations in the block copolymers. It was also found that there was a good linear relationship between the EC_{50s} and EC_{50} , as shown in Fig. 7-A. The difference between the EC_{50} and EC_{50s} might be related to the testing conditions of the EC_{50s} , in which the polymer chains have more opportunities and sufficient contact with soil and Foc4 spores, and effective contact between fungicides and spores would result in better antifungal activities. These results provide us with some inspiration for designing and synthesizing cationic polymers with high zeta potentials to obtain fungicides with better antifungal activity.

The rapid spread of Foc4 caused by agricultural production (banana seedling transportation, the use of production equipment, etc.) was one of the main reasons for the rapid spread of banana Fusarium wilt; thus, the ability to continuously and repeatedly inhibit newly transmitted Foc4 spores, i.e., the persistence of fungicides on Foc4 in soil, should be important for the control of banana Fusarium wilt. Therefore, by adding a Foc4 spore suspension to soil every 10 d, the persistence of different concentrations of fungicides in the soil was evaluated. As shown in Figure S3, both PDMS-g-AH and PDMS-g-GH were unable to kill all the

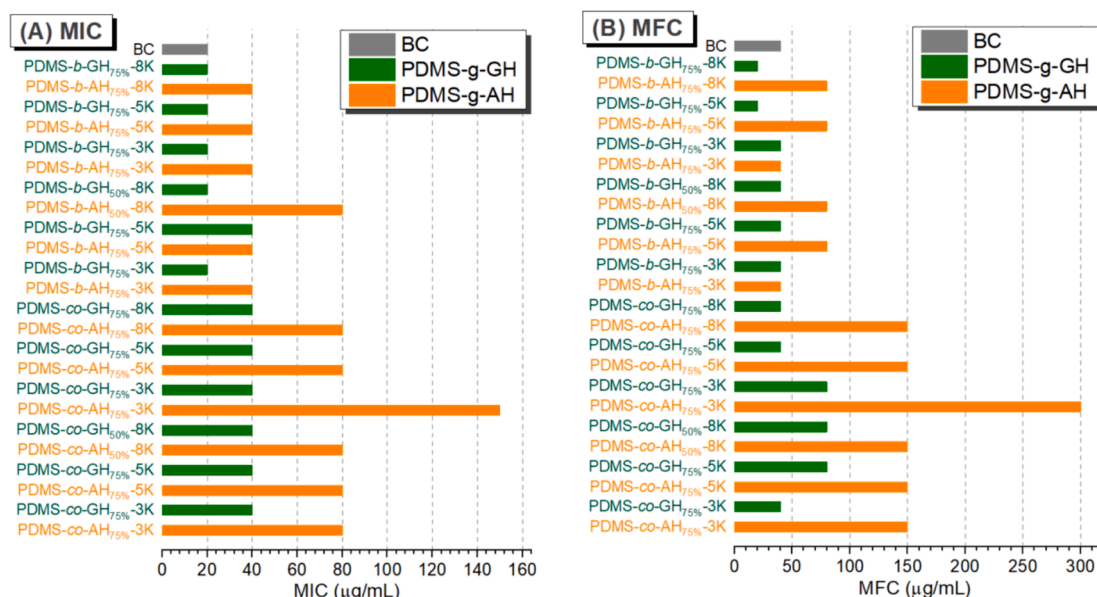


Fig. 4. MICs (A) and MFCs (B) of PDMS-g-GH and PDMS-g-AH against Foc4.

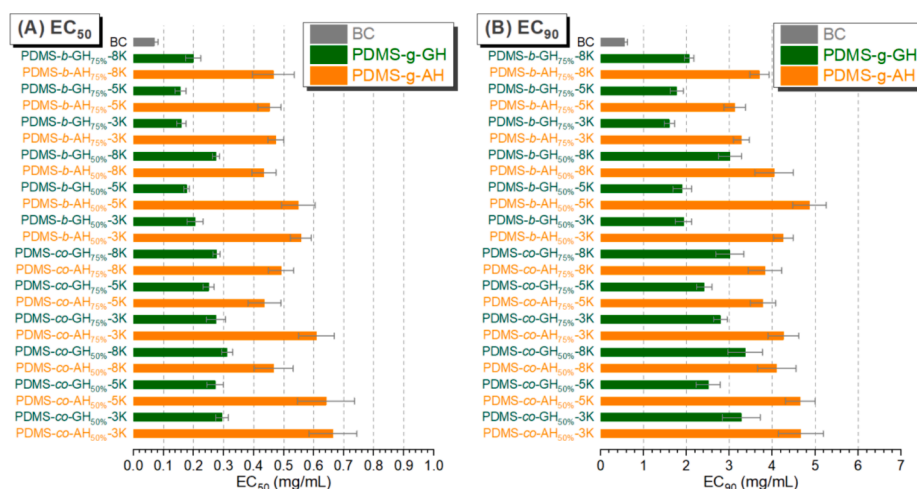


Fig. 5. EC_{50} and EC_{90} of PDMS-g-GH and PDMS-g-AH against Foc4 (Vertical bars represent the standard error of the means.).

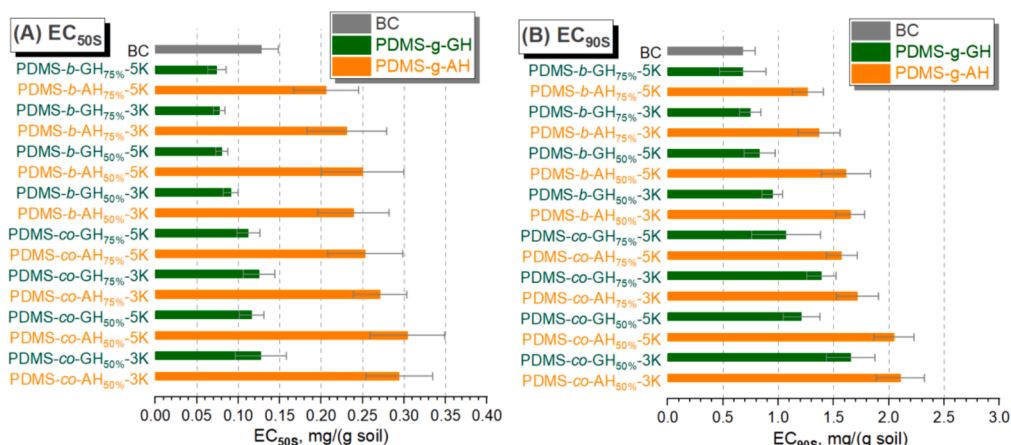


Fig. 6. EC_{50S} (A) and EC_{90S} (B) of PDMS-g-GH and PDMS-g-AH against Foc4 in soil (Vertical bars represent the standard error of the means.).

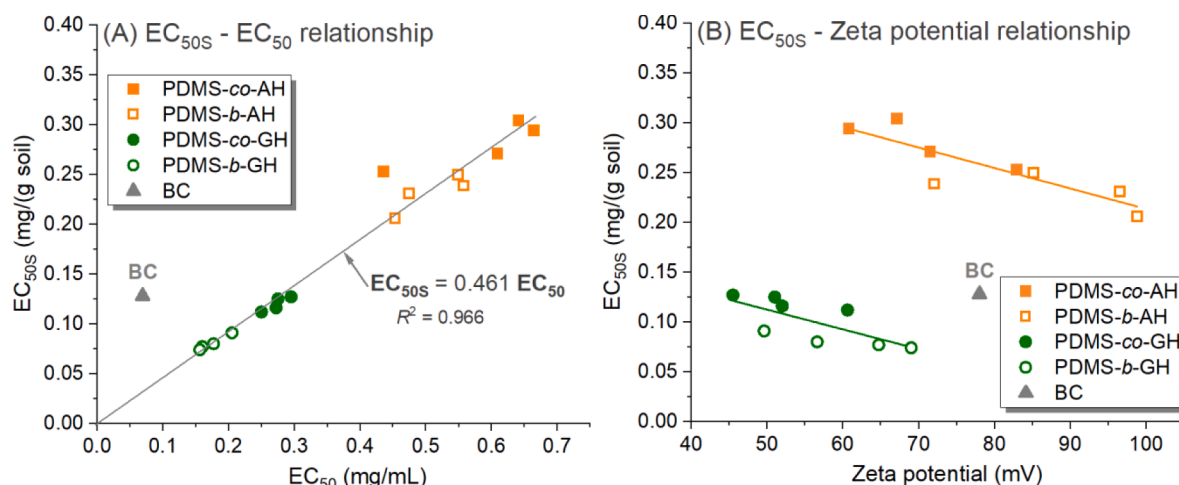


Fig. 7. The EC_{50S} – EC_{50} relationship (A) and the EC_{50S} – zeta potential relationship (B) of PDMS-g-GH and PDMS-g-AH.

Foc4 spores in the soil at concentrations of $1 \times EC_{50S}$ and $4 \times EC_{50S}$. When the concentration exceeded $16 \times EC_{50S}$, it could effectively kill Foc4 spores in the soil for a duration of 30 d. However, for BC, after the second addition of Foc4 spores, Foc4 colonies appeared on PDA media at 20 d, indicating that compared with PDMS-g-AH and PDMS-g-GH, BC

had a shorter persistence of Foc4 in soil. The results indicate that lower concentrations of PDMS-g-AH and PDMS-g-GH can effectively inhibit Foc4 spores in soil for longer durations.

3.5. The environmental impact of PDMS-g-GH

The development of antimicrobial agents with low toxicity and high efficiency is one of the important principles for the design of fungicides. Here, so-called low toxicity refers to minimizing the impact on other living organisms in the environment, such as soil microorganisms, environmental water that is in direct contact with soil, and the fish that survive in the environment, while suppressing pathogenic fungi.

Fig. 8 shows the effects of the PDMS-g-AH, PDMS-g-GH and BC treatments on the total number of culturable populations of bacteria, fungi and actinomycetes in the soil. Compared to BC, PDMS-g-AH and PDMS-g-GH effectively inhibited fungal growth, while the total number of bacterial and actinomycete communities increased. PDMS-g-GH had a greater inhibitory effect on the total number of fungal colonies than did PDMS-g-AH.

The influence of BC, PDMS-g-AH and PDMS-g-GH on the number of soil microbes might be related to the stable adsorption of PDMS-g-AH and PDMS-g-GH in soil and their antifungal activities in soil. As mentioned above, most of the PDMS-g-AH and PDMS-g-GH chains were stably adsorbed on the surface of the soil particles, which greatly reduced the effective contact probability between the free polymer chains and the microorganisms in the soil; thus, the antimicrobial activities of these cation polymers would be reduced and prolonged. In comparison, the weaker absorption of BC in soil might help to maintain the strong antimicrobial activities of BC, thus resulting in broad-spectrum inhibition of microorganisms in soil.

One possible explanation is that the bacteria, fungi, and actinomycetes in the soil ecosystem are in a dynamic equilibrium relationship. Since both PDMS-g-AH and PDMS-g-GH have different inhibitory effects on microorganisms in the soil, when they have a good inhibitory effect on fungi and greatly reduce their number, the bacteria and actinomycetes in the soil will be relatively conducive to reproduction and increase due to the reduction in competition. [14] In summary, the application of PDMS-g-GH in soil can shift the soil toward bacterial soil, which is beneficial for plant growth. Notably, the detailed strains of bacteria, fungi and actinomycetes after treatment with BC, PDMS-g-AH and PDMS-g-GH should be intensively investigated in the future.

Fig. 9 shows the acute toxicity of PDMS-g-AH and PDMS-g-GH to zebrafish under different conditions, i.e., direct toxicity (LC_{50}), soil/water mixture (LC_{50S}) and leachate of soil (LC_{50L}). Compared to the high toxicity of BC ($LC_{50} < 1.0$ mg/L), the direct toxicity of PDMS-g-AH was

lower and remained in the moderate toxicity range ($1.0 < LC_{50} < 10.0$ mg/L), while the direct toxicity of PDMS-g-GH was much lower and already located in the low toxicity range ($LC_{50} > 10.0$ mg/L), indicating that the conversion of primary amine salts (AH) to guanidine salts (GH) is beneficial for reducing the biological toxicity of PDMS-g-GH. In addition to direct application to aqueous solutions, considering that PDMS-g-GH is mainly applied to soil in the form of aqueous solutions, we also measured the toxicity of PDMS-g-AH, PDMS-g-GH, and BC after being adsorbed by soil and leached into environmental water by rainwater, namely, LC_{50L} and LC_{50S} . As shown in Fig. 9, due to the strong adsorption effect of these three fungicides in the soil, the amount of free fungicides lost to the environment after soil adsorption is significantly reduced, resulting in a significant reduction in their environmental toxicity. The LC_{50L} and LC_{50S} of BC were 50 mg/(kg soil) and 110 mg/(kg soil), respectively, reaching the range of low toxicity or practically nontoxic, while for PDMS-g-AH and PDMS-g-GH, their LC_{50L} and LC_{50S} are greater than 600 mg/(kg soil), which means that they are practically nontoxic and can be safely used in farmland soil.

4. Conclusions

In this paper, a series of random and block-type polysiloxane graft guanidine salts (PDMS-g-GHs) with tunable molecular weights, grafting degrees, and chain structures (random or block) were synthesized based on the guanidine reaction of polysiloxane graft primary amine salts (PDMS-g-AHs). Compared with PDMS-g-AH, PDMS-g-GH showed stronger antifungal activity against Foc4 and long-term antifungal activity against Foc4 in soil, but its environmental toxicity was significantly reduced. Block-type PDMS-g-GH, i.e., PDMS-b-GH, showed greater zeta potential, stronger anti-Foc4 activity and lower environmental toxicity than did the random type (PDMS-co-GH). These results support the potential application of PDMS-g-GH for the prevention and control of banana Fusarium wilt and other soil-borne fungal diseases.

CRediT authorship contribution statement

Yaling Lin: Writing – review & editing, Writing – original draft, Supervision, Funding acquisition, Conceptualization. **Shiqi He:** Writing – original draft, Methodology, Data curation. **Mingyang Wu:** Data curation. **Meng Hou:** Data curation. **Rui Li:** Writing – original draft, Methodology, Data curation. **Anqiang Zhang:** Writing – review &

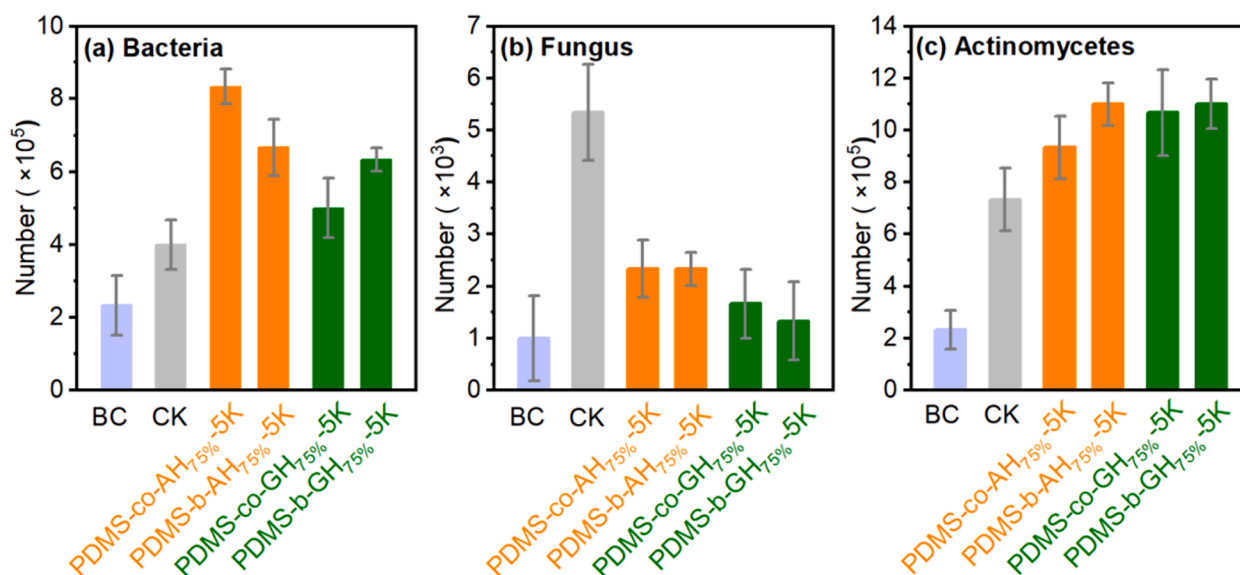


Fig. 8. Culturable populations of bacteria (A), fungi (B) and actinomycetes (C) in soil from the PDMS-g-GH and PDMS-g-AH treatments (Vertical bars represent the standard error of the means.)

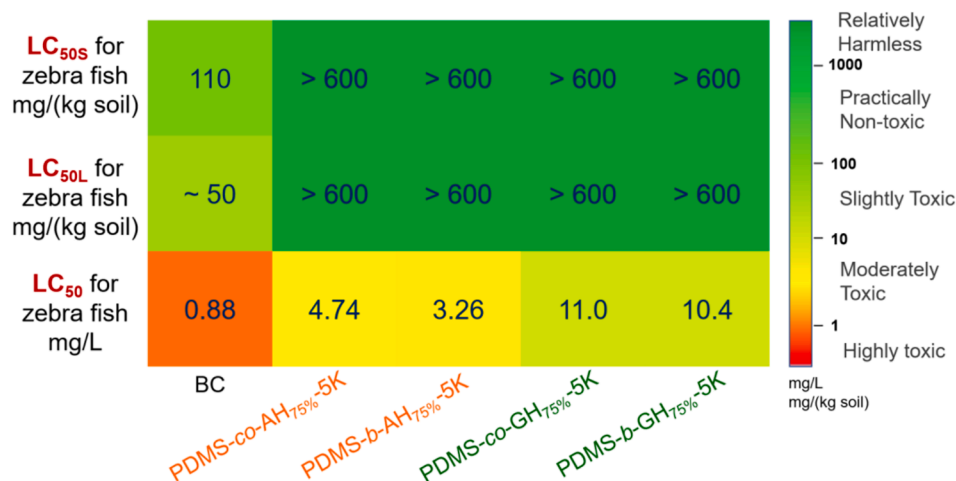


Fig. 9. LC₅₀, LC_{50L}, and LC_{50S} of PDMS-g-AH, PDMS-g-GH and BC for zebrafish (*Danio rerio*) (96 h) (Potassium dichromate and chloroacetamide were used as zebrafish and earthworm reference poisons, respectively. BC was used as a positive control. Average of three replicates.).

editing, Supervision, Methodology, Funding acquisition, Conceptualization.

Declaration of competing interest

The authors declare that they have no known competing financial interests or personal relationships that could have appeared to influence the work reported in this paper.

Data availability

Data will be made available on request.

Acknowledgements

The authors acknowledge the financial support from the National Natural Science Foundation of China (Nos. 52073098 and 31772202) and the Scientific and Technological Planning Project of Guangzhou City (201803020015).

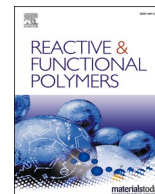
Appendix A. Supplementary material

Detailed methods and results including molecular weight of PDMS-co-PVMS and PDMS-b-PVMS, the methods for soil-polymer interaction experiments, the methods for evaluation of antifungal activities, the methods and results for the evaluation of persistence of PDMS-g-AH and PDMS-g-GH on Foc4 in soil, the methods for biotoxicity evaluation, can be found in Supporting Information. Supplementary data to this article can be found online at <https://doi.org/10.1016/j.eurpolymj.2024.113258>.

References

- [1] R.C. Ploetz, Fusarium wilt of banana is caused by several pathogens referred to as *Fusarium oxysporum* f. sp. *cubense*, *Phytopathology* 96 (6) (2006) 653–656.
- [2] Janet MR, Lilia CC, Cecilia O'D, Vivian AR, Andre D. Diagnostics of Fusarium wilt in banana: Current status and challenges. *Plant Pathology*. 2024, 1-17, DOI: 10.1111/ppa.13863.
- [3] B.G. Siddhesh, K.S.S. Upendra, R.G. Thumballi, Fusarium wilt of banana: Biology, epidemiology and management, *Int. J. Pest Manage.* 61 (3) (2017) 250–263.
- [4] D. Miguel, B. Marcia, H. Daniel, S. Eduardo, P.S. Charles, Fusarium wilt of banana: current knowledge on epidemiology and research needs toward sustainable disease management, *Front. Plant Sci.* 9 (10) (2018) 146.
- [5] W.M. Li, M. Dita, W. Wu, G.B. Hu, X.J. Ge, Resistance sources to *Fusarium oxysporum* f. sp. *cubense* tropical race 4 in banana wild relatives, *Plant Pathol.* 64 (5) (2015) 1061–1067.
- [6] S. Hong, H.L. Jv, M. Lu, B.B. Wang, Y.Z. Ruan, Significant decline in banana Fusarium wilt disease is associated with soil microbiome reconstruction under chilli pepper-banana rotation, *Eur. J. Soil Biol.* 97 (2020) 103154.
- [7] Z.Z. Shen, C.R. Penton, N.N. Lv, C. Xue, X.F. Yuan, Y.Z. Ruan, R. Li, Q.R. Shen, Banana Fusarium wilt disease incidence is influenced by shifts of soil microbial communities under different monoculture spans, *Microb. Ecol.* 75 (2018) 739–750.
- [8] T.V. Nguyen, L.T.T. Tran-Nguyen, C.L. Wright, et al., Evaluation of the efficacy of commercial disinfectants against *Fusarium oxysporum* f. sp. *cubense* race 1 and tropical race 4 propagules, *Plant Dis.* 103 (4) (2019) 721–728.
- [9] T. Bratec, N. Kirchhübel, N. Baranovskaya, et al., Towards integrating toxicity characterization into environmental studies: case study of bromine in soils, *Environ. Sci. Pollut. Res.* 26 (2019) 19814–19827.
- [10] G.Q. Lu, D.C. Wu, R.W. Fu, Studies on the synthesis and antibacterial activities of polymeric quaternary ammonium salts from dimethylaminoethyl methacrylate, *React. Funct. Polym.* 67 (4) (2007) 355–366.
- [11] W.Q. Zhong, Y. Chang, Y.L. Lin, A.Q. Zhang, Synthesis and antifungal activities of hydrophilic cationic polymers against *Rhizoctonia solani*, *Fungal Biol.* 124 (2020) 735–741.
- [12] Y.Y. Chang, W.Q. Zhong, J.Q. Liang, A.Q. Zhang, Y.L. Lin, Polydimethylsiloxane-polymethacrylate block copolymers containing quaternary ammonium salts against *Fusarium oxysporum* f. sp. *cubense* race 4 in soil: Antifungal activities and pot experiments, *React. Funct. Polym.* 160 (2021) 104848.
- [13] X.Q. Yin, P.F. Tan, Z.P. Gu, Z.M. Liu, L. Tan, Polymeric antibacterial materials: design, platforms and applications, *J. Mater. Chem. B* 9 (12) (2021) 2802–2815.
- [14] Y.L. Lin, D.Q. Zhang, S.J. Shan, W. Zhang, R. Li, A.Q. Zhang, Fluorine-containing amphiphilic quaternary ammonium salts for the suppression of Banana fusarium wilt, *React. Funct. Polym.* 182 (2023) 105488.
- [15] W. Zhang, J.G. Yu, M.Y. Wu, R. Li, A.Q. Zhang, Y.L. Lin, Polyacrylamide quaternary ammonium salts based on stable adsorption in soil and its application on the control of soil-borne fungal disease, *Eur. Polym. J.* 202 (2024) 112604.
- [16] S.Q. He, M. Hou, S.J. Shan, R. Li, N. Yu, Y.L. Lin, A.Q. Zhang, Synthesis and antibacterial/fungal activities of amphiphilic polysiloxanes primary ammonium salts, *React. Funct. Polym.* 183 (2023) 105495.
- [17] Y.L. Lin, W.Q. Zhong, C.Y. Dong, C. Zhang, X.X. Feng, A.Q. Zhang, Synthesis and antifungal activities of amphiphilic PDMS-b-QPDMAEMA copolymers on *Rhizoctonia solani*, *ACS Appl. Bio Mater.* 1 (6) (2018) 2062–2072.
- [18] K. Kuroda, W.F. DeGrado, Amphiphilic polymethacrylate derivatives as antimicrobial agents, *J. Am. Chem. Soc.* 127 (2005) 4128–4129.
- [19] G.J. Gabriel, A.E. Madkour, J.M. Dabkowski, et al., Synthetic mimic of antimicrobial peptide with nonmembrane-disrupting antibacterial properties, *Biomacromolecules* 9 (2008) 2980–2983.
- [20] K.E.S. Locock, T.D. Michl, J.D.P. Valentin, et al., Guanylated polymethacrylates: A class of potent antimicrobial polymers with low hemolytic activity, *Biomacromolecules* 14 (2013) 4021–4031.
- [21] H. Liu, M.M. Han, X. Liu, S.X. Ji, Guanylation significantly enhances the antifungal activity of poly(L-lysine), *ACS Appl. Mater. Interfaces* 4 (10) (2022) 7508–7517.
- [22] X.Y. Zhou, J. He, C.C. Zhou, Strategies from nature: polycaprolactone-based mimetic antimicrobial peptide block copolymers with low cytotoxicity and excellent antibacterial efficiency, *Polym. Chem.* 10 (8) (2019) 945–953.
- [23] X. Liu, Y.L. Yang, M.M. Han, J.W. Guo, et al., Guanylated hyperbranched polylysines with high *in vitro* and *in vivo* antifungal activity, *Adv. Healthc. Mater.* 11 (2022) 2201091.

- [24] P. Pham, S. Oliver, C. Boyer, Design of antimicrobial polymers, *Macromol. Chem. Phys.* 224 (3) (2023) 1–28.
- [25] H. Choi, K.J. Kim, D.G. Lee, Antifungal activity of the cationic antimicrobial polymer-polyhexamethylene guanidine hydrochloride and its mode of action, *Fungal Biol.* 121 (2017) 53–60.
- [26] N.D. Koromilas, G.C. Lainioti, G. Vasilopoulos, A. Vantarakis, J.K. Kallitsis, Synthesis of antimicrobial block copolymers bearing immobilized bacteriostatic groups, *Polym. Chem.* 7 (2016) 3562–3575.



Fluorine-containing amphiphilic quaternary ammonium salts for the suppression of Banana fusarium wilt

Yaling Lin^{a,*}, Deqiang Zhang^b, Shijie Shan^b, Wei Zhang^a, Rui Li^b, Anqiang Zhang^{b,*}

^a College of Materials and Energy, South China Agricultural University, 483 Wushan Rd., Guangzhou 510642, Guangdong, China

^b School of Materials Science and Engineering, South China University of Technology, 381 Wushan Rd., Guangzhou 510641, Guangdong, China

ARTICLE INFO

Keywords:

Polymeric quaternary ammonium salt
Fluoroalkyl group
Banana fusarium wilt
Antifungal activities

ABSTRACT

As the pathogen of banana Fusarium wilt, *Fusarium oxysporum* f. sp. *cubense* race 4 (Foc4) has the strongest toxicity and pathogenicity due to its long-term viability in soil, but there is still no effective way to control it at present. Based on the activity parameters of polymeric quaternary ammonium salt in our previous work, this paper hopes to enhance the amphiphilicity of polymeric quaternary ammonium salt by introducing a fluoroalkyl group to improve the antifungal property of polymeric quaternary ammonium salt and achieve stable adsorption and long-term inhibition of saprophytic Foc4 conidia in soil. Here, we prepared a series of fluorine-containing ammonium salts with random and block structures by atom transfer radical polymerization (ATRP), and we systematically studied the effects of the introduction of fluoroalkyl groups, the proportion of hydrophobic segments and polymer structure on micelle properties, antifungal properties, adsorption, migration and long-term antifungal properties against Foc4 in soil. Finally, the preferred polymeric quaternary ammonium salts were selected for pot experiments in the prevention and control of banana Fusarium wilt caused by Foc4, and positive experimental results were achieved. In conclusion, we made an exploratory attempt at the practical application of polymeric amphiphilic quaternary ammonium salt in plant disease control.

1. Introduction

Banana Fusarium wilt is a common soil-borne disease in banana plantations that causes immeasurable losses to the agricultural economy every year. *Fusarium oxysporum* f. sp. *cubense* race 4 (Foc4) has the strongest toxicity and pathogenicity due to its strict asexual reproduction ability and long-term viability in soil. Foc4 initially infects a plant by invading the xylem of the plant and establishing a biological nutritional relationship with the host. Then, the plant is killed by transforming the host tissue into necrotic nutrients [1–3]. Infected plants continue to release pathogens into the surrounding soil and infect surrounding plants or exist in the soil as chlamydospores for a long time. Once the environment changes, they infect the plants again and cause disease [4].

Two methods of chemical control used in practice are as follows. The first uses chemical agents to inhibit the number of pathogens in the soil. Some small-molecule drugs screened based on indoor virulence determination and pot experiments such as prochloraz, propiconazole, and pentachloronitrobenzene have a certain control effect on Foc4. However, small-molecule drugs easily lose their effect on soil erosion and

decomposition in soil. As a result, the control effect in practice is poor [5,6]. The second method can be called “soil disinfection,” where all microorganisms in the soil are killed by physical, chemical, or biological methods such as soil heating and fumigation. Among them, fumigation with small-molecule chemicals represented by minocycline (tetrahydro-3,5-dimethyl-2-h-1,3,5-thiadiazine-2-thione) [7], lime nitrogen (calcium cyanamide), and chlorine dioxide is the main method of field control at present. However, this method completely destroys the microbial community structure in the soil, so it is necessary to introduce new organic matter to restore the soil after treatment, which is not conducive to the stability of the soil ecosystem. In addition, biological control and crop rotation are difficult to implement effectively on a large scale due to the high economic cost and the inability to plant continuously [8,9]. As a result, there is no economically feasible way to treat Foc4 while maintaining the diversity of the soil ecosystem [10–12].

Based on the severe situation of Foc4 and the lack of strategies of small-molecule drugs, polymeric quaternary ammonium salts, which are also used as antifungal agents [13], have become a research hot spot of plant disease control. Compared with small-molecule antibiotics, the amphiphilic structure of antibacterial cationic polymers can make them

* Corresponding authors.

E-mail addresses: linyaling@scau.edu.cn (Y. Lin), aqzhang@scut.edu.cn (A. Zhang).

<https://doi.org/10.1016/j.reactfunctpolym.2022.105488>

Received 8 October 2022; Received in revised form 11 December 2022; Accepted 12 December 2022

Available online 15 December 2022

1381-5148/© 2022 Published by Elsevier B.V.

fold into a secondary structure with surface affinity and cations to produce a strong interaction with biofilm [14,15]. In addition, the structure and performance of antifungal cationic polymers have advantages such as the possibility of regulation, low synthesis cost, non-volatility, impermeability to skin, long circulation time, strong biological activity, stability, low residual toxicity to the environment, and delayed development of drug resistance. In the past ten years, new antifungal cationic polymers and their related research have developed rapidly [16,17].

In our previous work, we obtained a series of polymeric quaternary ammonium salts by changing the main chain structure, molecular weight, cationic group, hydrophilic-hydrophobic ratio, and other parameters of antibacterial cationic polymers [18–20]. It was found that the appropriate molecular weight and hydrophilic-hydrophobic balance might have an important impact on the antibacterial activity of antifungal cationic polymers [21,25]. In addition, the type of hydrophobic group seriously affected the antifungal activity. A series of studies were conducted on the relationship between quaternary ammonium salt structures [26,27], hydrophilic-hydrophobic balance, molecular weight [28,29], lateral base length [30], anti-ion [31,32], and antifungal activity. However, research on the effects of strong hydrophobic fluoroalkyl groups in quaternary ammonium salts has rarely been reported.

Compared with conventional antibacterial or antifungal agents, the antifungal agents for soil-borne disease have to face the complex interactions with soil, such as adsorption and inactivation, which might obviously affect their antifungal efficacy. Although our previous studies have confirmed that amphiphilic polymeric quaternary ammonium salts showed strong adsorption in soil [41,42], it is still unclear on the effect of the introduction of fluorine containing hydrophobic groups. As a potential antifungal agents for the control of banana *Fusarium* wilt, the environmental impact, such as the effect on the microbial diversity in soil, the toxicity of its leaching solution to zebra fish, and also including the pot experiments, should be comprehensively evaluated.

In this work, fluoroalkyl segments, which are more hydrophobic than carbon-hydrogen chains, are introduced into polymeric quaternary ammonium salts. Two types of polymeric fluorine-containing quaternary ammonium salts, i.e., F_1 -co- Q_5 and F_1 -b- Q_5 , are obtained by controlling the feeding sequence and reaction time in an atom transfer radical polymerization method (ATRP). We hope that the introduction of fluoroalkyl groups into polymeric quaternary ammonium salts will enhance the amphiphilicity of polymers with lower surface tension, excellent water-soluble stability, good adsorption in soil, and low environmental toxicity, and thus enhance long-term antifungal activities in soil. We systematically studied the effect of the fluoroalkyl group ratio and position of the fluoroalkyl group in the polymer chain on antifungal activities against *Foc4* in vitro or in soil, biological toxicity, soil adsorption, and migration characteristics. Then, pot experiments were conducted to confirm the growth-promoting effect of the synthesized fluorine-containing polymeric quaternary ammonium salts on normal banana plants and the control effect on *Foc4*.

2. Experimental

2.1. Materials

2-(Dimethylamino)ethyl methacrylate (DMAEMA, 99%), 2,2,2-trifluoroethyl methacrylate (DMAFMA, 99%), ethyl 2-bromoisobutyrate (EtBrIB, 98%), N, N, N', N'', N''-pentamethyldiethylenetriamine (PMDETA, 98%), and copper(I) bromide (CuBr, 99%) were purchased from Aladdin (Shanghai, China). Benzyl chloride and 2,3,5-triphenyltetrazolium chloride (TTC) were purchased from Sangon Biotech (Shanghai) Co., Ltd. (Shanghai, China). Potato dextrose agar medium (PDA) and beef extract peptone medium were prepared according to [20,22]. The fungal strain *Fusarium oxysporum* f. sp. *cubense* race 4 (*Foc4*), *Candida albicans* (*C. albicans*), and the bacterial strains *Escherichia coli* (*E. coli*) and *Staphylococcus albus* (*S. albus*) used in this study

were kindly supplied by the Fungal Laboratory of the University of South China Agricultural. Soil samples and banana seedlings were obtained from the Institute of Fruit Trees, Guangdong Academy of Agricultural Sciences, China.

2.2. Synthesis of QPDMAEMA (Q_5)

PDMAEMA (D_3) was synthesized as shown in Scheme 1.

The polymerization procedure was as follows: A calculated amount of EtBrIB, PMDETA, and CuBr was added to 80 g mixed solvent (toluene/ethanol = 1/1, m/m) in a 250-mL Schlenk flask. After three freeze-pump-thaw cycles, the reaction system was filled with nitrogen, DMAEMA was injected into the mixture, and the reaction mixture was stirred at 50 °C for a set time. Subsequently, the reaction mixture was exposed to air, and the catalyst was removed by neutral alumina column chromatography with acetone as the eluent. Then, the reaction mixture was dried under vacuum at 130 °C for 3 h, and the product (D_3) was obtained (ca. yield 73%). Here, the number average molecular weight of PDMAEMA was designed as approximately 3 kDa, so it is abbreviated as D_3 , and the antifungal activity of D_3 after quaternization is better according to [18].

^1H NMR (400 MHz, CDCl_3 , δ , ppm): 0.9–1.25 (s, C- CH_3), 1.82–1.94 (s, C- CH_2 -C), 2.28 (s, N(CH_3) $_2$), 2.57 (t, N- CH_2 - CH_2), 4.06 (t, O- CH_2 - CH_2). FT-IR (KBr, ν , cm^{-1}): 2952–2773 (ν_{CH}), 1730 ($\nu_{\text{C=O}}$).

QPDMAEMA (Q_5) was designed with a number average molecular weight of 5 kDa and synthesized via a quaternization reaction between D_3 and benzyl chloride: D_3 was dissolved in 80 g mixed solvent (toluene/ethanol = 1/1, m/m) in a 250-mL Schlenk flask. After three freeze-pump-thaw cycles, the reaction system was filled with a nitrogen atmosphere, then 4 times the amount of BC was injected into the mixture, and the reaction system was stirred at 70 °C for 48 h. Subsequently, the reaction system was dried under vacuum at 70 °C to remove most of the solvent, and anhydrous diethyl ether was added to the mixture to precipitate the product. After washing with diethyl ether three times, the precipitate was dried under vacuum at 40 °C overnight (ca. yield 90%).

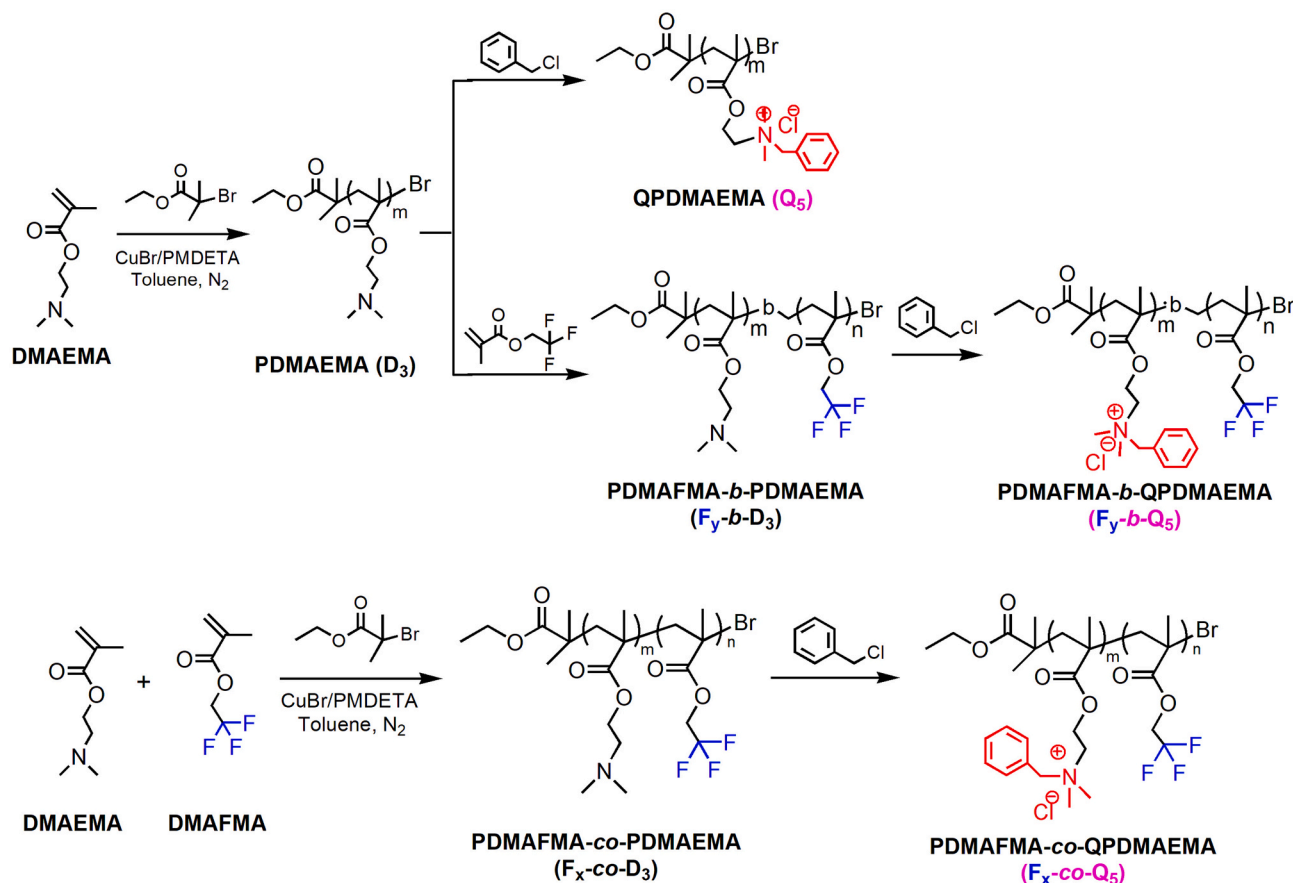
^1H NMR (600 MHz, methanol- d_4 , δ , ppm): 1.2 (s, C- CH_3), 3.28 (s, N $^+$ (CH_3) $_2$), 4.05 (t, CH_2 - CH_2 -N $^+$), 4.65 (m, CH_2 - CH_2 -N $^+$), 7.56, 7.72 (s, Φ -H). FT-IR (KBr, ν , cm^{-1}): 2983 (ν_{CH}), 1734 ($\nu_{\text{C=O}}$), 717, 768 ($\nu_{\Phi\text{-H}}$).

2.3. Synthesis of PDMAFMA-co-QPDMAEMA (F_x -co- Q_5) and PDMAFMA-b-QPDMAEMA (F_y -b- Q_5)

PDMAFMA-b-PDMAEMA (labeled F_y -b- D_3) and PDMAFMA-co-PDMAEMA (labeled F_x -co- D_3) were synthesized by atom transfer free radical polymerization similar to the synthesis route of D_3 . The difference is that the synthesis of F_y -b- D_3 is a two-step process. First, the calculated DMAEMA monomer is added to the reaction system and reacts to a set time, and then the DMAFMA monomer is added to react. The F_x -co- D_3 is synthesized by adding the calculated DMAEMA and DMAFMA monomers into the reaction system together through a one-step method, reacting to the set time and processing to obtain the product (ca. yield 70–75%). For F_y -b- D_3 and F_x -co- D_3 , the subscript “3” indicates that the designed molecular weight of the DMAEMA unit is approximately 3 kDa, and the subscripts “x (1 to 5)” and “y (1 to 5)” indicate that the designed molecular weights of the DMAFMA unit are 1, 2, 3, and 5 kDa, respectively.

^1H NMR (600 MHz, CDCl_3 , δ , ppm): 4.36 ppm (s, 2H, CH_2CF_3 from PDMAFMA); 4.07 ppm (s, 2H, $\text{CH}_2\text{CH}_2\text{N}(\text{CH}_3)_2$ from PDMAEMA); 2.56 ppm (s, 2H, $\text{CH}_2\text{CH}_2\text{N}(\text{CH}_3)_2$ from PDMAEMA); 2.21 ppm (s, 6H, $\text{CH}_2\text{CH}_2\text{N}(\text{CH}_3)_2$ from PDMAEMA); 1.92 to 1.50 ppm (m, 2H, CH_2 -from backbone); 1.25 to 0.81 ppm (m, 3H, CH_3 from backbone). FT-IR (KBr, ν , cm^{-1}): 2955–2773 (ν_{CH}), 1725 ($\nu_{\text{C=O}}$), 660 ($\delta_{\text{C-F}}$).

F_x -co- Q_5 and F_y -b- Q_5 were synthesized via a quaternization reaction between F_x -co- D_3 , F_y -b- D_3 and benzyl chloride, respectively. The F_x -co- D_3 and F_y -b- D_3 were dissolved in 80 g mixed solvent (toluene/ethanol = 1/1, m/m) in a 250-mL Schlenk flask. After three freeze-pump-thaw



Scheme 1. Synthesis routes of QPDMAEMA (Q₅), PDMAFMA-b-QPDMAEMA (F_y-b-Q₅), and PDMAFMA-co-QPDMAEMA (F_x-co-Q₅).

cycles, 4 times the amount of benzyl chloride was injected into the mixture, and the reaction system was stirred at 70 °C under a nitrogen atmosphere for 48 h. Subsequently, the reaction system was dried under vacuum at 70 °C to remove most of the solvent, and anhydrous diethyl ether was added to the mixture to precipitate the product. After washing with diethyl ether three times, the precipitate was dried under vacuum at 40 °C overnight (ca. yield 87% ~ 91%).

¹H NMR (600 MHz, methanol-D₄, δ , ppm): 1.15, 1.95 (s, C-CH₃), 3.24 (s, N⁺(CH₃)₂), 4.01 (t, CH₂-CH₂-N⁺), 4.59 (m, CH₂-CH₂-N⁺, O-CH₂-CF₃), 7.56, 7.72 (s, Φ -H). FT-IR (KBr, ν , cm⁻¹): 3011–2963 (ν CH), 1726 (ν C=O), 717, 768 (γ Φ -H).

2.4. Characterization

¹H NMR spectra were collected in CDCl₃ or methanol-d₄ solvent using a Bruker Avance III-600 (Bruker Instrument Corp., Germany) spectrometer. Size exclusion chromatography (SEC) with simultaneous ultraviolet (UV) and refraction index (RI) detection was conducted in THF at 35 °C using two identical 7.5 mm \times 300 mm columns (PLgel, 5 μ m, Mixed-C) at a flow rate of 1 mL/min (1260 Infinity, Agilent). This was calibrated with a series of polystyrene standards to obtain the apparent number-average molecular weight ($M_{n, SEC}$) and molar mass distribution (D). FT-IR spectra were obtained on a Nicolet iS5 spectrometer (Thermo Fisher, USA) by using KBr pellets. Critical micelle concentrations (CMC) were determined by using a DDS-11A conductivity meter (Shanghai Hongyi Instrument Co. Ltd., China) [23,24]. Zeta potentials and particle size distributions were analyzed by using a Brookhaven BI-90 Plus particle size analyzer (Brookhaven Instrument Corp., USA) using ultrapure water as the solvent.

Detailed characterization results on the products and the methods of antifungal testing, adsorption and migration characteristics, antifungal

bioassays in soil, toxicity tests, and pot experiments are provided in the Supporting Information.

3. Results and discussion

3.1. Structure characterization of Q₅, F_x-co-Q₅, and F_y-b-Q₅

Since there were many factors affecting the polymeric quaternary antifungal properties, we know that hydrophilic-hydrophobic balance [21,25] is a necessary condition for good antifungal properties of polymeric quaternary ammonium salts. This conclusion is based on research work regarding the design and antifungal structure of quaternary ammonium salt in our group [18–20]. There is a series of studies on the effects of quaternary ammonium salt structures, rope, molecular weight, lateral base length, anti-ion, and other parameters. The preliminary results showed that the polymeric quaternary had better antifungal properties when using ohmic chloride as a counterion. There is a series of studies on the relationship between quaternary ammonium salt structures [26,27], hydrophilic-hydrophobic balance, molecular weight [28,29], lateral base length [30], anti-ion [31,32], and antifungal activity. However, research reports on the effects of strong hydrophobic fluoroalkyl groups in quaternary ammonium salts are relatively rare. Here, the fluoroalkyl group is introduced into the quaternary ammonium salt. On the one hand, this could improve the structure and chemical stability of the quaternary ammonium salt, which had lower surface tension and excellent water solubility. On the other hand, the biological activity of the quaternary ammonium salt could promote its binding and enhance permeability.

For Q₅, F_x-co-Q₅, and F_y-b-Q₅, the number average molecular weight of the D₃ chain was designed as 3 kDa [18], and the molecular weights of the DMAFMA chain were designed as 1–5 kDa. The molecular weights of

Q₅, F_x-co-Q₅, and F_y-b-Q₅ are listed in Table 1 and are basically consistent with the design. The ¹H NMR and FT-IR spectra of the products are shown in Fig. 1. As shown in Figs. 1, 2988, 1725, 1640, 1146 cm⁻¹, and 774 and 720 cm⁻¹ are the infrared absorption bands of saturated -CH₂-, C=O, C=C, C-N, and C-H on the benzene ring, respectively, and F_x-co-Q₅ and F_y-b-Q₅ have infrared absorption peaks of C-F at 658 and 564 cm⁻¹, while Q₅ does not. The signals for the CH₂CH₂N(CH₃)₂, O-CH₂-CF₃ protons appear at 4.36 and 4.07 ppm in F_x-co-D₃, F_y-b-D₃ and move to 4.59 ppm after quaternization. The proton signal of benzene ring in benzyl group appears at 7.56 and 7.72 ppm after quaternization. Thus, Q₅, F_x-co-Q₅, and F_y-b-Q₅ were synthesized as expected.

3.2. Micellar conformation of Q₅, F_x-co-Q₅ and F_y-b-Q₅ in water

The characteristics of Q₅, F_x-co-Q₅ and F_y-b-Q₅ in aqueous solution are shown in Fig. 2. From the conductivity test data of Q₅, F_x-co-Q₅ and F_y-b-Q₅ in Fig. 2(a), it can be seen that the introduction of fluoroalkyl groups is conducive to the formation of micelles. In terms of the same molecular weight and fluorine segment, the CMC of the block structure fluorine-containing quaternary ammonium salt is smaller than that of the random structure. This is because when the fluorine-containing ammonium salt concentration is relatively low, the polymeric quaternary ammonium salt is present in a single molecule or several-molecule aggregate. As the polymeric quaternary ammonium salt concentration is increased in solution, it gradually reaches saturation to aggregate to form a micelle. As a result, the higher molecular weight, higher fluorine-containing segment, and stronger block structure fluorine-containing quaternary ammonium salt are more easily aggregated to form a micelle core and grow. Therefore, the CMC is lower [33].

The zeta potential [Fig. 2(b)] of fluorine-containing quaternary ammonium salt with random and block structures shows that the formed micelle zeta potential and dynamic stability of the micelles [34] constantly improve as the hydrophobicity increases. A schematic diagram of the particle size distribution [Fig. 2(c)] and transmission electron microscopy of fluorine-containing ammonium salt (Fig. S3) indicate that with increasing molecular weight and fluoroalkyl groups, the space position between fluorine-containing side groups increases, which prevents the main chain of quaternary ammonium salts from bending greatly. The micelles are prone to hollow phenomena and form vesicles. The shape orientation is irregular, and the particle size of micelles is relatively large.

3.3. Antifungal activities of Q₅, F_x-co-Q₅, and F_y-b-Q₅

3.3.1. Antifungal activities against *Foc4*

The MIC and MFC of fluorine-containing quaternary ammonium salts and BC against *Foc4* are shown in Fig. 3 using the TTC coloration

Table 1

Molecular weights of Q₅, F_x-co-Q₅ and F_y-b-Q₅ prepared at different [DMAEMA]/[DMAFMA] feeding ratios.

Samples	[DMAEMA]/ [DMAFMA] feeding molar ratio	<i>M_n</i> , SEC of [PDMAEMA] (kDa)	<i>M_n</i> , SEC of final sample (kDa)	<i>D</i> (<i>M_w</i> / <i>M_n</i>)
Q ₅	1.00	3.0	5.4	1.29
F ₁ -co-Q ₅	0.34	–	6.2	1.36
F ₂ -co-Q ₅	0.68	–	7.3	1.55
F ₃ -co-Q ₅	1.00	–	7.9	1.53
F ₅ -co-Q ₅	1.70	–	11.3	1.61
F ₁ -b-Q ₅	0.34	2.8	6.3	1.34
F ₂ -b-Q ₅	0.68	2.8	7.6	1.41
F ₃ -b-Q ₅	1.00	2.9	8.4	1.39
F ₅ -b-Q ₅	1.70	3.1	11.6	1.58

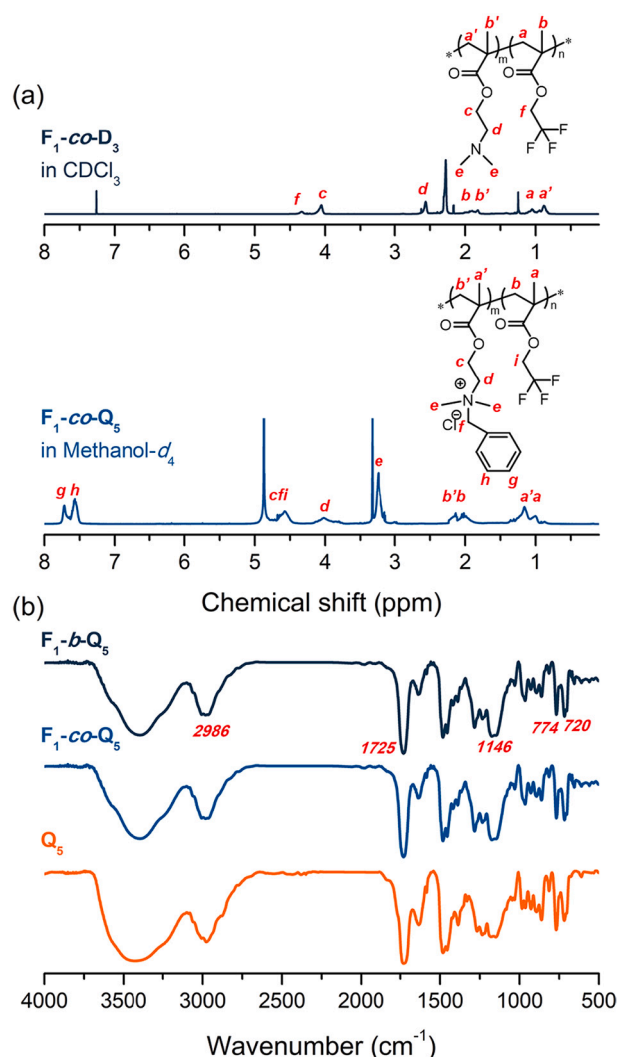


Fig. 1. (a) ¹H NMR spectra and (b) FT-IR spectra of Q₅, F₁-co-Q₅, and F₁-b-Q₅.

method [13]. From the experimental data, we can see that Q₅, F₁-co-Q₅, and F₁-b-Q₅ have a positive inhibitory effect on *Foc4* in vitro, in which F₁-co-Q₅ is equivalent to BC against *Foc4* with both at 40 μg/mL. In addition, the fluorine-containing ammonium salts exhibited a trend of antifungal activities with hydrophobicity: the antifungal activity of the quaternary ammonium salt increased at first and then decreased with increasing hydrophobicity of the quaternary ammonium salt. The fluoroalkyl group of quaternary ammonium salt with a better antifungal activity is preferably approximately 15%, the Q₅ is free of fluoroalkyl group, and the antifungal activity is poor, which also illustrates an element necessary for the hydrophobic segment to exhibit good antifungal performance. Additionally, in the case of similar hydrophobic (fluorine-containing) segments, the random structural antifungal properties are generally better than those of the block. This may be related to the micelle morphology and antifungal mechanism of quaternary ammonium salt in aqueous solution.

The 50% and 90% maximum inhibitory concentrations represent the concentrations of quaternary ammonium salt at which 50% or 90% of *Foc4* growth is inhibited. For the convenience of distinction, we define the concentrations of 50% and 90% inhibition of fluorine-containing quaternary ammonium salt against *Foc4* measured in vitro and in soil as IC₅₀, IC₉₀ and IC_{50S}, and IC_{90S}, respectively. The ratio of the growth inhibition of *Foc4* by typical mycelial growth in vitro and the spot plate method in soil on PDA medium are shown in Fig. 4. The experimental results show that the 50% and 90% maximum inhibitory concentrations

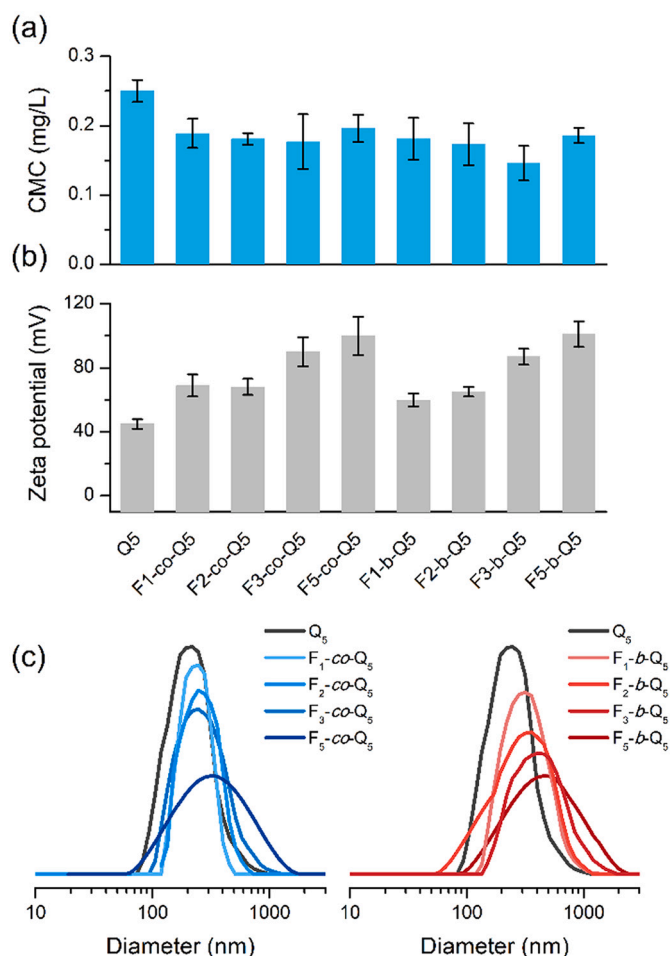


Fig. 2. (a) CMC values of Q5, F_x-co-Q5 and F_y-b-Q5 with different molecular weights and fluorine segments. (b) Zeta potentials and (c) particle size distributions of Q5, F_x-co-Q5 and F_y-b-Q5 with different molecular weights and fluorine segments.

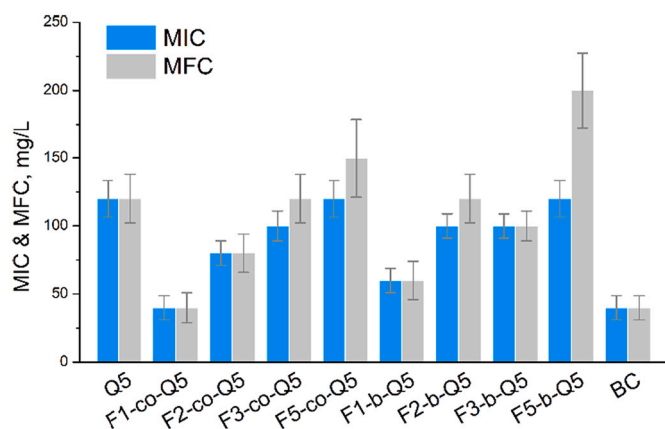


Fig. 3. MIC and MBC (for bacteria) or MFC (for fungi) values of Q5, F_x-co-Q5 and F_y-b-Q5 against Foc4.

of fluorine-containing quaternary ammonium salt are positively correlated with the antifungal activity (MIC) both in vitro and in soil. The difference is that the 50% and 90% maximum inhibitory concentrations of fluorine-containing quaternary ammonium salt are much higher than those of BC. This may occur because the mobility of fluorine-containing polymeric quaternary ammonium salt is much worse than that of BC,

resulting in its reduced utility. Additionally, it can be seen that the IC₅₀s and IC₉₀s of quaternary ammonium salt in soil are much smaller than the IC₅₀ and IC₉₀, which may be explained as follows: IC₅₀ and IC₉₀ were measured by the poison plate test method. In the test process, the quaternary ammonium salts and medium were mixed evenly to make culture medium, and the Foc4 mushroom dish was inoculated on the prepared culture medium. Then, in the process of inhibiting the growth of Foc4 mycelium, the quaternary ammonium salt on the surface of the medium plays a greater role because the solid medium limits the movement of quaternary ammonium salt drugs to a certain extent. In contrast, in the process of testing IC₅₀s and IC₉₀s, it is easier for quaternary ammonium salts to contact and interact with Foc4 in soil through shock culture. Therefore, the measured IC₅₀s is smaller than the IC₅₀.

3.3.2. Antimicrobial activities against *C. albicans*, *E. coli*, and *S. albus*

To explore the wide range of antimicrobial activities of Q5, F_x-co-Q5, and F_y-b-Q5, another fungus, *C. albicans*, and bacteria (*E. coli* and *S. albus*) were selected to determine their MIC and MFC (MBC) using the TTC coloration method [13]. The results are shown in Fig. S1. The MBC/MIC (or MFC/MIC) ratio of Q5, F_x-co-Q5, and F_y-b-Q5 against the three kinds of microbial is less than 4, which indicates that they have bactericidal/fungicidal effects. Specifically, the antifungal and antibacterial activities of both F_x-co-Q5 and F_y-b-Q5 showed a trend of first increasing and then decreasing with the increase of hydrophobicity, in which F1-co-Q5, F2-co-Q5, and F1-b-Q5/F1-co-Q5 showed the best antimicrobial activities on *C. albicans*, *E. coli* and *S. albus*, respectively.

The different antimicrobial activities of amphiphilic polymeric quaternary ammonium salt on different bacterial/fungal strains is different, which is related to the bacteriostatic/fungistatic mechanism and the structure of different kinds of bacteria/fungi. For example, compared with *S. albus*, the structure and components of the outer membrane of *E. coli* are more complex, and the resistant to the damage of quaternary ammonium cations would be stronger.

3.3.3. Effect on microbial diversity in soil

Traditional low-molecular-weight antimicrobial agents are typically used to kill pests and microorganisms in terms of plant protection, but low-molecular-weight antimicrobial agents kill all microorganisms and destroy the soil ecosystem due to their strong efficacy and toxicity. To explore the effect of fluorine-containing quaternary ammonium salts when used in the control of Banana Fusarium wilt, an experiment of preferred quaternary ammonium salt on microorganisms in soil is carried out [35]. Fig. 5 shows the number of bacteria, fungi, and actinomycetes in the soil after the addition of quaternary ammonium salts and BC. It can be seen from the chart that the number of bacteria, fungi, and actinomycetes were greatly reduced after BC application, while the number of bacteria and actinomycetes increased and the number of fungi decreased after the effect of the preferred quaternary ammonium salt on microorganisms in the soil. One possible explanation is that the bacteria, fungi, and actinomycetes in the soil ecosystem are in a dynamic equilibrium relationship. The prepared fluorine-containing quaternary ammonium salts have different inhibitory properties on microorganisms in the soil. When quaternary ammonium salts have a good inhibitory effect on fungi and greatly reduce their number, the bacteria and actinomycetes in the soil will be relatively conducive to reproduction and increase due to the reduction in competition.

3.3.4. Persistence of preferred quaternary ammonium salt on Foc4 in soil

In the practical application of fluorine-containing quaternary ammonium salt toward the prevention and control of Foc4 in plant protection, the stability and efficacy persistence are also very important parameter indicators. In this experiment, the preferred quaternary ammonium salts were mixed with soil, Foc4 was calculated, and the persistence of fluorine-containing quaternary ammonium salt was explored. Fig. S5 is a schematic diagram of the sampling and coating

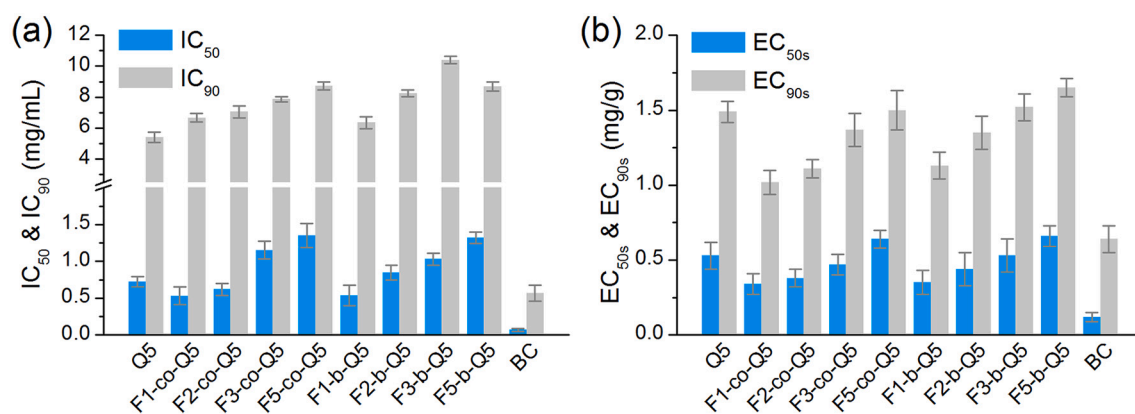


Fig. 4. (a) IC_{50} & IC_{90} and (b) EC_{50s} & EC_{90s} of Q_5 , F_x-co-Q_5 , and F_y-b-Q_5 .

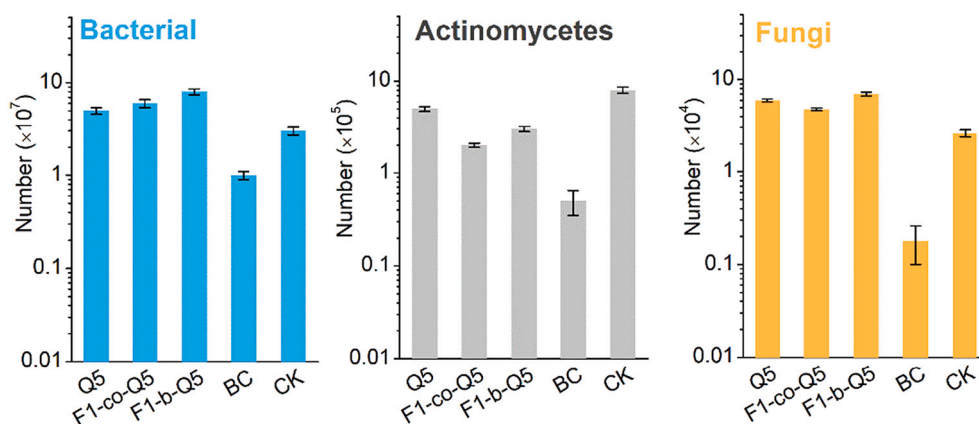


Fig. 5. Number of bacterial, actinomycetes, and fungi of Q_5 , F_x-co-Q_5 , F_y-b-Q_5 , BC, and CK as references.

results on PDA medium of the preferred quaternary ammonium salt at different concentrations after a certain time. The figure shows that the quaternary ammonium salt cannot kill all Foc4 in the soil at low concentrations, and there are still a certain number of Foc4 after coating on PDA medium. When the concentration of quaternary ammonium salt is more than 6 times that of IC_{50s} , it can effectively kill most bacteria in the soil and has a persistence of up to 30 days. This may be because the preferred quaternary ammonium salt is easy to adsorb in the soil and is not easy to migrate, which is conducive to its long-term role in the soil and the achievement of long-term antifungal performance at a high concentration against Foc4.

3.4. Adsorption and migration characteristics in soil

The physical and chemical properties of soil are important factors [36–38] that affect the interaction of Q_5 , F_x-co-Q_5 , and F_y-b-Q_5 with soil and then affect their characteristics in the soil environment. The characteristics of Q_5 , F_x-co-Q_5 , and F_y-b-Q_5 in agricultural soil can be detected according to the 260-nm absorption peak in the UV spectrophotometer due to the benzene ring structure.

Fig. 6(a)–(b) shows the adsorption curves of Q_5 , F_x-co-Q_5 , F_y-b-Q_5 , and BC in soil. We find that the adsorption process of quaternary ammonium salt in soil mainly occurs in the first 120 min, and the adsorption amount changes little with time after 120 min, reaching the saturated adsorption state between 8 and 10 h. The adsorption of fluorine-containing quaternary ammonium salt in soil is affected by many factors including electrostatic interactions, hydrophobic interactions, hydrogen bonding, physical and chemical properties of soil, and adsorption mechanisms. In the experiment, we selected the soil to

explore the effects of electrostatic interactions, hydrophobic interactions, and hydrogen bonding on the adsorption of fluorine-containing quaternary ammonium salts. An explanation of the saturated adsorption capacity and adsorption kinetic process is as follows: the experimental soil is negatively charged and has high cation exchange capacity on its surface. Therefore, when adsorbed with the soil, the fluorine-containing cationic quaternary ammonium salt is combined with the soil through electrostatic adsorption, which is the rapid adsorption stage of ion exchange. Then, the fluorocarbon chain is adsorbed and combined with the soil through hydrophobic interactions and hydrogen bonding. This is a relatively slow process. Figs. S2 and S3 show that the cation content of fluorine-containing amphiphilic quaternary ammonium salt mainly affects its adsorption rate, and the hydrophobic and electrostatic effects of fluorine-containing chain segments are more conducive to combination and desorption. This is consistent with the stronger hydrophobic effect, larger adsorption coefficient, and greater adsorption capacity [39,40].

The migration of Q_5 , F_x-co-Q_5 , and F_y-b-Q_5 with rainwater in soil is an important factor that affects their long-term antifungal performance against Foc4 in plant protection. The soil migration experiment simulates the leaching of quaternary ammonium salt in the soil layer by rainwater and explores the retention capacity of Q_5 , F_x-co-Q_5 , F_y-b-Q_5 , and BC in soil. Fig. 6(c)–(d) is a relationship chart showing the migration depth and leaching rate of Q_5 , F_x-co-Q_5 , F_y-b-Q_5 , and BC in soil. The migration capacity of fluorine-containing quaternary ammonium salt and BC in soil is poor, and the maximum leaching depth is less than 10 cm from the experimental data. The outflow rate R1 (0–10 cm) of various fluorine-containing quaternary ammonium salts and leaching solutions is more than 50%, which is difficult to leach according to GB

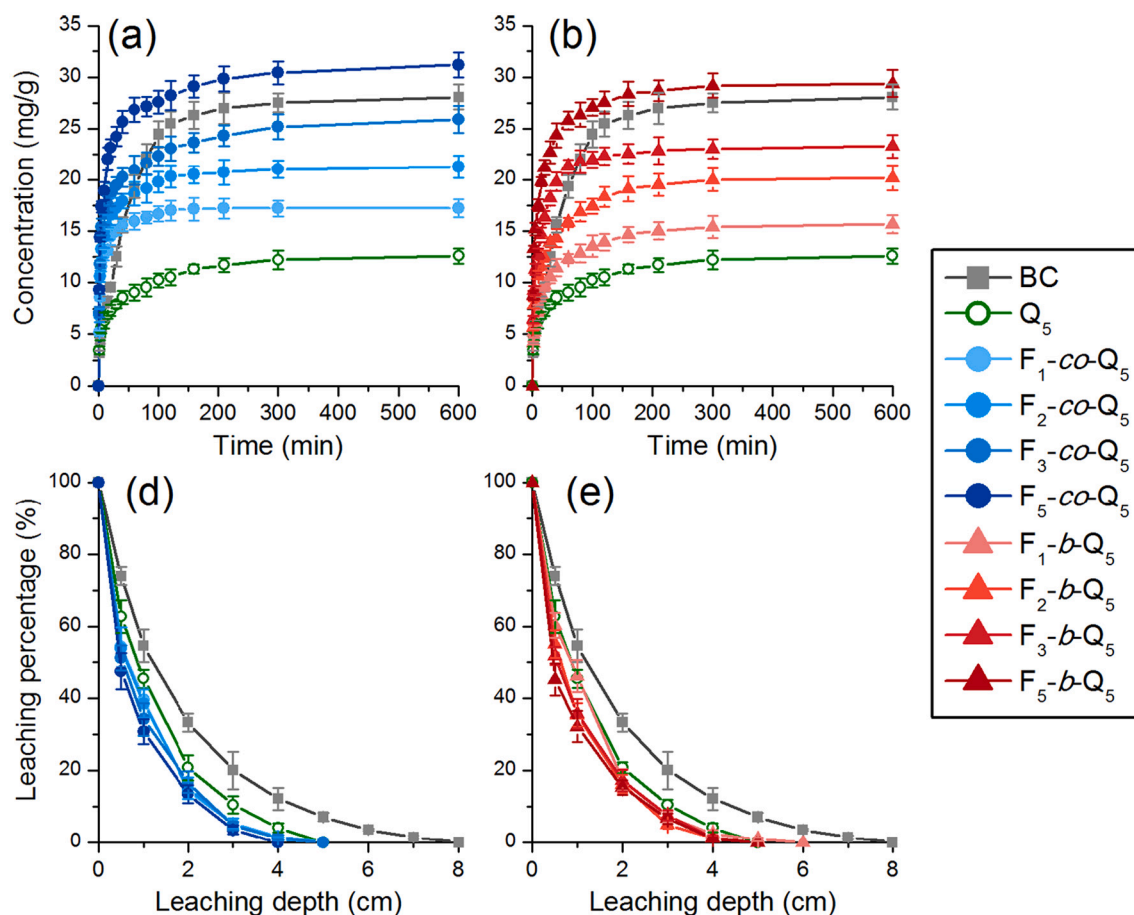


Fig. 6. (a-c) Saturated adsorption capacity of Q₅, F_x-co-Q₅, F_y-b-Q₅, and BC in soil. (d-f) Typical leaching curves of leaching depth against leaching percentage of Q₅, F_x-co-Q₅, and F_y-b-Q₅.

31270.5–2014. Therefore, Q₅, F_x-co-Q₅, and F_y-b-Q₅ do not easily migrate with water in the soil and can stay in the soil stably for a long time. This is conducive to long-term antifungal performance against Foc4.

3.5. Toxicity tests

Fig. 7 shows the toxicity data of Q₅, F_x-co-Q₅, F_y-b-Q₅, and BC to zebrafish according to GB/T 31270.12–2014. The oral toxicity LC₅₀ data of Q₅, F_x-co-Q₅, and F_y-b-Q₅ to zebrafish are between 1 and 10 mg/L,

showing an acute oral toxicity to zebrafish according to the classification standard of toxicity level. In addition, the oral acute toxicity LC₅₀ data of Q₅, F_x-co-Q₅, and F_y-b-Q₅ to zebrafish decreased as time elapsed, which indicates that the toxicity and side effects of Q₅, F_x-co-Q₅, and F_y-b-Q₅ on zebrafish are cumulative and long-lasting. Based on Q₅, F_x-co-Q₅ and F_y-b-Q₅ are easy to adsorb and difficult to migrate in the soil, and the toxicity LC₅₀ of quaternary ammonium salt in soil to zebrafish after soil adsorption and rainwater leaching is greater than 10 mg/L. This indicates that Q₅, F_x-co-Q₅, and F_y-b-Q₅ have great application prospects in the prevention and control of Foc4 in plant protection.

3.6. Pot experiments

In a pot experiment regarding the prevention and control effects of the preferred quaternary ammonium salt on Foc4 during the growth of banana seedlings, we set the growth of banana seedlings in four experimental groups (Table S2). Fig. 8(a), Fig. S6(a), and Fig. S7(a) show that when Foc4 is not inoculated, banana seedlings grow healthily, which indicates that fluorine-containing quaternary ammonium salts have little effect on the growth of banana seedlings under the experimental conditions without Foc4. Fig. 8(b), Fig. S6(b), and Fig. S7(b) indicate that when Foc4 is inoculated, the symptoms of Foc4 infection in banana seedlings are different: banana seedlings have better growth and fewer disease symptoms under higher concentrations of quaternary ammonium salt but have relatively poor growth under low concentrations of drugs. Fig. 8(b) shows that the leaves of banana seedlings turned yellow or withered seriously, and the pseudostem appeared as a dark or brown area at a concentration of IC_{50S} quaternary ammonium salt. The infection of Foc4 in banana seedling roots and leaves was relatively mild

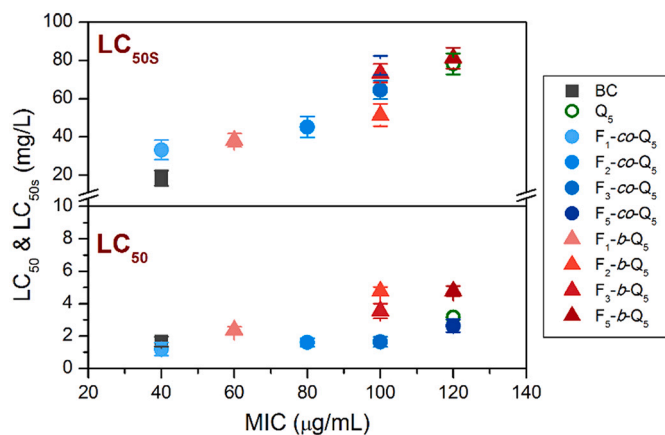


Fig. 7. Distribution of antifungal activity against Foc4 and biotoxicity to zebrafish: (a) acute toxicity and (b) toxicity after adsorption of soil.

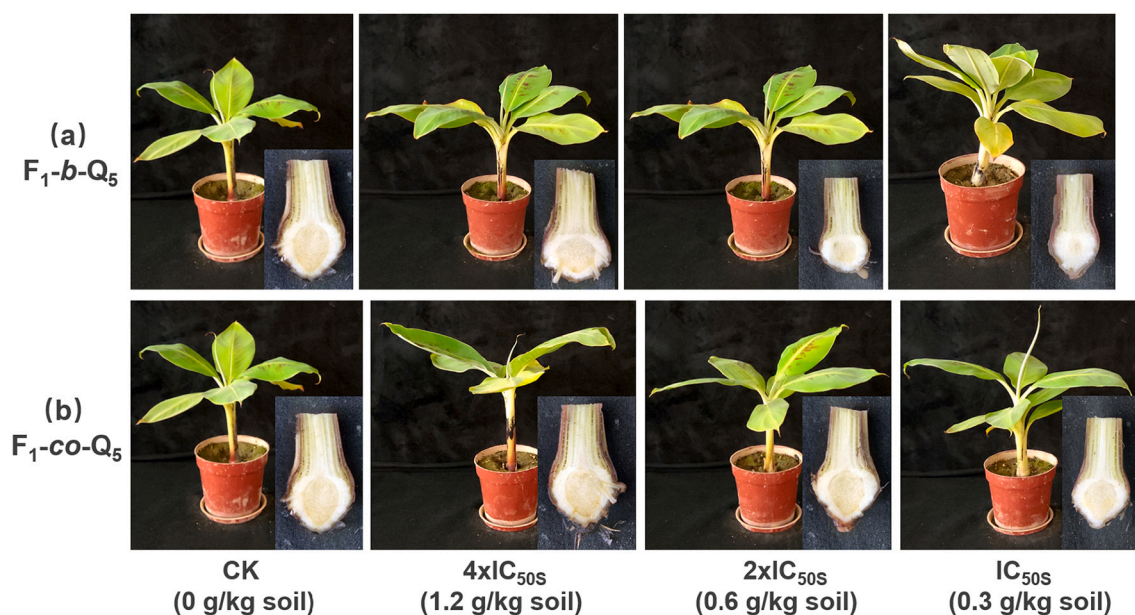


Fig. 8. Classic diagram of effect of (a) F_1-b-Q_5 and (b) F_1-co-Q_5 on growth of banana seedlings after 40 d. Small illustration in lower right corner shows longitudinal bisection of corms.

under a $4 \times IC_{50S}$ concentration of F_1-co-Q_5 . This may be because the high concentration of quaternary ammonium salt easily contacts Foc4 more fully in the soil and kills most of the Foc4, which leads to a small amount of residual Foc4 causing mild and minor infection of banana seedlings. (See Fig. 9.)

The $4 \times IC_{50S}$ concentration of quaternary ammonium salt is roughly equivalent to the IC_{90S} value measured by antifungal properties against Foc4 in soil (Fig. 4). At this concentration, fluorine-containing quaternary ammonium salt can kill most of the Foc4 in the soil, which is consistent with the growth of banana seedlings in the pot experiment. In addition, comparing the effect of Q_5 , F_1-co-Q_5 , and F_1-b-Q_5 on the growth parameters of banana seedlings in the process of controlling banana Fusarium wilt in Table S3 and Fig. S8, we found that the disease

index of banana seedlings under the $4 \times IC_{50S}$ (1.2 mg/g soil) action of F_1-co-Q_5 and F_1-b-Q_5 decreased to disease grade I (the degree of infection was approximately 11%). This indicated that the introduction of quaternary ammonium salt with an appropriate proportion of fluorine groups can enhance its antifungal performance to better control banana Fusarium wilt during the growth of banana seedlings.

4. Conclusions

This study showed that fluorine-containing amphiphilic quaternary ammonium salts with random and block structures (Q_5 , F_x-co-Q_5 , and F_y-b-Q_5) have good broad-spectrum antimicrobial properties, especially the fluoroalkyl group introduced into quaternary ammonium salt, which

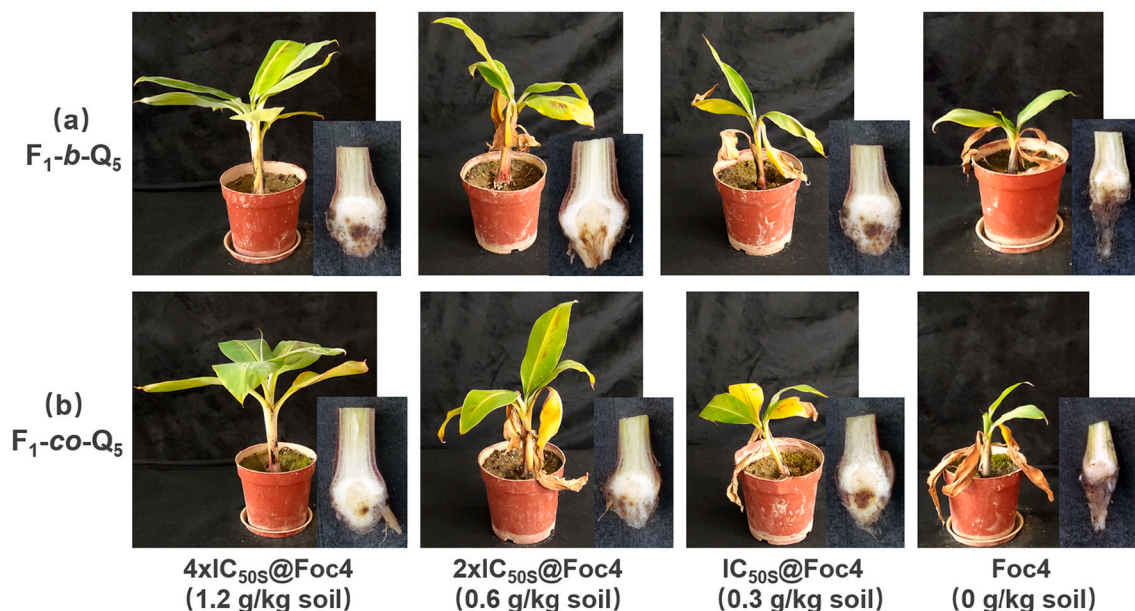


Fig. 9. Classic diagram of effect of (a) F_1-b-Q_5 and (b) F_1-co-Q_5 on growth of banana seedlings after 40 d under different concentrations of fluorine-containing amphiphilic quaternary ammonium salts, in which Foc4 conidia concentration is 2×10^6 conidia/g soil. Small illustration in lower right corner shows longitudinal bisection of corms.

exhibits better antifungal performance on Foc4, as the MIC of F_{1-co-Q5} is equivalent to BC. In addition, Q₅, F_{x-co-Q5}, and F_{y-b-Q5} are easy to adsorb in the soil and will not move, which is conducive to their long-term stable existence in the soil. In addition, they are unlikely to flow into groundwater to cause water pollution. This verified their low toxicity to zebrafish and long-term antifungal performance against Foc4 after application. Additionally, the application of fluorine-containing polymeric quaternary ammonium salt does not destroy the diversity of the microbial system in soil. Finally, the results of a pot experiment showed that the fluorine-containing quaternary ammonium salt had a more positive effect on the control of Foc4, while the fluoroalkyl group was introduced into the quaternary ammonium salt. Through the systematic characterization and research of fluorine-containing amphiphilic quaternary ammonium salts with random and block structures (Q₅, F_{x-co-Q5}, and F_{y-b-Q5}), we hope to provide a new way to protect banana plants against banana Fusarium wilt and promote the healthy and stable development of the banana industry.

Notes

The authors declare no competing financial interest.

Author contributions

The manuscript was written through the contributions of all authors.

Declaration of Competing Interest

The authors declare that they have no known competing financial interests or personal relationships that could have appeared to influence the work reported in this paper.

Data availability

No data was used for the research described in the article.

Acknowledgements

The authors acknowledge the financial support from the National Natural Science Foundation of China (Nos. 31772202 and 52073098) and the Scientific and Technological Planning Project of Guangzhou City (201803020015).

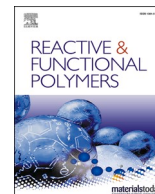
Appendix B. Supplementary data

Detailed methods for the antimicrobial testing; the characterization of F_{x-co-Q5} and F_{y-b-Q5}, D₃ and Q₅; the adsorption and migration characteristics of Q₅, F_{x-co-Q5} and F_{y-b-Q5} in agricultural soil; the antifungal properties against Foc4 in soil; the toxicity test; the methods & results for pot experiments, can be seen in Supporting Information. Supplementary data to this article can be found online at <https://doi.org/10.1016/j.reactfunctpolym.2022.105488>.

References

- J.P. Jones, S.S. Woltz, Fusarium wilt of tomato: interaction of soil liming and micronutrient amendments on disease development, *Phytopathology* 60 (2) (1970) 812–813.
- E.I. Jonathan, G. Rajendran, Interaction of *Meloidogyne incognita* and *Fusarium oxysporum* f. sp. *cubense* on banana, *Nematol. Mediterr.* 26 (1) (1998) 9–11.
- M. Dita, M. Barquero, D. Heck, E.S.G. Mizubuti, C.P. Staver, Fusarium wilt of banana: current knowledge on epidemiology and research needs toward sustainable disease management, *Front. Plant Sci.* 9 (2018) 1468.
- C.E. Alvarez, V. Garcia, J. Robles, Influence of soil characteristics on the incidence of Panama disease, *Fruits* 36 (2) (1981) 71–81.
- Y. Qi, X. Zhang, J. Pu, H. Zhang, Y. Xie, Inactivation effect of 10 compounds on *Fusarium oxysporum* f. sp. *cubense* and its toxin, *Int. J. Fruit Sci.* 25 (3) (2008) 78–82.
- Y. Pushpavathi, S.N. Dash, Y.A. Reddy, V. Triveni, Evaluation of fungicides and biocontrol agents for potential application in fusarium wilt management of banana cv Bantal, *Int. J. Farm Sci.* 7 (2) (2017) 115–118.
- M. Rokunuzzaman, A. Hayakawa, S. Yamane, S. Tanaka, K. Ohnishi, Effect of soil disinfection with chemical and biological methods on bacterial communities, *Egyptian J. Basic & Appl. Sci.* 3 (2) (2016) 141–148.
- T. Raguchander, V. Shanmugam, R. Samiyappan, Biological control of Panama wilt disease of banana, *Madras Agric. J.* 87 (4) (2000) 320–321.
- Z. Shen, Y. Ruan, X. Chao, J. Zhang, R. Li, Q. Shen, Rhizosphere microbial community manipulated by 2 years of consecutive biofertilizer application associated with banana fusarium wilt disease suppression, *Biol. Fertil. Soils* 51 (5) (2015) 553–562.
- T. Chang, R. Chang, Generation of volatile ammonia from urea fungicidal to *Phellinus noxius* in infested wood in soil under controlled conditions, *Plant Pathol.* 48 (3) (1999) 337–344.
- A.B. Pattison, C.L. Wright, T.L. Kukulies, A.B. Molina, Ground cover management alters development of fusarium wilt symptoms in Ducasse bananas, *Australas. Plant Pathol.* 43 (4) (2014) 465–476.
- A.K. Sharma, D. Sharma, A.K. Chopra, An overview of pesticides in the development of agriculture crops, *J. Appl. Nat. Sci.* 12 (2) (2020) 101–109.
- Z. Huang, R. Liuyang, C. Dong, Y. Lei, A. Zhang, Y. Lin, Polymeric quaternary ammonium salt activity against *Fusarium oxysporum* f. sp. *cubense* race 4: synthesis, structure-activity relationship and mode of action, *React. Funct. Polym.* 114 (2017) 13–22.
- M. Schulz, A. Olubummo, W.H. Binder, Beyond the lipid-bilayer: interaction of polymers and nanoparticles with membranes, *Soft Matter* 8 (2012) 4849–4864.
- K.A. Brogden, Antifungal peptides: pore formers or metabolic inhibitors in bacteria? *Nat. Rev. Microbiol.* 3 (3) (2005) 238–250.
- P. Gilbert, L.E. Moore, Cationic antiseptics: diversity of action under a common epithet, *J. Appl. Microbiol.* 99 (4) (2005) 703–715.
- E.R. Kenawy, F.I. Abdel-Hay, A.E.R.R. El-Shanshoury, M.H. El-Newehy, Biologically active polymers. V. Synthesis and antifungal activity of modified poly (glycidyl methacrylate-co-2-hydroxyethyl methacrylate) derivatives with quaternary ammonium and phosphonium salts, *J. Polym. Sci. A Polym. Chem.* 40 (14) (2002) 2384–2393.
- W. Zhong, C. Dong, R. Liuyang, Q. Guo, H. Zeng, Y. Lin, A. Zhang, Controllable synthesis and antifungal activities of acrylate polymers containing quaternary ammonium salts, *React. Funct. Polym.* 121 (2017) 110–118.
- Y. Lin, W. Zhong, C. Dong, C. Zhang, X. Feng, A. Zhang, Synthesis and antifungal activities of amphiphilic PDMS-b-QPDMAEMA copolymers on *Rhizoctonia solani*, *ACS Appl. Bio Mater.* 1 (2018) 2062–2072.
- A. Zhang, Q. Liu, Y. Lei, S. Hong, Y. Lin, Synthesis and antifungal activities of acrylamide polymers containing quaternary ammonium salts on bacteria and phytopathogenic fungi, *React. Funct. Polym.* 88 (2015) 39–46.
- E. Palermo, I. Sovadinova, K. Kuroda, Structural determinants of antifungal activity and biocompatibility in membrane-disrupting methacrylamide random copolymers, *Biomacromolecules* 10 (11) (2009) 3098–3107.
- Y. Lin, Q. Liu, L. Cheng, Y. Lei, A. Zhang, Synthesis and antifungal activities of polysiloxane-containing quaternary ammonium salts on bacteria and phytopathogenic fungi, *React. Funct. Polym.* 85 (2014) 36–44.
- A. Dominguez, A. Fernandez, N. Gonzalez, E. Iglesias, L. Montenegro, Determination of critical micelle concentration of some surfactants by three techniques, *J. Chem. Educ.* 74 (10) (1997) 1227–1231.
- A.M. Khan, S.S. Shah, Determination of critical micelle concentration (CMC) of sodium dodecyl sulfate (SDS) and the effect of low concentration of pyrene on its CMC using origin software, *J. Chem. Soc. Pak.* 30 (2) (2008) 186–191.
- C. Cheng, J. Wang, R. Kausik, K. Lee, S. Han, Nature of interactions between PEO-PPO-PEO triblock copolymers and lipid membranes: (II) role of hydration dynamics revealed by dynamic nuclear polarization, *Biomacromolecules* 13 (9) (2012) 2624–2633.
- K.E.S. Locock, T.D. Michl, J.D.P. Valentin, K. Vasilev, J.D. Hayball, Y. Qu, A. Traven, H.J. Griesser, L. Meagher, M. Haeussler, Guanylated polymethacrylates: a class of potent antifungal polymers with low hemolytic activity, *Biomacromolecules* 14 (11) (2013) 4021–4031.
- K.E.S. Locock, T.D. Michl, N. Stevens, J.D. Hayball, K. Vasilev, A. Postma, H. J. Griesser, L. Meagher, M. Haeussler, Antifungal polymethacrylates synthesized as mimics of tryptophan-rich cationic peptides, *ACS Macro Lett.* 3 (4) (2014) 319–323.
- Y. Chen, P.A. Wilbon, Y.P. Chen, Z.H. Zhou, M. Nagarkatti, C.P. Wang, F.X. Chu, A. W. Decho, C.B. Tang, Amphipathic antibacterial agents using cationic methacrylic polymers with natural rosin as pendant group, *RSC Adv.* 2 (27) (2012) 10275–10282.
- K. Kuroda, G.A. Caputo, W.F. DeGrado, The role of hydrophobicity in the antifungal and hemolytic activities of polymethacrylate derivatives, *Chemistry-a, Eur. J. Dermatol.* 15 (5) (2009) 1123–1133.
- A. King, S. Chakrabarty, W. Zhang, X.M. Zeng, D.E. Ohman, L.F. Wood, S. Abraham, R. Rao, K.J. Wynne, High antifungal effectiveness with low hemolytic and cytotoxic activity for PEG/quaternary copolyoxetanes, *Biomacromolecules* 15 (2) (2014) 456–467.
- W. Jaeger, J. Bohrisch, A. Laschewsky, Synthetic polymers with quaternary nitrogen atoms—synthesis and structure of the most used type of cationic polyelectrolytes, *Prog. Polym. Sci.* 35 (5) (2010) 511–577.
- M. Werner, J.U. Sommer, V.A. Baulin, Homo-polymers with balanced hydrophobicity translocate through lipid bilayers and enhance local solvent permeability, *Soft Matter* 8 (46) (2012) 11714–11722.

- [33] S.C. Owen, D. Chan, M.S. Shoichet, Polymeric micelle stability, *Nano Today* 7 (1) (2012) 53–65.
- [34] S. Creutz, J.V. Stam, F.C.D. Schryver, R. Jérôme, Dynamics of poly ((dimethylamino) alkyl methacrylate-block-sodium methacrylate) micelles. Influence of hydrophobicity and molecular architecture on the exchange rate of copolymer molecules, *Macromolecules* 31 (3) (1998) 681–689.
- [35] M. Teimouri, P. Mohammadi, A. Jalili, Microbial properties and dehydrogenase activity in semiarid area, Kerman Province, Iran, *Polish J. Environ. Stud.* 28 (2) (2019) 853–860.
- [36] S. Paria, K.C. Khilar, A review on experimental studies of surfactant adsorption at the hydrophilic solid-water interface, *Adv. Colloid Interf. Sci.* 110 (3) (2004) 75–95.
- [37] S. Xu, S.A. Boyd, Cationic surfactant sorption to a vermiculitic subsoil via hydrophobic bonding, *Environ. Sci. Technol.* 29 (2) (1995) 312–320.
- [38] S. Xu, S.A. Boyd, Cationic surfactant adsorption by swelling and nonswelling layer silicates, *Langmuir* 11 (7) (1995) 2508–2514.
- [39] V.C. Hand, G.K. Williams, Structure-activity relationships for sorption of linear alkylbenzenesulfonates, *Environ. Sci. Technol.* 21 (4) (1987) 370–373.
- [40] C.P. Higgins, R.G. Luthy, Sorption of perfluorinated surfactants on sediments, *Environ. Sci. Technol.* 40 (23) (2006) 7251–7256.
- [41] Y. Chang, W. Zhong, J. Liang, A. Zhang, Y. Lin, Polydimethylsiloxane-polymethacrylate block copolymers containing quaternary ammonium salts against *fusarium oxysporum* f. sp. *cubense* race 4 in soil: antifungal activities and pot experiments, *React. Funct. Polym.* 160 (2021), 104848.
- [42] W. Zhang, Y. Chang, W. Zhong, A. Zhang, Y. Lin, Antifungal mechanisms of polymeric quaternary ammonium salts against conidia of *fusarium oxysporum* f. sp. *cubense*, race 4, *Eur. J. Plant Pathol.* (2022), <https://doi.org/10.1007/s10658-022-02608-5>.



Polymeric diallyl quaternary ammonium salts for inhibiting banana Fusarium wilt

Yaling Lin^{a,*}, Chang Zhang^b, Meng Hou^a, Rui Li^b, Anqiang Zhang^{b,*}

^a College of Material and Energy, South China Agricultural University, 483 Wushan Rd., Guangzhou 510642, Guangdong, China

^b School of Material Science and Engineering, South China University of Technology, 381 Wushan Rd., Guangzhou 510641, Guangdong, China

ARTICLE INFO

Keywords:

Polymeric diallyl quaternary ammonium salt
Banana Fusarium wilt
Antifungal activity
Biototoxicity
Long-term inhibition

ABSTRACT

Banana Fusarium wilt is a typical soil-borne pathogen disease caused by *Fusarium oxysporum* f. sp. *cubense* (Foc) and is difficult to control because Foc conidia can survive for many years in soil. Thus, the inhibition of Foc conidia in soil would be an effective and possible way to control banana Fusarium wilt. In this work, three kinds of poly(N,N-diene propyl quaternary ammonium salts) (PDPQASs), namely, poly(methyl butyl diallyl ammonium chloride) (PM), poly(methyl benzyl diallyl ammonium chloride) (PB) and poly(dimethyl diallyl ammonium chloride) (PD), were synthesized, and the antifungal activities on Foc4, the adsorption and leaching properties in soil, and the biotoxieties on silkworms, zebrafish and mice were evaluated. It was found that the three kinds of PDPQAS showed obvious and stronger inhibiting effects on Foc4 conidia, and they were essentially nontoxic to silkworms and mice. Their toxicities were much lower than that of benzalkonium chloride (BC, a typical commercial small molecular QAS) to zebrafish, in which PB showed the best comprehensive properties in antifungal activities and biotoxieties. Benefitting from the stronger polymer-soil interaction, PB could absorb in soil more easily and hardly be leached from the soil, which helped PB stay in the soil more stably and effectively inhibited Foc4 conidia in the long term, giving PB a potential application in the control of banana Fusarium wilt.

1. Introduction

Banana Fusarium wilt is caused by *Fusarium oxysporum* f. sp. *cubense* (Foc). There are four categories of pathogenic fungi, among which tropical race 4 (Foc4) shows the strongest pathogenicity and can infect all the current banana varieties [1,2]. Banana Fusarium wilt is a typical soil-borne disease. Once Foc4 conidia enter a banana garden, they will reproduce in the soil, penetrate the intercellular space of the root epidermis cell walls and colonized the root vascular tissues of corms of bananas, leading to water blockage and resulting in pseudostem and leaf wilting [3]. So, in a conducive soil even low levels of pathogen inoculum can cause serious damages [4]. Thus, banana Fusarium wilt is considered a “cancer” in the banana growing industry, which has greatly restricted the development of the banana industry in South China and even in the world.

At present, chemical control and biological control are two important methods to control banana Fusarium wilt. For biological control, some fungi and bacteria that have antagonistic effects on the target pathogen have been used, but the current research is still mainly in the laboratory stage; furthermore, the fungi that have antagonistic effects on banana Fusarium wilt might change with the environment in the actual soil, showing instability [5]. For chemical control, the inhibitory effects of chemical reagents on banana Fusarium wilt have been studied. However, most of the chemical reagents used in chemical control are single and small molecules, which are prone to be lost with rain in the process of chemical control, making it difficult to achieve the effect of killing Foc conidia in the soil over a period of time [5,6]. Polymeric quaternary ammonium salts (PQASs) are novel antimicrobial agents. Due to their long molecular chain length and higher charge density, their immigration ability is lower than those of small molecule

Abbreviations: Foc, *Fusarium oxysporum* f. sp. *cubense*; Foc4, *Fusarium oxysporum* f. sp. *cubense* race 4; QAS, quaternary ammonium salts; PQAS, polymeric quaternary ammonium salts; PDPQASs, poly(N,N-diene propyl quaternary ammonium salts); MBDAC, methyl butyl diallyl ammonium chloride; PB, methyl benzyl diallyl ammonium chloride; DMDAC, dimethyl diallyl ammonium chloride; PM, poly(methyl butyl diallyl ammonium chloride); PB, poly(methyl benzyl diallyl ammonium chloride); PD, poly(dimethyl diallyl ammonium chloride); LC₅₀, median lethal concentration; LD₅₀, median lethal dose; MIC, minimum inhibitory concentration; MFC, minimal fungicidal concentration; TTC, 2,3,5-triphenyltetrazolium chloride..

* Corresponding authors.

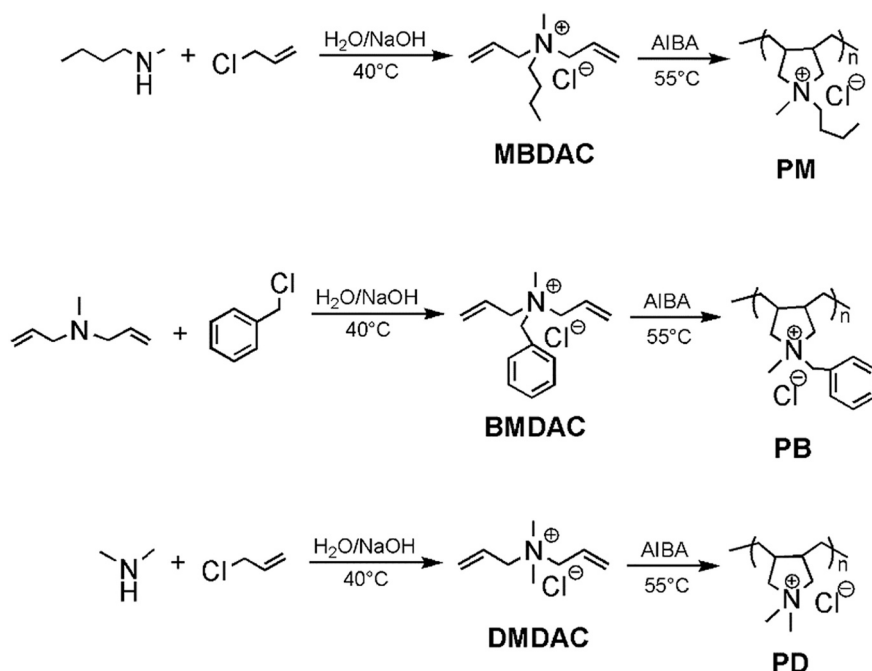
E-mail addresses: linyaling@scau.edu.cn (Y. Lin), aqzhang@scut.edu.cn (A. Zhang).

<https://doi.org/10.1016/j.reactfunctpolym.2022.105174>

Received 8 October 2021; Received in revised form 7 January 2022; Accepted 10 January 2022

Available online 20 January 2022

1381-5148/© 2022 Elsevier B.V. All rights reserved.



Scheme 1. Structures and synthesis routes of MBDAC, BMDAC, DMDAC, PM, PB and PD.

quaternary ammonium salts (SQASs); thus, the inhibitory effect might be prolonged [7,8].

According to the position of quaternary ammonium (N^+) in the macromolecules, PQAS can be divided into three categories: main chain type, side chain type and branch type [9]. In main chain cationic polymers, multiple cationic centers densely appear in the polymer skeleton, which can enhance the polymer's adsorption to the microbial membrane surface. Liu [10] and Cakmak [11] found that the main chain cationic polymers could greatly inhibit the growth of most pathogenic bacteria. There are many types of main chain cationic polymers, including polyguanidine [12,13], polyimidazole [10], diallyl quaternary ammonium polymer [14] and other main-chain macromolecular quaternary ammonium salts [11,15].

Compared with the side-chain quaternary ammonium salts most studied now [16], diallyl polymeric quaternary ammonium salt showed higher charge density, for example, the average molecular per quaternary ammonium (N^+) for polyacrylamide-based QAS (such as PQD-BC) [17] and the PDPQASs discussed in the work (such as PB), are about 280 and 227, respectively. Thus the PDPQASs have stronger adsorption characteristics to bacteria or fungi, and its antibacterial/antifungal activities could be further improved to meet the current needs of efficient sterilization. In addition, most of the current main chain type PQASs were synthesized based on the condensation method [18,19], while N,N-diene propyl types of PQASs (PDPQASs) can be obtained by traditional radical polymerization via a ring-closing mechanism, and the molecular weights are easy to control [20,21]. In addition, the polymerization of PDPQASs can be carried out in water without organic solvent, which is low cost and environmentally friendly and makes the synthetic method highly advantageous to a wide range of development and application in the future [22,23].

Although SQASs have been studied for decades, the applications of SQASs in the control of soil-borne disease have rarely been reported [24,25], which might be due to their broad-spectrum antimicrobial activity and their potential pollution to soil and water environments. Therefore, in this work, based on the synthesis of a series of N,N-diene propyl quaternary ammonium salts (DPQASs) with different side groups and the corresponding homopolymers (PDPQASs), the influence of molecular structure on the antifungal activities, biotoxicities (including toxicities to fish, silkworm and mice), polymer-soil

interactions and long-term antifungal properties of PDPQASs in Foc4-containing soil were studied in detail. We hope this work will help to further the understanding of the relationship between polymer structure and long-term antifungal properties and will assist in finding potential polymeric antimicrobial agents for plant protection.

2. Experimental

2.1. Materials

N-methyldiallyl amine (98%), azodiisobutyramidine hydrochloride (AIBA), benzyl chloride, dimethylamine, N-methyl-butylamine, and benzalkonium chloride (BC) were purchased from Shanghai Macklin Biochemical Technology Co., Ltd. (Shanghai, China). 2,3,5-Triphenyltetrazolium chloride (TTC) was purchased from BBI Life Sciences. *Fusarium oxysporum* f. sp. *cubense* race 4 (Foc4) was donated by the Fungal Laboratory, Department of Plant Pathology, South China Agricultural University and subcultured on potato dextrose agar medium (PDA). The soil (crushed and screened through a 20-mesh sieve) was taken from the banana field of the Institute of Fruit Tree Research, Guangdong Academy of Agricultural Sciences. The physicochemical properties of the tested soil are shown in Table S1.

2.2. Synthesis of quaternary ammonium monomers and their homopolymers

N, N-methyl butyl diallyl ammonium chloride (MBDAC) and its homopolymer (PM), N,N-dimethyl benzyl diallyl ammonium chloride (BMDAC) and its homopolymer (PB), and N,N-dimethyl diallyl ammonium chloride (DMDAC) and its homopolymer (PD) were synthesized according to Scheme 1, and the synthesis procedures were described briefly in the Supporting Information (Part S1).

2.3. Characterization

FT-IR spectra were collected on a Nicolet iS5 (Thermo Fisher Scientific Corp., USA) using KBr pellets. ^1H NMR spectra were obtained using a Bruker Avance III-400 (Bruker Instrument Corp., Germany) spectrometer with D_2O as the solvent. Size exclusion chromatography

Table 1

Molecular weights and distributions of PD, PM and PB.

Sample	M_n^a	M_w^a	$D (M_w/M_n)^a$
PD	7.36×10^3	12.9×10^3	1.95
PM	4.93×10^3	8.19×10^3	2.06
PB	2.41×10^3	4.37×10^3	2.11

 α : based on GPC testing.

(SEC) was performed on a Waters 515–2414 system (Waters Corp., USA) equipped with Ultrahydrogel 250 columns, and the samples were measured at 40 °C using 0.5 M acetic acid and 0.5 M sodium acetate solution as the eluent, and the instrument was calibrated using PEG standards.

2.4. Antifungal properties of the PDPQASs on *Foc4*

The antifungal activities of PDPQASs, namely PM, PB, and PD, were evaluated based on the method of inhibition of mycelial growth and the TTC coloration method [26]. The 50% inhibitory concentration (IC_{50}) and 90% inhibitory concentration (IC_{90}) were determined by the hyphal growth inhibition test to measure the diameters of the fungal colonies on PDA plates with different concentrations of PDPQASs; the minimum inhibitory concentrations (MICs) of PDPQASs on *Foc4* were determined by the broth microdilution method with 2,3,5-triphenyltetrazolium chloride (TTC), and the minimal fungicidal concentrations (MFCs) on *Foc4* were determined by the spot plate method [26]. All tests were conducted in triplicate.

2.5. Biototoxicity evaluation methods

The evaluation methods for determining the biotoxicities of PM, PB, PD and BC on insects (silkworms), fish (zebrafish) and mammals (Kunming mice) are listed in detail in the Supporting Information, Part S2.

2.6. Characterization of the interaction between PDPQASs and soil

The testing methods for the adsorption and leaching properties of PB in soil [7] and the inhibition characteristics of PB on *Foc4* in soil are listed in the Supporting Information (Part S3).

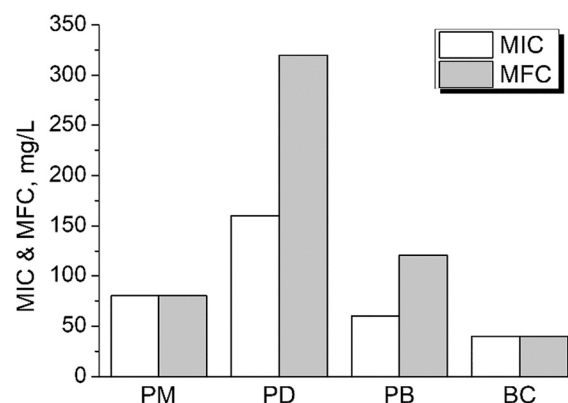


Fig. 2. MICs and MFCs of PD, PM, PB and BC against *Foc4* based on the TTC coloration method.

3. Results and discussion

3.1. Synthesis and characterization of PD, PM and PB

The FTIR and 1H NMR spectra of the three kinds of monomers, namely, DMDAC, MBDAC and BMDAC, are shown in Figs. S3 and S4, respectively. In which, the peaks in 958 cm^{-1} in the FTIR spectra, and the 5.60 ppm & 5.95 ppm in the 1H NMR spectra were assigned to the vinyl group of the monomers, and peaks in 1640 cm^{-1} were assigned to the N^+ groups.

Generally, the hygroscopic nature of quaternary ammonium salts was demonstrated strongly, and there was a wide water peak at 3422 cm^{-1} for each monomer. The characteristic peaks marked in Figs. S3 and S4 show that the monomers had the expected structure.

The homopolymers, namely, PD, PM and PB, were synthesized from DMDAC, MBDAC and BMDAC based on radical polymerizations, and their FTIR and 1H NMR spectra are shown in Figs. S5 and S6, respectively. The peaks for $C=C$ bonds (958 cm^{-1} in the FTIR spectra, and 5.60 ppm & 5.95 ppm in the 1H NMR spectra) almost disappeared, demonstrating the successful synthesis of the polymers. The molecular weights and distributions of PD, PM and PB are shown in Table 1. Table S2 showed that with different feed ratio of the monomers/initiators, overall, the polymerization activity decreased with increasing volume of the side group. And we noticed that although the molecular weight would be different, the molecular weight distribution and their anti-bacterial or antifungal activities were almost the same, which mean the molecular weight of PDPQASs was not the significant factor. Thus in

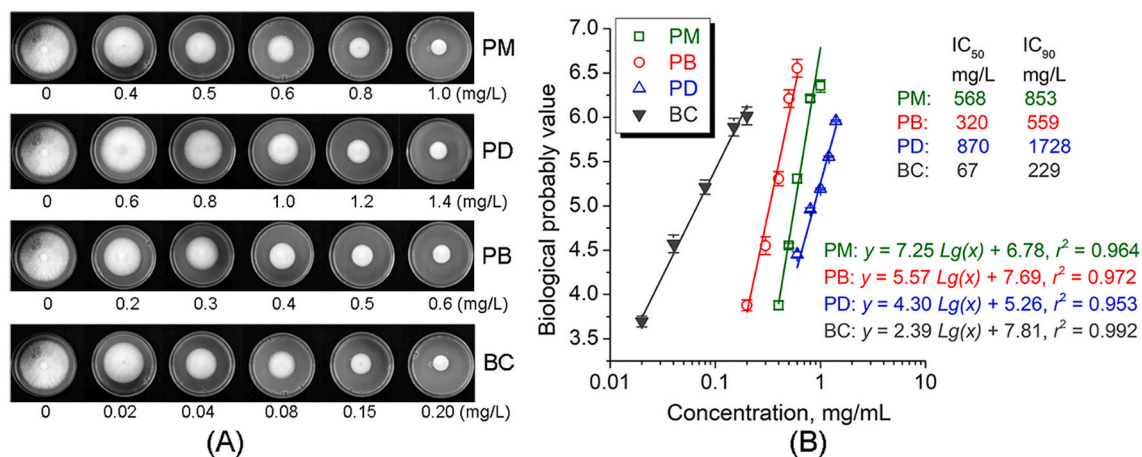


Fig. 1. (A) Antifungal activities of PD, PM, PB and BC against *Foc4* (after incubation for 5 d) based on the method of inhibition of mycelial growth and (B) the fitting curves and results of IC_{50} and IC_{90} .

Table 2

Toxicities of PD, PM, PB and BC to silkworm, zebrafish and Kunming mice.

Sample	LC ₅₀ for silkworm, mg/L	LC ₅₀ for zebrafish, mg/L	LD ₅₀ for Kunming mice, mg/kg
PM	> 2000	3.45	4500
PD	> 2000	4.31	> 5000
PB	> 2000	2.29	2000
BC	1320	1.79	555

this paper, for each polymer, only one sample was pick out for representative, as shown in Table 1.

3.2. Anti-fungal activities of PDPQASs on *Foc4*

The IC₅₀ and IC₉₀ are regarded as the two most important indicators for antifungal drugs [26]. Fig. 1-(A) shows the growth state of the typical fungus dish after being injected into the solid medium with the drug for 5 d. The inhibitory effect of the drug on mycelial growth was reflected in the size of mycelial growth under different concentrations. Fig. 1-(B) shows the fitting curves, and the IC₅₀ and IC₉₀ values could be calculated from the curves. Although BC showed the lowest IC₅₀ and IC₉₀, PB seemed to have the best anti-*Foc4* activities among the three kinds of PDPQASs. Similar results are shown in Fig. 2. PB also showed the lowest MIC among the three PDPQASs, which was slightly higher than that of BC. The differences between IC₅₀ & IC₉₀ and MIC & MFC for the same drug are mainly due to the testing methods; for the former, the fungal mycelium only contacts one side of the PDA plates containing drugs, while for the latter, the mycelium could mix with the drugs in solution uniformly, thus resulting in a much lower inhibitory concentration.

According to the mechanisms of electrostatic adsorption and bacteriostatic inhibition [27], the strength of the inhibition effect is determined by the binding property between the molecular chain and the outer membrane when the polymer adsorbs on the surface of the fungus. The stronger the hydrophobicity is, the more favorable it is to combine the polymer chain with the phospholipid layer of the fungal membrane structure through hydrophobic effects to destroy the integrity. The above three types of PDPQASs have a certain inhibitory effect on *Foc4* mycelia, and their inhibitory activity will decrease with increasing molecular weight. The stronger the side group hydrophobicity is, the better the inhibitory effect will be [17,28].

3.3. Biotoxicities of PDPQASs

As a typical cationic ammonium salt bacteriostatic agent, both the bacteriostatic effect and the biotoxicity should be evaluated. In this work, BC was chosen as a reference commercial cationic ammonium salt bacteriostatic agent, and the toxicity test results of BC and three kinds of

PDPQASs on silkworms, zebrafish and mice are shown in Table 2.

As shown in Table 2, the LC₅₀ values of PD, PM and PB for silkworms were greater than 2000 mg/L, indicating that the acute toxicity to silkworms was essentially nontoxic, while BC showed low toxicity to silkworms, which was consistent with the literature [29,30]. For zebrafish, although both PDPQASs and BC are labeled “moderate toxicity” (1–10 mg/L), the toxicity of PDPQASs is slightly lower than that of BC. PB showed a lower LC₅₀ for zebrafish, which might be due to the higher hydrophobicity, indicating that the toxicity would also be enhanced with the improvement of hydrophobicity of the side groups of PDPQASs [31,32]. This regularity between side group and toxicity could also be found in the toxicity to mice; the LD₅₀ of PD was greater than 5000 mg/kg, indicating that it was nontoxic to mice, and although PB had the lowest LD₅₀ of the three kinds of PDPQASs, LD₅₀ values of 2000 mg/kg or more indicate that they have low toxicity to mammals and are much safer than BC.

Based on the comprehensive evaluation of the antifungal activities and biotoxicities of the three kinds of PDPQASs, PB could be considered an ideal cationic ammonium salt bacteriostatic agent with higher anti-*Foc4* activities and lower biotoxicities and was chosen for further polymer-soil interaction studies.

3.4. Adsorption and leaching properties of PB

As a typical soil-borne pathogen, *Foc4* spores can survive in soil for several years, and anti-fungi agents should be applied in soil; thus, the interaction between polymeric cationic ammonium salts (here, PB was chosen for extensive study) and soil, including adsorption and leaching properties, should be evaluated. Although both PB and BC had good water solubility, the adsorption and leaching properties of PB were much different from those of BC, as shown in Fig. 3-(A). The saturated absorption (C_s) of PB was much higher than that of BC, while the time for equilibrium adsorption was also longer (approximately 16 h) than that of BC (approximately 9 h). Due to the broad-spectrum bacteriostatic effect, the drugs applied in soil hope to show good adsorption and should hardly be leached and lost from the soil, as shown in Fig. 3-(B). Compared with BC, the leaching rate of PB was much lower (the 350 mL leaching volume is equivalent to 70 mm rainfall in a day, that is, the level of a rainstorm), indicating that PB could easily absorb in soil and hardly be leached from soil [33].

3.5. Long-term anti-*Foc4* properties of PB in soil

Different loadings of PB with varied water/soil ratios were applied to the soil, where the initial concentration of *Foc4* spores in the soil was set as 2.25×10^5 conidia/(g dry soil). At this concentration, banana seedlings were susceptible to banana *Fusarium* wilt. By checking whether

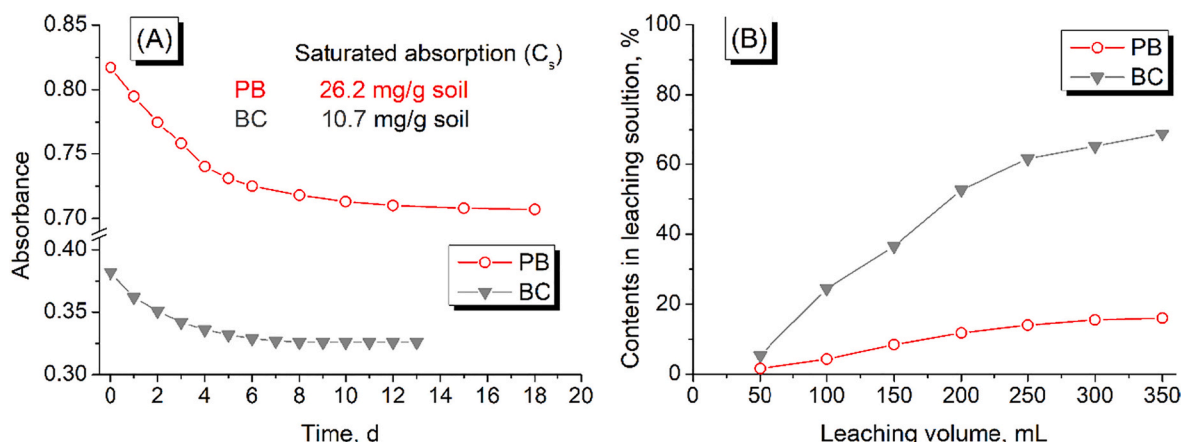


Fig. 3. Absorbance (A) and leaching (B) properties of PB and BC in soil.

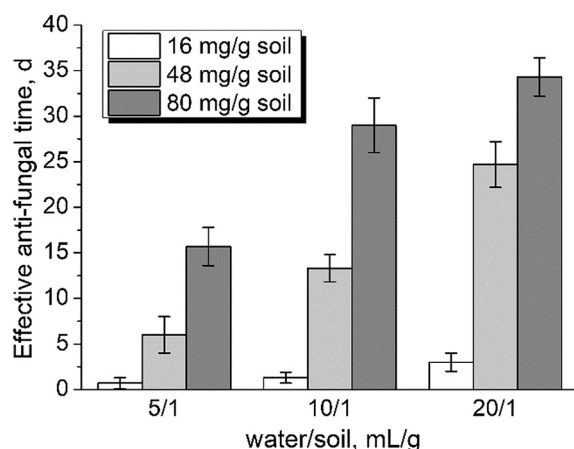


Fig. 4. Influence of PB loadings and the water/soil ratio on the long-term anti-Foc4 time of PB in soil.

there were live Foc4 conidia in the soil, the effective anti-Foc4 time in the soil could be determined. Fig. 4 shows that at a PB loading of 16 mg/(g dry soil) (roughly equivalent to $10 \times IC_{50}$), the effective anti-Foc4 time was very short under different water/soil ratios, which was mainly due to the PB loading of 16 mg/(g soil) being much lower than the saturated absorption (C_s) of PB in the soil (26.2 mg/g soil, as shown in Fig. 3-(A)). Thus, most of the PB was adsorbed on the surface of the soil particles, and PB chains were free in water, resulting in a poor anti-fungal effect. When the PB loadings were larger than C_s , with the increase in PB loading and water/soil ratio, more PB chains could be free in the soil/water mixture and result in better long-term anti-Foc4 properties. When the PB loading reached 80 mg/(g dry soil) (roughly equivalent to $50 \times IC_{50}$) under a water/soil ratio of 20/1, the effective anti-Foc4 time could be longer than one month, making PB a potential long-term anti-Foc4 agent.

4. Conclusions

In this work, three kinds of poly(N,N-diene propyl quaternary ammonium salts) with different side groups, namely, PM, PD and PB, were synthesized, and then the anti-Foc4 activities and biotoxicities were evaluated. PB showed higher anti-Foc4 activities and lower biotoxicities than small molecular quaternary ammonium salts, such as BC. Benefitting from the stronger polymer-soil interaction, PB could more easily absorb in soil and hardly be leached from soil, which helped PB remain in soil more stably and effectively inhibited Foc4 conidia. The more than one-month antifungal persistence time showed that PB had potential application prospects in the prevention of Foc4.

Author contribution statement

Yaling LIN: Conceptualization, writing- reviewing and editing, supervision; Chang ZHANG: Data collecting and writing; Meng HOU: Data collecting and writing; Rui LI: Data collecting and writing; Anqiang ZHANG: Conceptualization, writing- reviewing and editing, supervision.

Declaration of Competing Interest

The authors declare that they have no known competing financial interests or personal relationships that could have appeared to influence the work reported in this paper.

Acknowledgments

This work was supported by the National Natural Science Foundation of China under grant 31772202; the Scientific and Technological

Planning Project of Guangzhou City under grants 201803020015.

Appendix A. Supplementary data

Supplementary data to this article can be found online at <https://doi.org/10.1016/j.reactfunctpolym.2022.105174>.

References

- [1] K. Pegg, L. Coates, W. O'Neill, D. Turner, The epidemiology of Fusarium wilt of banana, *Front. Plant Sci.* 10 (2019) 1395.
- [2] R. Ploetz, Fusarium wilt of banana, *Phytopathology* 105 (2015) 1512–1521.
- [3] L. Zhang, T. Yuan, Y. Wang, D. Zhang, T. Bai, S. Xu, Y. Wang, W. Tang, S. Zheng, Identification and evaluation of resistance to *Fusarium oxysporum* f. sp. *cubense* tropical race 4 in *Musa acuminata* Pahang, *Euphytica* 214 (2018) 106.
- [4] M. Dita, M. Barquero, D. Heck, E.S. Mizubuti, C.P. Staver, Fusarium wilt of banana: current knowledge on epidemiology and research needs toward sustainable disease management, *Front. Plant Sci.* 9 (2018) 1468.
- [5] R. Ploetz, S. Freeman, J. Konkol, A. Al-Abed, Z. Naser, K. Shalan, R. Barakat, Y. Israeli, Tropical race 4 of Panama disease in the Middle East, *Phytoparasitica* 43 (2015) 283–293.
- [6] B. Wang, J. Yuan, J. Zhang, Z. Shen, M. Zhang, R. Li, Y. Ruan, Q. Shen, Effect of novel bioorganic fertilizer produced by *Bacillus amyloliquefaciens* W19 on antagonism of *Fusarium* wilt of banana, *Biol. Fertil. Soils* 49 (2013) 435.
- [7] Y. Chang, W. Zhong, J. Liang, A. Zhang, Y. Lin, Polydimethylsiloxane-polymethacrylate block copolymers containing quaternary ammonium salts against *Fusarium oxysporum* f. sp. *cubense* race 4 in soil: antifungal activities and pot experiments, *React. Funct. Polym.* 160 (2021) 104848.
- [8] Y. Jiao, L. Niu, S. Ma, J. Li, R. Fanklin, J. Chen, Quaternary ammonium-based biomedical materials: state-of-the-art, toxicological aspects and antimicrobial resistance, *Prog. Polym. Sci.* 71 (2017) 53–90.
- [9] Y. Xue, H. Xiao, Y. Zhang, Antimicrobial polymeric materials with quaternary ammonium and phosphonium salts, *Int. J. Mol. Sci.* 16 (2015) 3626–3655.
- [10] L. Liu, Y. Huang, S. Riduan, S. Gao, Y. Yang, W. Fan, Y. Zhan, Main-chain imidazolium oligomer material as a selective biomimetic antimicrobial agent, *Biomaterials* 33 (2012) 8625–8631.
- [11] I. Cakmak, Z. Ulukanli, M. Tuzcu, S. Karabuga, K. Genctav, Synthesis and characterization of novel antimicrobial cationic polyelectrolytes, *Eur. Polym. J.* 40 (2004) 2373–2379.
- [12] Y. Zhang, J. Jiang, Y. Chen, Synthesis and antimicrobial activity of polymeric guanidine and biguanidine salts, *Polymer* 40 (1999) 6189–6198.
- [13] M. Ahmed, T. Annamalai, X. Li, A. Seddek, P. Teng, Y. Tse-Dinh, J. Moon, Synthesis of antimicrobial poly(guanylurea)s, *Bioconjug. Chem.* 29 (2018) 1006–1009.
- [14] J. Olsson, T. Pham, P. Jannasch, Poly(N,N-diallylazacycloalkane)s for anion-exchange membranes functionalized with n-spirocyclic quaternary ammonium cations, *Macromolecules* 50 (2017) 2784–2793.
- [15] Y. Zhu, C. Xu, N. Zhang, X. Ding, B. Yu, F. Xu, Polycationic synergistic antibacterial agents with multiple functional components for efficient anti-infective therapy, *Adv. Funct. Mater.* 28 (2018) 1706709.
- [16] Y. Oda, S. Kanaoka, T. Sato, S. Aoshima, K. Kuroda, Block versus random amphiphilic copolymers as antibacterial agents, *Biomacromolecules* 12 (2011) 3581–3591.
- [17] A. Zhang, Q. Liu, Y. Lei, S. Hong, Y. Lin, Synthesis and antimicrobial activities of acrylamide polymers containing quaternary ammonium salts on bacteria and phytopathogenic fungi, *React. Funct. Polym.* 88 (2015) 39–46.
- [18] W. Jaeger, J. Bohrisch, A. Laschewsky, Synthetic polymers with quaternary nitrogen atoms-synthesis and structure of the most used type of cationic polyelectrolytes, *Prog. Polym. Sci.* 35 (2010) 511–577.
- [19] Y. Yang, J. Enbert, Synthesis and catalytic properties of hydrophobically modified poly(alkylmethyl diallyl ammoniumbromides), *J. Organomet. Chem.* 56 (1990) 4300–4304.
- [20] C. Wandrey, J. Hernandez-Barajas, D. Hunkeler, Diallyldimethylammonium chloride and its polymers, in: I. Capek, J. Hernández-Barajas, D. Hunkeler, J. L. Reddinger, J.R. Reynolds, C. Wandrey (Eds.), *Radical Polymerisation Polyelectrolytes. Advances in Polymer Science* 145, Springer, Berlin, Heidelberg, 1999, pp. 123–182, https://doi.org/10.1007/3-540-70733-6_3.
- [21] R. Losada, C. Wandrey, Copolymerization of a cationic double-charged monomer and electrochemical properties of the copolymers, *Macromolecules* 42 (2009) 3285–3293.
- [22] Y. Yang, B.F.N. Jan, Engberts. Synthesis and catalytic properties of hydrophobically modified poly(alkylmethylallylammonium bromides), *J. Organomet. Chem.* 56 (1991) 4300–4304.
- [23] G. Wang, B.F.N. Jan, Engberts. Synthesis and catalytic properties of hydrophobically modified poly(alkylmethyl-diallylammonium chlorides), *Eur. Polym. J.* 31 (1995) 409–417.
- [24] R. Meldrum, A. Daly, L. Tran-Nguyen, E. Aitken, The effect of surface sterilants on spore germination of *Fusarium oxysporum* f. sp. *cubense* tropical race 4, *Crop Prot.* 54 (2013) 194–198.
- [25] B. Nela, C. Steinberg, N. Labuschagne, A. Viljoena, Evaluation of fungicides and sterilants for potential application in the management of Fusarium wilt of banana, *Crop Prot.* 26 (2007) 697–705.
- [26] Z. Huang, R. Liuyang, C. Dong, Y. Lei, A. Zhang, Y. Lin, Polymeric quaternary ammonium salt activity against *Fusarium oxysporum* f. sp. *cubense* race 4: synthesis,

- structure-activity relationship and mode of action, *React. Funct. Polym.* 114 (2017) 13–22.
- [27] B. Mowery, S. Lee, D. Kissounko, R. Epand, R. Epand, B. Weisblum, S. Stahl, S. Gellman, Mimicry of antimicrobial host-defense peptides by random copolymers, *J. Am. Chem. Soc.* 129 (2007) 5474–5476.
- [28] D. Sha, J. Xu, X. Yang, Y. Xue, X. Liu, C. Li, M. Wei, Z. Liang, K. Shi, B. Wang, Y. Tang, X. Ji, Synthesis and antibacterial activities of quaternary ammonium salts with different alkyl chain lengths grafted on polyvinyl alcohol-formaldehyde sponges, *React. Funct. Polym.* 158 (2021) 104797.
- [29] Punyavathi Sudhakumari, C. Das, M. Bhat, H. Manjunatha, evaluation of the medically important compounds TASKI protasan and combatan for its efficacy using *Bombyx mori* as a model system, *J. Pharm. Res.* 7 (2013) 184–188.
- [30] Y. Lin, W. Zhong, C. Dong, C. Zhang, X. Feng, A. Zhang, Synthesis and antifungal activities of amphiphilic PDMS-*b*-QPDMAEMA copolymers on *Rhizoctonia solani*, *ACS Appl. Bio Mater.* 1 (2018) 2062–2072.
- [31] A. Engler, J. Tan, Z. Ong, D. Coady, V. Ng, Y. Yang, J. Hedrick, Antimicrobial polycarbonates: investigating the impact of balancing charge and hydrophobicity using a same-centered polymer approach, *Biomacromolecules* 14 (2013) 4331–4339.
- [32] M. Ganewatta, C. Tang, Controlling macromolecular structures towards effective antimicrobial polymers, *Polymer* 63 (2015) A1–A29.
- [33] Y. Wang, H. Gao, Z. Xie, L. Zhang, X. Ma, Effects of different agronomic practices on the selective soil properties and nitrogen leaching of black soil in Northeast China, *Sci Rep-UK*. 10 (2020) 14939.

Molecularly Imprinted Photonic Crystals Based on Fusaric Acid for the Detection of Banana Fusarium Wilt

Yaling Lin,* Xixiang Feng, Wei Zhang, Rui Li, and Anqiang Zhang*

Cite This: *ACS Appl. Polym. Mater.* 2021, 3, 5818–5825

Read Online

ACCESS |



Metrics & More



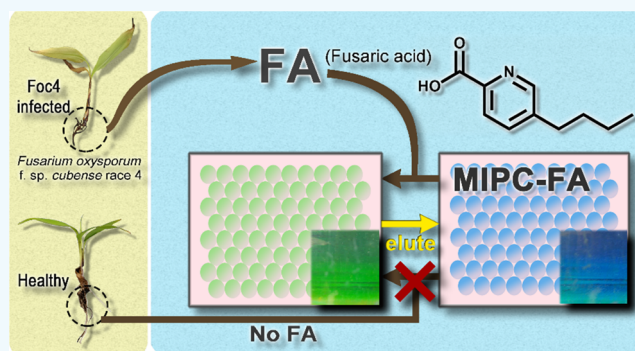
Article Recommendations



Supporting Information

ABSTRACT: Banana Fusarium wilt is a soil-borne disease caused by *Fusarium oxysporum* f. sp. *cubense* (Foc) in which *F. oxysporum* f. sp. *cubense* race 4 (Foc4) could infect all kinds of banana and has caused great damage to the banana planting industry. The most important means to prevent and control banana Fusarium wilt in agricultural production is to control the spread and invasion of pathogens. Among them, the detection and determination of banana Fusarium wilt in the field is essential and thus is the basis of protection. Since fusaric acid (FA) is one of the specific products present during the metabolic processing of Fusarium wilt pathogens, by combining FA with molecularly imprinted photonic crystal (MIPC) technologies, a series of MIPCs based on monodispersed silica, FA, and cross-linked polymers, i.e., MIPC-FA, which could be recycled, were designed and prepared. It was found that the responses of MIPC-FA were affected by the cross-linking degree of the polymer matrix and the pH values. The results showed that MIPC-FA could effectively detect FA in a solution of FA in a minute scale, Foc4-containing medium, and banana plants infected by Foc4, and the response was related to the FA concentration, which makes it an effective and fast method to detect and determine banana Fusarium wilt caused by Foc4 in the field.

KEYWORDS: molecularly imprinted photonic crystal, banana Fusarium wilt, fusaric acid, Foc4, field testing



1. INTRODUCTION

Banana Fusarium wilt is a typical vascular wilt disease caused by a special species of a complex of *Fusarium oxysporum* f. sp. *cubense* (Foc).¹ According to banana planting technology and the perennial and single-variety cultivation characteristics of banana plantations, it is obvious that the management of banana wilt is not simple.² At present, there are no effective fungicides or other eradication methods that can eradicate *F. oxysporum* f. sp. *cubense* race 4 (Foc4), and the affected plants lead to a rapid decline in the output of an entire banana plantation.

Banana wilt is considered to be a “polycyclic” plant disease,³ which means that the invasion of a small amount of pathogens may cause large-scale losses. Proactive prevention, containment of the disease, and isolation of infected plants appear to be extremely important. Therefore, the fast detection of infected plants is particularly important.

The detection of banana Fusarium wilt traditionally relies on the identification of disease symptoms. The main feature is that the leaves are yellow and the banana pseudostems become reddish brown.⁴ However, due to the long incubation period of the pathogen, by the time symptoms are found in the banana host, the pathogen has already begun to spread.⁵ The routine diagnosis of Foc requires long-term culture, microscopy and

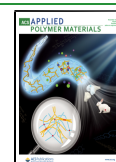
pathogenicity tests, and distinguishing Foc from other *Fusarium* species based on its morphological characteristics, which requires testing personnel to have an excellent *Fusarium* species research background. This method cannot distinguish between pathogenic and nonpathogenic strains.⁶ The pathogenicity test can distinguish whether it is pathogenic but this test is extremely time-consuming, and different environments may bring different results.

DNA-based diagnosis can effectively improve the speed and accuracy of testing. Polymerase chain reaction (PCR) using specific primers is a relatively common method of identification, but it requires cultivation and can only provide qualitative results.⁷ Quantitative PCR was developed to solve the shortcomings of conventional PCR and is often applied to the quantification of pathogen DNA in environmental samples.⁸ Lin and co-workers⁹ developed the SCAR primer set FocSc-1/FocSc-2, and primers for real-time PCR

Received: August 16, 2021

Accepted: October 5, 2021

Published: October 15, 2021



amplification can be applied to the quantitative detection of Foc4. The Food and Agriculture Organization (FAO) uses a PCR technique that uses specific primers to detect FocTR4-F/FocTR4-R.¹⁰ This specific method is only for FocTR4 (VCG-01213), which causes great damage to Cavendish bananas. This detection method can detect infected plants and soil- and water-containing pathogens.

In the process of Foc invading banana plants, the pathogen produces a series of phytotoxins to invade the host. Among them, fusaric acid (FA) is a phytotoxin produced by several species of *Fusarium*.¹¹ In banana *Fusarium* wilt, FA is closely related to the symptoms of banana *Fusarium* wilt. FA may destroy the cell membrane of the host cell at the stage when the bacteria causing banana *Fusarium* wilt invades the plant and causes an imbalance in the water level in the leaves.¹² Some studies also suggest that FA is related to the destruction of chloroplasts, and the reduction of photosynthesis and the presence of FA can be detected in leaves showing yellowing.¹³ It is believed that FA plays a very important role in the infection cycle of banana *Fusarium* wilt, which means that FA can be used as a target substance to detect banana *Fusarium* wilt caused by Foc.

Molecularly imprinted polymers (MIPs) are considered to be the closest synthetic analogues of the antibody–antigen system in biological systems. A molecularly imprinted polymer identifies the selective binding of the template molecule in the synthesis process through the “lock–key” structure.^{14,15} MIP provides the specificity of natural biological receptors and is inexpensive.

Currently, to solve the signal problem after molecular imprinting recognition, an increasing number of reports use electrochemical¹⁶ and optical technologies¹⁶ to transform molecular imprinted materials into “sensors”. Molecularly imprinted photonic crystals (MIPCs) prepared by combining molecular imprinting technology and photonic crystals are an ideal sensing material with high selectivity and fast response, and the most significant advantage of MIPCs is that their response signal can be directly observed by the naked eye. MIPCs based on many recognition molecules have been synthesized for the recognition of specific compounds, such as nitrobenzene,¹⁷ ethanol,¹⁸ formaldehyde,¹⁹ cocaine,²⁰ deltamethrin,²¹ etc. MIPC sensors enable low-cost, small, and rugged identification systems and could be suitable for portable systems for drug detection and environmental monitoring.

This work was designed to synthesize molecularly imprinted photonic crystals (MIPCs) using fusaric acid (FA) as a template molecule and to detect fusaric acid in a standard solution, Foc4 culture medium, and Foc4-infected seedlings.

2. MATERIALS AND METHODS

2.1. Chemicals and Materials. Tetraethyl orthosilicate (TEOS), methacrylic acid (MAA), ethylene glycol dimethacrylate (EGDMA), 2,2'-azobis(2-methylpropionitrile) (AIBN), and hydrofluoric acid (HF, 40%) were purchased from Macklin (Shanghai, China) and used directly. 5-Butylpicolinic acid (fusaric acid, FA) was purchased from Biosynth Carbosynth (Suzhou, China). Phosphate buffer solution (PBS, 0.01 M, pH 7.6) was prepared by dissolving Na₂HPO₄ and KH₂PO₄ in Milli-Q water. Glass slides (25 × 70 × 2 mm³) were immersed in a 98% H₂SO₄/30% H₂O₂ (70/30, v/v) mixture for 12 h, rinsed three times with deionized water in an ultrasonic bath, and then dried before use. Poly(methyl methacrylate) (PMMA) slides (50 × 25 × 2 mm³) were cleaned with anhydrous ethanol. All of the solvents and chemicals used were of reagent quality and used without further purification unless indicated.

2.2. Preparation of Monodispersed Silica. The multistep preparation method of monodispersed silica preceded based on the Stober method.^{22–24} In brief, 27.5 mL of anhydrous ethanol, 3.5 mL of ammonia, and 16 mL of deionized water were mixed in a 250 mL flask, stirred intensively with a magnetic stirrer, and then 50 mL of anhydrous ethanol and 3 mL of TEOS were added and the mixture was made to react for 4 h. After that, 2 mL of TEOS and 0.32 mL of deionized water were added every 4 h to the reaction. After repeating feeding eight times, monodispersed silica particles were obtained by centrifugation and resuspended in anhydrous ethanol five times. Afterward, the obtained monodispersed particles were fully dispersed in anhydrous ethanol with concentrations by weight of approximately 10–30%.

2.3. Preparation of the SiO₂ Photonic Crystal. The above-synthesized monodispersed SiO₂ ethanol concentrated emulsion was diluted to a 0.5–2% SiO₂ ethanol emulsion with anhydrous ethanol in a 25 mL beaker. A glass slide treated with piranha solution was inserted vertically into the beaker with the SiO₂ emulsion. After ethanol completely evaporated naturally, SiO₂ photonic crystals were prepared on both sides of the glass slide.

2.4. Fabrication of Molecularly Imprinted Photonic Crystal Films. In this work, we fabricated four kinds of MIPC-FA films and one nonmolecularly imprinted photonic crystal (N-MIPCs) film. The MIPC-FA films were imprinted with fusaric acid under different polymer compositions (including MAA, EGDMA, methanol, and water), while for the N-MIPC film, FA was not added during the preparation of polymers, as shown in Table 1. The scheme of the

Table 1. Formula for the Preparation of MIPC-FA Using a 250 nm SiO₂ Photonic Crystal as the Matrix

sample	FA (mmol)	MAA (mmol)	EGDMA (mmol)	methanol (μL)	water (μL)
MIPC-FA-1	1	4	1	400	100
MIPC-FA-2	1	6	1	400	100
MIPC-FA-3	1	6	1	500	0
MIPC-FA-4	1	8	1	400	100
N-MIPC	0	6	1	400	100

synthesis process of MIPCs is shown in Figure 1. For the fabrication of MIPC-FA, fusaric acid, MAA, and EGDMA were mixed with methanol and deionized water and stored at 6 °C overnight. Then, 0.01 g of AIBN was added to the stored homogeneous monomer mixtures and degassed with nitrogen for 10 min. The prepared glass slide with SiO₂ photonic crystals was closely attached to a PMMA

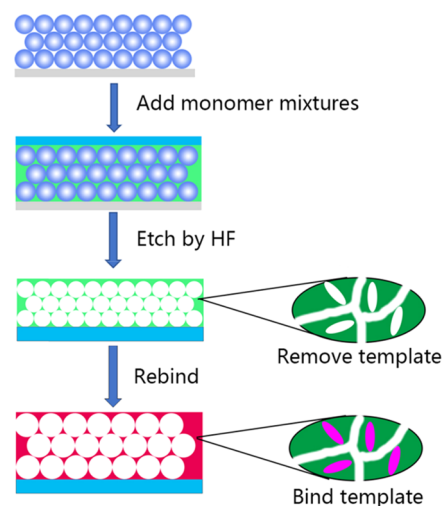


Figure 1. Schematic diagram of the preparation process of the MIPC-FA polymer film.²⁷

slide to form a sandwich structure, and the edge of the sandwich was immersed into the prepared mixture until the sandwich structure became transparent. The homogeneous monomer mixtures entered the gap of the photonic crystal due to capillary action. Then, the "sandwich" structure was fixed with clamps, and the remaining mixture was photopolymerized at 2 °C under UV light at 365 nm for 2 h.

After photopolymerization, the sandwiches were immersed in 1% hydrofluoric acid for 2 h until the two slides separated and the silica particles were etched fully. After rinsing the PMMA slide with deionized water for 3 min, the PMMA slide was immersed in an acetic acid/methanol (1/9, v/v) mixture for 2 h to remove the template molecules on the imprinted polymer. After removing the template, the PMMA slides were immersed in PBS to reach an equilibrium state for storage.

The fabrication of N-MIPCs is the same as that for the others except that no fusaric acid is added.

2.5. Determination of MIPC-FA Films toward Recognition.

All of the concentrations of the analytes were prepared with the same PBS (0.01 M, pH 7.6). For determination in a competitive environment, the analytes were changed to a mixture of PB buffer and extracted with the original concentration. For each analyte, testing began from the blank state of MIPC-FA films and followed a sequence from low to high concentrations to eliminate interference. After testing the highest concentration, the MIPC-FA films were soaked in an acetic acid/methanol mixture for recovery.

2.6. Extraction of Crude Toxin from Foc4. To extract the crude toxin of Foc4, Foc4 was inoculated in 200 mL of Czapek-Dox Medium (10^6 CFU/mL) for 7 days at 28 °C on a shaker at 180 rpm. The resulting medium was filtered through four layers of gauze, and the filtered liquor was collected and centrifuged at 8000g for 20 min. The supernatant was collected. The centrifugations were passed through a 0.45 μ m filter membrane, and the filtrate was collected. The filtrate was adjusted to pH 2.0 with 2 M HCl and then extracted five times with ethyl acetate to obtain the metabolite extract. Then, the solvent was removed by rotary evaporation at 40 °C under vacuum. The dried residue was dissolved in 5 mL of methanol and then filtered through a 0.45 μ m filter to obtain a methanol solution of the crude toxin.

2.7. Plant Cultivation. Banana seedlings (*Musa AAA Cavendish* cv. *Brazil*) were obtained from the South China Botanical Garden in Guangdong Province, China. Potted soil was provided by the Crop Nutrition and Fertilization Laboratory of South China Agricultural University.

The soil samples were sieved over a 5 mm mesh and then divided into two groups: an infected group and a blank group (each group contained 20 replications). The total amount of soil in the pot for each replication was 300 g in which Foc4 conidial suspension in the infected group and deionized water in the blank group were mixed with soil before being added to the pots (upper diameter of 7 cm, lower diameter of 5 cm, and height of 10 cm). Banana seedlings with a height of \sim 10 cm (2–3 leaves) were transplanted to the pots. Then, 200 mL of tap water was added, and 75 mL of tap water was added every afternoon to each pot. All potted plants were cultured in a greenhouse at a typical temperature of 28 °C and humidity of 60–80% under natural sunshine for \sim 12 h. After 15 days of banana seedling growth, various parts of the banana were prepared for observation and extraction.

2.8. Extraction of Fusaric Acid from Banana Seedlings. The cultivated banana plants were removed from the soil, and then banana seedlings were washed to remove the soil. Then, the roots, pseudostems, and leaves of the banana seedlings were separated. After pretreatment, the obtained roots, pseudostems and leaves were washed, dried, and weighed, and the weight was recorded; then, the extract was prepared in methanol/1% K_2HPO_4 with a volume ratio of 1:1 (pH = 2.5). Then, 3 mL of the extract was added to the weighed roots, pseudostems, and leaves, and they were ground until there were no obvious lumps. After grinding, the slurry was centrifuged at 8000g for 30 min, and the supernatant was collected and acidified with 2 M HCl to pH = 2.5. After acidification, excess ethyl acetate was added in

three extractions, the organic phases were finally combined, and ethyl acetate was removed by rotary evaporation under reduced pressure. The dried residue was dissolved in 3 mL of methanol to obtain a methanol extract of the banana roots, pseudostems, and leaves.

2.9. Crude Extraction Analysis by High-Performance Liquid Chromatography (HPLC). To identify the presence of FA in crude toxin extracted from the pathogen culture and seedlings, we employed an HPLC system (Waters 600s-2998, Waters Corporation) with a Hypersil ODS-2 column (4.6×250 mm², Thermo Fisher Scientific). Aliquots of 10 μ L of the extracts were injected and eluted with MeOH/0.43% H_3PO_4 (68/32, v/v) for 10 min with a UV detector at 280 nm. The flow rate was 1 mL/min. Before injection, the samples were filtered through 0.45 μ m filters.

2.10. Testing Procedure for the MIPC-FA Slide. Before testing, the extract of crude toxin from Foc4, the extract of fusaric acid from banana seedlings, or the FA standard solution should be diluted using phosphate buffer solution to the set concentration. After immersing the MIPC-FA slide into the above solution for about 1 min until the color of MIPC-FA no longer changes, the slide was taken out to observe with naked eyes or test using a UV–vis spectrometer. After testing, the MIPC-FA slide was soaked in acetic acid/methanol (1/9, v/v) solution for 20 min until the color of MIPC-FA no longer changes, and then the MIPC-FA slide was soaked in phosphate buffer solution for storage and reuse.

2.11. Instrumentation. The morphologies of SiO₂ templates and the obtained MIPC films were viewed by a scanning electron microscope (ZEISS EVO18, Germany) operating at 10 kV. UV–vis spectra were recorded using a PerkinElmer Lambda 950 spectrometer. A common digital camera was used to obtain the color image of MIPCs. The particle size of SiO₂ was measured by a nanoparticle size analyzer (HORIBA SZ-100Z, Japan).

3. RESULTS AND DISCUSSION

3.1. Characterization of Silica Photonic Crystals and MIPCs. The preparation of monodispersed silica photonic crystals and the influence of silica particle sizes on the reflectance spectra of silica photonic crystals are discussed in the Supporting Information (Parts S1 and S2).

Molecularly imprinted photonic crystals (MIPCs) can be prepared using SiO₂ photonic crystals as a template, filling the prepolymer, and etching and removing the SiO₂ microspheres after polymerization. As shown in Figure S3B, the molecularly imprinted polymer occupied the gaps in the original SiO₂ arrangement and became rigid using EGDMA as a cross-linking agent after silica was etched. In the end, a molecularly imprinted polymer with a certain rigidity and maintaining a highly ordered and periodic structure is obtained, and this photonic crystal structure is called an inverse opal.²⁵

Finally, considering the visible light wavelength range of the human eye and human sensitivity to different colors of light,²⁶ we chose the 250 nm SiO₂ microspheres as a template to prepare MIPCs and for further testing.

3.2. Recognition of MIPCs in Relation to pH. As mentioned before, MIPC-FA was prepared based on methacrylic acid (MAA) as a functional monomer. The typical pH response performance of MIPC-FA based on SiO₂ photonic crystals was tested and is shown in Figure S4. As shown in Figure S4A, the Bragg diffraction peak of MIPCs gradually shifts to red with increasing pH, and the intensity of the diffraction peaks reaches a maximum when pH = 5. This phenomenon may be caused by the irregular volume change of MIPCs. When pH = 3–11, the position of the diffraction peak changes in a roughly linear pattern with the pH value, and when pH is higher than 11 or lower than 3, the position of the diffraction peak appears more shifted, as shown in Figure S4B. This result indicated that the carboxyl group of the functional

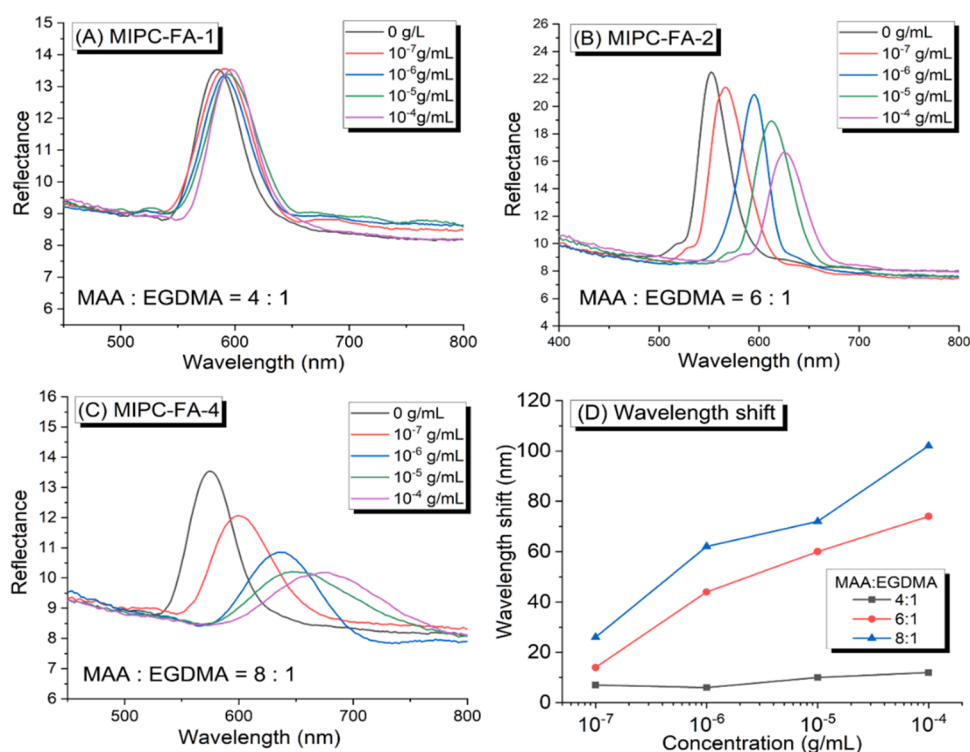


Figure 2. Reflectance spectra of MAA/EGDMA = 4:1 (A), 6:1 (B), and 8:1 (C) MIPC-FA to fusaric acid and chart of the diffraction peak shift (D).

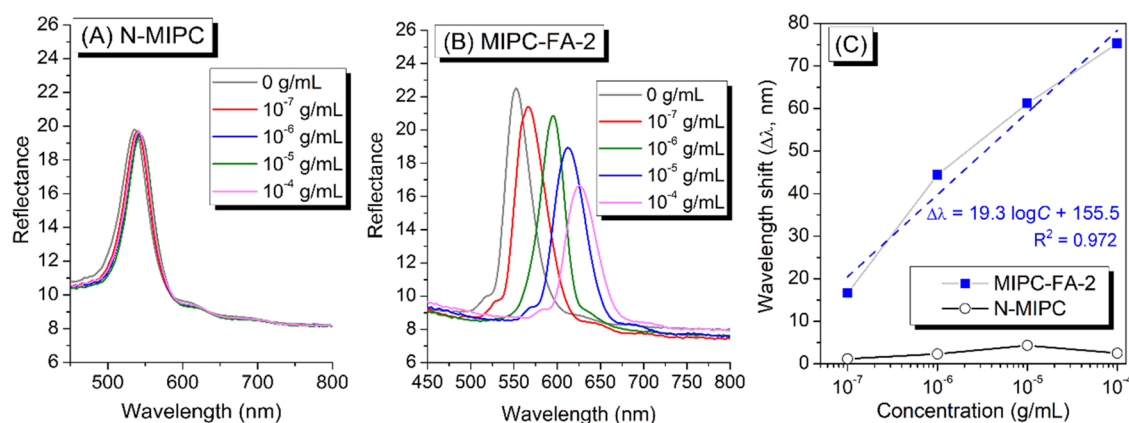


Figure 3. Responses of N-MIPC (A) and MIPC-FA-2 (B) and wavelength changes between N-MIPC and MIPC-FA-2 (C).

monomer (MAA) might be neutralized in an acid–base environment, which caused the swelling or shrinkage of MIPC-FA.

Based on this result, a phosphate buffer solution (PBS, pH = 7.6) is used as the test solvent in subsequent responsive experiments of MIPC to avoid the influence of the changes in diffraction peaks caused by pH changes.

3.3. Influence of Polymer Precursors on Response.

Figure 2 presents the response of MIPCs to fusaric acid under different cross-linking degrees. Different degrees of cross-linking were achieved at different ratios of MMA and EGDMA. As shown in Figure 2A, MIPC-FA-1 with MAA/EGDMA = 4:1 still has no obvious response under 10^{-4} g/mL fusaric acid (diffraction peak shift is only 8 nm under 10^{-4} g/mL). MIPC-FA-4 with MAA/EGDMA = 8:1 is obviously more responsive to fusaric acid, as illustrated in Figure 2C (diffraction peak shifts above 100 nm at 10^{-4} g/mL), but it can also be observed

that the diffraction peak intensity decreases and the peak width gradually widens with increasing FA concentration. Figure 2D indicates that the degrees of cross-linking of the imprinted polymer has a strong effect on the response. High degrees of cross-linking will cause little deformation of the polymer but a high degree of mechanical stability and low degrees of cross-linking will have the opposite effect. Therefore, a moderate cross-linking degree of the polymer (Figure 2B) can be used to obtain MIPCs that can cause deformation without significantly changing the ordered structure. Therefore, MIPC-FA-2, which has the best performance and with moderate cross-linking, is used for the following preparations.

According to the mechanism of molecularly imprinted photonic crystals, the response of MIPCs is based on hydrogen bonding between functional and template molecules. Water, as a highly polar substance, will affect the adsorption function of the molecularly imprinted polymer. The responses of the

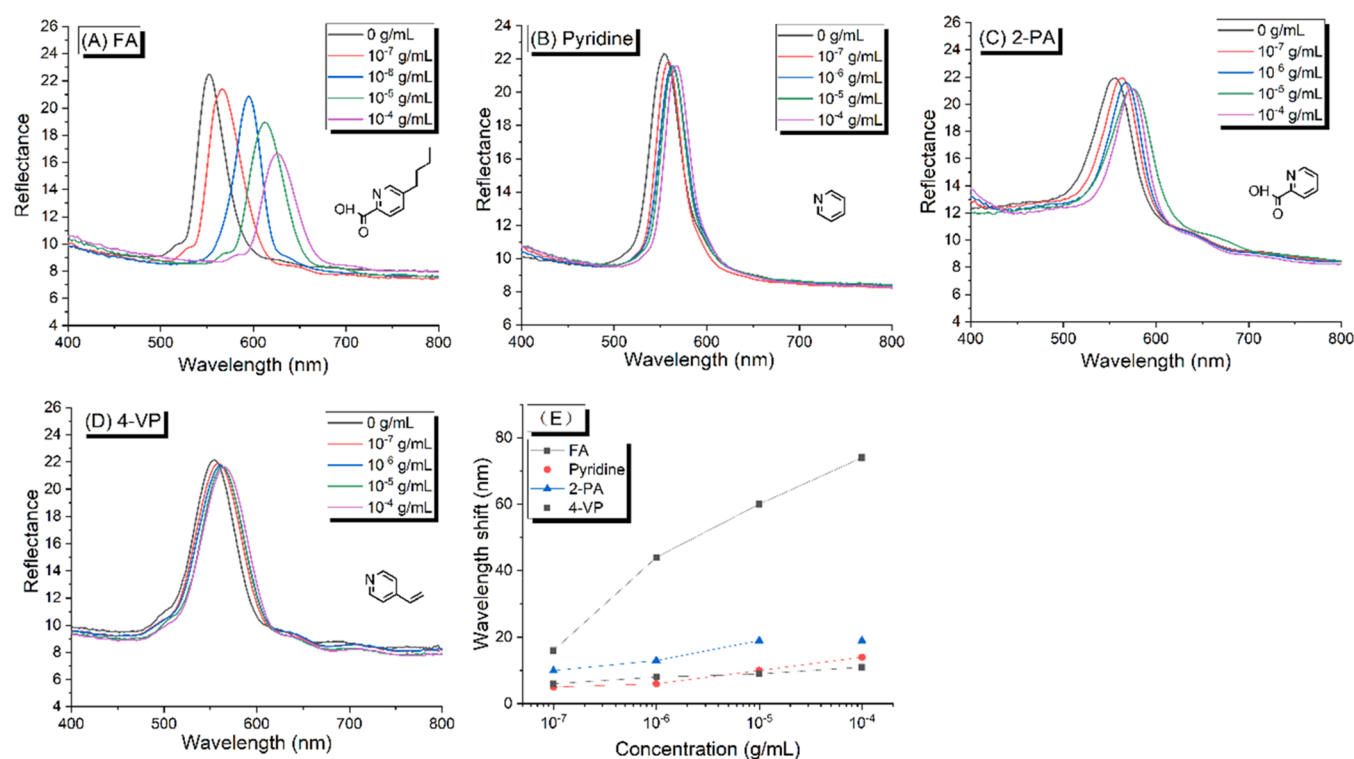


Figure 4. Response spectra of MIPC-FA caused by fusaric acid (A), pyridine (B), 2-picolinic acid (C), and 4-vinylpyridine (D) and wavelength shift chart (E); the insert picture is the corresponding chemical structure of the target molecule.

MIPCs with and without water during the preparation technique are shown in Figure S5. The response performance of MIPCs actually decreases without water, and a sudden decrease in diffraction peak intensity and shift can be observed at high concentrations of FA (Figure S5A). This phenomenon may be caused by water affecting the bonding of MIPCs and fusaric acid as well as the permeability in the test environment. A small amount of water can improve the permeability of the entire MIPC system in water (Figure S5B), which may offset the adverse effects caused by water molecules.

Finally, the wavelength changes of nonmolecularly imprinted photonic crystals (N-MIPCs) and MIPC-FA-2 under the same ratio of mixture in addition to the template molecule (FA) under fusaric acid are shown in Figure 3. This result indicates that the wavelength change caused by the molecularly imprinted polymer is caused by the template molecule selected during its synthesis, and N-MIPCs do not have the ability to recognize or change the diffraction peak. And for MIPC-FA-2, the relationship between the wavelength shift ($\Delta\lambda$) with the logarithmic concentrations of FA solutions ($\log C$) was almost linear, as shown in Figure 3C.

Based on the above discussion, the optimal synthesis process of MIPC-FA is determined as follows: SiO₂ photonic crystals with a particle size of 250 nm are selected to prepare templates; thus, λ_{\max} at different FA concentrations (0–10⁻⁴ g/mL) would be between 550 and 650 nm, and the polymerization ratio of MIPC-FA-2 is used to prepare molecularly imprinted photonic crystals to synthesize MIPC-FA.

3.4. Specificity of Molecularly Imprinted Photonic Crystals. The specificity of MIPC-FA depends on the recognition selectivity of the molecular imprinting technique and the changes in photonic crystal properties caused by recognition. To study the specificity of MIPCs based on fusaric

acid, MIPC-FA was used to respond to fusaric acid, pyridine, 2-picolinic acid, and 4-vinylpyridine, as shown in Figure 4A–D, respectively, which have pyridine ring but different side groups.

All of the substances used were prepared in the same concentration series. Compared with the result with fusaric acid (Figure 4A), a slight shift was observed when MIPC-FA was immersed in solutions of other substances. For example, the maximum red shift reached only 20 nm when the concentration of 2-picolinic acid was up to 10⁻⁴ g/mL, as shown in Figure 4B. The wavelength change caused by other substances hardly changes with the change in concentration. From the wavelength comparison in Figure 4E, it can be found that compared with the reaction to other substances, MIPC-FA shows obvious specificity to fusaric acid.

3.5. Recoverability of Molecularly Imprinted Photonic Crystals. It is known that the response of photonic crystals mainly depends on hydrogen bonding between the molecularly imprinted polymer and the template molecule, and this hydrogen bonding is reversible. Therefore, the recoverability of MIPC-FA was tested under a 1 × 10⁻⁴ g/mL fusaric acid combine-elute cycle. The spectrum of the repeated test and wavelength changes are shown in Figure S6. After five cycles of elute and response, MIPC-FA showed great reproducibility, and this reproducibility also showed that the structure of MIPC-FA is highly stable.

3.6. Analysis of Crude Toxin of the Foc4 Culture Medium. Former research results¹³ show that Foc4 produces a large number of metabolites during proliferation among which fusaric acid is typical. Following extraction of the crude toxin in the Foc4 culture medium, it was further tested by HPLC, as shown in Figure S7. Fusaric acid was found in the crude toxin after the extraction method, and then the standard curve was corrected according to the standard sample. The

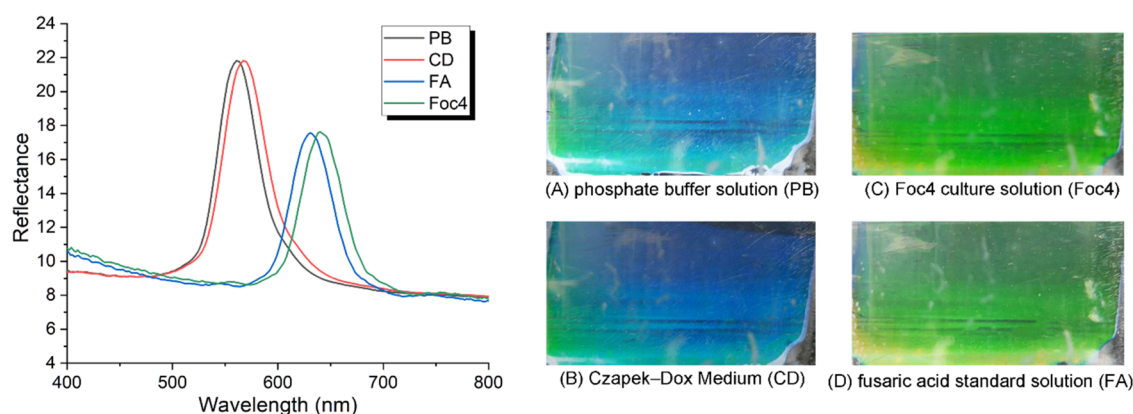


Figure 5. Comparison of the spectra of fusaric acid MIPC against phosphate buffer (PB) solution (A), Czapek-Dox (CD) Medium (B), Foc4 culture solution (C), and fusaric acid (FA) standard solution (D).

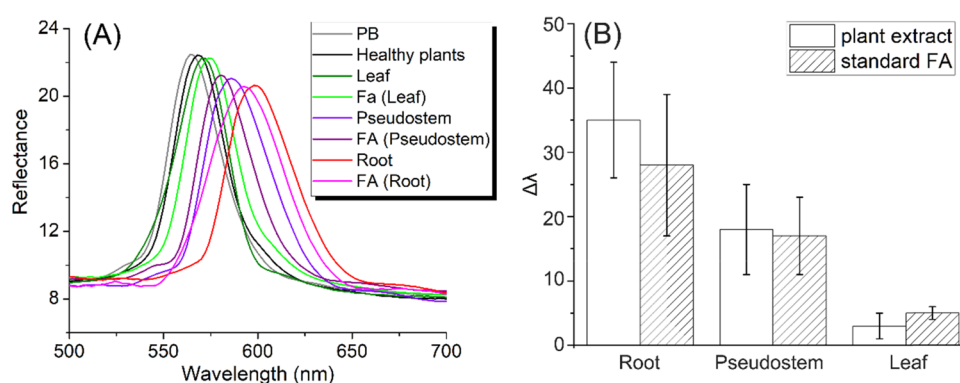


Figure 6. Reflectance spectrum (A) and Bragg diffraction peak shift (B) responses by plant extract and FA standard solution with the same concentration measured by HPLC.

concentration of fusaric acid in the Foc4 culture medium was $145.8 \pm 20.6 \mu\text{g/mL}$.

3.7. Response of MIPC-FA to Foc4 Culture Medium.

MIPC-FA was used to test the blank phosphate buffer solution and phosphate buffer solution of the blank Czapek-Dox medium, Foc4 culture medium, and FA standard solution with the same FA concentration (determined by the HPLC method) as the Foc4 culture medium. The results of the wavelength change and the corresponding MIPC-FA discoloration are shown in Figure 5.

Figure 5 shows that the Foc4 culture medium and FA standard solution with the same FA concentration ($145.8 \mu\text{g/mL}$, measured by HPLC) can cause obvious and similar wavelength shifts (69–75 nm) of MIPC-FA, while the Czapek-Dox medium causes almost no wavelength shifts. This result indicates that the FA in the Foc4 culture medium is the main reason for the wavelength shifts, which again verifies the specificity of MIPC-FA for fusaric acid.

In Figure 5A, about 15 nm shift can be observed between FA and Foc4, so we guess that it might be due to the complex components of the Foc4 culture medium, compared to the single component of the standard FA solution.

3.8. Distribution of Fusaric Acid in Banana Plants.

In Figure S8, it can be seen that the growth status of the banana seedlings inoculated with Foc4 was obviously worse: the roots of the plants inoculated with Foc4 were severely atrophied and almost brown, and there was no new root development; the pseudostems of the inoculated plant were relatively small, and there were spots similar to those seen in diseased plants; the

leaves of the inoculated plants obviously turned yellow from the top.

The inside of the banana was also observed by cutting the bulbs of different banana plants along the center part, as shown in Figure S8C,D. The bulbs of the inoculated plants were smaller than those of healthy bananas. After zooming in on the roots of the inoculated plants, it can be seen that the roots of the inoculated banana seedlings turned red, which may be due to xylem infection. In general, Foc4 banana seedlings were successfully infected based on multiple symptoms.

The phytotoxins in the banana plants from roots, pseudostems, and leaves were extracted separately, and the concentrations were analyzed by HPLC, as shown in Figure S9A. In contrast to the cultured Foc4 medium, there are more complex substances in plants. However, there was still a clear difference between the inoculated plant and the blank plant near 4.1 min. Comparing the peak time (4.1 min) of the fusaric acid standard under the same conditions, it was determined that the peak was the characteristic peak of fusaric acid. Finally, the concentration of fusaric acid was detected in three different positions from the roots, pseudostems, and leaves of the infected plants. As shown in Figure S9B, the distribution of fusaric acid was not uniform in banana plants, which may be related to the invasion stage of Foc4. The infection of Foc4 in plants started from the roots and gradually moved upward, which may cause uneven concentrations in banana seedlings.

3.9. Response of MIPC-FA to Extracts of Banana Plants. The extracts of plant roots, pseudostems, and leaves were selected for responsiveness experiments, and the same

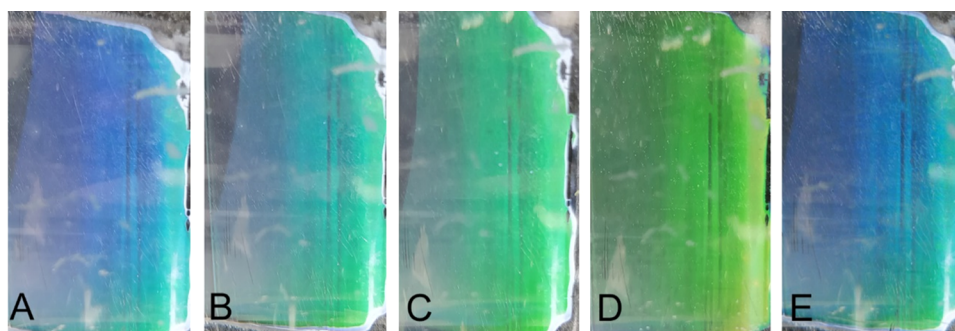


Figure 7. Color changes of MIPC-FA in blank PBS (A), leaves (B), pseudostems (C), and roots (D) of Foc4-infected and healthy banana seedlings (E).

concentration of fusaric acid obtained by HPLC was used for testing and comparison. The eluted MIPC-FA diffraction peak was used as the zero point to record the diffraction peak shift ($\Delta\lambda$) of different groups. The Bragg diffraction peak shift is shown in Figure 6, and the corresponding color changes of MIPC-FA are shown in Figure 7.

Comparing the HPLC data with the shift of the Bragg diffraction peak, it can be found that the difference between the peak shifts of the plant extracts is almost the same as the extraction concentration measured by HPLC. The diffraction peak shift caused by the root extract with FA concentration of about 150 ng/mL reached 35 nm, while the shift for pseudostem extract with FA concentration of about 50 ng/mL reached 28 nm. These degrees of diffraction peak shift can be observed with the naked eye, but the leaf extract with FA concentration of about 0.2×10^{-7} g/mL (as shown in Figure S9) only showed a 5 nm diffraction peak shift, which is difficult to identify by the naked eye, as shown in Figure 7B. Thus, the lower detection limit of MIPC-FA could be roughly inferred as about 50 ng/mL (0.5×10^{-7} g/mL).

Comparing the diffraction peak shifts of the fusaric acid standard and the extracted liquid at the same point, we found that the shift caused by root extraction was larger than that of the FA standard solution (5–15 nm), as shown in Figure 6A. The reason for this obvious gap might be that fusaric acid homologues or precursors are produced during toxin metabolism in Foc4 infection, and the presence of these similar substances may affect the detection. The gap between the peaks of other extracts and the corresponding standard solution was significantly smaller, which indicated that after Foc4 enters the vasculature, the Foc4 living environment has relatively less resistance, so the concentration of fusaric acid produced becomes low.

4. CONCLUSIONS

In conclusion, molecularly imprinted photonic crystals (MIPCs) of fusaric acid and their response to fusaric acid and to extracts of Foc4 culture medium and banana seedlings infected by Foc4 were studied. Monodispersed silica particles synthesized by a multistep method were used to fabricate silica photonic crystals by vertical deposition to provide templates for MIPCs. The degree of cross-linking of the polymer matrix and polymerization process parameters were adjusted to optimize the stability and response ability in fabricating the appropriate MIPC. The fabricated MIPCs show both a certain color change and spectroscopic differences under fusaric acid and have a specific response to FA. MIPC-FA can detect the concentrations of fusaric acid in the Foc4 culture medium and

Foc4-infected banana seedling extract, thus verifying that Foc4 produces fusaric acid in infected banana plants. Thus, we could afford a fast and effective field testing method, which could qualitatively or semiquantitatively determine whether a banana plant is infected by Foc4 or not and the approximate concentration of FA in the plant.

■ ASSOCIATED CONTENT

Supporting Information

The Supporting Information is available free of charge at <https://pubs.acs.org/doi/10.1021/acsapm.1c01032>.

Characterization of silica microspheres; SEM photographs of the photonic crystals; results for the influence of pH and water on the recognition of MIPCs; recoverability of MIPC-FA; determination of FA in the crude toxin of Foc4 culture medium; overall view of healthy and Foc4-infected banana seedlings (PDF)

■ AUTHOR INFORMATION

Corresponding Authors

Yaling Lin – College of Material and Energy, South China Agricultural University, Guangzhou 510642 Guangdong, China; orcid.org/0000-0002-5289-4304; Email: linyaling@scau.edu.cn

Anqiang Zhang – School of Materials Science and Engineering, South China University of Technology, Guangzhou 510641 Guangdong, China; orcid.org/0000-0001-7499-8406; Email: aqzhang@scut.edu.cn

Authors

Xixiang Feng – School of Materials Science and Engineering, South China University of Technology, Guangzhou 510641 Guangdong, China

Wei Zhang – College of Material and Energy, South China Agricultural University, Guangzhou 510642 Guangdong, China; orcid.org/0000-0003-1583-1555

Rui Li – School of Materials Science and Engineering, South China University of Technology, Guangzhou 510641 Guangdong, China; orcid.org/0000-0003-4866-5821

Complete contact information is available at:

<https://pubs.acs.org/doi/10.1021/acsapm.1c01032>

Notes

The authors declare no competing financial interest.

■ ACKNOWLEDGMENTS

The authors acknowledge the financial support from the National Natural Science Foundation of China (Nos. 31772202 and 52073098) and the Scientific and Technological Planning Project of Guangzhou City (201803020015).

■ ABBREVIATIONS

Foc, *Fusarium oxysporum* f. sp. *cubense*; Foc4, *Fusarium oxysporum* f. sp. *cubense* race 4; TEOS, tetraethyl orthosilicate; MAA, methacrylic acid; EGDMA, ethylene glycol dimethacrylate; PMMA, poly(methyl methacrylate); FA, fusaric acid (5-butylpicolinic acid); MIPs, molecularly imprinted polymers; MIPCs, molecularly imprinted photonic crystals; UV, ultra-violet; HPLC, high-performance liquid chromatography

■ REFERENCES

- (1) Ploetz, R. C. Fusarium wilt of banana is caused by several pathogens referred to as *Fusarium oxysporum* f. sp. *cubense*. *Phytopathology* **2006**, *96*, 653–656.
- (2) D'hont, A.; Denoeud, F.; Aury, J. M.; Baurens, F. C.; Carreel, F.; Garsmeur, O.; Noel, B.; Bocs, S.; Droc, G.; Rouard, M.; Da Silva, C.; Jabbari, K.; Cardi, C.; Poulain, J.; Souquet, M.; Labadie, K.; Jourda, C.; Lengelle, J.; Rodier-Goud, M.; Alberti, A.; Bernard, M.; Correa, M.; Ayyampalayam, S.; McKain, M. R.; Leebens-Mack, J.; Burgess, D.; Freeling, M.; Mbeguie-A-Mbeguie, D.; Chabannes, M.; Wicker, T.; Panaud, O.; Barbosa, J.; Hribova, E.; Heslop-Harrison, P.; Habas, R.; Rivallan, R.; Francois, P.; Poirion, C.; Kilian, A.; Burthia, D.; Jenny, C.; Bakry, F.; Brown, S.; Guignon, V.; Kema, G.; Dita, M.; Waalwijk, C.; Joseph, S.; Dievert, A.; Jaillon, O.; Leclercq, J.; Argout, X.; Lyons, E.; Almeida, A.; Jeridi, M.; Dolezel, J.; Roux, N.; Risterucci, A. M.; Weissenbach, J.; Ruiz, M.; Glaszmann, J. C.; Quetier, F.; Yahiaoui, N.; Wincker, P. The banana (*Musa acuminata*) genome and the evolution of monocotyledonous plants. *Nature* **2012**, *488*, 213–217.
- (3) Ploetz, R. C. Management of Fusarium wilt of banana: A review with special reference to tropical race 4. *Crop Prot.* **2015**, *73*, 7–15.
- (4) Gordon, T. R. *Fusarium oxysporum* and the Fusarium wilt syndrome. *Annu. Rev. Phytopathol.* **2017**, *55*, 23–39.
- (5) Dita, M. A.; Waalwijk, C.; Buddenhagen, I. W.; Souza, J. M. T.; Kema, G. H. J. A molecular diagnostic for tropical race 4 of the banana fusarium wilt pathogen. *Plant Pathol.* **2010**, *59*, 348–357.
- (6) Meldrum, R. A.; Fraser-Smith, S.; Tran-Nguyen, L. T. T.; Daly, A. M.; Aitken, E. A. B. Presence of putative pathogenicity genes in isolates of *Fusarium oxysporum* f. sp. *cubense* from Australia. *Australas. Plant Pathol.* **2012**, *41*, 551–557.
- (7) Niu, G.; Zhang, J.; Zhao, S.; Liu, H.; Boon, N.; Zhou, N. Bioaugmentation of a 4-chloronitrobenzene contaminated soil with *Pseudomonas putida* ZWL73. *Environ. Pollut.* **2009**, *157*, 763–771.
- (8) Pabinger, S.; Rödiger, S.; Kriegner, A.; Vierlinger, K.; Weinhäusel, A. A survey of tools for the analysis of quantitative PCR (qPCR) data. *Biomol. Detect. Quantif.* **2014**, *1*, 23–33.
- (9) Lin, Y.; Su, C.; Chao, C.; Chen, C.; Chang, C.; Huang, J.; Chang, P. A molecular diagnosis method using real-time PCR for quantification and detection of *Fusarium oxysporum* f. sp. *cubense* race 4. *Eur. J. Plant Pathol.* **2013**, *135*, 395–405.
- (10) Magdama, F.; Monserrate-Maggi, L.; Serrano, L.; Sosa, D.; Jiménez-Gasco, M. D. M. Comparative analysis uncovers the limitations of current molecular detection methods for *Fusarium oxysporum* f. sp. *cubense* race 4 strains. *PLoS One* **2019**, *14*, No. e0222727.
- (11) Fakhouri, W.; Walker, F.; Armbruster, W.; Heinrich, B. Detoxification of fusaric acid by a nonpathogenic *Colletotrichum* sp. *Physiol. Mol. Plant Pathol.* **2003**, *63*, 263–269.
- (12) Singh, V. K.; Singh, H. B.; Upadhyay, R. S. Role of fusaric acid in the development of 'Fusarium wilt' symptoms in tomato: Physiological, biochemical and proteomic perspectives. *Plant Physiol. Biochem.* **2017**, *118*, 320–332.
- (13) Dong, X.; Ling, N.; Wang, M.; Shen, Q.; Guo, S. Fusaric acid is a crucial factor in the disturbance of leaf water imbalance in Fusarium-infected banana plants. *Plant Physiol. Biochem.* **2012**, *60*, 171–179.
- (14) Andersson, L.; Sellergren, B.; Mosbach, K. Imprinting of amino acid derivatives in macroporous polymers. *Tetrahedron Lett.* **1984**, *25*, 5211–5214.
- (15) Wulff, G.; Oberkobusch, D.; Minárik, M. Enzyme-analogue built polymers, 18 chiral cavities in polymer layers coated on wide-pore silica. *React. Polym., Ion Exch., Sorbents* **1985**, *3*, 261–275.
- (16) Wang, J.; Pinkse, P. W. H.; Segerink, L. I.; Eijkel Jan, C. T. Bottom-up Assembled Photonic Crystals for Structure-Enabled Label-Free Sensing. *ACS Nano* **2021**, *15*, 9299–9327.
- (17) Alizadeh, T.; Hamedsoltani, L. Graphene/graphite/molecularly imprinted polymer nanocomposite as the highly selective gas sensor for nitrobenzene vapor recognition. *J. Environ. Chem. Eng.* **2014**, *2*, 1514–1526.
- (18) Alizadeh, T.; Rezaloo, F. A new chemiresistor sensor based on a blend of carbon nanotube, nano-sized molecularly imprinted polymer and poly methyl methacrylate for the selective and sensitive determination of ethanol vapor. *Sens. Actuators, B* **2013**, *176*, 28–37.
- (19) Tang, X.; Raskin, J.-P.; Lahem, D.; Krumpmann, A.; Decroly, A.; Debligny, M. A formaldehyde sensor based on molecularly-imprinted polymer on a TiO₂ nanotube array. *Sensors* **2017**, *17*, No. 675.
- (20) Smolinska-Kempisty, K.; Ahmad, O. S.; Guerreiro, A.; Karim, K.; Piletska, E.; Piletsky, S. New potentiometric sensor based on molecularly imprinted nanoparticles for cocaine detection. *Biosens. Bioelectron.* **2017**, *96*, 49–54.
- (21) Martins, N.; Carreiro, E. P.; Locati, A.; Ramalho, J. P. P.; Cabrita, M. J.; Burke, A. J.; Garcia, R. Design and development of molecularly imprinted polymers for the selective extraction of deltamethrin in olive oil: An integrated computational-assisted approach. *J. Chromatogr. A* **2015**, *1409*, 1–10.
- (22) Masalov, V. M.; Sukhinina, N. S.; Kudrenko, E. A.; Emelchenko, G. A. Mechanism of formation and nanostructure of Stöber silica particles. *Nanotechnology* **2011**, *22*, No. 275718.
- (23) Han, Y.; Lu, Z.; Teng, Z.; Liang, J.; Guo, Z.; Wang, D.; Han, M.; Yang, W. Unraveling the growth mechanism of silica particles in the stöber method: In situ seeded growth model. *Langmuir* **2017**, *33*, 5879–5890.
- (24) Weidemüller, M.; Hemmerich, A.; Görlitz, A.; Esslinger, T.; Hänsch, T. W. Bragg diffraction in an atomic lattice bound by light. *Phys. Rev. Lett.* **1995**, *75*, 4583–4586.
- (25) Schrodien, R. C.; Al-Daous, M.; Blanford, C. F.; Stein, A. Optical properties of inverse opal photonic crystals. *Chem. Mater.* **2002**, *14*, 3305–3315.
- (26) Biersdorf, W. R.; Armington, J. C. Response of the human eye to sudden changes in the wavelength of stimulation. *J. Opt. Soc. Am.* **1957**, *47*, 208–215.
- (27) Wu, Z.; Hu, X.; Tao, C.-a.; Li, Y.; Liu, J.; Yang, C.; Shen, D.; Li, G. Direct and label-free detection of cholic acid based on molecularly imprinted photonic hydrogels. *J. Mater. Chem.* **2008**, *18*, 5452–5458.

The interactions between bovine serum albumin and carboxybetaine-functionalized polysiloxanes in solution

Yaling Lin¹ · Weiyan Huang² · Yang You² · Yufeng Lei² · Anqiang Zhang²

Received: 25 August 2016 / Revised: 8 October 2016 / Accepted: 17 October 2016 / Published online: 27 October 2016
© Springer-Verlag Berlin Heidelberg 2016

Abstract The interactions between carboxybetaine-functionalized polydimethylsiloxanes (PDMS-g-CB) and bovine serum albumin (BSA) in water solution were investigated from varied aspects based on different techniques, including fluorescence spectroscopy, UV-Vis spectroscopy, circular dichroism spectroscopy, isothermal titration calorimetry, and atomic force microscopy. Due to the weak interaction between PDMS-g-CB and BSA, another polymer with similar structure as PDMS-g-CB, i.e., quaternary ammonium salt-functionalized polydimethylsiloxanes (PDMS-g-QAS), was synthesized and chosen as the positive control, and the results indicated that the free PDMS-g-CB in solution could exhibit good resistance against proteins, which was mainly due to the zwitterions-side groups' binding ability between PDMS chain and protein. Both the characterization methods and the results could help us to understand the interaction between free water-soluble polymers and protein, and extend the application of PDMS-g-CB and design new antifouling materials.

Electronic supplementary material The online version of this article (doi:10.1007/s00396-016-3969-5) contains supplementary material, which is available to authorized users.

✉ Yaling Lin
linyaling@scau.edu.cn

✉ Anqiang Zhang
aqzhang@scut.edu.cn

¹ College of Materials and Energy, South China Agricultural University, 483 Wushan Rd., Guangzhou, Guangdong 510642, China

² College of Material Science and Engineering, South China University of Technology, 381 Wushan Rd., Guangzhou, Guangdong 510641, China

Keywords Carboxybetaine functionalized polydimethylsiloxanes · Protein · Polymer/protein interactions · Fluorescence spectroscopy · Isothermal titration calorimetry

Introduction

Proteins exist extensively in plants, animals, and many other creatures and play vital roles in life processes. Polymer-protein interactions are important for the design and preparation of polymer materials for biomedical applications. The strength of polymer-protein interactions should be tailored depending on the application. Appropriate protein absorption to polymers is required in polymer scaffolds and targeted drug and gene delivery [1–3]. The interactions between polymers and proteins should be weak for marine coating, antifouling membranes, implanted devices, and drug delivery carriers [4–7]. PEG-based polymers, a type of hydrophilic polymer materials, have been widely studied as an antifouling material [8–11], and the hydration induced by hydrogen bonds between water molecules and such materials can be used to account for their antifouling behavior [12, 13]. However, their chemical instability restricts the application of this group of materials [14].

Polybetaine is a new generation of antifouling material [14–16]. With a negative and positive charge on a monomer unit, polybetaines are electrically neutral and hydrophilic and can bind water molecules more tightly via ionic solvation, which is stronger than hydrogen bond [13, 17, 18]. Polybetaines exhibit excellent protein-resistance properties and stabilities [19]. In recent years, antifouling materials based on polybetaines, such as poly(carboxylbetaine) (pCB) and poly(sulfobetaine) (pSB), have received an increasing amount of attention because of the inexpensive raw material and

excellent antifouling properties [20–26]. However, in most cases, these polybetaines have been immobilized on a certain surface, and their antifouling properties are evaluated through quartz crystal microbalance (QCM), surface plasmon resonance (SPR) methods [27, 28]. Thus, the interactions between proteins and free polybetaines in solution have rarely been reported.

In our previous work, water-soluble carboxybetaine-functionalized polydimethylsiloxanes (PDMS-g-CB), which consisted of a PDMS backbone and carboxybetaine pendant-side groups, were synthesized and were mixed with PDMS or grafted on PDMS surface, which could significantly improve the material's ability of resisting protein and bacterial absorption [29, 30]. The carboxybetaine-side group electrostatically combined with water, and the induced hydration layer resisted the absorption of protein and bacteria. Considering spraying operation would be more acceptable for some applications like plant protection, thus the interactions of free and water-soluble polymers with protein were more expected, unfortunately, it's rarely reported.

PDMS-g-CB is considered to be a potential environmentally friendly pesticide. A soluble antifouling material can be an excellent out way to pest prevention. Insects, such as *Spodoptera exigua* (beet armyworm), secrete mucus on the abaxial leaf surface to assist in the adhesion of eggs, and this mucus mainly contains water, proteins, and a small amount of carbohydrates [31]. We believe that it is possible to form an antifouling coating on leaf surfaces by spraying a PDMS-g-CB solution, thus resisting the adhesion of insect eggs and restraining the reproduction of pests. Thus, the interactions between proteins and free PDMS-g-CB are a fundamental issue.

In this study, experiments were conducted to gain an understanding of the interaction between free PDMS-g-CB and protein. Bovine serum albumin (BSA), a convenient and widely studied model globular protein in biological process, was chosen as the model protein for its well water-solubility, unique ligand-binding properties, and well-established structure [32]. We detected the interaction in solution between BSA and PDMS-g-CB using different analytical methods, including fluorescence spectroscopy, UV-Vis spectroscopy, circular dichroism spectroscopy, isothermal titration calorimetry, and atomic force microscopy. PDMS-g-QAS, [33] which is similar to PDMS-g-CB in structure, containing a PDMS backbone and quaternary ammonium salt pendant-side groups was chosen as the positive comparison. The results obtained from different measurements showed that the interactions between PDMS-g-CB and proteins in solution were weak, or even too weak to be detected, benefiting the design and application of this group of antifouling materials.

Experimental

Materials

Octamethylcyclotetrasiloxane (D^4 , >99.5 %, Dow Corning, USA), 1, 3, 5, 7-tetramethylcyclotetrasiloxane (D^4_H , >99 %, Hangzhou Silong Material Technology Co. Ltd., China), and hexamethyldisiloxane (MM, >99 %, Dow Corning, USA) were dried before use. N, N-Dimethylallylamino (DMAA, >99 %, Haining City Huangshan Chemical Industry Co. Ltd., China) was purified by distillation before use. Benzyl chloride (GC, >99 %) and sodium chloroacetate (SC) were purchased from Aladdin Reagent Co. Ltd. (Shanghai, China) and were used as received. Platinum (0)-1, 3-divinyl-1, 1, 3, 3-tetramethyldisiloxane complex solution (Karstedt's catalyst solution, Pt~2 %, Aladdin Reagent Co. Ltd., China) was used as the catalyst for the hydrosilylation reaction. Purolite™ CT175 (Purolite (China) Co. Ltd) is a clay containing sulfonic acid and was used as received. Other solvents, such as isopropanol, were used without any pretreatment. Bovine serum albumin (BSA) was purchased from the Bio Science & Technology Co. Ltd. (Shanghai, China). Water used in these experiments was purified by an Ultrapure water purification system with a minimum resistivity of 18.0 MΩ.cm. The phosphate buffer solution (PBS) had a pH of 7.0 and an ionic strength of 0.01 mol/L.

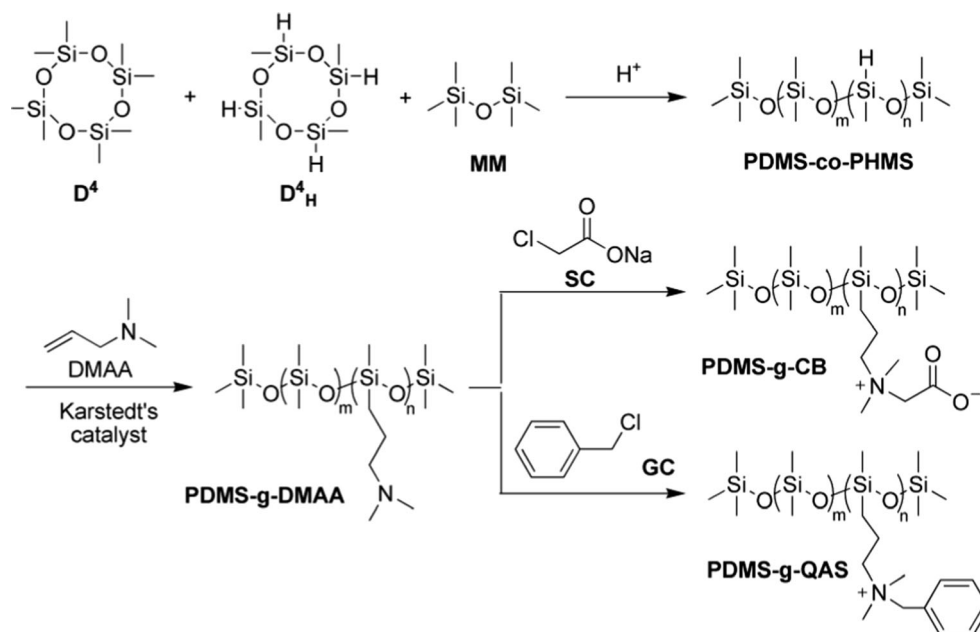
Syntheses of PDMS-g-CB and PDMS-g-QAS

In this paper, PDMS-g-CB series and PDMS-g-QAS were synthesized via a three-step procedure according to our previous report (Scheme 1) [29, 33]. The two polymers shared the same first two steps, but were different from each other when it comes in the third step.

Firstly, hydrogen-containing polysiloxanes (PDMS-co-PHMS) were synthesized through ring-opening polymerization of D^4 and D^4_H . Secondly, DMAA was grafted to PDMS-co-PHMS via a hydrosilylation reaction in the presence of Karstedt's catalyst to obtain PDMS-g-DMAA. Finally, carboxybetaine-functionalized polysiloxanes (PDMS-g-CB) were prepared by subsequent quaternization reaction with sodium chloroacetate (SC), while benzyldimethylaminopropyl chloride grafted polysiloxane (PDMS-g-QAS) were prepared with benzyl chloride (GC).

The control group for the series of experiments in this paper was PDMS-g-QAS, which had a similar construction to PDMS-g-CB and has been shown to interact with proteins [33].

The grafting ratio and molecular weight (determined by GPC) of the polymers are presented in Table 1.

Scheme 1 The synthetic route of PDMS-g-CB and PDMS-g-QAS

Fluorescence spectroscopy

Steady-state fluorescence experiments were carried out with an FM-4P spectrofluorometer (HORIBA, France) using a 1.0-cm quartz cell at 25 °C. Fluorescence spectra were measured upon adding different amounts of polymers to a fixed BSA solution of 0.1 mg/mL, and the mass ratio of the polymer/BSA was varied from 0 to 0.1, 0.5, 1, 2, 4, and 8. The samples were prepared with PBS with pH = 7.0 and incubated for 5 h before analyses. Intrinsic fluorescence spectra were recorded between 310 and 400 nm with an excitation wavelength of 275 nm, where the contribution of polymers was negligible. Excitation and emission slits comprised of nominal 2 nm bandwidths. The fluorescence spectra were acquired as an average of three repeated scans.

Circular dichroism spectroscopy

Far-UV circular dichroism (CD) spectroscopy was performed using a Chirascan CD spectropolarimeter (Applied Photophysics Ltd., UK) in a wavelength range of 190–260 nm. Considering the accuracy of the CD spectra, we used

a fixed BSA solution of 0.3 mg/mL, and the mass ratio of polymer/BSA was varied from 0 to 1/30, 5/30, 10/30, 20/30, 40/30, and 80/30. The samples were prepared with PBS with pH = 7.0 and incubated for 5 h before testing. The samples were filled in a 0.1-cm path length cuvette where the temperature was kept at 25 °C with a circulation water bath. The CD spectra were acquired as an average of three repeated scans with a scanning rate, response time, and step of 20 nm/min, 0.5 s, and 1 nm, respectively. The recorded spectra were corrected for background signals using buffer solution.

UV–Vis spectroscopy

UV-Vis spectra were obtained using a UV-2550 spectrometer (Shimadzu, Japan) with a 1.0-cm quartz cell at 25 °C. The spectra were recorded in a wavelength range from 200 to 300 nm with a step of 1 nm. The measurements used the same concentration series as the fluorescence spectroscopy measurements. The solutions were incubated at 25 °C for 5 h before analyses. A buffer solution was used as a blank to eliminate the disturbance from the adsorption of polymers. The UV-Vis spectra were acquired as an average of three repeated scans.

Isothermal titration calorimetry

The calorimeter used was the Nano ITC (TA Instruments, USA). A 2 μ L aliquot of a BSA solution was added stepwise using an automatic injection syringe containing 50 μ L of a 0.02 mg/mL BSA solution into a cell of 300 μ L that contained either water or a polymer solution with a 3-min interval between each injection at 25 °C. The concentrations of the

Table 1 Molecular weight and grafting ratio of polymers

Sample	Molecular weight (Mn)	Grafting ratio
PDMS-g-CB _{1/3}	4.85×10^3	1/3
PDMS-g-CB _{1/4}	3.10×10^3	1/4
PDMS-g-CB _{1/6}	2.22×10^3	1/6
PDMS-g-CB _{1/8}	3.69×10^3	1/8
PDMS-g-QAS	2.22×10^3	1/6

polymer solutions were four times their CMC values, i.e., 0.2, 0.3, 0.2, 0.25, and 0.2 mg/mL for PDMS-g-CB_{1/3}, PDMS-g-CB_{1/4}, PDMS-g-CB_{1/6}, PDMS-g-CB_{1/8}, and PDMS-g-QAS, respectively [29]. The solution was prepared with ultrapure water and degassed before testing.

Atomic force microscopy

Morphological changes of the proteins in the absence and presence of polymers were imaged using tapping-mode AFM. A drop of the mixed protein–polymer solution with a polymer/BSA mass ratio of 10/1 (BSA concentration of 0.05 mg/mL) was deposited on fresh peeled mica and dried for 24 h (under the normal conditions) before AFM imaging. AFM images were acquired by a Bruker Multimode 8. Commercial Si cantilever (Bruker) with an elastic modulus of 40 N/m was used. All images were acquired at a typical scan rate of 1.0 Hz and scan angle of 0°. Representative images of each sample were collected by scanning at least three different locations.

Results and discussion

The interactions between the polymers and proteins could be evaluated from different aspects. The addition of a polymer may change the conformation of a protein, which consists of tertiary and secondary structures, resulting in the release of heat or aggregation. Here, we used varied detection methods to evaluate the interaction between PDMS-g-CB (or PDMS-g-QAS) and BSA, as discussed in the following.

Fluorescent spectroscopy

The fluorescent spectroscopy of proteins was used to measure the change in the tertiary structure of the protein induced by different polymers. The intrinsic fluorescence of BSA recorded in the range of 280–480 nm mainly results from aromatic amino acids residues of Tyr and Trp [34]. Once the protein undergoes a conformational change, the fluorescence of the aromatic amino acids depends not only on the exposure or accessibility of their residues but also on the local protein environment immediately surrounding the aromatic amino acids [28]. Here, the polymer-induced conformational changes of proteins at different polymer/protein mass ratios (i.e., 0, 0.1, 0.5, 1, 2, 4, and 8) as a function of polymer grafting ratios was monitored by observing changes in the intensity of BSA fluorescence (Fig. 1). A blue shift from 348 to 329 nm was observed in PDMS-g-QAS/BSA systems (Fig. 1e), which suggests that the fluorescence residues were surrounded by a more hydrophobic environment resulting from the absorption of PDMS-g-

QAS molecules near the amino acid residues. The fluorescence intensity decreased with an increase in polymer concentration, as illustrated by Fig. 1e, where PDMS-g-QAS demonstrated a stronger ability to induce fluorescence quenching of BSA.

In contrast, for any PDMS-g-CB/BSA mixtures, the fluorescence curves of different concentrations were almost overlapped. There were no detectable red/blue shifts or clear intensity changes (Fig. 1a–d, f), which illustrated that PDMS-g-CB did not influence the microenvironment of aromatic amino acids or induce fluorescence quenching of BSA. It also illustrated that the faint influence of PDMS-g-CB on BSA aromatic amino acids residues was independent of its grafting ratio. The fluorescence intensities of PDMS-g-CB/BSA systems slightly decreased, which may have been induced by shading of the high concentration solution.

Different interactions between proteins and PDMS-g-CB or PDMS-g-QAS are likely attributed to their different side groups. PDMS-g-QAS is a polymeric quaternary ammonium salt, where the polymer chain is positively charged in aqueous media. While BSA is a negatively charged protein [35] and can combine with PDMS-g-QAS through electrostatic interactions and form aggregates in solution, resulting fluorescence quenching. PDMS-g-CB is a zwitterionic polymer, and the polymer chain is electrically neutral in solution. Additionally, the amount of carboxybetaine side groups is large and allows water molecules to bind strongly via ionic solvation, which can block the adhesion of protein molecules.

Circular dichroism spectroscopy

Far-UV circular dichroism (CD) spectroscopy is a useful tool for detecting changes in the secondary structure of BSA, which is composed of an α -helix, β -sheet, β -turn, and random coil [36]. The CD spectra for the PDMS-g-CB/BSA and PDMS-g-QA/BSA systems in the range of 190–260 nm are shown in Fig. 2. Two negative bands at approximately 210 and 222 nm were characteristic CD spectra of a BSA α -helix. The negative molar ellipticity decreased with an increase in the polymer concentration, indicating a decrease in the α -helix content [34]. The CD spectra curves of all PDMS-g-CB/BSA solution mixtures at different polymer concentrations were almost overlapping (Fig. 2a–d). The negative molar ellipticity decreased with an increase in the PDMS-g-QAS/BSA mass ratio (Fig. 2e), indicating that the addition of PDMS-g-QAS induced an α -helix transformation. The calculated contents of α -helix, β -sheet, β -turn, and random coil structures at the lowest and highest polymer concentrations (Fig. 2f) showed that PDMS-g-CB almost did not affect the secondary structure of BSA, while the 0.8 mg/mL PDMS-g-

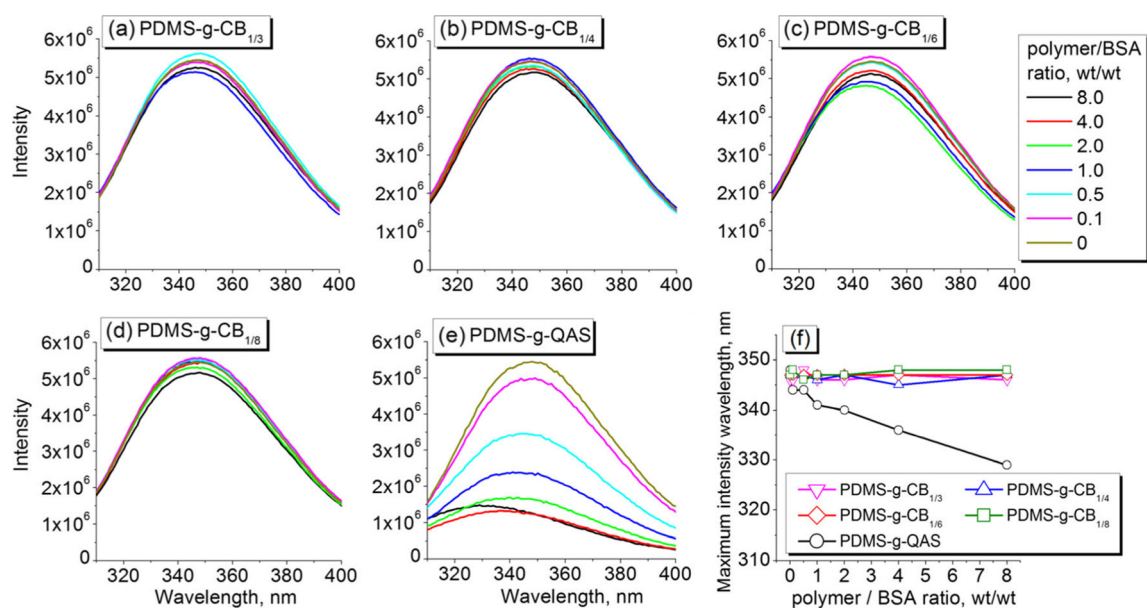


Fig. 1 The fluorescence curves of different polymer/BSA mixture solutions in varied concentrations **a** PDMS-g-CB_{1/3}, **b** PDMS-g-CB_{1/4}, **c** PDMS-g-CB_{1/6}, **d** PDMS-g-CB_{1/8}, **e** PDMS-g-QAS, and **f** the maximum intensity wavelength vs. polymer/BSA ratios

QAS could introduce a 50 % drop in the α -helix content, indicating the strong ability of PDMS-g-QAS in unfolding the BSA molecule.

UV-Vis measurements

Except for detecting the microenvironment of aromatic amino acid residues, UV-Vis spectroscopy can also detect changes in polypeptide backbone structures. Figure 3 shows the UV-Vis spectra for the polymer/BSA mixture

solutions, where two absorption peaks at approximately 204 and 278 nm are clearly presented. In PDMS-g-CB/BSA mixture solutions, the absorbance curves of different polymer concentrations were almost overlapped, and no red/blue shift and absorbance changes were observed at either 204 or 278 nm (Fig. 3a–d, and Fig. 4). For the PDMS-g-QAS/BSA mixtures, the addition of PDMS-g-QAS into the BSA buffer solution resulted in a significant red shift ($\Delta\lambda_{\max} \sim +8$ nm) of the maximum absorbance peak accompanied with an intensity increase at

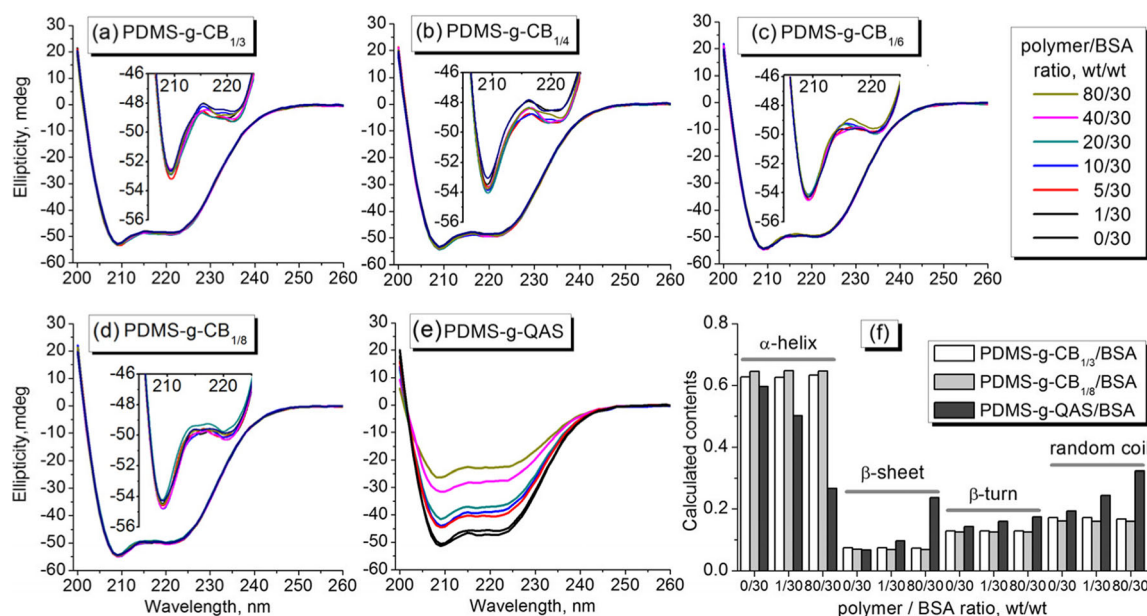
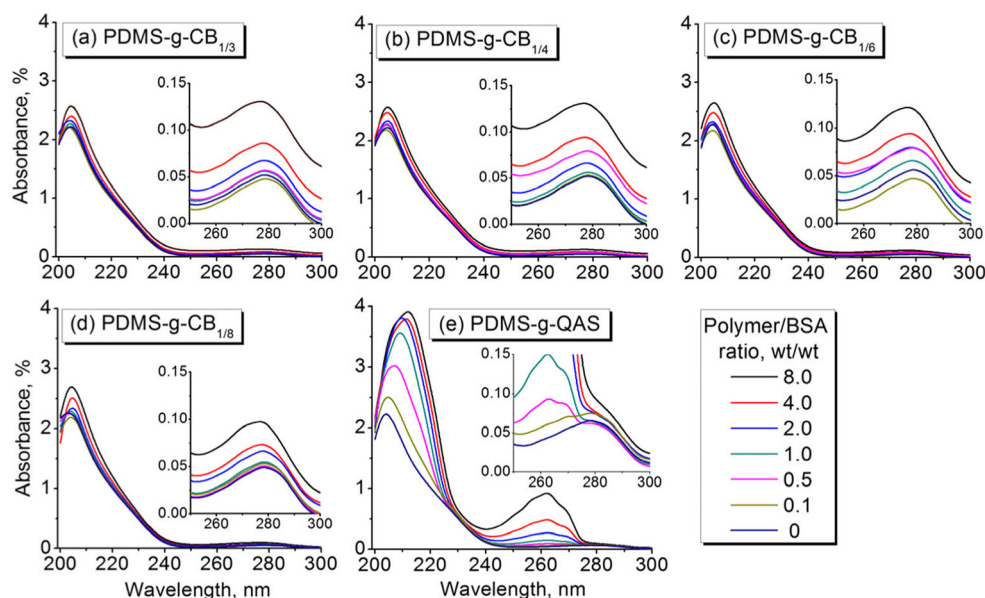


Fig. 2 CD spectra of polymer/BSA solution in varied polymer/BSA ratio **a** PDMS-g-CB_{1/3}, **b** PDMS-g-CB_{1/4}, **c** PDMS-g-CB_{1/6}, **d** PDMS-g-CB_{1/8}, **e** PDMS-g-QAS, and **f** The calculated contents of α -helix, β -sheet, β -turn, and random coil, with BSA concentration of 0.3 mg/mL

Fig. 3 The UV-Vis spectra of polymer/BSA solutions with different polymer/BSA ratio **a** PDMS-g-CB_{1/3}, **b** PDMS-g-CB_{1/4}, **c** PDMS-g-CB_{1/6}, **d** PDMS-g-CB_{1/8}, and **e** PDMS-g-QAS, with BSA concentration of 0.1 mg/mL



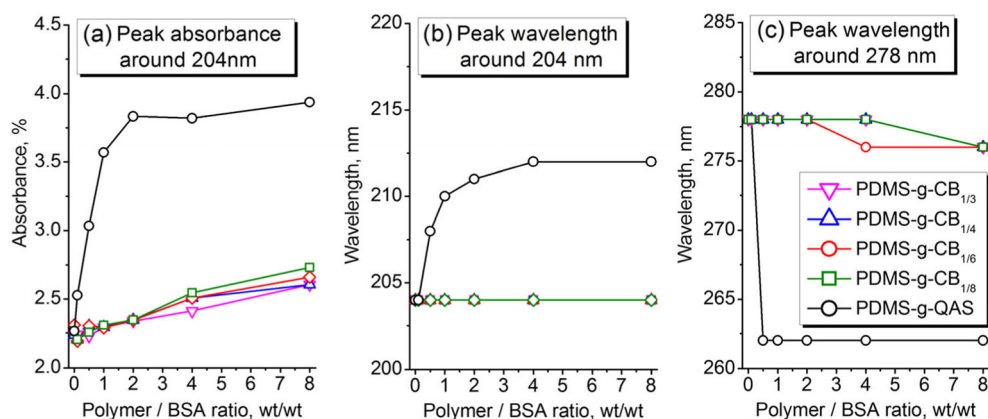
204 nm (Fig. 4a), which was attributed to the π - π^* transition of the polypeptide backbone structure ($C=O$) of BSA. It is reported that π^* electron clouds have higher polarity than that of π ; therefore, in a polar solvent, the energy of π^* should decrease more than that of π , which would reduce the energy gap between π^* and π and result in a red shift of absorbance at approximately 204 nm (Fig. 4b) [34]. These observations and CD measurements suggested that BSA was unfolded by PDMS-g-QAS and exposed the structures in a more polar environment.

There was also a blue shift ($\Delta\lambda_{\max} \sim -16$ nm) and intensity increase of the maximum absorbance peak at approximately 278 nm (Fig. 4b), which was due to the n - π^* transition of the aromatic amino acid residues [34]. This observation was consistent with the fluorescence spectra, and the aromatic amino acid residues were found to be surrounded by a more hydrophobic environment.

Isothermal titration calorimetry

From a macro perspective, heat absorption and emissions are always observed in the presence of reactions. Figure 5 shows the calorimetric titration curves upon the addition of a 0.2 mg/mL BSA solution into water and the polymer solutions (detailed titration curves are shown in Fig. S1, Electronic Supplementary Material). The curves of all the PDMS-g-CB/BSA systems almost overlapped, which suggested that the heat release of PDMS-g-CB/BSA systems was independent of polymer grafting ratios. Moreover, the curve shapes of the BSA/water and BSA/polymer mixtures were similar except for PDMS-g-QAS, as shown in Fig. S1a~f. When BSA was added to any of the PDMS-g-CB solutions, there was a heat release difference of approximately 1.5 μ J/mol between the BSA/water and BSA/PDMS-g-CB systems, which can be attributed to changes in the solution environments. PDMS-g-QAS had a

Fig. 4 The polymer maximum absorbance of varied grafting ratio at different concentration (a) and corresponding wavelength near 204 (b), and 278 nm (c), respectively



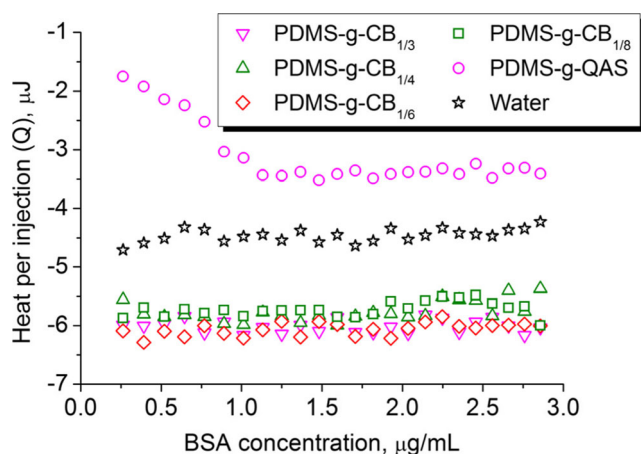


Fig. 5 ITC data for titration of BSA (0.2 mg/mL) into different polymer solution or water at 25 °C

different curve shape: the heat per injection (Q) decreased with an increase in protein content and then appeared to plateau. In the beginning, BSA interacted with PDMS-g-QAS and this process was exothermic. With an increase in the protein concentration in a sample cell, the bond reached saturation, as shown in Fig. S1f.

AFM experiments

AFM protocols provide morphological reproduction of microsurfaces and are generally used to characterize protein interactions with polymers. Thus, the morphological changes of the proteins upon incubation with polymers (PDMS-g-CB and PDMS-g-QAS) were examined. The mass ratio of polymer/BSA was 10/1, and the sample had a BSA concentration of 0.05 mg/mL. The morphologies of the deposited aggregates firmly adsorbed on mica were then analyzed by tapping-mode AFM. For BSA-involved systems, some small and uniform sphere-like molecules of 5–8 nm were observed in pure BSA solutions (Fig. 6a). Upon incubation of BSA with PDMS-g-CB, spherical particles similar in size, shape, and quantity were clearly observed (Fig. 6b). Conversely, a mixture of BSA and PDMS-g-QAS

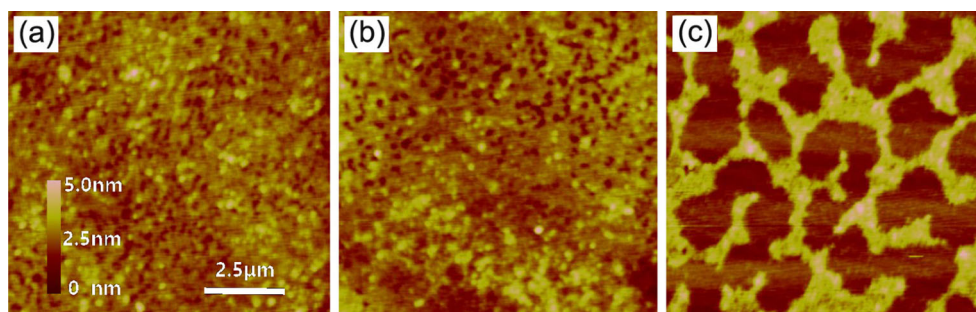
produced irregular aggregation, in sharp contrast to the morphologies of pure BSA and mixed BSA-PDMS-g-CB solutions (Fig. 6c). The aggregation of BSA may account for PDMS-g-QAS unfolding BSA molecules and changing the charge around the protein surface.

Overall, qualitative AFM images provided additional evidence that PDMS-g-CB had a relatively faint interaction with proteins than PDMS-g-QAS, complementary to the more quantitative results from all the experiments described above. Similar morphologies between protein and protein/PDMS-g-CB systems indicated that PDMS-g-CB in aqueous solutions did not induce morphological changes of proteins.

Conclusions

In this work, we studied the interaction between BSA and PDMS-g-CB or PDMS-g-QAS in solution from different aspects via optical techniques, ITC, and AFM. The CD spectra and UV-Vis spectra demonstrated that PDMS-g-QAS could unfold protein molecules, which consequently resulted in the exposure of aromatic amino acid residues to more hydrophobic environments, as observed in the fluorescence spectra. The ITC curves confirmed that interactions occurred between PDMS-g-QAS and BSA, and AFM protocols showed that this type of interaction induced protein aggregation. From a wide analysis of the data, we did not detect dramatic interactions between PDMS-g-CB and BSA compared with PDMS-g-QAS, which was attributed to its strong ability to bind with water molecules via the zwitterions on the side groups. The optical spectra and ITC results demonstrated that the grafting ratio did not influence the ability of PDMS-g-CB to resist the absorption of proteins and made it obvious that PDMS-g-CB had good anti-fouling properties. Because the PDMS-g-CBs were obtained by modified polyorganosiloxane (PDMS) through grafting betaine, the bio-inert properties of the PDMS backbone, and the super-hydrophilic side carboxybetaine groups allowed for effective insect prevention. This work helped clarify our understanding of the interaction

Fig. 6 AFM images of **a** pure BSA, **b** PDMS-g-CB_{1/6}/BSA, and **c** PDMS-g-QAS/BSA with BSA concentration of 0.05 mg/mL and polymer/BSA ratio of 10/1 (wt/wt)



between polymers and proteins in solution and can serve as a guide for the design and syntheses of anti-fouling materials applied in solution.

Acknowledgments This work was supported by the National Natural Science Foundation of China under Grant 31201552 and 51473051; the Specialized Research Fund for the Doctoral Program of Higher Education under Grant 20124404120025; and the Science and Technology Planning Project of Guangdong Province under Grant 2016A020210105.

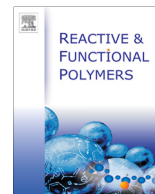
Compliance with ethical standards

Conflict of interest The authors declare that they have no conflict of interest.

References

- Place ES, George JH, Williams CK, Stevens MM (2009) Synthetic polymer scaffolds for tissue engineering. *Chem Soc Rev* 38:1139–1151
- Ma Z, Mao Z, Gao C (2007) Surface modification and property analysis of biomedical polymers used for tissue engineering. *Colloid Surface B* 60:137–157
- Kabanov AV, Batrakova EV, Alakhov VY (2002) Pluronic® block copolymers as novel polymer therapeutics for drug and gene delivery. *J Control Release* 82:189–212
- Yang WJ, Neoh K, Kang E, Teo SL, Rittschof D (2014) Polymer brush coatings for combating marine biofouling. *Prog Polym Sci* 39:1017–1042
- Zhao Y, Zhu L, Yi Z, Zhu B, Xu Y (2013) Improving the hydrophilicity and fouling-resistance of polysulfone ultrafiltration membranes via surface zwitterionization mediated by polysulfone-based triblock copolymer additive. *J Membrane Sci* 440:40–47
- Shen M, Wagner MS, Castner DG, Ratner BD, Horbett TA (2003) Multivariate surface analysis of plasma-deposited tetraglyme for reduction of protein adsorption and monocyte adhesion. *Langmuir* 19:1692–1699
- Yuan Y, Mao C, Du X, Du J, Wang F, Wang J (2012) Surface charge switchable nanoparticles based on zwitterionic polymer for enhanced drug delivery to tumor. *Adv Mater* 24:5476–5480
- Pale-Grosdemange C, Simon ES, Prime KL, Whitesides GM (1991) Formation of self-assembled monolayers by chemisorption of derivatives of oligo (ethylene glycol) of structure $\text{HS}(\text{CH}_2)_{11}(\text{OCH}_2\text{CH}_2)_m\text{OH}$ on gold. *J Am Chem Soc* 113:12–20
- Prime KL, Whitesides GM (1993) Adsorption of proteins onto surfaces containing end-attached oligo (ethylene oxide): a model system using self-assembled monolayers. *J Am Chem Soc* 115:10714–10721
- Guo D, Han H, Wang J, Xiao S, Dai Z (2007) Surface-hydrophilic and protein-resistant silicone elastomers prepared by hydrosilylation of vinyl poly (ethylene glycol) on hydrosilanes-poly (dimethylsiloxane) surfaces. *Colloids Surfaces A* 308:129–135
- Kingshott P, Thissen H, Griesser HJ (2002) Effects of cloud-point grafting, chain length, and density of PEG layers on competitive adsorption of ocular proteins. *Biomaterials* 23:2043–2056
- Ostuni E, Chapman RG, Holmin RE, Takayama S, Whitesides GM (2001) A survey of structure-property relationships of surfaces that resist the adsorption of protein. *Langmuir* 17:5605–5620
- Chen S, Li L, Zhao C, Zheng J (2010) Surface hydration: principles and applications toward low-fouling/nonfouling biomaterials. *Polymer* 51:5283–5293
- Jiang S, Cao Z (2010) Ultralow-fouling, functionalizable, and hydrolyzable zwitterionic materials and their derivatives for biological applications. *Adv Mater* 22:920–932
- Chen S, Jiang S (2008) A new avenue to nonfouling materials. *Adv Mater* 20:335–338
- Cheng G, Zhang Z, Chen S, Bryers JD, Jiang S (2007) Inhibition of bacterial adhesion and biofilm formation on zwitterionic surfaces. *Biomaterials* 28:4192–4199
- Leng C, Han X, Shao Q, Zhu Y, Li Y, Jiang S, Chen Z (2015) In situ probing of the surface hydration of zwitterionic polymer brushes: structural and environmental effects. *J Phys Chem C* 118:15840–15845
- Leng C, Hung H, Sieggreen OA, Li Y, Jiang S, Chen Z (2015) Probing the surface hydration of nonfouling zwitterionic and poly (ethylene glycol) materials with isotopic dilution spectroscopy. *J Phys Chem C* 119:8775–8780
- Cheng G, Li G, Xue H, Chen S, Bryers JD, Jiang S (2009) Zwitterionic carboxybetaine polymer surfaces and their resistance to long-term biofilm formation. *Biomaterials* 30:5234–5240
- Chen S, Chang Y, Lee K, Wei T, Higuchi A, Ho F, Tsou C, Ho H, Lai J (2012) Hemocompatible control of sulfobetaine-grafted polypropylene fibrous membranes in human whole blood via plasma-induced surface zwitterionization. *Langmuir* 28:17733–17742
- Yang W, Chen S, Cheng G, Vaisocherov H, Xue H, Li W, Zhang J, Jiang S (2008) Film thickness dependence of protein adsorption from blood serum and plasma onto poly (sulfobetaine)-grafted surfaces. *Langmuir* 24:9211–9214
- Zhang Z, Finlay JA, Wang L, Gao Y, Callow JA, Callow ME, Jiang S (2009) Polysulfobetaine-grafted surfaces as environmentally benign ultralow fouling marine coatings. *Langmuir* 25:13516–13521
- Wang M, Yuan J, Huang X, Cai X, Li L, Shen J (2013) Grafting of carboxybetaine brush onto cellulose membranes via surface-initiated ARGET-ATRP for improving blood compatibility. *Colloid Surface B* 103:52–58
- Quintana R, Gosa M, Jańczewski D, Kutnyanszky E, Vancso GJ (2013) Enhanced stability of low fouling zwitterionic polymer brushes in seawater with diblock architecture. *Langmuir* 29:10859–10867
- Sin M, Sun Y, Chang Y (2014) Zwitterionic-based stainless steel with well-defined polysulfobetaine brushes for general bioadhesive control. *ACS Appl Mater Inter* 6:861–873
- Chang Y, Chang W, Shih Y, Wei T, Hsue G (2011) Zwitterionic sulfobetaine-grafted poly (vinylidene fluoride) membrane with highly effective blood compatibility via atmospheric plasma-induced surface copolymerization. *ACS Appl Mater Inter* 3:1228–1237
- Leng C, Hung H, Sun S, Wang D, Li Y, Jiang S, Chen Z (2015) Probing the surface hydration of nonfouling zwitterionic and PEG materials in contact with proteins. *ACS Appl Mater Inter* 7:16881–16888
- Wu J, Zhao C, Hu R, Lin W, Wang Q, Zhao J, Bilinovich SM, Leeper TC, Li L, Cheung HM, Chen S, Zheng J (2014) Probing the weak interaction of proteins with neutral and zwitterionic anti-fouling polymers. *Acta Biomater* 10:751–760
- Cheng L, Liu Q, Lei Y, Lin Y, Zhang A (2014) The synthesis and characterization of carboxybetaine functionalized polysiloxanes for the preparation of anti-fouling surfaces. *RSC Adv* 4:54372–54381
- Zhang A, Cheng L, Hong S, Yang C, Lin Y (2015) Preparation of anti-fouling silicone elastomers by covalent immobilization of carboxybetaine. *RSC Adv* 5:88456–88463

31. Jin F, Ji B, Liu S, Tian L, Gao J (2009) Deposition modes, components and functions of secretions associated with oviposition in insects. *Acta Entomol Sin* 52:1008–1016
32. Bujacz A (2012) Structures of bovine, equine and leporine serum albumin. *Acta Crystallogr D Biol Crystallogr* 68: 1278–1289
33. Lin Y, Liu Q, Cheng L, Lei Y, Zhang A (2014) Synthesis and antimicrobial activities of polysiloxane-containing quaternary ammonium salts on bacteria and phytopathogenic fungi. *React Funct Polym* 85:36–44
34. Yin T, Qin M, Shen W (2014) Physicochemical investigations on the interactions between gemini/single-chain cationic surfactants and bovine serum albumin. *Colloid Surf A* 461:22–29
35. Martin VI, Rodriguez A, Maestre A, Moya ML (2013) Binding of cationic single-chain and dimeric surfactants to bovine serum albumin. *Langmuir* 29:7629–7641
36. Sreerama N, Woody R (2000) Estimation of protein secondary structure from circular dichroism spectra: comparison of CONTIN, SELCON, and CDSSTR methods with an expanded reference set. *Anal Biochem* 287:252–260



Synthesis and antimicrobial activities of polysiloxane-containing quaternary ammonium salts on bacteria and phytopathogenic fungi



Yaling Lin^{a,*}, Qiongqiong Liu^b, Liujun Cheng^b, Yufeng Lei^b, Anqiang Zhang^{b,*}

^a Department of Pharmaceutical Engineering, College of Resource and Environment, South China Agriculture University, 483 Wushan Rd., Guangzhou 510642, Guangdong, China

^b Department of Polymer Material Science and Engineering, College of Material Science and Engineering, South China University of Technology, 381 Wushan Rd., Guangzhou 510641, Guangdong, China

ARTICLE INFO

Article history:

Received 26 July 2014

Received in revised form 30 September 2014

Accepted 6 October 2014

Available online 14 October 2014

Keywords:

Polysiloxane graft quaternary ammonium salts

Antimicrobial activity

Phytopathogenic fungi

ABSTRACT

A series of dimethylaminopropyl benzyl chloride grafted polysiloxanes (PDMS-g-BCs) with tunable molecular weights and cationic content were synthesized, and the effect of polymer structure on the antimicrobial activities against bacteria (*Escherichia coli* (*E. coli*) and *Staphylococcus albus* (*S. albus*)) and phytopathogenic fungi (*Rhizoctonia solani* (*R. solani*) and *Fusarium oxysporum* f. sp. *cubense* race 4 (*Foc4*)) were systematically assessed. The antibacterial activity was evaluated by determining the minimum inhibitory concentration (MIC) against *E. coli* and *S. albus* by the broth dilution method, and the antifungal activity was measured by mycelia growth inhibition as well as by the MIC and minimum fungicidal concentration (MFC) values. The molecular weight and cationic content were major determinants of the activities of PDMS-g-BCs; when the molecular weight was approximately 2500 g/mol and the cationic content was approximately 20 mol% of the total siloxane units, PDMS-g-BCs gained strong antimicrobial activities toward both *E. coli* and *Foc4*, comparable to those of a commonly used broad-spectrum microbicide benzalkonium chloride, making PDMS-g-BCs promising fungicidal agents for plant disease control.

© 2014 Elsevier B.V. All rights reserved.

1. Introduction

Antimicrobial agents generate a great deal of interest from researchers in both academia and industry, as these agents are capable of destroying or inhibiting the growth of microbes. Quaternary ammonium salts (QASs) are widely used as disinfectants to control microbial growth. Both ionic and hydrophobic interactions between the QASs and microbial walls or cytoplasmic membranes lead to cell death or malfunctions in cellular processes [1]. However, low-molecular-weight QASs suffer from many disadvantages, including toxicity to the environment and short-lived antimicrobial activity [2]. Therefore, antimicrobial agents are often designed to contain reactive functional groups for covalent linkage to polymers.

Polymers with antimicrobial groups chemically bonded to the polymer chain have attracted a great deal of attention, as they effectively inhibit the growth of bacteria and other microbes without releasing toxic low-molar-mass compounds to the environment. The strong antimicrobial potency of these polymers is a

result of the high local concentration of active groups [2–4]. Their antimicrobial activity is attributed to the destructive interaction through electrostatic forces with the negatively charged microbial cell wall, cytoplasmic membrane, or both [2].

Among the polycationic antimicrobial agents, polysiloxanes are particularly attractive, as they show exceptionally high static and dynamic flexibility in many solvents as well as high permeability and unusual surface properties. All of these features make the QAS groups attached to the backbone readily available for the destructive interaction with microbial walls [5,6]. In addition, polysiloxanes are physiologically inert, chemically stable and, after modification with the ionic QAS groups, water-soluble [1].

To our knowledge, although polysiloxane QASs [5–10] are effective for inhibiting bacteria that cause diseases in humans and animals, few reports have been published about QAS-containing polysiloxanes as antifungal polymers applied to control phytopathogenic fungi that cause plant diseases.

To this end, in this paper, we synthesized dimethylaminopropyl benzyl chloride grafted polysiloxanes (PDMS-g-BCs) with tunable molecular weights and cationic content through three steps, and systematically investigated the structure and antibacterial (gram-positive bacteria *Staphylococcus albus* (*S. albus*) and the gram-negative bacteria *Escherichia coli* (*E. coli*)) and antifungal

* Corresponding authors. Tel./fax: +86 20 8711 2466.

E-mail addresses: linyaling@scau.edu.cn (Y. Lin), aqzhang@scut.edu.cn (A. Zhang).

(phytopathogenic fungi, including rice sheath blight pathogen (*Rhizoctonia solani*, *R. solani*) and banana fusarium wilt (*Fusarium oxysporum* f. sp. *cubense* race 4, *Foc4*)) properties of the PDMS-g-BCs.

2. Experimental

2.1. Materials

Benzalkonium chloride (dodecylbenzyltrimethylammonium chloride) and Karstedt's catalyst were supplied by Aladdin Reagent Co Ltd. (Shanghai, China). Octamethylcyclotetrasiloxane (D_4 , 99%) and 1,1,1,3,3,3-hexamethyldisiloxane (MM, 98%) was supplied by Dow Corning in USA. 1,3,5,7-tetramethylcyclotetrasiloxane (D_4^H , 99%) was supplied by Hangzhou Sloan Materials Technology Co, Ltd. (Hangzhou, China). Strong-acid cation exchange resin (Purolite® CT175) was supplied by Purolite (China) Co Ltd. N,N-dimethylallylamine (DMAA, 98%) was supplied by Haining Huangshan Chemical Co Ltd. (Haining, China). Beef extract was supplied by Sinopharm Chemical Reagent Co Ltd. (Shanghai, China). Peptone was supplied by Guangdong Ring Kay Microbial Technology Co Ltd. (Guangzhou, China). Agar was supplied by MYM Biological Technology Company (Shanghai, China). RPMI-1640 liquid medium was supplied by America Hyclone Company. All of the microorganisms were kindly supplied by the Fungus Laboratory, Department of Plant Pathology, South China Agricultural University.

2.2. Synthesis of benzyldimethylaminopropyl chloride grafted polysiloxane (PDMS-g-BC)

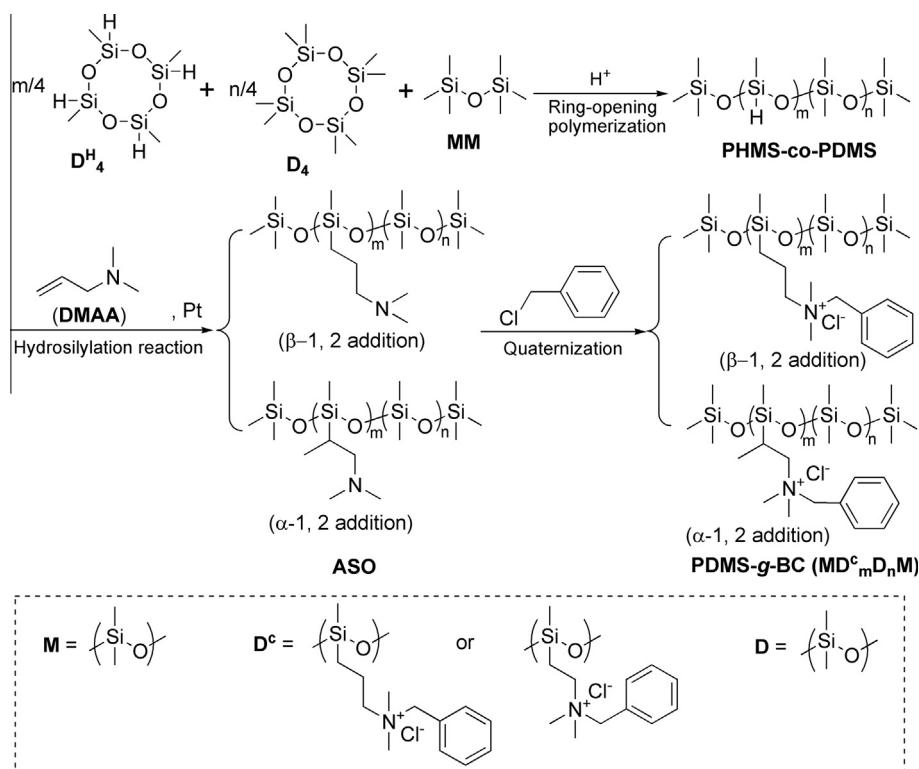
PDMS-g-BC series were prepared through the three-step process presented in Scheme 1.

Poly(hydromethylsiloxane-co-dimethylsiloxane) terminated by trimethylsiloxane groups (PHMS-co-PDMS) was synthesized by ring-opening polymerization. Calculated D_4 , D_4^H , MM and Purolite® CT175 (1 wt.%) were charged into a three-necked flask and stirred at 65 °C under a nitrogen atmosphere for 12 h. Then, the mixture was

filtered to remove the catalyst, and the volatile oligomers were distilled off under reduced pressure at 150 °C. ^1H NMR (400 MHz, CDCl_3 , δ , ppm): 0.07–0.09 (m, Si- CH_3), 4.68 (s, Si-H). FT-IR (ν , cm^{-1}): 2154 ($\nu_{\text{Si-H}}$), 1260 ($\nu_{\text{Si-CH}_3}$), 1027–1094 ($\nu_{\text{Si-O-Si}}$).

Tertiary amine substituted silicone oil (ASO) was obtained by the hydrosilylation reaction between PHMS-co-PDMS and DMAA. First, calculated N,N-dimethylallylamine (DMAA) and Karstedt's catalyst was charged into a three-neck flask equipped with a condenser, a magnetic stirrer and a nitrogen inlet. After purging the flask with nitrogen, PHMS-co-PDMS was dripped via the dropping funnel, and the mixture was heated to 100 °C. During the course of the reaction, samples were removed periodically, and conversions were monitored by FT-IR spectroscopy. The reaction was conducted until no Si-H absorption (2154 cm^{-1}) was detected by FT-IR spectroscopy. Then, the resulting mixture was distilled under reduced pressure to remove the remaining DMAA. ^1H NMR (400 MHz, CDCl_3 , δ , ppm): 0.05–0.09 (m, Si- CH_3), 0.49 (t, Si- CH_2CH_2), 0.91 (m, Si- CH), 0.98 (d, $\text{CH}_3\text{-CH}$), 1.51 (m, $\text{CH}_2\text{-CH}_2\text{-CH}_2$), 2.17–2.22 (m, $\text{N}^+(\text{CH}_3)_2$), 2.27 (m, $\text{CH}_2\text{-CH}_2\text{-CH}_2$). FT-IR (ν , cm^{-1}): 2771 ($\nu_{\text{N}(\text{CH}_3)_2}$), 1260 ($\nu_{\text{Si-CH}_3}$), 1027–1094 ($\nu_{\text{Si-O-Si}}$).

Benzyldimethylaminopropyl chloride grafted polysiloxane (PDMS-g-BC) was synthesized by the quaternization reaction. ASO and anhydrous ethanol were charged into a three-necked flask with a condenser, a magnetic stirrer and a nitrogen inlet, and the mixture was heated to 90 °C under nitrogen. Then, benzyl chloride (BC) dissolved in anhydrous ethanol was dripped via the dropping funnel, and the reaction was maintained at 90 °C for 30 h. After removing the solvent, the resulting product was dissolved in distilled water and washed with petroleum ether several times to remove the remaining BC. Finally, the mixture was subjected to rotary evaporation and vacuum drying to obtain a purified product of PDMS-g-BC. For simplicity of nomenclature, each polymer was given a letter based on its cationic content and molecular weight. For example, PDMS-g-BC_{17L}, composed of 17 mol% quaternary ammonium units, was named 17L, with "L" representing low molecular weight and the "17" representing mole percentage of



Scheme 1. Synthesis of PDMS-g-BCs.

Table 1

Characterization of PDMS-g-BCs with different molecular weights and cationic content.

Samples	MD _m D _n M	Molecular weight (g/mol)	m/(m + n)	Yield (%)
PDMS-g-BC _{17L}	MD ₅ D ₂₀ M	2700	1/6	58.6
PDMS-g-BC _{20L}	MD ₄ D ₁₆ M	2400	1/5	61.9
PDMS-g-BC _{25L}	MD ₄ D ₁₂ M	2100	1/4	62.5
PDMS-g-BC _{33L}	MD ₄ D ₈ M	1800	1/3	63.7
PDMS-g-BC _{50L}	MD ₈ D ₈ M	2900	1/2	53.4
PDMS-g-BC _{17H}	MD ₁₀ D ₅₀ M	6600	1/6	23.3
PDMS-g-BC _{20H}	MD ₁₂ D ₄₈ M	7000	1/5	6.5
PDMS-g-BC _{25H}	MD ₁₆ D ₄₈ M	8100	1/5	18.25

quaternary ammonium salt units. Similarly, the letter “H” represented the high-molecular-weight polymers. The characterization of PDMS-g-BC is presented in Table 1. ¹H NMR (400 MHz, D₂O, δ, ppm): 0.06 (m, Si-CH₃), 0.53 (m, Si-CH₂CH₂), 1.01 (m, Si-CH), 1.22 (d, CH₃-CH), 1.84 (m, CH₂-CH₂-CH₂), 2.98 (m, N⁺(CH₃)₂), 3.15 (m, CH₂-CH₂-CH₂), 4.41 (s, CH₂-Φ), 7.48 (s, Φ-H). FT-IR (ν, cm⁻¹): 3010 (ν_{Φ-H}), 1260 (ν_{Si-CH₃}), 1082 (ν_{Si-O-Si}), 704, 736 (ν_{Φ-H}).

2.3. Characterization

FT-IR spectra were obtained with a VERTEX spectrometer (Bruker Instrument Corp., Germany) by the KBr disk method. ¹H NMR spectra were obtained using an AV-400 FT-NMR (Bruker Instrument Corp., Germany) and D₂O or CDCl₃ as a solvent. GPC experiments were performed in chloroform (1 mL/min) at room temperature with an Elite EC2000 GPC apparatus (Dalian, China) equipped with a Shodex K-G guard column and a Shodex K-804L chromatographic column. The molecular weights were estimated with a polystyrene calibration.

2.4. Antimicrobial tests

2.4.1. Test microorganisms

The microorganisms included the gram-positive bacteria *S. albus* and the gram-negative bacteria *E. coli*. The phytopathogenic fungi associated with plant diseases included the rice sheath blight pathogen (*R. solani*) and the banana fusarium wilt (*Foc4*).

2.4.2. Media

Beef extract peptone medium was used as the growth medium for the tested bacteria and was prepared as follows: 3.0 g of beef extract, 10.0 g of tryptone, and 5.0 g of NaCl were added into 1000 mL of distilled water and heated to dissolve, and the solution's pH was adjusted to 7.0. To the solution, 15–20 g of agar powder was added to obtain solid medium. Then, the medium was sterilized by autoclaving (HVE-50, Japan Hirayama Corporation) at 121 °C for 20 min and cooled down.

Potato dextrose agar (PDA) was used as the growth medium for the tested fungi, and the PDA was prepared as follows: 200 g of sliced potato was boiled in water for 30 min, and the liquid was then strained through a cheese-cloth. Distilled water was added to adjust the total volume of suspension to 1000 mL, and then 20 g of dextrose and 15 to 20 g of agar powder were added. Finally, the medium was transferred to a flask, sealed, sterilized by autoclaving at 121 °C for 30 min and cooled down.

RPMI-1640 liquid medium was obtained by buffering RPMI-1640 (with L-glutamine and without bicarbonate) with 10 M NaOH to pH 7.0; the medium was sterilized by filtering with a 0.22-μm membrane.

2.4.3. Determination of minimum inhibitory concentration (MIC)

The antibacterial properties of PDMS-g-BCs against *E. coli* and *S. albus* were quantitatively evaluated using the broth dilution

method [11]. Bacterial growth rates were determined by measuring the optical density at 600 nm (OD₆₀₀) using a UV-vis spectrophotometer (UV-2300, Shanghai Techcomp Instrument Co Ltd.) based on the turbidity of the cell suspension. The minimum inhibitory concentration (MIC) against the tested bacteria was defined as the concentration of PDMS-g-BC at which bacterial growth was completely inhibited. The main procedures were as follows. The sterilized tubes were grouped and bundled according to concentrations; each group consisted of four bundles, and each bundle consisted of a number of branches (number determined by the sampling time), of which three bundles were parallel experiments, and the fourth was the control. Different concentrations of the sample solution were added to the corresponding tubes: 4 mL was added into the reference group, and 2 mL was added into the parallel group; then, 2 mL of the bacteria suspension was charged into the parallel group, and 4 mL of medium was charged into the reference group. The initial optical density (OD₆₀₀) from one tube from each bundle was tested using an UV spectrophotometer, with the solution in the corresponding reference tube as the reference solution. The remaining tubes were incubated at 37 °C in a shaker incubator (DHZ-D, Taicang Experimental Equipment Factory, China) under 120 rpm. During incubation, the OD₆₀₀ of one tube from each bundle was tested to record the bacterial suspension concentration. The MIC was the lowest concentration at which there was no visible growth of bacteria, i.e. the OD₆₀₀ did not change with time compared with the initial value.

2.4.4. Determination of mycelial growth inhibition

The antifungal activities of the samples were tested by the inhibition of mycelial growth. To prepare solutions of different concentrations, the samples were dissolved in sterilized water, mixed with PDA and poured onto sterile Petri dishes (with diameter of 9 cm). Control plates consisted of PDA only. A 5-mm disc containing mycelia was transferred to the center of the PDA plate containing the samples and incubated at 28 °C. Sterilized water was used as a negative control. Each experiment was conducted in three replicates. The diameter of fungal colonies was measured three times and averaged. Growth inhibition was calculated according to Formulas (1) and (2).

$$\text{Radial growth (mm)} = \text{The average fungi colony diameter (mm)} - 5 \text{ mm} \quad (1)$$

$$\text{Mycelia growth inhibition} = (C - T)/T \times 100\% \quad (2)$$

whereby C = radial growth of fungi in the control plate, T = radial growth of fungi in the treatment plate.

2.4.5. Determination of minimum inhibitory concentration (MIC) and minimum fungicidal concentration (MFC)

Foc4 was chosen as the tested microorganism to determine the MIC and MFC values of the samples. *Foc4* microorganisms were incubated at 28 °C for 7 days in PDA medium; the fungal suspension was prepared by adding 1 mL of 0.85% saline containing 0.01 mL of Tween 20 to the incubated colony. Then, the upper homogeneous liquid was transferred to a sterilized tube and diluted with RPMI-1640 liquid medium to give inoculation suspensions of 0.4×10^4 – 5×10^5 CFU/mL with twice the final concentration. The broth microdilution method was used to determine the MIC of the samples. The samples were dissolved in water and diluted in RPMI-1640 medium. The sample solution (100 μL) with concentrations ranging from 5×10^{-5} to 3 mg/mL was added into 96-well plates. The same volume of mycelial suspension containing approximately 0.4×10^4 – 5×10^5 CFU/mL was incubated at 28 °C for 46–50 h. In addition, a reference liquid medium without samples was used as a negative control. MIC was measured at least

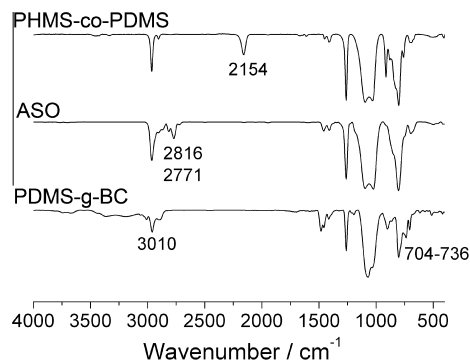


Fig. 1. FT-IR spectra of PHMS-co-PDMS, ASO and PDMS-g-BC.

three times and recorded as the lowest concentration that completely inhibited visible growth [12].

The MFC test was the most common estimation of fungicidal activity and was defined as the lowest concentration of antimicrobial agent needed to kill 99.9% of the initial inoculums after incubation [13]. To determine the MFC, 100 μ L from each of the wells at or above the MIC was plated on PDA and incubated at 28 $^{\circ}$ C for 48 h. The MFC was defined as the lowest concentration at which no colonies were detected on the PDA.

3. Results and discussions

3.1. Design, synthesis and characterization of PDMS-g-BC

By designing and synthesizing a series of polysiloxane QASs with controllable compositions, we examined the relationship between antimicrobial activities and the structure (molecular weight and cationic content) of polysiloxane QASs. Polysiloxane QASs possess rather flexible hydrophobic backbones, allowing potent antimicrobial activities to be achieved by finely tuning the molecular weight and cationic content. Thus, polysiloxane QASs (PDMS-g-BCs) were synthesized through three steps as described in Scheme 1. First, PHMS-co-PDMS was synthesized by the ring-opening polymerization of D_4 , D_4^H and MM, followed by a hydrosilylation reaction between PHMS-co-PDMS and *N,N*-dimethylallylamine (DMAA). PDMS-g-BC was finally obtained after the quaternization

of ASO with benzyl chloride (BC). The chemical structures of products were confirmed by FT-IR and 1 H NMR spectroscopy.

By adjusting the mole ratio of D_4 , D_4^H and MM, a series of PHMS-co-PDMS with various molecular weights and hydrogen content were synthesized by ring-opening polymerization. As shown in Figs. 1 and 2, the adsorption peaks at 2154, 1260, 1094 and 1027 cm^{-1} represented the stretching vibration of Si-H, Si-CH₃ and Si-O-Si, respectively, and the signal of Si-H protons appeared at $\delta = 4.68$ ppm and Si-CH₃ protons at $\delta = 0.07$ –0.09 ppm. The molecular weights of PHMS-co-PDMSs were determined by GPC, and the low- and high-molecular-weight serial PHMS-co-PDMSs varied from approximately 1600 to 2500 and from approximately 6300 to 7900, respectively.

ASO was synthesized by the hydrosilylation reaction of PHMS-co-PDMS with DMAA in the presence of Karstedt's catalyst. The disappearance of Si-H absorption (at 2154 cm^{-1}) and the appearance of $N(\text{CH}_3)_2$ (at 2816 and 2771 cm^{-1}) in the FT-IR analysis (Fig. 1) and the disappearance of a Si-H proton (at $\delta = 4.68$ ppm) and the appearance of a series of C-H protons in 1 H NMR analysis (Fig. 2) confirmed the reaction of PHMS-co-PDMS with DMAA leading to ASO.

A series of PDMS-g-BCs were obtained by the quaternization reaction between ASO and benzyl chloride (BC). In the FT-IR analysis (Fig. 1), Φ -H absorption at 704–736 and 3010 cm^{-1} appeared, and $N(\text{CH}_3)_2$ absorption at 2816 and 2771 cm^{-1} disappeared. In the 1 H NMR analysis (Fig. 2), after the quaternization reaction, the $N(\text{CH}_3)_2$ protons signals shifted from approximately 2.20 ppm to 2.98 ppm completely, and the characteristic protons signals of BC ($\delta = 4.41$ ppm and $\delta = 7.48$ ppm) appeared, which indicated the structure of PDMS-g-BC agreed well with our expectation. The characterization of PDMS-g-BC is presented in Table 1.

3.2. Antibacterial activities of PDMS-g-BCs

To investigate the antibacterial properties (MIC values) of PDMS-g-BCs, different concentrations of PDMS-g-BCs were added to the medium. Bacterial growth was monitored by measuring the optical density at 600 nm (OD_{600}) based on the turbidity of the cell suspension. In this experiment, OD_{600} curves were recorded in different concentrations of PDMS-g-BCs with medium, and the effect of PDMS-g-BCs on the bacterial growth was assessed from the curves. Taking PDMS-g-BC_{17L} (Fig. 3(A)) as an example, bacteria were first grown to $\text{OD}_{600} = 0.2$, and the bacterial growth

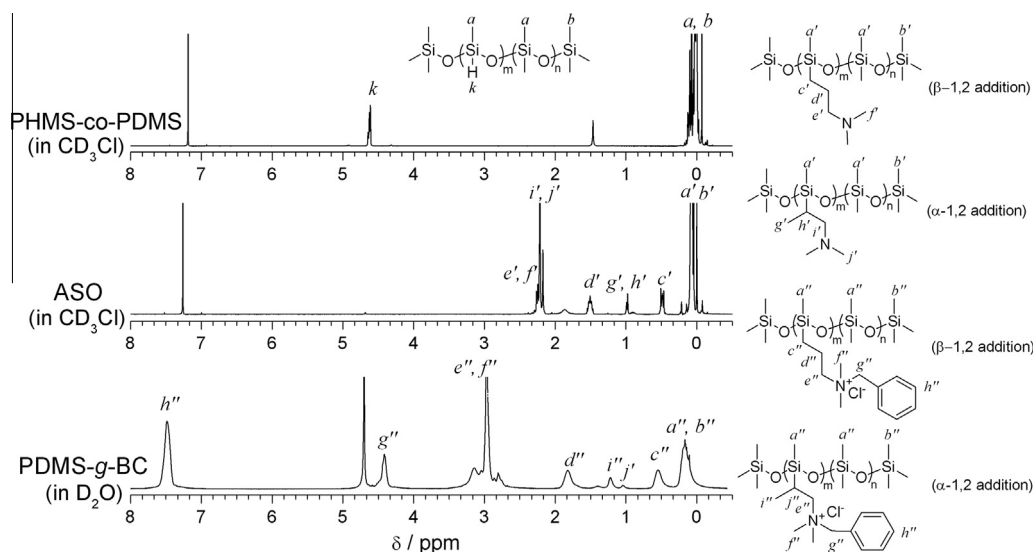


Fig. 2. 1 H NMR spectra of PHMS-co-PDMS, ASO and PDMS-g-BC.

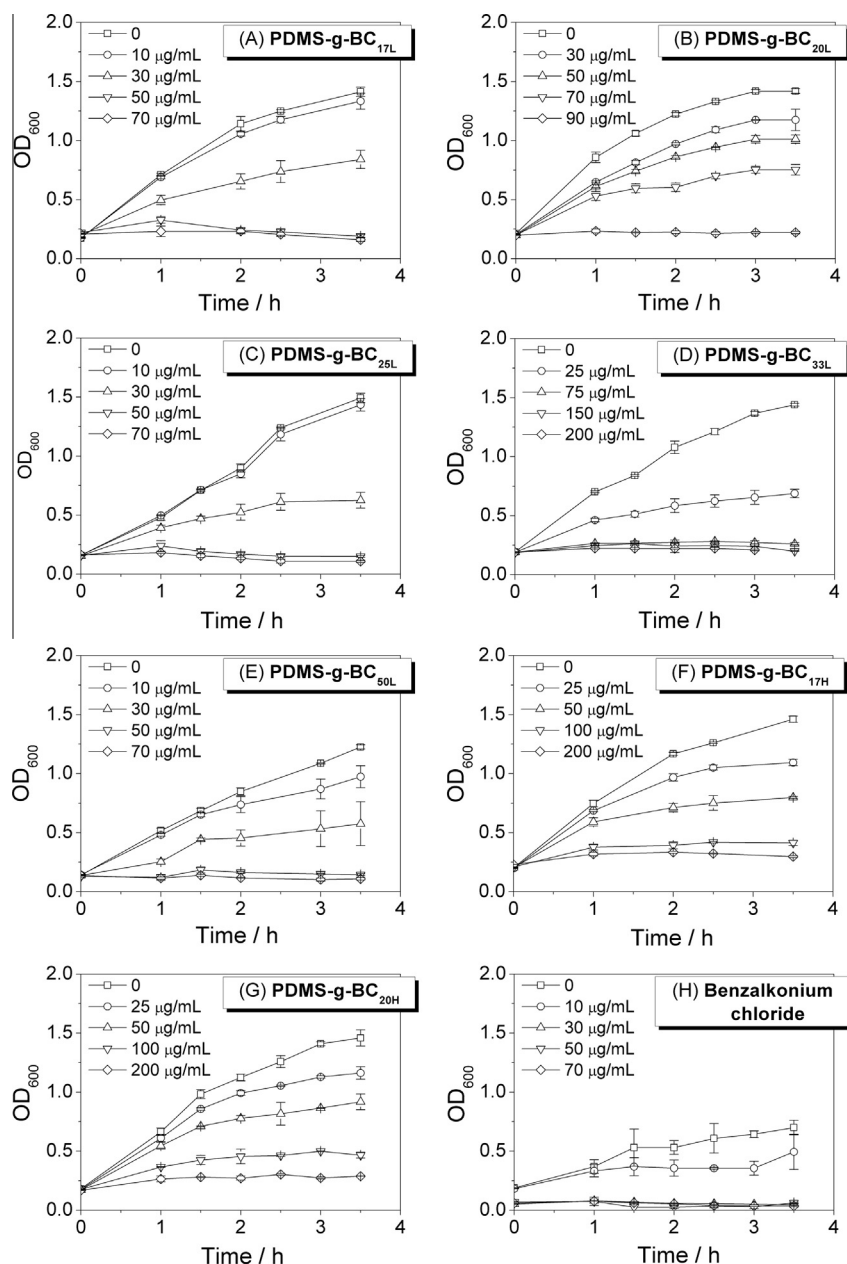


Fig. 3. MIC values for PDMS-g-BC and benzalkonium chloride against *E. coli*: (A) PDMS-g-BC_{17L}, (B) PDMS-g-BC_{20L}, (C) PDMS-g-BC_{25L}, (D) PDMS-g-BC_{33L}, (E) PDMS-g-BC_{50L}, (F) PDMS-g-BC_{17H}, (G) PDMS-g-BC_{20H}, and (H) benzalkonium chloride.

slowed as the concentration of PDMS-g-BC_{17L} increased, indicating that 10 µg/mL was able to slow the growth of *E. coli*. When the concentration of PDMS-g-BC_{17L} was increased to 50 µg/mL, the bacterial growth was completely inhibited. Thus, the minimal inhibition concentration (MIC) of PDMS-g-BC_{17L} was 50 µg/mL against *E. coli*.

The MIC values for PDMS-g-BCs against *E. coli* and *S. albus* are shown in Figs. 3 and 4, and the results are summarized in Tables 2 and 3.

As shown in Table 2, low-molecular-weight PDMS-g-BC_L (except PDMS-g-BC_{33L}) had low MIC values compared to those of benzalkonium chloride (dodecylbenzyltrimethylammonium chloride, a broad-spectrum and highly effective biocide, widely used in medical or industrial treatment), in which PDMS-g-BC_{25L} and PDMS-g-BC_{17L} had the best antibacterial effect, with MIC values of 50 µg/mL. Additionally, MIC values varied with cationic content, but there was no direct correlation between cationic content and MIC values.

MIC values of PDMS-g-BC_L demonstrated the importance of cationic content, hydrophobicity and molecular weight in the antimicrobial performance of polysiloxane QASs. PDMS-g-BC_L (except for PDMS-g-BC_{33L}) had potent antibacterial activities against *E. coli*, with the cationic content ranging between 17% and 50%, and the molecular weight of approximately 2500 g/mol. In addition, the molecular weight of polycations has been shown to profoundly impact the efficacy of many antimicrobial quaternized macromolecular systems, and an optimal molecular weight range exists for the biocidal action of polycations. Generally, the antimicrobial properties of conventional polymer biocides have a bell-shape dependence on molecular weight, while dendrimer biocides have a parabolic dependence. Ikeda found that the antibacterial activities of polycations strongly depended on molecular weight and had a bell-like shape [14]. Cooper and co-workers discovered a parabolic dependence on the molecular weight of the antimicrobial properties of the quaternary ammonium functionalized poly(pro-

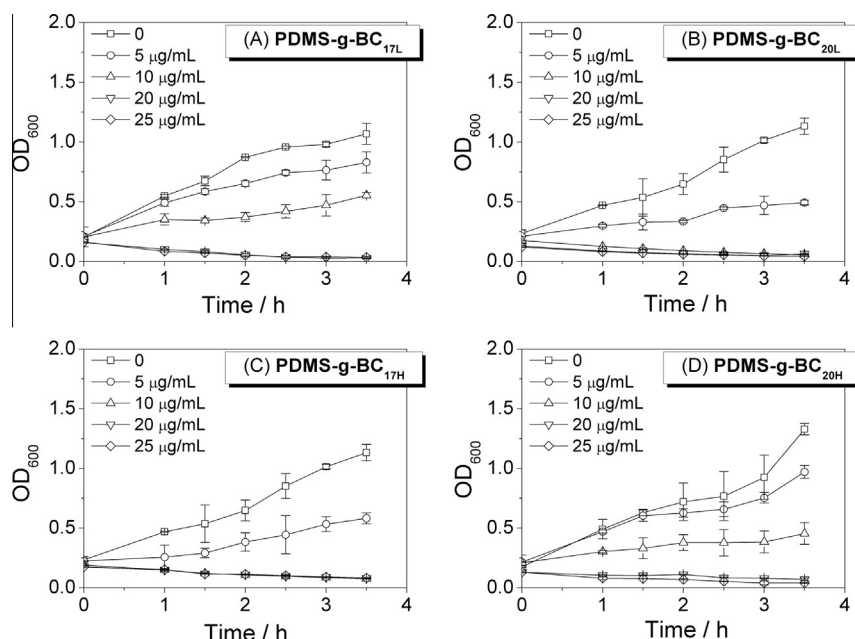


Fig. 4. MIC values for PDMS-g-BC against *S. albus*: (A) PDMS-g-BC_{17L}, (B) PDMS-g-BC_{20L}, (C) PDMS-g-BC_{17H}, (D) PDMS-g-BC_{20H}.

Table 2

MIC values of PDMS-g-BCs against *E. coli*.

Samples	Molecular weight (g/mol)	MIC (µg/mL)
PDMS-g-BC _{17L}	2700	50
PDMS-g-BC _{20L}	2400	90
PDMS-g-BC _{25L}	2100	50
PDMS-g-BC _{33L}	1800	200
PDMS-g-BC _{50L}	2900	70
PDMS-g-BC _{17H}	6600	200
PDMS-g-BC _{20H}	7000	200
Benzalkonium chloride	340	30

Table 3

Comparison of MIC values of PDMS-g-BCs against *E. coli* and *S. albus*.

Samples	MIC (µg/mL)	
	<i>E. coli</i>	<i>S. albus</i>
PDMS-g-BC _{17L} (<i>M</i> ~ 2700)	50	20
PDMS-g-BC _{20L} (<i>M</i> ~ 2400)	90	5
PDMS-g-BC _{17H} (<i>M</i> ~ 6600)	200	20
PDMS-g-BC _{20H} (<i>M</i> ~ 7000)	200	100

pyleneimine) dendrimers [3]. In our report, by comparing MIC values of low-molecular-weight PDMS-g-BC_L with high-molecular-weight PDMS-g-BC_H, we found that PDMS-g-BC_H had weaker antibacterial activities (displayed by higher MIC values) compared with those of PDMS-g-BC_L.

From Table 3, we found that PDMS-g-BCs showed lower MIC values against *S. albus* than against *E. coli*, which suggests that PDMS-g-BCs were more active against gram-positive bacteria *S. albus* than against gram-negative *E. coli* because of the difference in the structure of their cell walls [5,15]. Gram-positive bacteria possess a loosely packed polyglycane outer layer, which facilitated the deep penetration of PDMS-g-BC chains inside of the cell to interact with the cytoplasmic membrane, whereas gram-negative bacteria, with an additional membrane outside, protect the inner cytoplasmic membrane to a greater extent against the disruptive action of PDMS-g-BCs.

Polymers with QASs require sufficient hydrophobicity to impart substantial antimicrobial activity. In this article, the route of using

a flexible polysiloxane backbone was successful in endowing poly-cations with antibacterial properties as potent as those of the widely used broad-spectrum biocide (benzalkonium chloride). The high activity of the polysiloxane QASs can be explained by the larger conformational freedom of their chains, which was substantial in flexible dimethylsiloxane units. The high flexibility of the polymer chains facilitated the contact of the QAS groups with the microorganism, allowing polymers to adopt conformations favorable for the interaction with the bacterial wall [5,16,17]. Another important point is their amphiphilic character, with the hydrophilic inorganic portion and the hydrophobic organic groups, which augmented the concentration of the QAS groups in the vicinity of the microorganism cell wall.

3.3. Antifungal activities of PDMS-g-BCs

3.3.1. Effect of PDMS-g-BCs on mycelia growth of phytopathogenic fungi

Antifungal activities of PDMS-g-BC series were tested by the disc diffusion method. Fig. 5 displays the antifungal effect of PDMS-g-BCs against *R. solani* and *Foc4*, and the results are summarized in Fig. 6.

Fig. 6 demonstrates the antifungal activities of low-molecular-weight PDMS-g-BC_L against two phytopathogenic fungi, *R. solani* and *Foc4*. All of the samples exhibited a concentration-dependent inhibitory effect on the hyphal growth of *R. solani* and *Foc4*. When using a concentration of 1.6 mg/mL, there was a marked mycelial growth inhibition for PDMS-g-BC_{17L}, PDMS-g-BC_{20L}, PDMS-g-BC_{25L}, PDMS-g-BC_{33L} and PDMS-g-BC_{50L}, with a mycelial growth inhibition of approximately 80%. In particular, PDMS-g-BC_{25L} showed the highest activity toward both *R. solani* and *Foc4*. In addition, all PDMS-g-BCs exhibited significantly better inhibition ability against *R. solani* than against *Foc4*.

The effects of molecular weight on antifungal activity are evaluated in Figs. 7 and 8. The antifungal activity of higher-molecular-weight PDMS-g-BC_H tended to decrease compared to that of lower-molecular-weight PDMS-g-BC_L with the same cationic content.

Based on the above results, it is reasonable to infer that PDMS-g-BCs with relatively lower cationic content (20 mol% of the total

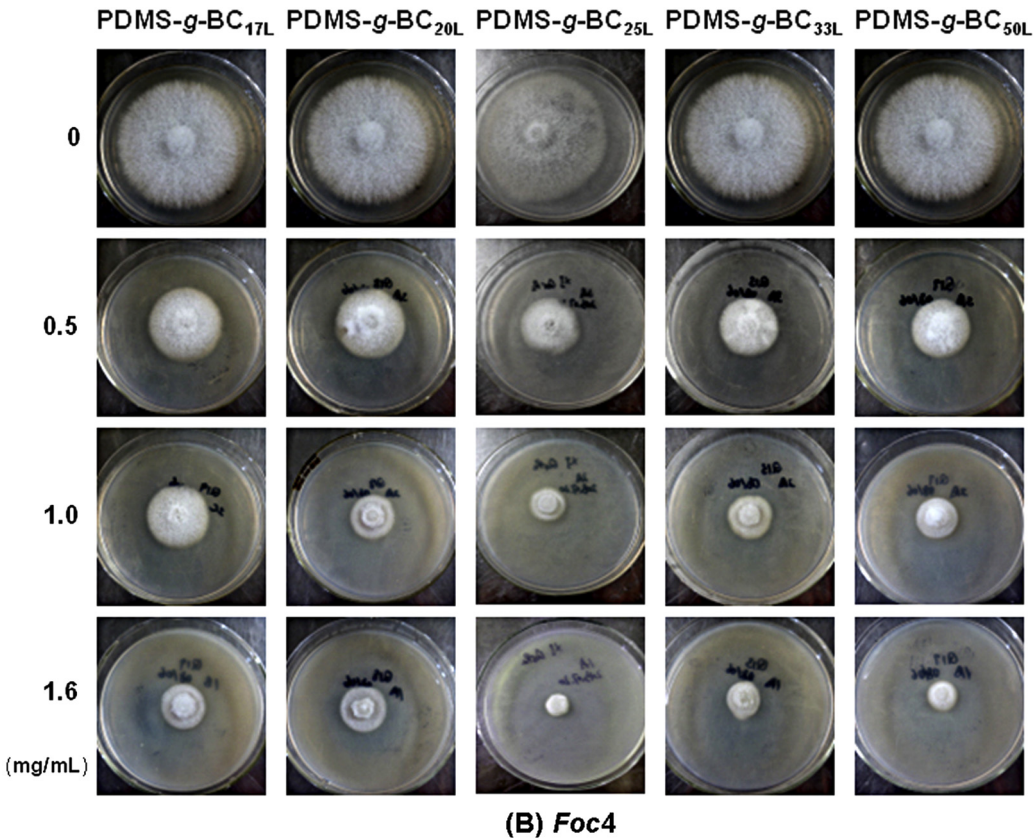
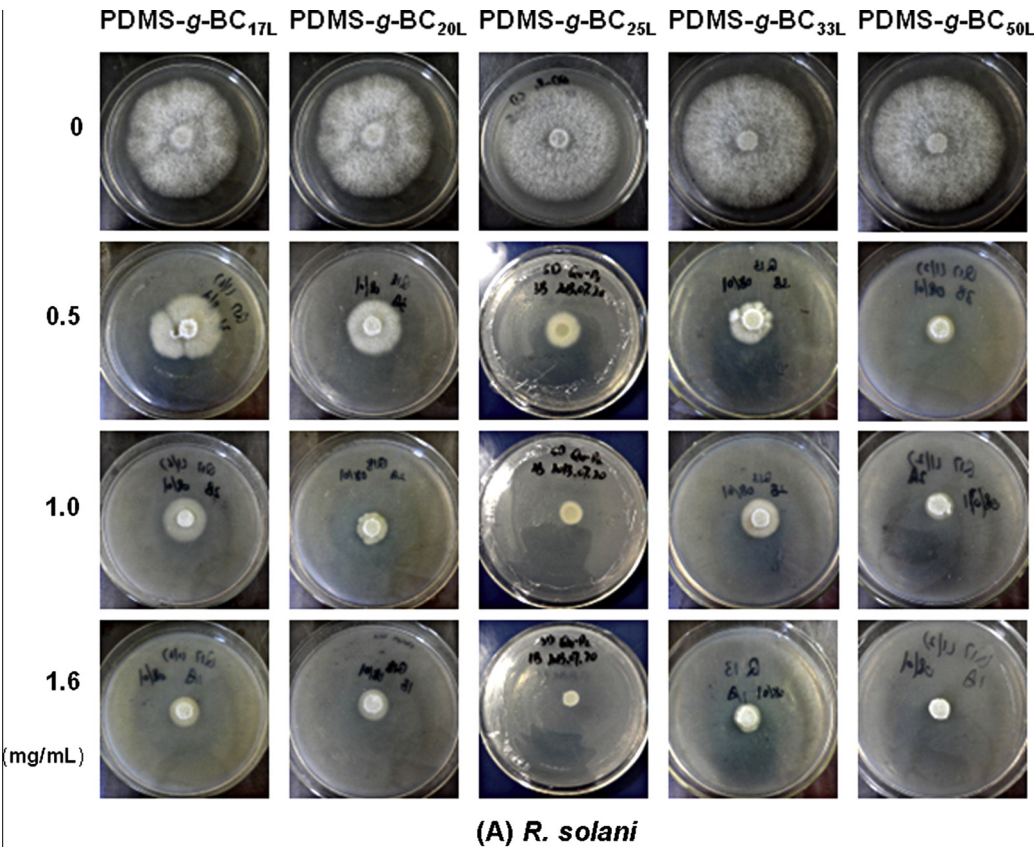


Fig. 5. Antifungal effects of PDMS-g-BC_L against (A) *R. solani* and (B) *Foc4*.

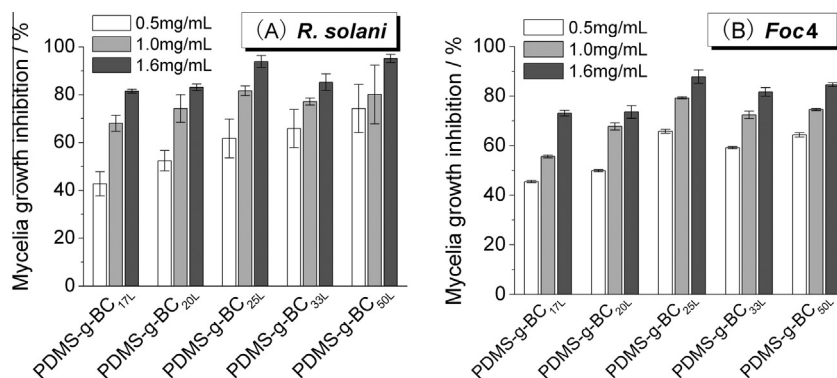


Fig. 6. Mycelial growth inhibition of PDMS-g-BC_L against (A) *R. solani* and (B) *Foc4*.

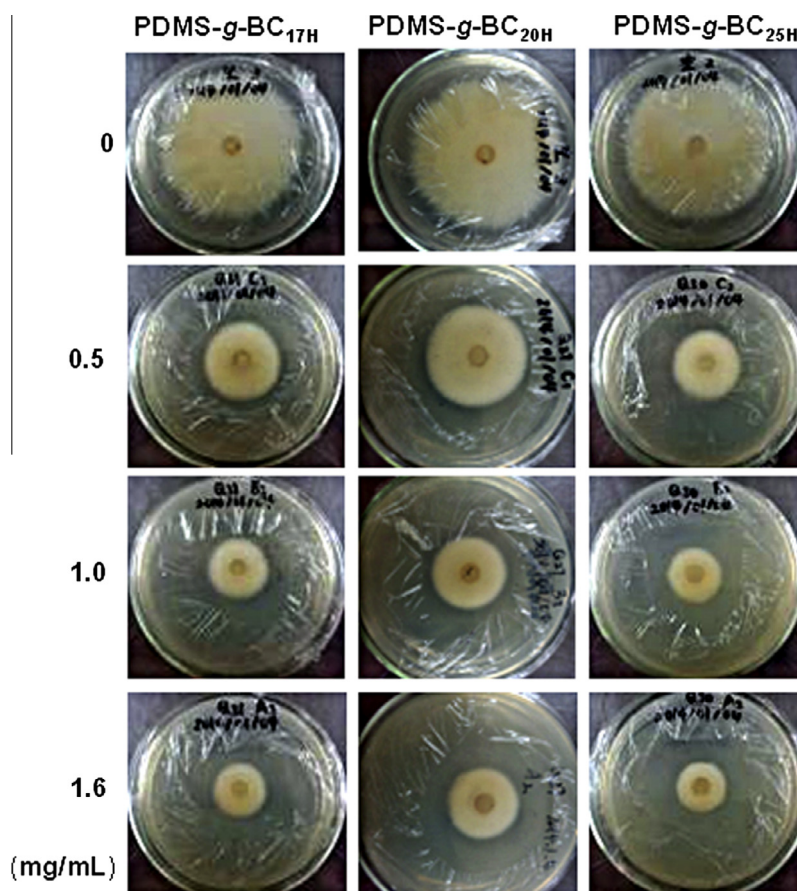


Fig. 7. Antifungal effects of PDMS-g-BC_H against *Foc4*.

siloxane units) and lower molecular weight (2500 g/mol) exhibit high inhibitory activity against the phytopathogenic fungi *Foc4*.

3.3.2. Minimum inhibitory concentration (MIC) and minimum fungicidal concentration (MFC) of PDMS-g-BC against *Foc4*

Based on the above results, the inhibitory effects of acrylamide QASs against *Foc4* were further estimated by the microdilution broth method. MIC was the minimum concentration that could completely inhibit fungal growth; MFC was the lowest concentration at which 99.9% of the fungi could be killed. The MFC/MIC ratio reflects the fungicidal activity of an antimicrobial agent: an antimicrobial agent has fungicidal activity when the MFC/MIC ratio is less or equal to 4, whereas an antimicrobial agent

only has fungistatic activity when the MFC/MIC ratio was greater than 4.

A series of sample solutions with concentration ranging from 0.05 to 3000 µg/mL mixed with a *Foc4* suspension was incubated in 96-well plates at 28 °C for 46–50 h. (MIC was defined as the lowest concentration that completely inhibited visible growth). The mixed liquid in each of the wells at or above the MIC was plated on PDA and incubated at 28 °C for 48 h, and MFC was defined as the lowest concentration at which no colony was detected.

PDMS-g-BCs had different molecular weights and cationic content, which indeed resulted in differences in their antifungal activities. The antifungal results, expressed in MIC and MFC values against *Foc4*, are grouped in Table 4.

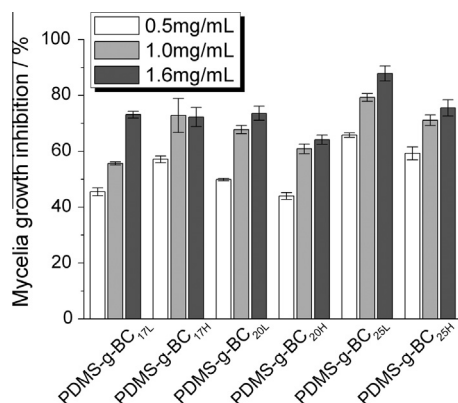


Fig. 8. Mycelial growth inhibition of PDMS-g-BC_L and PDMS-g-BC_H against *Foc4*.

Table 4

MIC and MFC values of PDMS-g-BCs against *Foc4*.

Samples	Molecular weight (g/mol)	MIC (μg/mL)	MFC (μg/mL)	MFC/MIC
PDMS-g-BC _{17L}	2700	5	25	5
PDMS-g-BC _{20L}	2400	5	5	1
PDMS-g-BC _{33L}	1800	250	1000	4
PDMS-g-BC _{50L}	2900	100	250	2.5
PDMS-g-BC _{17H}	6600	250	500	2
PDMS-g-BC _{20H}	7000	250	1000	4
PDMS-g-BC _{25H}	8100	50	100	2
Benzalkonium chloride	340	5	25	5

Low-molecular-weight PDMS-g-BC_L, PDMS-g-BC_{17L} and PDMS-g-BC_{20L} demonstrated better antifungal activities, with MIC and MFC values of 5.25 μg/mL and 5.5 μg/mL, respectively, compared to that of benzalkonium chloride (dodecyl benzyl dimethyl ammonium chloride), with MIC and MFC values of 5.25 μg/mL. Similar to the antibacterial effect of PDMS-g-BC_L, high-molecular-weight PDMS-g-BC_H had a molecular weight ranging from 6000 to 8000 g/mol but low antifungal effect, with MIC and MFC values between 50 and 1000 μg/mL. These results imply that a high molecular weight causes the loss of antifungal activity of PDMS-g-BCs, which is opposite to that of the quaternized chitosan [18]. The antifungal activities differed with regard to molecular weight and cationic content, and an appropriate molecular design of PDMS-g-BCs could strengthen their antifungal activity effectively. In addition, the MFC/MIC ratios of PDMS-g-BC_{20L}, PDMS-g-BC_{33L}, PDMS-g-BC_{50L}, PDMS-g-BC_{17H}, PDMS-g-BC_{20H} and PDMS-g-BC_{25H} are less than 4, implying that they are fungicidal agents.

4. Conclusions

In this experiment, benzyldimethylaminopropyl chloride grafted polysiloxane (PDMS-g-BCs) with tunable molecular weights and cationic content were synthesized successfully in

three steps. This paper systematically investigated the structure and antibacterial (gram-positive bacteria *S. albus* and gram-negative bacteria *E. coli*) and antifungal (phytopathogenic fungi, *R. solani* and *Foc4*) properties of the PDMS-g-BCs.

Antimicrobial results demonstrated the importance of cationic content and molecular weight in the antimicrobial performance of PDMS-g-BCs. With a cationic content of approximately 20 mol% of the total siloxane units and a molecular weight of approximately 2500 g/mol, PDMS-g-BC_L had great antimicrobial activities against *E. coli* and *Foc4* compared to that of a commonly used broad-spectrum microbicide benzalkonium chloride.

We conclude that polysiloxane QASs are worthy of further study as effective fungicidal agents to control plant diseases. Adequate control of phytopathogenic fungi growth using polysiloxane QASs requires an extensive knowledge of the factors that determine polysiloxane QAS performance.

Acknowledgments

The authors acknowledge financial support from the National Natural Science Foundation of China (Grants 31201552 and 51003032) and the Specialized Research Fund for the Doctoral Program of Higher Education (Grant 20124404120025).

References

- [1] G. Sauvet, S. Dupond, K. Kazmierski, J. Chojnowski, J. Appl. Polym. Sci. 75 (2000) 1005–1012.
- [2] E. Kenawy, S.D. Worley, R. Broughton, Biomacromolecules 8 (2007) 1359–1384.
- [3] C.Z. Chen, N.C. Beck-Tan, P. Dhurjati, T.K. van Dyk, R.A. LaRossa, S.L. Cooper, Biomacromolecules 1 (2000) 473–480.
- [4] A.M. Klibanov, J. Mater. Chem. 17 (2007) 2479–2482.
- [5] U. Mizerska, W. Fortuniak, J. Chojnowski, R. Hałasa, A. Konopacka, W. Werel, Eur. Polym. J. 45 (2009) 779–787.
- [6] K. Różga-Wijas, U. Mizerska, W. Fortuniak, J. Chojnowski, R. Hałasa, W. Werel, J. Inorg. Organomet. Polym. 17 (2007) 605–613.
- [7] P. Majumdar, J. He, E. Lee, A. Kallam, N. Gubbins, S.J. Stafslie, J. Daniels, B.J. Chisholm, J. Coat. Technol. Res. 7 (2009) 455–467.
- [8] U. Mizerska, W. Fortuniak, J. Chojnowski, K. Turecka, A. Konopacka, W. Werel, J. Inorg. Organomet. Polym. 20 (2010) 554–563.
- [9] L. Kou, J. Liang, X. Ren, H.B. Kocer, S.D. Worley, Y.M. Tzou, T.S. Huang, Ind. Eng. Chem. Res. 48 (2009) 6521–6526.
- [10] P. Majumdar, E. Crowley, M. Htet, S.J. Stafslie, J. Daniels, L. VanderWal, B. Chisholm, ACS Comb. Sci. 13 (2011) 298–309.
- [11] S.G. Chen, S.J. Chen, S. Jiang, Y.M. Mo, J.X. Luo, J.N. Tang, Z.C. Ge, Colloid Surf. B Biointerfaces 85 (2011) 323–329.
- [12] P. Plodpai, S. Chuenchitt, V. Petcharat, S. Chakthong, S.P. Voravuthikunchai, Crop Prot. 43 (2013) 65–71.
- [13] W. Sajomsang, P. Gonil, S. Saesoo, C. Ovatlarnporn, Int. J. Biol. Macromol. 50 (2012) 263–269.
- [14] T. Ikeda, H. Hirayama, H. Yamaguchi, S. Tazuke, M. Watanabe, Antimicrob. Agents Chemother. 30 (1986) 132–136.
- [15] T. Ikeda, S. Tazuke, Macromol. Chem. 185 (1984) 869–876.
- [16] W. Fortuniak, U. Mizerska, J. Chojnowski, T. Basinska, S. Slomkowski, M.M. Chehimi, A. Konopacka, K. Turecka, W. Werel, J. Inorg. Organomet. Polym. Mater. 21 (2011) 576–589.
- [17] P. Majumdar, E. Lee, N. Patel, S.J. Stafslie, J. Daniels, B.J. Chisholm, J. Coat. Technol. Res. 5 (2008) 405–417.
- [18] Z. Guo, R. Xing, S. Liu, Z. Zhong, X. Ji, L. Wang, P. Li, Carbohydr. Polym. 71 (2008) 694–697.

ISSN 1000-7555

CN 51-1293/06

CODEN GCKGEI

高分子材料 科学与工程

POLYMER MATERIALS SCIENCE & ENGINEERING

2013 Vol. 29 No. 11

目次

合成实验·工艺

- 正交试验法优化 BTDA-TDI/MDI 三元共聚聚酰亚胺聚合工艺 郭炳花, 陈 蕾, 于俊荣等(1)
- 超支化偶氮聚酯的合成及光致变色性能 冯宗财, 宋秀美, 王跃川等(6)
- 藻烷基端羟基聚醚的合成与表征 杜莉娟, 杨晓琴, 曾 韬等(10)
- 氧鎓离子法合成端羟基聚四氢呋喃-聚环氧丙烷嵌段共聚醚 汪存东, 潘洪波, 苏 玲等(15)
- 溶剂热法合成含异氰酸酯基的聚丙烯大分子相容剂 李 浩, 朱士洋, 张先明等(19)
- 聚氨酯/苯乙烯弹性体复合材料的合成及性能 赵亚丽, 李 莉, 李晓云等(24)
- 红外光谱法实时跟踪支化聚乙烯亚胺/甲基丙烯酸缩水甘油酯的官能团反应 茅群龙, 张 艳, 张 弢(28)

结构·性能

- 原位固相接枝 CaCO_3 /聚丙烯复合材料中界面相互作用与力学性能的关系 朱德钦, 生 瑜, 邹寅将等(31)
- 电袋复合除尘器内烟气成分对聚苯硫醚滤料的影响 黄 炜, 郑奎照, 郑辉东等(36)
- 预矿化丝素/壳聚糖复合支架的表征及细胞相容性 施李杨, 邓连霞, 杨明英等(42)
- 核壳型银/聚苯胺纳米复合材料的导电性能 李芝华, 华斯嘉, 卢健体(46)
- 液体橡胶增韧环氧树脂的力学性能及增韧机理 周恒石, 徐世爱(50)
- 氢氧化甲基丙烯酸锌/炭黑协同增强氢化丁腈橡胶硫化过程中的形态演变及性能 武守鹏, 纪彦玲, 徐文龙等(54)
- 石墨烯/碳纤维/聚偏氟乙烯导电复合材料的电性能 胡洪亮, 张 国, 陈 英等(58)
- 二元季铵盐化合物与明胶的相互作用 孟祥建, 崔月芝, 乔从德等(62)
- 多臂星形聚乙二醇-聚乳酸嵌段共聚物的降解特性 林雅铃, 吴敏儿, 邱艳舞等(67)
- 原位测量聚苯乙烯薄膜在溶剂气氛下的动态变化过程 李海东, 吕 鹤, 赖宇晴(71)
- 动态热机械分析法在材料耐老化性能分析中的应用 孟祥艳, 魏莉萍, 刘运传等(76)
- 材料测试·加工·应用
- 超高分子量聚乙烯-聚氨酯泡沫复合材料的抗爆实验与数值模拟 蔡军锋, 傅孝忠, 易建政(79)
- 模塑制品内部成型收缩特性的可视化测定方法 姜开宇, 孙合庆, 段 飞(84)
- 几种聚合物熔体黏度与超声波声速关系的表征 胡 坤, 王克俭(88)
- 基于响应面法的酚醛树脂固化条件优化 黄剑峰, 陈奶荣, 林巧佳等(92)
- 聚苯硫醚纤维氯甲基化反应条件的优化 周冬菊, 代立波, 惠跟雷等(97)
- 用于固体火箭发动机衬层固化过程监测的超声缓冲杆 杨亚军, 王召巴(101)

多臂星形聚乙二醇-聚乳酸嵌段共聚物的降解特性

林雅铃¹, 吴敏儿¹, 邱艳舞², 张安强²

(1. 华南农业大学资源环境学院制药工程系, 广东 广州 510642; 2. 华南理工大学材料科学与工程学院高分子系, 广东 广州 510641)

摘要:采用直接法合成了线型和多臂星形聚乙二醇-聚 L-乳酸嵌段共聚物((PLLA-b-PEG-b-PLLA 和 sPEG-b-PLLA)。研究了 3 种嵌段共聚物在 37 ℃、pH=7.2 的磷酸盐缓冲液中的降解机理。结果表明,共聚物降解后失重明显,亲水性降低;降解一定时间后共聚物的相对分子质量分布呈双峰分布,随着降解的进行,较低相对分子质量组分的相对分子质量并没有发生明显的变化。XRD 数据表明,降解前后的主要组成为结晶 PLLA 嵌段;¹H-NMR 分析证实,共聚物的降解过程中 PEG 嵌段和 PLLA 嵌段内部的降解程度很小。说明 sPEG-b-PLLA 在中性水性体系中的降解主要发生在连接 PLLA 和 PEG 的酯键上,而 PLLA 嵌段则由于处于结晶态,降解程度很低。

关键词:星形聚乙二醇-聚 L-乳酸嵌段共聚物;降解机理;结晶

中图分类号:TQ316.6⁺1

文献标识码:A

文章编号:1000-7555(2013)11-0067-04

聚乙二醇-聚乳酸嵌段共聚物(PEG-b-PLA)因其良好的两亲性、生物相容性和生物可吸收性,已被广泛应用于药物负载、组织工程等领域^[1~3]。与相同相对分子质量的线型共聚物相比,星形聚合物具有较小的流体力学体积,较高的热稳定性和较快的降解速率,更有利于药物的负载与输送。有关 PEG-PLA 嵌段共聚物的合成及降解已有广泛的研究^[3~8],但大部分的研究主要集中在不同形态的线型嵌段共聚物上,关于星形多臂 PEG-PLLA 共聚物降解行为的研究尚较少^[3]。本文在前期采用直接熔融缩聚法合成线型聚乙二醇-聚 L-乳酸三嵌段共聚物(PLLA-b-PEG-b-PLLA)和具有星形结构的多臂星形聚乙二醇-聚乳酸嵌段共聚物(sPEG-b-PLLA)的基础上,采用 FT-IR、GPC、¹H-NMR、接触角、降解失重等表征手段研究了上述线型和多臂星形 PEG-PLA 嵌段共聚物薄膜在中性 PBS 溶液(模拟体液)中的降解特性和降解规律。

1 实验部分

1.1 原料与试剂

线形聚乙二醇(PEG): $\bar{M}_n = 6000$, $\bar{M}_w/\bar{M}_n = 1.06$, Sigma-Aldrich 公司提供;四臂星形聚乙二醇(sPEG1): $\bar{M}_n = 0.43 \times 10^4$, $\bar{M}_w/\bar{M}_n = 1.05$, 黎明化工研究院提供;三臂星形聚乙二醇(sPEG2): $\bar{M}_n = 0.32 \times 10^4$, $\bar{M}_w/\bar{M}_n = 1.05$, 黎明化工研究院提供,使

用前用二氯甲烷溶解,冰乙醚沉析提纯 2 次,40 ℃真空干燥 48h 后备用;L-乳酸(LLA):耐热级,含水量约为 12%,武汉三江固德有限公司提供,采用文献[6]的方法制备得到提纯 LLA;辛酸亚锡($\text{Sn}(\text{Oct})_2$, 95%):Sigma-Aldrich 公司提供;pH=7.2 磷酸盐缓冲液(PBS):实验室配制;透析袋:截留相对分子质量 3500,上海绿鸟科技有限公司;其它试剂均为市售分析纯试剂。

1.2 仪器设备

Nicolet 6700 型红外光谱仪:美国 Thermo-Fisher 公司;Avance DRX-600 型核磁共振仪:瑞士 Bruker 公司;1515-2414 型凝胶渗透色谱仪:美国 Waters 公司;JC2000C 表面接触角分析仪:上海中晨数字技术设备有限公司;X'Pert Pro 型 X 射线衍射仪:荷兰 PANalytical 公司。

1.3 sPEG-b-PLLA 与 PLLA-b-PEG-b-PLLA 的合成

按文献[8]所述的方法合成。在装备冷凝器、机械搅拌的三口烧瓶中加入已提纯的 LLA 90g(1000 mmol),sPEG1 10g(2.33 mmol),按 LLA 质量的 1% 加入催化剂 $\text{Sn}(\text{Oct})_2$,从 120 ℃、10kPa 开始逐步升温聚合,每小时升温 5 ℃,至 165 ℃熔融聚合 9h。产物用二氯甲烷溶解、冰乙醚沉析 2 次,真空干燥后得到产物 sPEG1-b-PLLA。将 sPEG1 替换为 sPEG2 或 PEG 6000,可分别得到 sPEG2-b-PLLA 和 PLLA-b-PEG-b-

收稿日期:2013-01-14

基金项目:国家自然科学基金资助项目(51072055,51003032);广东省自然科学基金资助项目(07300675)

通讯联系人:林雅铃,主要从事药用高分子材料和药物分析的教学与研究, E-mail: linyaling@scau.edu.cn

PLLA。合成路线如 Fig.1 所示。

sPEG1-b-PLLA: FT-IR (KBr, cm^{-1}): 2960 ($-\text{CH}_3$); 2946 ($-\text{CH}-$); 2880 ($-\text{CH}_2-$); 1758 ($>\text{C}=\text{O}$); 1110 ($-\text{C}-\text{O}-$)。 $^1\text{H-NMR}$ (CDCl_3), δ : 5.17(a, 1H); 1.58(b, 6H); 3.64(c, 6H); 4.35(a', 1H); 3.41(c', 2H)。GPC(g/mol): $\bar{M}_n = 0.90 \times 10^4$, $\bar{M}_w = 1.29 \times 10^4$, $\bar{M}_w/\bar{M}_n = 1.43$ 。

sPEG2-b-PLLA: FT-IR (KBr, cm^{-1}): 2960 ($-\text{CH}_3$); 2946 ($-\text{CH}-$); 2880 ($-\text{CH}_2-$); 1758 ($>\text{C}=\text{O}$); 1110 ($-\text{C}-\text{O}-$)。 $^1\text{H-NMR}$ (CDCl_3) δ : 5.16(a, 1H); 1.58(b, 6H); 3.64(c, 6H); 4.36(a', 1H); 3.29(c', 2H)。GPC(g/mol): $\bar{M}_n = 1.07 \times 10^4$, $\bar{M}_w = 1.46 \times 10^4$, $\bar{M}_w/\bar{M}_n = 1.36$ 。

PLLA-b-PEG-b-PLLA: FT-IR(KBr, cm^{-1}): 2960 ($-\text{CH}_3$); 2946 ($-\text{CH}-$); 2880 ($-\text{CH}_2-$); 1758 ($>\text{C}=\text{O}$); 1110 ($-\text{C}-\text{O}-$)。 $^1\text{H-NMR}$ (CDCl_3) δ : 5.15(a, 1H); 1.57(b, 6H); 3.64(c, 6H); 4.35(a', 1H)。GPC(g/mol): $\bar{M}_n = 0.99 \times 10^4$, $\bar{M}_w = 1.48 \times 10^4$, $\bar{M}_w/\bar{M}_n = 1.50$ 。

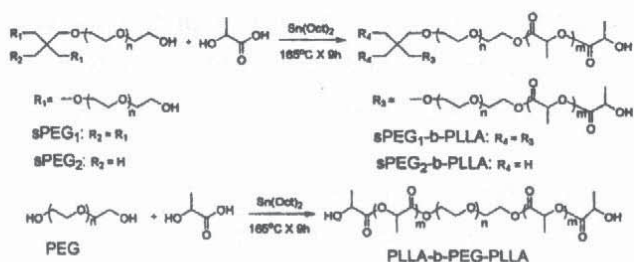


Fig.1 The Synthesis Route of sPEG-b-PLLA and PLLA-b-PEG-b-PLLA Copolymers

1.4 降解试验

将嵌段共聚物溶于二氯甲烷,配制成质量分数约为 10% 的溶液,将其倾倒在聚四氟乙烯平板上,涂抹均匀,待大部分溶剂自然挥干后,在真空干燥箱中常温

干燥 24 h,制得厚度约为 $40\ \mu\text{m}$ 的共聚物薄膜。将其剪裁成质量约为 100 mg 的 $50\text{mm} \times 50\text{mm}$ 的降解试验用薄膜。将降解试验用薄膜装入透析袋中,加入 1 mL PBS 缓冲溶液,两端密封,放入含有 150mL PBS 缓冲溶液的锥形瓶中,瓶口用 Parafilm 薄膜密封,置于 $(37 \pm 0.5)^\circ\text{C}$ 水浴恒温振荡摇床(100 r/min)中进行降解。间隔一定时间取出样品,真空干燥后记录样品的质量,按式(1)计算共聚物的失重率(Mass loss),并对样品进行相应的结构表征。

$$\text{Mass loss} = (m_i - m_t) / m_i \quad (1)$$

式中: m_i ——降解前共聚物的质量, g; m_t —— t 时刻共聚物的质量, g。

1.5 sPEG-b-PLLA 及其降解产物的结构表征

采用 Nicolet 6700 型红外光谱仪(KBr 压片)、Avance DRX-600 型核磁共振仪(CDCl_3 为溶剂,四甲基硅烷为内标)分别测定降解产物的 FT-IR 谱图和 $^1\text{H-NMR}$ 谱图。采用 Waters 1515-2414 型凝胶渗透色谱仪(以四氢呋喃为流动相,单分散聚苯乙烯作为标样,流速 1mL/min ,柱温 40°C)测定产物的相对分子质量及其分布。用 X' Pert Pro 型 X 射线衍射仪测定产物的结构参数, $\text{Cu K}\alpha$ 辐射,采用连续扫描方式,扫描步长 0.033° ,扫描范围 $5^\circ \sim 50^\circ$ 。用 JC2000C 表面接触角分析仪测定共聚物降解前后的接触角。

2 结果与讨论

2.1 共聚物降解过程中的结构变化

3 种嵌段共聚物在 $\text{pH} = 7.2$ 的 PBS 溶液中降解不同时间(0d~60d)后的 FT-IR 谱图如图 Fig.2 所示。由图中可见,归属于 PEG 嵌段或 sPEG 嵌段的亚甲基峰($-\text{CH}_2-$, $2880\ \text{cm}^{-1}$)与 PLLA 嵌段的酯羰基峰($>\text{C}=\text{O}$, $1758\ \text{cm}^{-1}$)的峰强度之比随着降解时间的延长而出现近似线性的下降趋势,说明残留在降解产物中的聚乙二醇嵌段的比例下降。

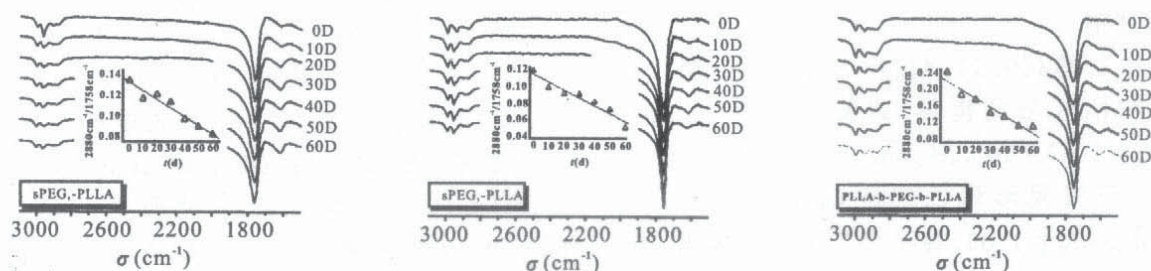


Fig.2 FT-IR Spectra of sPEG1-b-PLLA, sPEG2-b-PLLA, and PLLA-b-PEG-b-PLLA After 0d, 10d, 20d, 30d, 40d, 50d and 60d Degradation, and the Intensity Ratio of Peak $2880\ \text{cm}^{-1}$ and $1758\ \text{cm}^{-1}$

由 Fig.3 可见,所有的共聚物在降解前的 GPC 曲

线都大致呈单峰分布,随着降解的进行,共聚物的相对

分子质量变小,出现较低相对分子质量的物质。其中, sPEG1-b-PLLA 降解 10d 后分子量分布变宽,开始出现较低相对分子质量的物质,降解 20d 时出现明显的双峰分布,继续降解,双峰分布稳定,低相对分子质量聚合物的相对分子质量基本保持不变, sPEG2-b-PLLA

和 PLLA-b-PEG-b-PLLA 的降解行为类似。3 种嵌段共聚物降解前后的 XRD 谱图均主要表现为结晶性 PLLA 嵌段的特征峰,且峰形未出现明显的变化,如 Fig.4 所示。

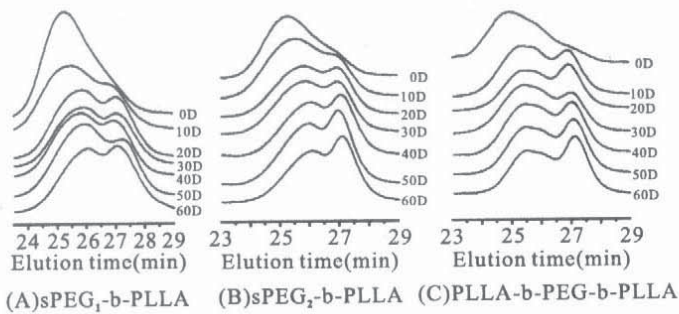


Fig. 3 GPC Curves of PEG-PLLA Copolymers After 0d, 10d, 20d, 30d, 40d, 50d, and 60d Degradation

由 Fig. 5(A)可见,共聚物中 PEG 嵌段降解前 $[c]/[c'] = 4n/2 = 2.47/0.06 = 41.2$;降解 60d 后, $[c]/[c'] = 4n/2 = 1.14/0.03 = 38.0$;降解前 PLLA 嵌段中 $[a]/[a'] = m = 1/0.05 = 20$;降解 60d 后 $[a]/[a'] = m = 1/0.05 = 20$,由此可知,降解前后的 n 值和

m 值变化小,说明在 PBS 缓冲液中,PEG 嵌段和 PLLA 嵌段的降解程度很小。sPEG2-b-PLLA(Fig. 5(B))和 PLLA-b-PEG-b-PLLA(Fig. 5(C))的 $^1\text{H-NMR}$ 谱图也有相似的结果。

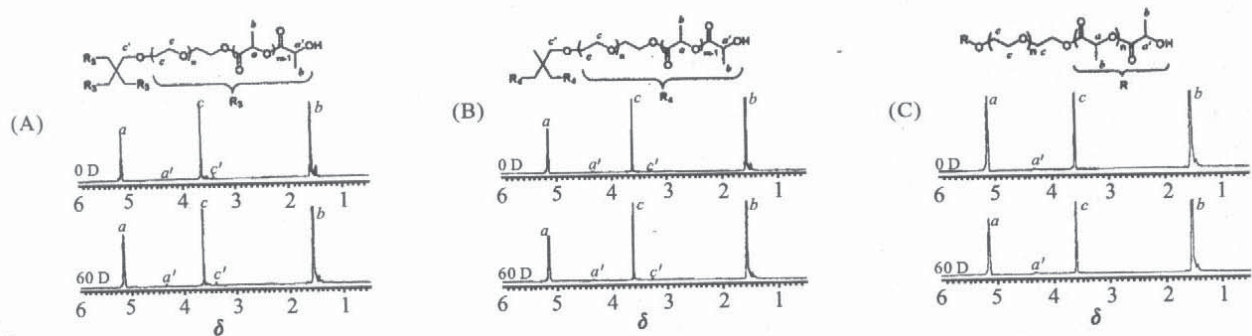


Fig. 5 $^1\text{H-NMR}$ Spectra of PEG-PLLA Copolymers Before and After 60d Degradation
(A): sPEG1-b-PLLA; (B): sPEG2-b-PLLA; (C): PLLA-b-PEG-b-PLLA

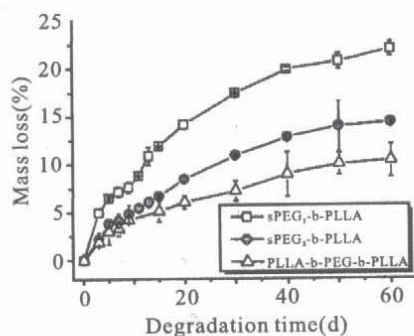


Fig. 6 Mass Loss of Different PEG-PLLA Films After Degradation in PBS (pH = 7.2)

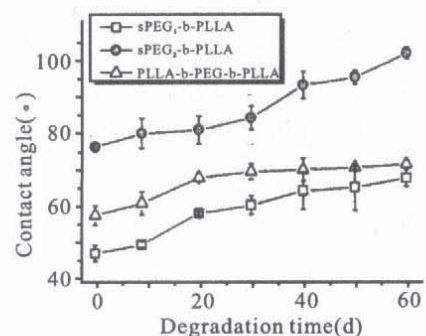


Fig. 7 The Contact Angle of PEG-PLLA Copolymers

共聚物的降解行为在宏观上表现为失重和亲水性的变化。Fig.6 是 3 种嵌段共聚物在降解过程中的失重行为,3 种嵌段共聚物在降解过程中都有明显的失重,且随着 PEG 臂数的增加,失重速率加快。这主要是由于 PEG 臂数的增加所引起的单位体积内连接 PLLA 嵌段与 PEG 嵌段的酯键密度增加所致。同时,降解产物的亲水性亦逐步降低,如 Fig.7 所示。接触角的变化趋势与 FT-IR 谱图(Fig.2)中亚甲基/羰基峰强度之比随着降解时间的延长而下降的现象相吻合。

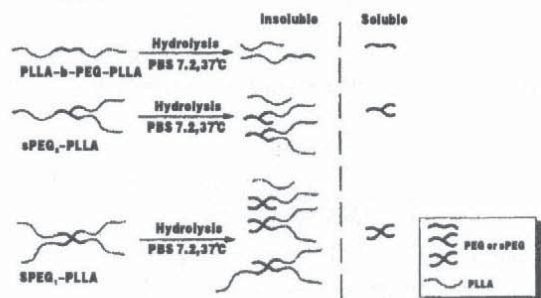


Fig. 8 The Degradation Mechanism of Star-Branched PEG-PLLA Copolymers

2.2 sPEG-PLLA 嵌段共聚物的降解机理

PEG-PLLA 嵌段共聚物在中性 PBS 中降解的基础是酯基的水解,而酯基水解的前提是水与酯基发生有效接触。PLLA 嵌段中有大量的酯基,但 PLLA 嵌段大多处于结晶态,水难以渗入,无法与 PLLA 嵌段内部的酯基发生有效接触,这也是 PLLA 嵌段的相对分子质量和结晶态结构在 PLLA-PEG 嵌段共聚物降解 60d 后依然未发生明显改变的主要原因。基于上述讨论,笔者推断,以 PLLA 为主体的线型和多臂星形 PEG-PLLA 嵌段共聚物在中性缓冲溶液中的降解机理主要为:PEG 嵌段与 PLLA 嵌段之间的酯键水解导致部分 PEG 嵌段完全从嵌段共聚物中游离出来,因其溶于水而流失,其他未完全水解的 PLLA-PEG 嵌段及残余的 PLLA 嵌段则因其水溶性不佳而未从降解产物中溶出,从而使得降解产物中 PEG 嵌段的含量降低、亲水性下降;而 PLLA 嵌段内部由于结晶度较高则未出现明显的降解(水解)。PEG-PLLA 嵌段共聚物在中性缓冲溶液中的降解过程如 Fig.8 所示。

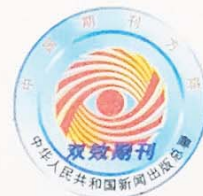
3 结论

采用直接熔融缩聚合成了线型和星形 PEG-PLLA 嵌段共聚物。通过考察其在 37 ℃、pH=7.2 的 PBS 缓冲液(模拟体液)中的降解行为,证实了线型和星形 PEG-PLLA 嵌段共聚物的降解主要发生在连接 PLLA 嵌段和 PEG 嵌段的酯键上,而 PLLA 嵌段则由于处于结晶态,降解(水解)程度很低。

参考文献:

- [1] 林雅铃, 张安强, 观富宜, 等. sPEG-b-PLLA/布洛芬微球的制备与体外释放研究[J]. 药学学报, 2010, 45(12): 1570-1575.
Lin Y L, Zhang A Q, Guan F Y, *et al.* Preparation of ibuprofen/sPEG-b-PLLA copolymer microspheres and its in vitro release properties[J]. Acta Pharmaceutica Sinica, 2010, 45 (12): 1570-1575.
- [2] Jie P, Venkatraman S S, Min F, *et al.* Micelle-like nanoparticles of star-branched PEO-PLA copolymers as chemotherapeutic carrier[J]. Journal of Controlled Release, 2005, 110 (1): 20-33.
- [3] Salaam L T E, Dean D, Bray T L. In vitro degradation behavior of biodegradable 4-star micelles [J]. Polymer, 2006, 47 (1): 310-318.
- [4] Li S, Rashkov I, Espartero J, *et al.* Synthesis, characterization, and hydrolytic degradation of PLA/PEO/PLA triblock copolymers with long poly (L-lactic acid) blocks [J]. Macromolecules, 1996, 29 (1): 57-62.
- [5] Cai C, Wang L, Dong C M. Synthesis, characterization, effect of architecture on crystallization, and spherulitic growth of poly (L-lactide)-b-poly (ethylene oxide) copolymers with different branch arms [J]. Journal of Polymer Science Part A: Polymer Chemistry, 2006, 44 (6): 2034-2044.
- [6] 林雅铃, 张安强, 王炼石. 载药用聚外消旋乳酸的合成方法: 中国, 200810026430.5 [P]. 2010-11-10.
- [7] Lin Y L, Zhang A Q, Wang L S. Synthesis and characterization of star-shaped poly (ethylene glycol)-block-poly (L-lactic acid) copolymers by melt polycondensation [J]. Journal of Applied Polymer Science, 2012, 124(6): 4496-4501.
- [8] 张安强, 林雅铃, 魏芬芬, 等. 星形聚乙二醇-聚乳酸嵌段共聚物的合成与表征[J]. 高分子材料科学与工程, 2011, 27(11): 84-88.
Zhang A Q, Lin Y L, Wei F F, *et al.* Synthesis and characterization of multi-arm star-shaped poly (ethyleneglycol)-b-poly (L-lactide) copolymer prepared by ring-opening polymerization [J]. Polymer Materials Science & Engineering, 2011, 27(11): 84-88.

(下转第 75 页. to be continued on P.75)



《高分子材料科学与工程》征稿简则

1. 本刊系经国家科委批准、公开发行的专业性学术刊物。办刊宗旨为面向国民经济,注重学术性、信息性、实用性。读者对象是从事与高分子材料有关的具有大专以上文化程度的科研、教学、生产及科技管理人员,有关专业的大学生及研究生等。

本刊是全国核心期刊,进入了 Ei Compendex 数据库、CA、《俄罗斯文摘杂志》、美国《剑桥科学文摘》等国际检索系统,连续入选美国 CA 千名表。2008 年荣获中国科技期刊精品奖,进入全国科技期刊 300 强行列。

2. 本刊登载与高分子材料科学与工程领域有关的高分子化学、高分子物理和物化、反应工程、结构与性能、成型加工理论与技术、材料应用与技术开发、研究方法 & 测试技术等方面的研究成果,设有以下栏目:

专论·综述 刊登对高分子材料学科具有重要指导意义的专论和综述性文章。

合成实验·工艺 刊登有关高分子材料的合成实验、合成工艺、反应工程等方面具有创意的研究论文。

结构·性能 刊登有关高分子材料的结构与性能研究以及高分子物理方面的具有创意的研究论文。

材料测试·加工·应用 刊登有关高分子的测试技术、成型加工理论与技术,以及材料应用方面具有创意的研究论文。

新技术·产品开发 刊登紧密结合高分子材料工业生产的新技术、新产品的开发成果。

教学讨论 刊登有关高分子专业的教学研究与讨论。 研究快讯 刊登有关高分子材料科学与工程方面的最新科研成果。

3. 来稿应具有创新性、学术性、科学性、规范性。论文力求主题明确,内容充实,数据可靠,文字精练,文责由作者自负,论文请控制在 8000 字以内(包括图、表,参考文献在内)。

4. 作者须同意将该文的复制权,发行权,信息网络传播权,汇编权等转让给本刊编辑部,编辑部所付稿酬中包含了其著作权在印刷版,光盘版和网络版等各种使用方式的使用报酬,以后不再另付作者。

5. 文稿自收到之日起,审稿期限为 3 个月,若超过期限收不到录用通知,请及时向编辑部查询。查询电话:028-85401653。

高 分 子 材 料 科 学 与 工 程

GAOFENZI CAILIAO KEXUE YU GONGCHENG

POLYMER MATERIALS SCIENCE AND ENGINEERING

(月刊, 1985 年创刊)

第 29 卷 第 11 期 2013 年 11 月

· 公开发行 ·

Vol. 29, No. 11 Nov. 2013

主 管: 中华人民共和国教育部

主 办: 中国石油化工股份有限公司科技开发部

国家自然科学基金委员会化学科学部

高分子材料工程国家重点实验室

四川大学高分子研究所(中国·成都)

主 编: 徐 偃

副主编: 袁晴棠 赵一雯

编 辑 出 版 《高分子材料科学与工程》编辑部

地址: 四川大学(西区)高分子研究所

邮政编码: 610065 电话: (028) 85401653

总 发 行 处 四川省报刊发行局

订 购 处 全国各地邮局

国 外 发 行 中国国际图书贸易集团有限公司

印 刷 中国核动力院印刷厂

Edited & Published by Editorial Board of Polymer Materials Science & Engineering

(Address: Polymer Research Institute, Sichuan University, Chengdu 610065, China)

Editor-in-Chief Xu Xi

Distributed Abroad by China National Publications Import & Export Corporation

(P.O. Box 88, Beijing, China)

<http://pmse.scu.edu.cn>

Email: GFZCLBJB@163.net

ISSN 1000-7555



11>

ISSN 1000-7555

刊号: CN 51-1293/O6

邮发刊号 62-67

国外代号: M6669

每期定价: 28.00 元 全年定价 336.00 元



Polyacrylamide quaternary ammonium salts based on stable adsorption in soil and its application on the control of soil-borne fungal disease

Wei Zhang^{a,1}, Jiangang Yu^{b,1}, Mingyang Wu^a, Rui Li^c, Anqiang Zhang^{c,*}, Yaling Lin^{a,*}

^a College of Materials and Energy, South China Agricultural University, 483 Wushan Rd., Guangzhou 510642, Guangdong, China

^b College of Natural Resources and Environment, South China Agricultural University, 483 Wushan Rd., Guangzhou 510642, Guangdong, China

^c School of Materials Science and Engineering, South China University of Technology, 381 Wushan Rd., Guangzhou 510641, Guangdong, China

ARTICLE INFO

Keywords:

Polyacrylamide quaternary ammonium salt
Polymer/soil interaction
Soil-borne fungal disease
Banana Fusarium wilt

ABSTRACT

Currently, soil-borne fungal disease (SBFD) have caused a huge damage in agriculture, and small molecule soil disinfectants have been widely used for the prevention and control of SBFD, which could not only kill the chlamydospore of pathogenic fungi, but also completely destroy the microbial community and its functional diversity in the soil, and is not conducive to subsequent plant planting. Therefore, how to effectively inhibit plant pathogenic fungi while maintaining the general balance of microbial population in the soil to facilitate subsequent plant planting come to be critical problem in the prevention and control of SBFD. In this work, a series of polyacrylamide containing quaternary ammonium salts (PAM-X) were synthesized based on the radical copolymerization of acrylamide (AM) and acrylamide containing different quaternary ammonium salts groups (AMX). Owing to the entanglement between polymer chains and soil, PAM-X could be stably absorbed in the soil, thus effectively delaying the free migration of PAM-X chains in soil, and reducing the probability of being leached from soil, which might be the key to obtain novel polymeric quaternary ammonium salts that have less impact on the environment. Banana Fusarium wilt, also known as “banana cancer”, caused by *Fusarium oxysporum* f. sp. *cubense* (Foc), was chosen as a typical soil-borne pathogen disease to verify the rationality of the above thoughts. The results showed PAM-X had well anti-Foc4 activities in soil, and could maintain the general balance of microbial population in the soil, which are almost non-toxic to earthworms in soil and fish, thus provides a new prevention and control method for SBFD.

1. Introduction

Soil-borne fungal disease (SBFD) is caused by plant pathogenic fungi (such as *Fusarium*, *Verticillium*, *Sclerotinia*, *Gaeumannomyces*) that can survive in the soil for a long time (up to 10 years), it is hard to control for the reason that the pathogenic fungi can survive in soil in the form of chlamydospore, and is becoming a key factor to restrict sustainable development of agricultural production in the world. [1] Due to the

complexity of soil, many chemicals could not show ideal inhibitory effects on pathogenic fungi in soil, although they might show inhibitory effects on the SBFD in the laboratory. [2] Therefore, currently, SBFDs are prevented and controlled using the method of soil disinfection, i.e., killing all microorganisms in the soil. [3] For example, soil fungicides or soil disinfectants, such as methyl bromide or calcium cyanamide were usually used to control banana Fusarium wilt, also known as “Panama disease” and “banana cancer”, which is one of the most destructive soil-

Abbreviations: Foc, *Fusarium oxysporum* f. sp. *cubense*; Foc4, *Fusarium oxysporum* f. sp. *cubense* “tropical” race 4; AM, acrylamide; AMX, acrylamide quaternary ammonium salts; AMBB, (2-methacrylamido) propyltetrahydroxydimethylammonium bromide; AMHEB, (2-methacrylamido) propyltetrahydroxydimethylammonium bromide; AMBC, (2-methacrylamido) propyltetrahydroxydimethylammonium chloride; PAM-X, random copolymers of AM and AMX; PAM-BB, random copolymer of AM and AMBB; PAM-HEB, random copolymer of AM and AMHEB; PAM-BC, random copolymer of AM and AMBC; PAM-X-FL, fluorescently labelled PAM-X; PQASs, polymeric quaternary ammonium salts; BC, benzalkonium chloride; MIC, minimum inhibitory concentration; MFC, minimal fungicidal concentration; IC₅₀, the 50% maximal inhibitory concentration against Foc4; IC₉₀, the 90% maximal inhibitory concentration against Foc4; IC_{50S}, the 50% maximal inhibitory concentration against Foc4 in soil; IC_{90S}, the 90% maximal inhibitory concentration against Foc4 in soil; LC₅₀, the median lethal concentration; LC_{50S}, the median lethal concentration of the chemical/soil mixture; LC_{50L}, the median lethal concentration of the soil leaching solution.

* Corresponding authors.

E-mail addresses: aqzhang@scut.edu.cn (A. Zhang), linyaling@scau.edu.cn (Y. Lin).

¹ These authors contributed equally.

<https://doi.org/10.1016/j.eurpolymj.2023.112604>

Received 15 August 2023; Received in revised form 14 November 2023; Accepted 17 November 2023

Available online 24 November 2023

0014-3057/© 2023 Elsevier Ltd. All rights reserved.

borne vascular diseases of banana in South China and even in the world, and is caused by *Fusarium oxysporum* f. sp. *cubense* (Foc), in which tropical race 4 (Foc4) has a significant impact on global banana production. [4–5] Normally, the soil disinfectants are small molecule which showed strong broad-spectrum antibacterial/fungi activities, could not only kill the chlamydospore of pathogenic fungi, but also kill most microorganisms (including beneficial microorganisms) in the soil, thus completely destroy the microbial community and its functional diversity in the soil, and is not conducive to subsequent plant planting. [6] New organic fertilizer needs to be introduced to restore the soil in order to replant bananas, [7–8] and the fumigated areas might eventually be re-attacked by the pathogen, making the next fruit production impossible. [9–10] Moreover, the volatilization or leaching of the small molecule soil disinfectants might cause serious environmental hazards, such as air pollution, water pollution, soil residual pollution, etc. [6,11] Therefore, how to effectively inhibit plant pathogenic fungi in soil while maintaining the general balance of microbial population in the soil, and reduce the environmental hazards to facilitate subsequent plant planting come to be critical problem in the prevention and control of SBFD. [1,2,4,8,11–13].

Quaternary ammonium salts (QASs) have been widely valued as daily disinfectants for their broad-spectrum anti-microorganism activities. [14–15] Although several type of QASs were applied to control plant pathogenic fungi in lab, when they were applied in soil, it may kill most microorganisms in the soil, [16] thus cause serious environmental risks and is detrimental to the subsequent planting. [16–17] Compared with small molecular QASs, by connecting the QASs groups with polymer chain to afford polymeric quaternary ammonium salts (PQASs) have attract more and more attentions for their excellent anti-microorganism properties, such as low toxicity, good environmental stability, none skin irritation, prolonged residence time and better biological activity. [18–21] However, they are less used in the prevention and control of plant diseases, especially soil-borne diseases. [22–24] On the other hand, polymeric compounds might improve soil structure by enhancing soil cohesion and increasing the stability and content of soil water-stable aggregates. For example, polyacrylamide (PAM) with different molecular weights has different effects on soil improvement, and all are effective. It maintains soil moisture and soil fertility, increases the content of soil water-stable aggregates, reduces soil bulk density, has no acute toxicity to aquatic organisms, and can promote the growth of corn plants after application. [25] Likewise, researchers have also reported the potential of crosslinked PAM for absorbing, retaining, and releasing extremely large amounts of water relative to its own weight. [26–27].

Therefore, we combined the virtue of PQASs with PAM, compared with previously reported PQASs, [18–19,24,31–32] the molecular weight of PAM is 1–3 orders of magnitude higher, which could help to enhance the interaction between polymer and soil particles, and effectively reduce the risk of quaternary ammonium salts loss by leaching, thus afford a serials polyacrylamide quaternary ammonium salts that have less impact on the environment. As talked above, PAM has been widely used for soil improvement for its good adsorption and aggregation properties on soil, thus it might be a suitable carrier for PQASs. According to this thought, a series of polyacrylamide copolymers (PAM-X) based on acrylamide (AM) and acrylamide containing different quaternary ammonium salts (AMX) [24] were synthesized via simple radical copolymerization, the adsorption and migration properties of PAM-X in soil, its impact on soil physical and chemical properties were studied in detail, and the biological and environmental toxicities were also evaluated by its impact on microbial population diversity in soil, earthworms and zebrafish. As for the persistency of PAM-X in soil, PAM-X could be considered as stable and none obvious harm to the environment before its degradation due to the PAM is hard to degrade in soil. Then, Foc4 was chosen as the typical pathogenic fungi of SBFD, and the anti-Foc4 activities both *in vitro* and *in vivo* (in soil) of PAM-X were evaluated intensively. This work has taken an exploratory step towards

the subsequent practical application of PAM-X, especially in sustainable prevention and control of SBFD.

2. Experimental

2.1. Materials

N, N-dimethylamine propyl methacrylamide (DMPMA), *n*-butyl bromide (BB, > 98 %), 1-hexyl bromide (HEB, 99 %), benzyl chloride (BC, 99 %) and 2,3,5-triphenyltetrazolium chloride (TTC, > 95 %), 2,2'-azobis(2-methylpropionamidine) dihydrochloride (AIBA, 98 %) and acrylamide (AM, 98 %), allyl chloride (99 %), 1-methylpiperazine (98 %), propylamine (98 %), 4-bromo-1,8-naphthalic anhydride (95 %) and ethylene glycol monomethyl ether (99 %) were purchased from Shanghai Macklin Biochemical Technology Co., Ltd. (Shanghai, China).

Fusarium oxysporum f. sp. *cubense* race 4 (Foc4) was donated by the Fungal Laboratory, Department of Plant Pathology, South China Agricultural University. The soil (crushed and screened through a 20-mesh sieve) was taken from the vegetable field of scientific research base of South China Agricultural University. The physicochemical properties of the soil are shown in Table S2, all the soil samples were passed through a 20-mesh sieve before using. Banana seedlings (*Musa AAA Cavendish* cv. *Brazil*) used in this experiment were provided by the South China Botanical Garden, Chinese Academy of Sciences. Zebrafish were purchased from Shanghai Feixi Biotechnology Co., Ltd., with a total length of 2 ± 0.5 cm and a weight of 0.2 ± 0.1 g. The earthworm species was *Eisenia foetida*, purchased from Xinyida Earthworm Farm in Hebei Province, China, with a total length of 5–8 cm and a weight of 0.3–0.6 g. Other chemical agents were used as received.

2.2. Synthesis of AMX (AMBB, AMHEB and AMBC)

The acrylamide quaternary ammonium salts, i.e., the AMX monomers, including (2-methacrylamido) propyltetrabutyldimethylammonium bromide (AMBB), (2-methacrylamido) propyltetrahexyldimethylammonium bromide (AMHEB), and (2-methacrylamido) propyltetrabenzyldimethylammonium chloride (AMBC), were synthesized by the quaternization reaction of DMPMA with halogenated reagents, including *n*-butyl bromide, 1-hexyl bromide and benzyl chloride, according to the our previous work,²⁴ as shown in Scheme 1. The detailed synthesis procedure of AM was shown in Part S1 of Supporting Information.

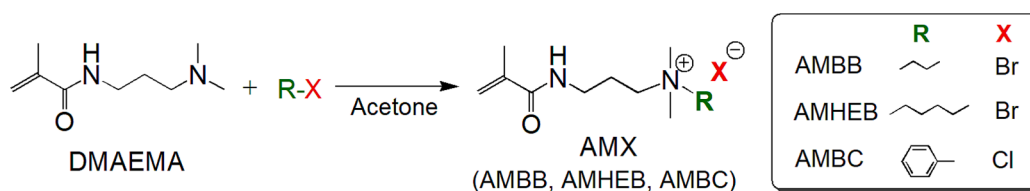
2.3. Synthesis of PAM-X (PAM-BB, PAM-HEB, and PAM-BC)

The random copolymer (PAM-X) of acrylamide (AM) and AMX (AMBB, AMHEB, and AMBC) with different AM / AMX feeding ratios were synthesized by radical copolymerization presented in Scheme 2.

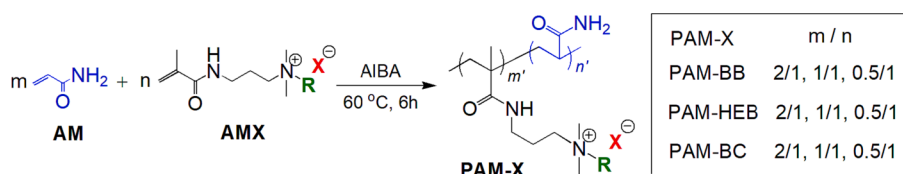
Taking PAM-BB with AM / AMBB feeding ratios (m/n) of 1/1 as the example, the typical procedure of PAM-BB was briefly stated as follows: first, under nitrogen atmosphere, AMBB (15.36 g, 0.05 mol) and AM (3.55 g, 0.05 mol) dissolved in sterile water (70 mL) was charged into a three-necked flask with a condenser, a magnetic stirrer and a nitrogen inlet, then heated to 60 °C under nitrogen atmosphere, and 0.28 g AIBA (dissolved in 5 mL sterile water) was dripped via the dropping funnel, and the reaction temperature was maintained at 60 °C for 6 h. After that, the mixture was condensed and added into acetone to precipitate the copolymers, the sticky copolymers were collected and then dried under vacuum at 70 °C for 24 h, and the product was denoted as PAM-BB. Similarly, PAM-HEB and PAM-BC with different AM / AMX feeding ratios were synthesized by identical procedure as above.

PAM-BB: ¹H NMR (600 MHz, D₂O, δ , ppm): 0.98–1.11 (bm, CH₂-C(CH₃), -CH₃), 1.39 (bs, -CH₂-CH₃), 1.75 (bs, -CH₂-CH₂-CH₃), 2.00 (bs, CH₂-C(CH₃), CH₂-CH₂-CH₂), 3.08 (bs, N⁺(CH₃)₂), 3.19 ~ 3.32 (bm, NH-CH₂, -CH₂-N⁺-CH₂). FT-IR (ν , cm⁻¹): 1661 (ν C=O amide), 1217 (ν C-N).

PAM-HEB: ¹H NMR (600 MHz, D₂O, δ , ppm): 0.89–1.10 (bm, CH₂-C



Scheme 1. The chemical structure and synthesis routine of the AMX (AMBB, AMHEB, and AMBC) monomers.



Scheme 2. The synthesis routine of polyacrylamide quaternary ammonium salts (PAM-X).

(CH₃), -CH₃), 1.35 (bs, -CH₂-(CH₂)₃-CH₃), 1.76–1.89 (bs, N⁺-CH₂-CH₂), 2.02 (bs, CH₂-C(CH₃), CH₂-CH₂-CH₂), 2.85 ~ 3.20 (bs, N⁺(CH₃)₂, NH-CH₂, -CH₂-N⁺-CH₂). FT-IR (ν, cm⁻¹): 1666 (ν C=O amide), 1215 (ν C-N).

PAM-BC: ¹H NMR (600 MHz, D₂O, δ, ppm): 0.96–1.13 (bm, CH₂-C(CH₃)), 1.53 ~ 1.96 (bm, CH₂-C(CH₃), 2.88 ~ 3.56 (bm, CH₂-CH₂-CH₂-N⁺-CH₂(CH₃)₂), 4.33 (bs, CH₂-Φ), 7.50 (bs, Φ-H). FT-IR (ν, cm⁻¹): 1665 (ν C=O amide), 1215 (ν C-N), 704, 734 (γ Φ-H).

The measurement residual monomers of PAM-X were shown in the [Supporting Information \(Part S4\)](#).

In order to realize the visualization of PAM-X, a very small amount of fluorescent group (FL) were introduced into PAM-X to obtain fluorescent labelled polyacrylamide quaternary ammonium salt (PAM-X-FL), and the detailed synthesis procedures of PAM-X-FL were shown in the [Supporting Information \(Part S2\)](#).

2.4. Characterization and methods

FT-IR spectra were collected on a Nicolet iS5 Fourier-Transform Infrared Spectrometer (Thermo Scientific, USA) equipped with an iD7-ZnSe ATR accessory. ¹H NMR spectra were obtained using a Bruker Avance III HD 600 (Bruker Instrument Corp., Germany) spectrometer with D₂O as the solvent. The viscosity average molecular weights (M_v) was measured using a capillary viscometer under 30 °C according GB/T 12005.1–1992.

The other methods, including the testing method for the soil/PAM-X interaction (adsorption, and migration), antifungal assay of PAM-X on *Foc4* (*in vitro* and in soil), biotoxicity evaluation (culturable microbes in soil, earthworm acute toxicity and fish acute toxicity evaluation), are detailed in the [Supporting Information \(Part S6 to S8\)](#).

3. Results and discussion

3.1. Structural characterization of PAM-X and anti-*Foc4* activities screening

To obtain high antifungal activities and improve soil characteristics, we designed and synthesized a series of polyacrylamide quaternary ammonium salts with different structures. The molecular structures of the target compounds were determined by ¹H NMR, FT-IR and fluorescence spectra, as detailed in the [Supporting Information \(Figures S2 and S3\)](#). As shown in [Figure S2](#), the peaks for C = C bonds (5.60 and 5.95 ppm in the ¹H NMR spectra) almost disappeared, and the absorption peaks at 1661, 1215 and 2881 cm⁻¹ represented the infrared absorption bands of -CONH- and -CH- of PAM-BB, PAM-HEB and PAM-BC ([Figure S3](#)), respectively. The spectra of the products were in complete

agreement with the expected structures and showed essentially no contaminants, which demonstrated the successful synthesis of the polymers.

As shown in [Table 1](#), the proportion of AMX monomer units in PAM-X was lower than that of the feeding ratio, and the viscosity average molecular weights of PAM-X were decrease with the increasing of AM/AMX feeding ratios, which mainly due to the steric hindrance effect of the bigger quaternary ammonium salt side groups. Due to the low contents of FL groups in PAM-X-FL (the feed ratio of FL-3 in the monomers was less than 1 wt%), although it is difficult to distinguish the characteristic peaks of FL groups in the FTIR and ¹H NMR spectra, we found that the maximum emission wavelength of PAM-X-FL moved from 523 nm (for FL-3) to 515 nm ([Figure S1](#)), indicating the copolymerization between AMX and FL-3.

In order to simplified the soil adsorption and environmental toxicity of PAM-X with different QASs structures, the *in vitro* anti-*Foc4* activities of PAM-X with different AM/AMX feeding ratios were tested based on the classical broth microdilution method with 2,3,5-triphenyl-tetrazoliumchloride (TTC), the results were shown [Table 1](#). It was found that for different PAM-X, the products with the feeding ratio of AM/AMX = 1/1 (mol/mol) showed the best anti-*Foc4* activities, thus in the following discussion, without special explanation, PAM-X refer to the products that are synthesized with the feeding ratio of AM/AMX = 1/1 (mol/mol).

3.2. The interactions between PAM-X and soil

Due to the weak light-absorbing properties of PAM-X, PAM-X containing fluorescent groups, i.e., PAM-X-FL, was chosen to determine the

Table 1
Molecular weight and anti-*Foc4* activities of PAM-X.

PAM-X	m / n ^a	m' / n' ^b	M _v ^c (kDa)	MIC (mg/mL)	MFC (mg/mL)	MFC/MIC
PAM-BB	2/1	2.67/1	320	0.04	0.08	2
	1/1	1.30/1	300	0.04	0.04	1
	0.5/1	0.57/1	200	0.04	0.16	4
PAM-HEB	2/1	2.9/1	330	0.04	0.04	1
	1/1	1.18/1	290	0.04	0.04	1
	0.5/1	0.53/1	180	0.08	0.16	2
PAM-BC	2/1	2.77/1	330	0.04	0.04	1
	1/1	1.35/1	290	0.02	0.02	1
	0.5/1	0.51/1	180	0.02	0.04	2

a. The feeding ratio of AM / AMX (m / n, mol / mol).

b. The proportion of AM units / AMX units in PAM-X (m' / n', mol / mol) based on ¹H NMR measurements.

c. The viscosity average molecular weights (M_v) based on capillary viscometer.

adsorption kinetics of PAM-X in soil. Fig. 1 shows the sorption kinetics of 100 mg/L PAM-X-FL in soils. In less than 5 h, the equilibrium adsorption of the three kinds of PAM-X-FL in soil was observed, and afterward, the concentration of PAM-X-FL in the soil was almost unchanged, and the entire adsorption kinetics of these three PAM-X on the soil conformed to the pseudo-second-order model with coefficients of correlation (R^2) above 0.995 (Fig. 1-B). Both the Freundlich and Langmuir models were selected to fit the results (Fig. 1-C, D and Table 1), where the Freundlich model showed a better regression coefficient (R^2), indicating that the adsorption of PAM-X to the tested soil is more tend to be a multilayer adsorption process. The Freundlich constant ($1/n$) (Table 2) is related to the adsorption strength of the adsorbent: $1/n$ values of 0.1–0.5, 0.5–1.0, and > 1.0 indicate that adsorption is good, easy to adsorb, and difficult to adsorb, respectively. Thus, the $1/n$ value of the three PAM-X is PAM-HEB (0.366) $<$ PAM-BB (0.608) $<$ PAM-BC (0.685), indicating that these three kinds of PAM-X can be easily adsorbed in soil, in which PAM-HEB shows an excellent adsorption effect.

In addition to the absorption properties, the migration and leaching behaviour of PAM-X in soil are also important for polymer/soil and polymer/fungi interactions. Fig. 2 shows the fluorescence curves of the PAM-X-FL solution and the leachates of soil containing PAM-X-FL, from which we can see that the PAM-X-FL solution emitted bright green light under ultraviolet lamp irradiation and had a strong fluorescence intensity at 515 nm, while after leaching, the leachates of soil were only light blue under the ultraviolet lamp (365 nm) irradiation, and there was no fluorescence intensity at 515 nm. Thus, it can be concluded that PAM-X-FL is difficult to move in soil.

Both the soil adsorption and soil migration assays demonstrated that PAM-X is easily adsorbed and relatively immobile in soil, which might be mainly due to two aspects: first, the positive charge carried by PAM-X can combine with the negative charge normally carried by soil particles

Table 2

Sorption isotherm parameters of PAM-X sorption to soils.

	Freundlich parameters			Langmuir isotherm		
	K_f (mmol/g)	$1/n$	R^2	q_{\max} (mg/g)	b	R^2
PAM-BB	1.57	0.608	0.9981	64.1	0.0084	0.9671
PAM-HEB	3.54	0.366	0.9909	69.4	0.0046	0.9974
PAM-BC	0.68	0.685	0.9996	64.9	0.0037	0.9478

(such as sludge and sediments), and second, the long chain of polymers and the entanglement between polymer chains and soil particles. Compared with alkyl groups, the presence of benzyl groups might strengthen the hydrophobic characteristics of quaternary ammonium salts and weaken the adsorption of polymeric quaternary ammonium salts in soil. These results are similar to previous studies on the behaviour of QASs in soil. [28–29].

The addition of polymers can change the physical conditions of soil for the interaction between soil particles and polymeric substances, and enhance the stability of aggregates by adhesions and adsorptions. Polymer adsorptions of soil particles could reduce the repulsive force between soil particles, and adhesions of polymers could bind the soil particles. [30] Thus the addition of PAM-X was assumed to act as a binding agent to stabilize the soil aggregates.

3.3. Anti-Foc4 activities of PAM-X

To evaluate the anti-fungal activities of chemicals, several antifungal parameters, such as the minimum inhibitory concentration (MIC) and minimal fungicidal concentration (MFC) based on the broth micro-dilution procedure with 2,3,5-triphenyl-tetrazoliumchloride (TTC), 50

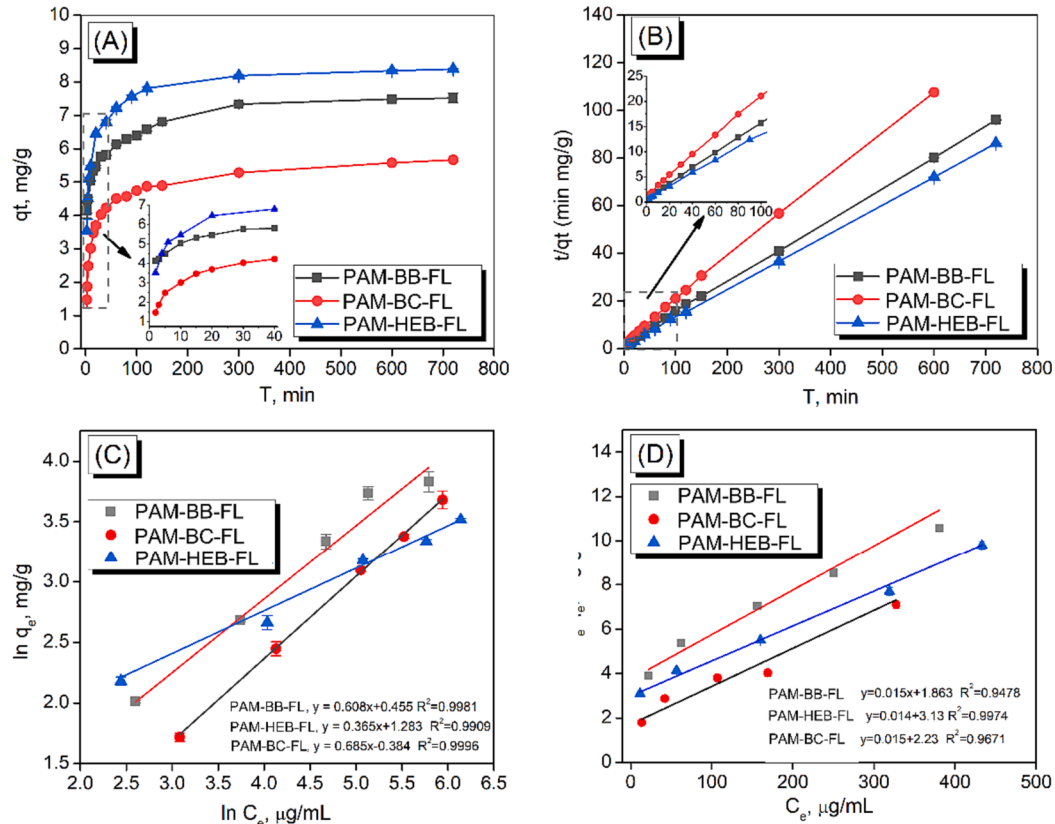


Fig. 1. Sorption kinetics and isotherms of PAM-X-FL (PAM-BB-FL, PAM-BC-FL and PAM-HEB-FL) in soils: (A) relationships between the sampling time and the PAM-X-FL concentration in soils; (B) the pseudo-second-order model fit to PAM-X-FL sorption kinetics data; (C) Freundlich sorption isotherms and (D) Langmuir sorption isotherms.

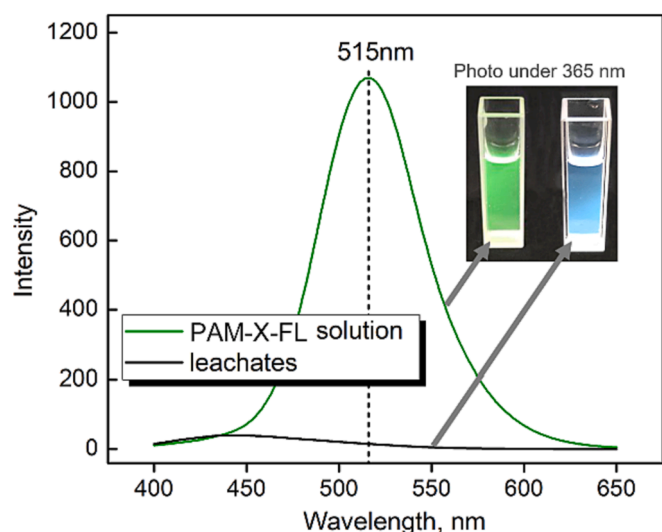


Fig. 2. Leaching behaviour of PAM-X-FL in soil.

% inhibitory concentration (IC_{50}) and 90 % inhibitory concentration (IC_{90}) based on the mycelia growth inhibition method, were often used. The culture media for these antifungal parameters were different: the culture media for MIC and MFC was liquid potato-dextrose (PD) media in which the chemicals could meet the *Foc4* conidia freely, while IC_{50} and IC_{90} were tested on solid potato-dextrose-agar (PDA) media, where the chemicals could meet the *Foc4* hyphae only on the surface of the PDA media. It should be noted that the *Foc4* conidia remained in the soil, which is much different from the culture media mentioned above; thus, we developed a new method in which the *Foc4* conidia were cultured in a mixture of sterilized soil and water, as detailed in the Part S8 of SI. This test condition is most similar to the actual environment of *Foc4* conidia in soil, and the results were labelled as IC_{50s} and IC_{90s} , in which the subscript “s” represents “Soil”. Fig. 3 shows the above mentioned typical anti-*Foc4* activities of PAM-X with different QAS structures in which a commercial bactericidal agent, benzalkonium chloride (BC),

was chosen as the positive control.

The results demonstrated that PAM-X exhibited antifungal activity against *Foc4* with MIC values ranging from 0.02 to 0.04 mg/mL, and the MFC/ IC_{50} ratios of the compounds were less than 4, indicating that both PAM-X and BC were fungicidally effective. [31] Although the IC_{50} values of PAM-X ranged from 0.56 to 0.65 mg/mL, which are much higher than those of BC, the difference between the IC_{50s} of PAM-X and BC was much smaller, as shown in Fig. 3, which demonstrates the good actual anti-*Foc4* activities of PAM-X in soil. We also noticed that compared with IC_{50} & IC_{90} , the IC_{50s} & IC_{90s} of BC increased, while the IC_{50s} & IC_{90s} of PAM-X decreased, which might be due to the better interaction of *Foc4* conidia and PAM-X in soil than in PDA media.

Although BC showed the lowest IC_{50} and IC_{90} in PDA media, in soil, PAM-X showed better sustained anti-*Foc4* activities. As mentioned above, during the measurements of IC_{50} & IC_{90} , the fungal mycelium only contacts one side of the PDA plates containing drugs, while for the IC_{50s} & IC_{90s} , the *Foc4* conidia could mix with the drugs in soil uniformly. [32] According to the mechanisms of fungistatic, the fungistasis of quaternary ammonium salts is a typical contact fungicidal, [33] and the effective contact between the fungistatic and the conidia is an important factor affecting its actual fungistatic activity in soil. Compared with BC, PAM-X was more easily adsorbed in soil and gradually desorbed, thus effectively promoting the effective contact between free PAM-X and *Foc4* conidia, resulting in increased antifungal activity. In particular, the slow desorption of the polymer chains is an important basis for the long-lasting antifungal activity of PAM-X. [34] This means that a single application of PAM-X in the field could prevent *Foc4* from invading banana plants through the soil for a certain period, and the results matched well with those of previous studies. [24,31–32].

3.4. Biototoxicity evaluation of PAM-X in the soil environment

Due to the broad-spectrum microbial inhibition characteristics of quaternary ammonium salt, the application of traditional small molecular quaternary ammonium salt in agriculture, especially in soil, is greatly limited due to its high environmental toxicity. Compared with small molecular quaternary ammonium salts, polymeric quaternary ammonium salts with higher molecular weight, such as the polyacrylamide-containing quaternary ammonium salt groups designed in this study, i.e., PAM-X, showed much difference in antifungal activities and soil adsorption properties, so it is necessary to evaluate their impact on the soil environments, including the impact on the culturable microbial populations in the soil, the effect on earthworms in soil and the acute toxicity of soil leachate containing PAM-X to fish.

The populations of total bacteria, fungi and actinomycetes in soil can also be used as indicators of soil health. [12–13,35] An appropriate microbial community structure is conducive to improving crop yield and soil defence ability. The effect of PAM-X on soil culturable microbial populations was evaluated based on plate counting methods in different media. After colony counting, the number of biological colonies in soil treated with PAM-X for 2 d was compared with that in untreated soil. The results of the culturable microbial analysis of soil amended with different PAM-X are presented in Fig. 4 A–C, which shows that PAM-X treatment increased the number of bacteria and actinomycetes in the soil in the order of PAM-BB > PAM-HEB > PAM-BC, and the total number of fungi decreased relatively, followed by PAM-BC > PAM-HEB > PAM-BB. Compared with PAM-X, traditional small molecular quaternary ammonium salts, such as benzalkonium chloride (BC), which has been widely commercially available, showed classic broad-spectrum bactericidal and fungicidal characteristics (Fig. 4: the culturable populations of bacteria, fungi and actinomycetes have decreased significantly; that is, BC could not only effectively inhibit *Foc4* conidia in soil but also destroy the ecology of the original microbial population in the soil, which is obviously not conducive to the growth of banana plants and not a sustainable way to control banana Fusarium wilt.

The changes in soil microbial numbers might be related to the stable

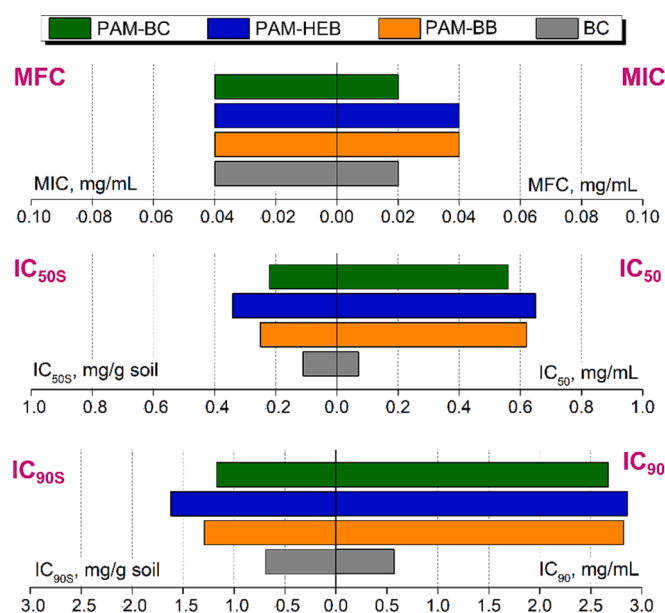


Fig. 3. Typical anti-*Foc4* activity parameters: (A) MIC & MFC, (B) IC_{50} & IC_{50s} and (C) IC_{90} & IC_{90s} of PAM-X and BC. (All the values are the average of 3 replicates; the data of the fungicidal activities were statistically analysed using Excel to give the IC_{50} & IC_{50s} and IC_{90} & IC_{90s} values.).

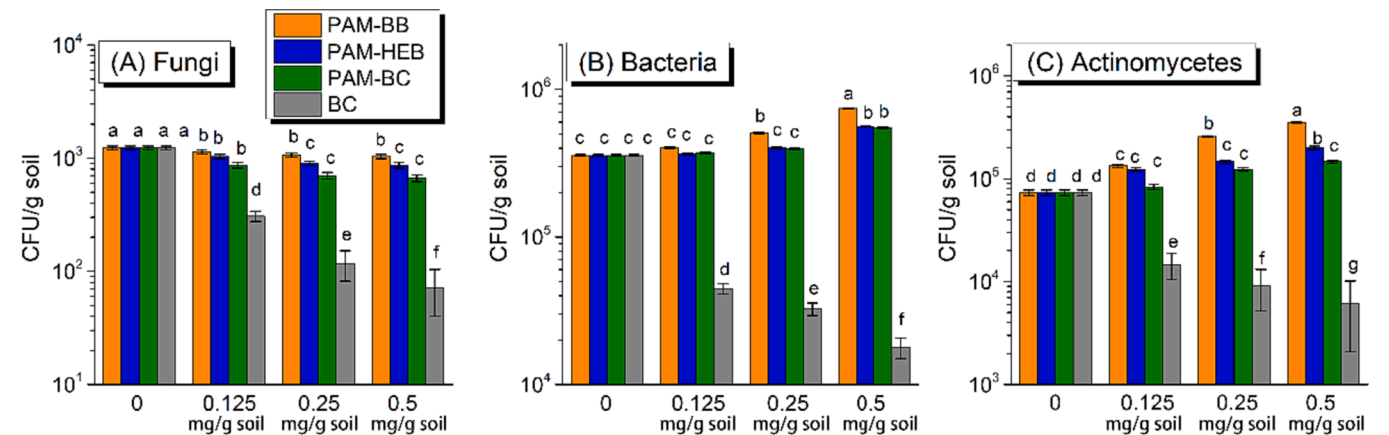


Fig. 4. Culturable populations of fungi (A), bacteria (B) and actinomycetes (C) in soils from the PAM-X treatments. (Vertical bars represent the standard error of the means. Treatments followed by different letters are significantly different according to Duncan's multiple range test ($p < 0.05$)).

adsorption of PAM-X in soil: due to the good adsorption of PAM-X in soil, most of the PAM-X chains were stably adsorbed on the surface of soil particles, which greatly reduces the effective contact probability between free PAM-X chains and microorganisms in soil. The increased bacterial numbers and decreased fungal numbers following PAM-X application represent an increase in soil fertility, possibly resulting in greater inhibition of *Foc4*.

In addition to the effect on the microbial community in the soil, the application of PAM-X to the soil also affected the earthworms living in the soil and the natural water environment in contact with the soil. Although quaternary ammonium salt showed high aquatic acute toxicity (e.g., zebrafish acute toxicity), considering that PAM-X is not directly applicable to natural water but applied to field soil, the only way to enter natural water (such as ponds and streams) is to be brought into or leached away by irrigation or rainwater. Therefore, in addition to routine evaluation of fish acute toxicity (LC_{50}) of PAM-X solutions, the fish acute toxicity of simulated rain leaching solution containing PAM-X soil (LC_{50L}) and a suspension containing PAM-X and soil (LC_{50S}) were also evaluated, which could help to simulate the actual application conditions of PAM-X in the field.

Fig. 5 shows the acute toxicities of three types of PAM-X, PAM-BB, PAM-HEB and PAM-BC on earthworms and zebrafish in which BC was chosen as the positive control. After 14 d of culture, the LC_{50} values for PAM-X and BC to earthworms were > 600 mg/kg and 150 mg/kg,

respectively, which means that both PAM-X and BC had no acute toxicity to earthworms. The acute toxicity of PAM-X and BC to zebra fish (*D. rerio*) is quite high; the LC_{50} of the three kinds of PAM-X is in the range of 1 to 10 mg/L (moderately toxic), and the LC_{50} of BC is less than 1 mg/L (highly toxic). After the application in soil, due to the good absorption of PAM-X in soil, the acute toxicity of both the leachate solution of the soil/PAM-X mixture (LC_{50L}) and the suspension of water/soil/PAM-X (LC_{50S}) could be significantly reduced: the LC_{50L} and LC_{50S} of three kinds of PAM-X were more than 600 mg/(kg soil), which is the actual maximum dosage of PAM-X in soil. For comparison, the LC_{50L} and LC_{50S} of BC under the same conditions are 70 mg/L and 150 mg/L. This means that the leaching solutions of the soil/PAM-X mixture and soil/BC mixture are non-acute-toxic and low-acute-toxic for zebra fish, respectively, according to GB/T 31270.12 (Test guidelines on environmental safety assessment for chemical pesticides).

4. Conclusions

Taken together, combining the strong adsorption effect of polyacrylamide in soil and the good anti-fungi activities of polymeric quaternary ammonium salts, polyacrylamide containing quaternary ammonium salts (PAM-X, including PAM-BB, PAM-HEB and PAM-BC) show strong soil-adsorption effect and exhibit inhibitory effects on the mycelial and conidial growth of *Foc4*, in which PAM-BC with a benzyl

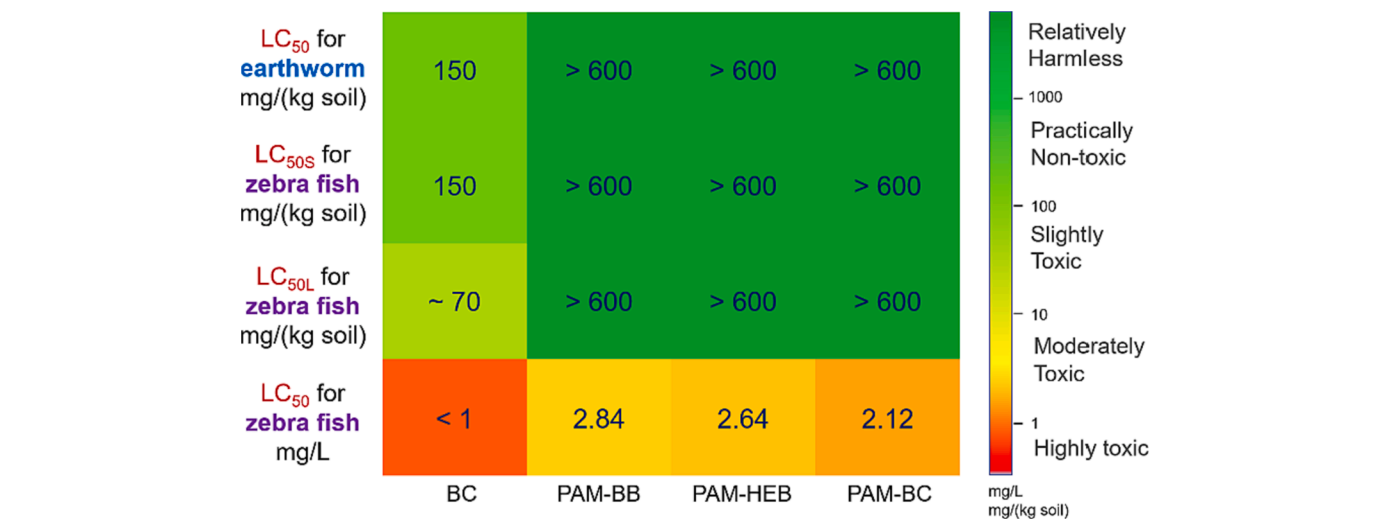


Fig. 5. LC_{50} , LC_{50L} , and LC_{50S} of PAM-X for zebrafish (*Danio rerio*) and earthworms (96 h). (Potassium dichromate and chloroacetamide were used as zebrafish and earthworm reference poisons, respectively. BC was used as a positive control. Average of three replicates.).

structure has better inhibitory and fungicidal effects. Due to the long chain of PAM-X, it exhibits easy adsorption in soil and is hard to move in soil, which makes it unlikely to flow into groundwater and cause water pollution. The IC_{50S} of PAM-X in soil is lower and more stable than that in indoor medium and can resist the invasion of *Foc4* conidia in soil. Unlike small molecule quaternary ammonium salts (such as benzalkonium chloride), which can kill almost all microorganisms in the soil, the adding of PAM-X can maintain the general balance of microbial population in the soil, in which the fungal population was effectively inhibited, while the bacteria and actinomycetes population was promoted, thus help to obtain a “bacterial soil” that is more conducive to plant growth. The good adsorption and difficult migration in the soil of PAM-X greatly reduce its impact on earthworms in the soil, and the soil drenching solution and soil suspension containing PAM-X are nontoxic to fish, which provides a new prevention and control method for SBF. It is also noticed that although PAM-X showed well anti-*Foc4* activities in soil and have less impact on environment, the non-degradability of PAM-X might be a risk for its application in soil, and degradable materials might be considered in the future work.

Declaration of competing interest

The authors declare that they have no known competing financial interests or personal relationships that could have appeared to influence the work reported in this paper.

Data availability

Data will be made available on request.

Acknowledgements

The authors acknowledge the financial support from the National Natural Science Foundation of China (Nos. 52073098 and 31772202) and the Scientific and Technological Planning Project of Guangzhou City (201803020015).

Appendix A. Supplementary data

Supplementary data to this article can be found online at <https://doi.org/10.1016/j.eurpolymj.2023.112604>.

References

- [1] W.W. Bockus, J.P. Shroyer, The impact of reduced tillage on soilborne plant pathogens, *Annu. Rev. Phytopathol.* 36 (1) (1998) 485–500.
- [2] H. Li, J. Huang, H. Yuan, Advances in control of plant soil-borne diseases by organic amendments, *Acta Phytopathologica Sinica* 32 (4) (2002) 289–295.
- [3] P. Gay, P. Piccarolo, D.R. Aimonino, C. Tortia, A high efficacy steam soil disinfection system, part II: Design and testing, *Biosyst. Eng.* 107 (3) (2010) 194–201.
- [4] B.G. Siddhesh, K.S.S. Upendra, R.G. Thumballi, Fusarium wilt of banana: biology, epidemiology and management, *International Journal of Pest Management* 61 (3) (2017) 250–263.
- [5] L. Teixeira, E. Nomura, E. Damatto, et al., Effectiveness of soil management practices on Fusarium wilt of banana in the Ribeira Valley, Brazil, *Tropical Plant Pathology* 47 (3) (2022) 1–10.
- [6] T. Bratec, N. Kirchhübel, N. Baranovskaya, et al., Towards integrating toxicity characterization into environmental studies: case study of bromine in soils, *Environ. Sci. Pollut. Res.* 26 (2019) 19814–19827.
- [7] T.V. Nguyen, L.T.T. Tran-Nguyen, C.L. Wright, et al., Evaluation of the efficacy of commercial disinfectants against *Fusarium oxysporum* f. sp. cubense race 1 and tropical race 4 propagules, *Plant Dis.* 103 (4) (2019) 721–728.
- [8] Z.Z. Shen, C. Xue, P.W.J. Taylor, Y.N. Ou, B.B. Wang, Y. Zhao, Y.Z. Ruan, R. Li, Q. R. Shen, Soil pre-fumigation could effectively improve the disease suppressiveness of biofertilizer to banana Fusarium wilt disease by reshaping the soil microbiome, *Biol. Fertil. Soils* 54 (2018) 793–806.
- [9] R.A. Segura, J.J. Stoorvogel, F.A. Blanco, J.A. Sandoval, A medium-term field experiment to study the effect of managing soil chemical properties on Fusarium wilt in banana (Musa AAA), *Journal of Fungi* 7 (2021) 261.
- [10] B. Nel, C. Steinberg, N. Labuschagne, et al., The potential of nonpathogenic *Fusarium oxysporum* and other biological control organisms for suppressing fusarium wilt of banana, *Plant Pathol.* 55 (2) (2006) 217–223.
- [11] L.F. Izquierdo-García, S.L. Carmona, P. Zuluaga, G. Rodríguez, M. Dita, M. Betancourt, M. Soto-Suárez, Efficacy of disinfectants against *Fusarium oxysporum* f. sp. cubense tropical race 4 isolated from La Guajira, Colombia, *Journal of Fungi* 7 (2021) 297.
- [12] S. Hong, H.L. Jv, M. Lu, B.B. Wang, Y.Z. Ruan, Significant decline in banana Fusarium wilt disease is associated with soil microbiome reconstruction under chilli pepper-banana rotation, *Eur. J. Soil Biol.* 97 (2020), 103154.
- [13] J. Yang, Y. Duan, X. Liu, et al., Reduction of banana fusarium wilt associated with soil microbiome reconstruction through green manure intercropping, *Agr Ecosyst Environ* 337 (2022), 108065.
- [14] J.W. Jr, B. Heldreth, W.F. Bergfeld, et al., Safety assessment of polyquaternium-22 and polyquaternium-39 as used in cosmetics, *Int. J. Toxicol.* 35 (s3) (2016) 47–53.
- [15] Y. Jiao, L.N. Niu, S. Ma, J. Li, R.T. Franklin, J.H. Chen, Quaternary ammonium-based biomedical materials: State-of-the-art, toxicological aspects and antimicrobial resistance, *Prog. Polym. Sci.* 71 (2017) 53–90.
- [16] C. Zhang, U. Tezel, K. Li, et al., Evaluation and modeling of benzalkonium chloride inhibition and biodegradation in activated sludge, *Water Res.* 45 (3) (2011) 1238–1246.
- [17] B. Sarkar, M. Megharaj, Y. Xi, et al., Sorption of quaternary ammonium compounds in soils: implications to the soil microbial activities, *J. Hazard. Mater.* 184 (1–3) (2010) 448–456.
- [18] G.Q. Lu, D.C. Wu, R.W. Fu, Studies on the synthesis and antibacterial activities of polymeric quaternary ammonium salts from dimethylaminoethyl methacrylate, *React. Funct. Polym.* 67 (4) (2007) 355–366.
- [19] Y. Lei, S. Zhou, C. Dong, et al., PDMS tri-block copolymers bearing quaternary ammonium salts for epidermal antimicrobial agents: Synthesis, surface adsorption and non-skin-penetration, *React. Funct. Polym.* 124 (2018) 20–28.
- [20] C.C. Zhou, H. Wang, H.T. Bai, P.B. Zhang, L.B. Liu, S. Wang, Y.L. Wang, Tuning antibacterial activity of cyclodextrin-attached cationic ammonium surfactants by a supramolecular approach, *ACS Appl. Mater. Interfaces* 9 (2017) 31657–31666.
- [21] C.J. Raorane, Y. Kim, T. Periyasamy, J.H. Lee, S. Ulaganathan, T.J. Nam, S.C. Kim, J. Lee, Quaternary ammonium salt (QAS)-modified thermoresponsive PNIPAM-PDMAEA copolymer for antibiofilm and antimicrobial applications, *Polymer* 281 (2023), 126104.
- [22] W. Ji, R.R. Koepsel, H. Murata, et al., Bactericidal specificity and resistance profile of poly(quaternary ammonium) polymers and protein-poly(quaternary ammonium) conjugates, *Biomacromolecules* 18 (8) (2017) 2583–2593.
- [23] M. Rahman, M. Bam, E. Luat, et al., Macromolecular-clustered facial amphiphilic antimicrobials, *Nature, Communications* 9 (2018) 5231.
- [24] A. Zhang, Q. Liu, Y. Lei, et al., Synthesis and antimicrobial activities of acrylamide polymers containing quaternary ammonium salts on bacteria and phytopathogenic fungi, *React. Funct. Polym.* 88 (2015) 39–46.
- [25] A.I. Mamedov, S. Beckmann, C. Huang, G.J. Levy, Aggregate stability as affected by polyacrylamide molecular weight, soil texture, and water quality, *Soil Sci. Soc. Am. J.* 71 (6) (2007) 1909–1918.
- [26] A.I. Mamedov, C.H. Huang, F.A. Aliev, et al., Aggregate stability and water retention near saturation characteristics as affected by soil texture, aggregate size and polyacrylamide application, *Land Degrad. Dev.* 28 (2) (2017) 543–552.
- [27] B. Kebede, A. Tsunekawa, N. Haregeweyn, et al., Effectiveness of polyacrylamide in reducing runoff and soil loss under consecutive rainfall storms, *Sustainability* 12 (4) (2020) 1597.
- [28] Z.Z. Ismail, U. Tezel, S.G. Pavlostathis, Sorption of quaternary ammonium compounds to municipal sludge, *Water Res.* 44 (7) (2010) 2303–2313.
- [29] H. Jiang, L. Xu, Y. Hu, et al., Flotation and adsorption of quaternary ammonium cationic collectors on diaspore and kaolinite, *Trans. Nonferrous Met. Soc. Chin.* 21 (11) (2011) 2528–2534.
- [30] F.L. Santos, J.L. Reis, O.C. Martins, et al., Comparative assessment of infiltration, runoff and erosion of sprinkler irrigated soils, *Biosyst. Eng.* 86 (3) (2003) 355–364.
- [31] Z. Huang, R. Liuyang, C. Dong, et al., Polymeric quaternary ammonium salt activity against *Fusarium oxysporum* f. sp. cubense race 4: Synthesis, structure-activity relationship and mode of action, *React. Funct. Polym.* 114 (2017) 13–22.
- [32] Y.Y. Chang, W.Q. Zhong, J.Q. Liang, A.Q. Zhang, Y.L. Lin, Polydimethylsiloxane-polymethacrylate block copolymers containing quaternary ammonium salts against *Fusarium oxysporum* f. sp. cubense race 4 in soil: Antifungal activities and pot experiments, *React. Funct. Polym.* 160 (2021), 104848.
- [33] B.P. Mowery, S.E. Lee, D.A. Kissounko, et al., Mimicry of antimicrobial host-defense peptides by random copolymers, *J. Am. Chem. Soc.* 129 (50) (2007) 15474–15476.
- [34] M.T. Garcia, I. Ribosa, T. Guindulain, et al., Fate and effect of monoalkyl quaternary ammonium surfactants in the aquatic environment, *Environ. Pollut.* 111 (1) (2001) 169–175.
- [35] G. Bonanomi, V. Antignani, M. Capodilupo, et al., Identifying the characteristics of organic soil amendments that suppress soilborne plant diseases, *Soil Biol. Biochem.* 42 (2) (2010) 136–144.



Antifungal mechanisms of polymeric quaternary ammonium salts against conidia of *Fusarium oxysporum* f. sp. *cubense*, race 4

Wei Zhang · Yaoyao Chang · Weiqiang Zhong · Anqiang Zhang · Yaling Lin

Accepted: 1 October 2022 / Published online: 8 October 2022
 © Koninklijke Nederlandse Planteziektenkundige Vereniging 2022

Abstract *Fusarium* wilt of banana is a devastating disease caused by *Fusarium oxysporum* f. sp. *cubense* (*Foc*), of which the “tropical” race 4 strain (*Foc4*) has a significant impact on the banana industry worldwide. Due to the strong persistence of *Foc4* conidia, there is no effective chemical control method up to now. Quaternary ammonium salts (QASs), as cationic fungicides, have great application prospects in the field of inhibiting plant diseases and our previous work showed that polymeric quaternary ammonium salts (PQASs) could effectively inhibit *Foc4* conidia in soil. In this paper, we investigate the effects of two kinds of PQASs, i.e. polydimethylsiloxane-polymethacrylate block copolymers, containing quaternary ammonium salts (PDMS-*b*-QPDMAEMA), poly(methacrylamido propylbenzyl dimethylammonium chloride) (PQD-BC), on the antifungal activities against *Foc4*, using antifungal bioassays and microscopy. It was found that PQASs had high inhibitory effects on conidia and worked fast. Microscopy showed that PQASs could not only rapidly enter conidia, but also stably adsorb to the surface of conidia and penetrate newly grown hyphae. It was also found that PQASs could affect the hydrophobicity of conidial surfaces, change the composition of the cell wall and destroy its

integrity. Over all, this work provides valuable information for the application of PQASs as antifungal agents for inhibiting *Foc4*.

Keywords *Fusarium* wilt of banana · *Foc4* conidia · Polymeric quaternary ammonium salts · Antifungal mechanisms

Abbreviations

<i>Foc4</i>	<i>Fusarium oxysporum</i> f. sp. <i>cubense</i> “tropical” race 4
QAS	quaternary ammonium salts
SQAS	single & small molecular containing quaternary ammonium salt groups
PQASs	polymeric quaternary ammonium salts
PDMS- <i>b</i> -QPDMAEMA (S_nQ_5)	polydimethylsiloxane-polymethacrylate block copolymers containing quaternary ammonium salts
PQD-BC	poly(methacrylamido propylbenzyl dimethylammonium chloride)
BC	benzalkonium chloride
MIC	minimum inhibitory concentration
MFC	minimal fungicidal concentration
IC ₅₀	the 50% maximal inhibitory concentration

W. Zhang · Y. Chang · Y. Lin (✉)
 College of Materials and Energy, South China Agricultural University, 483 Wushan Rd, Guangzhou 510642 Guangdong, China
 e-mail: linyaling@scau.edu.cn

W. Zhong · A. Zhang
 School of Materials Science and Engineering, South China University of Technology, 381 Wushan Rd, Guangzhou 510641 Guangdong, China

IC₉₀ the 90% maximal inhibitory concentration

Introduction

Fusarium wilt of banana is a serious soil-borne vascular disease caused by *Fusarium oxysporum* f. sp. *cubense* (*Foc*), of which the tropical race 4 (*Foc4*) is the most destructive (Shen et al., 2019). The pathogen can survive in the soil as chlamydospores for more than 20 years and infect banana roots at an appropriate time and therefore, it is very difficult to control this disease (Dita et al., 2018; Nel et al., 2006). The spread of *Foc4* is mainly caused by passive movement of pathogen propagules over short or long distances, with human activity being the main responsible factor, through planting material, workers, vehicles, movement of spore-bearing soil, irrigation and flooding (Dita et al., 2018). Even if a small amount of pathogen infects the field, it can cause devastating losses (Ploetz et al., 2015). Surface disinfectants have been found to eliminate the pathogen from infested tools, but effective prophylactic or therapeutic fungicides are not common although there are reports (Meldrum et al., 2013; Nel et al., 2007; Nguyen et al., 2019).

Quaternary ammonium salts (QASs) are rapidly becoming important antimicrobial solutions due to their substantial efficacy (Abid et al., 2017). Therefore, they have been widely used as disinfectants in agricultural fields, public places as well as in medical and health contexts (Buffet-Bataillon et al., 2012). The QASs can be divided into two types depending on molecular weight. The first group comprise single and small molecules containing quaternary ammonium salt groups (referred as SQASs) such as benzalkonium chloride (BC), alkyldimethylbenzylammonium chloride and didecyldimethylammonium chloride. The second group comprises polymeric quaternary ammonium salts (referred as PQASs), i.e. macromolecules containing quaternary ammonium salt groups such as the homopolymer of methacrylamido propylbenzyl dimethylammonium chloride (PQD-BC), dimethylaminopropyl benzyl chloride-grafted polysiloxanes and poly(acryloyloxydodecylpyridinium bromide) (Lin et al., 2014; Zhang et al., 2015, b). Antibacterial and antifungal activities and mechanisms of SQASs have been reported and a widely recognized mechanism is based on cationic immobilization. This means that the positive charge carried by SQASs combines with the negative charge on the surface of the

fungi/bacteria, resulting in a disorder of charge distribution on the cell membrane surface, thus destroying the cell membrane structure, leading to the leakage of cytoplasmic components and eventually death (Gou et al., 2018; Jiao et al., 2017). Gilbert and Moore (2005) showed that SQASs could interfere with the physiological functions of the bacterial cell membrane surface, such as respiration, solute transport and cell wall biosynthesis and thus dissolve all cell contents and kill cells. Ioannou et al. (2007) found that alkyldimethylbenzylammonium chloride and didecyldimethylammonium chloride could be adsorbed to the cell surface of microorganisms and the long carbon chains of SQASs could dissolve phospholipid bilayers and steroid compounds in the cell membrane. However, SQASs are toxic to the environment and have poor chemical stability (Jiao et al., 2017; Lei et al., 2018; Zhang et al., 2015, b). To solve these problems, combining QAS groups with high molecular weight polymer chains to produce PQAS, give the advantages of good curative effects, low toxicity, non-volatility, high chemical stability and prolonged action time, thus having broad application prospects (Lin et al., 2018; Xue et al., 2015).

The suppression mechanisms of PQASs are similar to those of SQASs. They can also have destructive interactions with negatively charged biofilms and cause leakage of intracellular components (Jiao et al., 2017). Compared with SQASs, PQASs have a higher positive charge density. A higher quaternary ammonium group content can promote the rapid adsorption of PQASs to the surface of pathogenic microorganisms and destroy the cell membrane, thereby significantly enhancing the antimicrobial activity (Lei et al., 2018). Rembaum et al. (1977) revealed that the bactericidal effect of PQASs was accompanied by bacterial cell adhesion, aggregation and cleavage as well as complex formation with DNA. Narita et al. (2001) studied the destruction of yeast protoplasts by PQASs with different charge densities and hydrophobic chain segments. They found that hydrophobicity was crucial to induction of cell disruption. Huang et al. (2017) measured the effects of PQD-BC and dimethylaminopropyl benzyl chloride-grafted polysiloxanes on *Foc4* cell walls and cell membrane integrity, mitochondrial function and genome. They found that these two PQASs could induce *Foc4* cell death by destroying cell structural integrity, leading to the release of cell contents, inducing mitochondrial dysfunction and interfering with the synthesis of

genomic DNA. PQD-BC is a typical hydrophilic homopolymer and its main chain is polyacrylamide (Zhang et al., 2015, b), which has a strong hydrophilicity that may not be conducive for the adsorption in soil. Dimethylaminopropyl benzyl chloride-grafted polysiloxane is an amphiphilic polymeric quaternary ammonium salt with hydrophobic polydimethylsiloxane as the main chain and a hydrophilic N, N-dimethyl benzyl chloride quaternary ammonium salt as the side group (Lin et al., 2014). Due to the random distribution of the hydrophilic side groups on the hydrophobic chain, it is difficult accurately to control the structure of dimethylaminopropyl benzyl chloride-grafted polysiloxanes.

As described above, the *Foc4* conidia have a long survival time in the soil, which makes it difficult to control the pathogen. Therefore, inhibiting the spread of conidia or killing them in the soil is of great significance to control Fusarium wilt. In previous studies, QASs were generally not considered sporicidal (Jiao et al., 2017). In our previous study, we synthesized an amphiphilic polydimethylsiloxane-polymethacrylate block copolymer containing quaternary ammonium salts (PDMS-*b*-QPDMAEMA) with good adsorption properties in soil and found that it could not only kill *Foc4* conidia, but also inhibit them in soil for 90 days when the pathogen was applied every 10 days (Chang et al., 2021; Lin et al., 2018). In this work, we focus on *Foc4* conidia and study the mechanisms of inhibition of PQAS on *Foc4* conidia. We hope this work will help to understand further the relationship between polymer structure and sporicidal activity and will assist in finding potential polymeric antimicrobial agents for plant protection.

Materials and methods

Strains and culture conditions

The fungal strain used in this study was *Fusarium oxysporum* f. sp. *cubense* (E. F. Smith) Snyder & Hansen, Tropical race 4 (*Foc4*), donated by the Fungal Laboratory of South China Agricultural University and sub-cultured on potato dextrose agar medium (PDA). *Foc4* conidia were obtained from agar cultures after 5 d growth at 28 °C. The concentrations of conidial suspensions were determined using a haemocytometer.

Chemicals

Three kinds of QASs were used in the work, i.e. polydimethylsiloxane-polymethacrylate block copolymers containing quaternary ammonium salts (PDMS-*b*-QPDMAEMA, labelled as S_nQ_5 , $n = 0, 5$ or 10 , which means that the molecular weight of the polydimethylsiloxane block is 0, 5 or 10 kDa), poly(methacrylamido propylbenzyl dimethylammonium chloride) (PQD-BC) and benzalkonium chloride (BC). For direct observation of the migration of PQASs into *Foc4* conidia, part of the benzyl group (< 2%) in the QAS structure was replaced by a fluorescein group (-FL), allowing green fluorescence emission under the excitation of ultraviolet light (365 nm) and the corresponding compounds were labelled as S_5Q_5 -FL, PQD-BC-FL and BC-FL, respectively. All QASs except BC were synthesized according to literature (Lin et al., 2018; Zhang et al., 2015, b; Zhong et al., 2017). Their structural characterization and antifungal properties are shown in Supplementary Information (**Part S1–S2**). BC, 2,3,5-triphenyltetrazolium chloride (TTC), kelp polysaccharide and mannose were obtained from Macklin Biotech Co. Ltd., Shanghai, China. Glucosamine hydrochloride was obtained from Sangon Biotech (Shanghai) Co., Ltd. (Shanghai, China). The alkaline phosphatase (ALP) kit was supplied by Nanjing Jiancheng Institute of Bioengineering (Nanjing, Jiangsu, China).

Influence of PQASs on conidial germination

Under sterile conditions, fungal culture plates were flooded with sterile water and the resulting conidial suspension was filtered through three layers of sterile 200-mesh gauze to separate the microconidia from the mycelium. The suspension was adjusted to 4×10^6 microconidia/mL using a haemocytometer. Equal volumes of the microconidial suspension were mixed with PQASs and the final concentrations of PQASs were 5, 10, 20 and 40 µg/mL (three wells per sample). The mixed suspensions were incubated in a constant temperature shock incubator at 28 °C and 120 rpm for 8 h and then observed under differential interference microscopy (DICM, Eclipse 80i microscope, Nikon, Japan). Two-hundred spores in each well were randomly examined for the presence of germ tubes. A microconidium was considered germinated if the germ tube length was at least as long as the spore (Steinkellner

et al., 2005). Sterile water was used as a negative control and the same concentration of BC was used as a positive control. The experiment was performed twice. The germination inhibition rate was calculated according to eqs. (1):

Germination inhibition rate

$$= (C_0 - C_t) / C_0 \times 100\% \quad (1)$$

where C_0 is the number of conidia in the negative control (water), C_t is the number of germinated conidia in the suspension treated with PQASs or BC.

*Inactivation kinetics of PQASs on *Foc4* conidia*

The QAS solutions and a *Foc4* microconidial suspension were mixed in equal amounts in sterile 1.5 mL microcentrifuge tubes, giving a final concentration of *Foc4* conidia of 10^6 conidia/mL and a final concentration of QASs of 30 $\mu\text{g/mL}$. Tubes were incubated for 3, 5, 7, 9, 19, 25 or 31 min and at each sampling time, 100 μL aliquots of the mixed suspensions were taken out and spread on PDA plates with a glass spreader. The plates were then incubated in darkness for 2 d at 28 °C and samples cultured in the absence of a QAS solution were used as control. The colonies grown on the plate were counted using the Image J software. There were three replications for each treatment and the experiment was performed twice. The effect of QASs on the inactivation of *Foc4* conidia is expressed as the inactivation efficiency at different times:

$$\text{Inactivation efficiency} = (N_0 - N_t) / N_0 \times 100\% \quad (2)$$

Where N_0 is the number of fungal colonies without QAS at time 0 and N_t is the number of fungal colonies at time t .

The Chick-Watson model (Dalrymple et al., 2010) conveys the primary principle of disinfection processes, which is described as a linear relationship between the inactivation effect and the exposure time (Leite et al., 2015; Wen et al., 2017):

$$\ln(N_t/N_0) = k C t \quad (3)$$

where k , the slope of the line, is the pseudo-first order inactivation rate constant ($\text{mL } \mu\text{g}^{-1} \cdot \text{min}^{-1}$); C is the concentration of QASs ($\mu\text{g/mL}$); and t is the QASs treatment time (min).

*Microscopy of the interaction between PQASs and *Foc4* conidia*

BC-FL, PQD-BC-FL and S_5Q_5 -FL were mixed with sterile distilled water to prepare 40 mg/mL QAS-FL solutions. *Foc4* was cultured for 5 d, removed from the incubator and then 0.5 mL prepared QAS-FL solution was added and the suspension incubated for 3 min or 3 h. After incubation, conidia were scraped onto a slide with a cover glass and slowly washed several times with sterile water. *Foc4* conidia were incubated for 3 min for each treatment and germination of 200 conidia were studied using DICM. Furthermore, germination of 100 *Foc4* conidia incubated for 3 h for each treatment were studied in a confocal laser scanning microscope (CLSM, TCS SP8 STED 3X, Leica, Germany) with 40x and 100x magnification (Sun et al., 2015, b).

In addition, after treating *Foc4* conidia with 0.1 mg/mL S_5Q_5 -FL for 2 d, about 20 μL conidial suspension was taken out, washed and S_5Q_5 -FL removed, then germination of 200 *Foc4* conidia were studied using DICM.

*Effects of QASs on the cell walls of *Foc4* conidia*

*Changes in the surface potential and hydrophobicity of *Foc4* conidia*

Fungal disks (each 7 mm in diameter), obtained from the periphery of 5-day-old cultures of *Foc4*, were inverted on the centre of each PDA plate and cultured in a 28 °C thermostatic incubator for 2–9 d. Under sterile conditions, fungal culture plates were flooded with sterile water and the resulting conidial suspension filtered through three layers of sterile 200-mesh gauze to separate the microconidia from mycelium. The suspension was adjusted to $(2 \sim 3) \times 10^6$ microconidia/mL using a haemocytometer.

Some conidial suspensions were used to determine changes in the spore surface potential. A zeta potential analyser (Horiba SZ-100Z, Horiba, Japan) with a stent temperature of 25 °C was used, with water as the dispersion medium. The *Foc4* conidial suspension was transferred to the electrode pool and when the instrument temperature was stable, the surface potential of the conidia was determined (Halder et al., 2015).

The remaining conidial suspensions were used to determine changes in the conidial hydrophobicity rates through an improved two-phase extraction method

(Girardin et al., 1999; Shah et al., 2007). The detailed steps were: 6 mL *Foc4* conidial suspension was added to a round-bottom glass colorimetric tube (soaked overnight in hydrochloric acid, cleaned and sterilised after use). A volume of 1.2 mL *n*-hexadecane was added as the oil phase and the tube was sealed with a glass plug. The suspension was oscillated vigorously for 60 s and then transferred to a funnel for 90 min. After the suspension was stratified, the aqueous phase was collected and mixed. Then, the concentration of conidia in the aqueous phase was determined with a haemocytometer. The concentration of conidia without oil phase mixing was used as the control. The conidial hydrophobicity was calculated from eq. (4) (Shan, 2009):

$$\text{Conidial hydrophobicity} = (N_0 - N) / N_0 \times 100\% \quad (4)$$

where N_0 is the initial concentration of *Foc4* conidia without oil phase mixing and N is the final concentration of *Foc4* conidia in aqueous phase.

In order to evaluate the effect of QASs on conidial surface hydrophobicity, a *Foc4* conidial suspension with a concentration of $10^6 \sim 10^8$ microconidia/mL was added to the QAS solution. After incubation for 1 h, 5 mL culture solution was removed and added to the centrifuge tube. The supernatant was centrifuged at $19600 \times g$ for 3 min and then, 3 mL sterile water was added to re-suspend. This process was repeated twice to wash away the residual QASs. Sterile water was added again, the conidia was suspended in the tube and then hydrophobicity was determined by an improved two-phase extraction method described in the previous paragraph. There were three replications for each treatment and the experiment was performed twice.

Sorbitol assay

Fifty- μ L potato dextrose broth was added aseptically to each well of a 96-well plate. Subsequently, 50 μ L BC solution with different concentrations was added into each horizontal row of the wells to obtain the concentrations of 5, 2.5, 1.25, 0.6, 0.3, 0.15, 0.08, 0.04, 0.02, 0.01 and 0 mg/mL. Next, 100 μ L conidial suspension with concentration of 4×10^6 microconidia/mL was added to all wells of the plate except the first horizontal row of the wells. For the group of “BC + sorbitol”, 25 μ L sorbitol solution was added into wells of the plate to obtain a final concentration of 0.8 M, while for the group “BC”, 25 μ L potato dextrose broth instead of

sorbitol solution was added. Sterility control of the medium was performed by adding 100 μ L potato dextrose broth in the first horizontal row of wells of all 96-well plates in the absence of *Foc4*. The 96-well plate was incubated in darkness for 2 d at 28 °C. Then, 20 μ L 2,3,5-triphenyl tetrazolium chloride dye solution (5%, w/v) (Turecka et al., 2018) was added to the well and the plate incubated in darkness for 2 h at 28 °C. The minimum inhibitory concentration (MIC) value is the lowest concentration at which there was no visible growth, i.e. there was no red colour in the well. There were three replications for each treatment and the experiment was performed twice.

The mycelium growth inhibition method (Zhong et al., 2017) was also used to evaluate effects of sorbitol on the growth rate of mycelium on potato dextrose agar (PDA) medium. The experiment was divided into 4 groups. In the first group, the medium contained 0.8 M sorbitol; in the second group, it contained 0.04 mg/mL BC; in the third group, it contained 0.04 mg/mL BC and 0.8 M sorbitol and the last group was pure medium (control). Each mixture was poured into 9 cm diameter sterile Petri dishes and left to solidify. Fungal disks (each 6 mm in diameter) obtained from the periphery of 5-day-old cultures of *Foc4* were inverted on the centre of each plate. All plates were incubated at 28 °C for 5 d. The radial diameter (mm) of each colony was measured in two directions at right angles using a calliper. The percent mycelial inhibition of the radial growth of *Foc4* by the compounds compared with the control was calculated using the following formula:

Percent mycelial inhibition

$$= (D_c - D_t) / D_c \times 100\% \quad (5)$$

where D_c is the mean colony diameter of the control group and D_t is the mean colony diameter of the treatment group. There were three replications for each treatment and the experiment was performed twice.

Conidial cell-wall disruption assay

Damage to the external cell wall layers cause release of alkaline phosphatase (ALP) from the cell (Cheng et al., 1970). The effect of PQASs on *Foc4* conidial cell wall was determined by assaying ALP in the supernatant (Dong et al., 2018). A conidial suspension and QAS solutions were added to 2 mL centrifuge tubes. The final QAS concentrations were equivalent to the minimum inhibitory

concentration, the 50% inhibitory concentration and the 90% inhibitory concentration. The test methods to obtain these data are described briefly in Supporting Information (Part S2). The final concentration of *Foc4* was 10^6 conidia/mL. The same volume of sterile distilled water was added instead of a QAS solution as a control. The samples were incubated at 28 °C and 200 rpm for 2 d on a rotary shaker (MQT-60R, Shanghai Minquan Instrument Co. Ltd., China) and centrifuged at $19600\times g$ for 3 min to collect the supernatant from each centrifuge tube. Then, 50 μ L supernatant was taken to determine the alkaline phosphatase content for each treatment by using an alkaline phosphatase kit (Nanjing Jiancheng Institute of Bio-engineering, Nanjing, Jiangsu, China). According to the instructions of manufacturer, the activity of ALP in the supernatant was measured with a UV-vis spectrophotometer at 405 nm (UV2300, Techcomp, Shanghai, China) and calculated by eq. (6) (Shao et al., 2013). There were three replications for each treatment and the experiment was performed twice.

$$\text{ALP activity} = \frac{OD_{\text{standard value}}}{OD_{\text{estimated value}}} \times 0.005\text{mg} \times \frac{100\text{mL}}{0.05\text{mL}} \quad (6)$$

where $OD_{\text{standard value}}$ refers to the measured absorbance of the standard solution prepared according to the instructions ($A = 0.242$).

Effects of PQASs on the Foc4 conidial cell wall components

The QAS solutions and a *Foc4* microconidial suspension were mixed in equal amounts in 2 mL centrifuge tubes. The final QAS concentrations were equivalent to the minimum inhibitory concentration, the 50% inhibitory concentration and the 90% inhibitory concentration. The final concentration of *Foc4* conidia was 3×10^6 conidia/mL. The same volume of sterile distilled water was added instead of QAS solution as a control. The samples were incubated at 28 °C and 200 rpm for 2 h on a rotary shaker, then centrifuged at $19600\times g$ for 3 min at 4 °C. The supernatant of each centrifuge tube was collected for subsequent determination of chitin, glucan and mannose in the cell walls.

The chitin content in the cell walls was determined by measuring the amount of GlcNAc (N-acetylglucosamine) released by acid hydrolysis of fungal cell walls (Guerriero

et al., 2010; Liu et al., 2007; Liu et al., 2021). One-mL supernatant was suspended in 0.5 mL 0.8 M potassium tetraborate solution and heated to 100 °C for 3 min. After cooling to room temperature, 3 mL 1% (w/v) 4-dimethylaminobenzaldehyde (P-DMAB) reagent was added and the tubes were kept in a water bath at 36 °C for 20 min. Then the absorbance was measured at 544 nm with a UV-vis spectrophotometer. The chitin content is expressed as the microgram content of glucosamine hydrochloride per millilitre supernatant and was calculated according to a standard curve (as shown in Fig. S7), prepared with a known amount of glucosamine hydrochloride.

The glucan content in the cell walls was determined by the aniline blue assay (Fernandes et al., 2021; Han et al., 2014; Kahn et al., 2006). Two-mL 0.04% (w/v) aniline blue solution was added to 1 mL supernatant and incubated in a water bath at 80 °C in the darkness for 15 min. After cooling to room temperature for 30 min, the fluorescence absorbance intensities at 503.5 nm were measured using a fluorescence spectrophotometer (F2700, HITACHI, Japan). The glucan content (μ g/mL) was calculated according to a standard curve (as shown in Fig. S8) prepared with a known amount of kelp polysaccharide as the standard sample (Han et al., 2014).

The mannose content in the cell walls was determined by an ultraviolet spectrometry method (Lin et al., 2015; Matsuoka et al., 2014). A volume of 3.0 mL of 72% sulphuric acid was added to 1.0 mL supernatant and treated in an ultrasonic cleaner for 30 min (KQ-250DE, Kunshan ultrasonic instruments Co. Ltd., Jiangsu, China). The suspension was kept in a water bath at 100 °C for 4 h to allow the cell walls to be hydrolysed with sulphuric acid. After cooling to room temperature, 0.5 mL 8 M NaOH was added to neutralise the solution ($\text{pH} = 7$). A volume of 0.2 mL of the above solution and 0.2 mL NaCl-H₃BO₃ solution (mixed solution of 12% NaCl (w/v) and 2% H₃BO₃ (w/v)) were added to 10 mL test tubes. As a control, 0.2 mL distilled water instead of 0.2 mL NaCl-H₃BO₃ solution was used. Then 4.6 mL 90% (w/w) H₂SO₄ was added to each tube and mixed by vortexing for 30 s. The tubes were placed in a 70 °C water bath and incubated for 30 min, taken out and cooled with running water. The absorbance of samples was measured by a UV-vis spectrophotometer (UV2300, Techcomp, Shanghai, China) at 280 nm. The difference between absorption with and without NaCl-H₃BO₃ is directly proportional to the mannose

concentration. The content of mannose ($\mu\text{g/mL}$) in the sample was calculated according to a standard curve (as shown in Fig. S9) with known concentrations of mannose. There were three replications for each treatment and the experiment was performed twice.

Data analysis

Data obtained were analysed by SPSS version 22 (SPSS Inc., Chicago, IL, USA). Duncan's multiple range test was used to separate means ($P < 0.05$). A linear regression model ($y = ax$, where a is the slope) was used to relate the inactivation effect ($\ln(N_t / N_0)$) with the exposure time (t). All experiments were performed twice and there were three replications for each treatment. Figures show averages of the two independent experiments. This was possible to show since there were no significant interactions between treatments and experiments. Error bars show the standard error of the mean (SEM) and treatments followed by different letters are statistically at $P < 0.05$.

Results

Effect of PQASs on *Foc4* conidial germination

The effect of PQASs on germination of *Foc4* conidia after 8 h treatment is shown in Fig. 1. An increase of QAS concentration, for benzalkonium chloride (BC), poly(methacrylamido propylbenzyl dimethylammonium chloride) (PQD-BC), polydimethylsiloxane-polymethacrylate block copolymers containing quaternary ammonium salts with 0 kDa, 5 kDa and 10 kDa of polydimethylsiloxane block (S_0Q_5 , S_5Q_5 and $S_{10}Q_5$), resulted in a gradually increased inhibition of spore germination for each QAS. QAS at a concentration of 40 $\mu\text{g/mL}$ could completely inhibit *Foc4* spore germination. BC showed better inhibition of germination at lower concentrations.

Inactivation kinetics of QASs on *Foc4* conidia

The inactivation efficiency and inactivation kinetics of QASs on *Foc4* conidia were evaluated by measuring the survival of *Foc4* conidia treated with QASs after plating on PDA. Figure 2A shows that the number of colonies in the plates decreased gradually with the extension of

treatment time. Each PQAS can kill *Foc4* very quickly, as shown in Fig. 2B. To inhibit conidial growth completely (99.99%), the incubation time was approximately 10 min for S_0Q_5 and S_5Q_5 and approximately 25 min for $S_{10}Q_5$ or PQD-BC. For BC, incubating the conidia for 31 min gave an inhibition rate of only 99%. The Chick-Watson model fitting of inactivation kinetics of QASs (30 $\mu\text{g/mL}$) on *Foc4* conidia is shown in Fig. 2B. The Chick-Watson model described fungal inactivation well, with correlation coefficients (R^2) greater than 0.9. The inactivation rate constants (k) of BC, PQD-BC, S_0Q_5 , S_5Q_5 and $S_{10}Q_5$ were 0.1271, 0.3897, 1.005, 0.9058 and 0.4038, respectively. The efficiencies of inactivation were in the order: $S_0Q_5 > S_5Q_5 > S_{10}Q_5 > \text{PQD-BC} > \text{BC}$.

Staining of *Foc4* conidia by PQASs

After the benzyl group in the QAS structure was replaced by a fluorescein group (-FL), green fluorescence was emitted under the excitation of ultraviolet light. PQAS-FL treatment of *Foc4* conidia for 3 min is shown in Fig. 3A. Green fluorescence was seen in all conidia, indicating that QASs-FL was able to enter the *Foc4* conidia quickly. Furthermore, *Foc4* conidia were treated with QASs-FL for 3 h and observed under CLSM. The clear green fluorescence in conidia treated with BC-FL, PQD-BC-FL and S_5Q_5 -FL can be seen in Fig. 3B,

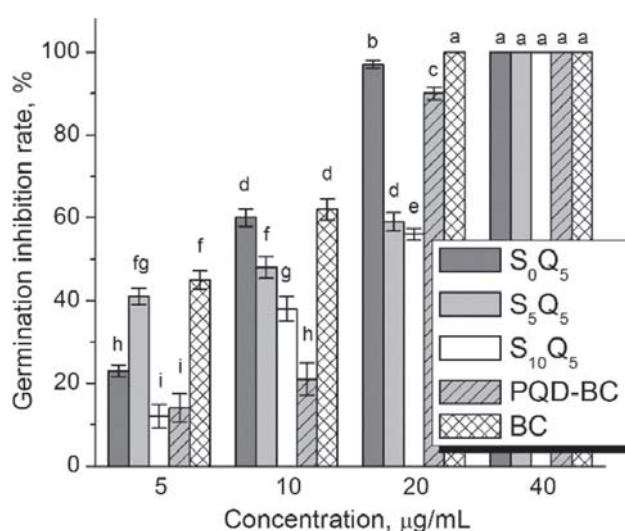


Fig. 1 Inhibition of germination of *Foc4* conidia in S_nQ_5 , PQD-BC and BC. The experiment was performed twice with three replications for each treatment. The figure shows averages of the two experiments. Error bars represent the standard error of the mean. Treatments followed by different letters are statistically different at $P < 0.05$

indicating that QASs-FL can enter and remain inside the *Foc4* conidia. Conidia treated with PQD-BC-FL and S₅Q₅-FL showed a clear outline and fluorescence on the cell surface, as indicated by the red arrow in Fig. 3B. The outer contour of conidia treated with BC-FL was blurred and there was no obvious fluorescence on the cell surface. This indicates that PQASs cannot only enter the conidia, but also bind to the cell surface of the spores and the small molecule QASs can enter conidia through cell wall and cell membrane, but is less adsorbed to conidial surfaces. Compared with the small molecule QAS, PQAS had better adsorption performance on conidial cell wall.

After being treated with 0.1 mg/mL S₅Q₅-FL for two days, *Foc4* conidia were observed by DICM. The results are shown in Fig. 4. There was fluorescence not only in the fragments of conidia, but also in the newly germinated hyphae, indicating that S₅Q₅-FL can continue to be taken up by the newly formed hyphae.

Effect of PQAS on the cell walls of *Foc4* conidia

Changes in the Foc4 conidial surface potential and hydrophilicity

The detection results of the zeta potential and hydrophobicity of conidia are shown in Fig. 5A, B. Figure 5A shows that the potential of the conidial surface decreased continuously with the extension of culture time. Figure 5B shows that the conidial hydrophobicity was approximately 20% and did not change with the extension of culture time. The change in the conidial hydrophobicity after 1 h of QAS treatment at the minimum inhibitory concentration (MIC) is shown in Fig. 5C. Thus, the conidial hydrophobicity after treatment with BC decreased, whereas the conidial hydrophobicity after treatment with PQD-BC, S₀Q₅, S₅Q₅ and S₁₀Q₅ increased.

Sorbitol assay

Sorbitol, as a substance to maintain proper osmotic pressure, provides a suitable environment for the cell wall biosynthetic pathways. It is often used to test the effect of drugs on the cell wall. The effect of sorbitol on the BC inhibition properties is presented in Fig. 6. Figure 6A shows that the minimum inhibitory concentration (MIC) of BC for the conidia was 0.04 mg/mL and after adding sorbitol, the value was 0.02 mg/mL.

The decrease in MIC indicated that sorbitol increased the inhibition of BC on conidia. In order to confirm this, the mycelium growth inhibition method was used and the results are shown in Fig. 6B. A concentration of 0.8 M sorbitol had no effect on the growth of *Foc4* hyphae. The inhibition rate of mycelium growth was 35.2% for BC at the MIC and with the addition of 0.8 M sorbitol to BC, the inhibition of mycelial growth was 51.3%. The increase in the inhibition further indicated that sorbitol and BC had a synergistic effect on the inhibition of *Foc4* mycelial growth. Therefore, the widely used method of adding sorbitol to evaluate whether a compound destroys the conidial cell wall was not suitable for QASs.

Effect of QASs on Foc4 conidia alkaline phosphatase (ALP) leakage

In conidia, ALP exists between the cell wall and cell membrane. When the cell wall is destroyed, the ALP will leak out of the cell, so the integrity of the conidial cell wall can be evaluated by detecting the ALP activity in the culture medium. Figure 6C shows that the ALP content in the culture medium treated with BC was low and did not change significantly with the increase of BC dosage. ALP content in the culture medium treated with high concentrations of PQASs increased significantly and PQD-BC was the most destructive compound to the cell walls of *Foc4* conidia.

Effects of PQASs on cell wall components

Chitin, glucan and mannose are the main components of the cell walls of fungi. They are polysaccharides polymerised from monosaccharides. Effects of PQASs on the cell wall components of *Foc4* conidia can be evaluated by determining the content of these polysaccharides in the culture medium, as shown in Fig. 7. After being treated with QASs at the minimum inhibitory concentration (MIC), 50% inhibitory concentration (IC₅₀) and 90% inhibitory concentration (IC₉₀), the content of chitin, glucan and mannose in the culture medium all increased with the increase of QAS concentration. This indicates that each QAS can act on the components of the cell wall of the *Foc4* conidia, with glucan being most severely affected. The effects of PQASs on the components of *Foc4* cell wall were significantly greater than that of BC.

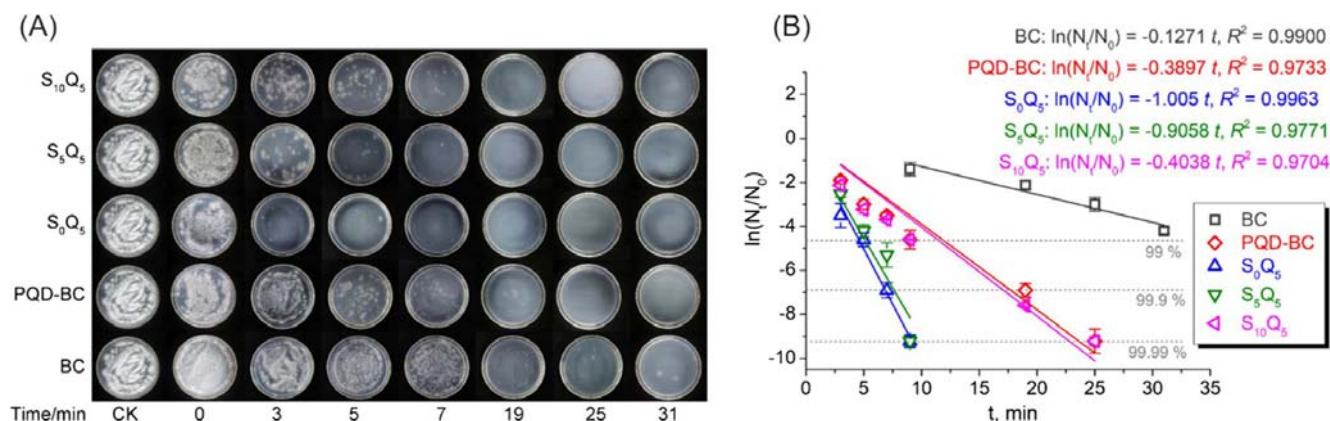


Fig. 2 **a** Growth of *Foc4* conidia on agar plates after S_5Q_5 , PQD-BC and BC treatment (30 $\mu\text{g/mL}$). With the extension of the incubation time, the number of colonies in the 100 μL mixture in the plate gradually decreased. **b** Inactivation kinetics of S_5Q_5 , PQD-BC and BC (30 $\mu\text{g/mL}$) on *Foc4* conidia. (The missing data point for BC at 3 to 7 min was because the number of colonies in

the Petri dish was too large to count). All experiments were performed twice with three replications for each treatment. Representative results from one experiment are shown in (A) whereas the average of the two experiments are shown in (B). Error bars represent the standard error of the mean

Discussion

The continuing development of fungicide resistance in plants necessitates the discovery of new fungicides with new or different modes of action (Ammar et al., 2013). Cationic polymers possess potent broad-spectrum

antimicrobial activity (Peng et al., 2019; Venkataraman et al., 2019) and do not elicit fungicide resistance (Lou et al., 2018). It has been found that cationic polymers have good inhibitory effects on fungi and the structure of the polymer is one of the key factors that determine its antifungal properties (Gilbert & Moore, 2005; Jiao et al.,

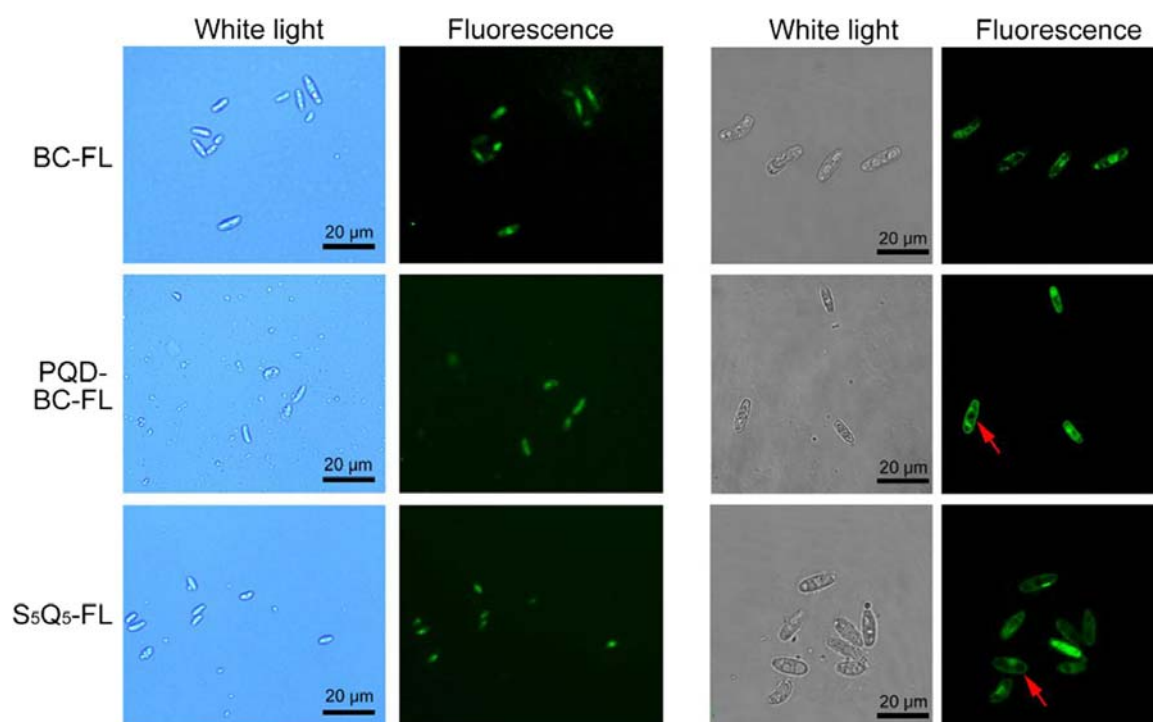
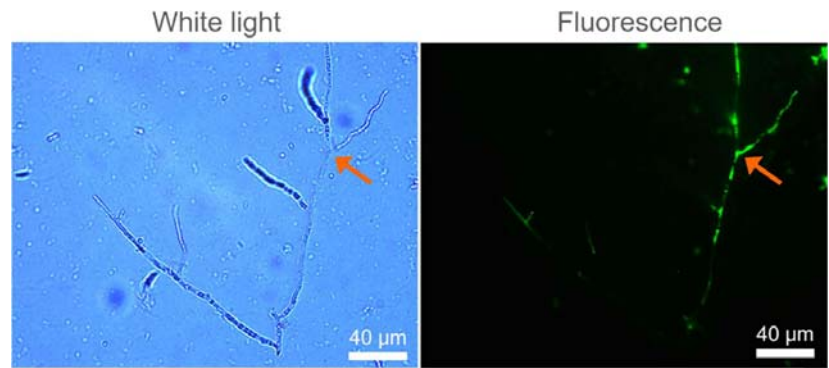


Fig. 3 **a** Differential interference microscopy micrographs of *Foc4* conidia. After *Foc4* conidia were treated with BC-FL, PQD-BC-FL or S_5Q_5 -FL at a concentration of 40 mg/mL for 3 min, clear green fluorescence was seen in all conidia. **b** Confocal microscopy of QASs-FL entering *Foc4* conidia. Conidia treated

with PQD-BC-FL and S_5Q_5 -FL showed clear outlines and fluorescence in the cell wall or cell membrane, as shown by the red arrow. The outer edge of the conidia treated with BC-FL was fuzzy and there was no obvious fluorescence in the cell wall or cell membrane

Fig. 4 Differential interference microscopy micrographs of *Foc4* conidia. After *Foc4* conidia were treated with S_nQ_5 -FL at a concentration of 0.1 mg/mL for 2 d, clear green fluorescence was seen in the newly formed hyphae



2017). Studies of how the polymers inhibit fungi are helpful to understand the relationship between the structure and antifungal activity and will be helpful for the development of new cationic polymers that can be used to control plant diseases.

Fusarium wilt of bananas is a serious soil-borne fungal disease and pathogen spores is an obvious target for controlling the disease. Thus, inhibiting or killing the *Foc4* conidia in soil is of great significance to the control of banana Fusarium wilt (Xue et al., 2015). Izquierdo-García et al. (2021) found that in the absence of soil, 10 kinds of commercial small molecular quaternary ammonium compounds showed 100% biocidal efficiency against microconidia, macroconidia and chlamydospores at both <1 and 15 min, while the presence of soil significantly decreased the efficacy of most of the disinfectants. Different from the commercial small molecular quaternary ammonium compounds, we previously found that if *Foc4* was added to the soil every second day, the inhibitory effect of polydimethylsiloxane-polymethacrylate block copolymers containing quaternary ammonium salts (S_nQ_5) could be maintained for 30 days and if *Foc4* was

added to the soil every 10 days, the inhibitory effect of S_nQ_5 could be maintained for 90 days. The impact of S_nQ_5 on the number of three types of microbial species (i.e. bacteria, fungi and actinomycetes) in the soil was evaluated (Chang et al., 2021). It was found that the number of fungi was reduced whereas the number of bacteria and actinomycetes was increased. This indicates that S_nQ_5 may not have a devastating impact on the microbial population in the soil, meaning that the impact may be acceptable. Most of the control methods based on soil fungicides and soil fumigation, such as methyl bromide or calcium cyanamide treatments, could kill almost all the microorganisms (including *Foc4*) in soil in a short time, but this would also completely destroy the microbial community and its functional diversity in the soil and the fumigated areas might eventually be re-attacked by the pathogen, making the next fruit production impossible (Herbert & Marx, 1990). Furthermore, compared with the soil disinfectant, the environmental toxicity risk is greatly reduced after soil adsorption because S_nQ_5 can be adsorbed in the soil. Pot experiments also showed that S_nQ_5 had a good control effect on Fusarium wilt of

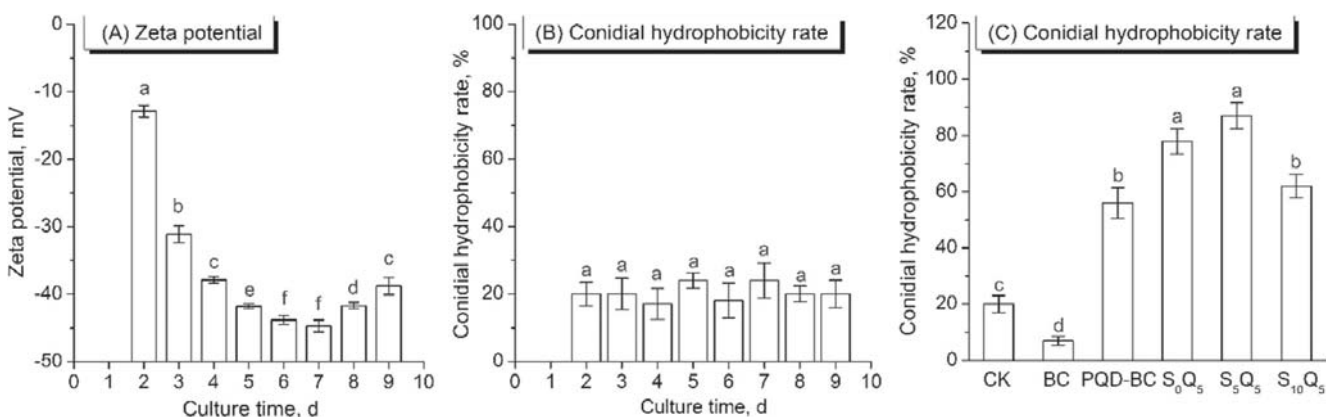


Fig. 5 Effect of culture time (days) in sterile water on: (A) The zeta potential of the *Foc4* conidial surfaces; (B) Conidial hydrophobicity and; (C) Effect of S_nQ_5 , PQD-BC and BC treatments on the conidial hydrophobicity. All experiments were performed

twice with three replications for each treatment. The figure show averages of the two experiments. Error bars represent the standard error of the mean. Treatments followed by different letters are statistically different at $P < 0.05$

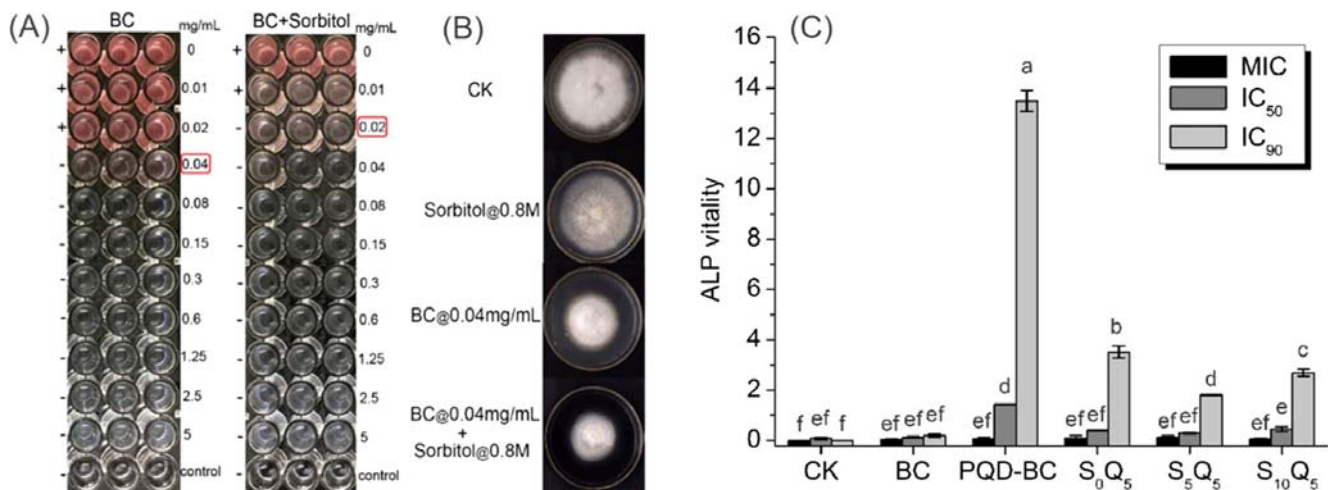


Fig. 6 **A** The minimum inhibitory concentration (MIC) of sorbitol and BC against *Foc4* based on the 2,3,5-triphenyl tetrazolium chloride colorimetric method; (+) indicates live cells in the plate and (–) indicates fewer or no cells in the plate. **B** The typical mycelial growth of *Foc4* on PDA medium after sorbitol and BC were applied. The experiments were performed twice and representative results are shown. **C** Effect of S_nQ₅, PQD-BC and BC on

alkaline phosphatase (ALP) content in *Foc4* culture medium. All experiments were performed twice with three replications for each treatment. Averages of the two experiments are shown in (C). Error bars represent the standard error of the mean. Treatments followed by different letters are statistically different at $P < 0.05$

banana and did not harm banana seedlings (Chang et al., 2021). These results show the potential of S_nQ₅ in banana fields to long term prevention of invasion by *Foc4*.

In this study, we further investigated the inactivation kinetics of S_nQ₅ on *Foc4* conidia and the adsorption and destruction of S_nQ₅ on the cell wall of *Foc4* conidia. Conidial germination was completely inhibited when the S_nQ₅ concentration was more than 40 µg/mL (Fig. 1). Meldrum et al. (2013) also found Sporekill™, which contain a quaternary ammonium compound as an active ingredient, could inhibit the germination of *Foc4* spores. The efficiency of killing fungal spores would be an important factor to evaluate the performance of fungicides. Our study also

found that S_nQ₅ could kill *Foc4* spores completely within 10 min (Fig. 2) and therefore, it shows promise as a sporicide against *Foc4*. The amphiphilic polymeric quaternary ammonium salts (S_nQ₅) had the highest inactivation efficiencies on *Foc4* conidia, followed by the hydrophilic macromolecular quaternary ammonium salt (PQD-BC) and finally the small molecular quaternary ammonium salt (BC) (Fig. 2). As described in the literature, structural parameters such as hydrophobicity/hydrophilicity balance, molecular weight and the length of carbon chain likely affect the antifungal activities (Muñoz-Bonilla & Fernández-García, 2012; Obłak et al., 2013; Ganewatta & Tang, 2015). Compared with BC, S_nQ₅ showed rapid fungicidal efficiency, which is

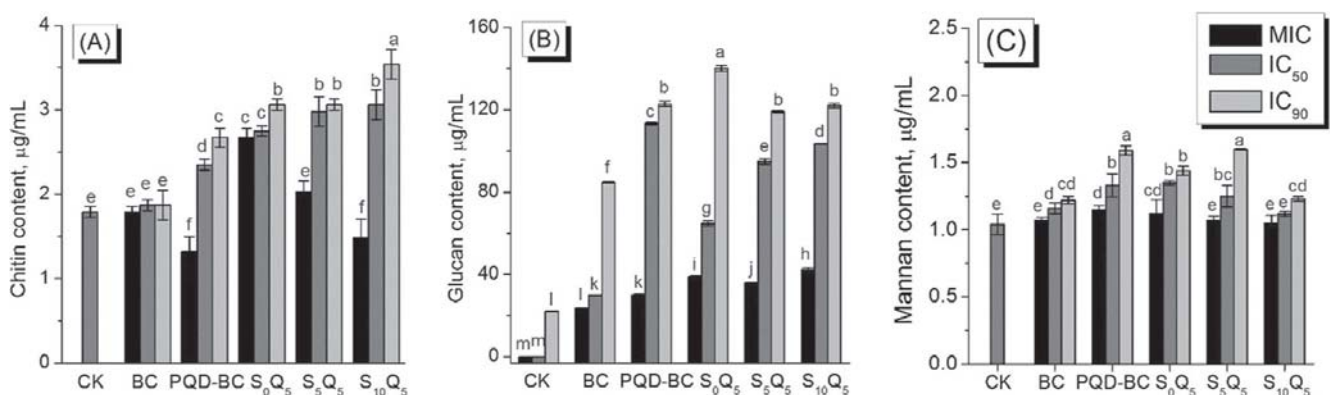


Fig. 7 Effects of S_nQ₅, PQD-BC and BC on cell wall components of *Foc4* conidia. **A** Chitin. **B** Glucan. **C** Mannose. All experiments were performed twice with three replications for each treatment.

The figure show averages of the two experiments. Error bars represent the standard error of the mean. Treatments followed by different letters are statistically different at $P < 0.05$

mainly due to the polymeric structure and the increasing proportion of hydrophobic segments.

The cell wall is essential for maintaining fungal cell shape and integrity (Ivey et al., 2017). It is often considered as one of the targets of drugs attacking fungi (Cortés et al., 2019; Zuo et al., 2015). To cause fungal death, the quaternary ammonium salts (QASs) have to be absorbed onto the cell and alter the inherent charge of the cell wall (Jiao et al., 2017). Microscopy (Fig. 3) demonstrated that S_nQ_5 could not only enter the interior of *Foc4* conidia, but also effectively adsorb to the surface of conidia. This effective adsorption is mainly achieved through the following steps: firstly, the conidial surface is negatively charged (Fig. 5A) and S_nQ_5 is positively charged, so they have electrostatic adsorption; secondly, our study found that S_nQ_5 could significantly change the conidial hydrophobicity (Fig. 5C). Like other filamentous fungi (Shan, 2009; Wösten, 2001), the hydrophobin in the *Foc4* conidial wall endows it with hydrophobic characteristics (Fig. 5B). The hydrophilic groups of S_nQ_5 can be combined with the *Foc4* conidial wall, making the hydrophobic groups of S_nQ_5 face the aqueous solution. It is reported that the hydrophobicity of spores could prevent fungi from losing water and play a role in preventing disinfectants from entering the spores during disinfection (Wen et al., 2019). The ability to change the conidial hydrophobicity is the difference between S_nQ_5 and other disinfectants (including chlorine and other small molecular cationic compounds) in the mechanism of inhibiting spores (Nguyen et al., 2019; Shen et al., 2019). In this study, we found that S_5Q_5 -FL could be taken up continually by the newly formed hypha (Fig. 4) and affect the internal structure of hypha and inhibit their activity (Dong et al., 2018). In our future work, the impact of invasive S_5Q_5 on the internal structure and activity of new hyphae will be further studied.

Cell wall integrity plays an important role in responses to external stress and in fungal growth and pathogenicity (Malavazi et al., 2014). The effect of fungicides on fungal cell wall integrity is often evaluated by the sorbitol protection test (Turecka et al., 2018). The increase of minimum inhibitory concentration (MIC) in the experiments with sorbitol could indicate the cell wall as a potential target of action of the compound (Leite et al., 2015; Turecka et al., 2018). We found that when *Foc4* was treated with BC in a medium supplemented with sorbitol, the MIC decreased after two days of incubation compared to the MIC in medium without sorbitol (Fig. 6A).

The experimental results using the mycelium growth inhibition method (Zhong et al., 2017) further confirmed that sorbitol and BC had a synergistic effect on the inhibition of *Foc4* mycelium growth (Fig. 6B). Therefore, this method might not be suitable for QASs. Alkaline phosphatase (ALP) is an enzyme produced in the cytoplasm and leaked into the periplasmic space. Generally, ALP is released from fungal cells with impaired cell wall permeability (Ouyang et al., 2019). In our previous work, we found that BC caused leakage of ALP and thus damaged the cell wall integrity of *Foc4* hyphae (Huang et al., 2017). In this study, BC could hardly cause leakage of ALP from *Foc4* conidia and a significantly higher ALP activity was observed in PQAS treatments, indicating that PQASs disrupted the cell wall permeability of *Foc4* conidia.

The fungal cell wall contains glucan, mannose and chitins, in which chitin is considered as one of the core polysaccharide components of the fungal cell wall. Glucan is a conserved “stealth” molecule in the cell walls of phytopathogenic fungi, which protects the intruder from being recognised by the host plant and melanin is a dark-pigmented proteinaceous polymer that provides appressoria of numerous plant-pathogenic fungi with their characteristic dark brown/black appearance (Cortés et al., 2019; Ivey et al., 2017). In this study, S_nQ_5 was adsorbed to the conidial cell wall and destroyed the cell wall structure, resulting in a significantly increased concentration of chitin, mannose and other components of the cell wall in the extracellular solution (Fig. 7). Therefore, the cell wall might be one of the targets of S_nQ_5 copolymers attacking conidia. Limited by methodological difficulties, the exact target points in cell wall are still poorly understood, but we hope to explore this further in the future. Also, from a practical point of view, although pot experiments have been performed in our previous work (Chang et al., 2021), field testing still needs to be carried out.

Collectively, our results revealed that three kinds of QASs (S_nQ_5 , PQD-BC and BC) had strong inhibitory effects on the growth and germination of *Foc4* conidia and the effect was rapid. Among these QASs, the destruction of conidial morphology by S_nQ_5 containing hydrophobic blocks was stronger and faster than that by the SQAS (BC). S_nQ_5 can increase the hydrophobic ratio of the conidial surface, act on the main components of the conidial cell wall and destroy the integrity of the cell wall. The addition of hydrophobic segments can enhance the inhibitory strength and inhibitory rate of PQASs, which was beneficial for guiding the synthesis of PQASs

with improved performance and promoting the application of PQASs in the control of Fusarium wilt in banana.

Supplementary Information The online version contains supplementary material available at <https://doi.org/10.1007/s10658-022-02608-5>.

Acknowledgments This work was supported by the National Natural Science Foundation of China under grant 31772202; the Scientific and Technological Planning Project of Guangzhou City (201803020015).

Author contribution Wei ZHANG: methodology, data curation, writing, original draft preparation; Yaoyao CHANG: methodology, data curation, writing, original draft preparation; Weiqiang ZHONG: data curation; Anqiang ZHANG: conceptualization, writing, reviewing and editing, supervision; Yaling LIN: conceptualization, writing, reviewing and editing, supervision.

Declarations

Competing interests The authors declare that they have no known competing financial interests or personal relationships that could have appeared to influence the work reported in this paper.

References

- Abid, C. Z., Jain, S., Jackeray, R., Chattopadhyay, S., & Singh, H. (2017). Formulation and characterization of antimicrobial quaternary ammonium dendrimer in poly(methyl methacrylate) bone cement. *Journal of Biomedical Materials Research Part B: Applied Biomaterials*, 105(3), 521–530. <https://doi.org/10.1002/jbm.b.33553>
- Ammar, M. I., Nenaah, G. E., & Mohamed, A. H. H. (2013). Antifungal activity of prenylated flavonoids isolated from *Tephrosia apollinea* L. against four phytopathogenic fungi. *Crop Protection*, 49, 21–25. <https://doi.org/10.1016/j.cropro.2013.02.012>
- Buffet-Bataillon, S., Tattevin, P., Bonnaure-Mallet, M., & Jolivet-Gougeon, A. (2012). Emergence of resistance to antibacterial agents: The role of quaternary ammonium compounds—A critical review. *International Journal of Antimicrobial Agents*, 39(5), 381–389. <https://doi.org/10.1016/j.ijantimicag.2012.01.011>
- Chang, Y., Zhong, W., Liang, J., Zhang, A., & Lin, Y. (2021). Polydimethylsiloxane-polymethacrylate block copolymers containing quaternary ammonium salts against *Fusarium oxysporum* f. sp. *cubense* race 4 in soil: Antifungal activities and pot experiments. *Reactive and Functional Polymers*, 160, 104848. <https://doi.org/10.1016/j.reactfunctpolym.2021.104848>
- Cheng, K. J., Ingram, J. M., & Costerton, J. W. (1970). Release of alkaline phosphatase from cells of *Pseudomonas aeruginosa* by manipulation of cation concentration and of pH. *Journal of Bacteriology*, 104, 748–753.
- Cortés, J., Curto, M., Carvalho, V., Pérez, P., & Ribas, J. (2019). The fungal cell wall as a target for development of new antifungal therapies. *Biotechnology Advances*, 37, 107352. <https://doi.org/10.1016/j.biotechadv.2019.02.008>
- Dalrymple, O. K., Stefanakos, E., Trotz, M. A., & Goswami, D. Y. (2010). A review of the mechanisms and modeling of photocatalytic disinfection. *Applied Catalysis B: Environmental*, 98(1–2), 27–38. <https://doi.org/10.1016/j.apcatb.2010.05.001>
- Dita, M., Barquero, M., Heck, D., Mizubuti, E. S., & Staver, C. P. (2018). Fusarium wilt of banana: Current knowledge on epidemiology and research needs toward sustainable disease management. *Frontiers in Plant Science*, 9, 1468. <https://doi.org/10.3389/fpls.2018.01468>
- Dong, C., You, W., Liuyang, R., Lei, Y., Zhang, A., & Lin, Y. (2018). Anti-*Rhizoctonia solani* activity by polymeric quaternary ammonium salt and its mechanism of action. *Reactive and Functional Polymers*, 125, 1–10. <https://doi.org/10.1016/j.reactfunctpolym.2018.01.020>
- Fernandes, C., Mota, M., Barros, L., Dias, M. I., Ferreira, I. C., Piedade, A. P., Casadevall, A., & Gonçalves, T. (2021). Pyomelanin synthesis in *Alternaria alternata* inhibits DHN-melanin synthesis and decreases cell wall chitin content and thickness. *Frontiers in Microbiology*, 12, 691433. <https://doi.org/10.3389/fmicb.2021.691433>
- Ganewatta, M., & Tang, C. (2015). Controlling macromolecular structures towards effective antimicrobial polymers. *Polymer*, 63, A1–A29. <https://doi.org/10.1016/j.polymer.2015.03.007>
- Gilbert, P., & Moore, L. E. (2005). Cationic antiseptics: Diversity of action under a common epithet. *Journal of Applied Microbiology*, 99(4), 703–715. <https://doi.org/10.1111/j.1365-2672.2005.02664.x>
- Girardin, H., Paris, S., Rault, J., Bellon-Fontaine, M. N., & Latgé, J. P. (1999). The role of the rodlet structure on the physicochemical properties of *aspergillus* conidia. *Letters in Applied Microbiology*, 29(6), 364–369. <https://doi.org/10.1046/j.1472-765x.1999.00643.x>
- Gou, Y. P., Meghil, M. M., Pucci, C. R., Breschi, L., Pashley, D. H., Cutler, C. W., Niu, L., Li, J., & Tay, F. R. (2018). Optimizing resin-dentin bond stability using a bioactive adhesive with concomitant antibacterial properties and anti-proteolytic activities. *Acta Biomaterialia*, 75, 171–182. <https://doi.org/10.1016/j.actbio.2018.06.008>
- Guerriero, G., Avino, M., Zhou, Q., Fugelstad, J., Clergeot, P. H., & Bulone, V. (2010). Chitin synthases from *Saprolegnia* are involved in tip growth and represent a potential target for anti-oomycete drugs. *PLoS Pathogens*, 6(8), e1001070. <https://doi.org/10.1371/journal.ppat.1001070>
- Halder, S., Yadav, K. K., Sarkar, R., Mukherjee, S., Saha, P., Haldar, S., Karmakar, S., & Sen, T. (2015). Alteration of zeta potential and membrane permeability in bacteria: A study with cationic agents. *SpringerPlus*, 4(1), 1–14. <https://doi.org/10.1186/s40064-015-1476-7>
- Han, S., He, L., Liu, Y., Cheng, J., & Yang, L. (2014). Quick determination of β -glucan from phellinus by fluorometry method. *Modern Chemical Industry*, 34, 156–158. (in Chinese). <https://doi.org/10.16606/j.cnki.issn0253-4320.2014.06.005>
- Herbert, J. A., & Marx, D. (1990). Short-term control of Panama disease of bananas in South Africa. *Phytophylactica*, 22(3), 339–340.

- Huang, Z., Liuyang, R., Dong, C., Lei, Y., Zhang, A., & Lin, Y. (2017). Polymeric quaternary ammonium salt activity against *fusarium oxysporum* f. sp. *cubense* race 4: Synthesis, structure-activity relationship and mode of action. *Reactive and Functional Polymers*, 114, 13–22. <https://doi.org/10.1016/j.reactfunctpolym.2017.02.013>
- Ioannou, C. J., Hanlon, G. W., & Denyer, S. P. (2007). Action of disinfectant quaternary ammonium compounds against *Staphylococcus aureus*. *Antimicrobial Agents and Chemotherapy*, 51(1), 296–306. <https://doi.org/10.1128/AAC.00375-06>
- Ivey, G., Gero, S., & Sarah, G. (2017). The role of the fungal Cell Wall in the infection of plants. *Trends in Microbiology*, 25(12), 957–967. <https://doi.org/10.1016/j.tim.2017.05.015>
- Izquierdo-García, L. F., Carmona, S. L., Zuluaga, P., Rodríguez, G., Dita, M., Betancourt, M., & Soto-Suárez, M. (2021). Efficacy of disinfectants against *fusarium oxysporum* f. sp. *cubense* tropical race 4 isolated from La Guajira, Colombia. *Journal of Fungi*, 7, 297. <https://doi.org/10.3390/jof7040297>
- Jiao, Y., Niu, L. N., Ma, S., Li, J., Tay, F. R., & Chen, J. H. (2017). Quaternary ammonium-based biomedical materials: State-of-the-art, toxicological aspects and antimicrobial resistance. *Progress in Polymer Science*, 71, 53–90. <https://doi.org/10.1016/j.progpolymsci.2017.03.001>
- Kahn, J. N., Hsu, M. J., Racine, F., Giacobbe, R., & Motyl, M. (2006). Caspofungin susceptibility in *aspergillus* and non-*aspergillus* molds: Inhibition of glucan synthase and reduction of β -d-1, 3 glucan levels in culture. *Antimicrobial Agents and Chemotherapy*, 50(6), 2214–2216. <https://doi.org/10.1128/aac.01610-05>
- Lei, Y., Zhou, S., Dong, C., Zhang, A., & Lin, Y. (2018). PDMS tri-block copolymers bearing quaternary ammonium salts for epidermal antimicrobial agents: Synthesis, surface adsorption and non-skin-penetration. *Reactive and Functional Polymers*, 124, 20–28. <https://doi.org/10.1016/j.reactfunctpolym.2018.01.007>
- Leite, M. C. A., de Brito Bezerra, A. P., de Sousa, J. P., & de Oliveira Lima, E. (2015). Investigating the antifungal activity and mechanism(s) of geraniol against *Candida albicans* strains. *Medical Mycology*, 53(3), 275–284. <https://doi.org/10.1093/mmy/myu078>
- Lin, Q., Zheng, J., Cai, D., Lin, Y., Xia, B., & Zhang, F. (2015). Determination of Mannan and β -glucan in yeast Cell Wall by HPLC with pre-column derivatization. *Journal of Instrumental Analysis*, 34, 106–110. (in Chinese). <https://doi.org/10.3969/j.issn.1004-4957.2015.01.017>
- Lin, Y., Liu, Q., Cheng, L., Lei, Y., & Zhang, A. (2014). Synthesis and antimicrobial activities of polysiloxane-containing quaternary ammonium salts on bacteria and phytopathogenic fungi. *Reactive and Functional Polymers*, 85, 19–30. <https://doi.org/10.1016/j.reactfunctpolym.2014.10.002>
- Lin, Y., Zhong, W., Dong, C., Zhang, C., Feng, X., & Zhang, A. (2018). Synthesis and antifungal activities of amphiphilic PDMS-*b*-QPMAEMA copolymers on *Rhizoctonia solani*. *ACS Applied Bio Materials*, 1(6), 2062–2072. <https://doi.org/10.1021/acsabm.8b00545>
- Liu, F., Diao, C., Song, B., Yang, S., Hu, D., Wang, J., Zeng, S., & Huang, R. (2007). Inhibition activity and mechanism primary study of Guangkuling 3% AS to *fusarium oxysporum* f.sp. *capsicum*. *Agrochemicals*, 89–91. (in Chinese). <https://doi.org/10.16820/j.cnki.1006-0413.2007.02.005>
- Liu, X., Bao, T., Zheng, L., Kgosi, V. T., Liu, X., & Liu, H. (2021). Cell wall integrity in *Magnaporthe oryzae* is weakened by proteins secreted by *bacillus licheniformis* BL06. *Biological Control*, 157, 104582. <https://doi.org/10.1016/j.biocontrol.2021.104582>
- Lou, W., Venkataraman, S., Zhong, G., Ding, B., Tan, J. P., Xu, L., Fan, W., & Yang, Y. Y. (2018). Antimicrobial polymers as therapeutics for treatment of multidrug-resistant *Klebsiella pneumoniae* lung infection. *Acta Biomaterialia*, 78, 78–88. <https://doi.org/10.1016/j.actbio.2018.07.038>
- Malavazi, I., Goldman, G. H., & Brown, N. A. (2014). The importance of connections between the cell wall integrity pathway and the unfolded protein response in filamentous fungi. *Briefings in Functional Genomics*, 13, 456–470. <https://doi.org/10.1093/bfpg/elu027>
- Matsuoka, H., Hashimoto, K., Saijo, A., Takada, Y., Kondo, A., Ueda, M., Ooshima, H., Tachibana, T., & Azuma, M. (2014). Cell wall structure suitable for surface display of proteins in *Saccharomyces cerevisiae*. *Yeast*, 31(2), 67–76. <https://doi.org/10.1002/yea.2995>
- Meldrum, R. A., Daly, A. M., Tran-Nguyen, L. T. T., & Aitken, E. A. B. (2013). The effect of surface sterilants on spore germination of *fusarium oxysporum* f. sp. *cubense* tropical race 4. *Crop Protection*, 54, 194–198. <https://doi.org/10.1016/j.cropro.2013.08.014>
- Muñoz-Bonilla, A., & Fernández-García, M. (2012). Polymeric materials with antimicrobial activity. *Progress in Polymer Science*, 37(2), 281–339. <https://doi.org/10.1016/j.progpolymsci.2011.08.005>
- Narita, T., Ohtakeyama, R., Matsukata, M., Gong, J. P., & Osada, Y. (2001). Kinetic study of cell disruption by ionic polymers with varied charge density. *Colloid and Polymer Science*, 279(2), 178–183. <https://doi.org/10.1007/s003960000411>
- Nel, B., Steinberg, C., Labuschagne, N., & Viljoen, A. (2006). The potential of nonpathogenic *fusarium oxysporum* and other biological control organisms for suppressing fusarium wilt of banana. *Plant Pathology*, 55(2), 217–223. <https://doi.org/10.1111/j.1365-3059.2006.01344.x>
- Nel, B., Steinberg, C., Labuschagne, N., & Viljoen, A. (2007). Evaluation of fungicides and sterilants for potential application in the management of fusarium wilt of banana. *Crop Protection*, 26(4), 697–705. <https://doi.org/10.1016/j.cropro.2006.06.008>
- Nguyen, T. V., Tran-Nguyen, L. T. T., Wright, C. L., Trevorow, P., & Grice, K. (2019). Evaluation of the efficacy of commercial disinfectants against *fusarium oxysporum* f. sp. *cubense* race 1 and tropical race 4 propagules. *Plant Disease*, 103(4), 721–728. <https://doi.org/10.1094/pdis-03-18-0453-re>
- Oblak, E., Piecuch, A., Krasowska, A., & Łuczyński, J. (2013). Antifungal activity of gemini quaternary ammonium salts. *Microbiological Research*, 168(10), 630–638. <https://doi.org/10.1016/j.progpolymsci.2011.08.005>
- Ouyang, Q. L., Duan, X. F., & Tao, N. G. (2019). Cinnamaldehyde exerts its antifungal activity by disrupting the cell wall integrity of *Geotrichum citri-aurantii*. *Frontiers in Microbiology*, 10, 55. <https://doi.org/10.3389/fmicb.2019.00055>
- Peng, C., Vishwakarma, A., Mankoci, S., Barton, H. A., & Joy, A. (2019). Structure-activity study of antibacterial poly (ester urethane) s with uniform distribution of hydrophobic and

- cationic groups. *Biomacromolecules*, 20(4), 1675–1682. <https://doi.org/10.1021/acs.biomac.9b00029>
- Ploetz, R., Freeman, S., Konkol, J., Al-Abed, A., Naser, Z., Shalan, K., Barakat, R., & Israeli, Y. (2015). Tropical race 4 of Panama disease in the Middle East. *Phytoparasitica*, 43(3), 283–293. <https://doi.org/10.1007/s12600-015-0470-5>
- Rembaum, A. S. A. E., Senyei, A. E., & Rajaraman, R. (1977). Interaction of living cells with polyionenes and polyionene-coated surfaces. *Journal of Biomedical Materials Research*, 11(1), 101–110. <https://doi.org/10.1002/jbm.820110110>
- Shah, F. A., Allen, N., Wright, C. J., & Butt, T. M. (2007). Repeated *in vitro* subculturing alters spore surface properties and virulence of *Metarhizium anisopliae*. *FEMS Microbiology Letters*, 276(1), 60–66. <https://doi.org/10.1111/j.1574-6968.2007.00927.x>
- Shan, L. (2009). Biocontrol potential of *Metarhizium* isolates against aphids and hydrophobicity-related traits of *Beauveria bassiana*, *Metarhizium* spp. and *Paecilomyces fumosoroseus* for use in microbial control. *Ph.D. Dissertation. Zhejiang University*. Hangzhou, China (in Chinese).
- Shao, X., Cheng, S., Wang, H., Yu, D., & Mungai, C. (2013). The possible mechanism of antifungal action of tea tree oil on *Botrytis cinerea*. *Journal of Applied Microbiology*, 114(6), 1642–1649. <https://doi.org/10.1111/jam.12193>
- Shen, Z., Xue, C., Penton, C. R., Thomashow, L. S., Zhang, N., Wang, B., & Shen, Q. (2019). Suppression of banana Panama disease induced by soil microbiome reconstruction through an integrated agricultural strategy. *Soil Biology and Biochemistry*, 128, 164–174. <https://doi.org/10.1016/j.soilbio.2018.10.016>
- Steinkellner, S., Mammerler, R., & Vierheilig, H. (2005). Microconidia germination of the tomato pathogen *fusarium oxysporum* in the presence of root exudates. *Journal of Plant Interactions*, 1(1), 23–30. <https://doi.org/10.1080/17429140500134334>
- Sun, L., Song, S., Fu, L., Deng, X., Wang, D., Liang, X., Li, R., & Shen, Q. (2015). Exploring a soil fumigation strategy based on ammonium bicarbonate to control fusarium wilts of cucurbits. *Crop Protection*, 70, 53–60. <https://doi.org/10.1016/j.cropro.2015.01.004>
- Sun, Y., Dong, W., Sun, L., Ma, L., & Shang, D. (2015). Insights into the membrane interaction mechanism and antibacterial properties of chensinin-1b. *Biomaterials*, 37, 299–311. <https://doi.org/10.1016/j.biomaterials.2014.10.041>
- Turecka, K., Chylewska, A., Kawiak, A., & Waleron, K. F. (2018). Antifungal activity and mechanism of action of the co (III) coordination complexes with diamine chelate ligands against reference and clinical strains of *Candida* spp. *Frontiers in Microbiology*, 9, 1594. <https://doi.org/10.3389/fmicb.2018.01594>
- Venkataraman, S., Tan, J. P., Chong, S. T., Chu, C. Y., Wilianto, E. A., Cheng, C. X., & Yang, Y. Y. (2019). Identification of structural attributes contributing to the potency and selectivity of antimicrobial polyionenes: Amides are better than esters. *Biomacromolecules*, 20(7), 2737–2742. <https://doi.org/10.1021/acs.biomac.9b00489>
- Wen, G., Xu, X., Zhu, H., Huang, T., & Ma, J. (2017). Inactivation of four genera of dominant fungal spores in groundwater using UV and UV/PMS: Efficiency and mechanisms. *Chemical Engineering Journal*, 328, 619–628. <https://doi.org/10.1016/j.cej.2017.07.055>
- Wen, G., Zhao, D., Xu, X. Q., Chen, Z. H., Huang, T. L., & Ma, J. (2019). Inactivation of fungi from four typical genera in groundwater using PMS/cl⁻ system: Efficacy, kinetics and mechanisms. *Chemical Engineering Journal*, 357, 567–578. <https://doi.org/10.1016/j.cej.2018.09.195>
- Wösten, H. A. B. (2001). Hydrophobins: multipurpose proteins. *Annual Review in Microbiology*, 55, 625–646. <https://doi.org/10.1146/annurev.micro.55.1.625>
- Xue, Y., Xiao, H., & Zhang, Y. (2015). Antimicrobial polymeric materials with quaternary ammonium and phosphonium salts. *International Journal of Molecular Sciences*, 16(2), 3626–3655. <https://doi.org/10.3390/ijms16023626>
- Zhang, A., Liu, Q., Lei, Y., Hong, S., & Lin, Y. (2015). Synthesis and antimicrobial activities of acrylamide polymers containing quaternary ammonium salts on bacteria and phytopathogenic fungi. *Reactive and Functional Polymers*, 88, 39–46. <https://doi.org/10.1016/j.reactfunctpolym.2015.02.005>
- Zhang, C., Cui, F., Zeng, G., Jiang, M., Yang, Z., Yu, Z., Zhu, M., & Shen, L. (2015). Quaternary ammonium compounds (QACs): A review on occurrence, fate and toxicity in the environment. *Science of the Total Environment*, 518, 352–362. <https://doi.org/10.1016/j.scitotenv.2015.03.007>
- Zhong, W., Dong, C., Liuyang, R., Guo, Q., Zeng, H., Lin, Y., & Zhang, A. (2017). Controllable synthesis and antimicrobial activities of acrylate polymers containing quaternary ammonium salts. *Reactive and Functional Polymers*, 121, 110–118. <https://doi.org/10.1016/j.reactfunctpolym.2017.10.010>
- Zuo, C., Li, C., Li, B., Wei, Y., Hu, C., Yang, Q., Yang, J., Sheng, O., Kuang, R., Deng, G., Biswas, M. K., & Yi, G. (2015). The toxic mechanism and bioactive components of Chinese leek root exudates acting against *fusarium oxysporum* f. sp. *cubense* tropical race 4. *European Journal of Plant Pathology*, 143(3), 447–460. <https://doi.org/10.1007/s10658-015-0697-5>

Springer Nature or its licensor holds exclusive rights to this article under a publishing agreement with the author(s) or other rightsholder(s); author self-archiving of the accepted manuscript version of this article is solely governed by the terms of such publishing agreement and applicable law.



ISSN 1000-2030
CN 32-1148/S
CODEN NNDXEI

南京农业大学学报

JOURNAL OF NANJING AGRICULTURAL UNIVERSITY

第 44 卷 第 6 期
Vol. 44 No. 6

2021 年 11 月
Nov. 2021

6
2021



全国中文核心期刊
CSCD 来源期刊
中国精品科技期刊
百种中国杰出学术期刊

目次

• 综述 •

小麦籽粒品质空间分布异质性及其形成机制研究进展

..... 姜东,仲迎鑫,蔡剑,周琴,王笑,戴廷波,曹卫星(1013)

surfactin 生物合成及应用的研究进展 陈晓宇,赵洪源,陆兆新(1024)

• 植物科学 •

水稻白穗突变体 *wp8* 的表型鉴定及候选基因定位和功能分析

..... 刘林,朱泽,王致远,刘世家,田云录,周时荣,江玲,刘玲珑,万建民(1035)

一种快速添加或替换蛋白标签的新方法及应用

..... 张皓,刘雪莹,钱铭,高鸿儒,汤超,张华,王鹏,张绍铃,吴巨友(1046)

菊花苗期氮高效品种资源筛选及氮效率评价体系建立

..... 葛礼姣,方馨妍,张云月,罗孟婷,管志勇,陈素梅,房伟民,陈发棣,赵爽(1054)

切花百合耐热性评价及越夏栽培技术研究 蓝令,吴泽,张德花,滕年军(1063)

辣椒胶孢炭疽菌 CFEM 效应因子鉴定及转录组分析

..... 刘思珍,欧阳超,满益龙,盛家伟,陈岳,张鑫,郑立敏,李智强,
李大伟,张德咏,刘勇,王运生,谭新球(1074)

基于磁性纳米探针的莠去津残留荧光检测方法 刘金彤,蒲虹辰,叶林瑶,莫艳阳,杨红(1083)

超声细胞破碎法快速提取真菌中的麦角甾醇 霍理坚,冯祖睿,林雅铃(1090)

• 生物与环境 •

ZFP36 互作蛋白基因 *OsGRP1* 的克隆及其在 ABA 诱导的抗氧化防护途径中的功能分析

..... 陆秋萍,季锴,蒋明义(1097)



霍理坚, 冯祖睿, 林雅铃. 超声细胞粉碎法快速提取真菌中的麦角甾醇[J]. 南京农业大学学报, 2021, 44(6): 1090–1096.

HUO Lijian, FENG Zurui, LIN Yaling. Rapid extraction of ergosterol from fungi by ultrasonic cell disruption [J]. Journal of Nanjing Agricultural University, 2021, 44(6): 1090–1096.

超声细胞粉碎法快速提取真菌中的麦角甾醇

霍理坚, 冯祖睿, 林雅铃*

(华南农业大学材料与能源学院, 广东 广州 510642)

摘要: [目的] 本文旨在尝试用超声细胞粉碎法从真菌中提取麦角甾醇, 以寻找比以往更快速测定真菌中麦角甾醇含量的方法。[方法] 以甲醇为溶剂, 选择料液比、超声前浸泡时间、超声时间和超声功率为影响因素, 以高效液相色谱法测定含量, 通过正交试验确定以超声细胞粉碎法从水稻纹枯病菌(*Rhizoctonia solani*) 中提取麦角甾醇的最佳条件。将其结果与传统的皂化回流法提取进行比较。进而分别以超声细胞粉碎法、超声辅助提取法、皂化回流法从金针菇(*Flammulina velutipes*) 中提取麦角甾醇并进行比较。[结果] 通过正交试验确定超声细胞粉碎法以甲醇作溶剂从水稻纹枯病菌中提取麦角甾醇的最佳条件为: 料液比 1/50(每 50 mL 甲醇中加入 1 g 菌丝, 下同), 超声前浸泡 20 min, 超声功率 200 W, 超声时间 4 min, 测得菌丝中麦角甾醇含量约为 $2.59 \text{ mg} \cdot \text{g}^{-1}$; 而以皂化回流法提取测得麦角甾醇含量为 $2.18 \text{ mg} \cdot \text{g}^{-1}$ 。采用超声细胞粉碎法以甲醇作溶剂从金针菇中提取麦角甾醇的条件是: 料液比 1/50, 超声前浸泡 20 min, 超声功率 250 W, 超声时间 8 min, 提取率为 $3.27 \text{ mg} \cdot \text{g}^{-1}$ 。超声辅助提取法和皂化回流法的提取率分别为 3.01 和 $2.82 \text{ mg} \cdot \text{g}^{-1}$ 。以超声细胞粉碎法提取率最高, 且差异极显著。[结论] 以超声细胞粉碎法从 2 种真菌中获得麦角甾醇的量均比皂化回流法提取高, 且试剂用量少, 操作省时简便, 有望成为快速测定真菌中麦角甾醇含量的方法。

关键词: 水稻纹枯病菌; 金针菇; 麦角甾醇; 超声细胞粉碎法; 高效液相色谱法

中图分类号: S432.4⁺4

文献标志码: A

文章编号: 1000-2030(2021)06-1090-07

Rapid extraction of ergosterol from fungi by ultrasonic cell disruption

HUO Lijian, FENG Zurui, LIN Yaling*

(College of Material and Energy, South China Agricultural University, Guangzhou 510642, China)

Abstract: [Objectives] In order to find a more rapid method to determine the content of ergosterol in fungi, this paper attempted to extract ergosterol from fungi by ultrasonic cell disruption method. [Methods] Using methanol as the solvent, the effects of material-to-liquid ratio, immersion time before ultrasonic extraction, ultrasonic time and ultrasonic power on the extraction of ergosterol from *Rhizoctonia solani* by ultrasonic cell disruption method were investigated through orthogonal experiment design. The contents of ergosterol in the extract under the optimum extraction conditions were determined by HPLC, and the results were compared with the traditional saponification reflux extraction method. Furthermore, ergosterol was extracted from *Flammulina velutipes* by ultrasonic cell disruption method, ultrasonic assisted extraction method and saponification reflux method, and their contents were compared. [Results] The optimal conditions for ultrasonic cell disruption method to extract ergosterol from *R. solani* were: the ratio of material-to-liquid was 1/50(1 g mycelium was added per 50 mL of methanol, the same below), mycelium was immersed for 20 min before ultrasonic extraction, ultrasonic power was 200 W, and ultrasonic time was 4 min. Under this extraction condition, the content of ergosterol was about $2.59 \text{ mg} \cdot \text{g}^{-1}$; and the content of ergosterol extracted by saponification reflux method was about $2.18 \text{ mg} \cdot \text{g}^{-1}$. Using methanol as the solvent, when the material-to-liquid ratio was 1/50, the immersion time before ultrasonic was 20 min, the ultrasonic time was 8 min, and the ultrasonic power was 250 W, the average content of ergosterol extracted by ultrasonic crushing method was about $3.27 \text{ mg} \cdot \text{g}^{-1}$. However, the average contents of ergosterol extracted from *F. velutipes* by ultrasonic assisted extraction method and saponification reflux extraction method were $3.01 \text{ mg} \cdot \text{g}^{-1}$ and $2.82 \text{ mg} \cdot \text{g}^{-1}$, respectively. Ultrasonic cell disruption had the highest extraction rate, and the difference was extremely significant. [Conclusions] The amount of ergosterol extracted from the two kinds of fungi by ultrasonic cell disruption method was higher than that of saponification reflux extraction method. Ultrasonic cell disruption method had the advantages of less reagent consumption, time-saving and simple operation. It was expected to be a rapid method for determining the content of ergosterol in fungi.

Keywords: *Rhizoctonia solani*; *Flammulina velutipes*; ergosterol; ultrasonic cell disruption; high performance liquid chromatography

收稿日期: 2021-01-14

基金项目: 国家自然科学基金项目(31772202); 广州市科技计划项目(201803020015, 201704020084)

作者简介: 霍理坚, 硕士, 实验师, 从事分析化学研究, E-mail: huolijian@scau.edu.cn。* 通信作者: 林雅铃, 博士, 副教授, 研究方向为植物病害化学防治, E-mail: linyaling@scau.edu.cn。

(C)1994-2021 China Academic Journal Electronic Publishing House. All rights reserved. http://www.cnki.net

麦角甾醇,别名麦角固醇,是真菌细胞膜的重要组成成分,因其结构稳定,专一性强,可以将其含量作为真菌生物量的指标^[1]。抗真菌药通过与麦角甾醇生物合成途径中的各种酶作用,干扰或阻断麦角甾醇生物合成,破坏真菌细胞膜结构而达到抑菌、杀菌目的^[2-3]。麦角甾醇也是一种重要的医药化工原料,可用于生产可的松、激素黄体酮等甾醇类药物。为提高麦角甾醇的产量,国内外学者广泛开展了微生物发酵合成麦角甾醇的研究^[4]。因此,无论是在真菌病害防治领域,还是药物生产领域,找到一种从真菌中快速提取麦角甾醇并准确测定其含量的方法是十分必要的。

目前,麦角甾醇的提取方法有皂化回流法、超声辅助提取法、微波萃取法或超临界流体 CO₂ 萃取法等^[4],其中以皂化回流法最常见。皂化回流法存在提取时间长、温度高、有机溶剂使用量大、安全系数小等缺点^[5]。超声波是一种高频机械振荡波,其能量会引起萃取溶剂的空化,而空化作用能加速传热和传质速率,从而破坏细胞膜^[6]。目前超声波法的常用设备是超声清洗机^[7-9],其超声波能量分布不集中,细胞粉碎效率不高,若能提高超声粉碎效率则有望缩短提取时间,提高工作效率。

水稻纹枯病菌(*Rhizoctonia solani*) 引发的水稻纹枯病是全球范围内危害最为严重的水稻真菌病害之一^[10]。金针菇(*Flammulina velutipes*) 是常见的食药两用菌类,其富含维生素、氨基酸、纤维素等成分,具有很高的营养价值和药用价值,在功能性食品、医药保健品开发上具有很大潜力^[11]。本研究先以水稻纹枯病菌为对象,采用具有较大超声粉碎功率的超声细胞粉碎仪,以甲醇为溶剂,探索和改进超声细胞粉碎法提取麦角甾醇的条件,用 HPLC 法测定提取后麦角甾醇含量;然后将优化的超声细胞粉碎法用于金针菇麦角甾醇的提取,以期能找到一种可替代传统皂化回流法且简单可行的麦角甾醇提取与测定方法。

1 材料与方法

1.1 试验材料

水稻纹枯病菌(*Rhizoctonia solani*) 由华南农业大学植物保护学院植物病理系真菌研究室提供。金针菇(毛柄金线菌,*Flammulina velutipes*) 购自华南农业大学农贸市场。

1.2 试剂和仪器

麦角甾醇标准品(纯度 98.0%) 购自成都乐美天医药科技有限公司;甲醇(色谱纯)、氢氧化钾、维生素 C、氯化钠、无水乙醇、石油醚(60~90 °C)、无水硫酸钠均为分析纯,购自上海麦克林生化科技有限公司。试剂配制:2 mol·L⁻¹ 氢氧化钾-乙醇溶液(KOH-EtOH),取 KOH 11.2 g,加入 EtOH 溶解成 100 mL;0.1 mol·L⁻¹ 维生素 C 溶液,取维生素 C 0.176 g,加无水乙醇 100 mL;饱和 NaCl 溶液,取 NaCl 25 g,加水 50 mL 振荡溶解,静置后取上清液;麦角甾醇标准溶液,精确称取麦角甾醇标准品 5 mg,加色谱甲醇稀释定容至 50 mL,质量浓度为 0.1 mg·mL⁻¹。

仪器:高效液相色谱仪(Waters 600-2998);Hypersil ODS 250×4.6 mm 5 μm 色谱柱;JY92-IIIDN 超声细胞粉碎仪(宁波新芝生物科技股份有限公司);KQ-250DE 型数控超声波清洗器(昆山市超声仪器有限公司);BSA124S 万分之一电子天平(赛多利斯科学仪器北京有限公司)。

1.3 麦角甾醇含量的测定方法

参照李治建等^[12]方法,采用 HPLC 法,以甲醇为流动相,流速为 1 mL·min⁻¹,检测波长为 260 nm,进样量 10 μL,室温测定。以 0.1 mg·mL⁻¹ 麦角甾醇标准溶液作对照,外标法计算供试液中麦角甾醇的含量。

1.4 皂化回流法提取 *R. solani* 中的麦角甾醇

参照 Heleno 等^[13]方法,称取约 0.2 g 菌丝干粉,精密称量,加入 2 mol·L⁻¹ KOH-EtOH 溶液 10 mL,0.1 mg·mL⁻¹ 维生素 C 溶液 2.5 mL,60 °C 下恒温皂化 45 min。皂化液放冷至室温,加入 5 mL NaCl 饱和溶液,以 10 mL 石油醚萃取 3 次,收集有机相,加少量无水 Na₂SO₄ 除水,40 °C 旋蒸至干,以甲醇溶解转移至 10 mL 容量瓶定容。

1.5 超声细胞粉碎法提取 *R. solani* 中的麦角甾醇

1.5.1 正交试验确定最佳提取条件 在前期预试验中,发现菌丝(g)与溶剂(mL)的比例(简称为料液比)、菌丝干粉超声粉碎前浸泡在溶剂中的时间、超声粉碎的功率、超声粉碎的时间等对麦角甾醇的提取率有一定的影响,故初步确定 4 个变量,即:料液比(A)、超声粉碎前浸泡时间(B)、超声功率(C)和超声时间(D),其变量水平见表 1,选用 L₁₆(4⁵) 正交试验评价上述 4 个变量对提取率的影响并获得最优提取条件。

表1 正交优化试验因素与水平表
Table 1 Level and factors in the $L_{16}(4^5)$ orthogonal experiments

水平 Level	料液比(A) Material-to-liquid ratio	超声前浸泡时间(B) /min Immersion time before ultrasonic extraction	超声功率(C) /W Ultrasonic power	超声时间(D) /min Ultrasonic time
1	1/10	0	100	2
2	1/30	20	200	4
3	1/50	40	300	6
4	1/70	60	400	8

超声细胞粉碎法提取麦角甾醇的试验步骤: 将 *R. solani* 菌丝冻干, 研细成粉, 待用。考虑到麦角甾醇易溶于甲醇, HPLC 法测定也以甲醇作为流动相, 故在超声提取时, 采用色谱纯甲醇作为溶剂。根据设定的变量条件, 分别精密称取干燥 *R. solani* 菌丝冻干粉, 置于 15 mL 离心管, 准确移取设定量的甲醇, 浸泡规定时间, 称量; 在设定的功率条件下, 冰浴中超声处理设定的时间, 放置室温后再次称量, 滴加甲醇补足减失的量; 摇匀, 取溶液适量以 0.45 μm 尼龙滤膜过滤, 得到供试溶液, 用 HPLC 测定麦角甾醇含量。每个试验条件重复 3 次, 取平均值。

1.5.2 含量测定方法学考察 最佳提取条件的加样回收试验: 取约 0.20 g *R. solani* 菌丝干粉 9 份, 精密称定, 分为高、中、低 3 个浓度组, 分别加入含标准品 0.75、0.50、0.25 mg 的甲醇溶液, 按 1.5.1 节中确定的最佳提取条件下进行提取, 根据测定结果计算加样回收率。

重复性试验: 取约 0.20 g 的 *R. solani* 菌丝干粉 5 份, 精密称定, 以上述最佳提取条件平行操作得供试溶液, 测定并计算提取率及相对标准偏差(RSD)。

1.6 提取金针菇中麦角甾醇的方法

超声细胞粉碎法: 取约 0.20 g 金针菇冻干粉 3 份, 精密称定, 置于 15 mL 离心管, 准确移取 10 mL 甲醇, 充分混合后浸泡 20 min, 称量; 超声细胞粉碎仪超声(250 W, 冰浴)处理 8 min, 放置室温, 再次称量, 滴加甲醇补足减失的量, 摇匀, 以微孔滤膜过滤, 测定含量。

超声辅助提取法: 取约 0.20 g 金针菇冻干粉 3 份, 精密称定, 置于 15 mL 离心管, 准确移取 10 mL 甲醇, 摇匀, 称量, 超声清洗机超声(250 W, 40 $^{\circ}\text{C}$ 水浴)处理 40 min, 放置室温, 再次称量, 滴加甲醇补足减失的量, 摇匀, 以微孔滤膜过滤, 测定含量^[7,14]。

皂化回流提取法: 取约 0.20 g 金针菇冻干粉 3 份, 精密称定, 加入 2 mol·L⁻¹ KOH-EtOH 10 mL, 在 85~90 $^{\circ}\text{C}$ 下皂化 3 h^[7]。冷却后转移至分液漏斗, 加入 10 mL 石油醚萃取 2 次, 收集上层石油醚^[15], 旋转蒸发至干, 用甲醇溶解转移至 10 mL 容量瓶定容。溶液以微孔滤膜过滤, 测定含量。

上述提取试验均重复 3 次, 取平均值, 计算其 RSD 值并进行方差分析。

1.7 数据分析

采用 Excel 2010 软件进行绘图和处理分析数据。

2 结果与分析

2.1 麦角甾醇 HPLC 检测方法的建立

在 1.3 节所述的 HPLC 色谱条件下, 得到麦角甾醇标准溶液(0.1 mg·mL⁻¹)和菌丝提取液中麦角甾醇的色谱图(图 1)。由图 1 可以看出: 麦角甾醇色谱峰的保留时间约为 14.423 min, 样品峰与其他物质峰完全分离, 分离度大于 1.5。

麦角甾醇在 0.010~0.200 mg·mL⁻¹线性关系良好, 标准曲线的回归方程为:

$$Y = 15\,181X + 31\,335, R^2 = 0.999\,9。$$

在相同条件下, 0.1 mg·mL⁻¹标准品溶液连续进样 3 次, 麦角甾醇峰面积的相对标准偏差(RSD)为 0.59%, 说明本色谱条件满足检测要求。

2.2 皂化回流法提取 *R. solani* 中麦角甾醇

根据文献所述的皂化法, 按 1.4 节所述条件从 *R. solani* 菌丝中提取麦角甾醇, 并采用 1.3 节中所述的方法进行含量测定。3 次重复测试结果显示: 菌丝中麦角甾醇含量约为 2.18 mg·g⁻¹, RSD 为 2.28%。

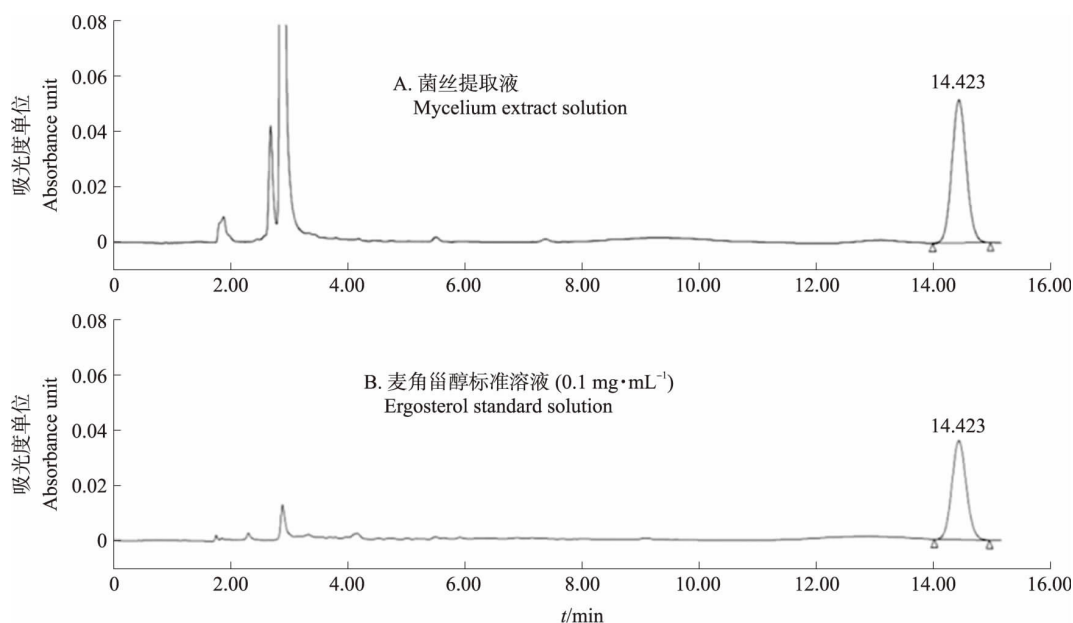


图 1 菌丝提取液和麦角甾醇标准溶液的 HPLC 色谱图

Fig. 1 HPLC chromatograms of mycelium extract solution and ergosterol standard solution

2.3 超声细胞粉碎法提取 *R. solani* 中麦角甾醇的正交试验结果及其提取条件优化

由表 2 中极差 (R) 值可知: 料液比 (A) 对麦角甾醇的提取率影响最大, 其次为超声前浸泡时间 (B)、超声时间 (D), 超声功率 (C) 的影响最小。由表 3 方差分析结果可知: 料液比、超声前浸泡时间对麦角甾醇提取率的影响较显著, 而超声功率与超声时间对麦角甾醇的提取率影响不显著。基于此, 确定以超声细胞粉碎法提取水稻纹枯病菌中麦角甾醇的最佳条件为 $A_3B_2C_2D_2$, 即: 料液比 1/50, 超声前浸泡 20 min, 超声功率 200 W, 超声时间 4 min。

表 2 正交优化试验结果分析表

Table 2 Analysis of the results from orthogonal experiment

试验号 Number	因素 Factors				麦角甾醇含量 / (mg·g ⁻¹) Ergosterol content
	A	B	C	D	
T1	1	1	1	1	1.47
T2	1	2	2	2	1.83
T3	1	3	3	3	1.57
T4	1	4	4	4	1.33
T5	2	1	2	3	2.56
T6	2	2	1	4	2.48
T7	2	3	4	1	2.47
T8	2	4	3	2	2.34
T9	3	1	3	4	2.63
T10	3	2	4	3	2.65
T11	3	3	1	2	2.57
T12	3	4	2	1	2.44
T13	4	1	4	2	1.95
T14	4	2	3	1	1.81
T15	4	3	2	4	1.75
T16	4	4	1	3	1.61
水平 1 下的偏差均值 (k_1)	1.55	2.15	2.03	2.05	—
水平 2 下的偏差均值 (k_2)	2.46	2.19	2.15	2.17	—
水平 3 下的偏差均值 (k_3)	2.57	2.09	2.09	2.10	—
水平 4 下的偏差均值 (k_4)	1.78	1.93	2.10	2.05	—
极差 R	1.02	0.27	0.11	0.12	—
因素主次 Factor priority	$A > B > D > C$				
最优方案 Best plan	$A_3B_2C_2D_2$				

表 3 方差分析表
Table 3 Analysis results of variance

因素 Factor	偏差平方和 Sum of square(SS)	自由度 Freedom(DF)	F 值 F-value	显著性 Level of significance
料液比 Material-to-liquid ratio	3.039	3	178.765	*
超声前浸泡时间 Immersion time before ultrasonic	0.166	3	9.765	*
超声功率 Ultrasonic power	0.026	3	1.529	
超声时间 Ultrasonic time	0.040	3	2.353	
偏差 Error	0.020	3		

2.4 超声细胞粉碎法的准确度和精密度

由表 4 加样回收试验结果可知: 在超声细胞粉碎法的最佳提取条件下, 麦角甾醇的加样回收率为 92.22%~101.13%, 平均回收率为 96.53%, *RSD* 为 2.68%。由表 5 重复性试验结果可见: 在最佳提取条件下其麦角甾醇的平均含量为 2.59 mg·g⁻¹, *RSD* 为 0.88%。试验结果均符合相关规定要求, 说明此提取方法准确度高, 重复性好。

表 4 超声细胞粉碎法加样回收试验结果
Table 4 Test results of sample recovery rate of ultrasonic cell disruption method

组别 Group	平均峰面积 Average peak area	菌丝量/g Mycelium weighing	回收率/% Recovery rate	平均回收率/% Average recovery rate	<i>RSD</i> /%
低浓度组 Low concentration group	973 759 988 990 992 368	0.199 9 0.201 1 0.200 9	97.63 100.02 101.13	96.53	2.68
中浓度组 Medium concentration group	1 347 605 1 341 389 1 352 413	0.200 6 0.200 3 0.200 9	96.02 95.48 96.37		
高浓度组 High concentration group	1 670 465 1 700 077 1 711 026	0.199 5 0.200 0 0.199 7	92.22 94.39 95.54		

表 5 超声细胞粉碎法重复性试验结果
Table 5 Reproducibility test results of ultrasonic cell disruption method

编号 Number	平均峰面积 Average peak area	菌丝量/g Mycelium weighing	麦角甾醇含量/(mg·g ⁻¹) Ergosterol content	平均含量/(mg·g ⁻¹) Average content	<i>RSD</i> /%
1	599 097	0.200 7	2.59	2.59	0.88
2	593 776	0.200 1	2.57		
3	593 779	0.201 3	2.56		
4	603 096	0.201 1	2.60		
5	607 890	0.201 5	2.62		

2.5 3 种方法提取金针菇中麦角甾醇的比较结果

由表 6 可看出: 3 种提取方法中, 以超声细胞粉碎法提取率最高, 需时最少, 且重现性良好。方差分析结果显示, 超声细胞粉碎法提取麦角甾醇的提取率与皂化回流法和超声辅助法提取麦角甾醇的提取率差异极显著(*P*<0.01)。

表 6 皂化回流法、超声辅助法及超声细胞粉碎法提取金针菇中麦角甾醇的比较及方差分析
Table 6 Comparison of extraction of ergosterol from *Flammulina velutipes* with saponification reflux, ultrasound assisted and ultrasonic cell crushing and analysis results of variance

方法 Methods	平均峰面积 Average peak area	菌丝量/g Mycelium weighing	麦角甾醇含量/ (mg·g ⁻¹) Ergosterol content	麦角甾醇平均含量/ (mg·g ⁻¹) Average content of ergosterol	<i>RSD</i> /%	与超声细胞粉碎法比较 Compare with ultrasonic cell crushing				
						偏差平方和 SS	自由度 DF	均方 MS	F 值 F-value	P 值 P-value
皂化回流法 Saponification reflux	902 288 843 671 856 555	0.200 4 0.199 8 0.200 2	2.93 2.74 2.78	2.82	3.40	0.30	1	0.31	54.40	0.002
超声辅助法 Ultrasound assisted	942 803 906 658 929 845	0.200 6 0.200 3 0.199 8	3.05 2.94 3.02							
超声细胞粉碎法 Ultrasonic cell crushing	994 814 1 001 496 1 020 542	0.199 5 0.199 7 0.200 5	3.24 3.26 3.31							

3 结论与讨论

麦角甾醇存在于真菌的菌丝细胞中,对其进行有效提取的前提是麦角甾醇必须能从细胞中溶出。超声波的机械效应、空化效应、热效应等作用有利于细胞的粉碎,促使麦角甾醇从菌丝细胞中溶出并迅速分散在提取液中。故相对于皂化回流法,超声辅助提取和超声细胞粉碎提取法的提取量均有所增加。一般认为,超声前的浸泡有利于甲醇与菌丝的充分接触,有利于超声波能量的传导,提高菌丝细胞的粉碎率,正交试验结果亦证实了这一点。当超声的功率达到一定值(250 W)时,已经基本实现对菌丝细胞的有效粉碎,故进一步提高超声功率和超声时间,对麦角甾醇的提取影响不显著。本试验还发现,当料液比为1/20时,供试样品中可见有未完全粉碎的菌丝,说明减少料液比(即增加溶剂的用量)也有利于菌丝在超声条件下的充分粉碎,麦角甾醇更易溶出,提取更充分。

利用超声波提取,以往常用超声清洗机进行超声辅助提取,其操作是把菌丝、提取液混合至容器(如锥形瓶)中,浸入清洗槽水浴超声。超声波从清洗槽底部的振子发出,透过水浴(体积相对较大)和容器才到达提取液,在此过程中能量分散弱化,要使细胞粉碎率高需时较长。而超声细胞粉碎仪的工作原理是超声波通过浸入在样品溶液中的钛合金变幅杆对容器中的细胞、提取液直接产生作用,能量集中,细胞粉碎效率高。试验结果证实了这一点,超声细胞粉碎提取进一步缩短了提取时间,且麦角甾醇提取率也有提高。

借助超声波进行提取比传统的皂化回流法用时大幅减少,且操作简单,溶剂使用量少。相比于超声清洗机,由于超声细胞粉碎仪可提供能量更为集中的超声波,因此用超声细胞粉碎法可得到更高的提取率,且试验结果显示该方法的准确度及重复性均达到相关规定。综上所述,超声细胞粉碎法可作为真菌菌丝中麦角甾醇含量快速测试的参考方法。本研究仅选择了较有代表性的植物致病菌和食用菌各1种作为试验材料,将来要对多种真菌进行研究,进一步确定超声细胞粉碎法应用于真菌中提取麦角甾醇的可行性。

参考文献 References:

- [1] Verma B, Robarts R D, Headley J V, et al. Extraction efficiencies and determination of ergosterol in a variety of environmental matrices [J]. *Communications in Soil Science and Plant Analysis*, 2002, 33(15/16/17/18) : 3261–3275.
- [2] 马养民, 赵洁, 周雪宁. 植物内生真菌抗植物病原真菌活性物质的研究 [J]. *化学进展*, 2010, 22(增刊 1) : 440–448.
Ma Y M, Zhao J, Zhou X N. Anti-plant pathogenic fungal compounds from endophytic fungi [J]. *Progress in Chemistry*, 2010, 22(Suppl 1) : 440–448(in Chinese with English abstract) .
- [3] Song X M, Zhu X Y, Li T, et al. Dehydrozingerone inspired discovery of potential broad-spectrum fungicidal agents as ergosterol biosynthesis inhibitors [J]. *Journal of Agricultural and Food Chemistry*, 2019, 67(41) : 11354–11363.
- [4] 曹龙辉, 李晓珺, 赵文红, 等. 麦角甾醇的研究进展 [J]. *中国酿造*, 2014, 33(4) : 9–12.
Cao L H, Li X J, Zhao W H, et al. Research progress on ergosterol [J]. *China Brewing*, 2014, 33(4) : 9–12(in Chinese with English abstract) .
- [5] 郭瑞, 饶斌, 吴琴燕, 等. 超声辅助皂化提取禾谷镰孢菌中麦角甾醇及其 HPLC 分析 [J]. *分析实验室*, 2019, 38(11) : 1353–1358.
Guo R, Rao B, Wu Q Y, et al. Optimization of saponification assisted ultrasonic extraction and HPLC analysis of ergosterol from *Fusarium graminearum* [J]. *Chinese Journal of Analysis Laboratory*, 2019, 38(11) : 1353–1358(in Chinese with English abstract) .
- [6] Zhao T J, Chen J, Shi Y P. Holistic analysis of Liuwei Dihuang pills using ultrasonic cell grinder extraction and ultra-performance liquid chromatography [J]. *Chinese Journal of Chromatography*, 2017, 35(1) : 32–46.
- [7] 胡代花, 张嘉昕, 李翠丽, 等. 超声辅助提取金针菇中麦角甾醇及其 HPLC 测定方法 [J]. *食品工业科技*, 2017, 38(23) : 192–197.
Hu D H, Zhang J X, Li C L, et al. Optimization of ultrasonic-assisted extraction process of ergosterol from *Flammulina velutipes* and its determination by HPLC [J]. *Science and Technology of Food Industry*, 2017, 38(23) : 192–197(in Chinese with English abstract) .
- [8] 谢翎, 陈红梅, 陈安徽, 等. 超声波破碎法提取球孢白僵菌麦角甾醇的条件优化研究 [J]. *徐州工程学院学报*, 2007, 22(2) : 10–13.
Xie L, Chen H M, Chen A H, et al. Study of the optimization conditions for the extraction of ergosterol from *Beauveria bassiana* by using ultrasonic [J]. *Journal of Xuzhou Institute of Technology*, 2007, 22(2) : 10–13(in Chinese with English abstract) .
- [9] 董笑菲. HPLC 法测定发酵冬虫夏草菌丝粉中麦角甾醇的含量 [J]. *现代食品*, 2019(18) : 154–157.
Dong X F. Determination of ergosterol in fermented *Cordyceps sinensis* mycelial powder by HPLC [J]. *Modern Food*, 2019(18) : 154–157(in Chinese with English abstract) .
- [10] 吴志明, 李昆太. 水稻纹枯病的危害及其微生物防治概述 [J]. *生物灾害科学*, 2018, 41(2) : 81–88.
Wu Z M, Li K T. The damage of rice sheath blight and its microbial control [J]. *Biological Disaster Science*, 2018, 41(2) : 81–88(in Chinese with English abstract) .
- [11] 谭一罗, 杨和川, 苏文英, 等. 金针菇活性成分及药理活性研究进展 [J]. *江苏农业学报*, 2018, 34(5) : 1191–1197.

- Tan Y L, Yang H C, Su W Y et al. Research progress on bioactive composition and pharmacological activity of *Flammulina velutipes* [J]. Jiangsu Journal of Agricultural Sciences, 2018, 34(5) : 1191-1197(in Chinese with English abstract) .
- [12] 李治建, 古力娜·达吾提, 斯拉甫·艾白, 等. 高效液相色谱法分析红色毛癣菌麦角甾醇的含量 [J]. 石河子大学学报(自然科学版), 2009, 27(1) : 73-76.
- Li Z J, Gulina D, Silapu A, et al. Determination of ergosterol in mycelium of *Trichophyton rubrum* by high performance liquid chromatography [J]. Journal of Shihezi University(Natural Science), 2009, 27(1) : 73-76(in Chinese with English abstract) .
- [13] Heleno S A, Diz P, Prieto M A, et al. Optimization of ultrasound-assisted extraction to obtain mycosterols from *Agaricus bisporus* L. by response surface methodology and comparison with conventional Soxhlet extraction [J]. Food Chemistry, 2016, 197: 1054-1063.
- [14] 易承学, 童珊珊, 徐希明, 等. HPLC 法同时测定金针菇中麦角甾醇和 22, 23-二氢麦角甾醇的含量 [J]. 江苏大学学报(医学版), 2014, 24(2) : 126-128.
- Yi C X, Tong S S, Xu X M, et al. High performance liquid chromatography for simultaneous determination of ergosterol and 22, 23-dihydroergosterol in *Flammulina velutipes* [J]. Journal of Jiangsu University(Medicine Edition), 2014, 24(2) : 126-128(in Chinese with English abstract) .
- [15] 高虹, 谷文英, 丁霄霖. 利用微波辅助提取测定姬松茸中麦角甾醇含量 [J]. 浙江大学学报(农业与生命科学版), 2007, 33(1) : 113-118.
- Gao H, Gu W Y, Ding X L. Optimization of microwave-assisted extraction for determination of ergosterol in *Agaricus brasiliensis* [J]. Journal of Zhejiang University(Agriculture and Life Sciences), 2007, 33(1) : 113-118(in Chinese with English abstract) .

责任编辑: 夏爱红

《南京农业大学学报》第九届编辑委员会

顾问: 盖钧铭 万建民

主任委员: 陈发棣

副主任委员: 丁艳锋 沈其荣 沈波

委员: (以姓氏笔画为序)

丁艳锋 王丽平 王秀娥 王源超 叶永浩 兰叶青 朱艳 朱伟云
刘凤权 刘文斌 刘永杰 刘红林 刘泽文 刘斐 刘裕强 刘蓉
刘满强 李英 李春保 李艳 李祥瑞 吴磊 杨红 杨晓静
汪小昆 沈波 沈文飏 沈其荣 沈明霞 沈振国 张正光 张红生
张绍铃 陈发棣 周立祥 周光宏 郑永华 赵方杰 胡水金 柳李旺
姜东 洪晓月 徐国华 高峰 高志红 郭世荣 郭旺珍 陶小荣
曹瑞兵 崔中利 章元明 章文华 屠康 强 胜

主编: 沈其荣

副主编: 陈发棣 丁艳锋 沈波(常务)

南京农业大学学报

Nanjing Nongye Daxue Xuebao

1956年9月创刊

第44卷 第6期 2021年 双月刊

JOURNAL OF NANJING
AGRICULTURAL UNIVERSITY

Started in 1956

Bimonthly, Vol. 44 No. 6 2021

主管单位 中华人民共和国教育部
主办单位 南京农业大学
主 编 沈其荣
编辑出版 《南京农业大学学报》编辑部
地 址 南京市卫岗1号, 210095
电 话 (025) 84395214
电子信箱 nauxb@njau.edu.cn
网 址 <http://nauxb.njau.edu.cn>
印刷单位 江苏省地质测绘院
发行范围 公开发行
国内发行 江苏省邮政局
国外发行 中国国际图书贸易总公司
订 阅 全国各地邮政局

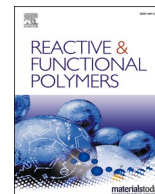
Administrated by Ministry of Education, P. R. China
Sponsored by Nanjing Agricultural University
Chief Editor: Shen Qirong
Edited and Published by Editorial Department of Journal of
Nanjing Agricultural University
Address: No. 1 Weigang, Nanjing 210095 Jiangsu, China
Tel: +86-25-84395214
E-mail: nauxb@njau.edu.cn
Web Site: <http://nauxb.njau.edu.cn>
Printed by Jiangsu Geologic Surveying and Mapping Institute
Distributed Abroad by International Book Trading Corporation
P. O. Box 399, Beijing, P. R. China

中国标准连续出版物号: ISSN 1000-2030 国内邮发代号: 28-53
CN 32-1148/S 国外发行代号: Q5785

2021年11月30日出版 定价: 20.00元

ISSN 1000-2030





Perspective Article

Polydimethylsiloxane-polymethacrylate block copolymers containing quaternary ammonium salts against *Fusarium oxysporum* f. sp. *cubense* race 4 in soil: Antifungal activities and pot experiments

Yaoyao Chang^a, Weiqiang Zhong^b, Jiaqi Liang^a, Anqiang Zhang^{b,*}, Yaling Lin^{a,*}

^a College of Materials and Energy, South China Agricultural University, 483 Wushan Rd., Guangzhou 510642, Guangdong, China

^b School of Material Science and Engineering, South China University of Technology, 381 Wushan Rd., Guangzhou 510641, Guangdong, China

ARTICLE INFO

Keywords:

Banana Fusarium wilt
Polymeric quaternary ammonium salts
Adsorption
Migration
Antifungal activity
Persistence

ABSTRACT

Fusarium oxysporum f. sp. *cubense* race 4 (Foc4) has significant impacts on banana production. Foc4 conidia can survive for many years in the soil, making control difficult. Thus, the inhibition of the conidia that serve as a continual source of inoculum in soil should be an effective way to control banana Fusarium wilt. In this paper, we first investigated the activities of polydimethylsiloxane-polymethacrylate block copolymers containing quaternary ammonium salts (PDMS-*b*-QPDMAEMA, labeled Si_xQ₅) against Foc4 with microbroth dilution and toxicity plate assays. Then, the environmental behavior of these compounds, i.e., their adsorption and migration in soils, was further studied. Later, the effect and duration of Si_xQ₅ on Foc4 in soil and the effects of Si_xQ₅ on soil microbial diversity were evaluated. In addition, we conducted pot experiments to study the effect of Si₅Q₅ on banana Fusarium wilt. The results showed that Si_xQ₅ showed a good inhibitory effect on Foc4, was easily adsorbed by the soil and was relatively immobile in soil. The inhibitory effect of Si_xQ₅ on Foc4 was maintained for 30 d under continual inoculation of Foc4 into the soil (Foc4 addition every 2 d), and Si_xQ₅ remained active in the soil for 90 d with Foc4 addition every 10 d. Soil microbial population analysis revealed that the culturable total fungal and bacterial populations increased and the culturable actinobacterial population decreased Si_xQ₅ with addition. Pot experiments showed that Si₅Q₅ can reduce Foc4 infection in banana seedlings and does not harm banana seedlings. The stability and inhibitory effects on Foc4 demonstrate the potential application of Si_xQ₅ in banana fields to prevent Foc4 conidial infection in the long term.

1. Introduction

Banana Fusarium wilt (aka Panama disease) is one of the most destructive soil-borne diseases of banana and is caused by *Fusarium oxysporum* f. sp. *cubense* (Foc); specifically, tropical race 4 (Foc4) has been distributed throughout the world's main banana production areas and infects almost all bananas [1]. Foc4 can infect the roots and vascular systems of plants [2], and the pathogen conidia are highly resistant to stress. Once this pathogen has colonized the soil, Foc4 can survive for approximately 20 years even without banana hosts [3,4] and even 40 years under extreme conditions [5]. Panama wilt is a perennial and polycyclic disease, which means that there are limited prevention and control methods for it [6]. One of the most effective methods is eradicating Foc4 from infested soil. Therefore, soil treatments are essential. People sterilize the soil by burning rice husks in the Philippines and

Indonesia, but there is no efficacy data for this method. Other soil treatment methods, such as solarization, fumigation and flood fallowing, can effectively kill Foc4 in soil; however, the effects can only be maintained for a single fruiting cycle, and Foc4 rapidly reinvests the area [1,6]. Soils that inhibit the occurrence of Fusarium wilt have been identified. The diversity of the microbial community in the soil and soil enzyme activity can strengthen the resistance of soil to Foc4 invasion. Bacteria are the most diverse and abundant group of microorganisms in the soil and have the most antagonistic effect against Fusarium pathogens [7–9]. Therefore, to support sustainable crop production, it is essential to effectively kill Foc4 in the long term while exerting no significant effect on the disease-suppressive bacterial community in the rhizosphere.

Since soil is a complex and dynamic environment, the adsorption and desorption of fungicides in soils are important processes that

* Corresponding authors.

E-mail addresses: aqzhang@scut.edu.cn (A. Zhang), linyaling@scau.edu.cn (Y. Lin).

<https://doi.org/10.1016/j.reactfunctpolym.2021.104848>

Received 12 November 2020; Received in revised form 5 February 2021; Accepted 6 February 2021

Available online 10 February 2021

1381-5148/© 2021 Elsevier B.V. All rights reserved.

characterize the mobility and transport of fungicides in the soil sub-surface. These behaviors have an important impact on the persistence of fungicides. Therefore, it is of great significance to study the environmental behavior of fungicides entering the soil and analyze the factors influencing the fungicides' persistent fungicidal activity against Foc4 infection.

Although cationic polymers with quaternary ammonium salt groups (PQASs) have attracted a great deal of attention in recent years for their they exhibit good environmental stability [10] and various antimicrobial activities via the modifications of their chemical side chains, structures and properties [11–16], the application of PQASs, especially biodegradable PQASs, in phytopathogenic fungi was rarely reported. In our previous work, a serial of PQASs, including the homopolymer of acrylamide quaternary ammonium salt (PQD-BC) [16,23,53], dimethylaminopropyl benzyl chloride-grafted polysiloxanes (PDMS-g-BC) [19], and hydrophilic cationic polymers with different charge density and molecular weights [60] were synthesized, and the antifungal effect on Foc4 and *Rhizoctonia solani* (*R. solani*) were discussed. These works could help us understand the relationship between polymer structures and antifungal activities, in which the amphiphilic structure, molecular weights and QAS groups showed significantly effect on the antifungal activities. We previously described the synthesis of polydimethylsiloxane-polymethacrylate block copolymers containing quaternary ammonium salts (PDMS-*b*-QPDMAEMA, labeled Si_xQ₅), which are environmental-friendly and show nontoxic or nearly nontoxic to silkworms and Kunming mice and have antifungal activities against *R. solani*, the pathogen responsible for rice sheath blight [17]. Since the PDMS block is hydrophobic and the QPDMAEMA block is hydrophilic, PDMS-*b*-QPDMAEMA is a typical amphiphilic cationic block copolymer and shows strong adsorption ability. However, the morphological characteristics and life cycles of Foc4 and *R. solani* are very different. As mentioned above, Foc4 is the banana wilt pathogen and can infect and propagate by producing conidia as well as chlamydoconidia that can survive in soil or nonhost plants for many years [18]. To date, the antimicrobial activities and environmental behaviors of PDMS-*b*-QPDMAEMA in soils have not been reported.

In this paper, we investigated the activities of PDMS-*b*-QPDMAEMA against Foc4 and its environmental behavior with respect to its adsorption and migration in soil. These data are important for evaluating the impact of PDMS-*b*-QPDMAEMA on Foc4 and for future field studies. In addition, the effects of PDMS-*b*-QPDMAEMA on Foc4, the indigenous microorganisms in soil and their persistent fungicidal activities against Foc4 infection in soils were evaluated. Finally, pot experiments were conducted to evaluate the long-term effect of PDMS-*b*-QPDMAEMA on banana Fusarium wilt and banana seedlings in soil. These results are expected to provide a theoretical basis for the further application of PQASs in Foc4 prevention and control.

2. Experiments

2.1. Materials

2,3,5-Triphenyltetrazolium chloride (TTC) was obtained from Sangon Biotech (Shanghai) Co., Ltd. (Shanghai, China). Gause No. 1 medium and Martin's Bengal rose agar medium were supplied by Qingdao Hope Bio-Technology Co., Ltd. (Shandong, China). Beef extract peptone medium and potato dextrose agar medium (PDA) were prepared according to previous references [19]. The fungal strain used in this study, *Fusarium oxysporum* f. sp. *cubense* (E. F. Smith) Snyder & Hansen, race 4 (Foc4), was donated by the University of South China Agricultural University's Fungal Laboratory and subcultured on potato dextrose agar medium (PDA). Foc4 conidia were obtained from the surface of the agar after culture for 5 d at 28 °C. The concentrations of the conidial suspensions were determined using a hemocytometer. Soil samples were taken from banana plantations at the Institute of Fruit Trees, Guangdong Academy of Agricultural Sciences, China. A five-point sampling method

Table 1

Soil physicochemical properties.

Sand (%)	Silt (%)	Clay (%)	pH (1:2.5)	Organic matter (%)	CEC ^a (mmol/kg)
>0.05 mm	0.005–0.05 mm	<0.005 mm			
49.4%	18.2%	32.4%	5.0	1.9%	104

^a CEC, cation exchange capacity, mmol/kg.

was used to collect soil at a depth of approximately 0–30 cm from the soil surface, after which the soil samples were air-dried at room temperature, homogenized and sieved through a 2-mm mesh. Some basic physicochemical properties of the samples are listed in Table 1. The percentages of clay, silt and sand were measured using a hydrometer [20]. The cation exchange capacity was measured with a standard acetate ammonium procedure. The soil organic matter content was determined using the dichromate digestion method. The pH was measured in a soil:H₂O (1:2.5) solution [21]. Since the cation exchange capacity (CEC) was less than 160 mmol/kg, the soil samples could be classified as Ferallsols according to the WRB (World Reference Base for Soil Resources) [22].

PDMS-*b*-QPDMAEMA (Si_xQ₅, x = 0, 2, 5, 10, x represent the molecular weights of the PDMS blocks, i.e., 0, 2000, 5000 or 10,000, respectively) and fluorescence-labeled PDMS-*b*-QPDMAEMA (Si_xQ₅-FL) were synthesized via anionic ring-opening polymerization and atom transfer radical polymerization (ATRP) [17], and the specific procedures are described in SI (Part S1).

2.2. Antifungal bioassay

The effect of Si_xQ₅ on the mycelial growth of Foc4 was determined by a hyphal growth inhibition test in vitro. The minimum inhibitory concentration (MIC) of Si_xQ₅ on Foc4 was determined by the broth micro-dilution method with 2,3,5-triphenyltetrazolium chloride (TTC), and the minimal fungicidal concentration (MFC) of Si_xQ₅ against Foc4 was determined by the spot plate method [23]. All tests were conducted in triplicate.

2.3. Adsorption and migration characteristics of Si_xQ₅ in agricultural soil

2.3.1. Adsorption tests

According to the method described in the OECD106 guide, the adsorption - desorption with batch equilibrium desorption method was used to carry out the soil adsorption test [24]. The soil was weighed (1.000 ± 0.001 g) into a conical flask, and 100 mL of 0.01 M CaCl₂ aqueous solution containing Si_xQ₅ was added to make a soil/water ratio of 1:100. The concentration of Si_xQ₅ ranged from 0 to 1000 µg/mL, and 0.01 M CaCl₂ aqueous solution was used as a background solution to minimize changes in ionic strength and avoid dispersion. Each conical flask was shaken with a shaker at 200 rpm at 25 °C for 24 h, and then the supernatant was centrifuged at a relative centrifugal force (RCF) of 3000 g for 10 min. The supernatant concentration from each tube was analyzed by a micro ultraviolet spectrophotometer (SMA5000, Merinton). The absorbance was measured at 210 nm [25]. There were two blank controls: one control (Si_xQ₅ solution, no soil) test to assess the loss of compounds as a result of adsorption on the container wall; and another experiment was conducted to determine the interference due to the 0.01 M CaCl₂ aqueous solution and soil. Each treatment was conducted in triplicate.

The amount of Si_xQ₅ adsorbed was determined according to the difference between the initial and final concentrations of Si_xQ₅ in the supernatant. The quantity of Si_xQ₅ adsorbed by soil was calculated by Eq. (1):

$$C_s = \frac{C_0V - C_eV}{1000 \cdot m} \quad (1)$$

Table 2Equations used to study Si_xQ₅ sorption in soils.

Model	Equation	Eq.	Description
Langmuir	$C_s = \frac{KM_s C_e}{1 + KC_e}$	(2)	K , Langmuir coefficient (L/mg); M_s , the maximum amount of Si _x Q ₅ adsorbed on soil solids as a monolayer (mg/g).
Freundlich	$C_s = K_f C_e^{\frac{1}{n}}$	(3)	K_f and n , Freundlich capacity and intensity factors, respectively.
Temkin	$C_s = K_1 \ln(K_2 C_e)$	(4)	K_1 and K_2 , Temkin sorption constants.

where C_s is the amount of Si_xQ₅ adsorbed per unit weight of soil (mg/g), C_0 is the initial concentration of Si_xQ₅ in the treatment solution, and C_e is the concentration of Si_xQ₅ present in the supernatant at equilibrium (μg/mL). V is the volume of the treatment solution (mL), and m is the mass of the soil (g).

The adsorption data obtained from intermittent experiments were analyzed by using the Langmuir, Freundlich and Temkin isotherm model [26], as shown in Table 2.

2.3.2. Migration tests

The migration potential of Si_xQ₅ in soil was studied by thin layer chromatography (TLC). Thin-layer plates of soil were prepared according to a previously reported method [27]. The air dried plate was marked with two horizontal lines at a distance from the base of 3 cm (baseline) and 18 cm (endpoint). A droplet of 10.0 μg Si_xQ₅-FL solution prepared in alcohol was spotted onto the baseline of the plate. The plates were immersed with the base down at a certain angle from vertical in a closed glass chamber containing distilled water at a height of 0.5 cm. Distilled water was used as the developing solvent. After the developing solvent migrated to a distance of 18 cm from the base, the plates were removed from the glass chambers and laid flat to dry at room temperature. Autoradiograms were obtained by irradiation with an ultraviolet lamp (365 nm). Each Si_xQ₅-FL was treated in triplicate. The mobility factor (R_f) of Si_xQ₅-FL on the plates was calculated by the following formula [28]:

$$R_f = \frac{L}{L_{\max}} \quad (5)$$

where L is the average moving distance of Si_xQ₅-FL from the starting point, and L_{\max} is the moving distance of the developing solvent from the starting point.

2.4. Antifungal bioassay in soil

2.4.1. Optimization of antifungal conditions based on the uniform design method

The optimum soil conditions for the maximum antifungal activity of Si_xQ₅ were determined by a uniform design method according to a previous study [29]. Experiments for the optimization of the antifungal conditions involved three factors, including the Si_xQ₅ concentration (mg/g, X_1), shaking speed of shaker (rpm, X_2) and water/soil ratio (mL/g, X_3). The levels of each factor (Table S3) were selected according to the experimental results of the pre-experiments. A U_{10}^5 uniform design table was used to arrange the 10 experiments (Table 3), where the contents in brackets indicate the level of the factor, and the contents outside of the brackets indicate the exact concentration, shaking speed or water/soil ratio of each factor.

The testing was conducted as follows: the collected soil samples were first sterilized in a 121 °C high-temperature and high-pressure sterilizer for 20 min and then inoculated with Foc4 conidial suspension to obtain a soil/Foc4 mixture in the range of 2.25×10^5 conidia/(g dry soil) [30]. According to the uniform design table (Table 2), for each test, 0.5 g air dried soil containing Foc4 conidia prepared as described above was

Table 3Experiments based on uniform design table (U_{10}^5).

No.	X_1 (Si _x Q ₅ concentration, mg/g) ^a	X_2 , (shaking speed, rpm)	X_3 , water/soil ratio (mL/g)
T1	(10xIC ₅₀)	(175)	(3/1)
T2	(10xIC ₅₀)	(200)	(10/1)
T3	(20xIC ₅₀)	(250)	(1/1)
T4	(20xIC ₅₀)	(150)	(9/1)
T5	(30xIC ₅₀)	(175)	(18/1)
T6	(30xIC ₅₀)	(225)	(1/1)
T7	(40xIC ₅₀)	(250)	(9/1)
T8	(40xIC ₅₀)	(150)	(18/1)
T9	(50xIC ₅₀)	(200)	(3/1)
T10	(50xIC ₅₀)	(225)	(10/1)

^a The IC₅₀ values for Si₀Q₅, Si₅Q₅ and Si₁₀Q₅ were 0.73, 0.76, and 0.94 mg/mL, respectively, as shown in Table 5.

mixed with sterile distilled water containing Si_xQ₅ in a 5-mL tube with a lid, and the experiments were carried out at 28 °C. A total of 25 μL of solution was taken from each sample every 2 d to confirm whether it contained live Foc4 conidia by the dilution plate coating method. If no live Foc4 conidia could be found, another 25 μL of Foc4 suspension was added to the tube to maintain the conidia concentration at 2.25×10^5 conidia/(g dry soil). If live Foc4 conidia were found, then the time was defined as the effective antifungal time (Y, day) of Si_xQ₅ and recorded. Each treatment was conducted in triplicate.

Regression analyses of the data were performed using SAS software (SAS 8.01, SAS Institute Inc., USA.), wherein the stepwise regression model was chosen to analyze the data; the variable listed in Eq. (6) was eliminated if the significance parameter of a variable was lower than 0.1.

$$Y = a_1 X_1 + a_2 X_2 + a_3 X_3 + a_4 X_1 X_2 + a_5 X_1 X_3 + a_6 X_2 X_3 + a_7 X_1^2 + a_8 X_2^2 + a_9 X_3^2 + a_{10} \quad (6)$$

where a_1 to a_9 are the coefficients for the variables from X_1 to X_3^2 , respectively, and a_{10} is the constant.

2.4.2. Determination of the effects of Si_xQ₅ on soil microbial diversity

Fresh soil samples (0.5 g) were incubated with potato dextrose broth medium (0.5 mL) for 24 h at room temperature to develop the microbial populations in the soil and then added to 5 mL of sterilized distilled water containing Si_xQ₅ at different concentrations (10xIC₅₀, 20xIC₅₀ and 30xIC₅₀). The samples were cultured for 2 d at 28 °C on a shaker with a shaking speed of 225 rpm. Then, the number of cultivable microorganisms in the soil was determined using two methods, including the traditional plate count method [31] and gene sequencing.

For the plate count method, 25 μL of the soil suspension was inoculated into an agar plate containing suitable medium (including beef extract peptone medium, Gause No. 1 medium, and Martin's bengal rose agar medium, which were chosen for the culture of bacteria, actinomycetes and fungi, respectively), the number of living microbes was counted, and the population number was determined. The total number of microorganisms was determined by counting the number of colony forming units (CFU/g dry soil). Each treatment was conducted in triplicate.

For the gene sequencing method, after the samples were centrifuged at 10,000 r/min for 3 min, the upper liquid was collected and filtered using a 0.22 μm filter membrane, and both the soil sample and the filter membrane were sent for gene sequencing. The soil fungal community structure was analyzed using Illumina MiSeq sequencing (Sangon Biotech Co., Ltd., Shanghai, China). The gene-specific primers ITS1F/ITS2R were used to amplify the fungal ITS1-ITS2 region [32]. The details of the procedure are recorded in the Supporting Information.

2.4.3. Persistence of Si_xQ₅ on Foc4 in soil

To perform antifungal bioassays of Si_xQ₅ in soil over time, 0.5 g of

Table 4
Groups for pot experiments.

Groups	Foc4 conidia in soil, CFU/g soil	Si ₅ Q ₅ in soil, mg/g soil
CK	0	0
Group 1	0	IC ₅₀ (0.76)
Group 2	1 × 10 ⁵	0
Group 3	1 × 10 ⁵	IC ₅₀ (0.76)

sterilized dry soil was mixed with sterile distilled water containing Si_xQ₅ in a 5-mL tube with a lid, and then Foc4 conidial suspension was added at 2.25×10^5 conidia/(g dry soil). Then, the experiments were carried out at 28 °C. A total of 25 µL of solution was taken from each sample every 10 d to confirm whether it contained live Foc4 conidia by the dilution plate coating method [33]. If no live Foc4 conidia were found, another 25 µL of Foc4 suspension was added to the tube to maintain the conidia concentration at 2.25×10^5 conidia/(g dry soil). If live Foc4 conidia were found, then the time was defined as the antifungal persistence time (d) of Si_xQ₅ and recorded. Each treatment was conducted in triplicate.

2.5. Pot experiment

Potted soil was provided by the Crop Nutrition and Fertilization Laboratory of South China Agricultural University. The basic parameters of the soil are shown in Table S4.

The soil samples were sieved over a 5 mm mesh and then divided into 4 groups, i.e., 3 treatment groups (Groups 1, 2 and 3) and a CK according to Table 4, in which CK refers to normal samples (without the addition of Foc4 conidia or the addition of Si₅Q₅; each group contained 10 replications), and the total amount of soil in the pot for each replication was 700 g, in which Si₅Q₅ solution and Foc4 conidial suspension were mixed with soil before being added to the pots (upper diameter 13 cm, lower diameter 10 cm, height 13 cm) [32]. After banana seedlings (*Musa* AAA Cavendish cv. Brazil, purchased from South China Botanical Garden, Chinese Academy of Sciences, Guangzhou (Huang et al., 2019) with a height of approximately 15 cm (4–5 leaves) were transplanted to the pots, 200 mL tap water was added, and then 75 mL tap water was added every afternoon to each pot. All potted plants were cultured in the greenhouse at a typical temperature of 25 to 35 °C and humidity of 55–95% under natural sunshine for approximately 12 h. After 90 d of banana seedling growth, the plant height, false stem circumference, total leaf number, green leaf number, fresh weight and dry weight of each seedling were recorded. Based on the degree of corm browning and leaf chlorosis, disease classification was carried out, and the disease index of the banana seedlings was calculated by Eq. (7).

$$\text{Disease index} = \frac{\sum \text{Number of cases at all levels} \times \text{Relative values}}{\text{Total number of plants} \times \text{Maximum value}} \times 100\% \quad (7)$$

3. Results and discussion

3.1. Antifungal activities of Si_xQ₅ on Foc4

Since Si_xQ₅ is a typical amphiphilic cationic block copolymer, which is moisture-absorbing and easy to dissolve in water. In fact, it could be “miscible” with water when the concentration is larger than critical micelle concentration (CMC, range from 0.06 to 0.09 mg/mL for Si_xQ₅ [17]): at this time, most of the polymer exists in the aqueous solution in the form of micelles. The effects of Si_xQ₅ on the mycelial growth of Foc4 were determined by the hyphal growth inhibition test in which the colony diameter was measured on PDA plates with different concentrations of Si_xQ₅. Si_xQ₅ inhibited the growth of Foc4 in the concentration range of 0.3–1.5 mg/mL. As the concentration of Si_xQ₅ increased, the diameter of each treatment group decreased. The 50% maximum

Table 5
The antifungal effect of Si_xQ₅ against Foc4.

	MIC ^a , mg/mL	MFC ^a , mg/mL	MIC/MFC	IC ₅₀ ^a , mg/mL	IC ₉₀ ^a , mg/mL
Si ₀ Q ₅	0.15	0.6	4	0.73	4.73
Si ₅ Q ₅	0.15	0.6	4	0.76	2.96
Si ₁₀ Q ₅	0.15	0.3	2	0.94	3.20

^a MIC: Minimum inhibitory concentration, MFC: Minimal fungicidal concentration, IC₅₀: 50% maximum inhibitory concentration, IC₉₀: 90% inhibitory concentration.

inhibitory concentration (IC₅₀) represents the concentration of Si_xQ₅ at which 50% of Foc4 growth is inhibited, and the 90% inhibitory concentration (IC₉₀) represents the concentration of Si_xQ₅ at which 90% of Foc4 growth is inhibited [34]. After 5 d of incubation, Si_xQ₅ displayed antifungal effects (Fig. S1-A, B and Table 5), and the results indicated that although both Si₀Q₅ (IC₅₀ = 0.73 mg/mL) and Si₅Q₅ (IC₅₀ = 0.76 mg/mL) showed better inhibition effect than that of Si₁₀Q₅ (IC₅₀ = 0.94 mg/mL) at 50% inhibition of mycelial growth, Si₅Q₅ (IC₉₀ = 2.96 mg/mL) exhibited the greatest effect against Foc4, compared with Si₀Q₅ (IC₉₀ = 4.73 mg/mL) and Si₁₀Q₅ (IC₅₀ = 3.20 mg/mL) at 90% inhibition of mycelial growth. The antifungal efficacy results also showed that Si₀Q₅, Si₅Q₅ and Si₁₀Q₅ inhibited the mycelial growth of Foc4 in a dose-dependent manner.

The MIC and MFC are the principal measures of in vitro activity. We subsequently tested the MIC and MFC of Si_xQ₅ against Foc4, as shown in Fig. S1-C, D and Table 5. The in vitro studies showed that Si_xQ₅ had an inhibitory effect on Foc4. The ratio of MFC/MIC can reflect the fungicidal activity; when the ratio was less than or equal to 4, Si_xQ₅ showed fungicidal activity; otherwise, Si_xQ₅ had antifungal activity [35]. Si_xQ₅ showed lower MIC and MFC values and MFC/MIC ratios ≤ 4, indicating that the compounds were fungicidally effective. This finding indicated that PDMS-*b*-QPDMAEMA (Si_xQ₅) has promise for application as an antifungal agent against plant pathogens.

The antifungal experiment showed that Si_xQ₅ had good antifungal effects on Foc4. Quaternary ammonium salts compounds (QASSs) are widely used in agricultural production, textile printing and dyeing, and mining flotation because of their good surface activity and bactericidal effect [36]. Previous studies have shown that QASSs are effective biological fungicides that can bind to proteins and nucleic acids, destroy the integrity of the cell membrane, and lead to the leakage of cytoplasmic ions and macromolecules [37–39]. In our previously studies, the effect of the homopolymer of (2-methacrylamido) propyltetra-benzyltrimethylammoniumchloride (PQD-BC) and dimethylamino-propyl benzyl chloride-grafted polysiloxanes (PDMS-g-BC) on Foc4 were discussed in detail [23]. In which, the polymeric QASSs were found to induce cell death in Foc4 by disrupting the cellular structure integrity, such as the loss of the cell wall and plasma membrane integrity and oxidative stress (lipid peroxidation), leading to the release of intracellular contents and inducing mitochondrial dysfunction and interference with genomic DNA. Comparing with PQD-BC, Si_xQ₅ containing a hydrophobic PDMS “tail” and showed similar amphiphilic structure as that of PDMS-g-BC, which help Si_xQ₅ to achieve smaller MIC and IC₉₀ on Foc4 than PQD-BC [23]. And due to the similar hydrophilic QPDMAEMA block containing QASSs as PQD-BC, it could be expected that Si_xQ₅ would have an antifungal effect on Foc4 with the similar mechanism as PQD-BC and PDMS-g-BC.

3.2. The adsorption and migration characteristics of Si_xQ₅ in agricultural soil

3.2.1. Soil adsorption properties of Si_xQ₅

Adsorption isotherms (Fig. 1-A) were drawn from the concentration (*C*₀) and soil adsorption capacity (*C*_s) at adsorption equilibrium and then analyzed using the Langmuir, Freundlich and Temkin isotherm models

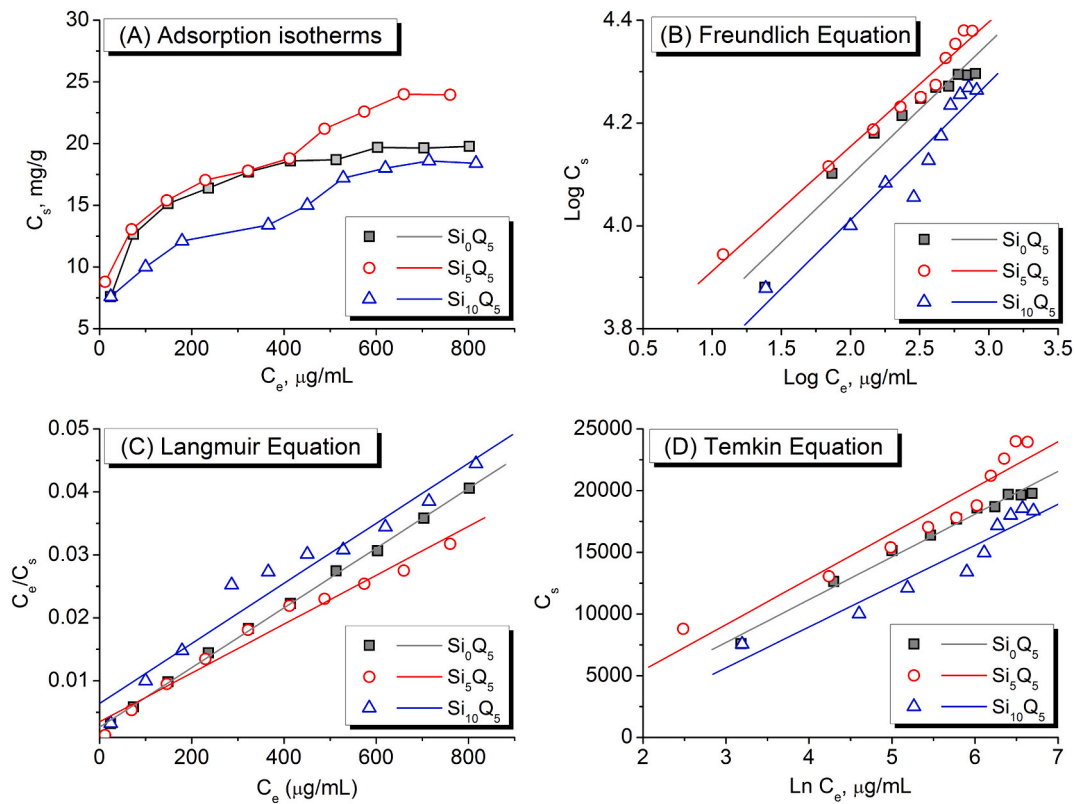


Fig. 1. The adsorption isotherms of Si_xQ_5 in soil with the (A) Freundlich equation model (B), Langmuir equation model (C), and Temkin equation model (D).

(Fig. 1-B, C and D, respectively). With the increase in the adsorbed amount in soil, the adsorption behavior of quaternary ammonium salt in soil weakens until the soil is saturated; thus, the inflection point can be found in Fig. 1-A. The interferences from the background soil organic matter and 0.01 M CaCl_2 aqueous solution were consistently very low (absorbance ~ 0.001) in all experiments. From Fig. 1-A, the adsorption isotherms at 25 °C followed L-type characteristics, reflecting the relatively high affinity between Si_xQ_5 and the soils. Table 6 presents the constants of the Langmuir, Freundlich and Temkin isotherm models.

From the determined parameters of the Freundlich, Langmuir and Temkin equations, the Langmuir model yielded the best fit, with all the correlation coefficients (R^2 values) greater than 0.95. The M_s values of Si_0Q_5 , Si_5Q_5 and Si_{10}Q_5 were 21,097 $\mu\text{g/mL}$, 25,773 $\mu\text{g/mL}$ and 20,964 $\mu\text{g/mL}$, respectively, indicating that $\text{Si}_5\text{Q}_5 > \text{Si}_0\text{Q}_5 > \text{Si}_{10}\text{Q}_5$. The adsorption data were also fitted to the Freundlich and Temkin equations, and the correlation coefficients suggested that the Freundlich ($R^2 = 0.92\text{--}0.98$) and Temkin ($R^2 = 0.91\text{--}0.98$) equations could well describe the adsorption data [40]. The Freundlich parameters $1/n$ followed the order $\text{Si}_5\text{Q}_5 < \text{Si}_0\text{Q}_5 < \text{Si}_{10}\text{Q}_5$. Universally, the lower $1/n$ is, the higher the binding affinity to the soil. This relationship is consistent with the description of the Langmuir equation. The sorption parameter K_f has a strong dependence on organic matter; the higher the content of organic matter in soil, the greater the K_f . The relation describing the adsorption of a given molecule can be illustrated in a different manner in which the K_f value is standardized according to the soil organic carbon (OC%)

content to obtain the organic carbon-normalized adsorption coefficient (K_{oc}) according to the following formula [41]:

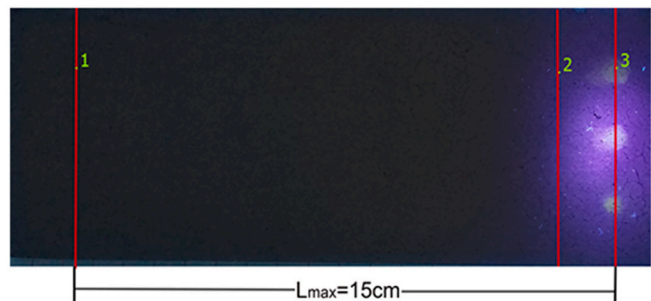
$$K_{oc} = \frac{1.724K_f}{OM\%} \quad (8)$$

where 1.724 is the conversion coefficient between the soil organic matter and organic carbon contents. Through calculation, the K_{oc} values of Si_0Q_5 , Si_5Q_5 and Si_{10}Q_5 were determined to be 344,813, 424,408 and 272,448, respectively, all of which are greater than 20,000. According to Chinese National Standard GB/T 31270.4–2014, the adsorption properties indicate that Si_xQ_5 is easily adsorbed in soil.

Adsorption isotherms can explain the distribution of an adsorbate between the liquid and solid phases, and the possibility of the interaction between the adsorbed species can be determined by this mathematical model [26]. The adsorption isotherms show that the adsorption of Si_xQ_5 can be considered monolayer adsorption, which indicates that the binding force of Si_xQ_5 to soil is strong. The adsorption capacity of Si_xQ_5 in soil increases with increasing concentration, but when it reaches a certain point, the adsorption capacity will no longer increase [42]. The adsorption isotherm model of Si_xQ_5 is more suitable for the Langmuir model than the Freundlich and Temkin equations, and the Langmuir isotherm model is appropriate for monolayer adsorption onto a surface with a limited number of identical sites. That is, the whole adsorption process of Si_xQ_5 in soil is monolayer adsorption. The experimental results are consistent with the existing adsorption results for

Table 6
Freundlich, Langmuir and Temkin equation model parameters.

Sample	Freundlich equation			Langmuir equation			Temkin equation		
	K_f	$1/n$	R^2	M_s	K	R^2	K_1	K_2	R^2
Si_0Q_5	3800	0.2587	0.9400	21,097	0.018	0.9990	3466	0.46	0.9851
Si_5Q_5	4677	0.2422	0.9816	25,773	0.011	0.9738	3706	0.59	0.9227
Si_{10}Q_5	3002	0.267	0.9259	20,964	0.007	0.9529	3311	0.27	0.9179



Line 1: the maximum distance of distilled water migration (endpoint);
Line 2: boundaries with R_f values less than 0.1;
Line 3: the starting position (baseline) of the migration.

Fig. 2. Results of soil thin layer chromatography.

quaternary ammonium salts in soil [43,44].

In summary, Si_xQ_5 belongs to the group of compounds that are easily adsorbed by soil. The adsorption properties of Si_xQ_5 in soil follow the order $\text{Si}_5\text{Q}_5 > \text{Si}_{10}\text{Q}_5 > \text{Si}_{10}\text{Q}_5$, which shows that with certain length (about 5 k for the PDMS block) of the hydrophobic segment, the best adsorption performance of PDMS-*b*-QPDMAEMA in soil could be achieved.

3.2.2. Soil migration

Fig. 2 shows the soil adsorption and soil thin layer chromatography of Si_xQ_5 -FL in soil. The distance covered by Si_xQ_5 -FL on a thin layer compared to that covered by water, i.e., the R_f value, was measured by using a 365 nm ultraviolet lamp. The distance between Si_xQ_5 -FL and the thin layer was less than 1 cm, so the R_f value was less than 0.1; thus, it can be concluded that Si_xQ_5 -FL does not move in soil.

From soil adsorption assays and soil thin layer chromatography, it can be concluded that Si_xQ_5 is easily adsorbed and relatively immobile in soil, which might be mainly due to the positive charge of quaternary nitrogen atoms, while the soil particles (such as sludge and sediments) normally bear negative charges. These results are similar to those of many previous studies on the behavior of QASs in soil [45–50]. The easy adsorption and immobility of Si_xQ_5 in soil indicate that Si_xQ_5 is not easily lost in soil, which is beneficial for the long-term control of banana Fusarium wilt, and the negative impacts of its presence will be the subject of further study.

Table 7
Results of regression analysis.

Si_xQ_5	Regression equation	Standard error	Correlation coefficient (R^2)
Si_0Q_5	$Y = -1.5614 + 0.07069 X_1X_3$	2.75	0.9618
Si_5Q_5	$Y = 0.02896 + 0.06911 X_1X_3$	3.84	0.9290
Si_{10}Q_5	$Y = -1.523 + 0.07381 X_1X_3 - 0.05965 \times \frac{2}{3}$	3.51	0.9330

3.3. Antifungal bioassay in soil

3.3.1. Optimization of antifungal conditions

The uniform design method (UD) was first established by Chinese mathematicians Kaitai Fang and Yuan Wang by combining number theory with multivariate statistics and is usually applied in multifactor and multilevel experimental design [58]. Compared with the traditional orthogonal design method, the uniform design method is capable of selecting experimental points that are uniform throughout the experimental region and highly representative in the experimental domain, so that higher reliability can be achieved with the same number of tests. As an efficient way to optimize various processes, the uniform design method is widely used in materials preparation and optimization of test conditions [59]. In this work, the Si_xQ_5 concentration (X_1 , mg/g), shaking speed (X_2 , rpm) and water/soil ratio (X_3 , mL/g) were selected as the factors that might affect the final results, i.e., the effective antifungal time (Y , day). The results of the uniform design are shown in Fig. 3, in which the effective antifungal time (Y) varied considerably from 0 to 32 d under different conditions. The final regression equations based on the stepwise regression model are shown in Table 7, in which the variables whose significance parameters were lower than 0.1 have been eliminated. The high R^2 values indicated a strong relationship between the experimental and predicted values in this experiment. Therefore, the model is suitable for describing the relationship between antifungal conditions and significant factors for optimization. The Si_xQ_5 concentration (X_1) and water/soil ratio (X_3) were the main factors affecting Si_xQ_5 in soil. That is, when the Si_xQ_5 concentration (X_1) and water/soil ratio (X_3) were both high, the sustained antifungal time (Y) of Si_xQ_5 in the soil was the longest. Within the range of experimental conditions, shaking speed (X_2) had no significant effect. The longest antifungal times (28 d, 32 d, and 30 d) were obtained when the major factors were as follows: a Si_xQ_5 concentration of $50\times\text{IC}_{50}$ and water/soil ratio of 10/1. Since shaking speed (X_2) was not a significant factor, the shaking speed was chosen as 225 r/min.

Confirmation experiments were carried out under these conditions,

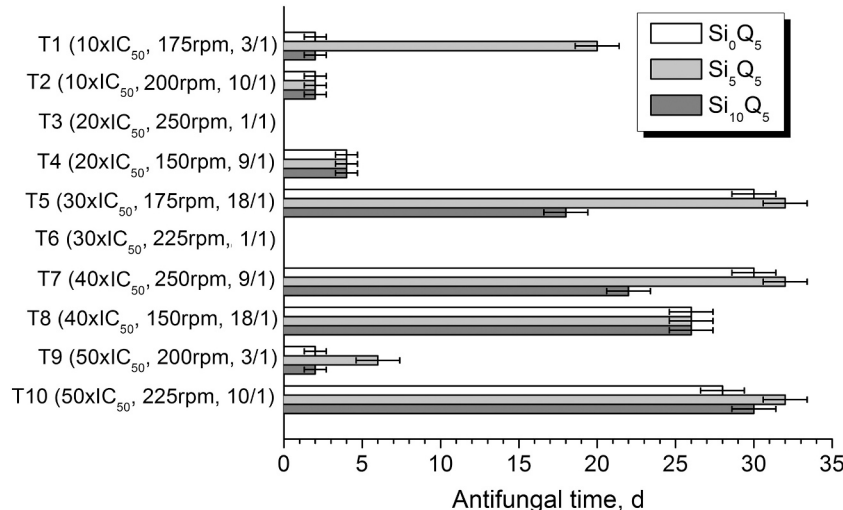


Fig. 3. Uniform design results.

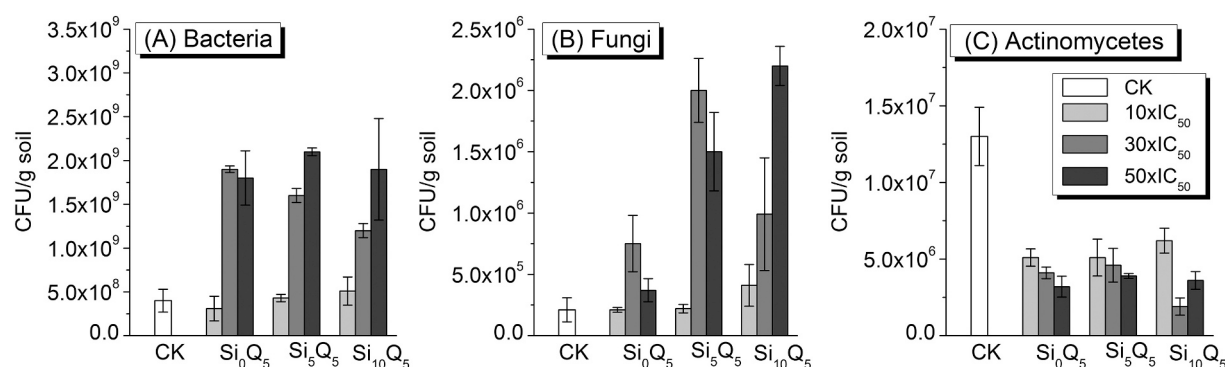


Fig. 4. Microbial biomass in soil.

and the corresponding times were 28 ± 1.4 d, 32 ± 1.4 d and 30 ± 1.4 d, respectively. The relative error between the verification test and the regression model was predicted, and the results demonstrated that a uniform design method can be used for the optimization of antifungal conditions. The results also showed that when Foc4 conidia were continuously inoculated into the soil, Si_xQ₅ could resist the pathogen for 30 d. The longevity of this antifungal activity makes the long-term prevention of banana Fusarium wilt feasible.

One of the reasons why banana Fusarium wilt is difficult to control is that Foc4 continues to invade plantations, and the existing soil treatment methods cannot effectively prevent the invasion of Foc4 for a long time. Therefore, we are committed to the study of methods that can effectively kill Foc4 conidia in soil after multiple infestations of Foc4. Through the experiment, we found that the antifungal effect of Si_xQ₅ under continuous addition of Foc4 every 2 d could be maintained for 30 d under the optimal antifungal conditions.

When the time interval of the continuous addition of Foc4 increased from 2 d to 10 d, Si₀Q₅, Si₅Q₅ and Si₁₀Q₅ maintained antifungal activity in soil for 90, 90 and 80 d, respectively, as shown in Fig. S4, reflecting the stability of these compounds in soil, which enables their application in banana fields to prevent Foc4 conidia invasion over the long term. Clara and Garcia also showed that QASs are not easily degraded in the environment [51], especially under anaerobic conditions (such as those found in sludge, sediment, etc.) [52].

This sustained antimicrobial activity of Si_xQ₅ against Foc4 in soil means that, in the field, a single application of Si_xQ₅ can prevent Foc4 from invading banana plants through the soil for a certain period of time, and the results matched well with those previous studies [53–57], in which quaternary ammonium dendrimer in poly(methyl methacrylate) bone cement showed continuous antibacterial activity against common hospital-acquired bacteria.

3.3.2. Effect of Si_xQ₅ on soil microbial diversity

Since small molecular quaternary ammonium salts are normally considered broad-spectrum fungicides, the effect of Si_xQ₅ on soil microbial diversity was evaluated based on plate counting methods in different media. After colony counting, the number of biological colonies in soil treated with Si_xQ₅ for 2 d was compared with that in soil without Si_xQ₅ treatment. The typical microbial biomasses, including bacteria, fungi and actinomycetes, in soil after the Si_xQ₅ treatments are shown in Fig. S2, and the results based on statistics are shown in Fig. 4, which shows that the microbial volume of actinomycetes decreased with increasing Si_xQ₅ concentrations. However, Si_xQ₅ significantly increased the total amount of bacteria and fungi in the soil.

In addition to the classical plate counting methods, gene sequencing was also chosen for evaluation. Soil microorganisms treated with Si₅Q₅ underwent DNA extraction, library construction, and macrogenome biological sequencing, and finally, bioinformatics analysis was performed to evaluate the differences in fungal community composition structure and diversity in the treated soil. The richness and diversity of

microbial communities can be reflected by diversity analysis of single samples (alpha diversity), as shown in Table S1. The results show that, compared with those of CK, with increasing Si₅Q₅ concentrations in soil, the richness of microbial species in soil increases, and the diversity decreases. On the basis of the taxonomic analysis, the community composition of each sample at each taxonomic level was counted. The sequences of the first 15 genera are shown in Table S2 and Fig. S3. We found that the sequence numbers of *Fusarium*, *Apiotrichum*, *Cylindrocladiella*, *Corallomycetella*, *Heterophoma*, *Humicola*, and *Plectosphaerella* decreased with increasing concentrations of Si₅Q₅, while the number of *Pichia* sequences increased. The results indicate that although Si₅Q₅ could inhibit the growth of part of the fungi including *Fusarium*, the growth of yeast-like fungi such as *Pichia* could be facilitated, thus the microorganisms in soil could be maintained in a certain state, instead of killing them all, which help to maintain the balance of natural resource.

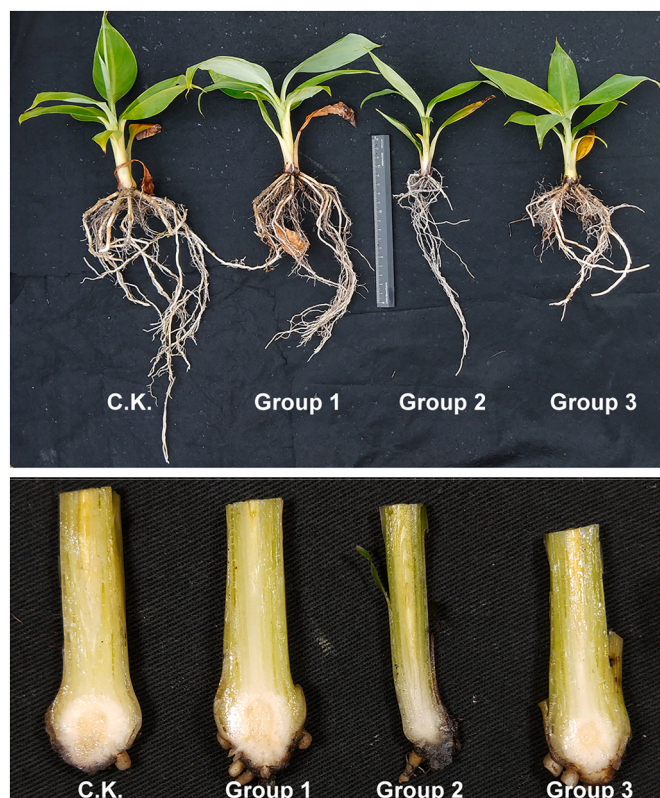


Fig. 5. Comparison of the growth of banana seedlings.

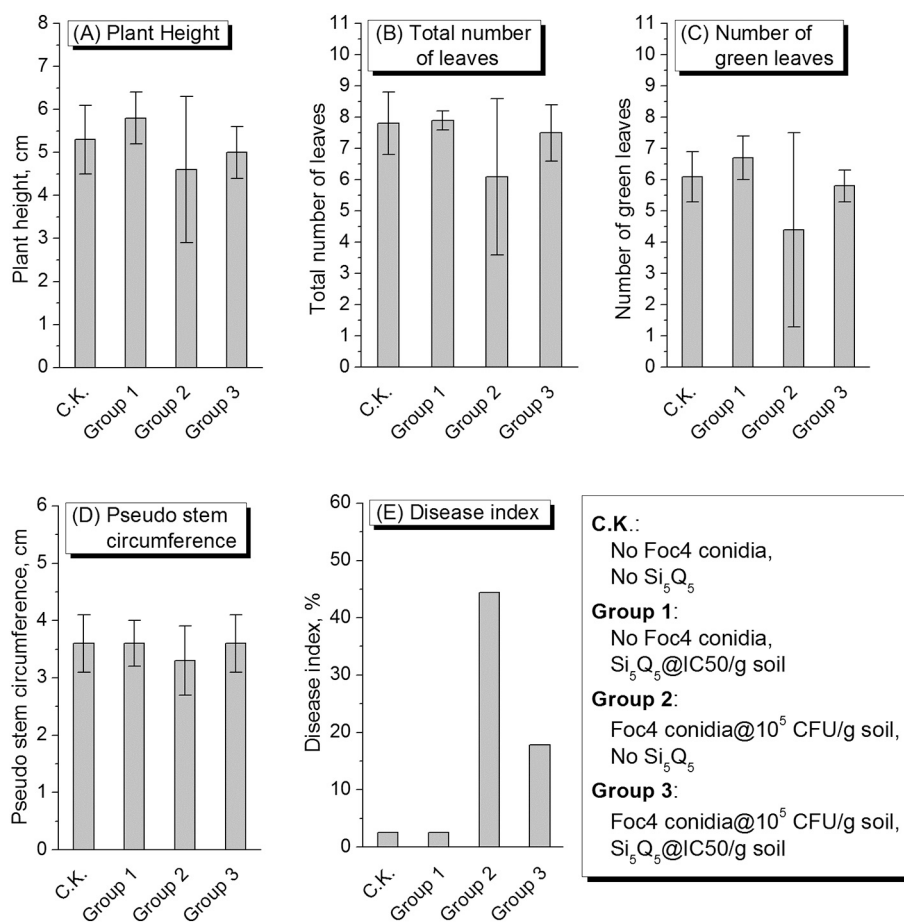


Fig. 6. The effect of Si_5Q_5 and Foc4 on banana seedlings based on pot experiments: (A) Plant height, (B) Total number of leaves, (C) Number of green leaves, (D) Pseudo stem circumference and (E) Disease index. (For interpretation of the references to colour in this figure legend, the reader is referred to the web version of this article.)

3.4. Pot experiments

The results of the pot experiment are shown in Figs. 5 and 6. From the results of banana plant height, total leaf number, green leaf number, pseudo stem circumference and disease index, it could be seen that the growth of banana seedlings treated with Si_5Q_5 at $1\text{C}_{50}/\text{g}$ soil (**Group 1**) showed no difference from those obtained with the water control (CK), indicating that Si_5Q_5 with a concentration of $1\text{C}_{50}/\text{g}$ soil will not cause phytotoxicity to banana seedlings. The disease index of banana seedlings treated with Foc4 conidia of 10^5 CFU/g soil (**Group 2**) reached 44.4%, and that of banana seedlings treated with Si_5Q_5 (**Group 3**) was 17.8%. As shown in Fig. 5, the Foc4 conidia-treated banana seedlings (**Group 2**) grew shorter, the stems were thinner, and the cut corms were dark brown, while those of the other groups grew healthy, and the cut corms had no brown or dark brown lesions, indicating that Si_5Q_5 did not harm banana seedlings and could reduce the infection of banana seedlings by Fusarium wilt.

From left to right: **CK** (No Foc4 conidia, No Si_5Q_5), **Group 1** (No Foc4 conidia, Si_5Q_5 @ $1\text{C}_{50}/\text{g}$ soil), **Group 2** (Foc4 conidia @ 10^5 CFU/g soil, No Si_5Q_5), and **Group 3** (Foc4 conidia @ 10^5 CFU/g soil, Si_5Q_5 @ $1\text{C}_{50}/\text{g}$ soil).

4. Conclusions

Taken together, the results of this study show that polydimethylsiloxane-polymethacrylate block copolymers containing quaternary ammonium salts, i.e., PDMS-*b*-QPMAEMA (Si_xQ_5), are fungicidally effective against Foc4; Si_xQ_5 exhibits easy soil adsorption in

soil and does not move in soil, which makes it unlikely to flow into groundwater and cause water pollution. The inhibitory effect of Si_xQ_5 on Foc4 can be maintained for 30 d under continuous inoculation of Foc4 into soil (every 2 d) or remains active in the soil for 90 d under continuous inoculation of Foc4 (every 10 d), which reflects the stability of Si_xQ_5 in soil and shows its potential application in banana fields to prevent the invasion of Foc4 conidia over the long term. Although Si_xQ_5 could inhibit Foc4 conidia in soil effectively and showed a certain inhibitory effect on actinomycetes, it had no obvious inhibitory effect on culturable total fungal and bacterial populations, which are conducive to improving soil fertility. Pot experiments showed that Si_5Q_5 had a good control effect on banana Fusarium wilt and did not harm banana seedlings.

We hope that the study of PDMS-*b*-QPMAEMA in soil can provide a new way to protect soil from banana Fusarium wilt and eradicate the banana wilt pathogen in diseased soil to promote the healthy and steady development of the banana industry.

Data availability

All data included in this study are available from the corresponding author upon request.

Declaration of Competing Interest

The authors declare that they have no known competing financial interests or personal relationships that could have appeared to influence the work reported in this paper.

Acknowledgments

This work was supported by the Science and Technology Program of Guangzhou, China, under grants 201803020015; the National Natural Science Foundation of China under grant 31772202; and the Science and Technology Planning Project of Guangdong Province, China under grant 2016A020210105.

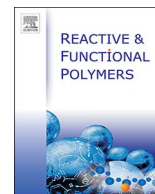
Appendix A. Supplementary data

Supplementary data to this article can be found online at <https://doi.org/10.1016/j.reactfunctpolym.2021.104848>.

References

- [1] R. Ploetz, *Fusarium wilt of banana is caused by several pathogens referred to as Fusarium oxysporum f. sp. cubense*, *Phytopathology* 96 (2006) 653–656.
- [2] Z. Shen, B. Wang, J. Zhu, H. Hu, C. Tao, Y. Ou, X. Deng, N. Ling, R. Li, Q. Shen, Lime and ammonium carbonate fumigation coupled with bio-organic fertilizer application steered banana rhizosphere to assemble a unique microbiome against Panama disease, *Microb. Biotechnol.* 12 (2019) 515–527.
- [3] I. Buddenhagen, Understanding strain diversity in *Fusarium oxysporum f. sp. cubense* and history of introduction of “tropical race 4” to better manage banana production, *ISHS Acta Hort.* 828 (2009) 193–204.
- [4] B. Huang, D. Yan, X. Wang, X. Wang, W. Fang, D. Zhang, C. Ouyang, Q. Wang, A. Cao, Soil fumigation alters adsorption and degradation behavior of pesticides in soil, *Environ. Pollut.* 246 (2019) 264–273.
- [5] L. Zhang, T. Yuan, Y. Wang, D. Zhang, T. Bai, S. Xu, Y. Wang, W. Tang, S. Zheng, Identification and evaluation of resistance to *Fusarium oxysporum f. sp. cubense* tropical race 4 in *Musa acuminata* Pahang, *Euphytica* 214 (2018) 106.
- [6] R. Ploetz, S. Freeman, J. Konkola, A. Al-Abed, Z. Naser, K. Shalan, R. Barakat, Y. Israeli, Tropical race 4 of Panama disease in the Middle East, *Phytoparasitica* 43 (2015) 283–293.
- [7] J.M. Raaijmakers, T.C. Paulitz, C. Steinberg, C. Alabouvette, Y. Moënné-Loccoz, The rhizosphere: a playground and battlefield for soilborne pathogens and beneficial microorganisms, *Plant Soil* 321 (2009) 341–361.
- [8] D. Zhang, X. Ji, Z. Meng, W. Qi, K. Qiao, Effects of fumigation with 1,3-dichloro-propene on soil enzyme activities and microbial communities in continuous-cropping soil, *Ecotoxicol. Environ. Saf.* 169 (2019) 730–736.
- [9] D. Zhou, T. Jing, Y. Chen, F. Wang, D. Qi, R. Feng, J. Xie, H. Li, Deciphering microbial diversity associated with *Fusarium wilt*-diseased and disease-free banana rhizosphere soil, *BMC Microbiol.* 19 (2019) 161.
- [10] B. Dizman, M.O. Elasm, L.J. Mathias, Synthesis and antibacterial activities of water-soluble methacrylate polymers containing quaternary ammonium compounds, *J. Polym. Sci. A* 44 (2006) 5965–5973.
- [11] C. Abbate, M. Arena, A. Baglieri, M. Gennari, Effects of organoclays on soil eubacterial community assessed by molecular approaches, *J. Hazard. Mater.* 168 (2009) 466–472.
- [12] C. Dong, W. You, R. Liuyang, Y. Lei, A. Zhang, Y. Lin, Anti-*Rhizoctonia solani* activity by polymeric quaternary ammonium salt and its mechanism of action, *React. Funct. Polym.* 125 (2018) 1–10.
- [13] J.V. Nye, W.F. Guerin, S.A. Boyd, Heterotrophic activity of microorganisms in soils treated with quaternary ammonium compounds, *Environ. Sci. Technol.* 28 (1994) 944–951.
- [14] B. Sarkar, M. Megharaj, Y. Xi, G.S.R. Krishnamurti, R. Naidu, Sorption of quaternary ammonium compounds in soils: implications to the soil microbial activities, *J. Hazard. Mater.* 184 (2010) 448–456.
- [15] C. Zhang, F. Cui, G. Zeng, M. Jiang, Z. Yang, Z. Yu, M. Zhu, L. Shen, Quaternary ammonium compounds (QACs): a review on occurrence, fate and toxicity in the environment, *Sci. Total Environ.* 518–519 (2015) 352–362.
- [16] W. Zhong, C. Dong, R. Liuyang, Q. Guo, H. Zeng, Y. Lin, A. Zhang, Controllable synthesis and antimicrobial activities of acrylate polymers containing quaternary ammonium salts, *React. Funct. Polym.* 121 (2017) 110–118.
- [17] Y. Lin, W. Zhong, C. Dong, C. Zhang, X. Feng, A. Zhang, Synthesis and antifungal activities of amphiphilic PDMS-b-QPDMAEMA copolymers on *Rhizoctonia solani*, *ACS Appl. Bio Mater.* 1 (2018) 2062–2072.
- [18] P. Deltour, S.C. Franca, O.L. Pereira, I. Cardoso, S. De Neve, J. Debode, M. Hofte, Disease suppressiveness to *Fusarium wilt* of banana in an agroforestry system: influence of soil characteristics and plant community, *Agric. Ecosyst. Environ.* 239 (2017) 173–181.
- [19] Y. Lin, Q. Liu, L. Cheng, Y. Lei, A. Zhang, Synthesis and antimicrobial activities of polysiloxane-containing quaternary ammonium salts on bacteria and phytopathogenic fungi, *React. Funct. Polym.* 85 (2014) 36–44.
- [20] S. Rzaşa, W. Owczarzak, Methods for the granulometric analysis of soil for science and practice, *Polish J. Soil Sci.* 46 (2013) 1–50.
- [21] J. Huang, Y. Pang, F. Zhang, Q. Huang, M. Zhang, S. Tang, H. Fu, P. Li, Suppression of *Fusarium wilt* of banana by combining acid soil ameliorant with biofertilizer made from *Bacillus velezensis* H-6, *Eur. J. Plant Pathol.* 154 (2019) 585–596.
- [22] Z.T. Gong, Z.C. Chen, G.L. Zhang, World soil resource reference base (WRB): establishment and development, *Soils* 4 (2003) 271–278.
- [23] Z. Huang, R. Liuyang, C. Dong, Y. Lei, A. Zhang, Y. Lin, Polymeric quaternary ammonium salt activity against *Fusarium oxysporum f. sp. cubense* race 4: synthesis, structure-activity relationship and mode of action, *React. Funct. Polym.* 114 (2017) 13–22.
- [24] OECD, Test No. 106: Adsorption - Desorption Using a Batch Equilibrium Method, OECD Publishing, Paris, 2000.
- [25] A.H. Khan, S.M. Macfie, M.B. Ray, Sorption and leaching of benzalkonium chlorides in agricultural soils, *J. Environ. Manag.* 196 (2017) 26–35.
- [26] M. Piri, E. Sepehr, Z. Rengel, Citric acid decreased and humic acid increased Zn sorption in soils, *Geoderma* 341 (2019) 39–45.
- [27] J.F. Guo, G.N. Zhu, J.J. Shi, J.H. Sun, Adsorption, desorption and mobility of fomesafen in Chinese soils, *Water Air Soil Pollut.* 148 (2003) 77–85.
- [28] S. Li, Y. Sun, T. Yang, W. Huangpu, Relationship between mobility factors (Rf) of two hydrophobic termiticides and selected field and artificial soil parameters, *Sci. Total Environ.* 388 (2007) 206–213.
- [29] J. Jiang, Y. Xiong, H. Jiang, D. Ye, Y. Song, F. Li, Soil microbial activity during secondary vegetation succession in semiarid abandoned lands of loess plateau, *Pedosphere* 19 (2009) 735–747.
- [30] H.X. Peng, K. Sivasithamparan, D.W. Turner, Chlamydoconidia germination and *Fusarium wilt* of banana plantlets in suppressive and conducive soils are affected by physical and chemical factors, *Soil Biol. Biochem.* 31 (1999) 1363–1374.
- [31] T. Wen, X. Huang, J. Zhang, T. Zhu, L. Meng, Z. Cai, Effects of water regime, crop residues, and application rates on control of *Fusarium oxysporum f. sp. cubense*, *J. Environ. Sci.* 31 (2015) 30–37.
- [32] Z. Shen, C.R. Penton, N. Lv, C. Xue, X. Yuan, Y. Ruan, R. Li, Q. Shen, Banana *Fusarium wilt* disease incidence is influenced by shifts of soil microbial communities under different monoculture spans, *Microb. Ecol.* 75 (2018) 739–750.
- [33] F. Sopena, C. Maqueda, E. Morillo, Formulation affecting alachlor efficacy and persistence in sandy soils, *Pest Manag. Sci.* 65 (2009) 761–768.
- [34] J.C. Sherris, Problems in vitro determination of antibiotic tolerance in clinical isolates, *Antimicrob. Agents Chemother.* 30 (1986) 633–637.
- [35] R. Swisher, G.C. Carroll, Fluorescein diacetate hydrolysis as an estimator of microbial biomass on coniferous needle surfaces, *Microb. Ecol.* 6 (1980) 217–226.
- [36] B. Sylvie, T. Pierre, B. Martine, J. Anne, Emergence of resistance to antibacterial agents: the role of quaternary ammonium compounds—a critical review, *Int. J. Antimicrob. Agents* 39 (2012) 381–389.
- [37] Y. Gou, M.M. Meghil, C.R. Pucci, L. Breschi, D.H. Pashley, C.W. Cutler, L. Niu, J. Li, F.R. Tay, Optimizing resin-dentin bond stability using a bioactive adhesive with concomitant antibacterial properties and anti-proteolytic activities, *Acta Biomater.* 75 (2018) 171–182.
- [38] Y. Jiao, L. Niu, S. Ma, J. Li, F.R. Tay, J. Chen, Quaternary ammonium-based biomedical materials: state-of-the-art, toxicological aspects and antimicrobial resistance, *Prog. Polym. Sci.* 71 (2017) 53–90.
- [39] S. Liu, L. Tonggu, L. Niu, S. Gong, B. Fan, L. Wang, J. Zhao, C. Huang, D.H. Pashley, F.R. Tay, Antimicrobial activity of a quaternary ammonium methacryloxy silicate-containing acrylic resin: a randomised clinical trial, *Sci. Rep.* 6 (2016) 21882.
- [40] B.H. Hameed, I.A.W. Tan, A.L. Ahmad, Adsorption isotherm, kinetic modeling and mechanism of 2,4,6-trichlorophenol on coconut husk-based activated carbon, *Chem. Eng. J.* 144 (2008) 235–244.
- [41] G. Pataklioutas, T.A. Albanis, Adsorption-desorption studies of alachlor, metolachlor, EPTC, chlorothalonil and pirimiphos-methyl in contrasting soils, *Pest Manag. Sci.* 58 (2002) 352–362.
- [42] W.C. Koskinen, D.M. Stone, A.R. Harris, Sorption of hexazinone, sulfometuron methyl, and tebutiuron on acid, low base saturated sands, *Chemosphere* 32 (1996) 1681–1689.
- [43] Z.Z. Ismail, U. Tezel, S.G. Pavlostathis, Sorption of quaternary ammonium compounds to municipal sludge, *Water Res.* 44 (2010) 2303–2313.
- [44] L. Xiang, T. Sun, M. Zheng, Y. Li, H. Li, M. Wong, Q. Cai, C. Mo, Sorption of dodecyltrimethylammonium chloride (DTAC) to agricultural soils, *Sci. Total Environ.* 560 (2016) 197–203.
- [45] M. Clara, S. Scharf, C. Scheffknecht, O. Gans, Occurrence of selected surfactants in untreated and treated sewage, *Water Res.* 41 (2007) 4339–4348.
- [46] A.F. Cirelli, C. Ojeda, M.J.L. Castro, M. Salgot, Surfactants in sludge-amended agricultural soils: a review, *Environ. Chem. Lett.* 6 (2008) 135–148.
- [47] A.C. Das, D. Mukherjee, Insecticidal effects on soil microorganisms and their biochemical processes related to soil fertility, *World J. Microbiol. Biotechnol.* 14 (1998) 903–909.
- [48] P.B. Hatzinger, M. Alexander, Effect of aging of chemicals in soil on their biodegradability and extractability, *Environ. Sci. Technol.* 29 (1995) 537–545.
- [49] I. Ferrer, E.T. Furlong, Accelerated solvent extraction followed by on-line solid-phase extraction coupled to ion trap LC/MS/MS for analysis of benzalkonium chlorides in sediment samples, *Anal. Chem.* 74 (2002) 1275–1280.
- [50] U. Tezel, J.A. Pierson, S.G. Pavlostathis, Fate and effect of quaternary ammonium compounds on a mixed methanogenic culture, *Water Res.* 40 (2006) 3660–3668.
- [51] M.T. Garcia, I. Ribosa, T. Guindulain, J. Sanchez-Leal, J. Vives-Rego, Fate and effect of monoalkyl quaternary ammonium surfactants in the aquatic environment, *Environ. Pollut.* 111 (2001) 169–175.
- [52] M.T. Garcia, E. Campos, J. Sánchez-Leal, I. Ribosa, Anaerobic degradation and toxicity of commercial cationic surfactants in anaerobic screening tests, *Chemosphere* 41 (2000) 705–710.
- [53] A. Zhang, Q. Liu, Y. Lei, S. Hong, Y. Lin, Synthesis and antimicrobial activities of acrylamide polymers containing quaternary ammonium salts on bacteria and phytopathogenic fungi, *React. Funct. Polym.* 88 (2015) 39–46.
- [54] C.K.V.Z. Abid, S. Jain, R. Jakeray, S. Chattopadhyay, H. Singh, Formulation and characterization of antimicrobial quaternary ammonium dendrimer in poly(methyl methacrylate) bone cement, *J. Biomed Mater Res B Appl Biomater* 105 (2017) 521–530.

- [55] G. Jing, Z. Zhou, J. Zhuo, Quantitative structure-activity relationship (QSAR) study of toxicity of quaternary ammonium compounds on *Chlorella pyrenoidosa* and *Scenedesmus quadricauda*, *Chemosphere*. 86 (2012) 76–82.
- [56] W. Jiang, C. Xu, S. Jiang, T. Zhang, S. Wang, B. Fang, Establishing a mathematical equations and improving the production of l-tert-leucine by uniform design and regression analysis, *Appl. Biochem. Biotechnol.* 181 (2017) 1454–1464.
- [57] M. Tandukar, S. Oh, U. Tezel, K.T. Konstantinidis, S.G. Pavlostathis, Long-term exposure to benzalkonium chloride disinfectants results in change of microbial community structure and increased antimicrobial resistance, *Environ. Sci. Technol.* 47 (2013) 9730–9738.
- [58] K. Fang, *Orthogonal and Uniform Experimental Design*, Science Press of China, 2001 (in Chinese).
- [59] Q. Xiao, H. Yan, Y. Wei, Y. Wang, F. Zeng, X. Zheng, Optimization of H₂O₂ dosage in microwave-H₂O₂ process for sludge pretreatment with uniform design method, *J. Environ. Sci.* 24 (2012) 2060–2067.
- [60] W. Zhong, Y. Chang, Y. Lin, A. Zhang, Synthesis and antifungal activities of hydrophilic cationic polymers against *Rhizoctonia solani*, *Fungal Biol.* 124 (2020) 735–741.



Anti-*Rhizoctonia solani* activity by polymeric quaternary ammonium salt and its mechanism of action

Chenyun Dong^a, Wanling You^a, Ruqi Liuyang^a, Yufeng Lei^b, Anqiang Zhang^{b,*}, Yaling Lin^{a,*}

^a College of Materials and Energy, South China Agricultural University, 483 Wushan Rd., Guangzhou 510642, Guangdong, China

^b College of Material Science and Engineering, South China University of Technology, 381 Wushan Rd., Guangzhou 510641, Guangdong, China

ARTICLE INFO

Keywords:

Acrylamide quaternary ammonium salt
Antifungal bioassay
Mechanism of antifungal action
Rhizoctonia solani

ABSTRACT

Polymeric quaternary ammonium salts (PQASs) exhibit antibacterial action and are less toxic, less stimulatory to the human body and have easier-to-modify functionalities than small molecular antibacterial agents. However, few studies on the structure-activity relationship and toxicity mechanism of PQASs against fungi have been reported. We previously described the synthesis of a novel PQAS, namely, a homopolymer of (2-methacrylamido)propyltetraethylammonium chloride (PQD-BC), and discovered that the polymer exhibits antifungal activities not only against *Fusarium oxysporum* f. sp. *Cubense* tropical race 4 (Foc 4), the pathogen of banana wilt, but also against *Rhizoctonia solani* (*R. solani*), the pathogen of rice sheath blight (RShB). Furthermore, we studied the mechanism of action of PQD-BC against Foc 4, which is markedly different from *R. solani* in morphology and life cycle. Therefore, the structure-antifungal activity relationship and toxicity mechanism of PQD-BC against *R. solani* were extensively studied in this work and compared with those of the low-molecular-weight quaternary ammonium salt benzyltrimethylammonium chloride (BC), and the results play an important role in identifying long-term and low-toxicity fungicides that can suppress the sclerotia of *R. solani*. The results showed that PQD-BC and BC can destroy the structural integrity and morphology of a cell, such as by loss of the cell wall and plasma membrane integrity, leading to the release of intracellular contents and can induce mitochondrial dysfunction and interference with genomic DNA and inhibit the formation of sclerotia. However, PQD-BC showed a special mechanism for causing the lipid peroxidation of the cell membrane; this mechanism was not observed with BC. The newly elucidated mechanism accounts for differences between polymers and small-molecule compounds and provides a theoretical basis for further application of PQAS against fungi and sclerotia.

1. Introduction

Rice, one of the primary staple food on earth, is subject to many diseases that often place major biological constraints on production. Rice sheath blight (RShB), a pervasive rice disease occurring throughout temperate and tropical production systems, is caused by *Rhizoctonia solani* (*R. solani*) Kühn, among which AG-1(IA) is the strongest and most harmful strain. Although the pathogen is soil borne, RShB develops into a major production limitation in an alarmingly brief timespan [1]. It has been reported to reduce yield by 15% - 44% in Texas, USA [2]. The most important factor for RShB epidemic is the formation of sclerotia. As the dormant structures of fungi, sclerotia are hard, asexual and resistant to unfavorable conditions as well as to chemical and biological degradation [3–6]. The high capability of sclerotial survival may be related to its special double layer [7] and secreted melanin [8]. The mycelia of *R. solani* forms sclerotia to survive

in soil when host plants are removed and the sclerotia germinate and infect new plants in the next growing season [3–6]. This cycle can follow on all the while. Without breaking the cycle, RShB is difficult to eradicate.

To date, the methods of controlling RShB mainly involve agricultural, biological and chemical managements. Agricultural managements which control RShB directly, such as salvage sclerotia [9], crop rotation [10] and duck-rice system [11,12], require a lot of time and manpower. Biological managements exploit microbes, such as *Trichoderma* [13], *Bacillus* [14] and *Pseudomonas* [15], to inhibit mycelial growth of *R. solani*. Their inhibiting effects are reported as evident and friendly to environment. However, the field application of microbes tends to be susceptible to other factors, and hard to achieve the laboratory effect. Chemical antimicrobial agents are the most adopted. Management of RShB using chemical agents has focused on killing hypha and preventing the formation of sclerotia, such as New-Ag-

* Corresponding authors.

E-mail addresses: aqzhang@scut.edu.cn (A. Zhang), linyaling@scau.edu.cn (Y. Lin).

<https://doi.org/10.1016/j.reactfunctpolym.2018.01.020>

Received 29 July 2017; Received in revised form 23 January 2018; Accepted 25 January 2018

Available online 01 February 2018

1381-5148/ © 2018 Elsevier B.V. All rights reserved.

antibiotic 702 [16] and *validamycin* [17]. Nevertheless, no methods have been reported to completely inhibit the growth of mycelia and the germination of *R. solani* sclerotia, especially from the aspect of taking advantage of functional polymers.

Quaternary ammonium salts (QASs) have been widely used as small molecular biocides with several advantages over other antibacterial agents, including excellent cell membrane penetration properties, lower toxicity, less skin irritation, better environmental stability, extended residence time and enhanced biological activity. Polymeric quaternary ammonium salts (PQASs) exhibit greater antimicrobial activities than the corresponding small molecular QASs. The higher activity of polymeric PQASs has been interpreted as follow: the net positive charge of PQASs and the net negative charge of bacterial cell membranes provide a stronger driving force for the initial attraction of the PQASs to the cell surface. After the PQASs bind to the negatively charged phospholipid, their hydrophobic moieties interact with the inner hydrophobic core of the bacterial membrane, leading to a disruption of the cytoplasmic membrane and a release of potassium and other constituents, which eventually causes cell death. Therefore, PQASs can be firmly adsorbed onto the surface of negatively charged surfaces, effectively restraining bacteria [18–20].

In addition, compared with small molecular compounds, functional polymers' properties can be manipulated through changes in their structure. PQASs can then be grafted from a hydrophilic group or hydrophobic groups and endowed with amphiphilicity. These materials not only deliver steric stabilization in solid dispersions and generate controlled surface structures upon arrangement of materials but also modify interfacial properties such as wetting and lubrication [21,22]. These properties might offer a path for inhibiting the germination of sclerotia, thereby controlling RShB epidemics.

Previously, we have revealed the antifungal activity of polymeric QAS against phytopathogenic fungi, including *Fusarium oxysporum* f. sp. *Cubense* tropical race 4 (Foc 4) and *R. solani* [19,20,23]. Foc 4 is the pathogen of fusarium wilt of banana, which can produce spores by asexual reproduction [23,24]. However, *R. solani* and Foc 4 belong to different classes and have different morphologies and life cycles. *R. solani* strains are reported to be tiny, multinucleated, seldom producing spores and infecting host plants by mycelia and sclerotia [1]. Therefore, the antifungal mechanism of the functional polymer against *R. solani* remains undiscovered, as well as the difference in the antifungal mechanism between PQASs and small molecular counterparts against filamentous fungi.

In this paper, poly((2-methacrylamido)propyl)tetra-benzyl-dimethylammonium chloride (PQD-BC) is synthesized (Scheme 1) [19], and its activities and mechanisms against the mycelial growth and sclerotial formation of *R. solani* AG-1(IA) are investigated and compared with those of a commercially available small-molecular QAS, benzalkonium chloride (BC), to provide a clearer direction for the application of polymeric antifungal agents and new choices for controlling RShB.

2. Experimental

2.1. Materials

Bovine serum albumin (BSA) was provided by Hangzhou Sijiqing Biological Engineering Materials Co. Ltd. (Hangzhou, China). 2,3,5-Triphenyltetrazolium chloride (TTC) and an Ezup Column Fungi Genomic DNA Purification Kit were purchased from Sangon Biotech

(Shanghai) Co., Ltd. (Shanghai, China). Propidium iodide (PI) was supplied by Aladdin Reagent Co. Ltd. (Shanghai, China). The fungal strain used in this study is *Rhizoctonia solani* Kühn AG-1(IA), which was donated by the Fungi Laboratory at the South China Agriculture University and was maintained on potato dextrose agar (PDA). *R. solani* mycelial suspensions were obtained from the surface of the agar after culturing for 2 days at 28 °C. The concentration of the mycelial suspensions was determined using a hemocytometer. Benzyl-dimethyl-dodecylammonium chloride (BC) with a purity > 99% was purchased from Shanghai Aladdin Bio-Chem Technology Co., Ltd. (Shanghai, China). Alkaline phosphatase (ALP), malondialdehyde (MDA) and succinate dehydrogenase (SDH) kits were purchased from the Nanjing Jiancheng Institute of Bioengineering (Nanjing, Jiangsu, China). A mitochondrial isolation kit and GoldView™ were purchased from the Beijing Solarbio Science & Technology Co. Ltd., Beijing, China. PQD-BC was synthesized using radical polymerization according to the method described in our previous study [19], the structure of PQD-BC and BC were shown in Scheme 1.

2.2. Antifungal bioassay

2.2.1. Mycelial growth inhibition

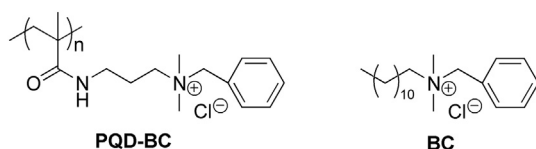
The antifungal efficiency of PQD-BC and BC on the mycelial growth of *R. solani* was measured using an *in vitro* mycelial growth inhibition assay [19]. Briefly, the compounds (PQD-BC and BC) were sterilized by passage through a 0.45 µm Millipore filter, diluted in different concentrations (PQD-BC: 0.25, 0.50, 0.75, 1.00, 1.25 and 1.5 mg/mL; BC: 0.015, 0.03, 0.045, 0.06, 0.075 and 0.2 mg/mL) and then mixed with molten agar (at a temperature > 60 °C); agar was diluted with distilled water for the control. Mycelial pieces (6 mm diameter) obtained from the periphery of 2-day-old cultures of *R. solani* were inverted on the center of each plate. Treated and untreated plates were incubated at 28 °C in triplicate. The efficacy of the treatment was determined by computing the average of two perpendicular diameters of each colony. The percent mycelial inhibition of the radial growth of the fungi by the compounds compared with the effect of the control was calculated at day 2 using the following formula:

$$\text{Percentage mycelial inhibition} = (D_c - D_t)/D_t \times 100\% \quad (1)$$

where D_c is the mean colony diameter of the control group and D_t is the mean colony diameter of the treatment group. Each measurement consisted of at least three replications.

2.2.2. Minimum inhibitory concentration (MIC)

The antimicrobial properties of the synthesized compounds were studied by the conventional procedure of broth microdilution with TTC. The TTC reagent is colorless; however, it gives off a bright-red color when reduced, indicating the presence of live fungi [25,26]. The fungistatic activity was characterized by the minimum inhibitory concentration (MIC) corresponding to the lowest serial dilution that resulted in the lack of visible microorganism growth. The synthetic compounds against *R. solani* were determined using *R. solani* cultured in sterile potato dextrose broth (PDB) medium for 3 days. Afterwards, the mycelia were suspended using a homogenizer. The sample solution (100 µL), in concentrations ranging from 5×10^{-3} to 0.3 mg/mL, was added to 96-well plates. The same volume of mycelial suspension containing approximately 10^5 – 10^6 CFU/mL was incubated at 28 °C for 2 days using a hemocytometer. Two control tests containing PDB medium supplemented with a tested strain and an equal volume of sterile PDB medium (negative control) were also performed. Then, 50 µL (5.0 mg/mL) of TTC solution (in PDB) was added to every well and the mycelia were cultured in the dark at 28 °C for another 2 h. The visual color changes were recorded before and after incubation to determine the MIC (mg/mL, present in the well). The color changes present in the well matched that in the blank well that was taken as the MIC for each fungus.



Scheme 1. Chemical structures of PQD-BC and BC.

2.2.3. Minimal fungicidal concentration (MFC)

In contrast to the MIC, the MFC of the synthetic compounds against *R. solani* was determined by the spot plate method. Aliquots from wells that appeared to contain few or no colonies were deposited and uniformly spread onto the agar surface of Petri dishes. Therefore, after the MIC experiment, 100 μ L of solution was collected from some wells and spotted onto the PDA plates. The PDA plates were cultured at 28 °C for 2 days. The lowest concentration of the samples that showed fewer than 5 growth colonies was assigned as the minimal fungicidal concentration (MFC) for each fungus.

2.3. Mechanism of antifungal action

2.3.1. Mycelial morphology and biomass assay

The morphology of mycelium treated with different concentrations of synthetic compounds (PQD-BC and BC) was observed by light microscopy. *R. solani* was cultured in PDB and rotated at 28 °C on a rotary shaker at 120 rpm for 3 days; it was then supplemented by three different concentrations of compounds (MIC, IC₅₀ and IC₉₀). After treatment for 48 h, the mycelia were harvested and moved to a glass slide, which was then covered by a slip and examined under a fluorescence microscope (Nikon Eclipse 80i, Japan), and the images were captured through a charge-coupled device camera. The dry weights (biomass) of mycelia were measured after drying for 6 h at room temperature. The data were based on three replicates.

2.3.2. Cell-wall disruption assay

The cell-wall integrity was expressed as the increased alkaline phosphatase (ALP) of the medium after compound treatments [27]. The mycelia of *R. solani* were prepared by being cultured in PDB medium (45 mL) and rotated at 28 °C on a rotary shaker at 120 rpm for 3 days. Afterward, the PDB medium supplemented with 5 mL of three different concentrations (MIC, IC₅₀, and IC₉₀) of polymers (PQD-BC and BC) was incubated under the same conditions for another 48 h in triplicate. The PDB medium added to the same volume of sterile distilled water was used as a control. The suspensions were obtained from the supernatants after being centrifuged at 4000 g for 10 min. An ALP kit was used to determine the effects of the polymers on the cell wall. The activity of ALP (A_{ALP}) in the supernatant was measured by a UV-vis spectrophotometer at 405 nm according to the manufacturer's instructions [27]. The activity of ALP was calculated according to the following formulas:

$$A_{ALP} = (\Delta OD_t - \Delta OD_b) \times F \quad (2)$$

$$F = (V \times 1000) / (V_s \times \varepsilon \times 1.0) \quad (3)$$

where ΔOD_t is the increase in OD (optical density, conceptually and numerically equivalent to absorbance) at 504 nm of the treated-sample after 1 min, ΔOD_b is the increase in OD of the reagent under the same conditions, V is the total volume (mL) of the reaction, V_s is the volume (mL) of the sample and ε is the molar extinction coefficient. The molar extinction coefficient of 4-nitrophenol at 504 nm is 18.5. The 1000 is the conversion coefficient from U/mL to U/L and 1.0 is the path length of the cuvette.

2.3.3. Cytoplasmic membrane disruption assay

To observe the effect of polymers against the plasma membrane integrity, we cultured *R. solani* in a sterile PDB medium at 28 °C on a rotary shaker at 120 rpm for 3 days. After that, 5 mL of three different concentrations (MIC, IC₅₀ and IC₉₀) of synthetic compounds (PQD-BC and BC) were added to PDB medium; the control was treated with the same quantity of sterile distilled water. Following incubation under constant shaking at 28 °C for 48 h in triplicate, the small amount of mycelia which was picked by tweezers, soaked in 1 mL of PBS and centrifuged at 10,000 rpm for 5 min; it was then washed twice with PBS (pH 7.4) on a rotary shaker. Next, 10 μ L of mycelia suspension was

mixed with 15 μ M of the red fluorescent nucleic acid stain PI, which is commonly used for detecting cellular membrane integrity [28], and placed in the dark for 1 h. To remove the PI, the medium was washed five times with PBS on a rotary shaker, and finally re-suspended in 100 μ L of PBS. The sample (5 μ L) was moved onto a glass slide and then covered with a slip, sealed, and observed under the oil objective (100 \times) of fluorescence microscope (Nikon Eclipse 80i, Japan). Excited by lasers at 543 nm, PI emissions were collected using a long-pass filter for PI at 590–800 nm. The images were captured using a charge-coupled device camera. Three fields of view were chosen randomly from each cover slip.

2.3.4. Cellular leakage assay

Membrane permeability was determined by the leakage level of cytoplasmic materials in the culture as a result of disruption of the fungal wall/membrane [29]. *R. solani* was grown in PDB medium in triplicate under shaking for 3 days at 28 °C. Then, the mycelia were harvested and washed twice with PBS (pH 7.4) using a Büchner funnel. The mass-washed mycelia were re-suspended in a 50 mL solution containing test compounds (PQD-BC and BC) diluted to three concentrations (MIC, IC₅₀, and IC₉₀) and were then incubated under shaking for another 24 h. Two control samples were prepared. One was treated with the same quantity of sterile distilled water, and the other was supplemented with three different concentrations of compounds (MIC, IC₅₀, and IC₉₀). Samples from the suspensions were collected and filtered at 2 h intervals during the incubation. The filtered solutions were used to determine the leakage of soluble proteins, carbohydrates and nucleic acids. A Bradford assay was performed to quantify the release of the proteins on the basis of the different concentrations of BSA as the standard [30]. Soluble carbohydrates were detected by the anthrone reaction, which uses glucose as the standard [31]. The electric conductivity of the resulting supernatant was measured using a conductivity meter (DDS-11A, Shanghai Precision Scientific Instrument Co., Ltd., Shanghai, China) [27].

2.3.5. Lipid peroxidation analysis

The lipid peroxidation in the cell membrane of *R. solani* was quantified on the basis of its malondialdehyde (MDA) levels [31–33]. The mycelia of *R. solani* were prepared by being cultured in PDB medium (45 mL) and rotated at 28 °C on a rotary shaker at 120 rpm for 3 days. The PDB medium was then mixed with three different concentrations (IC₉₀ \times 0.5, IC₉₀, and IC₉₀ \times 2) of compounds (PQD-BC and BC) and incubated under shaking for 24 h at 28 °C; no compounds were added in the control group. The fungal suspensions were centrifuged at 12,000 rpm for 5 min, and the pellet was then sonicated twice on ice with lysis buffer (2% Triton- \times 100, 1% SDS, 100 mM NaCl, 10 mM Tris-HCl, 1 Mm EDTA [pH 8.0]) and quartz sand in 5% trichloroacetic acid (TCA). After centrifugation, the supernatant of the fungal suspension was used as a crude MDA-mycelial solution. The MDA contents of the mycelia and medium were determined according the manufacturer's instructions provided with the MDA kit. MDA can react with freshly prepared thiobarbituric acid to form a colored complex, which has a maximum absorbance at 532 nm in a UV-vis spectrophotometer (UV2300, Techcomp, Shanghai, China) [31]. Each experiment was performed three times. The content of MDA was calculated using the following equation:

$$MDA = \Delta OD_t / \Delta OD_b \times Cr \times DF \quad (4)$$

where ΔOD_t is the reduction of the OD value of the treated sample after 1 min, ΔOD_b is the increase of the OD value of the reagent from the MDA kit after 1 min, Cr is the concentration of standard substance in the MDA kit (10 nmol/mL), and DF is the dilution factor of the sample before being tested. The MDA content was expressed as mmol per gram of mycelia.

2.3.6. Effect on mitochondrial function

The mitochondrial function of *R. solani* was expressed by the intracellular enzyme succinate dehydrogenase (SDH) activity (A_{SDH}) [29]. The mycelia of *R. solani* were prepared by being cultured in PDB medium (45 mL) and rotated at 28 °C on a rotary shaker at 120 rpm for 3 days. The PDB medium was then mixed with three different concentrations (MIC, IC_{50} and IC_{90}) of compounds (PQD-BC and BC) and incubated under shaking for 24 h at 28 °C; the same quantity of sterile distilled water was added to the PDB medium for the control group. After filtration, the mycelia were ground into powder under liquid nitrogen and used to isolate mitochondria with a mitochondrial isolation kit. The A_{SDH} was determined using the SDH kits and measured by UV–vis spectrophotometry at 600 nm. The total protein content was determined by the Bradford method [30]. Afterwards, the amount of protein was calculated according to the standard protein curve, which was measured with different concentrations of a protein standard. The A_{SDH} was calculated using the following equation:

$$A_{SDH} = (\Delta OD_{600}/100)/(C_s/10) \times 100\% \quad (5)$$

where ΔOD_{600} is the OD value of the sample and C_s is the protein concentration (mg/mL). One unit of SDH activity was defined as the amount of enzyme in 1 mL of fungal suspension after a 1 min reaction time that gave a reduction by 0.01 absorbance unit compared to the control reaction. Each treatment was performed in triplicate.

2.3.7. In vitro electrophoretic mobility shift assay (EMSA)

The DNA-binding activities of genomic DNA and the compounds were assessed by EMSA, which is widely used to research antimicrobial drugs, and is based on the observation that bound DNA complexes migrate through gels more slowly than unbound DNA fragments [34,35]. To obtain a significant amount of highly purified genomic DNA, *R. solani* was grown in PDB medium in triplicate under shaking for 3 days at 28 °C. The mycelia were then harvested and washed twice with PBS (pH 7.4) by Büchner funnel to remove the PDB medium. After the sample was freeze-dried, the total intracellular DNA was extracted with an Ezup Column Fungi Genomic DNA Purification Kit, and RNase was added. Genomic DNA being sufficiently free of protein gave a UV absorbance ratio of 1.8–2.0 at 260 and 280 nm (A_{260}/A_{280}). A total of 5 µg of highly purified genomic DNA in a fixed concentration (500 µg/mL) was mixed with the TE buffer (10 mM Tris-HCl + 1 mM EDTA, pH 8.0) treated with the compounds (PQD-BC and BC) at three different concentrations (MIC, IC_{50} , and IC_{90}). The addition of the same volume of PBS (pH 7.4) was set as the control test. Treated and untreated tests were incubated at room temperature for 10 min in triplicate. Agarose gel electrophoresis was used to examine the interaction between the compounds and genomic DNA; the TE buffer was incubated alone with DNA in the control. A 5 µL volume of GoldView™ was used as a fluorescent dye, and 1 mg of DNA was loaded onto the 1% gel; electrophoresis was performed in TAE (tris acetate EDTA) buffer for 20 min. The gel was visualized under UV light using a Bio-Rad Trans illuminator IEC 1010.

2.3.8. In vivo efficacy on genomic DNA

On the basis of the *in vitro* EMSA, to further confirm that genomic DNA combined with compounds in the agarose gel electrophoresis and to investigate whether the compounds penetrated the cell barriers and interacted with genomic DNA, we also studied the *in vivo* efficacy against the genomic DNA of *R. solani* after the compound treatments. The mycelia of *R. solani* were prepared by being cultured in PDB medium (45 mL) and rotated at 28 °C on a rotary shaker at 120 rpm for 3 days. Then, the PDB medium was mixed with three different concentrations (MIC, IC_{50} and IC_{90}) of compounds (PQD-BC and BC) and incubated in triplicate under shaking for 24 h at 28 °C; the same quantity of sterile distilled water was added for the control group. The mycelia were collected and washed twice with PBS (pH 7.4) to remove the medium, and then ground under liquid nitrogen. The total

intracellular DNA was extracted with assay kits and RNase was added. The *in vivo* interaction between the compounds and genomic DNA was studied by agarose gel electrophoresis.

2.4. Effect of inhibiting sclerotial formation

The effect of the synthetic compounds of PQD-BC and BC on the formation of sclerotia was determined based on the time of sclerotia information, the number of sclerotia per Petri dish and the dry weight of sclerotia. Specifically, a 6-mm-diameter Petri dish, which was cut with a sterile cork borer from the edge of an actively growing colony cultured on PDA plates for 7 days, was placed in the center of a 9-cm-diameter petri dish containing PDA medium with three different concentrations (MIC, IC_{50} and IC_{90}) of synthetic compounds (PQD-BC and BC). The same volume of PDB was added for the control. Each measurement consisted of at least three replicates. After being cultured for 7 days, the sclerotia were collected and counted. Finally, the sclerotia were dried at room temperature for 24 h before weighing.

2.5. Statistical analysis

SPSS software (SPSS Inc., Chicago, IL, USA) was used for the statistical analyses of the data. To determine the effects of the treatments, an analysis of variance (ANOVA) was performed. A Duncan's multiple range test was used for mean separations when the treatment effects were statistically significant ($P < 0.05$).

3. Results and discussion

3.1. Antifungal activity

The half-maximal inhibitory concentration (IC_{50}) is the drug safety indicator that could cause 50% fungal death, and the 90% inhibitory concentration (IC_{90}) is the concentration at which 90% of the fungi were killed. The addition of PQD-BC or BC to the PDA medium inhibited the mycelia growth of selected fungi significantly at all concentrations tested, as measured by the diameter of the treatment and control using the crossing method. The IC_{50} and IC_{90} have biological probability values of 0.5 and 6.2816, respectively. PQD-BC and BC inhibited the mycelial growth of *R. solani* in a dose-dependent manner at concentrations from 0.5 to 2 mg/mL (PQD-BC) and from 0.015 to 0.2 mg/mL (BC) (Fig. 1). As the concentrations of PQD-BC and BC increase, the diameter of each treatment group decreases. This result indicated that the compounds (PQD-BC and BC) can inhibit the growth of *R. solani* (Table 1). In *R. solani* cultured at 28 °C for 2 more days, the PQD-BC exerted antifungal effects with a IC_{50} of 0.73 mg/mL and a IC_{90} of 1.64 mg/mL, whereas BC exhibited antifungal activity with a IC_{50} of 0.048 mg/mL and a IC_{90} of 0.127 mg/mL.

Two principal measures of *in vitro* activity are the minimal inhibitory concentration (MIC) and the minimal fungicidal concentration (MFC). The MIC is the lowest concentration of drug that prevents visible fungal growth. High MICs indicate that stronger concentrations of antimycotic agents are required to inhibit fungal growth. The MIC of PQD-BC and BC was determined using the TTC coloration method and is defined as the lowest concentration able to inhibit visible microbial growth. TTC is a redox indicator used to differentiate between metabolically active and inactive cells; the colorless compound is enzymatically reduced to red TPF (1,3,5-triphenylformazan), which is stable and cannot be oxidized in the air in living cells because of the activity of various dehydrogenases. When the number of active cells is low, TTC cannot be reduced and the solution is colorless; it is therefore often used as a chromogenic agent to test whether viable cells are present [35]. Therefore, MIC was determined as the lowest concentration at which no red color was observed, as shown in Fig. 2–(A). MFC, also known as the minimum lethal concentration, is the concentration of drug that reduces the original fungal inoculum by 99.9%, as shown in

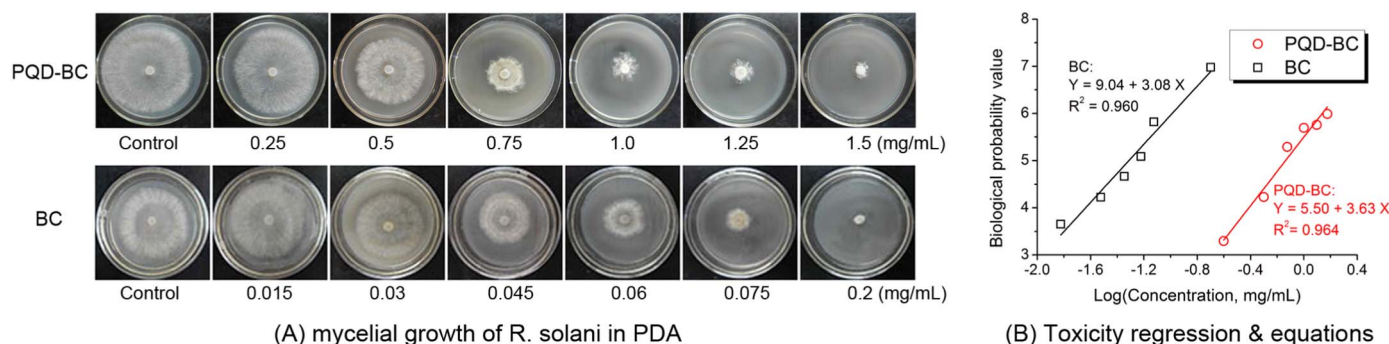


Fig. 1. (A) The typical mycelial growth of *R. solani* in PDA medium after PQD-BC and BC were applied, and (B) the corresponding toxicity regression curves and regression equations. The data were based on three replicates, and the test was repeated twice, with similar results.

Table 1

The antifungal effect of PQD-BC and BC against *R. solani*.

Compounds	Mycelial growth		Spore propagation		
	IC ₅₀ (mg/mL)	IC ₉₀ (mg/mL)	MIC (mg/mL)	MFC (mg/mL)	MFC/MIC
PQD-BC	0.73	1.64	0.2	0.2	1
BC	0.048	0.127	0.03	0.035	1.167

Fig. 2-(B). The ratio of MFC/MIC reflects the fungicidal activity. An antimicrobial agent exhibited fungicidal activity when the ratio of MFC/MIC was less than or equal to 4, otherwise the antimicrobial agent only had antifungal activity. The *in vitro* studies showed that PQD-BC displayed antifungal action against *R. solani*, with an MIC and MFC of 0.2 mg/mL; therefore, BC exerted antifungal activity against *R. solani*, with an MIC of 0.03 mg/mL and an MFC of 0.035 mg/mL. Thus, PQD-BC and BC were effective against *R. solani*, with low MIC and MFC values and MFC/MIC ratios of PQD-BC and BC < 4, indicating they were fungicidally effective, as shown in Table 1.

3.2. Mechanism of antifungal action

3.2.1. Mycelial morphology and biomass

The mycelial growth and morphology of *R. solani* was detected by light microscopy, as shown in Fig. 3. After being cultured for 48 h, the mycelia in the control were in good condition; the mycelia were smooth and full. However, the morphology of the mycelia that were treated with three different concentrations (MIC, IC₅₀ and IC₉₀) of PQD-BC had

changed, including increased branching of mycelia and shortened branch spacing and fewer large vacuoles in some mycelial cells. Some mycelial cells, after treatment with PQD-BC, produced particulate matter that could be a condensation of the cytoplasm [16], as shown in Fig. 3-(A1). However, the number and volume of vacuoles increased in the cells treated with increasing concentration of BC, as shown in Fig. 3-(A2). The BC treatment resulted in cytoplasmic vacuolation [36]. This difference between macromolecular compound (PQD-BC) and small molecular compound (BC) may be related to the different molecular weight, and thereby the different dispersion and density of cations in liquid. In addition, the mycelia treated with a high concentration (IC₅₀ and IC₉₀) of PQD-BC and BC became dark, the medium became cloudy, and the mycelia fractured easily when harvested. We suspected that Rs-melanin was produced during the incubation with PQD-BC and BC. Rs-melanin was reported to be stable to light, temperature reducer and other metal ions [8]. Therefore, mycelia of *R. solani* survives within the hostile environment, by producing Rs-melanin and forming sclerotia.

Furthermore, the biomass was measured using an electronic balance, as shown in Fig. 3-(B). The growth of mycelia during treatment was effectively inhibited by PQD-BC and BC, the growth production was strongly reduced in a dose-dependent manner. After being treated by small molecular QAS, the liquid occupied the main volume of the mycelia cell due to cytoplasmic vacuolation. The weight of mycelia reduced because of a massive loss of water through drying. However, the condensation of cytoplasm, caused by PQAS, maintained the mycelial dry weight.

3.2.2. Cell wall integrity

To determine if PQD-BC and BC led to the loss of cell wall integrity

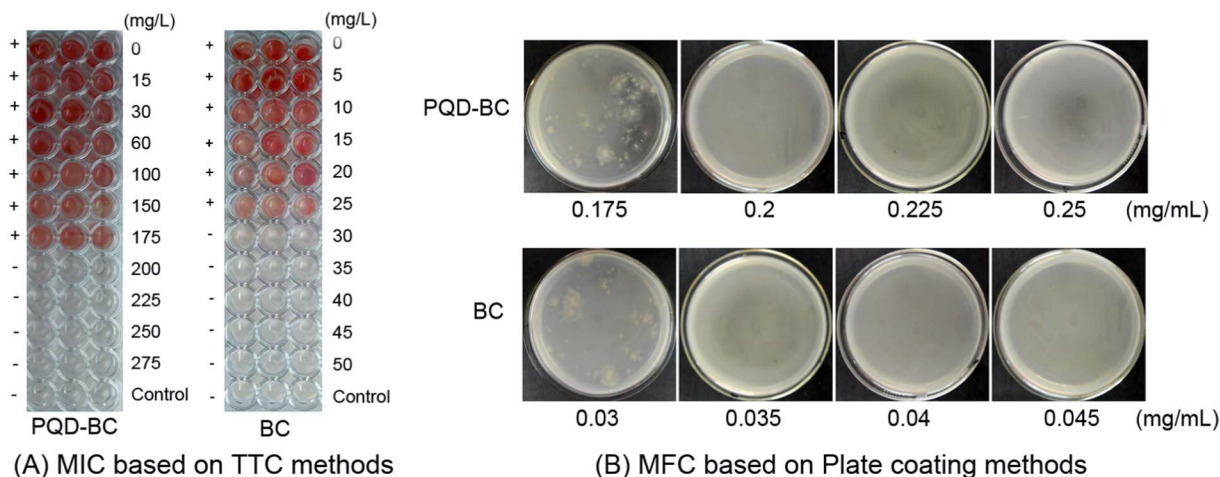


Fig. 2. (A) The MIC values of PQD-BC and BC against *R. solani* based on the TTC colorimetric method; (+) indicates certain cells on the plate and (–) indicates fewer or no cells on the plate. (B) The MFC values of PQD-BC and BC against *R. solani* based on the number of colonies in PDA.

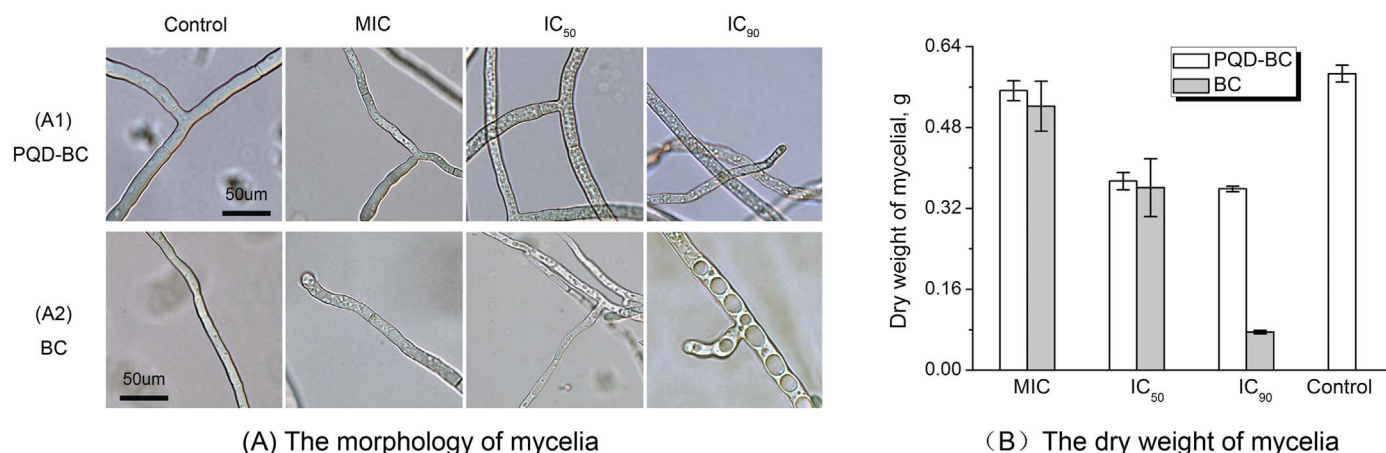


Fig. 3. The mycelial membrane structure (A) and dry weight (B) of *R. solani* mycelia after PQD-BC and BC treatments.

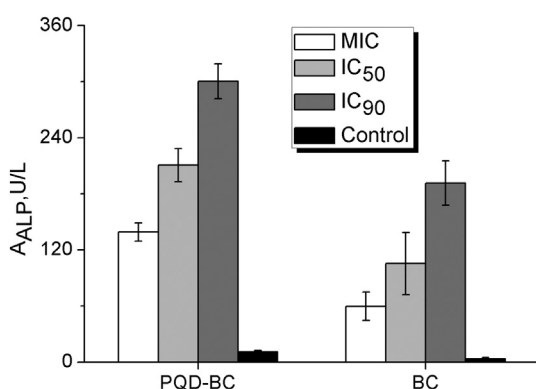


Fig. 4. Loss of cell-wall integrity in *R. solani* after PQD-BC or BC treatment. The alkaline phosphatase activity (AALP) was expressed as units per liter of filtered solution.

in *R. solani*, the ALP content, which is produced in the cytoplasm and cannot pass through the intact cell wall [37], was measured. Damage to the external cell wall layers can lead to the release of ALP from the cell [38]. After 3-day-old mycelia of *R. solani* were treated with four different concentrations (MIC, IC₅₀, IC₉₀ and 0), increased ALP activities of 0.2 mg/mL, 0.73 mg/mL and 1.64 mg/mL were observed in the medium at the MIC, IC₅₀ and IC₉₀, respectively, in the PQD-BC-treated cells. In BC-treated cells, the ALP activities were 0.03 mg/mL, 0.048 mg/mL and 0.127 mg/mL at the MIC, IC₅₀, IC₉₀, respectively. The PQD-BC- and BC-treated groups showed significantly higher ALP activity than the control after a 48 h treatment, which confirmed that the cell wall of *R. solani* was destroyed in a dose-dependent manner (Fig. 4). The data suggest that, after absorbing onto the cell surface, PQD-BC and BC could damage the cell walls of fungal pathogens and that they acted on the plasma membrane, leading to the release of intracellular contents like ALP, which led to eventual direct cell death.

3.2.3. Membrane-active mode of action

Quaternary ammonium salt treatments can rapidly lead to the disintegration of biological membranes in fungal pathogens, resulting in cell death [39]. To establish the mode of antifungal action, the cytoplasmic membrane integrity of *R. solani* was characterized using a fluorescent dye, propidium iodide (PI). PI is capable of combining with cell's genetic matters to produce a red fluorescence by green-light stimulation, but cannot permeate through the intact cytoplasmic membrane. As shown in Fig. 5, the cell nuclei were obviously stained with PI after treatment with PQD-BC at the MIC, IC₅₀ and IC₉₀ (0.2 mg/mL, 0.73 mg/mL and 1.64 mg/mL, respectively). By contrast, no red fluorescence appears in the control. In BC treatment, the cell nucleus can be stained with PI only at a IC₉₀. The microscopy results thus indicate that

the cationic polymer interacted with and subsequently disrupted the membrane integrity of the fungi [23]. Fluorescence microscopy images show that, compared with the control treatment, QASs treatment caused complete membrane permeabilization of the cells, as clearly indicated by red fluorescence; this observation indicates that the number of mycelia that lost plasma membrane integrity increased after the PQD-BC and BC treatments (Fig. 5). Compared with Foc 4 [23], only the spores could be seen in the fluorescence microscopy images. All of the cationic biocides were found to depolarize the membrane integrity of *R. solani*, and they may inhibit the growth of *R. solani* by directly damaging the plasma membrane and causing the cell death of the fungal pathogen.

Damage to the plasma membrane can lead to the loss of osmotic balance and to the influx of fluids and ions as well as to the loss of proteins and carbohydrates, eventually causing the onset of cell death [19]. To further confirm that PQD-BC and BC caused a loss in the cytoplasmic membrane integrity of *R. solani*, the leakage of cytoplasmic constituents was determined. The figure clearly shows that the two compound treatments significantly induced the leakage of soluble proteins (Fig. 6-(A)), carbohydrates (Fig. 6-(B)), and conductivity (Fig. 6-(C)) out of the *R. solani* mycelia. In general, the amount of leaked materials was positively correlated with the concentrations of PQD-BC and BC. The cellular leakage could be observed after 4 h of treatment, and it was generally constant over a period of 6 h for soluble proteins and carbohydrates. A similar trend was observed for the electrical conductivity. Because we observed the same physiological events with the release of cytoplasmic constituents, the mode of action of PQD-BC and BC is reasonably assumed to be interpretable on the basis of each elementary process: cationic biocides adsorb onto the fungal cell surface, diffuse through the cell wall, and subsequently bind to the cytoplasmic membrane, releasing the cytoplasmic constituents and finally inducing the cell death of the fungal pathogen.

3.2.4. Lipid peroxidation

To investigate the lipid damage, the levels of MDA, which is a decomposition product of polyunsaturated fatty acid hydroperoxidase and a biomarker of lipid peroxidation, were assessed [28]. MDA was primarily released into the medium when the plasma membrane lipid peroxidation was initiated; we determined MDA level to investigate whether lipid peroxidation was associated with membrane damage [31]. The mycelia cultured in PDB for 3 days, extracted from the medium, and washed twice with PBS (pH 7.4) were treated with four different concentrations of PQD-BC or BC at 1/2 × IC₉₀, IC₉₀ and 2 × IC₉₀ (0.82 mg/mL, 1.64 mg/mL and 3.28 mg/mL, respectively). As shown in Fig. 7-(A), the IC₉₀ of PQD-BC led to the highest release of MDA among treatment groups. The results show that, as the concentration of PQD-BC increases, so does the release of MDA. However,

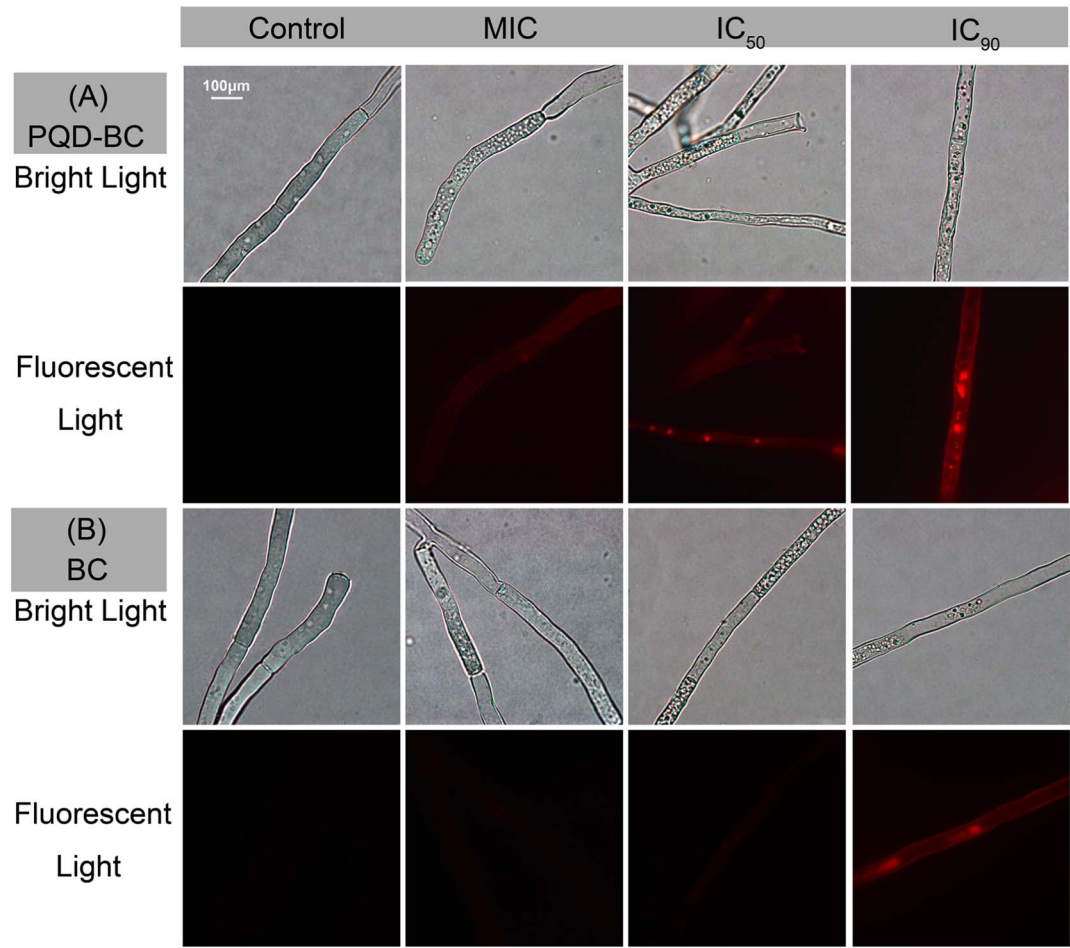


Fig. 5. Loss of plasma membrane integrity in *R. solani* after (A) PQD-BC and (B) BC treatments. The mycelia were stained with PI and observed with a fluorescence microscope. Mycelia with damaged plasma membranes fluoresced red. (For interpretation of the references to color in this figure legend, the reader is referred to the web version of this article.)

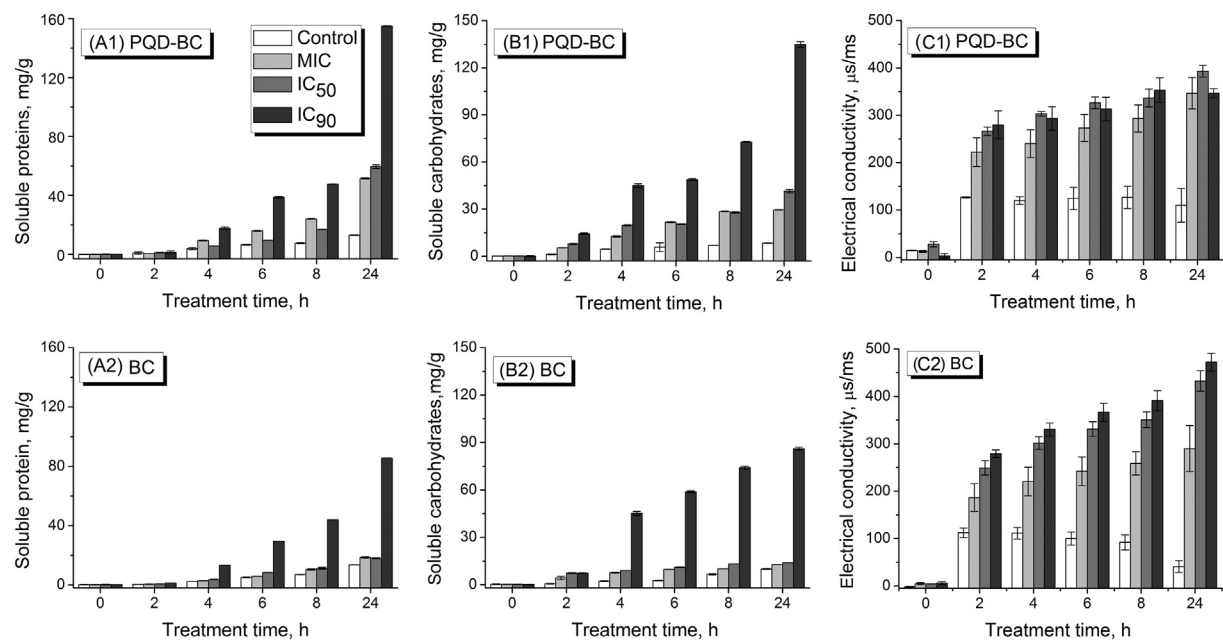


Fig. 6. Leakage of cytoplasmic contents: (A1, A2) soluble proteins, (B1, B2) carbohydrates and (C1, C2) electric conductivity from *R. solani* treated with PQD-BC and BC. Each data point is the mean \pm SE of three replicates.

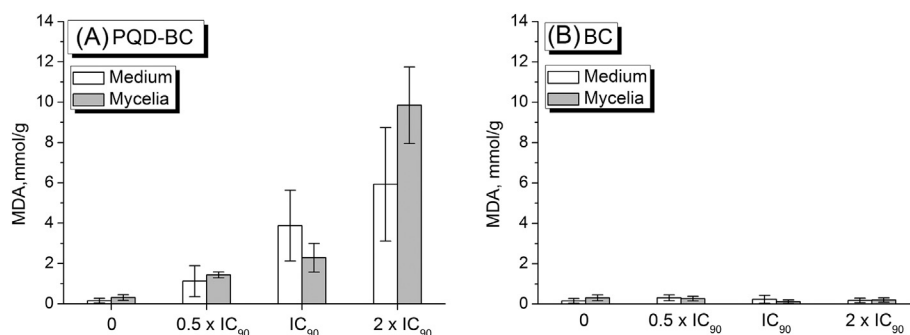


Fig. 7. Loss of cell wall integrity in *R. solani* after (A) PQD-BC and (B) BC treatments.

no obvious changing level of MDA on the BC-treated group was detected (Fig. 7).

Lipid peroxidation is the oxidative degradation of lipids, a process in which free radicals “steal” electrons from the lipids in cell membranes by a free radical chain reaction mechanism. In normal cells, reactive oxygen species (ROS), the byproducts of metabolism containing oxygen free radicals are dynamically balanced with antioxidants like glutathione (GSH). Hostile environmental factors, including UV, heat or chilling exposure, salinity and so on, can place a dramatic increment in ROS levels, cause the so-called oxidative stress. The result that the macromolecular PQD-BC can induce the lipid peroxidation, was similar to those of antimicrobial peptides (AMPs), such as Scolopendin 2 [31] and Glabridin [32]. It is reasonably assumed that the elevated local cationic density of macromolecular QAS (PQD-BC) are more likely to break the balance to give an oxidative stress and induce membrane lipid peroxidation in *R. solani*. By contrast, the small molecular QAS (BC) disperses in the liquid and lacks the ability of enriching around the mycelia and elevating the local density of cations. Therefore, BC did not induce the lipid peroxidation of treated mycelia. These results demonstrated the different mechanism between macromolecular and small molecular QAS in breaking the cytoplasmic membrane integrity.

3.2.5. Mitochondrial dysfunction

To assess changes in mitochondrial function, the SDH activity of *R. solani* cells exposed to the compounds was determined. SDH is the functional substance for the tricarboxylic acid cycle and aerobic respiration. Its activity is closely associated with bioenergy synthesis and mitochondrial function in various prokaryotic and eukaryotic cells [40]. The control group exhibited SDH activity, whereas the amount of SDH released from the cells to the culture medium decreased as the concentrations of the compounds (PQD-BC and BC) increased (Fig. 8). Therefore, PQD-BC and BC affect the bioenergy synthesis pathway of *R. solani* by inhibiting SDH activity. This finding suggests that the potential mechanism underlying their antifungal actions is inhibition of mitochondrial function.

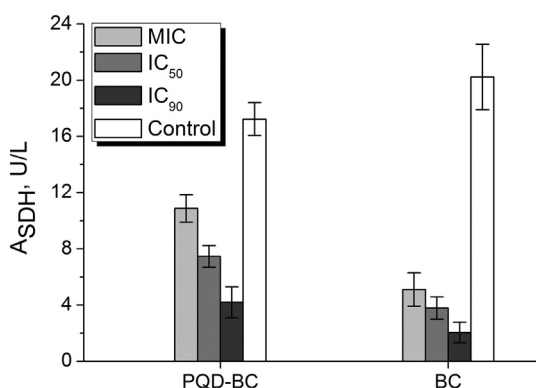


Fig. 8. Mitochondrial function (A_{SDH}) of *R. solani* after PQD-BC and BC treatments.

3.2.6. Interactions of genomic DNA with the compounds

As a carrier of genetic information, DNA is a major target for drug interactions because of its ability to interfere with transcription (gene expression and protein synthesis) and replication, a major step in cell growth and division [41–43]. In this study, the EMSA was used to test the affinity of DNA-binding polymers to investigate their efficacy against genomic DNA, and the mode of action was illustrated. When genomic DNA is separated by electrophoresis, rapid migration will be observed for unbound and cleaved DNA. By contrast, the complex produces a slower migration because of the increase of molecular weight and decrease of negative charge, which means that a constant amount of DNA was mixed with increasing amounts of compounds, tethered to compound-DNA-conjugated agarose beads. For the *in vitro* experiments, test compounds were immobilized with *R. solani* genomic DNA according to the results of the agarose electrophoresis experiments. In Fig. 9, Lanes 2–7 show genomic DNA incubated with the test compounds at three different concentrations (MIC, IC₅₀ and IC₉₀), whereas Lane 1 applies to untreated genomic DNA (control DNA). Compared with the control treatment, the compound treatments are very effective at changing the mobility and shape of genomic DNA. As shown in Fig. 9-(A), no obvious DNA bands were present in the lanes for the PQD-BC-treated group (Lanes 2–4), and the DNA loading buffer containing bromide blue indicator remained in the pore. GoldView™, a new type of nucleic acid dye that can replace ethidium bromide (EB), exhibits weak fluorescence; however, its emission intensity in the presence of DNA can be greatly enhanced because of its strong intercalation between the adjacent DNA base pairs. This enhanced fluorescence could be quenched, or at least partly quenched, by the addition of a second molecule with higher DNA-binding ability. This finding indicates that PQD-BC was immobilized strongly with genomic DNA, which caused the GoldView™ to be completely replaced by PQD-BC and led to an appreciable decrease in the emission intensity. BC could combine with genomic DNA strongly, increasing the weight of the composite molecule. Therefore, the speed of genomic DNA movement in electrophoresis slows and the phenomenon of tailing appears. Because of the combination of genomic DNA and synthetic compounds, the large molecules of genomic DNA were broken down and genomic DNA treated with compounds combined with TE buffer formed in the long tail in the gel. On the basis of the results of the assay of DNA interactions *in vitro*, the phenomenon of PQD-BC and BC against DNA *in vivo* (as shown in Fig. 9-(B)) was similar. On the basis of the aforementioned results, the binding site of PQD-BC and genomic DNA could be associated with the GoldView™ and genomic DNA: BC can bind with the genomic DNA of *R. solani* as a complex and destroy it.

3.3. Effect of inhibiting sclerotial formation

Sclerotia are the dormant structures of fungi and are also described as an aggregation of mycelia. Sclerotial formation can be divided into three stages: sclerotial initial (SI), sclerotial developing (SD), and sclerotial mature (SM) [44]. The PQD-BC and BC treatments at IC₉₀ and

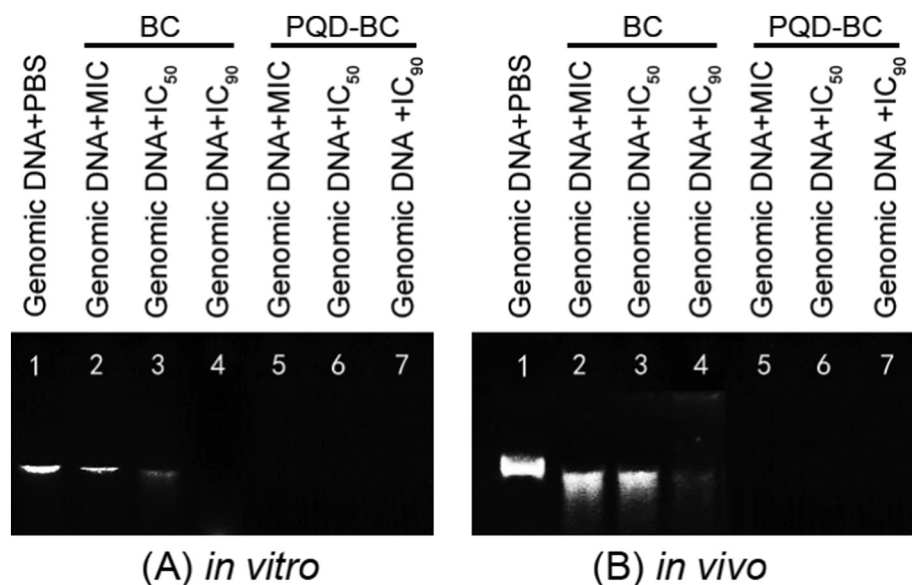


Fig. 9. Interaction of compounds (PQD-BC and BC) with *R. solani* genomic DNA (A) *in vitro* and (B) *in vivo*. Each lane contained 10 μ L of compounds: 10 μ L of DNA marker was moved to Lane 1: 10 μ L of genomic DNA with PBS (negative control), where the volume ratio is 6: 1. (A) *In vitro*, Lanes 2–4: genomic DNA with a fixed concentration was treated with TE buffer containing PQD-BC (volume: genomic DNA: TE buffer = 6: 1) at final concentrations matching the MIC, IC₅₀ and IC₉₀. For Lanes 5–7: genomic DNA with a fixed concentration was treated with 2 μ L of the TE buffer (6:1) containing BC at a final concentration matching the MIC, IC₅₀, and IC₉₀. (B) *In vivo*, PQD-BC was added to Lane 5–7; however, BC was added to Lanes 2–4. The data were based on three replicates, and the test was repeated twice with similar results. Representative results are shown.

the control are presented in Fig. 10. As shown in Fig. 10, the sclerotia treated with PQD-BC or BC at IC₉₀ reached the SI stage after 5 and 4 days of culturing, respectively. The other treated concentrations (MIC and IC₅₀) of compounds (PQD-BC and BC) were shown in Fig. S1 (as listed in the Supporting Information). The sclerotia reached the stage of SI formation on the third day of culturing (Fig. 11-(A)). This result indicates that PQD-BC and BC can delay sclerotia formation. In addition, under treatment with PQD-BC or BC, the number of sclerotia decreased significantly (Fig. 11-(B)), and the polymer at three different concentrations (MIC, IC₅₀ and IC₉₀) had no effect on the dry weight of sclerotia as the concentration increased compared with the effect of the treatment with BC (Fig. 11-(C)).

The sclerotia have a double-layer structure, in which the inner layer consists of a large number of living cells and the outer layer of empty cells [7]. Hence, we can infer that PQD-BC and BC can affect the formation of sclerotia, by causing the increasing number of empty cells in single sclerotium and forming heavier sclerotia to survive the harmful environment. Moreover, the heavier sclerotia formed in BC-treated groups indicated the more toxic environment that BC created.

4. Conclusions

We previously demonstrated methods for developing quaternary ammonium salt (PAD-BC) and small molecular quaternary ammonium salt (BC) that inactivate various fungi (*R. solani*). PQD-BC and BC were

found to actively inhibit mycelial growth and sclerotial formation in *R. solani*.

PQD-BC and BC destroyed the cell structure. We speculated that PQD-BC and BC can produce a destructive effect on the integrity of the cell wall and cell membrane of *R. solani* and on the formation of sclerotia because of the good biocompatibility. In particular, the macromolecule quaternary ammonium salt of PQD-BC can cause plasma membrane lipid peroxidation, unlike a small molecular quaternary ammonium salt such as BC. However, due to its large molecular weight, PQD-BC cannot easily traverse the cytoplasm membrane into the cell and attack the organelles. The mechanism of action suggests that the polymeric quaternary ammonium salts may act on a broad spectrum of fungal species, indicating a new strategy for preventing and controlling *Rhizoctonia solani* and establishing a base for studying the effect of the polymer on inhibiting microorganisms.

Acknowledgments

This work was supported by the Science and Technology Program of Guangzhou, China, under grant 201704020084; the Science and Technology Planning Project of Guangdong Province, China under grant 2016A020210105; and the National Natural Science Foundation of China under grant 31772202, 51473051.

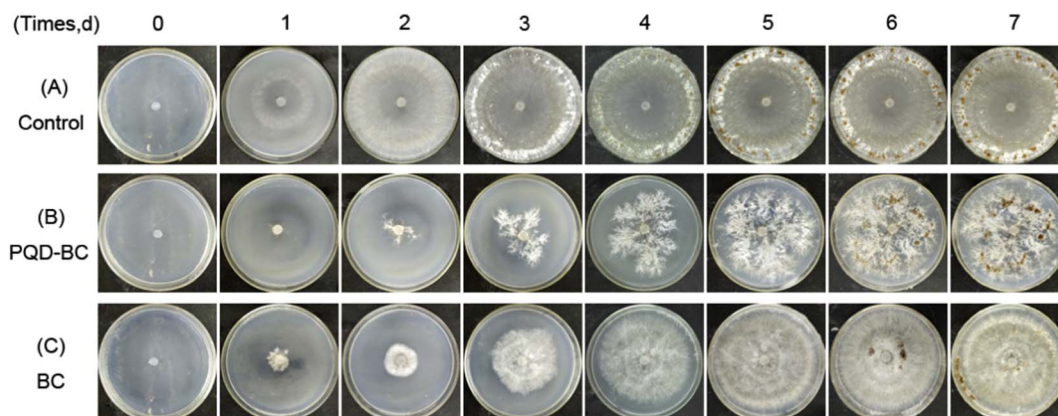


Fig. 10. The sclerotial formation of *R. solani* on PDA medium after applying (B) PQD-BC and (C) BC at IC₉₀, compared with the (A) control. The data were based on three replicates, and the test was repeated twice with similar results. Representative results are shown.

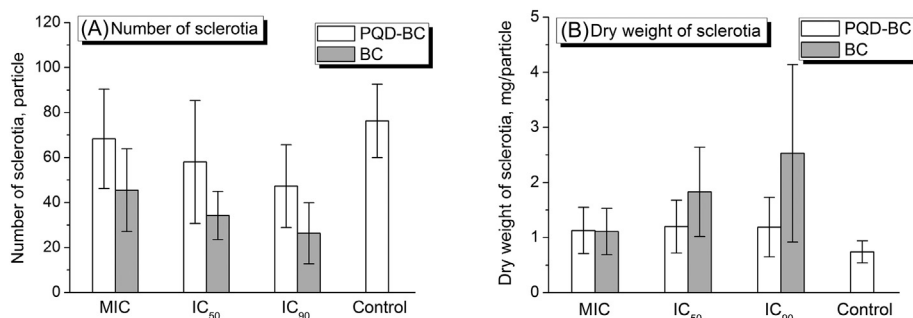


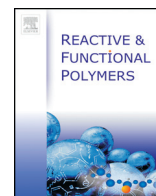
Fig. 11. The (A) number and (B) average dry weight of sclerotia of *R. solani* treated with three different concentrations of PQR-BC and BC.

Appendix A. Supplementary data

Supplementary data to this article can be found online at <https://doi.org/10.1016/j.reactfunctpolym.2018.01.020>.

References

- [1] F.N. Lee, M.C. Rush, Rice sheath blight: a major rice disease, *Plant Dis.* 67 (1983) 829–832.
- [2] M.A. Marchetti, C.N. Bollich, Quantification of the relationship between sheath blight severity and yield loss in rice, *Plant Dis.* 75 (1991) 773–775.
- [3] C.D. Georgiou, K.P. Petropoulou, Effect of the antioxidant ascorbic acid on sclerotial differentiation in *Rhizoctonia solani*, *Plant Pathol.* 50 (2001) 594–600.
- [4] S. Kumar, K. Sivasithamparan, M.W. Sweetingham, Proliferation of sclerotia in soil by *Rhizoctonia solani* anastomosis group (AG) 11 pathogenic on lupin, *Assoc. of Appl. Biologists* 141 (2002) 11–18.
- [5] A. Erental, M.B. Dickman, O. Yarden, Sclerotial development in *Sclerotinia sclerotiorum*: awakening molecular analysis of a “Dormant” structure, *Fungal Biol. Rev.* 22 (2008) 6–16.
- [6] M. Anees, V. Edel-Hermann, C. Steinberg, Build up of patches caused by *Rhizoctonia solani*, *Soil Biol. Biochem.* 42 (2010) 1661–1672.
- [7] T. Hashiba, Y. Tomio, S. Mogi, Biological and ecological studies on the sclerotium of *Pellicularia sasakii* (Shirai) S. Ito I. Floating on the water surface of sclerotium, *The Phytopathological Soc. of Japan* 38 (1972) 414–425.
- [8] J.Y. Chen, C.J.Z. Wang, C.W. Shu, et al., Isolation and characterization of a melanin from *Rhizoctonia solani*, the causal agent of rice sheath blight, *Eur. J. Plant Pathol.* 142 (2015) 281–290.
- [9] G.J. Tan, L. Chen, Y. Yang, et al., Study on the relationship between the sclerotial floatation characteristics and ultrastructure of rice sheath blight, *Anhui Nongye Daxue Xuebao/Journal of Anhui Agricultural University*, 27 (2000) 13–17.
- [10] J.P. Damicone, M.V. Patel, W.F. Moore, Density of sclerotia of *Rhizoctonia solani* and incidence of sheath blight in rice fields in Mississippi, *Plant Dis.* 77 (1993) 257–260.
- [11] M.X. Bui, R.B. Ogle, J.E. Lindberg, Studies on integrated duck-rice systems in the Mekong Delta of Vietnam, *J. Sustain. Agric.* 20 (2002) 27–40.
- [12] S.U. Pin, X.L. Liao, Y. Zhang, et al., Influencing factors on rice sheath blight epidemics in integrated rice-duck system, *J. Integr. Agric.* 11 (2012) 1462–1473.
- [13] S. Naeimi, S.M. Okhowat, M. Javan-Nikkah, et al., Biological control of *Rhizoctonia solani* AG-1A, the causal agent of rice sheath blight with *Trichoderma* strains, *Phytopathol. Mediterr.* 49 (2010).
- [14] L. Liu, M.Q. Liang, L. Lu, et al., Synergistic effects of the combined application of *Bacillus subtilis* H 158 and strobilurins for rice sheath blight control, *Biol. Control* 117 (2018) 182–187.
- [15] Y.Y. Yu, C.H. Jiang, C. Wang, et al., An improved strategy for stable biocontrol agents selecting to control rice sheath blight caused by *Rhizoctonia solani*, *Microbiol. Res.* 203 (2017) 1–9.
- [16] S.J. Wei, J. Xu, G.Q. Tu, The efficacy evaluation of Ag-antibiotic 702 in the treatment of rice pathogenic fungi, *Jiangxi Nongye Daxue Xuebao/Journal of Jiangxi Agricultural University*, 33 (2011) 488–492 (in Chinese).
- [17] H. Zhang, Q.H. Zhao, W.H. Tang, G.A. Wolf, The influence of Jinggangmycin A on the activities of resistance-related enzymes in rice, *Zhiwu Baohu Xuebao/Journal of Plant Conservation*, 24 (1992) 511–519 (in Chinese).
- [18] L.J. Cheng, Q.Q. Liu, Y.F. Lei, Y.L. Lin, A.Q. Zhang, The synthesis and characterization of carboxybetaine functionalized polysiloxanes for the preparation of anti-fouling surfaces, *RSC Adv.* 4 (2014) 54372–54381.
- [19] A.Q. Zhang, Q.Q. Liu, Y.F. Lei, S.H. Hong, Y.L. Lin, Synthesis and antimicrobial activities of acrylamide polymers containing quaternary ammonium salts on bacteria and phytopathogenic fungi, *React. Func. Polymers* 88 (2015) 39–46.
- [20] L.J. Cheng, Q.Q. Liu, L. Yang, Y.L. Lin, A.Q. Zhang, Synthesis and characterization of hydrogen-containing polysiloxanes (in Chinese), *Gaofenzi Cailiao Kexue Yu Gongcheng/Polymer, Mater. Sci. Eng.* 30 (2014) 25–28.
- [21] J. Wang, A. Sugawara-Narutaki, A. Shimajima, et al., Dendritic silica nanoparticles synthesized by a block copolymer-directed seed-regrowth approach, *Langmuir* 31 (2015) 1610–1614.
- [22] M. Fukao, A. Sugawara, A. Shimajima, et al., One-dimensional assembly of silica nanospheres mediated by block copolymer in liquid phase, *J. Am. Chem. Soc.* 131 (2009) 16344–16345.
- [23] Z.F. Huang, R.Q. Liuyang, C.Y. Dong, et al., Polymeric quaternary ammonium salt activity against *Fusarium oxysporum* f. sp. *Cubense* race 4: synthesis, structure-activity relationship and mode of action, *React. Func. Polym.* 114 (2017) 13–22.
- [24] Y.H. Lin, Y.J. Lin, T.D. Chang, et al., Development of a Taqman probe-based insulated isothermal polymerase chain reaction (iiPCR) assay for detection of *Fusarium oxysporum* f. sp. *cubense* race 4, *PLoS One* 11 (2016) 1–13.
- [25] C.C. Sollod, A.E. Daub, Cell surface redox potential as a mechanism of defense against photosensitizers in fungi, *Appl. Environ. Microbiol.* 58 (1992) 444–449.
- [26] K.J. Rao, S. Paria, Anti-Malassezia furfur activity of natural surfactant mediated in situ silver nanoparticles for a better antidandruff shampoo formulation, *RSC Adv.* 6 (2016) 11064–11069.
- [27] X. Shao, S. Cheng, H. Wang, et al., The possible mechanism of antifungal action of tea tree oil on *Botrytis cinerea*, *J. Appl. Microbiol.* 114 (2013) 1642–1649.
- [28] K.N. Fish, S.L. Schmid, H. Damke, Evidence that dynamin-2 functions as a signal-transducing GTPase, *J. Cell Biol.* 150 (2000) 145–154.
- [29] F. Wu, G.L. Meng, Jing He, et al., Antibiotic-loaded chitosan hydrogel with superior dual functions: antibacterial efficacy and osteoblastic cell responses, *ACS Appl. Mater. Interfaces* 6 (2014) 10005–10013.
- [30] M.M. Bradford, A rapid and sensitive method for the quantitation of microgram quantities of protein utilizing the principle of protein–dye binding, *Anal. Biochem.* 72 (1976) 248–254.
- [31] H.J. Lee, J.S. Hwang, D.G. Lee, Scolopendin 2 leads to cellular stress response in *Candida albicans*, *Apoptosis* 21 (2016) 856–865.
- [32] A. Singh, M.P. Pal, Darokar, a polyphenolic flavonoid glabridin: oxidative stress response in multidrug-resistant *Staphylococcus aureus*, *Free Radic. Biol. Med.* 87 (2015) 1–28.
- [33] R.H. Mohamed, R.A. Karam, H.A. Hagrass, et al., Anti-apoptotic effect of spermatogonial stem cells on doxorubicin-induced testicular toxicity in rats, *Gene* 561 (2015) 107–114.
- [34] J.H. Kim, Immobilized DNA-binding assay, an approach for *in vitro* DNA-binding assay, *Anal. Biochem.* 334 (2004) 401–402.
- [35] E.F. Palermo, I. Sovadinova, K. Kuroda, Structural determinants of antimicrobial activity and biocompatibility in membrane-disrupting Methacrylamide random copolymers, *Am. Chem. Soc.* 10 (2009) 3098–3107.
- [36] P. Plodpai, S. Chuenchitt, V. Petcharat, et al., Anti-*Rhizoctonia solani* activity by *Desmos chinensis* extracts and its mechanism of action, *Crop Prot.* 43 (2013) 65–71.
- [37] S.S. Lindsay, B. Wheeler, K.E. Sanderson, et al., The release of alkaline phosphatase and of lipopolysaccharide during the growth of rough and smooth strains of *Salmonella typhimurium*, *Can. J. Microbiol.* 19 (1973) 35–43.
- [38] K.J. Cheng, J.M. Ingram, J.W. Costerton, Release of alkaline phosphatase from cells of *Pseudomonas aeruginosa* by manipulation of cation concentration and of Ph, *J. Bacteriol.* 104 (1970) 748–753.
- [39] J. Zhang, G.B. Akcapinar, L. Atanasova, et al., The neutral metalloproteinase NMP1 of *Trichoderma guizhouense* is required for mycotrophy and self-defence, *Environ. Microbiol.* 18 (2015) 580–597.
- [40] W.W. Fan, G.Q. Yuan, Q.Q. Li, et al., Antibacterial mechanisms of methyl gallate against *Ralstonia solanacearum*, *Australas. Plant Pathol.* 43 (2014) 1–7.
- [41] Fatma Öztürk, Leyla Açı, İzzet Şener, Fikret Karci, Emine Kiliç, Antimicrobial properties and DNA interactions studies of 3-hetarylazoquinoline-2, 4-diol compounds, *Turk. J. Chem.* 36 (2012) 293–302.
- [42] B. Dede, I. Özmen, F. Karipcin, Synthesis, characterization, catalase functions and DNA cleavage studies of new homo and heteronuclear Schiff base copper (II) complexes, *Polyhedron* 28 (2009) 3967–3974.
- [43] E.E. İltir, N. Asmafiliz, Z. Kiliç, et al., Phosphorus–nitrogen compounds: part 19. Syntheses, structural and electrochemical investigations, biological activities, and DNA interactions of new spirocyclic monofluorocyclotriphosphazenes, *Polyhedron* 29 (2010) 2933–2944.
- [44] C.D. Georgiou, N. Patsoukis, et al., Sclerotial metamorphosis in filamentous fungi is induced by oxidative stress, *Integr. Comp. Biol.* 46 (2006) 691–712.



Polymeric quaternary ammonium salt activity against *Fusarium oxysporum* f. sp. *cubense* race 4: Synthesis, structure-activity relationship and mode of action

Zhenfeng Huang^{a,1}, Runqi Liuyang^{a,1}, Chengyun Dong^a, Yufeng Lei^b, Anqiang Zhang^b, Yaling Lin^{a,*}

^a College of Materials and Energy, South China Agricultural University, 483 Wushan Rd., Guangzhou 510642, Guangdong, China

^b College of Material Science and Engineering, South China University of Technology, 381 Wushan Rd., Guangzhou 510641, Guangdong, China

ARTICLE INFO

Article history:

Received 26 December 2016

Received in revised form 20 February 2017

Accepted 28 February 2017

Available online 03 March 2017

Keywords:

Polymeric quaternary ammonium salts

Antifungal bioassay

Mechanism of antifungal action

ABSTRACT

Polymeric quaternary ammonium salts (PQAS) have been widely used to prevent microbial contamination, but little is known about their activity against phytopathogenic fungi. Our previous report described the synthesis of two novel PQAS, namely a homopolymer of (2-methacrylamido) propyltetra benzyl dimethyl ammonium chloride (PQD-BC) and dimethylaminopropyl benzyl chloride-grafted polysiloxanes (PDMS-g-BC); we demonstrated their structure-activity relationship against phytopathogenic fungi such as *R. solani* and *Fusarium oxysporum* f. sp. *cubense* tropical race 4 (Foc4). Here, we analyzed the structure-activity relationship and toxicity mechanism of these compounds at the molecular level against Foc4 compared with the low molecular-weight quaternary ammonium salt benzalkonium chloride (BC). The results revealed that PQD-BC and PDMS-g-BC application inhibited the growth of Foc4 in a concentration-dependent manner and that PDMS-g-BC exhibited higher activity than PQD-BC. In addition, these polymers were found to induce cell death in Foc4 by disrupting the cellular structure integrity, such as the loss of the cell wall and plasma membrane integrity and oxidative stress (lipid peroxidation), leading to the release of intracellular contents and inducing mitochondrial dysfunction and interference with genomic DNA. The newly elucidated mechanism provides possible applications in which PQAS can be used against phytopathogenic fungi.

© 2017 Elsevier B.V. All rights reserved.

1. Introduction

Fusarium wilt is caused by *Fusarium oxysporum* f. sp. *cubense*, which is also known as Panama disease, and it is regarded as one of the most devastating soil-borne diseases affecting bananas [1–5]. Foc tropical race 4 (Foc4) is the most virulent race, and it can infect almost all commercial banana cultivars; at present, there are no completely effective control methods [2]. A number of studies have been performed to control *Fusarium* wilt with biotechnology, including the transfer of antifungal genes into bananas and using biocontrol agents to control fungal disease [4–6]. However, there are few studies on the use of synthetic fungicides to effectively prevent *Fusarium* wilt in field trials.

Cationic antimicrobials are well known for their use in self-sterilizing surfaces, and they are used for numerous applications such as hospital surfaces, surgical equipment, protective clothes in hospitals, medical implants, wound dressings, food packaging materials, and everyday consumer products. Nevertheless, small molecule cationic antimicrobials

can be highly toxic to the environment, and their protection is shown to be short-lived due to the difficulty involved in controlling their diffusion rate, and water-soluble antimicrobial compounds have led to the rapid emergence of resistant strains and environmental problems [7–9]. It is well known that the bacterial cell surface is negatively charged, and the adsorption of polycations onto the negatively charged cell surface is expected to be enhanced with the increasing molecule weight of the polymers due to the increasingly charged density of the polycations [10]. Given that their high microbicidal activity arises not only from highly cationic charges but also substantial hydrophobicity (*i.e.*, the alkyl chain length), modified polycations must possess a degree of hydrophilic/hydrophobic balance to ensure high activity and water insolubility; the hydrophobic chains must be able to trigger-gather, producing different adsorptions onto the cell surface [11]. In addition, the polymeric salts were more active than the corresponding monomer with the longest alkyl chain [10–13]. Among the most commonly used cationic antimicrobials, cationic polymers with quaternary ammonium groups show great promise in the field of antimicrobial coatings [11]. To create these coatings, a great deal of attention has recently been paid to polymeric quaternary ammonium compounds (PQAS), which are employed as biocides owing to their low toxicity and broad antimicrobial spectrum [14–16].

* Corresponding author.

E-mail address: linyinling@scau.edu.cn (Y. Lin).

¹ These authors contributed equally.

The mode of action of cationic biocides has been summarized as follows: (i) adsorption onto the bacterial cell surface, (ii) diffusion through the cell wall, (iii) binding to the cytoplasmic membrane, (iv) the release of the cytoplasmic constituents, and (v) the death of the cell [17]. The targets of antifungal agents are heavily focused, directly or indirectly, on the cell envelope (wall and plasma membrane), and particularly on the fungal membrane sterol and ergosterol, and on their biosynthesis. Therefore, targets located elsewhere in the cell would be a welcome innovation for systemically bioavailable antifungal agents [18–20]. Several reports have revealed that some antifungal agents specifically inhibit the synthesis of cell wall polysaccharides, particularly chitin or β -glucan, and some others are involved in synthesizing informational macromolecules, namely RNA or DNA, in susceptible fungi [3,21]. Although the antimicrobial effects of PQAS have been extensively investigated, little is known about the structure-activity relationship and the mechanism of antimicrobial action, especially the antifungal mechanism, which hindered their broader application in the antimicrobial field. To date, numerous reports have revealed that PQAS primarily targets the microbial membrane and accumulates in cells driven by the cell membrane potential, but there are no clear-cut reports on their mode of action elsewhere in the cell at the molecular level, which therefore must be investigated.

From this perspective, the synthesis of two novel PQAS with different structures and compositions, that is, the homopolymer of (2-methacrylamido) propyltetrabenzyl-dimethylammonium chloride (PQD-BC) and dimethylaminopropyl benzyl chloride grafted polysiloxanes (PDMS-g-BC), have previously been reported, and we have demonstrated their structure-activity relationship against phytopathogenic fungus such as *R. solani* and Foc4 [22–25]. The aim of the present study was to discuss their structure-activity relationship and toxic mechanism of action at the molecular level along with that of the broad-spectrum microbicide benzalkonium chloride (dodecyl dimethyl benzyl ammonium chloride, BC), which has the same key group (benzyl) as synthetic polymers. The antimicrobial activities of polymers were evaluated against Foc4, and the integrity of the cellular structure (the cytoplasmic membrane and cell wall) was detected to investigate the mode of antifungal action. To investigate the targets in detail elsewhere in the cell, in which polymers inhibited fungal growth, we investigated the interaction of the synthetic polymers and intracellular macromolecules, such as the intracellular enzyme activity (succinic dehydrogenase, SDH) and informational macromolecules (genomic DNA). It is meaningful to develop polymers with antifungal activity and study their structure-activity relationship for the future development of broad-spectrum multifunctional materials.

2. Experimental

2.1. Materials

Bovine serum albumin (BSA) was provided by Hangzhou Sijiqing Biological Engineering Materials Co. Ltd. (Hangzhou, China). TTC (2, 3, 5-triphenyltetrazolium chloride) was purchased from Sangon Biotech (Shanghai) Co., Ltd. (Shanghai, China). *N,N*-Dimethylamine propyl methacrylamide (DMPMA), benzyl chloride (99%), ammonium persulfate (APS, 99%), and PI (propidium iodide) were supplied by Aladdin Reagent Co. Ltd. (Shanghai, China). *N,N*-dimethylallylamine (DMAA, 98%) was supplied by Haining Huangshan Chemical Co. Ltd. (Haining, China). The fungal strain used in this study is *Fusarium oxysporum* f. sp. *cubense* (E. F. Smith) Snyder & Hansen (Foc4), which was donated by the Laboratory of Fungi at South China Agriculture University and maintained on potato dextrose agar (PDA). Foc4 spores were obtained from the surface of the agar after culture for 3 days at 28 °C and 5 days at 35 °C. The spores were suspended in 5 mL of sterile distilled water containing 0.05% (v/v) Tween 20. The concentration of the spore suspensions was determined using a hemocytometer. Benzalkonium chloride (BC) with a purity of over 95% was purchased

from Shanghai Aladdin Bio-Chem Technology Co., Ltd. (Shanghai, China).

2.2. Synthesis of PDMS-g-BC and PQD-BC

Dimethylaminopropyl benzyl chloride-grafted polysiloxanes (PDMS-g-BC) and the homopolymer of (2-methacrylamido) propyltetrabenzyl-dimethylammonium chloride (PQD-BC) were synthesized according to our previous articles [22–25], as shown in Schemes 1 and 2. In which, the PDMS-g-BC with specified molecular weights and structure ($M_n \sim 2.5 \times 10^3$ g/mol, M_w/M_n (DPI) ~ 2.1 , cationic content ($m/(m+n) \sim 20$ mol%), which showed optimized antimicrobial activities against Foc4, according to Ref [24], was synthesized and chosen as the sample for extensively studies. While for PQD-BC, the molecular weight (M_n) based on Ubbelohde capillary viscometer was about 3.2×10^5 g/mol, according to ref. [23].

2.3. Antifungal bioassay

2.3.1. Mycelia growth inhibition method

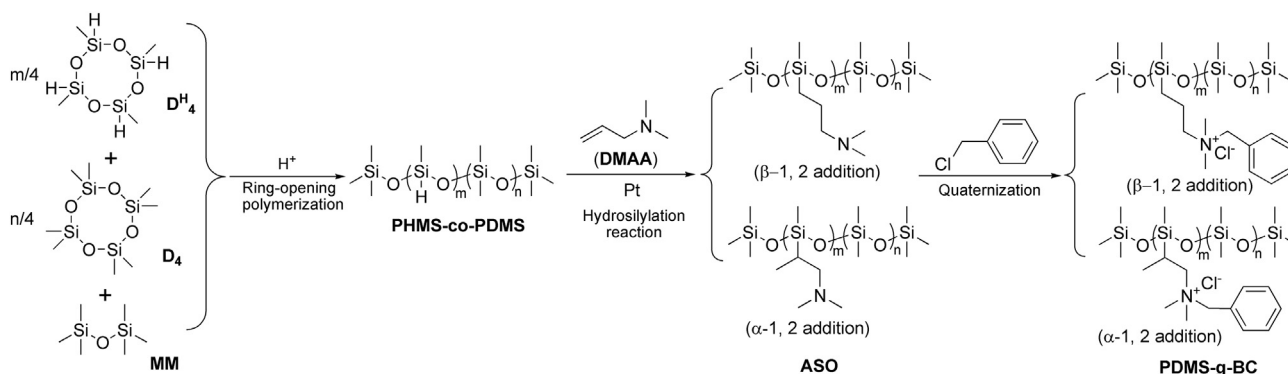
The effect of synthetic compounds (PDMS-g-BC, PQD-BC, and BC) on the mycelial growth of Foc4 was measured using an *in vitro* mycelial growth inhibition assay [26–28]. In brief, 6-mm-diameter disks of mycelial agar were cut with a sterile cork borer from the actively growing edge of 5-day-old cultures on PDA plates. Each one was then was placed in the center of each 9-cm-diameter Petri dish containing PDA medium with various concentrations of polymers (0–1.6 mg/mL). Before being mixed with molten agar at a temperature below 60 °C, the synthetic compound solutions were sterilized by passing them through a 0.45 μ m Millipore filter. The radial growth of Foc4 was detected after it was incubated at 28 °C for 5 days. Equal volumes of sterile distilled water were used as the negative control. Mycelial growth was expressed as the diameter of the fungal colony (mycelium) in the Petri dish minus the diameter of the agar plugs (6 mm). The inhibition percentage was calculated according to the following formula:

$$\text{Inhibitory rate} = \frac{D_c - D_t}{D_c} \times 100\% \quad (1)$$

where D_c is the mean colony diameter for the control set and D_t is the mean colony diameter for the treatment set. The concentration-dependent curve was the biological probability value of inhibition rates for the Y-axis against the log (test sample concentration) for the X-axis. The IC_{50} and IC_{90} values were defined as the concentration required for 50% and 90% inhibitions of mycelial growth, respectively (seen in Table 1). The antifungal effects of synthetic compounds were expressed as the IC_{50} and IC_{90} , which were evaluated further using the below-mentioned method. Each measurement consisted of at least three replicates. The mycelial growth picture is shown in Fig. 1.

2.3.2. Minimum inhibitory concentration (MIC)

The minimum inhibitory concentration (MIC) of the synthetic compounds against Foc4 was determined by using the broth microdilution procedure with 2, 3, 5-triphenyl-tetrazolium chloride (TTC). The TTC reagent is colorless, but it gives off a bright red color when reduced, indicating the presence of live fungi [29,30]. Foc4 spores were cultured in sterile potato dextrose (PD) medium (in liquid) with different concentrations of compounds solutions in 96-well plates (100 μ L of medium per well) at a concentration of approximately 1.0×10^5 cells/mL. After the spores were cultured for 24 h, 5 μ L (5.0 mg/mL) of TTC solution (in PD medium) was added to each well, and the 96-well plates were subsequently incubated in the dark at 28 °C for another 4 h. Two controls were set up; in one control, no spores were added to the wells (blank wells) containing an equal volume of sterile PD medium, and in the other, an equal volume of spores (1.0×10^5 cells/mL) was added to the wells with an equal volume of sterile PD medium without



Scheme 1. Synthesis routine for PDMS-g-BC. *m* and *n* are number of hydrogen-containing segments and number of non-hydrogen-containing segments, respectively.

the compounds (negative control). The visual color changes were recorded before and after incubation to determine the MIC (mg/mL, present in the well). The color changes present in the well matched that of the blank well that was taken as the MIC for each fungus.

2.3.3. Minimal fungicidal concentration (MFC)

To differentiate between the fungistatic and fungicidal effect of the compounds, the MFC of the polymers against *Foc4* was determined by spot plate method. Aliquots from wells that appeared to have fewer or no colonies were plated on PDA plates. For this purpose, 50 μ L of culture from each well was taken after the MIC experiment and spotted onto the PDA plates. The PDA plates were then incubated for 3 days at 28 $^{\circ}$ C to allow the cells to grow. The number of colonies present in the well for which no colony was observed on the PDA plates was taken as the minimal fungicidal concentration (MFC) for each fungus.

2.4. Mechanism of antifungal action

2.4.1. Cytoplasmic membrane disruption assay

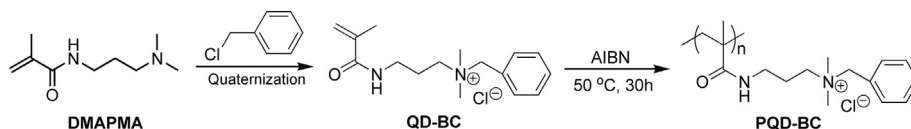
To observe the plasma membrane integrity, *Foc4* spores were cultured in sterile PD medium containing synthesis compounds at three different concentrations (the MIC, IC_{50} , and IC_{90}). The treatment concentration was chosen on the basis of the antifungal bioassay and a control was made in a similar manner in sterile PD medium without the test compounds. After incubation under constant shaking at 28 $^{\circ}$ C for 48 h, the spore suspension was harvested, washed twice with PBS (pH 7.4), and finally resuspended in 100 μ L of PBS. Then, 10 μ L of spore suspension was combined with 15 μ M of the red fluorescent nucleic acid stain propidium iodide (PI), which is commonly used for detecting the cellular membrane integrity [31]. After it was incubated in the dark for 15 min, the mixture was centrifuged, washed twice with PBS to remove residual dye and resuspended in 100 μ L of PBS. A 5 μ L aliquot was placed on a glass slide, which was then covered by a cover slip, sealed, and examined under a fluorescence microscope (Nikon Eclipse 80i, Japan). Excitation was performed for PI at 543 nm. Emissions were collected using a long pass filter for PI at 590–800 nm. The images were captured through a charge-coupled device camera. Three fields of view were chosen randomly from each cover slip. The experiment was repeated three times.

2.4.2. Cellular leakage assay

The leakage of cytoplasmic contents from the mycelia was determined to explain the changes in membrane permeabilization according to the method of Lewis and Papavizas with some modifications [32]. *Foc4* was cultured in PD medium on a rotary shaker at 120 rpm for 3 days at 28 $^{\circ}$ C. The mycelia were then harvested and washed with phosphate-buffered saline (PBS, pH 7.4). The equal mass-washed mycelia were re-suspended in 50 mL of sterile distilled water containing test compounds at three different concentrations (IC_{90} , $6 \times IC_{90}$ and $12 \times IC_{90}$, as seen in Table 1) and incubated on a rotary shaker for 8 h. The controls were treated with the same quantity of sterile distilled water. Samples from the suspensions were collected and filtered at 2 h intervals during the incubation. The filtered solutions were used to determine the leakage of soluble proteins, carbohydrates and nucleic acids. A Bradford assay was performed to quantify the release of the proteins, using BSA as the standard [33]. Soluble carbohydrates were detected by anthrone reaction, which uses glucose as the standard [34]. The electric conductivity of the resulting supernatant was measured in a conductivity meter (DDS-11A, Shanghai Precision Scientific Instrument Co., Ltd. Shanghai, China) [28]. Each measurement consisted of at least three replicates.

2.4.3. Lipid peroxidation analysis

The lipid peroxidation in the cell membrane of *Foc4* was quantified based on its malondialdehyde (MDA) levels [35–37]. *Foc4* was cultured in PD medium on a rotary shaker at 120 rpm for 3 days at 28 $^{\circ}$ C. To detect lipid peroxidation, the fungal suspensions were treated with compounds at three different concentrations ($1/2 \times IC_{90}$, IC_{90} , and $2 \times IC_{90}$, as seen in Table 1), with no addition to the control group. The fungal suspensions were incubated for another 24 h at 28 $^{\circ}$ C with shaking at 120 r/min. The fungal suspensions were centrifuged at 12,000 rpm for 5 min, after which the pellet was sonicated twice on ice with lysis buffer (2% Triton-X 100, 1% SDS, 100 mM NaCl, 10 mM Tris-HCl, 1 mM EDTA [pH 8.0]) in 5% trichloroacetic acid (TCA). The mixture was centrifuged, and the supernatant was harvested as a crude MDA-mycelial solution. The MDA contents of the mycelia and medium were determined using an MDA kit purchased from Nanjing Jiancheng Institute of Bioengineering (Nanjing, Jiangsu, China). MDA can react with freshly prepared thiobarbituric acid to form a colored complex, which has a maximum absorbance at 532 nm in a UV-Vis spectrophotometer (UV2300,



Scheme 2. Synthesis routine for PQD-BC.

Table 1
The antifungal effect of PQD-BC, PDMS-g-BC and BC against Foc4.

Compounds	Mycelial growth		Spore propagation		
	IC ₅₀ (mg/mL)	IC ₉₀ (mg/mL)	MIC (mg/mL)	MFC (mg/mL)	MFC/MIC
PQD-BC	1.0	2.78	0.3	2.0	6.67
PDMS-g-BC	0.64	7.05	0.15	0.4	2.67
BC	0.06	0.52	0.1	0.2	2.0

Techcomp, Shanghai, China) [35]. Each experiment was performed in triplicate.

2.4.4. Cell wall disruption assay

The cell wall integrity was expressed as the increased alkaline phosphatase (ALP) of the medium after compounds treatments [28]. Foc4 was cultured in PD medium and rotated at 28 °C on a rotary shaker at 120 rpm for 3 days. After that, 5 mL of sterile distilled water containing polymers was added to the above medium at three different concentrations (the MIC, IC₅₀, and IC₉₀) and incubated on a rotary shaker for another 48 h. The controls were treated with the same quantity of sterile distilled water. The suspensions were centrifuged at 4000 × g for 10 min to obtain the supernatants. To find the effects of the polymers on the cell wall, the activity of ALP in the supernatant was determined by using assay kits purchased from the Nanjing Jiancheng Institute of Bioengineering (Nanjing, Jiangsu, China) according to the manufacturer's instructions, and the result was recorded in U/L [28]. Each treatment had three replicates.

2.4.5. Efficacy on mitochondrial function

The mitochondrial function of Foc4 was expressed by the extracellular enzyme SDH activity (A_{SDH}) [38]. Foc4 was cultured in PD medium on a rotary shaker at 120 rpm for 3 days at 28 °C. Sterile distilled water-dissolved compounds were added to the fungal suspension to reach the final concentrations needed for the MIC, IC₅₀ and IC₉₀, and they were incubated on a rotary shaker for another 48 h. The controls received the same quantity of sterile distilled water. The mycelia were filtered and used to isolate mitochondria with a Mitochondrial Isolation Kit (Beijing Solarbio Science & Technology Co. Ltd., Beijing, China). Before the mitochondria were extracted, the mycelia were ground under liquid nitrogen. The A_{SDH} was determined using the assay kits purchased from the Nanjing Jiancheng Institute of Bioengineering (Nanjing, Jiangsu, China). The total protein content was determined by Bradford method [33]. Afterwards, the amount of protein was calculated according to the standard protein curve, which was measured with different

concentrations of a protein standard. The A_{SDH} was calculated using the following equation:

$$A_{SDH} = \frac{\Delta OD_{600} \times 100}{C_s/V_s} \quad (2)$$

where ΔOD_{600} is the reduction of OD (Optical density, conceptually and numerically equivalent to absorbance) value at 600 nm of the sample in 1 min, C_s is the protein concentration (mg/mL) and V_s is the volume of the sample (mL).

SDH can take part in reduction of 2, 6-dichlorophenolindophenol, which has a maximum absorbance at 600 nm in a UV-Vis spectrophotometer. One unit of SDH activity was defined as the amount of enzyme in 1 mL of fungal suspension with a 1 min reaction time that gave a reduction by 0.01 absorbance unit. Each treatment had three replicates.

2.4.6. In Vitro electrophoretic mobility shift assay (EMSA)

The DNA-binding activities of genomic DNA and the compounds were assessed by EMSA, which is widely used to research antimicrobial drugs, and it is based on the observation that bound DNA complexes migrate through gels more slowly than unbound DNA fragments [39–40]. To obtain a significant amount of highly purified genomic DNA, Foc4 was cultured in PD medium on a rotary shaker at 120 rpm for 3 days at 28 °C. The mycelia were then collected and washed twice with PBS (pH 7.4) to remove the medium. After freeze-drying, the total intracellular DNA was extracted with an Ezup Column Fungi Genomic DNA Purification Kit (Sangon Biotech Co., Ltd., Shanghai, China), and RNase was added. Genomic DNA gave a UV absorbance ratio of 1.8–1.9 at 260 and 280 nm (A_{260}/A_{280}), indicating that the DNA was sufficiently free of proteins. 5 µg highly purified genomic DNA with a fixed concentration (500 µg/mL) was incubated with the TE buffer containing aliquots of chemical compounds at three different concentrations (the MIC, IC₅₀, and IC₉₀) at room temperature for 10 min. The interaction between the compounds and genomic DNA was studied by agarose gel electrophoresis, and the TE buffer alone was incubated with a DNA control. A 5 µL volume of GoldView™ (Beijing Solarbio Science & Technology Co. Ltd., Beijing, China) was used as fluorescent dye and 1 mg of DNA was loaded onto the 1% gel; electrophoresis was performed in TAE (Tris Acetate EDTA) buffer for 60 min. The gel was visualized under UV light using a Bio-Rad Trans illuminator IEC 1010. All the experiments were repeated three times.

2.4.7. In vivo efficacy on genomic DNA

To investigate whether the compounds penetrated the cell barriers and interacted with genomic DNA, we also studied the *in vivo* efficacy against Foc4 genomic DNA after the compounds treatments. Foc4 was

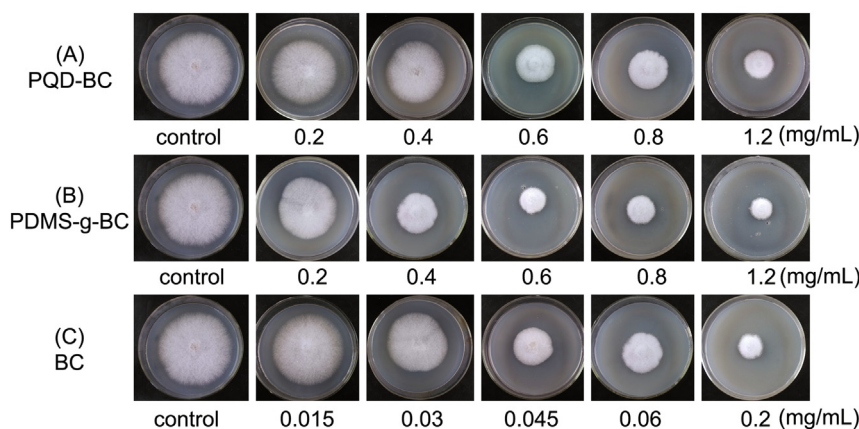


Fig. 1. The mycelial growth of Foc4 in PDA medium after applying PQD-BC (A), PDMS-g-BC (B) and BC (C). The data were based on three replicates, and the test was repeated twice with similar results. The representative results are shown.

cultured in PD medium on a rotary shaker at 120 rpm for 3 days at 28 °C. Sterile distilled water-dissolved compounds were added to the fungal suspension to reach the final concentrations needed for the MIC, IC₅₀ and IC₉₀ and they were incubated on a rotary shaker for another 48 h. The controls received the same quantity of sterile distilled water. The mycelia were collected and washed twice with PBS (pH 7.4) to remove the medium, and then ground under liquid nitrogen. The total intracellular DNA was extracted with assay kits (Sangon Biotech Co. Ltd., Shanghai, China), and RNase was added. The *in vivo* interaction between the compounds and genomic DNA was studied by agarose gel electrophoresis. All the experiments were repeated three times.

2.5. Statistical analysis

SPSS software (SPSS Inc., Chicago, IL, USA) was used for the statistical analyses of the data. To determine the effects of the treatments, an analysis of variance (ANOVA) was performed. A Duncan's multiple range test was used for mean separations when the treatment effects were statistically significant ($P < 0.05$).

3. Results and discussion

3.1. Antifungal activity

The effects of PQD-BC, PDMS-g-BC and BC on the mycelial growth of Foc4 were detected at various concentrations on PDA plates. The test compounds inhibited the growth of Foc4 in a dose-dependent manner at concentrations ranging from 0.2–1.2 mg/mL (PQD-BC and PDMS-g-BC) and from 0.015–0.2 mg/mL (BC) (Fig. 1). After 5-day incubation, the PQD-BC displayed antifungal effects with an IC₅₀ of 1.0 mg/mL and an IC₉₀ of 2.78 mg/mL, whereas PDMS-g-BC exhibited antifungal activity with an IC₅₀ of 0.64 mg/mL and an IC₉₀ of 7.05 mg/mL, which indicated that the inhibitory effect of PDMS-g-BC was greater than that of PQD-BC. BC exhibited the most active effect against Foc4 (IC₅₀ = 0.06 mg/mL, IC₉₀ = 0.52 mg/mL). The determination of the antifungal efficacy showed that PQD-BC, PDMS-g-BC and BC inhibit the mycelial growth of Foc4 in a dose-dependent manner.

We subsequently tested the MIC and MFC of PQD-BC, PDMS-g-BC and BC against Foc4 as shown in Fig. 2. The *in vitro* studies showed that PQD-BC exerted antifungal action against Foc4 with an MIC of 0.3 mg/mL and an MFC of 2 mg/mL. PDMS-g-BC displayed antifungal action against Foc4 with an MIC of 0.15 mg/mL and an MFC of 0.4 mg/mL. The MIC and MFC values of BC against Foc4 were 0.1 and 0.2 mg/mL, respectively.

The ratios of MFC to MIC were used to define an organism as tolerant. For comparable antifungal efficiency in PQD-BC with a polyacrylamide

backbone (MFC/MIC = 6.67) against Foc4, the MIC of PDMS-g-BC with a larger hydrophobic polydimethylsiloxane backbone against Foc4 is lower, which indicates that incorporating a more hydrophobic backbone into polymers is easier to trigger-gather adsorbance onto the cell surface and strengthen the antimicrobial activities of PQAS. This finding also indicated that PDMS-g-BC is a promising application for antifungal agents against plant pathogenic disease (MFC/MIC = 2.67, a ratio value of <4 corresponding to fungicide) [41], which can be compared to that of BC (MFC/MIC = 2). The fungal cell surfaces are negatively charged in the same way as the bacterial cell surface due to their components (chitin and β -glucan), and PQD-BC, PDMS-g-BC and BC with the same cationic group and different degrees of hydrophilicity are able to trigger-gather, leading to different degrees of adsorption onto the Foc4 cell surface according to the results of the mycelia growth inhibition method and the broth microdilution method. Taken together, the antifungal activities of PQAS are affected by certain molecular weights and degrees of hydrophobicity, and these results thus indicated that PQD-BC and PDMS-g-BC could be used to develop antifungal materials.

3.2. Mechanism of antifungal action

3.2.1. Membrane-active mode of action

Quaternary ammonium salts treatments can rapidly lead to the disintegration of biological membranes in fungal pathogens, resulting in cell death [6]. To establish the mode of antifungal action, the cytoplasmic membrane integrity was disrupted with compounds against Foc4 using a fluorescent dye (PI) by fluorescence microscopy. The PI is membrane-impermeable and is generally excluded from viable cells only when the fungal membrane is compromised, and the microscopy results thus indicated that the cationic polymer interacted with and subsequently disrupted the membrane integrity of the fungi. Fluorescence microscope images showed that in comparison with the control, the cells that were treated with the compounds showed complete membrane permeabilization as clearly indicated by red fluorescence, which shows that the numbers of spores that lost plasma membrane integrity increased after PQD-BC, PDMS-g-BC and BC treatments (Fig. 3). All the cationic biocides were found to depolarize the membrane integrity of Foc4, and they may inhibit the growth of Foc4 by directly damaging the plasma membrane and causing the cell death of the fungal pathogen.

Damage to the plasma membrane can lead to the loss of the osmotic balance and the influx of fluids and ions as well as the loss of proteins and carbohydrates, eventually causing the onset of cell death [24]. To confirm whether PQD-BC, PDMS-g-BC and BC caused a loss in the cytoplasmic membrane integrity of Foc4, the leakage of cytoplasmic

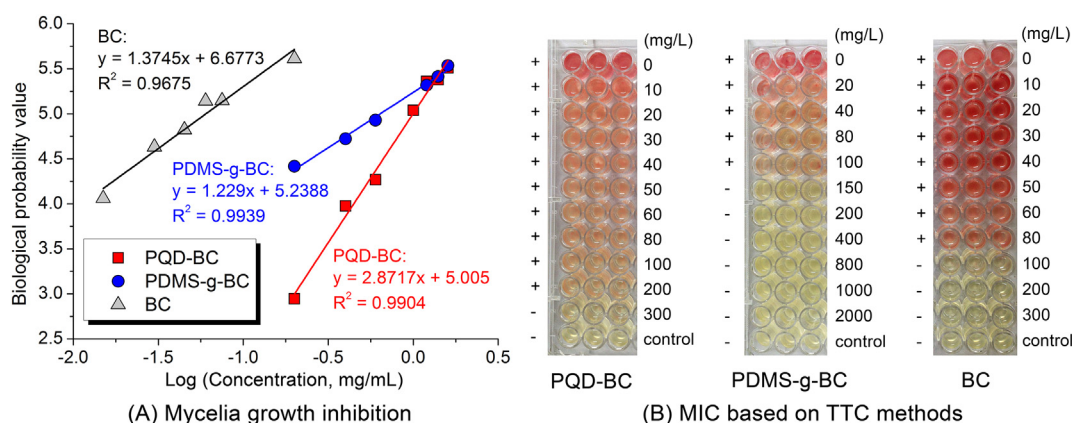


Fig. 2. (A) Effect of PQD-BC, PDMS-g-BC and BC on mycelial growth of Foc4 in PDA medium. The growth of Foc4 was measured after 5 days of incubation at 28 °C. The data were based on three replicates. Treatments followed by different letters within each sampling interval are significantly different according to Duncan's multiple range test ($P < 0.05$). (B) The MIC values of PQD-BC, PDMS-g-BC and BC against Foc4 based on the TTC colorimetric method. (+) indicates certain cells in the plate and (–) indicates fewer or no cells in the plate.

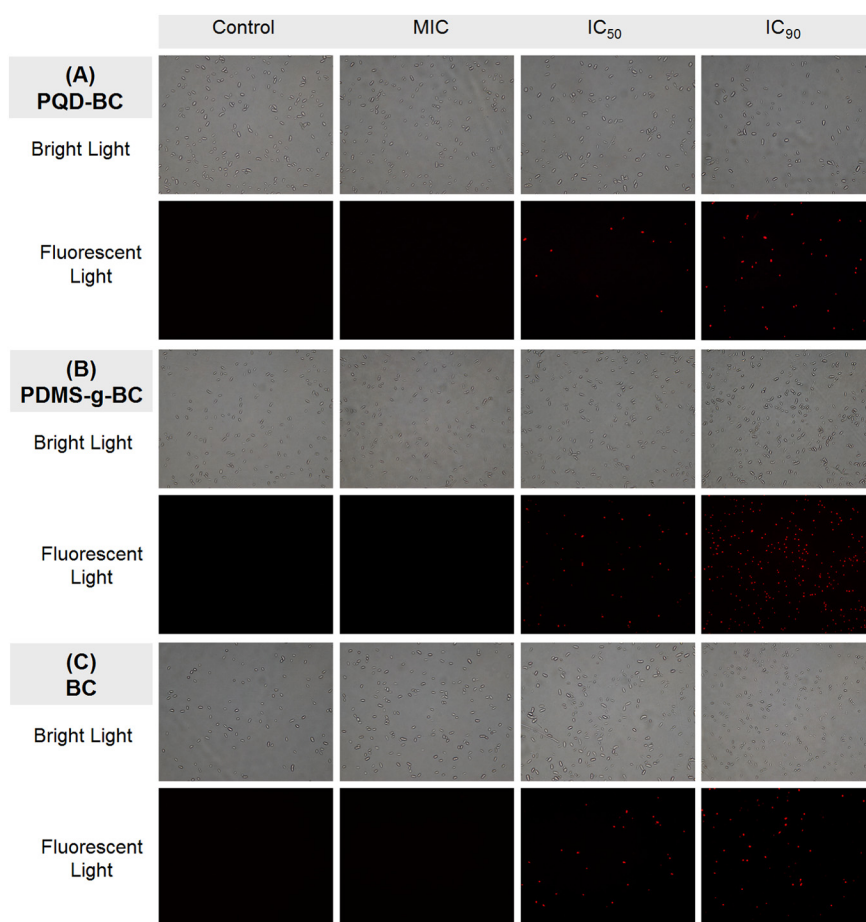


Fig. 3. Loss of plasma membrane integrity in Foc4 after PQD-BC (A), PDMS-g-BC (B) and BC (C) treatments. The spores were stained with PI and observed with a fluorescence microscope. The spores are magnified by 20 times life size. Spores with damaged plasma membranes fluoresced red. (For interpretation of the references to color in this figure legend, the reader is referred to the web version of this article.)

constituents was determined. As expected, it is clear from the figure that the three compound treatments significantly induced the leakage of soluble proteins (Fig. 4-A), carbohydrates (Fig. 4-B), and conductivity (Fig. 4-C) out of the Foc4 mycelia. In general, the amount of leaked materials was positively correlated with the concentrations of PQD-BC, PDMS-g-BC and BC. The cellular leakage could be observed after 4 h of treatment, and it was generally constant over a period of 6 h for soluble proteins, carbohydrates, and electric conductivity. Since we observed the same physiological events with the release of cytoplasmic constituents, it is quite reasonable to assume that the mode of action of PQD-BC, PDMS-g-BC and BC can be interpreted on the basis of each elementary process in which cationic biocides adsorb onto the fungal cell surface, diffusing through the cell wall, and subsequently binding to the cytoplasmic membrane, releasing the cytoplasmic constituents, and finally inducing the cell death of the fungal pathogen. The hydrophobicity of the polymers enabled them to partition into the lipids of the fungal cell membrane and mitochondria, rendering them permeable and leading to the leakage of the cell contents.

Taken together with the antifungal efficiency of PQD-BC and PDMS-g-BC, the penetration is intensively affected by the interaction of the ammonium group with the cytoplasmic membrane and the mobility of the functional group. With a stronger driving force, the ammonium group can reach the cytoplasmic membrane more easily. Therefore, the increase in antifungal efficiency with a longer hydrophobic polydimethylsiloxane backbone may be explained by the increasing hydrophobicity of the quaternary group, which may strengthen the interaction with the cytoplasmic membrane, therefore enhancing the ability to kill the fungal cell.

3.2.2. Lipid peroxidation

To investigate the lipid damage, the levels of MDA, a biomarker of lipid peroxidation and a decomposition product of polyunsaturated fatty acid hydroperoxidase, were assessed [35]. MDA, which was primarily released into the medium when the plasma membrane lipid peroxidation was set off, and it was determined to investigate whether lipid peroxidation was associated with membrane damage [36]. In the lipid peroxidation assay, exposure of Foc4 for 24 h to PQD-BC of $1/2 \times IC_{50}$, IC_{50} and IC_{90} led to a the highest release (4.58, 8.33 and 21.67 mmol/g, respectively) of MDA among treatment-groups, whereas exposure to PDMS-g-BC of $1/2 \times IC_{50}$, IC_{50} and IC_{90} led to the second-highest release (0.61, 2.39 and 20.4 mmol/g, respectively) of MDA. No obvious effect on the BC-treated group was detected (data not shown). The results show that significantly increased MDA levels occur as a result of the oxidative damage induced by exposing Foc4 to $1/2 \times IC_{90}$, IC_{90} and $2 \times IC_{90}$ of PQD-BC (Fig. 5-A) and PDMS-g-BC (Fig. 5-B) for 24 h in comparison with the control. The oxidative degradation caused by PQD-BC and PDMS-g-BC, which is referred to as lipid peroxidation, leads to a decrease in the cell membrane fluidity and an increase in membrane leakiness. This finding suggested that the toxicity of PQD-BC and PDMS-g-BC is linked to oxidative stress, which induces membrane lipid peroxidation and may cause the loss of plasma membrane integrity in Foc4, but BC had no effect on the plasma membranes of treated mycelia.

3.2.3. Cell wall integrity

To determine whether PQD-BC, PDMS-g-BC and BC led to the loss of cell wall integrity in Foc4, the ALP contents of the medium were

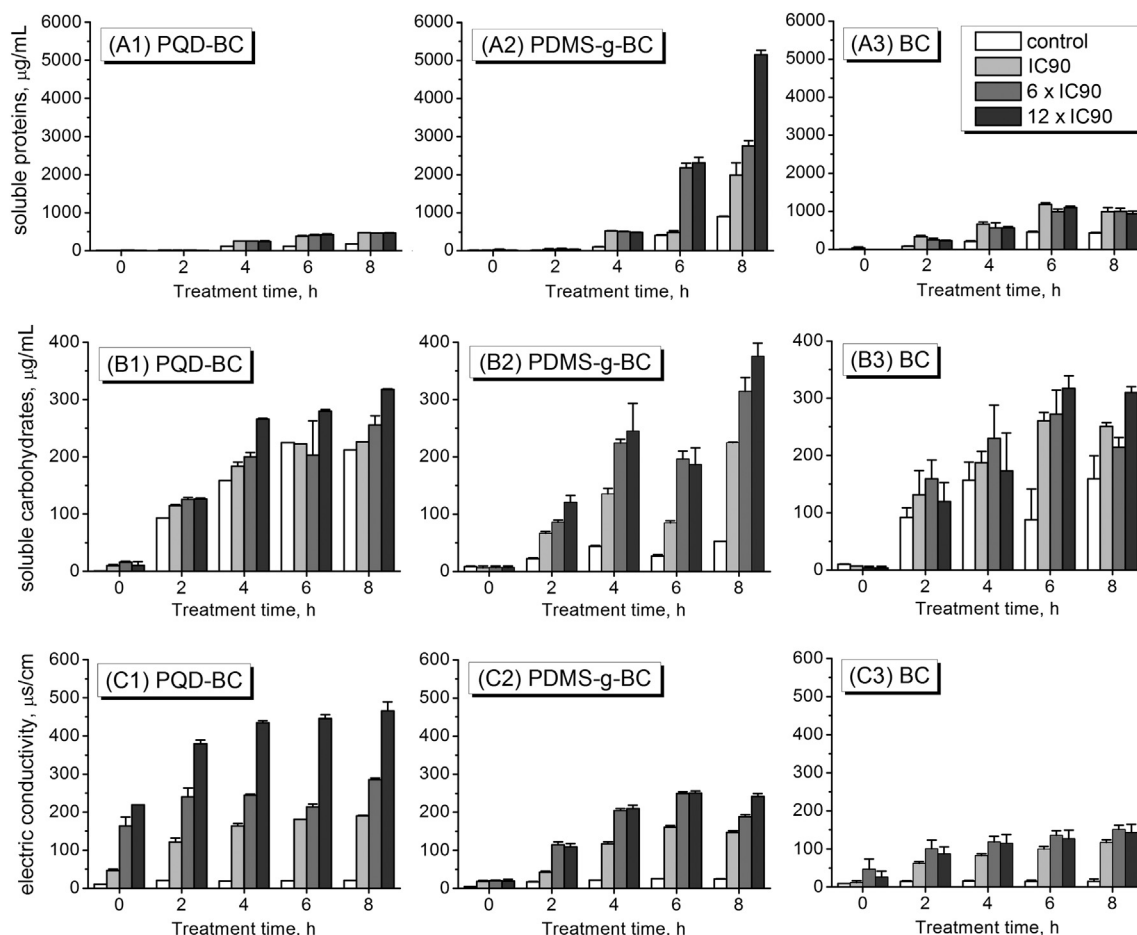


Fig. 4. Leakage of cytoplasmic contents from Foc4 treated with PQD-BC, PDMS-g-BC and BC. Mycelia were placed in distilled water supplements with different concentrations of antifungal agents and incubated at 28 °C for 0, 2, 4, 6 and 8 h. The cytoplasmic leakage of soluble proteins (A) and (B) was expressed as micrograms per milliliter of solution, while the leakage of electric conductivity (C) was monitored using an electrical conductivity meter. Each data point is the mean \pm SE of three replicates.

measured, which has been shown to be produced in the cytoplasm and secreted into the periplasmic space [42]. Damage to the external cell wall layers can lead to the release of ALP from the cell [43]. Increased ALP activities, which was observed in medium, were found to be 0.57, 1.24, and 3.66 U/L at MIC, IC₅₀ and IC₉₀, respectively, whereas in the PDMS-g-BC-treated cells were found to be 0.50, 1.87, and 6.39 U/L at

MIC, IC₅₀ and IC₉₀, respectively and in the BC-treated cells were found to be 0.73, 0.89, and 8.28 U/L at MIC, IC₅₀ and IC₉₀, respectively. The PQD-BC, PDMS-g-BC and BC treated groups showed higher ALP activity than the control after a 24-h treatment, which confirmed that the cell wall of Foc4 was destroyed in a dose-dependent manner (Fig. 6).

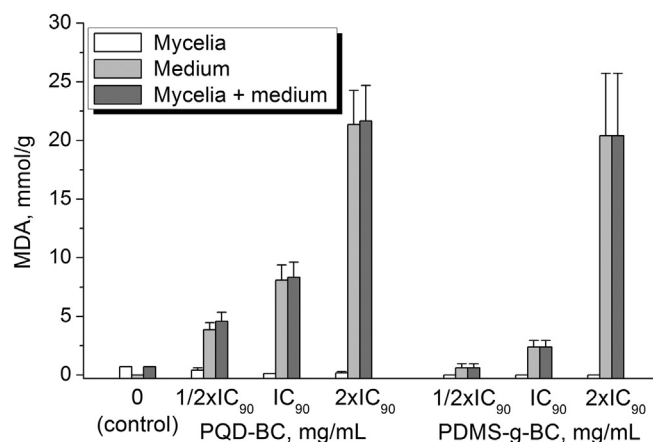


Fig. 5. Loss of cell wall integrity in Foc4 after PQD-BC and PDMS-g-BC treatments. Mycelia were placed in distilled PD medium supplement with different concentrations of antifungal agents and incubated at 28 °C for 48 h. The malonic aldehyde (MDA) content was expressed as the mmol per gram (mmol/g) of mycelia. The data were based on three replicates. Bars indicate standard errors.

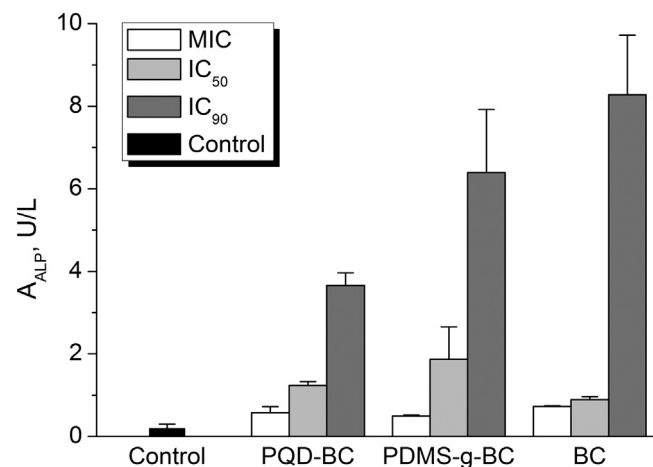


Fig. 6. Loss of cell wall integrity in Foc4 after PQD-BC, PDMS-g-BC and BC treatments. The mycelia were placed in distilled PD medium supplemented with different concentrations of antifungal agents and incubated at 28 °C for 48 h. The alkaline phosphatase activity was expressed as units per liter (U/L) of filtered solution. The data were based on three replicates. The bars indicate standard errors.

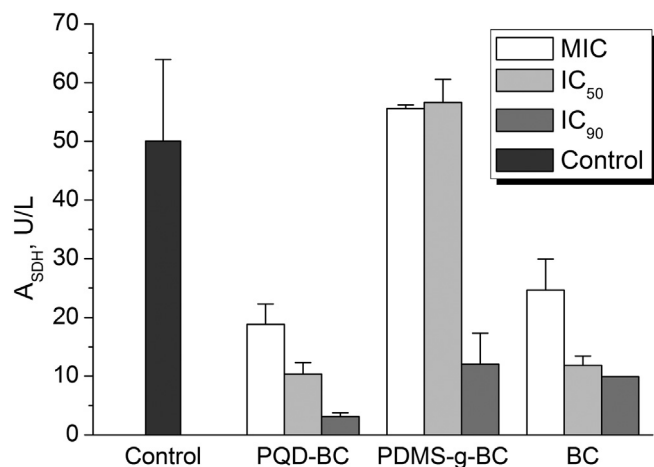


Fig. 7. Mitochondrial function of Foc4 after PQQ-BC, PDMS-g-BC and BC treatments. The mycelia were placed in distilled PD medium supplement with different concentrations of antifungal agents and incubated at 28 °C for 48 h. The succinate dehydrogenase activity was expressed as units per milligram of soluble protein. The data were based on three replicates. Bars indicate standard errors.

These data suggested that after absorption onto the cell surface, the PQQ-BC, PDMS-g-BC, and BC treatments were able to destroy the cell walls of fungal pathogens and they interacted with the plasma membrane, leading to the release of intracellular contents and ALP, which led to eventual direct cell death.

3.2.4. Mitochondrial dysfunction

To assess changes in mitochondrial function, the SDH activity of Foc4 cells that were exposed to the compounds was determined. SDH is the functional substance for the tricarboxylic acid cycle and aerobic respiration. Its activity is closely associated with bioenergy synthesis and mitochondrial function in a variety of prokaryotic and eukaryotic cells [38]. For SDH activity, the control group was active, while there was a substantial decrease in the treated groups in a dose-dependent manner following exposure to PQQ-BC and BC (Fig. 7). There were no significant effect after PDMS-g-BC treatment at the MIC and IC₅₀, while a higher concentration (IC₉₀) could significantly decrease SDH activity. Therefore, PQQ-BC, PDMS-g-BC and BC affect the bioenergy synthesis pathway of Foc4 by inhibiting SDH activity. This finding suggested that the potential mechanism underlying their antifungal actions were their inhibition of mitochondrial function.

3.2.5. Interactions of genomic DNA with the compounds

As a carrier of genetic information, DNA is a major target for drug interactions because of its ability to interfere with transcription (gene expression and protein synthesis) and replication, a major step in cell growth and division [44–46]. In this study, the EMSA was used to test the affinity of DNA-binding polymers to investigate their efficacy against genomic DNA, and the mode of action was illustrated. When genomic DNA is separated by electrophoresis, rapid migration will be observed for unbound and cleaved DNA. By contrast, the complex produces a slower migration due to the increase of molecular weight and decrease of negative charge, which means that a constant amount of DNA was mixed with increasing amounts of compounds, tethered to compound-DNA-conjugated agarose beads. For the *in vitro* test, test compounds were immobilized with Foc4 genomic DNA according to the observations made by agarose electrophoresis. Lanes 1–9 show genomic DNA that was incubated with the test compounds at three different concentrations (the MIC, IC₅₀ and IC₉₀), while Lane 10 applies to the untreated genomic DNA (control DNA). Compared with the control, the treatments are very effective at changing the mobility and shape of genomic DNA. As shown in Fig. 8-A, BC could partly retard genomic DNA at MIC and IC₅₀ and completely retard genomic DNA at IC₉₀ (in Lanes 4–6), while PDMS-g-BC partly retard genomic DNA at MIC and completely inhibit the electrophoretic mobility of genomic DNA at IC₉₀ (in Lanes 7–9). The result suggested that DNA was exposed to PDMS-g-BC and BC to form compound-DNA complexes through electrostatic interactions and thereby specifically results in a further reduction in the mobility of the compound-DNA complex (supershift). However, no obvious DNA bands were indicated in the lane for the PQQ-BC treated group (in Lanes 1–3), and the DNA loading buffer containing bromide blue indicator remained in the pore. The GoldView™ has weak fluorescence, but its emission intensity in the presence of DNA can be greatly enhanced because of its strong intercalation between the adjacent DNA base pairs. This enhanced fluorescence could be quenched, or at least partly quenched by the addition of a second molecule with higher DNA-binding ability. This finding indicated that PQQ-BC was immobilized strongly with genomic DNA, which caused the GoldView™ was completely replaced by PQQ-BC and appreciable decrease in the emission intensity. A similar finding occurs in the treated group when the concentration of PDMS-g-BC reached the IC₉₀ (in Lanes 9). The amount of bound DNA was increased with increasing amounts of both test compounds in the reaction.

Interactions between genomic DNA and test compounds at MIC, IC₅₀ and IC₉₀, respectively, were further investigated during *in vivo* analysis (Fig. 8-B). Notably, the genomic DNA that was exposed to PQQ-BC

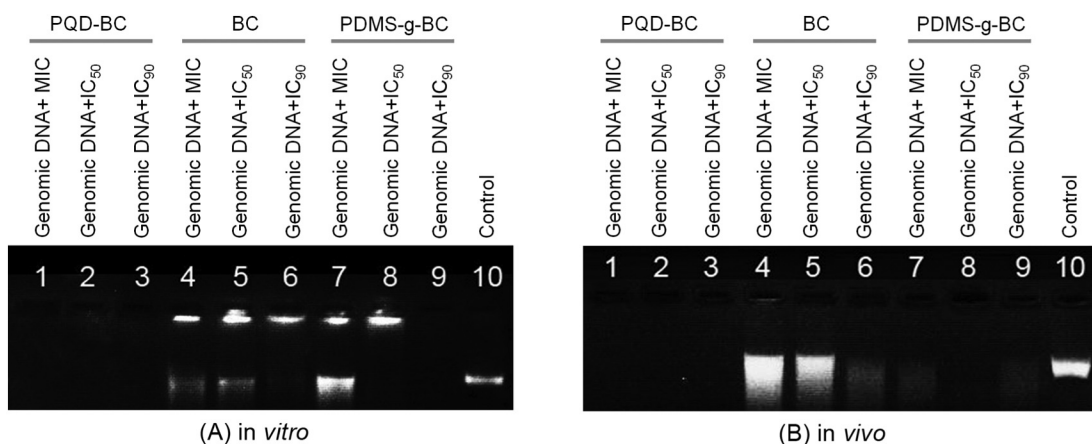


Fig. 8. Interaction of compounds (PQQ-BC, PDMS-g-BC and BC) with Foc4 genomic DNA *in vitro* (A) and *in vivo* (B). 25 µg of genomic DNA (5 µL of genomic DNA with a fixed concentration (500 µg/mL)) was used. For lanes 1–3: treated with 5 µL of TE buffer containing PQQ-BC at final concentrations matching the MIC, IC₅₀, and IC₉₀. For lanes 4–6: treated with 5 µL of TE buffer containing BC at final concentrations matching the MIC, IC₅₀, and IC₉₀. For lanes 7–9: treated with 5 µL of TE buffer containing PDMS-g-BC at final concentrations matching the MIC, IC₅₀, and IC₉₀. For lane 10: treated with 5 µL of TE buffer without test compound (negative control). The data were based on three replicates and the test was repeated twice with similar results. The representative results are shown.

show a similar situation to *in vitro* analysis that the genomic DNA was lost in all concentrations tested (in Lanes 1–3), whereas the genomic DNA was degraded upon the application of BC at all concentrations tested (in Lanes 4–6). The genomic DNA that was exposed to PDMS-g-BC was mostly being diminished (in Lanes 7–9). The different DNA cleavage efficiency of the compounds with different structures may be to the different binding affinity of the compounds to DNA. The experiment revealed the structure-activity relationship in the antifungal action in that BC was able to bind to DNA nonspecifically, while the PQD-BC treatment caused specific binding. The PDMS-g-BC treatment caused specific binding if the treated concentration reached the IC₉₀.

In conclusion, PQD-BC, PDMS-g-BC and BC were bound to DNA and created fractures in the DNA strands, causing changes that affected the structural and electrophoretic mobility of DNA, such as the DNA damage that inhibited the DNA replication and transcription that regulate the cell cycle, causing cell death indirectly.

4. Conclusions

In conclusion, we previously demonstrated methods for developing polyacrylamide quaternary ammonium salts (PQD-BC) and polydimethylsiloxane graft quaternary ammonium salts (PDMS-g-BC) that inactivate various fungi (*R. solani* and Foc4). The PQD-BC and PDMS-g-BC were found to actively inhibit mycelial growth and spore propagation against Foc4. The structure-activity relationship studies indicated that for a comparable antifungal efficiency in PQD-BC with a polyacrylamide backbone against Foc4, the antifungal efficiency of PDMS-g-BC with a more hydrophobic polydimethylsiloxane backbone against Foc4 is more active, which means that incorporating a more hydrophobic backbone into polymers can strengthen the antimicrobial activities of PQAS, and it showed the promising application for antifungal agents in plant pathogenic disease, which can be compared to BC. The potential mechanism underlying Foc4 involves several targets in the fungal cells, including the disruption of the cellular structure, such as the cell wall and plasma membrane, inducing lipid peroxidation, mitochondrial dysfunction and interference with genomic DNA. Understanding the mechanism of action may predict that the polymeric quaternary ammonium salts will act on a broad spectrum of fungal species and may provide a new strategy for preventing and controlling Fusarium wilt in bananas.

Acknowledgments

This work was supported by the Science and Technology Planning Project of Guangdong Province, China under grant 2016A020210105; the Science and Technology Program of Guangzhou, China, under grant 201605121117091; and the National Natural Science Foundation of China under grant 31201552.

References

- [1] C.W. Wardlaw, The biology of banana wilt (Panama disease). I. Root inoculation experiments, *Ann. Bot.* 44 (1930) 741–766.
- [2] Cunwu Zuo, Li Chunyu, Li Bin, et al., The toxic mechanism and bioactive components of Chinese leek root exudates acting against *Fusarium oxysporum* f. sp. *cubense* tropical race 4, *Eur. J. Plant Pathol.* 143 (2015) 447–460.
- [3] Chun-Hua Hu, Wei Yue-Rong, Huang Yong-Hong, et al., An efficient protocol for the production of chit42 transgenic Furenzhi banana (*Musa* spp. AA group) resistant to *Fusarium oxysporum*, *In Vitro Cell Dev. Biol. Plant* 49 (2013) 584–592.
- [4] Y.L. Wu, G.J. Yi, X.X. Peng, Rapid screening of *Musa* species for resistance to *Fusarium* wilt in an *in vitro* bioassay, *Eur. J. Plant Pathol.* 128 (2010) 409–415.
- [5] Shun Song, Chen Xin, Huang Dongmei, et al., Identification of miRNAs differentially expressed in *Fusarium* wilt-resistant and susceptible banana varieties, *S. Afr. J. Bot.* 106 (2016) 244–249.
- [6] Jian Zhang, Günseli Bayram Akcapinar, Lea Atanasova, et al., The neutral metalloproteinase NMP1 of *Trichoderma guizhouense* is required for mycotrophy and self-defence, *Appl. Environ. Microbiol.* 18 (2015) 580–597.
- [7] S.M. Iconomopoulou, G.A. Voyiatzis, The effect of the molecular orientation on the release of antimicrobial substances from uniaxially drawn polymer matrixes, *J. Control. Release* 103 (2015) 451–464.
- [8] Fang Wu, Guolong Meng, Jing He, et al., Antibiotic-loaded chitosan hydrogel with superior dual functions: antibacterial efficacy and osteoblastic cell responses, *ACS Appl. Mater. Interfaces* 6 (2014) 10005–10013.
- [9] Yun Kee Jo, Jeong Hyun Seo, Bong-Hyuk Choi, et al., Surface-independent antibacterial coating using silver nanoparticle-generating engineered mussel glue, *ACS Appl. Mater. Interfaces* 6 (2014) 20242–20253.
- [10] A. Katchalsky, Polyelectrolytes and their biological interaction, *Biophys. J.* 4 (1964) 9–41.
- [11] Jiaul Hoque, Akkapeddi Padma, Yadav Vikas, et al., Broad spectrum antibacterial and antifungal polymeric paint materials: synthesis, structure-activity relationship, and membrane-active mode of action, *ACS Appl. Mater. Interfaces* 7 (2015) 1804–1815.
- [12] Shan Jiang, Li Wang, Haojie Yu, et al., Preparation of crosslinked polystyrenes with quaternary ammonium and their antibacterial behavior, *React. Funct. Polym.* 62 (2005) 209–213.
- [13] Tomiki Ikeda, Hiroki Hirayama, Hideki Yamaguchi, et al., Polycationic biocides with pendant active group: molecular weight dependence of antibacterial activity, *Antimicrob. Agents Chemother.* 30 (1986) 132–136.
- [14] A. Vnitskikh Zh, Shklyayev Yu, T.F. Odegova, et al., Synthesis and antimicrobial activity of mono- and biquaternized derivatives of dipyriddylenes and dipyriddylenes, *Pharm. Chem. J.* 40 (2006) 19–22.
- [15] K. Róžga-Wijas, U. Mizerska, W. Fortuniak, J. Chojnowski, R. Hałas, W. Werel, Quaternary ammonium salts (QAS) modified polysiloxane biocide supported on silica materials, *J. Inorg. Organomet. Polym.* 17 (2007) 605–613.
- [16] L. Kou, J. Liang, X. Ren, H.B. Kocer, S.D. Worley, Y.M. Tzou, T.S. Huang, Synthesis of a water-soluble siloxane copolymer and its application for antimicrobial coatings, *Ind. Eng. Chem. Res.* 48 (2009) 6521–6526.
- [17] T.J. Franklin, G.A. Snow, Antiseptics, antibiotics and the cell membrane, *Biochemistry of Antifungal Action*, Springer US 1975, pp. 56–75.
- [18] B.E. Elewski, Mechanisms of action of systemic antifungal agents, *J. Am. Acad. Dermatol.* 28 (1993) S28–S34.
- [19] C.O. Frank, J.P. Alistair, Neil Brown, A.R. Gow, Antifungal agents: mechanisms of action, *Trends Microbiol.* 11 (2003) 272–279.
- [20] Wenqiang Chang, Ming Zhang, Ying Li, et al., Lichen endophyte derived pyridoxatin inactivates *Candida* growth by interfering with ergosterol biosynthesis, *Biochim. Biophys. Acta Gen. Subj.* 1850 (2015) 1762–1771.
- [21] A. Beauvais, S. Bozza, O. Knemeyer, C. Formosa, V. Balloy, et al., Deletion of the *a*-(1,3)-glucan synthase genes induces a restructuring of the conidial cell wall responsible for the avirulence of *Aspergillus fumigatus*, *PLoS Pathog.* 9 (2013) 1–14.
- [22] L.J. Cheng, Q.Q. Liu, Y.F. Lei, Y.L. Lin, A.Q. Zhang, The synthesis and characterization of carboxybetaine functionalized polysiloxanes for the preparation of anti-fouling surfaces, *RSC Adv.* 4 (2014) 54372–54381.
- [23] A.Q. Zhang, Q.Q. Liu, Y.F. Lei, S.H. Hong, Y.L. Lin, Synthesis and antimicrobial activities of acrylamide polymers containing quaternary ammonium salts on bacteria and phytopathogenic fungi, *React. Funct. Polym.* 88 (2015) 39–46.
- [24] Y.L. Lin, Q.Q. Liu, L.J. Cheng, Y.F. Lei, A.Q. Zhang, Synthesis and antimicrobial activities of polysiloxane-containing quaternary ammonium salts on bacteria and phytopathogenic fungi, *React. Funct. Polym.* 85 (2014) 19–30.
- [25] L.J. Cheng, Q.Q. Liu, L. Yang, Y.L. Lin, A.Q. Zhang, Synthesis and characterization of hydrogen-containing polysiloxanes (in Chinese), *Gaofenzi Cailiao Kexue Yu Gongcheng/Polym. Mater. Sci. Eng.* 30 (2014) 25–28.
- [26] Samir Drobny, Michael Wisniewski, Ahmed El Ghaouth, et al., Influence of food additives on the control of postharvest rots of apple and peach and efficacy of the yeast-based biocontrol product aspire, *Postharvest Biol. Technol.* 27 (2003) 127–135.
- [27] Du Shijie, Zaimin Tian, Dongyan Yang, et al., Synthesis, antifungal activity and structure-activity relationships of novel 3-(difluoromethyl)-1-methyl-1H-pyrazole-4-carboxylic acid amides, *Molecules* 20 (2015) 8395–8408.
- [28] X. Shao, S. Cheng, H. Wang, et al., The possible mechanism of antifungal action of tea tree oil on *Botrytis cinerea*, *J. Appl. Microbiol.* 114 (2013) 1642–1649.
- [29] C.C. Sollod, A.E. Jenns, M.E. Daub, Cell surface redox potential as a mechanism of defense against photosensitizers in fungi, *Appl. Environ. Microbiol.* 58 (1992) 444–449.
- [30] K. Jagajjani Rao, Santanu Paria, Anti-Malassezia furfur activity of natural surfactant mediated in situ silver nanoparticles for a better antidandruff shampoo formulation, *RSC Adv.* 6 (2016) 11064–11069.
- [31] K.N. Fish, S.L. Schmid, H. Damke, Evidence that dynamin-2 functions as a signal-transducing GTPase, *J. Cell Biol.* 150 (2000) 145–154.
- [32] J.A. Lewis, G.C. Papavizas, Permeability changes in hyphae of *Rhizoctonia solani* induced by germling preparations of *Trichoderma* and *Gliocladium*, *Phytopathology* 77 (1987) 699–703.
- [33] M.M. Bradford, A rapid and sensitive method for the quantitation of microgram quantities of protein utilizing the principle of protein-dye binding, *Anal. Biochem.* 72 (1976) 248–254.
- [34] D.L. Morris, Quantitative determination of carbohydrates with Dreywood's anthrone reagent, *Science* 107 (1948) 254–255.
- [35] Heejeong Lee, Jae-Sam Hwang, Dong Gun Lee, Scolopendin 2 leads to cellular stress response in *Candida albicans*, *Apoptosis* 21 (2016) 856–865.
- [36] V. Singh, A. Pal, M.P. Darokar, A polyphenolic flavonoid glabridin: oxidative stress response in multidrug-resistant *Staphylococcus aureus*, *Free Radic. Biol. Med.* 87 (2015) 48–5735.
- [37] R.H. Mohamed, R.A. Karam, H.A. Hagrass, et al., Anti-apoptotic effect of spermatogonial stem cells on doxorubicin-induced testicular toxicity in rats, *Gene* 561 (2015) 107–114.
- [38] W.W. Fan, G.Q. Yuan, Q.Q. Li, et al., Antibacterial mechanisms of methyl gallate against *Ralstonia solanacearum*, *Australas. Plant Pathol.* 43 (2014) 1–7.
- [39] Özge Yıldız, A.T. Çolak, M. Yılmaz, et al., The syntheses, characterization, antimicrobial, DNA cleavage and cytotoxic activities of novel terephthalate complexes, *J. Mol. Struct.* 1127 (2017) 668–674.

- [40] Jeong-Ho Kim, Immobilized DNA-binding assay, an approach for *in vitro* DNA-binding assay, *Anal. Biochem.* 334 (2004) 401–402.
- [41] J.C. Sherris, Problems in *in vitro* determination of antibiotic tolerance in clinical isolates, *Antimicrob. Agents Chemother.* 30 (1986) 633–637.
- [42] K.J. Cheng, J.M. Ingram, J.W. Costerton, Release of alkaline phosphatase from cells of *Pseudomonas aeruginosa* by manipulation of cation concentration and of pH, *J. Bacteriol.* 104 (1970) 748–753.
- [43] S.S. Lindsay, B. Wheeler, K.E. Sanderson, et al., The release of alkaline phosphatase and of lipopolysaccharide during the growth of rough and smooth strains of *Salmonella typhimurium*, *Can. J. Microbiol.* 19 (1973) 335–343.
- [44] Fatma Öztürk, Leyla Açık, İzzet Şener, Fikret Karcı, Emine Kılıç, Antimicrobial properties and DNA interactions studies of 3-hetarylazoquinoline-2, 4-diol compounds, *Türk. J. Chem.* 36 (2012) 293–302.
- [45] B. Dede, I. Özmen, F. Karipcin, Synthesis, characterization, catalase functions and DNA cleavage studies of new homo and heteronuclear Schiff base copper (II) complexes, *Polyhedron* 28 (2009) 3967–3974.
- [46] E.E. İlter, N. Asmafiliz, Z. Kılıç, et al., Phosphorus–nitrogen compounds: part 19. Syntheses, structural and electrochemical investigations, biological activities, and DNA interactions of new spirocyclic monoferrocenylcyclotriphosphazenes, *Polyhedron* 29 (2010) 2933–2944.

证书号第 3173335 号



发明专利证书

发明名称：大分子季铵盐在抑制水稻纹枯病菌菌核萌发中的用途

发明人：林雅铃；刘杨润琦；周盛文；刘琼琼；雷雨风；张安强

专利号：ZL 2016 1 0278530.1

专利申请日：2016 年 04 月 28 日

专利权人：华南农业大学

地址：510642 广东省广州市天河区五山路 483 号

授权公告日：2018 年 12 月 07 日

授权公告号：CN 105941463 B

国家知识产权局依照中华人民共和国专利法进行审查，决定授予专利权，颁发发明专利证书并在专利登记簿上予以登记。专利权自授权公告之日起生效。专利权期限为二十年，自申请日起算。

专利书记载专利权登记时的法律状况。专利权的转移、质押、无效、终止、恢复和专利权人的姓名或名称、国籍、地址变更等事项记载在专利登记簿上。



局长
申长雨

申长雨



第 1 页 (共 2 页)

其他事项参见背面

证书号第 3173335 号



专利权人应当依照专利法及其实施细则规定缴纳年费。本专利的年费应当在每年 04 月 28 日前缴纳。未按照规定缴纳年费的，专利权自应当缴纳年费期满之日起终止。

申请日时本专利记载的申请人、发明人信息如下：

申请人：

华南农业大学

发明人：

林雅铃；刘杨润琦；周盛文；刘琼琼；雷雨风；张安强

证书号第 3173334 号



发明专利证书

发明名称：嵌段大分子季铵盐在抑制香蕉枯萎病菌生长中的用途

发明人：林雅铃；周盛文；刘琼琼；刘杨润琦；金莲淳；洪双豪；雷雨风
张安强

专利号：ZL 2016 1 0278195.5

专利申请日：2016 年 04 月 28 日

专利权人：华南农业大学

地址：510642 广东省广州市天河区五山路 483 号

授权公告日：2018 年 12 月 07 日

授权公告号：CN 105901013 B

国家知识产权局依照中华人民共和国专利法进行审查，决定授予专利权，颁发发明专利证书并在专利登记簿上予以登记。专利权自授权公告之日起生效。专利权期限为二十年，自申请日起算。

专利书记载专利权登记时的法律状况。专利权的转移、质押、无效、终止、恢复和专利权人的姓名或名称、国籍、地址变更等事项记载在专利登记簿上。



局长
申长雨

申长雨



第 1 页 (共 2 页)

其他事项参见背面

证书号第 3173334 号



专利权人应当依照专利法及其实施细则规定缴纳年费。本专利的年费应当在每年 04 月 28 日前缴纳。未按照规定缴纳年费的，专利权自应当缴纳年费期满之日起终止。

申请日时本专利记载的申请人、发明人信息如下：

申请人：

华南农业大学

发明人：

林雅铃；周盛文；刘琼琼；刘杨润琦；金莲淳；洪双豪；雷雨风；张安强

证书号第 5025894 号



发明专利证书

发明名称：非渗透性的含聚硅氧烷的无规共聚物及其制备方法和应用

发明人：林雅铃;谭杏银;梁嘉琪;叶琪;侯萌;何诗琦;张德强
钟伟强;张安强

专利号：ZL 2020 1 1328953.2

专利申请日：2020 年 11 月 24 日

专利权人：华南农业大学

地址：510642 广东省广州市天河区五山路 483 号

授权公告日：2022 年 03 月 25 日

授权公告号：CN 112592478 B

国家知识产权局依照中华人民共和国专利法进行审查，决定授予专利权，颁发发明专利证书并在专利登记簿上予以登记。专利权自授权公告之日起生效。专利权期限为二十年，自申请日起算。

专利证书记载专利权登记时的法律状况。专利权的转移、质押、无效、终止、恢复和专利权人的姓名或名称、国籍、地址变更等事项记载在专利登记簿上。



局长
申长雨

申长雨



第 1 页 (共 2 页)

证书号 第 5025894 号



专利权人应当依照专利法及其实施细则规定缴纳年费。本专利的年费应当在每年 11 月 24 日前缴纳。未按照规定缴纳年费的，专利权自应当缴纳年费期满之日起终止。

申请日时本专利记载的申请人、发明人信息如下：

申请人：

华南农业大学

发明人：

林雅铃; 谭杏银; 梁嘉琪; 叶琪; 侯萌; 何诗琦; 张德强; 钟伟强; 张安强

证书号第6397045号



发明专利证书

发明名称：具有两嵌段结构的含氟大分子季铵盐及其制备方法和应用

发明人：林雅铃;侯萌;张德强;张安强

专利号：ZL 2022 1 0337163.3

专利申请日：2022年03月31日

专利权人：华南农业大学

地址：510642 广东省广州市天河区五山路483号

授权公告日：2023年10月13日

授权公告号：CN 114773504 B

国家知识产权局依照中华人民共和国专利法进行审查，决定授予专利权，颁发发明专利证书并在专利登记簿上予以登记。专利权自授权公告之日起生效。专利权期限为二十年，自申请日起算。

专利证书记载专利权登记时的法律状况。专利权的转移、质押、无效、终止、恢复和专利权人的姓名或名称、国籍、地址变更等事项记载在专利登记簿上。



局长
申长雨

申长雨



证书号 第6397045号

专利权人应当依照专利法及其实施细则规定缴纳年费。本专利的年费应当在每年03月31日前缴纳。
未按照规定缴纳年费的，专利权自应当缴纳年费期满之日起终止。

申请日时本专利记载的申请人、发明人信息如下：

申请人：

华南农业大学

发明人：

林雅铃;侯萌;张德强;张安强



荣誉证书

谭杏银、梁嘉琪、叶琪同学

在广东第十届大学生材料创新大赛中，荣获总决赛

三等奖

特发此证，以资鼓励。

作品名：一种新型的非渗透性皮肤消毒剂材料

指导老师：林雅铃、赵慧

主办单位：广东省材料研究学会

合作单位：广东省本科高校材料类专业教学指导委员会
(南方科技大学代章)

承办单位：广东工业大学材料与能源学院

二〇二〇年十二月二十日

HR

华南农业大学人力资源管

本科-课程论文(设计)

本科-毕业论文(设计)

讲授研究生课程

指导研究生折合学时

指导创新创业项目

近五年本科生评教

近五年研究生评教

评教结果排名情况

系统首页

职称评审

2024年度职称评审

林雅铃 (教职工)

表9-A 近五年本科生评教结果

帮助

重获数据

本页数据完整性校验

此数据来源于本科生院，按照时间倒叙排列，申报人无法填写或更改

	操作	学年学期	分数	参评人数	单位排名	开课单位	排名占比	数据来源	业绩审核意见	业绩审核意见说明
<input type="checkbox"/>	上移 下移	2019-2020学年第二...	91.2	114	75-51	材料与能源学院	68.00%	本科生院	通过	
<input type="checkbox"/>	上移 下移	2020-2021学年第一...	94.4	54	91-58	材料与能源学院	63.74%	本科生院	通过	
<input type="checkbox"/>	上移 下移	2020-2021学年第二...	96.64	56	84-1	材料与能源学院	1.20%	本科生院	通过	
<input type="checkbox"/>	上移 下移	2021-2022学年第一...	94.64	24	95-17	材料与能源学院	17.90%	本科生院	通过	
<input type="checkbox"/>	上移 下移	2021-2022学年第二...	96.07	66	86-1	材料与能源学院	1.16%	本科生院	通过	
<input type="checkbox"/>	上移 下移	2022-2023学年第一...	96.235	92	98-25	材料与能源学院	25.51%	本科生院	通过	
<input type="checkbox"/>	上移 下移	2023-2024学年第一...	98.255	82	89-10	材料与能源学院	11.24%	本科生院	通过	
<input type="checkbox"/>	上移 下移	2024-2025学年第一...	99.41	71	92-5	材料与能源学院	5.43%	本科生院	通过	